The Assessment of Surface Quality in Planed and Spindle Moulded Products

Keith Michael Maycock

A thesis submitted in partial fulfilment
of the requirements of De Montfort University
for the degree of Doctor of Philosophy

June 1993

De Montfort University

Acknowledgements

I would like to express my gratitude and thanks to the following people:

Prof. R M Parkin for giving me the opportunity to conduct this research and for his supervision throughout its duration.

Dr. T Buttery who, despite serious illness, continued to support my efforts.

Wadkin plc, Leicester for the use of their woodworking machinery and personnel; particularly **Michael Goddard** who saw a future in the project.

Kim Reeve for her encouragement and giving of her time, unselfishly.

Jo Cotterill for the hours she spent proof reading.

My parents, **Veronica and Garfield Maycock**, for their constant encouragement and moral support when times were difficult.

Paul "Have you finished it yet?!" **Bedford**, aged 6, for always asking.

Frank Cutri for what he did.

Each contribution has been very much appreciated.

SUMMARY

There are a lack of objective surface quality assessment standards in the timber planing industry. The current practice, that of visual and tactile inspection, results in a wide variance in what is classed as an acceptable or a defective surface finish. These methods, by their very nature, are subjective, and restricted to post-process application. Modern woodworking machines "extrude" timber at extremely high rates, often in excess of 140m/min. When the machining process develops a significant fault, a large quantity of defective timber is produced before the symptoms are detected by post-process inspection.

Evidently, there is a need to develop sensors capable of real-time, in-process monitoring of the surface quality. Thus, when process faults occur they are detected instantaneously, so that any necessary remedial action may be effected immediately.

Due to the high cutting speeds and vibration levels associated with wood machining, contact methods of in-process surface assessment are precluded; optical methods provided a more adequate bandwidth.

Discussions with woodworking machinery manufacturers and users reveal that the form and frequency variation of the planed surface are the critical factors that control its aesthetic qualities.

This thesis describes the development and validation of a non-contact, surface assessment system for planed and spindle moulded timber. The system uses a novel

Laser illumination and Machine Vision technique. The signal processing analyses the surface information using Fourier techniques to produce frequency "signature". These are then analysed to provide data on product quality.

The laser instrument, comprising, interface circuitry, optics and computer algorithms, to facilitate data capture from real surfaces, is a post-process device, designed using the principles of in-process assessment. A Fast Fourier Transform algorithm was used to convert the captured data to the frequency domain. In this form the data was further analysed, using tailored algorithms, to identify the nature and origins of any surface faults.

A mathematical model of the machining process was also developed and used as the nucleus around which a computer, surface simulation, algorithm was written. This model and algorithm was used as a tool to give insight into the nature of real machined surface profile faults, and to indicate their origins.

The laser instrument was validated by comparing its surface assessment results with that of an established standard engineering surface assessing system. Future work will include making the instrument more compact and adapting it for in-process use.

CONTENTS

LIST OF FIGURES vii

LIST OF TABLES x

1 INTRODUCTION 1

1.1 Early History of the Woodworking Industry 2

1.2 Planer - Moulder Evolution 5

1.3 Surface Quality. 10

1.4 Modern Planers and Moulders. 11

1.5 Research Objectives. 12

2 REVIEW OF PREVIOUS WORK 14

2.1 Introduction. 15

2.2 Performance Assessment. 16

2.3 Contact Methods of Surface Assessment. 17

2.4 Non-contact Methods of Surface Assessment. 19

2.5 Surface Analysis in the Woodworking Industry. 32

2.6 Application of Available Laser Techniques 36

3 PROPOSAL 38

3.1 Objective. 39

3.2 Proposed Instrument. 41

3.4 Proposed Development of Instrument 42

4 MATHEMATICAL MODEL OF THE PLANING PROCESS 44

4.1 Introduction 45

4.2 The Planing Process. 46

4.3 Curtate Trochoid Mathematical Model. 48

4.4 Loci Generation. 57

4.5 Loci Sampling. 58

4.6 Surface Profile Simulation. 65

5 DEVELOPMENT OF POST-PROCESS LASER INSTRUMENT 71

5.1 Introduction / General Description 73

5.2 Electronic Hardware. 76

5.3 Optical Hardware 88

5.4 Instrument Framework 94

5.5 Data Capture Software 97

5.6 Data Analysis Software 102

6 TIMBER MACHINING INVESTIGATION 132

6.1 Introduction 134

6.2 Planer - Moulder Machine 134

6.3 Machining Variables and Parameters 138

6.4 Machine Preparation and Condition 139

6.5 Timber Specification 141

6.6 Induced and Simulated Surface Finish Defects 142

6.7 Surface Finish Analysis 150

7 RESULTS 160

7.1 Introduction 161

7.2 Theoretical Results 161

7.3 Machined Timber Sample Results 162

8 DISCUSSION 165

8.1 Introduction 166

8.2 Hardware 166

8.3 Software 171

8.4 Machining Investigations 176

8.5 General Comments 199

9 CONCLUSIONS 200

9.1 Objectives Realised 201

9.2 Future Work 202

REFERENCES **204**

FIGURES **212**

TABLES **213**

APPENDICES **221**

LIST OF FIGURES

Figure 1.1: Early power-operated machinery was belt driven from lineshafts

Figure 1.2: Malcolm Muir's Planer, 1827

Figure 1.3: John McDowall's Planer, 1836

Figure 1.4: First Moulder with Integral Electric Motors, 1916

Figure 1.5: Elements of a Motorised Cutterhead with Spindle and Bearings

Figure 1.6: A Modern Moulding and Planing Machine

Figure 2.1: A Method of Assessing Surface Measuring Instrumentation

Figure 2.2: Multi-feature Measurement

Figure 2.3: Deutchke's Irregular Measurement System

Figure 2.4: Pneumatic Method

Figure 2.5: Capacitive Method

Figure 2.6: Schmaltz's First Method

Figure 2.7: Basic Principles of Optical Technique

Figure 2.8: Factors of various Optical Surface Assessment Methods

Figure 2.9: Glossmeter Principle

Figure 2.10: Mitsui's Instrument

Figure 2.11: Interference Method for examining Surface form

Figure 2.12: Optical Probe

Figure 2.13: Diffractometer

Figure 2.14: Foucault Knife-edge Method

Figure 2.15: Schematic of Heterodyne Method

Figure 3.1: Up-cutting Mode

Figure 3.2: Ideally Planed Surface

Figure 3.3: Proposed Method/Technique - In process

Figure 3.4: Proposed Method/Technique - Post process

Figure 4.1: Up-cutting Mode

Figure 4.2: Trochoid Family

Figure 4.3: Ideally Planed Surface Profile

Figure 4.4: Typical Surface Profile

Figure 4.5: Schematic of Cutterhead Action

Figure 4.6: Typical knife tip Loci from SSA - stage I

Figure 4.7: Typical knife tip Loci from SSA - stage I

Figure 4.8: Typical knife tip Loci from SSA - stage II

Figure 4.9: Typical knife tip Loci from SSA - stage III
Figure 4.10: Typical knife tip Loci from SSA

Figure 5.1.1: Schematic of the Post-Process System
Figure 5.2.1: Schematic of the BBC microcomputer
Figure 5.2.2: Schematic of the 6522 VIA
Figure 5.2.3: Read Handshake Timing Diagram for Port A Only
Figure 5.2.4: Write Handshake Timing Diagram
Figure 5.2.5: Schematic of Photodiode Array
Figure 5.2.6: Sensor Geometry and Idealised aperture Response Function
Figure 5.2.7: Photodiode Relative Spectral Response as Function of Wavelength
Figure 5.2.8: Photodiode Output Charges verses Exposure Characteristic
Figure 5.2.9: Power Supply Circuit Diagram
Figure 5.2.10:Timing Diagram for Photodiode Inputs and Outputs
Figure 5.2.11: Differential Amplifier used to extract "noise-free" signal
Figure 5.2.12: Sample and Hold Boxcar Video Signal
Figure 5.2.13: Timing Diagram - Data Capture

Figure 5.3.1: Beam Expander
Figure 5.3.2: Lens Maker's Formula: symbol definition
Figure 5.3.3: Beam Expander - The optical arrangement
Figure 5.3.4: Image Focusing - The optical arrangement
Figure 5.3.5: Graph of Focal Length against Image Distance
Figure 5.3.6: Lens Mount

Figure 5.4.1: Framework
Figure 5.4.2: Timber-Sample Clamping Device
Figure 5.4.3: Helium-neon Laser and "Floating" Carriage
Figure 5.4.4: Laser beam Incidence angle Adjustment
Figure 5.4.5: Image Alignment Mechanism
Figure 5.4.6: Dark-housing to exclude Ambient light

Figure 5.5.1: Determining Optimum Photodiode Integration Period

Figure 5.6.1: Time History of Sinusoid obtained with Oscilloscope
Figure 5.6.2: Time and Frequency Description of a Sine Wave
Figure 5.6.3: Summing Frequency Description of Sinusoids
Figure 5.6.4: Composing a Non-sinusoidal Waveform by Summing Sinusoids

Figure 5.6.5: Square Wave satisfies conditions for its Fourier Series to exist
Figure 5.6.6: Magnitude and Phase Spectra for Square Wave in figure 5.6.5a
Figure 5.6.7: Fourier Series and Fourier Integral
Figure 5.6.8: Relationship between Fourier Series and Fourier Integral
Figure 5.6.9: Comparison of diagram conventions: Series and Transform Spectrum
Figure 5.6.10: A Generalised Square Pulse and its Frequency-domain Magnitude and Phase
Figure 5.6.11: The Process of Rectangular Windowing
Figure 5.6.12: Zero-order Approximation
Figure 5.6.13: Result of the first step for an N=8 point decimation-in-time FFT
Figure 5.6.14: Result of the second step for an N=8 point decimation-in-time FFT
Figure 5.6.15: Final flow graph for an N=8 point decimation-in-time FFT
Figure 5.6.16: The Butterfly structure in the various stages of a decimation-in-time FFT
Figure 5.6.17: Modified Butterfly structure requiring only one complex multiplication
Figure 5.6.18: Rearrangement of figure 5.6.15: input in natural order, output bit-reversed
Figure 5.6.19 - 5.6.46 Validation of FFT Algorithm

Figure 6.1: The B-series 220 Planer - Moulder Machine
Figure 6.2: Head unit Specifications of the Modular "200B"
Figure 6.3: Final Top Head
Figure 6.4: Spindle Unit Bearing Assembly
Figure 6.5: Hydrogrip Planing Cutterblock and Cutterheads
Figure 6.6: Heavy Duty In-feedworks and In-feed Table
Figure 6.7: Out-feedworks
Figure 6.8: Chipbreaker
Figure 6.9: Side Pressure Rollers
Figure 6.10: Standard Jointer fitted to Top and Bottom Cutterheads
Figure 6.11: Dust Extractor System
Figure 6.12: Socket Screw Positions used to Induce Cutterhead Imbalance
Figure 6.13: An NX-grinder used for producing Proud-knives
Figure 6.14: Timber Sample Analysis by Laser Instrument
Figure 6.15: Timber Sample Analysis by Talyrond 200
Figure 6.16: Results from Profile Simulation - Proud-knife
Figure 6.17: Result of Pulse-train Simulation - Proud-knife

Figure 7.G0.S1 - Figure 7.G0.S6: Results: Theoretical Only
Figure 7.G1.S1 - Figure 7.G1.S8: Results: Single-knife finishes
Figure 7.G2.S1 - Figure 7.G2.S12: Results: Head Imbalance
Figure 7.G3.S1 - Figure 7.G3.S15: Results: Proud Knife finishes

Figure 7.G4.S1 - Figure 7.G4.S6: Results: Vibrational effects

Figure 7.G5.S1 - Figure 7.G5.S5: Results: Fault Combinations

LIST OF TABLES

TABLE 1: Calibration Table for micrometer-controlled Angle of Incidence of Timber Illumination

TABLE 2: Example of Bit Reversal for 3 bits

TABLE G1: Single knife finish

TABLE G2: Unbalanced Cutterhead

TABLE G3: Proud Knife

TABLE G4: Timber Vibration

TABLE G5: Fault Combinations

1 INTRODUCTION

1.1 Early History

1.1.1 Saw-mills

1.1.2 The Steam Engine

1.1.3 Rotating Cutterhead

1.1.4 Planing Machines

1.1.5 Lineshafts

1.1.6 Tongue and Grooving Machine

1.2 Planer - Moulder Evolution

1.2.1 Early Moulder Developments

1.2.2 Design Improvements

1.2.4 Electric Motors

1.2.5 Refinements and Modifications

1.2.6 Ball Bearing Electric Moulder

1.2.7 Spindle Design

1.3 Surface Quality

1.3.1 Defective Finish

1.3.2 Current Surface Analysis

1.4 Modern Planer Moulders

1.5 Research Objectives

1.1 Early History of the Woodworking Industry

1.1.1 Saw-mills

Saw-mills powered by water wheels were in general use in mainland Europe as early as the 14th Century. They were introduced in England much later; the delay was due to the fears that their use might have inflicted damage to the sawyers' trade.

These early mills used reciprocating saws; the cutting and shaping of timber products by machine is a comparatively recent practice. The spindle shaping and moulding of timber first became a practical proposition about 200 years ago when rotating cutting tools became available, coupled with an "available-on demand" source of power.

1.1.2 The Steam Engine

When the condensed steam engine was invented by Watt in 1769, for the first time there was a readily available source of power which could be installed in any appropriate location. The steam engine made possible, and paved the way for, the industrial revolution in which the large scale production of timber products featured.

1.1.3 Rotating Cutterhead

Initially, with the exception of hand tools used on lathes, there were no implements available which could be utilised in the machine cutting of wood. The major breakthrough occurred in 1777 when Samuel Miller invented the circular saw. When, over a decade later (in 1793), Samuel Bentham

developed the rotating cutterhead, the chief concern of the industry - improved surface quality coupled with increased throughput - became a possibility.

With the steam engine as a power source, the implication of the circular saw and rotating cutters set the stage for, and launched the woodworking industry into, a new era - an era which saw the development of continuous cutting woodwork machinery, enabling the mass production of items, the shapes of which could be diversely varied.

1.1.4 Planing Machines

The roots of most of the woodworking machinery in use today can be traced back to those invented between 1777 and 1850 (Mansfield J.H, 1952). Nine years after Samuel Bentham filed his patent in 1793, saw a further landmark in the evolution of woodworking machinery, bound to produce superior and consistent quality surface finish; in 1802 Joseph Bramah patented and started building planing machines; they were about 40 feet long and the timber was clamped to a table which moved backwards and forwards past a horizontal, primitive cutterhead.

1.1.5 Lineshafts

Early power-operated machinery was belt driven from lineshafts (figure 1.1). These in turn were driven from a prime mover; this was initially water power but was superseded by the steam engine.

The lineshaft's speed would vary from about 90 to 150 rev/min; some were made of wood, others of cast-iron; the driving pulleys were made of laminated wood. From the lineshaft there was a belt drive to the machine or to an intermediate countershaft.

1.1.6 Tongue and Grooving Machine

In 1827 Malcolm Muir invented a machine from which modern planers have been developed (figure 1.2); the timber was moved by an endless chain and passed through the machine. The timber first passed a rotating cutterhead carried on a vertical spindle which machined a datum face, and then over three bottom knife blocks containing fixed knives for planing the underside of the timber.

A tongue was then cut in the datum face by saws mounted on horizontal spindles (one above the board, the other below) each cutting to a depth of the tongue. The timber then passed through two horizontal saws on vertical spindles which cut through to the saw cuts made by the vertical saws; this produced a sawn out tongue.

On the opposite side to the datum face the board was cut to width by a saw; this widthing saw was followed by a grooving saw which cut the horizontal groove. The vertical spindles on each side of the machine (used for the tonguing and grooving operation) also carried revolving cutters which machined overlapping rebates on the top of the board; this determined the thickness of the board.

Although throughput on these machines increased, the surface finish of the products was inconsistent and generally of poor quality.

1.2 Planer - Moulder Evolution

1.2.1 Early Moulder Developments

John McDowall built machines to Malcolm Muir's designs but gradually introduced his own modifications. By 1836 when he filed his patent, his modifications had converted the original machine to the form of planers currently being manufactured (figure 1.3); feed rollers replaced the endless chain; rotary cutterheads replaced the tonguing and grooving saws. This brought the woodworking industry closer to the ideal - consistent, high quality surface finish combined with continuous, high speed production.

For many years, right into the 20th century, some woodworking machinery manufacturers produced machinery of wood framed construction. There was a theory abroad that wood was better than iron for this purpose because it more readily absorbed the vibration of fast running machinery which would otherwise be conveyed to the products surface finish; also, it was thought that it would be less easy to bruise the product if the machines were built of wood rather than metal.

As general technical knowledge increased, cast-iron frames were introduced followed by phosphor bronze bearings; the bearings ran in oil or grease; fat would sometimes be packed around the bearings so that if they did get hot, the fat would melt and, hopefully, prevent the bearings from seizing up.

Worn bearings would permit play between the bearing and the journal, with consequent deterioration, in the case of planing and moulding machines, in the quality of the product's surface finish.

1.2.2 Design Improvements

By the end of the 19th Century the progress in technology had made it possible to manufacture machinery much more accurately; the turn of the century saw many engineering developments taking place which greatly affected the quality of timber products and the rate at which they were manufactured. These included the appearance of precision ball bearings (Burnner H.E, 1929), higher spindle speeds and better tooling.

Circular cutterheads with thin knives replaced square cutterheads with thick knives; square cutterheads were limited to only four knives; circular blocks could accommodate higher rotating speeds, larger number of knives and consequently facilitate greater feed speeds for a given surface finish. The addition of feed rollers and pressure rollers permitted multiple feeding of narrow stock of slightly differing thicknesses.

1.2.4 Electric Motors

Electric motors were first used in woodwork machinery shops as a means of breaking down complicated transmissions powered from a single prime mover. Situations had developed where one shaft could be driving another, perhaps on another floor or in other buildings. Thus, the larger workshops were a maze of pulleys and overhead belting. Some of the smaller woodworking

plants presented a tidy appearance by hiding the lineshafts under the floor, but the maze of belts, though hidden, were still there and the machine positioning had to be related to the lineshaft and not to the convenience of work flow through the shop.

Woodworking machines, due to their comparatively high cutting speed requirement, readily lend themselves to being driven by a compact electric motor. Initially, the convenience of electric motors was used only to drive individual lineshafts; later, machines which had an integral electric motor were being designed and manufactured (figure 1.4).

1.2.5 Refinements and Modifications

The power transmission from a prime mover, via lineshaft and countershaft, to machine was extremely inefficient, with approximately half the power lost. This motivated the initial efforts towards individual drives (Mansfield J.H, 1952).

Many refinements followed the integral drive; the heads were provided with a brake to bring the spindle to rest rapidly; independent start and stop button controls replaced cumbersome belt striking gear and allowed only the required heads to be selected; direction of rotation could be selected, as required, at the push of a button; it was possible to provide motors with six different speeds, at the turn of a switch - this eliminated the use of multi-step gearboxes.

This type of machine was a great success; it only required one-third of the floor space of its belt driven counterpart, with its countershaft; it eliminated the problems of belting maintenance, which was considerable on the fast machines; there was no slowing down of spindles under load because the motor speed was relatively constant and the motors were designed to cope with a 100% overload. Thus, there was no tearing of the grain, as had been the experience with belt driven spindles which would slow down under sudden load, due to belt slippage. As a result product surface quality became more consistent.

1.2.6 Ball Bearing Electric Moulder.

The monumental breakthrough in woodworking technology happened when the ball bearing electric moulder was introduced, with a built-in motor mounted directly on each cutterhead arbour. The absence of belts made it possible to tilt all the heads to any desired angle and thus combine several cuts in one operation; previously this had been accomplished on a number of separate machines; there was also a 40% to 60% power saving.

Some of the early electric moulders were used in motor car body plant shops on components which were concealed, so that the knife mark spacing (a measure of the quality of the surface) was not very important. It was found that with the new electric moulders, the components could be fed up to four times as fast as the belt driven machines, with a more consistent depth, spacing and parallelism of the knife marks; also, there were fewer splinters and tears, despite the faster speeds. The reason for this was that the

spindles were mounted in close-fitting, anti-friction ball bearings, in contrast to spindles which float on a film of oil (as was the case with friction bearings); ball bearings restrict the spindle's end play; also, direct driven motorised spindles were rotated by balanced magnetic forces as opposed to being subject to the pulling and pounding of high speed belts.

1.2.7 Spindle Design.

As soon as the importance of spindle rotation was recognised as a contributory factor in surface finish, a great deal of attention was given to the design of the motorised spindle unit. Ball bearing tolerances were considered and it was found that the original allowances, specified for the first electric moulders, should be reduced by one-tenth (Burnner H.E, 1929).

It was found that the solution to spindle design was to use a large diameter spindle with a ball bearing at either end (figure 1.5); the cutter arbour projected beyond the main bearing at one end of the spindle and the rotor for the motor projected at the other. All of this was carried in a cylindrical frame (machined on the outside) with a flange mounting at one end to carry the motor's stator frame.

Thus, the whole motorised spindle unit could be mounted in a robust sleeve on the machine. The sleeve was designed to permit lateral movement of the motorised unit together with adjustment of cutterhead position; longitudinal movement of the whole unit, with its supporting sleeve, was also catered for. Thus the complete head was concentric and rigidly secured to a main frame,

which was also of rigid construction.

1.3 Surface Quality.

1.3.1 Defective Finish.

Although other improvements followed, such as the development of long-lived, high-speed steel tooling, the introduction of power feed units, hydraulic pressure pads, pivoting chip breakers, the application of electronics, microprocessors, etc, the superior design of a moulder, assessed in terms of the surface quality produced, still depends primarily on the degree to which the cutterhead can achieve perfect rotation. This end is pursued by improving the design of spindles, the means of applying power to them, and taking steps to eliminate vibration.

For high production rates, cutterblocks which carry a large number of knives are essential. During ideal cutting conditions, for a given rotational and feed speed, the surface finish required depends on the number of knives present on the cutterhead; increasing the number of knives will reduce the surface's knife-mark pitch and consequently improve its quality.

With multi-knife cutterblocks the probability that some will stand proud of, or below, the desired common cutting circle diameter is high; the repercussion, in multi-knife planing operations, is a defective surface finish. To alleviate this, "jointing" is employed. Jointing is analogous to the dressing of a grinding wheel in order to true eccentric running and expose new grits. In a similar way, the individual knives of the cutterhead are

dressed with a carborundum stick to remove eccentric tracking and produce a new cutting edge.

The surface finish of planed and spindle moulded products may also be affected by the degree to which the cutterhead is dynamically balanced. The locus of each knife on a cutterhead will be influenced by the fact that the block is unbalanced; this is significant because the height of the cusps produced by ideal cutting action is of the order of 10 to 25µm while the eccentricity effected by just a few grammes, at rotational speeds of 15000 rev/min, is in the region of 30µm to 50µm; this will obviously have a marked effect on the surface finish (Jackson M.R, 1986).

1.3.2 Current Surface Analysis.

The woodworking industry has not yet acquired a reliable method with which to quantify and categorise the surface quality of its planed and spindle moulded products. The current practice is that of visual and tactile inspection, which results in a wide variance in what is classed as an acceptable or defective surface finish; what one manufacturer may reject as an "unacceptable standard", another may accept as "good". These methods, by their very nature, are subjective and are restricted to post-process application.

1.4 Modern Planers and Moulders.

Modern woodworking machinery have benefitted extensively from the technological advances, developments and discoveries of the past (Timber

Trades Journal 1986a, 1990a, 1990b; Parkin R.M, 1988). The use of computers for the control of the production process is widespread (Bolzing D, Liu F, 1987; Thomlinson J, 1987; Cowdery M.J, 1990). Contrasted with those of the past, current spindle moulders and planers (figure 1.6) are highly sophisticated and complex machines, producing elaborate, extremely accurate and superior quality components (Timber Trades Journal, 1986; Cowdery M.J, 1990).

Ever increasing production rates are being demanded of modern machines; current maximum spindle speeds are of the order of 15000 rev/min, resulting in cutting speeds in the region of 100 metres per second (Timber Trades Journal, 1986b). With feed speeds in excess of 150 metres per minute, the spindle moulding process is comparable to that of an extrusion machine, the moulder employing a number of rotary heads to produce the profile, as opposed to a single die head used in the extrusion of plastics and aluminium.

1.5 Research Objectives.

Despite the application of the knowledge and expertise accrued during the history of the woodworking industry, there are still inherent faults and defects within the planing/moulding process which manifest themselves with undesirable frequency (Jackson M.R, 1986). With "extrusion" rates in excess of 150 metres per minute, when a process fault develops (eg. bearing failure, excessive vibration, proud knife, etc.) a considerably large quantity of sub-standard (defective surface finish) timber is produced before the symptoms are detected by post-process, visual/tactile inspection.

Evidently, to ensure consistent quality and economy, it is necessary to develop sensors capable of real-time, in-process monitoring the surface quality of the product (Goddard M, 1985). Thus, when process faults occur they are detected instantaneously, and any necessary remedial action effected immediately. Also, a practical and more precise method of specifying the surface finish of machined wood is required to ensure consistent quality of production (Jackson M.R, 1986; Goddard M, 1985).

This thesis is an account of investigations undertaken in the field of surface assessment of spindle moulded and planed products. The research sought to develop a low-cost, adequate sensor/transducer and appropriate analytical techniques for quantifying the surface finish produced by moulders/planers within the woodworking industry.

2 REVIEW OF PREVIOUS WORK

2.1 Introduction

2.2 Performance Assessment

2.3 Contact Methods of Surface Assessment

2.3.1 Stylus Technique

2.4 Non-contact Methods of Surface Assessment

2.4.1 Pneumatic Technique

2.4.2 Capacitance Technique

2.4.3 Ultrasonic Technique

2.4.4 Optoelectronic Techniques

2.4.4.1 Gloss Meters

2.4.4.2 Interferometers

2.4.4.3 Optical Probes

2.5 Surface Analysis in the Woodworking Industry

2.5.1 Visual-Tactile Methods

2.5.2 Stylus Instruments

2.5.3 Optical Techniques

2.6 Application of Available Laser Techniques

2.1 Introduction.

Only in the past 50 years has the importance of surface shape and texture received recognition (Harris P.G, Trigg A.D. 1987). Between 1940 and 1960 considerable research was carried out on tribology; in particular, work in contact phenomenon such as friction and wear was dominant (Hingle H. 1986). Much of the basic correlation relating such functions to the surface geometry was not discovered because of the inherent difficulty in measurement.

Another drawback was the limitation of the available instruments; only rudimentary surface parameters such as Roughness average (R_a) and, to a limited extent, peak features could be measured. It was only with the advent of digital methods that the breakthrough occurred.

There has been slow progress in the field of instrumentation required to measure surfaces effectively. This restriction was due to a number of problems: There was not a true understanding of surfaces and their functions; the limitation in data processing power; the limitations of the instruments themselves. In recent years these three areas have been brought together by the use of random process analysis, digital methods and contacting and non-contacting methods. This chapter reviews current trends in these areas and highlights their advantages, disadvantages and present applications.

2.2 Performance Assessment.

One of the ways in which the performance of surface measuring instruments can be assessed is shown on figure 2.1. There are two axes; the horizontal one is the range of the instrument divided by its resolution and the vertical one is its frequency response.

As can be seen from figure 2.1, a conventional instrument has a range to resolution of about one in one thousand and a frequency response of several hundred Hertz (Whitehouse D.J, 1972). This working point is more or less fixed, at present, for a good instrument design. Future instrument designs will tend to, and attempt to, move this working point.

The implication for the axes of figure 2.1 in terms of instrumentation in engineering metrology is as follows:

The horizontal axis is, in effect, an integrated measurement axis; the further the working point moves to the right the greater the possibility of integrating many features of the geometry together in one measurement.

The vertical axis is a measure of the instrument's potential for in-process application, implicating assessment while the workpiece is being manufactured.

2.3 Contact Methods of Surface Assessment.

2.3.1 Stylus Technique.

Great advances have been made in integrated measurement using the stylus method, ie. the moving of the working point to the right of figure 2.1. For instance, by having an instrument with a large dynamic range and high resolution (such as a range to resolution ratio of one million) it is now possible to assess the track of a ball race measuring not only the radius and surface finish and centres separately but to measure its total geometry simultaneously (figure 2.2). Previously this could only be achieved with the use of three separate instruments (Phillips M.J, Whitehouse D.J. 1977; Stevens D.M.G, 1989).

Thus, by attaching a digital computer to a wide-range transducer system it is possible to achieve an integrated measurement. This does not imply that just linking a computer to the instrument achieves anything; it has to be supported by appropriate mathematics.

The use of sophisticated mathematics is also a recent trend in the field of mechanical instrumentation. It is now possible to utilise some of the mathematics which, although established for many years, have been impossible to implement due to lack of computing power. One crucial element necessary to effect the calculations is a fast computer; their availability has enabled dramatic improvements in the stylus method when observed on the merit graph of figure 2.1.

As well as good mathematics and fast computers, it is also vital that excellent

sensors and transducers are employed. To this end one of the recent achievements has been the marriage of optical methods with mechanical methods which has produced stylus sensors having large dynamic ranges (Drews W.E, 1987). Typically, it is now possible to use an interferometer as part of the transducer (Stevens D.M.G, 1989; Sherrington I, Smith E.H, 1988). Of necessity, the interferometer has to be very small; with modern polishing techniques it is possible to manufacture miniature prisms and lenses. This implies that the components are of the order of millimetres as opposed to centimetres in size. So, having measured the workpiece totally it is possible to isolate certain features of interest, amplify them using the computer, and examine them in more detail (Babus, Probert, O'Callaghan and Evans, 1988).

The other direction in which stylus instruments can improve is in that of in-process measurement. Progress in this department has not been as dramatic as in integrated measurement. The main reason for this is that stylus instruments are sluggish in their response; they have an upper bandwidth of about 450 Hz (Whitehouse D.J, Bowen D.K, Chetwynd et al, 1987) and are of delicate construction making them unsuitable for the often hostile environment of production processes (Jackson M.R, 1986).

Some advances have been made, however, in developing more portable instruments. This entails making them small, capable of being hand-held and being easily transported to the locale of use. Small instruments are particularly useful for measurement on large components which cannot be

moved. For example, a shaft in a ship engine.

Today, typical instruments for measuring surfaces or measuring roundness in situ can be small enough to be carried in the pocket (Quality Today, 1986). These instruments are, clearly, not as sophisticated as those in inspection rooms but can be very effective from the point of view of quality control.

Despite the distinct stagnation in the progress towards the in-process use of stylus instruments, attempts are still being made to measure and assess surfaces while they are actually being produced. One such method, of German origin (Deutchke S.J et al, 1973), comprises of a drum which is pushed onto the workpiece (figure 2.3). Out of the drum protrudes a single probe with a transducer on the end. As the workpiece rotates and the drum is driven, the probe is forced to make contact with the workpiece once every one revolution of the drum. The amount by which the probe penetrates the circumscribed circle about the workpiece is recorded so that over many revolutions a picture of the surface distribution is accrued. Although this method has problems because of the influence of debris and coolants it is a step in the correct direction along the road to in-process gauging using stylus instruments.

2.4 Non-contact Methods of Surface Assessment.

A very good criterion for a sensor-transducer system is to maximise the change of energy per unit displacement; this enables a good signal-to-noise ratio to be achieved. With this criterion, the following non-contact methods

of assessing surfaces will be considered:

Pneumatic Technique,

Capacitive Technique,

Ultrasonic Technique.

2.4.1 Pneumatic Technique.

In this method air is blown onto the object surface via a measuring head and skirt. The air which escapes between the skirt and surface can be related to the surface finish (see figure 2.4a); in practice the leakage is proportional to the surface finish and the average distance between the skirt lip and the surface.

There are two ways in which pneumatics can be employed; one is to measure the air flow directly - monitor the flow to see how it changes with the surface finish (figure 2.4b). The second is to consider the effect of the surface finish on the back pressure in the air supply (figure 2.4c).

The use of pneumatic techniques for surface evaluation has disadvantages: The range to resolution of these devices is relatively low - about 100:1 - and therefore does not compare well with stylus methods. Their main advantage is that they do not contact the workpiece and are comparatively cheap. However, other problems are evident; for example the skirt geometry must approximately follow the average form of the workpiece, otherwise too much air escapes (due to mismatch of shape). Another problem is that unless the

air used is clean and dry, water can form when the air escapes from beneath the skirt of the instrument. For these reasons pneumatics are not generally considered to be viable as a method for assessing timber surface quality.

2.4.2 Capacitive Technique.

Another method is the use of capacitance; here an electrode is positioned above the surface to be analyzed in the presence of a dielectric between the two (figure 2.5). The capacitance between them can be used to assess the texture (Crookall J.R, Sherwood K.F, 1968). The relationship between capacitance and surface is not very straightforward - in fact, it is an inverse law in which there is an extra term, the average distance (**d**) of the electrode from the surface, is added to the denominator:

$$\text{capacitance} = \iint (d+f(x,y))^{-1} dx\, dy \qquad (2.1)$$

The capacitive method is very sensitive and can therefore be used quite effectively in various applications. There are problems however. The signal from the transducer is susceptible to extraneous electrical noise and therefore if very small or sensitive signals are being measured, effective shielding must be employed. Another problem is that the shape of the electrode must nominally follow the shape of the surface being assessed. Further to this, changes in moisture content or in ambient conditions of the material being assessed has a marked effect on the results obtained.

The capacitance technique does have advantages: it is non-contacting, very sensitive and it measures over an area; stylus methods, clearly, do not.

Nevertheless, for general purpose use in surface metrology it is not regarded as a preferred method.

2.4.3 Ultrasonic Technique.

In this method ultrasonic waves are projected onto the surface and the reflected, scattered waves are detected. From the captured signal the surface finish is assessed. One advantage of the method is that it is relatively easy and straightforward to obtain the phase as well as amplitude of the reflected signal; this is of benefit as it provides two sources of information from which to assess the surface.

In principle the method shows much promise, in practice problems arise. Ultrasonics are very difficult to propagate through air; the rate of attenuation is considerable. It is also very difficult to manufacture miniature ultrasonic sources and directionality of the received signal is hard to achieve. Research work is continuing in this field but to date no practical instrument has been realised (Smith P.F, Player M.A, Collie D.L.A, 1988).

2.4.4 Opto-electronic Techniques.

The "non-contact", "rapid-response" nature of light, coupled with recent advances in laser and opto-electronic technology, has brought about interesting and new possibilities for in-process assessment of product quality.

The very first optical method for assessing surface finish was that adopted by Schmaltz in 1927 (Schmaltz G, 1936); he projected a light source onto the

surface (from one angle) via a sharp edge (eg. a razor blade) and observed the interface between the illuminated and shadowed surface (from another angle), figure 2.6. This, in effect, produced a pseudo-profile which is indicative of the surface finish; the method is not quantitative.

The basic principles of most optical techniques are illustrated in figure 2.7; a ray of light (at angle of incidence θ) impinges upon, and rebounds off, the object surface. The degree to which the surface affects the reflected light can be used as a measure of the surface finish or texture. There are four main parameters or variables in this configuration:

1) The angle of incidence of the illuminating light beam.
2) The spot size illuminated by the light on the surface.
3) The scattering angle of the light reflected from the surface.
4) The type of light source.

Figure 2.8 represents the different possibilities of assessing surfaces using optics; the abscissa, in essence, represents the spot size; the ordinate denotes three functions:

1) Cost
2) Fidelity (the degree to which the reading is compatible with a reading of the same surface made with a stylus instrument).
3) Speed of Response.

At the extreme left ("the origin") of figure 2.8 is the stylus instrument which, by virtue of the above definition, has a fidelity of one. Then comes the optical probe, which is in effect a mimic of the stylus probe; because of factors such as polarization and variation in intensity of light, the highest fidelity

obtainable is about 0.9 (Arecchi F.T, Bertani D, Ciliberto S, 1979).

Further to the right of figure 2.8 is the laser scanner, diffraction (or interference methods) and gloss meter; moving to the right increases the area of illumination. It can be seen that the methods on the left-hand side of figure 2.8 are useful in the field of technology, giving absolute readings which are traceable to standards; this truth diminishes as instruments towards the right of the figure are considered. These instruments tend to be cheaper, less accurate and, consequently, they are mostly used as comparators rather than absolute measuring systems. They have, however, a much faster dynamic response and therefore more likely to be effective for in-process measurement.

2.4.4.1 Gloss Meter.

On the extreme right of figure 2.8 is the simple glossmeter; the principle of which is shown in figure 2.9. A light is shone onto the surface and is scattered from it. Two photo-detectors, A and B, detect the intensity of the light falling on them; detector A is positioned at the angle of specular reflection; this corresponds to the same angle from the normal as the incident light; detector B is positioned to detect diffused reflection.

By considering the way in which the surface scatters the light (ie the amount of reflected light that reaches the two detectors) the surface finish can be estimated. For example, from the very smooth surface of figure 2.9(a) most of the light is specularly reflected (as in a mirror) so the majority of the light will arrive at detector A and very little at detector B. So the calculation of

$$\text{value} = (A-B)/(A+B) \qquad (2.2)$$

will result in a value nearly equal to unity.

According to this rough scale, an optical finish would produce a surface having a value of 1. This quality of surface is only detectable if the surface roughness is about one-eighth of the wavelength of the illuminating light (Whitehouse D.J, 1985). As the surface gets rougher (say $\lambda/2$) more light gets scattered into B than in the case of the mirror finish and the ratio of the detectors give the value 0.5 rather than 1 (figure 2.9(b)). For very rough surfaces, where the surface finish is much bigger than the wavelength of the illuminating light, there is an equal probability of scattered light impinging detector B as hitting A. The result of the calculation in equation 2.2 will be a value of zero (figure 2.9(c)). Thus, it is possible to classify surfaces according to their roughness by illuminating them with light; a good surface results in a value of one, a bad surface produces a zero.

For a specified process it is possible to obtain good correlation between the R_a measured using a stylus instrument and the numerical value of the quotient, (A-B)/(A+B) (Whitehouse D.J, 1985); this is not necessarily linear but the curve would be constant for a particular process, albeit a different curve for every process. Thus, this merit value is not directly related to R_a; it can only be used as a comparator within a process and not for comparisons between processes.

A typical example of an in-process, surface assessment system being developed by Mitsui is shown in figure 2.10 (Mitsui K, 1986). Mitsui uses a He-Ne laser, of 1mW output, as a light source. The laser beam is directed onto the object surface through a series of mirrors and an objective (NA = 0.1, X5). For the detection of the reflected light position, a PIN photodiode array, which can measure centre position of the light spot directly as a voltage, is used. It is necessary to scan the array quickly enough to detect movement.

While Mitsui reports a measuring range of -30μm to 20μm with his measuring system, like other researchers in this field (Hattori M, 1981; Inasaki I, 1982), mention is made of the effect of surface vibration on the measurement/assessment technique.

Object surface vibration would have a marked effect, introducing spurious data and causing inaccurate results.

2.4.4.2 Interferometers.

More sophisticated methods employ coherent light to illuminate the surface and compare the reflected light with that from a reference (eg. a glass flat or an interferometer reference mirror). The reference flat can be positioned as in a Twyman Green interferometer (or a multiple beam interferometer) by laying it on the surface. Fringe contours can be observed which give a mapping of the surface (figure 2.11). Each contour line represents a line of constant height. Careful observation of the contours can give a real insight into the general shape of the surface and by use of suitable optical processing

it can be used to make a quantitative assessment of the surface finish.

The major disadvantage with the method is that it demands a considerable amount of operator skill to unravel the fringe pattern. This has been the biggest problem using interferometers and is why they have not been used more widely. However, there have been attempts to make the use of these interferometers more accessible.

One such development makes use of the mireau interferometer principle (Wyant J.C, 1985). This interferometer technique uses a photodiode or a television camera to view the interference fringe; the fringe pattern is stored. The viewing reference optics are then moved axially using a piezoelectric transducer; this moves the reference by one-third of the light's wavelength; the camera then takes another picture of the fringes, which is stored in the computer (figure 2.12). This is repeated a third time. The basic idea being that a number of movements are made in the z-direction covering one wavelength of the light.

The stored computer images of the fringes can be used to give the actual height at any position in the plane, resulting in either a profile or an area. The area method tends to have a relatively low resolution. Both can give ambiguous results if sharp edges are present on the surface; this is due to diffraction.

The method does, however, require a reasonable flat surface and there is the problem that when the objective is moved in the vertical direction it cannot be allowed to twist, otherwise the mechanical relationship between positions is lost, which results in a considerable depreciation in fidelity between the different pictures.

Another development which fits into the same family as interference methods is that of diffraction techniques. In one embodiment (Whitehouse D.J, 1972) a collimated beam of laser light is projected onto the surface (figure 2.13). This is scattered by the surface, collected optically and directed onto a photodiode array. The diode array is addressed by a computer so interrogation can take place.

The key to the technique is that the optics in the instrument have to be arranged such that light reflected from the surface at any one angle is imaged onto the detector at one spot. This is achieved by placing the detector in the back focal plane of the objective lens. This particular configuration has considerable benefit in metrology providing certain surface-finish conditions are met; the intensity pattern on the detector can be regarded as the power spectral density of the surface geometry provided the surface finish is relatively small compared with the wavelength of light; one-eighth of the light's wavelength is considered to be small.

One advantage of the technique is that small details on the surface tend to be scattered over very wide angles which produces a large displacement

signal on the detector. Therefore, large displacements on the detector corresponds to small distances on the surface; this is unusual in the sense that small details are normally more difficult to measure than large ones.

From the power spectrum it is possible to evaluate the surface roughness R_a value and the average or RMS slope of the surface and the RMS curvature (Rakels J.H, 1986)

There are practical problems with the technique. Because the angle of reflection rather than its position in the workpiece is being imaged the method is not sensitive to particular spots and blemishes. In fact, it measures the average surface properties and does not image directly in the same way as conventional optics, so movement of the workpiece can be tolerated; the workpiece can move in the X and Y directions and there is no effect on the detector. However, yaw of the specimen can pose a problem because the light scattered from the workpiece can miss the detector optics. Again, because an area is being assessed via scattered angles rather than an image system, any debris which emerges from the workpiece as it is being machined will have very little effect on the detector signal. This is because if one chip flies between the instrument and the component it will tend to restrict light coming from the surface at all angles by an equal amount. The result is that the total light falling on the detector drops very slightly but it drops over the whole detector and not just in one spot; all frequencies are attenuated equally. This is not important from the point of view of measuring surfaces, as it is the relative amplitudes of the spectrum which are

important not the absolute values.

The frequency response of the instrument is limited by the time taken to process the detected signal. The size of the device need not be large and bulky.

2.4.4.3 Optical Probes.

Optical probes are also an interesting area for consideration; in this technique an instrument has been devised in which the stylus tip is replaced by an optical spot.

The majority of instruments of this type have been achieved with a "follower" device in which, although the surface is not contacted, the sensor follows the surface at constant separation.

One method is based upon the Foucault knife-edge test (Dupuy M.O, 1967). In this method a laser is imaged onto the surface. This light is re-imaged from the surface onto a partial obstruction in the image plane (figure 2.14). Conventionally this obstruction is a knife edge but can be one from an assortment of masks.

When focused on the surface, the spot will be imaged onto the knife edge. This will produce a particular shadow pattern on the detectors which are placed behind the knife edge. If the surface has a deep valley and the spot drops into it then its image is formed in front of the knife edge. This

produces a different shadow pattern on the detectors. This difference in shadow pattern, from in focus to out of focus, operates a control system which moves the objective lens down to recreate the focus (vice versa for a peak). This is achieved using a piezoelectric device. By monitoring the movement of the objective lens and optical system it is possible to get a measure of the surface finish as a profile.

One of the most successful ways of devising an optical probe is the heterodyne methods which use common path interference in which two types of illumination come to bear on the surface simultaneously (figure 2.15). Invariably the light is split into two different wavelengths or different polarization (Sommargren G.E, 1981). The two rays of light, having different wavelengths or polarisation, focus in different places, either transversely or axially.

It is therefore possible to follow the surface geometry by examining how the surface affects the two focused spots. Using this principle (common path interference) some of the very finest surface finish measuring instruments have been made, measuring to tenths of a nanometre. They tend to be relatively slow, however, as adjustments within the instrument have to be made; also movement of the optical elements does limit the frequency response (typically less than 100 Hz) and hence the speed at which the surface can be followed. The use of different wavelengths and different polarization can cause problems as surfaces can react differently to electromagnetic waves.

In practice there is no guarantee that the same result obtained from a mechanical stylus would be repeated by an optical stylus because of the nature of each interaction with the surface is different. Both have inherent problems; with the mechanical method the surface has to be relatively hard, with the optical method the surface has to be reflective.

2.5 Surface Analysis in the Woodworking Industry.

The machining of wood, as compared to that of metals, has attracted very little research since the late nineteen fifties. The little research which has been done in this area is disjointed, un-coordinated and non-sequiturial in its history.

Woodwork machinery researchers have looked at the areas of cutting forces (Kivimaa E, 1950), chip formation (Koch P, 1964), surface wave theory and vibration (Petter C, 1954; Goodchild R, 1963; Mori M, Hoshi T, 1964) and factors which affect the surface quality of rotary planed timber components (Davis E.M, Nelson H, 1954).

Currently popular methods of surface analysis have their origins within the metalworking industry. Surface roughness measurements are normally made using stylus instruments having relatively short traverse lengths. Established analysis techniques offer a means of characterising profiles; broadly speaking the various methods may be divided into categories which define the amplitude, or the wavelength, variation, although some methods are found to deal with both regimes simultaneously (Peklenik J, 1968).

2.5.1 Visual/Tactile Methods.

Visual/tactile methods have been used since the early days of woodworking (Brown H.P, Panshin A.J, Forsaith C.C, 1952; Koch P, 1955)). Today it is still the most popular technique used, by customers and manufacturers alike, for assessing the quality of planed timber (Jackson M.R, 1986; Goddard M, 1985; Maycock K.M, et al, 1987). Because of its subjective nature, the method has many shortcomings. There is no quantitative assessment of the degree of waviness defects and, as such, no standards can be formulated. This results in a wide variance in the classification of surface finishes throughout the industry. The problem is compounded by the fact that there are no definite standards for the waviness quality of planed timber. Considerable conflict is thus caused between manufacturers and customers when each use their own, different, subjective assessment "standards" (Deal R.C, 1951).

Research into visual/tactile methods (Stumbo D.A, 1963; Knudsen V.O, 1928; Brown I.D, 1960; Schmaltz G, 1936) has shown that roughness values of the order of 0.5µm can be sensed by a combination of touch and sight. They also concluded that the eye is capable of sensing changes of angle of reflection of the order of 1.5 degrees on semi-transparent materials such as wood.

2.5.2 Stylus Instruments

Some researchers (Jackson M.R, 1986; Elmsorf A, Vaughan T.W, 1958; Stumbo D.A, 1960 and 1963), have used instruments from the metalworking industry to investigate the roughness of wood surfaces. Elmendorf and Vaughan (1958) found that the size of the stylus is critical when comparing

a Talysurf (diamond pyramid stylus, 0.002mm wide at the tip), with a Forster Instrument (stylus tip radius 0.055mm). The Forster instrument provides a more consistent profile of the surface since the trace rarely goes over range, under the tested conditions. The Talysurf, however, with its smaller stylus, is more prone to go over range, making the interpretation of results an arduous task.

Han (1957) and Goodchild (1963) investigated the development of two different stylus instruments. Using a larger stylus radius (3mm) Han (1957) was able to filter out the effects of primary texture (grain structure) in obtaining traces of particle board waviness. Goodchild (1963), using a similar instrument design technique (with a 0.05mm radius stylus), investigated the surface waves of rotary planed Beech (a very fine textured wood). A good degree of filtration was achieved using the 0.05mm stylus.

Stumbo (1960) and Peters and Cummings (1970), looked at the performance of True Datum devices (the alternative of the surface datum using skid follower systems) which remove the effects of workpiece bow or twist. Jackson(1986) used similar stylus instruments as research tools.

The surface parameters determined by stylus instruments such as Centre Line Average (R_a) or Root Mean Square (R_q) parameters are very limited for describing surface profiles, and is often misleading; profiles clearly different in form can have the same numerical value of R_a or R_q (Greenwood J.A, 1968).

Stylus instruments are undoubtedly of interest as a research tool; their in-process use in wood machining, with its high levels of vibration, is precluded by their small bandwidth and delicate construction. Even if stylus instruments were made more robust (Jackson M.R, 1986), their response (400Hz bandwidth) would be inadequate to track the traversing surface profiles; a stylus instrument having a bandwidth of 2.3kHz is required to accurately track a 1mm pitch profile (see Section 4.6.4) traversing at 140 m/min.

Extending the bandwidth of stylus instruments includes increasing the static stylus forces. This is likely to result in timber damage due to stylus "ploughing" (Han R.A, 1957).

2.5.3 Optical Techniques

Researchers Elmendorf and Vaughan(1958), Stumbo(1960) and Peters and Cummings(1970) have investigated the use of optical light sectioning as a technique for surface quality assessment. The method is quantitative in that measurements are taken using a microscope to assess the overall peak-to-valley height. The technique, which uses light incident at 35^0, is very time consuming, hence it has not been generally adopted by the woodworking industry, although furniture related industries have used this technique.

A variation on the optical light sectioning technique uses oblique lighting to illuminate the object surface. This provides visual enhancement of the appearance of the forms of defect, but not a quantitative assessment of

surface waviness. Oblique illumination is sometimes used to improve the ability of the eye to ascertain variation of surface waviness (Brown I.D, 1960), but is of limited use for in-process surface assessment.

2.6 Application of Available Laser Techniques

In recent years, laser techniques have been, and are being, developed to measure surface profile and roughness (Broadmann R, 1986; Hitoshi F, Toshimitsu A, 1977; Pryor T.R, Hageniers O.L, North W.P.T, 1972; Pernick B.J, 1979; Dobosz M, 1984; Harris P.G, Trigg A.D, 1987). The vast majority of the techniques monitor the reflection of a laser beam focused on the surface to be assessed. The angle of incidence of the beam is of the order of 45 degrees; photo-detectors record the variation of the reflected angle as the object surface is traversed.

Most of the laser surface assessment techniques are being investigated within the context of metal machining where the workpiece is rigidly fixed to the same datum (the machine table) as the measuring device, hence, minimising relative vibration. With wood-machining, however, the workpiece is not clamped to the machine table, but is traversed across it, using pressure rollers as guides, thus a comparatively high level of vibration prevails.

For these reasons, major difficulties are envisaged in adopting any of the laser techniques described above for the in-process assessment of the surface quality of machined timber. What is required is fast-response, non-contact, vibration-resistant method of surface quality assessment, including

parameter(s) which can readily indicate and identify machining defects.

3 PROPOSAL

3.1 Objective

3.2 Proposed Parameter

3.3 Proposed Instrument

3.4 Proposed Development of Instrument

3.1 Objective.

The anisotropic nature of wood, considered with respect to its rotary planing, causes inherent difficulties in assessing the quality of surfaces produced. One of the principle factors when planing wood is that the rotating knives do not constantly move in the direction of the timber fibres (or grain). Cutting conditions become even more complex with timber which exhibit natural defects such as wavy, curly, or diagonal grain (Petter C, 1954); these increase the difficulty in producing a good surface finish (Thomlinson R, Harrington J.S, 1960).

The objective of this project was to investigate the possibility of designing and manufacturing a non-contact transducer and associated signal conditioning, that would assess the surface form of machined timber, with considerations for in-process utilisation and adaptive control. Closely associated with the development of the transducer was the investigation of appropriate parameter/s that would readily indicate the quality of a machined timber surface profile. Coupled to the investigation was the need to mathematically model the timber planing process so that machine performance could be predicted/simulated, given specific machining faults. The simulated surface profiles could then be used as templates for comparison with actual surfaces.

3.2 Proposed Parameter.

The timber industry uses the up-cutting mode for machining its products (figure 3.1). Due to the kinematics of the planing process, the geometry of the machined surface consists of a series of cusps; their distribution and linear

spacing (periodicity) being dependent largely on the linear feed speed of the timber, the number of knives used on the final cutter head, the rotational speed of the cutterhead, etc. Figure 3.2 shows the ideal surface profile of timber planed under ideal conditions (ie. no knives proud, zero vibration, dynamically balanced cutterhead, concentric spindle, etc).

Because the cutting circle radius used on planing machines is relatively large (typically 150mm), the depth, **h**, of the cusps, produced on the surface (figure 3.2), is of the order of a few microns (typically 10 μm). These are very small amplitude variations and, as such, are not readily detectable by the naked eye. Amplitude variation, then, does not account for any "defects" as perceived by the human eye. However, the eye is extremely sensitive to changes in slope (Gonzalez R.C, Wintz P, 1977) ie. boundaries or lines on the surface. Hence, the eye detects the change from positive to negative slope at the apex of each cusp.

It is the consistency with which the apexes repeat that affect the aesthetic qualities of the machined surface; ie. any variation in the surface wavelength, or long periodic "beats" superposed thereon, are detectable by the eye and, as such, render the surface quality defective (Brown I.D. 1960; Elmdorf A, Vaughan T.W, 1958).

Therefore, it would seem reasonable to analyze the surface form in terms of the frequency information inherent on any machined (planed) timber surface.

3.2 Proposed Instrument.

The proposed technique would use laser light to highlight the apexes at the intersection of the surface "arcs" (figure 3.3). A broad beam of laser light would be directed at grazing incidence ($\theta < 1.5$ degrees) to the surface being machined, and in the same plane as the traversing workpiece. This would have the effect of highlighting the leading slopes of each cusp in the beams path and produce a pattern of bright and dark regions on the surface of the workpiece (figure 3.3). This pattern, which contains the periodic information of interest, would be traversed past a single photodiode as the workpiece is fed through the rotating cutterhead.

The output voltage of the photodiode is proportional to the intensity of the light incident upon it. This voltage would be sampled (utilising a rotary position encoder to precisely define the sampling points), digitised (using an Analogue to Digital Convertor) and stored in memory for subsequent analysis.

The data captured would not be prone to distortion due to vibration for two reasons:

1. The aperture of the beam is wide compared to the amplitude of timber vibration so the timber will at all times be illuminated.

2. The plane of vibration would be almost perpendicular to the illuminating, incident beam; the surface finish to be assessed is bigger than the wavelength of the laser, so, the reflected light to be monitored would be diffuse (as opposed to specular (see figure 2.9 and Section 2.4.4.1). Hence, any variation in workpiece position due to vibration will be insignificant.

With appropriate sampling frequency, the data captured over a given length of timber could be analyzed, in terms of its frequency content, using Fourier Analysis Techniques.

Fourier Analysis of the data involves transforming the data from the "time" domain to the frequency domain using a fast Fourier Transform (FFT) algorithm. A "fault finding algorithm" would then have to be developed to analyse the frequency domain data to detect any machining defects which may have been induced on the timber surface.

3.4 Proposed Development of Instrument

The initial investigations into the technique outlined above were to be undertaken in a microprocessor/instrumentation laboratory where there was no access to woodworking machinery. The high cost of operating such machinery also meant that the collaborating machinery manufacturers (Wadkin plc, Leicester) could not produce any significant amounts of machined timber.

The philosophy adopted, therefore, was to develop the instrument/surface-analysis technique on stationary, pre-machined timber samples (figure 3.4). This was to be accomplished by employing a linear array of photodiodes (instead of a single diode). "Traversing" was to be achieved by scanning the diode array, instead of traversing the timber.

Optical lenses were to be used to focus the image of a given illuminated length of timber on to the photodiode array. Scanning of the array would provide data which would then be captured for subsequent analysis.

The device thus investigated would be a post-process instrument, but, established using the principles of in-process measurement. This combination of grazing incidence laser illumination and the photodiode technique is innovative and was the subject of a Patent search and provisional application. This was not pursued due to lack of funds.

4 MATHEMATICAL MODEL OF THE PLANING PROCESS

4.1 Introduction

4.2 The Planing Process.

4.3 Curtate Trochoid Mathematical Model

4.3.1 Ideal Cutterhead Rotation

4.3.2 Cutterhead Eccentricity

4.3.3 Cutterhead Vibration

4.3.4 Knife Locus

4.3.4.1 Displacement Component in y-direction.

4.3.4.2 Displacement Component in x-direction.

4.4 Loci Generation

4.5 Loci Sampling

4.6 Surface Simulation Algorithm Development

4.6.1 Development Stage I

4.6.2 Development Stage II

4.6.3 Development Stage III

4.6.4 Development Stage IV

4.1 Introduction

Before describing the development of the proposed instrument and method of surface analysis of planed timber, as outlined in chapter 3, a study of the geometry of, and the mechanics associated with, the production process will be presented in order to generate a mathematical model which can be used to represent the geometry of a spindle machined surface. This mathematical model can then form the nucleus of a profile simulation algorithm; the simulation software can then be used to test the hypothesis of, and substantiate the philosophy behind, the proposed surface assessment method. It can also be used to predict surface profiles and hence FFT (or frequency signature) templates for machine performance determination or surface profile comparisons.

In this chapter is developed a versatile, cartesian-rigorous, mathematical model for surfaces produced by the wood planing process. This is presented in terms of the actual path taken by each knife as it cuts the workpiece. The mathematical model forms the foundation of a computer algorithm which simulate the resultant surface finish produced in the vast majority of wood planing situations.

Other investigators (Kivimaa E. 1950; Goodchild R. 1963; and Jackson M.R. 1986) have produced rather limited mathematical models of spindle planed surfaces without using the true locus of the cutting knives. For the sake of simplicity they have resorted to approximating the cutting motion by employing the circular arcs of adjacent circles on a common horizontal axis.

By comparison, the novel mathematical model developed here, although containing a deeper and greater input from the world of pure mathematics, more accurately represents the actual knife locus and hence the surface finish produced by the machining process.

4.2 The Planing Process.

The production of machined timber has some similarities with the milling of metals; the workpiece is fed into the revolving cutterhead (consisting of a number of knives clamped in a cylindrical body) which shears chips from the surface, in the up-cutting mode (figure 4.1). The finished surface, therefore, consists of a series of elemental surfaces generated by the individual cutting edge of each knife.

With wood, however, the feed (typically 100 m/min) and cutter speeds (typically 15000 rev/min) far exceed those of milling; also in metal machining the workpiece is clamped to a moving bed, whilst in wood machining the bed is fixed and the workpiece is traversed across it.

Because of the limited period of engagement of each knife, the chip removed is short and of a variable thickness; this results from the combination of translatory motion of the workpiece coupled with the rotation of the cutterhead. Thus, the direction of motion of the knife is continuously changing with respect to the direction of motion of the workpiece, so that the locus of the knife, with respects to the workpiece, is not circular but trochoidal.

"Trochoid" is the name given to a family of curves which are the locus of a point taken along a radial line, originating at the centre of a circle, generated while the circle rolls on a straight line (figure 4.2). The point chosen on this radial line at a distance from the centre of the circle may be either less, equal to, or greater than the radius of the circle and will generate, respectively, curves called, "prolate trochoid", "cycloid" and "curtate trochoid".

The cutting edge of each knife follows a curtate trochoid locus when viewed from the perspective of the workpiece which is travelling horizontally at constant linear velocity and intersecting with the cutting circle of the cutterhead.

Due to the kinematics of the planing process, the geometry of the machined surface consists of a series of cusps; their distribution and linear spacing being mainly dependent on the feed speed and the number of knives used on the final cutterhead. Figure 4.3 shows the ideal surface finish of timber planed under ideal conditions (ie. no knives proud ($R_1 = R_2 = R_3 = R_4$), no vibration, dynamically balanced spindles, etc) using a cutterhead having four knives (Jackson M.R, 1986).

As can be expected, in practice, the ideal surface is rarely achieved; vibration, spindle eccentricity, proud knives, etc, affect the locus of each knife, and hence the quality of surface profile produced. It follows that the greater the degree of vibration, dynamic imbalance, etc, the further the surface form departs from the ideal. A more typical profile of a planed surface is shown

in figure 4.4

4.3 Curtate Trochoid Mathematical Model.

Figure 4.5 shows a schematic diagram representing the action of a general cutterhead, having **N1** knives equi-spaced about its circumference and revolving at angular velocity **W1**. The cutting edges of the knives are positioned a nominal distance **Ri** from the centre of rotation, O. **H1** is the vertical distance between the machine table, CD, and the horizontal axis of the cutterhead spindle which passes through point O.

The workpiece, ABCD, of initial thickness **Tw**, travels from right to left at constant linear velocity, **V1**, and interferes with the cutting circle of the knives by a nominal distance, **d**, the depth of cut.

The cutting action of each knife is deemed to start at angular displacement, **F1** (measured from the conventional reference plane used in trigonometry) and end after having rotated through a further angular displacement **Ti**.

Thus

$$\mathbf{Ti = 2.arcCos((H1-Tw)/Ri)} \qquad \mathbf{(4.1)}$$

and the angular separation of the knives, **Lb**, is given by:

$$\mathbf{Lb = 2\pi/N1} \qquad \mathbf{(4.2)}$$

The general angular displacement, **Lg** (angle of lag), between the position that the first knife contacts the workpiece and the **I**th knife is given by

$$\mathbf{Lg = (I - 1).Lb} \qquad \mathbf{(4.3)}$$

4.3.1 Ideal Cutterhead Rotation.

Ideal rotation will occur if spindle eccentricity is zero (ie. the cutterhead is dynamically balanced and the spindle rotates concentrically) and the effects of vibration are absent. Under these conditions, provided the knives share a common cutting circle radius (ie. no knife stands proud), the instantaneous position, **I(t)**, of each knife relative to the point of first contact with the workpiece (see figure 4.5), resolved in the x and y direction can be expressed as

$$\mathbf{I(t)_x = Ri.Cos(F1 + W1.t) - Ri.Cos(F1)} \qquad \mathbf{(4.4a)}$$

$$\mathbf{I(t)_y = Ri.Sin(F1 + W1.t) - Ri.Sin(F1)} \qquad \mathbf{(4.4b)}$$

where the suffixes **x** and **y** indicate the direction of resolution.

4.3.2 Cutterhead Eccentricity

The cutterhead may rotate eccentrically due to a lack of spindle concentricity or dynamic imbalance; this would modify the cutterhead position in space and hence the loci of its knives. The value of the instantaneous modification in position, **E(t)**, for a given knife, is dependent on the cutterhead's angular orientation during rotation. The circle in figure 4.5, of radius **Re** and centred at J, is used here to represent the magnitude of the eccentric motion of the cutterhead due to dynamic imbalance and spindle concentricity. Viewed from the perspective of time the loci of each displacement is clearly sinusoidal. Resolved in the x and y directions, the amount by which the cutterhead

position modified (at time t) is described by:

$$E(t)_x = Re.Cos(n.W1.t) \qquad (4.5a)$$

$$E(t)_y = Re.Sin(n.W1.t) \qquad (4.5b)$$

where

the resolved direction is indicated by the suffices, **x** and **y**,

Re is the maximum amplitude of the displacement ,

n.W1 is the angular frequency of the eccentric action

and

t is instantaneous time.

The angle, **Ee**, measured from the conventional reference plane, is the angular position at which the displacement is deemed to start to affect the cutting action of the individual knife (it ceases to do so after rotating a further angular displacement, **Te**) This modifies the above equations (**4.5a** and **4.5b**) to:

$$E(t)_x = Re.Cos(Ee + n.W1.t) \qquad (4.6a)$$

$$E(t)_y = Re.Sin(Ee + n.W1.t) \qquad (4.6b)$$

Being more specific, if $Er(t)_x$ and $Er(t)_y$ are, respectively, the x and y components of displacement due to the spindles lack of concentricity (colloquially referred to as "spindle runout") and, similarly, $Ei(t)_x$ and $Ei(t)_y$ are displacements caused by dynamic imbalance, then

$$Er(t)_x = r1.Cos(E1 + n_1.W1.t) \qquad (4.7a)$$

$$Er(t)_y = r1.Sin(E1 + n_1.W1.t) \qquad (4.7b)$$

and

$$Ei(t)_x = r2.Cos(E2 + n_2.W1.t) \quad (4.8a)$$

$$Ei(t)_y = r2.Sin(E2 + n_2.W1.t) \quad (4.8b)$$

where $n_1.W1$ and $n_2.W1$ are respectively, the angular frequency of the eccentric action due to lack of spindle concentricity, and dynamic imbalance,

r1 and **r2** are the maximum magnitude of the corresponding displacements,

E1 and **E2** being the respective angular position at which each displacements are deemed to start affecting the knife's cutting action (**T1** and **T2** are respectively their angular duration).

4.3.3 Cutterhead Vibration

The instantaneous position of the cutterhead could also be affected by resonant vibration, structural vibration etc. The plane of this vibration would depend on the locale and operating conditions. The circle in figure 4.5, of radius **Rv** and centred at K, is used here to represent the magnitude of the cutterhead motion due to vibration. If the magnitude of the vibration is **Rv** and its frequency is **v1.W1**, then the instantaneous amount by which the cutterhead position is modified, **V(t)**, is given by

$$V(t) = Rv.Sin(v1.W1.t) \quad (4.9a)$$

For the purpose of this analysis, and to maintain generality, the plane of vibration is defined by the plane at angle **Gv** to the horizontal. Thus the components of displacement, due to vibration, resolved in the x and y directions are given by:

$$V(t)_x = (Rv.Sin\ (v1.W1.t))/(Tan(Gv)) \quad (4.9b)$$

$$V(t)_y = Rv.Sin\ (v1.W1.t) \quad (4.9c)$$

where the suffixes **x** and **y** indicate the direction of resolution.

4.3.4 Knife Locus.

The x-y co-ordinates for the locus of the cutting edge of a general knife on a cutterhead will now be defined. The knife action is viewed from the perspective of the moving workpiece and referenced with respect to the initial contact point of the first knife (point Q, see figure 4.5). Thus, the origin of the x-y plane is defined as follows:

The x-origin is the vertical plane passing through the point at which the first knife makes initial contact with the workpiece.

The y- origin is the horizontal plane of the machine bed

Thus, the x-origin moves leftwards as the cutting action progresses, while the y-origin remains fixed.

Alternatively, the workpiece, and hence the x-origin, can be considered to be stationary while the cutterhead is assumed to move rightward with linear velocity **V1**, rotating with angular velocity **W1**.

For the purposes of analysis the locus of the general knife, viewed relative to the workpiece, will be resolved into two components:

1) Component of displacement in the x-direction
2) Component of displacement in the y-direction

Hence the mathematical equation which describes the locus will be a function of time and in the parametric form:

$$x = f(t) \qquad (4.10a)$$

$$y = F(t) \qquad (4.10b)$$

The co-ordinates of the general knife edge in the x-y plane will be calculated using the finite difference method; that is, the difference between knife position at **t=0** (the x-y origin 0,0) and its position at **t=dt** (present position x,y). So, by varying the value of **dt**, the complete cutting action of each knife can be mapped.

4.3.4.1 Component of Displacement in the y-direction.

The displacement of the knife in the y-direction, y, during time **dt**, can be expressed as a summation of the various elements of which it is comprised.

Thus, during time period **dt**:

$$y = dI_y + dEr_y + dEi_y + dV_y \qquad (4.11)$$

where

dI_y = knife displacement due to Ideal cutterhead rotation,

dEr_y = knife displacement due to spindle Runout,

dEi_y = knife displacement due to Dynamic Imbalance,

and

dV_y = knife displacement due to Vibration.

Now, from equation **4.4b**

$$dI_y = Ri.Sin(F1 + W1.dt) - Ri.Sin(F1) \qquad (4.12)$$

from equation **4.7b**

$$dEr_y = r1.Sin(E1 + n_1.W1.dt) \qquad (4.13)$$

from equation **4.8b**

$$dEi_y = r2.Sin(E2 + n_2.W1.dt) \qquad (4.14)$$

from equation **4.9c**

$$dV_y = Rv.Sin(v1.W1.dt) \qquad (4.15)$$

So that:

$$y = Ri.Sin(F1 + W1.dt) - Ri.Sin(F1) + r1.Sin(E1 + n_1.W1.dt) + r2.Sin(E2 + n_2.W1.dt) + Rv.Sin(v1.W1.dt) \qquad (4.16)$$

4.3.4.2 Component of Displacement in x-direction.

The displacement of the knife, relative to the workpiece, in the x-direction, can be divided into two major elements:

1. Knife displacement.
2. Workpiece displacement.

So that the x-displacement, x, is given by:

$$\text{x=knife displacement + workpiece displacement} \qquad (4.17)$$

The knife displacement can be further sub-divided and expressed as a summation of its various elements of which it is comprised. Thus, during time

period **dt**:

$$\textbf{Knife displacement} = dI_x + dEr_x + dEi_x + dV_x \qquad (4.18)$$

where dI_x = knife displacement due to Ideal cutterhead rotation,

dEr_x = knife displacement due to spindle Runout,

dEi_x = knife displacement due to Dynamic Imbalance,

and dV_x = knife displacement due to Vibration

Now, from equation **4.4a**

$$dI_x = Ri.Cos(F1 + W1.dt) - Ri.Cos(F1) \qquad (4.19)$$

from equation **4.7a**

$$dEr_x = r1.Cos(E1 + n_1.W1.dt) - r1.Cos(E1) \qquad (4.20)$$

from equation **4.8a**

$$dEi_x = r2.Cos(E2 + n_2.W1.dt) - r2.Cos(E2) \qquad (4.21)$$

from equation **4.9b**

$$dV_x = (Rv.Sin(v1.W1.dt))/(Tan(Gv)) \qquad (4.22)$$

Hence

$$\begin{aligned}\textbf{knife displacement} = {} & Ri.[Cos(F1 + W1.dt) - Cos(F1)] \\ & + r1.[Cos(E1 + n_1.W1.dt) - Cos(E1)] \\ & + r2.[Cos(E2 + n_2.W1.dt) - Cos(E2)] \\ & + (Rv.Sin(v1.W1.dt))/(Tan(Gv))\end{aligned} \qquad (4.23)$$

The displacement of the workpiece can be calculated from the velocity-time relationship:

workpiece displacement = workpiece velocity x time taken

Since **Lg** is the general lag angle between the first cutter and the active cutter - the **Ith** cutter (see equation **4.3**) - and, **W1.dt** is the rotation angle during which cutting takes place, time taken to traverse angular displacement **(Lg + W1.dt)** is

$$(Lg + W1.dt)/W1$$

hence

$$\text{workpiece displacement} = V1.(Lg + W1.dt)/W1 \qquad (4.24)$$

So that

$$\begin{aligned} x = {} & Ri.[\cos(F1 + W1.dt) - \cos(F1)] \\ & + r1.[\cos(E1 + n_1.W1.dt) - \cos(E1)] \\ & + r2.[\cos(E2 + n_2.W1.dt) - \cos(E2)] \\ & + (Rv.\sin(v1.W1.dt))/(\tan(Gv)) \\ & + V1(Lg + W1.dt)/W1 \end{aligned} \qquad (4.25)$$

The x-displacement, **Xs**, at which the **Ith** knife starts to cut the workpiece is given by

$$Xs = V1.I.Lb/W1 \qquad (4.26)$$

The x-displacement, **Xe**, at which the **Ith** knife stops cutting the workpiece is given by

$$Xe = V1.(I.Lb + Ti)/W1 + Ri.\{Cos(F1 + Ti) - Cos(F1)\}$$
$$+ r1.\{Cos(E1 + T1) - Cos(E1)\}$$
$$+ r2.\{Cos(E2 + T2) - Cos(E2)\} \qquad (4.27)$$

4.4 Loci Generation.

The parametric equations **4.16** and **4.25**, derived above, can be used to produce the co-ordinates of the locus of each knife, relative to the traversing workpiece, as the cutterhead rotates. The computer algorithm, entitled "LOCI-0" and listed in Appendix A0, was written to achieve this. It was designed to simulate ideal spindle rotation coupled with uniform timber feed speeds; cutterhead vibration, imbalance non-concentricity etc. was ignored at this stage. Examples of knife loci generated is shown in figures 4.6a to 4.6h.

The locus of each knife (relative to the moving timber) was plotted in turn as the cutterhead rotated through 360 degrees (2π rad) starting from the location where the first knife engaged the timber. The angular velocity of the cutterhead and linear feedspeed of the timber were both constant.

"LOCI-0" is written in BBC BASIC and uses the following variable parameters:

N% - number of knives on cutterhead (integer)
R1 - knife radius (mm)
W1 - angular velocity of cutterhead (rad/s)
V1 - linear velocity of workpiece (feedspeed) (mm/s)
Tw - initial workpiece thickness (mm)
H1 - distance: cutterhead centreline to machine bed (mm)
I - knife number
F1 - angular displacement of knife at initial contact (rad)
Lb - angular displacement between successive knives (rad)
Lg - angular displacement between Ith knife and 1st (rad)
dt - increment of time (s)
XORG - x-origin of the graphics x-y plane

YORG - y-origin of the graphics x-y plane

The algorithm began by establishing the constant values of the various parameters, lines 20 to 50. The profile of the unplanned workpiece was then drawn, and, for convenience, the x-origin and y-origin was moved to coincide with the centreline of the cutterhead.

The algorithm made use of a double nested **FOR-NEXT** loop as follows:

The outer **FOR-NEXT** loop, lines 100 to 200, introduced each knife in turn, starting with the first and progressing incrementally to the **N1**th. The angular displacement, **Lg**, between the first knife and the **I**th (current) knife was calculated, line 110, as were the co-ordinates of its initial position, lines 120 and 130. A straight line was drawn between the cutterhead's centre and the initial position of the current knife, line 140; this diagrammatically represented the knife.

The inner **FOR-NEXT** loop, lines 150 to 190 was used to calculate the co-ordinates of the locus of the **I**th (current) knife edge, every 0.1 radians, as the cutterhead rotated, through 2π radians. The successive knife edge positions were plotted, in the x-y plane, and connected by straight lines (chord approximation).

4.5 Loci Sampling.

Equations **4.16** and **4.25** completely define the locus of each knife-tip as the cutterhead rotates. Thus, this mathematical model can be used to generate

simulated, machined surface profiles by considering only the sections of the knife's locus which corresponds with actual cutting taking place.

There was, however, a problem with sampling. Equations **4.16** and **4.25** describe the loci as a function of time. This description is unsatisfactory from the perspective of generating simulated surface profile data which can be sampled at uniform, linear intervals (in the x-direction); uniform sampling is essential for the subsequent Fourier analysis of the surface profile data; whilst the x-displacement of the workpiece with respect to time is uniform, the x-displacement of each knife edge is not; the x-velocity of each cutting edge varies in both magnitude and sense. Thus, if the coordinates of the profile are calculated (sampled) at regular time intervals, the x-displacement between calculations (sample points) would vary considerably with time; this was illustrated by modifying the computer algorithm "LOCI-0" such that the generated data was plotted as a histogram. The modified algorithm was called "LOCI-1" (see Appendix A1) and an example of the data generated is shown in figure 4.7. This clearly demonstrated the non-uniform-sampling-interval problem.

To alleviate this problem the displacement, **x**, in equation **4.25** had to become the independent variable (**dt** becoming the dependent variable, ie. **dt** = **f(x)**); so **dt** could be calculated for any given x-displacement. Thus the linear sampling interval in the x-direction could be regulated; the corresponding y-displacements could be calculated by substituting the particular value of **dt** in equation **4.16**. This was accomplish by using the trigonometric identity,

$$\mathbf{Cos(A+B) = Cos(A).Cos(B) - Sin(A).Sin(B)} \qquad \mathbf{(4.28)}$$

So

$$\mathbf{Cos(F1+W1.dt) = Cos(F1).Cos(dt) - Sin(F1).Sin(dt)} \qquad \mathbf{(4.29)}$$

$$\mathbf{Cos(E1+W1.dt) = Cos(E1).Cos(dt) - Sin(E1).Sin(dt)} \qquad \mathbf{(4.30)}$$

$$\mathbf{Cos(Z1+W1.dt) = Cos(Z1).Cos(dt) - Sin(Z1).Sin(dt)} \qquad \mathbf{(4.31)}$$

Substituting equations **4.29, 4.30** and **4.31** in equation **4.25** gives:

$$\begin{aligned}\mathbf{x} = {} & \mathbf{Ri\{[Cos(F1).Cos(W1.dt) - Sin(F1).Sin(W1.dt)]-Cos(F1)\}} \\ & \mathbf{+r1\{[Cos(E1).Cos(n_1.W1.dt)-Sin(E1).Sin(n_1.W1.dt)]-Cos(F1)\}} \\ & \mathbf{+r2\{[Cos(Z1).Cos(n_2.W1.dt)-Sin(Z1).Sin(n_1.W1.dt)]-Cos(Z1)\}} \\ & \mathbf{+Rv.\ Sin(v1.W1.dt).Cos(Gv)+V1.Lg/W1+V1.dt}\end{aligned}$$

Therefore

$$\begin{aligned}\mathbf{x} = {} & \mathbf{Ri.Cos(F1).Cos(W1.dt) - Ri.Sin(F1).Sin(W1.dt) - Ri.Cos(F1)} \\ & \mathbf{+r1.Cos(E1).Cos(n_1.W1.dt)-r1.Sin(E1).Sin(n_1.W1.dt)-r1.Cos(E1)} \\ & \mathbf{+r2.Cos(Z1).Cos(n_2.W1.dt)-r2.Sin(Z1).Sin(n_2.W1.dt)-r2.Cos(Z1)} \\ & \mathbf{+Rv.Sin(v1.W1.dt).Cos(Gv) + V1.Lg/W1 + V1.dt}\end{aligned} \qquad \mathbf{(4.32)}$$

Decomposing equation **4.32** further, so as to isolate **dt** from the **Sine** and **Cosine** functions, use is made of the Taylor polynomial (or series) of the respective functions:

For **m**, in general,

$$\mathbf{Cos(m) = 1 - \frac{m^2}{2!} + \frac{m^4}{4!} - \ .....} \qquad \mathbf{(4.33)}$$

and

$$\mathbf{Sin(m) = m - \frac{m^3}{3!} + \frac{m^5}{5!} - \ .....} \qquad \mathbf{(4.34)}$$

Truncating both polynomials at the second power of **m** gives:-

$$\mathbf{Cos(m) = 1 - \frac{m^2}{2!}} \qquad \mathbf{(4.35)}$$

$$\mathbf{Sin(m) = m} \qquad \mathbf{(4.36)}$$

Equations **4.35** and **4.36** are accurate to two decimal places for **m** less than 0.3 radians.

Substituting, as required, equations **4.35** and **4.36** into equation **4.32**, using as appropriate:-

$$\mathbf{m = W1.dt}$$

$$\mathbf{m = n_1.W1.dt}$$

$$\mathbf{m = n_2.W1.dt}$$

$$\mathbf{m = v1.W1.dt}$$

gives

$$\mathbf{x = Ri.Cos(F1)\{1 - W1^2.dt^2/2\} - Ri.Sin(F1).W1.dt - Ri.Cos(F1)}$$
$$\mathbf{+ r1.Cos(E1)\{1-n_1^2.W1^2.dt^2/2\} - r1.Sin(E1).n_1.W1.dt-r1.Cos(E1)}$$
$$\mathbf{+r2.Cos(Z1)\{1-n_1^2.W1^2.dt^2/2\} - r2.Sin(Z1).n_1.W1.dt - r1.Cos(Z1)}$$
$$\mathbf{+ Rv.v1.W1.dt.Cos(Gv) + V1.Lg/W1 + V1.dt}$$

Multiplying out and grouping matching terms to form a quadratic in **dt**:-

$$\mathbf{x = - Ri.W1^2/2.Cos(F1).dt^2 - Ri.W1.Sin(F1).dt}$$
$$\mathbf{- n_1^2.r1.W1^2/2.Cos(E1).dt^2 - n_1.r1.W1.Sin(E1).dt}$$
$$\mathbf{- n_2^2.r2.W1^2/2.Cos(Z1).dt^2 - n_2.r2.W1.Sin(Z1).dt}$$
$$\mathbf{+ v1.Rv.W1.Cos(Gv).dt}$$
$$\mathbf{+ V1.dt + V1.Lg/W1}$$

Factorising:-

$$x = -W1^2/2.\{Ri.Cos(F1)+n_1^2.r1.Cos(E1)+n_2^2.r2.Cos(Z1)\}.dt^2 + \{Rv.v1.W1.Cos(Gv)+V1 - W1[Ri.Sin(F1)+n_1.r1.Sin(E1)+n_2.r2.Sin(Z1)]\}.dt + V1.Lg/W1$$

Multiplying through by 2 and rearranging:-

$$0 = W1^2\{Ri.Cos(F1) + n_1^2.r1.Cos(E1) + n_2^2.r2.Cos(Z1)\}.dt^2 + 2\{W1.[Ri.Sin(F1) + n_1.r1.Sin(E1) + n_2.r2.Sin(Z1) - v1.Rv.Cos(Gv)] - V1\}.dt + 2\{x - V1.Lg/W1\}$$

Rewriting

$$0 = A.dt^2 + B.dt + C \qquad (4.37)$$

where

$$A = W1^2.\{Ri.Cos(F1) + n_1^2.r1.Cos(E1) + n_2^2.r2.Cos(Z1)\}$$

$$B = 2\{W1.[Ri.Sin(F1) + n_1.r1.Sin(E1) + n_2.r2.Sin(Z1) - v1.Rv.Cos(Gv)] - V1\}$$

and $C = 2\{x - V1.Lg/W1\}$

Equation 4.37 is a quadratic in dt and is of the general form

$$ax^2 + bx + c = 0,$$

the solution of which is:-

$$x = \frac{-b \pm \sqrt{(b^2 - 4.a.c)}}{2.a}$$

Therefore the solution of equation 4.37 is:-

$$dt = = \frac{-B \pm \sqrt{(B^2 - 4.A.C)}}{2.A} \qquad (4.38)$$

In general, equation **4.37** will have two roots (or solutions); which may be:

1) real and different
2) real and equal
3) complex

The roots will be real if the discriminant, **(B_2 - 4.A.C)** is positive or zero, and, complex if it is negative.

Examination of each term in the discriminant of equation **4.37** shows that:

B^2 is clearly always positive.

A is negative; the term **Ri.Cos(F1)** is negative because **F1** is between 180 degrees and 270 degrees. The amplitude of the other terms of which **A** is composed is very much smaller than **Ri** in reality. The **C** is positive; **V1.Lg/W1**, the displacement of the timber before the knife engages will always be leftward of **x** (on the x-y plane in which the motion is being analyzed). Hence **x** is always greater than **V1.Lg/W1** and the result of the subtraction always positive.

Hence the two roots of equation **4.37** are real and distinct because **A**, the coefficient of **dt^2**, is always negative, whilst **C**, the constant term, is always positive resulting in a discriminant which is always positive. Both roots are significant in terms of the complete knife locus, but only one relates to the actual surface profile. The required root is obtained by considering the nature (shape) of the function, **f(dt)**, associated with, equation **4.37** ie.

$$f(dt) = A.dt^2 + B.dt + C \qquad (4.39)$$

Factorising equation **4.39** gives

$$f(dt) = A\{dt^2 + B/A.dt + C/A\} \qquad (4.40)$$

Let the two distinct roots of equation **4.37** be **Ro1** and **Ro2** so that

$$f(dt) = A\{dt^2 + B/A.dt + C/A\} = A(dt - Ro1)(dt - Ro2)$$

ie.

$$f(dt) = A(dt - Ro1)(dt - Ro2) \qquad (4.41)$$

Now, let **Ro1 < Ro2** :-

when **dt < Ro1**:

(dt - Ro1) and **(dt - Ro2)** are both negative; therefore **f(dt)** has the same sign as **A**

when **Ro1 < dt < Ro2**:

(dt - Ro1) and **(dt - Ro2)** have opposite signs; therefore **f(dt)** has the opposite sign to **A**

when **dt > Ro2**:

(dt - Ro1) and **(dt - Ro2)** are both positive; therefore **f(dt)** has the same sign as **A**

The coefficients **A, B** and **C** of equations **4.37** and **4.39** can be evaluated by substituting typical values for the constituent variables of which they are comprised. Typically, equation **4.39** has two roots; one root is negative whilst the other is positive. The negative root is invalid as it relates to an instant in time prior to that of the initial engagement of the knife with the timber. The valid solution is therefore the positive root.

Thus, for the **I**th knife, **dt** can be calculated for any x-displacement between **Xs** and **Xe** (see equations **4.26** and **4.27**); this value of **dt** can then be

substituted into equation **4.16** to yield the corresponding y-coordinate.

4.6 Surface Profile Simulation.

The surface simulation algorithm (SSA) that was ultimately written, evolved through four main stages. At each stage various concepts were introduced and modifications made. What follows discusses the four stages of development and highlights, with subsequent solutions, the problems that were encountered.

4.6.1 Development Stage I

(Refer to algorithm LOCI-1 in Appendix A1)

In stage I, which has already been described, an algorithm was written which plots the locus of each knife as the cutterhead rotates through 360 degrees (2π radians). This algorithm proved unsatisfactory because the sampling rate was non-uniform (see figure 4.7).

4.6.2 Development Stage II

(Refer to algorithm LOCI-2, Appendix A2)

Stage II incorporated the solution to the non-uniform sampling rate problem (Section 4.5) and the sampled points were restricted to the vicinity or locale in which timber removal/cutting is deemed to take place, ie. between **Xs**, the x-displacement at which the knife is deemed to start engagement with the timber, and **Xe**, the x-displacement at which the knife is deemed to disengage with the timber (see lines 160 to 250 and figure 4.8a).

In stage II the idea of a single proud knife was introduced; this knife can be placed in any one of the **N1** positions available (lines 50 and 60) and described a cutting circle radius which is larger than that of the other knives (line 100).(see figure 4.8b).

One problem encountered in stage II was as follows:

Where, with respects to the x-axis, the cutting action of one knife overlapped with that of another, the sampled points of the first locus did not necessarily coincide with those of the second, within the region of overlap. This meant that, despite uniform sampling between localised start and end points (ie. **Xs** and **Xe**), when viewed as a whole, the generated profile data again exhibit a non-uniform sampling rate (see figure 4.8c and figure 4.8d).

The remedy to the "sample-point overlap coincidence" problem was to magnify the profile by a magnification factor, **m**, such that successive sample points (sample spacing), in the x-direction were unit distance apart. Hence, each sample point would fall on an integer value in the x-direction. Under this magnification **Xs** and **Xe**, for each knife cut, could be modified slightly so as to coincide with the nearest corresponding integer value; the positional error in displacement due to this adjustment, evaluated over a sample length of 0.125m (an adequate assessment length suggested by engineers in the woodworking industry (Goddard M, et al, 1986), see section 5.3.3), is between

0% and 0.8%/**m** (=1/(125x **m**)x 100%), where **m** is the magnification factor.

ASIDE:

The magnification factor, **m**, *calculated here, depends on the number of sample points employed between* **Xs** *and* **Xe**; *at this stage 16 sample points were used.*

Thus $$\mathbf{m} = \frac{1}{\Delta x} \qquad (4.42)$$

where $$\Delta x = \frac{(Xe - Xs)}{16}$$

and is the sample spacing before magnification.

Note:

The frequency content of the generated profile data is the parameter of major interest; magnification of the data has no effect on its frequency content.

4.6.3 Development Stage III

(Refer to algorithm LOCI-3, Appendix A3)

Stage III incorporated the solution to the "sample-point overlap coincidence" problem (lines 180 to 200 and line 290, also see figure 4.9a) and introduced the idea of eccentricity motion of the cutterhead spindle (lines 90, 350 and 370, also see figure 4.9b). The notion of a single proud knife, introduced in stage II, was expanded such that a number of proud knives and their respective positions on the cutterhead could be selected (see lines 80 and 240).

4.6.4 Development Stage IV

(Refer to algorithm SSA, Appendix A4)

The final stage, Stage IV, of development of the Surface Simulation Algorithm, saw the introduction of a standard sample length of 0.125m for each simulated data set. To satisfy the Nyquist sampling theorem criterion,

which states that the sampling frequency must be at least twice that of the highest frequency component in the waveform being sampled, the maximum sample spacing had to be 0.5mm; a surface wave of pitch 1.0mm is currently the highest quality finish produced in the woodworking industry (Goddard M, Garrett J, 1986). So, at least 250 equi-spaced sample points would be required in a 0.125m sample length.

The simulated data would subsequently be analyzed in terms of its frequency content using fast Fourier analysis techniques. The use of Cooley-Tukey method (Cooley J.W, Tukey J.W, 1965) to evaluate the Fourier Transform (ie. the fast Fourier transform (FFT)) requires that the number of sampled points to be transformed must be an integer power of 2 (ie 2^n where **n** is an integer). Hence 256 sample points satisfied both the Nyquist sampling and the FFT requirements.

The sample length (0.125m) was divided into 256 giving a sample spacing, Δx, before magnification, of 2.44×10^{-4} metres (=0.125/256 metres). The resulting magnification factor, **m**, is given by:

$$\mathbf{m} = \frac{\text{(No. of sample points)}}{\text{(sample length)}} \qquad (4.43)$$

$$= \frac{256}{0.125}$$

$$= 2048 \qquad \text{(see line 5090)}$$

{At this magnification the positional error in displacement, assessed over the sample length, is

3.9×10^{-4} % (=1/(125 x m) x 100%)}

The **FOR - NEXT** loop used in previous stages to indicate the number of knifemarks on the profile, was superseded in stage IV by a **REPEAT - UNTIL** loop (lines 5120 and 5430). The action of this loop is to monitor the simulated profiles length and terminate when this is greater than the effective sample length of 0.125 metres. This was effected by calculating the number of revolutions the cutterhead would describe during the time it took for the workpiece to travel a distance equal to the sample length. The reasoning was as follows:

Time (**t**) for workpiece, travelling at constant linear velocity (**V**), to traverse sample length (**smplth**) is given by:-

$$t = \frac{(smplth)}{V} \qquad (4.44)$$

Time period (T) for cutterhead, rotating at constant angular velocity (**W**), to complete one revolution is given by:-

$$T = \frac{2\pi}{W1} \qquad (4.45)$$

Therefore, the number of revolutions, **c**, made by the cutterhead in time **t** is given by:-

$$c = \frac{t}{T} \qquad (4.46)$$

So
$$c = \frac{(smplth \times W1)}{(V \times 2\pi)} \qquad (4.47)$$

The current number of revolutions, **nc**, made by the cutterhead is calculated by dividing the current total number of knifemarks on the profile (**I-1**) by the total number of knives on the cutterhead (**nN%**).

Hence

$$\mathbf{nc} = \frac{\mathbf{(I\text{-}1)}}{\mathbf{(nN\%)}} \qquad \mathbf{(4.49)}$$

Thus, the **REPEAT - UNTIL** loop is terminated when **nc** is greater than (**c+1**), see line 5430

Stage IV also saw the introduction of the effects of machine/timber vibration on the simulated profile; the machine/timber was deemed to vibrate in the vertical plane with amplitude, **vib**, and with a frequency which was some multiple, **rate**, of the cutterheads angular frequency, **W1** (see lines 4640 and 5300). Examples of profiles generated are shown in figures 4.10a to 4.10f.

5 DEVELOPMENT OF POST-PROCESS LASER INSTRUMENT

5.1 Introduction / General Description

5.2 Electronic Hardware

5.2.1 The Host Computer

5.2.1.1 General Description

5.2.1.2 Versatile Interface Adapter

5.2.2 Linear Photodiode Array

5.2.2.1 General Description

5.2.2.2 Photodiode Array Circuit

5.2.2.3 Sensor Geometry

5.2.2.4 Drive Requirements

5.2.2.5 Signal Extraction

5.2.2.6 Data Capture

5.2.2.7 Data Transfer

5.3 Optical Hardware

5.3.1 Laser Beam Production

5.3.2 Beam Expansion

5.3.3 Image Focusing and Sample Length

5.4 Instrument Framework

5.4.1 Introduction

5.4.2 Framework

5.4.3 Adjustment Mechanisms

5.4.3.1 Angle of Incidence

5.4.3.2 Object Position / Alignment

5.4.3.3 Image Focusing

5.4.3.4 Image Alignment

5.4.4 Dark-housing

5.5 Data Capture Software

5.5.1 Microcomputer Access to Auxiliary RAM

5.5.2 Optimum Photodiode Integration Period

5.6 Data Analysis Software

5.6.1 Fourier Transforms

5.6.1.1 Waveforms

5.6.1.2 Fourier Series

5.6.1.3 Discrete Spectra from Fourier Series

5.6.1.4 Spectral Diagrams

5.6.1.5 Non-periodic Waveforms.

5.6.1.6 Fourier Series to Fourier Integral

5.6.1.7 Frequency Domain Diagrams

5.6.1.8 Transforming Periodic Waveforms

5.6.1.9 Numerical Evaluation of Transform

5.6.2 Discrete Fourier Transforms

5.6.3 Fast Fourier Transforms

5.6.4 FFT Algorithm

5.6.5 Validating the FFT Algorithm

5.1 Introduction / General Description

The development of the post-process instrument was effected under three main headings:-

1) Hardware
2) Framework
3) Software

1) The hardware consisted of:-

(a) Host Computer - general purpose microcomputer (BBC Master Series) which, under program control, communicated with the electronic circuitry of the laser instrument, capturing, storing and analysing data samples.

(b) Laser Instrument Electronic Circuitry - photodiode array and peripheral array drivers, amplifier circuits, Analogue to Digital Converter (ADC), Auxiliary Memory, up-down counters, clocking circuits, sample-and hold circuits, power supplies, etc.

(c) Laser Instrument Optics - laser beam source and power supply, laser beam expander, image focusing lenses, etc.

2) The framework consists of:-

(a) A fabricated structure which supported the photodiode array, timber samples, laser light source and focusing lens in fixed, mutually orthogonal positions, and, associated adjustment and alignment mechanisms.

3) The software consists of:-

(a) Data Capture from Laser Instrument - calculation of appropriate photodiode integration period between start pulses, start pulse generation, the retrieval and storage of sampled surface data.

(b) Data Analysis - the Fast Fourier transformation (FFTs) of captured surface data to the frequency domain, the correlation/comparison of known surface defects with corresponding FFT results, the displaying of frequency signatures.

This chapter details the development of the laser, surface assessment, instrument.

Section 5.2 deals with the electronic hardware. The applicable electronic parts and functions of the host computer are described (Section 5.2.1), followed by a description of the photodiode array circuitry with which it interfaces (Section 5.2.2).

Details of the optical hardware - laser beam production, beam expansion, image focusing - are then given (Section 5.3).

Section 5.4 introduces the design of the framework and adjustment mechanisms associated with the laser instrument.

Section 5.5 deals with the software which controlled the laser instrument during the capture of data from the timber surface.

Section 5.6 describes the development of the software used in the Fourier analysis of the data.

5.2 Electronic Hardware.

The complete electronic hardware for the laser instrument is shown schematically in figure 5.1.1; for complete circuit diagram see Appendix C1. This section discusses the operation of the major elements of the electronic circuitry .

5.2.1 The Host Computer.

5.2.1.1 General Description.

The host computer used was a BBC Master Series general purpose microcomputer; its hardware consists of a large number of integrated circuits and various electronic components.

The general lay-out of the computer is shown in block diagram form in figure 5.2.1. At the centre of the system is the 6502 central processing unit (CPU). This chip executes all the programs, arithmetic and logical functions. It is connected to the rest of the system via three buses; the data bus, the address bus and the control bus. In figure 5.2.1 a bus is represented by double lines terminated by arrows at each major block and is simply electrical links connected in parallel to several devices.

Normally one of these devices is talking to another device on the bus. The communication protocols which enable data transfer to take place are set up by the control, address and data buses. The address bus has 16 separate lines hence the maximum amount of directly addressable memory on a 6502 CPU chip is 65536 bytes; the address bus is unidirectional because the 6502

CPU can only supply (not receive) addresses. The data bus has 8 lines so any number between 0 and 255 can be transferred across it. Communication between the peripherals, memory and the CPU occurs over the data bus; data transfer is bidirectional

In order to control the direction of data flow on the data bus a READ or WRITE signal is provided by the control bus. Thus, hardware connected to the system can determine whether it is being sent data, or, is meant to send data back to the 6502 CPU.

The other major control bus functions are those of providing a clock, interrupts and resets. The clock signal synchronises all the chips. The RESET line allows all the hardware to be initialised to some predefined state after reset. The interrupt is a signal sent from a peripheral to the 6502 CPU requesting some form of servicing. There are two types of interrupts; maskable (IRQ) and non-maskable (NMI). The 6502 CPU can ignore a maskable interrupt under software control; a non-maskable interrupt can never be ignored.

When power is first applied to the system, a reset is generated to ensure that all devices start up in there reset states. The 6502 CPU then starts to get instructions from the MOS ROM (machine operating system read only memory) which direct the 6502 CPU's activity. A variety of functions exist, enabling reading or writing of data to memory or to an input/output device or performing arithmetic and logical operations on the data. Once entered,

the MOS (machine operating system) program gains full control of the system.

5.2.1.2 Versatile Interface Adapter

(Refer to figure 5.2.1 and figure 5.2.2)

There are two 6522 Versatile Interface Adapters (VIA's) inside the BBC microcomputer. One is dedicated to the MOS and controls the keyboard, sound, speech, etc., while the other drives the parallel printer port and the user port. (The user port being the interface employed to link the BBC master to the laser instrument's electronic hardware.)

Each VIA is housed in a 40 pin package (figure 5.2.2) and contains two fully programable bidirectional 8-bit input/output ports (port A and port B) each with its own handshaking capability. There are two 16-bit programmable timer/counters, a serial/parallel or parallel/serial shift register and latched input/output registers.

On port A 8 lines (PA0 to PA7) can be individually programmed as inputs or outputs under the control of the Data Direction Register A (DDRA). The logic level on the output pins is controlled by an Output Register A (ORA) and the input data can be latched into an internal register under control of the CA1 line. These various modes of operation are controlled via internal function control registers, the peripheral control register (PCR) and the auxiliary control register (ACR), which are programmed by the 6502 CPU.

The 8 bidirectional port B lines (PB0 to PB7) are controlled by an output register (ORB) and a data direction register (DDRB) in a similar way to port A. The logic level of the PB7 output signal can also be controlled by one of the interval timers. The second timer can be programmed to count pulses on the PB6 input.

The port B control lines (CB1 and CB2) act as interrupt inputs, or, as handshake outputs (similar to port A). Each line controls an interrupt flag in the interrupt flag register (IFR) with a corresponding interrupt enable bit in the interrupt enable register (IER). The control lines can also be programmed to act as a serial port under the control of the shift register.

Operation of Port A and Port B

There are two data direction registers, DDRA and DDRB, which specify whether the peripheral pins are to operate as input or outputs. Placing a "0" in a bit of a DDR will cause the corresponding bit of that port to be defined as an input; a "1" defines it as an output.

Each of the port's input/output pins is controlled by a bit in an output register (ORA or ORB) and an input register (IRA or IRB). When configured as an output, a port line will be reflect the status of the corresponding bit in the output register. If the line is defined as an input, writing data to its output register will have no effect. Reading a port will cause the content of the input register (IRA or IRB) to be transferred onto the data bus.

Handshaking Data Transfer

The 6522 VIA allows data transfers between two asynchronous devices (in this case between the 6502 CPU and peripheral devices) through the operation of "handshake" lines. The port A lines, CA1 and CA2, handshake data on both "read" and "write" operations; port B lines, CB1 and CB2, handshake on the "write" operation only.

The "read" handshaking operates with "data ready" and "data taken" signals. The peripheral device must generate the "data ready" signal to the 6502 CPU, signifying that valid data is present on the peripheral port. This signal interrupts the 6502 CPU which then reads the data, causing the creation of a "data taken" signal. The peripheral device responds by making new data available. This process continues until the data transfer is complete (timing diagram figure 5.2.3). The "write" handshaking also operates with "data ready" and "data taken" signals. The 6522 VIA provides the "data ready" (CA2 or CB2) signal and accepts the "data taken" (CA1 or CB1) signal from a peripheral device. The "data taken" signal sets the interrupt flag and clears the "data ready" output (timing diagram figure 5.2.4). Selection of the operating modes for CA1, CA2, CB1 and CB2 is controlled by the PCR.

Timer Operation

Timer 1 consists of two 8 bit latches and a 16 bit counter. When it is loaded the counter decrements at the system clock rate (1 MHz) until it reaches zero. On reaching zero, if enabled, the interrupt flag will be set and an interrupt will be requested of the 6502 CPU. The timer then disables any further

interrupts, or, automatically transfers the contents of the latches to the counter and continues to decrement.

Interrupt Operation

Interrupt flags are set either by an interrupt in the chip (eg. Timer reaching zero) or an interrupt condition on an input to the chip (eg. handshake data transfer).

The interrupt flags remain in the set condition until the interrupt has been serviced. The source of the interrupt can be ascertained by reading the interrupt flags in order - from highest priority to lowest priority. This can be done by reading the interrupt flag register into the 6502 CPU's accumulator, shifting right (or left) and using conditional branch instructions to detect an active interrupt.

5.2.2 Linear Photodiode Array.

5.2.2.1 General description.

The linear photodiode is enclosed in an integrated type package with a ground and polished glass window. The device consists of a row of 1024 silicon photodiodes (25μm centre-to-centre spacing), each has an associated storage capacitor on with which to integrate photocurrent, and a multiplex switch for periodic readout via a shift register scanning circuit. A shift register clock driver is also integrated so that only a single Transistor Transistor Logic (TTL) clock is required for scanning. A row of dummy diodes is read out differentially with the photodiode to allow cancellation of the multiplex switching transients, providing a clean video signal.

The sensing elements are diffused p-n junctions (see Appendix B3) for high quantum efficiency and full silicon spectral response. Light incident on the photodiodes is converted to an electrical charge which is integrated and stored on the photodiode capacitance until readout.

5.2.2.2 Photodiode Array Circuit.

A circuit diagram of the linear photodiode array is shown in figure 5.2.5. Each cell consists of a photodiode and dummy photodiode, both with associated storage capacitance. These photodiodes are connected through Metal Oxide Semiconductor (MOS) multiplex switches to video and dummy recharge lines, which are common to all the cells. The switches are sequentially closed for one clock period by the shift register scanning circuit, thereby recharging each cell to -5 volts and storing about 3pC on its capacitor.

The scanning circuit is driven by a single phase TTL clock with a periodic TTL start pulse introduced to initiate each scan. The cell-to-cell sampling rate is the clock frequency, and the total time between scans is the interval between start pulses

During the period between start pulses the charge on each photodiode is gradually removed by photocurrent; the photocurrent being a product of photodiode sensitivity and incident light intensity. The total charge removed from each cell is the product of the photocurrent and the period between start pulses. This charge has to be replaced through the video recharge gate, when the photodiode is sampled and reset, once each scan.

As well as the signal charge, switching transients are capacitively coupled to the video line by the multiplex switches. The same switching transients are introduced to the dummy line and therefore can be removed from the signal by reading the video lines differentially (common mode rejection).

5.2.2.3 Sensor Geometry.

In the photodiode array, the light sensing area is a long, narrow, rectangular region covered by an opaque mask. Bar shaped photodiodes extend across the region and are connected to the storage capacitors and multiplex switches buried under the mask. The entire aperture is photo-sensitive; photocurrent generated by light incident between the photodiodes is collected by the nearest photodiode. Figure 5.2.6 shows the aperture geometry along with an idealized response function which would be obtained by scanning a point

source of visible light along the length of the aperture. Figure 5.2.7 shows the relative spectral response as a function of wavelength and a plot of charge output versus exposure is shown in figure 5.2.8

5.2.2.4 Drive Requirements.

The photodiode array require two power supplies; +5 volts and -15 volts (figure 5.2.9). The ARRAY-CLOCK, RESET (ie. recharge) and START timing signals were TTL signals supplied by external circuitry:

The ARRAY-CLOCK signal was generated by a 9602 multivibrator -the ARRAY-CLOCK signal was also used to drive the SAMPLE-PULSE delay circuit which in turn drove a SHUNT-PULSE pulse generator which supplied the recharge gate of the array with the RESET (or recharge) pulse (figure 5.1.1).

The START signal was initiated by the data capture algorithm stored in the BBC microcomputer; this was synchronised with the negative a going edge of the of the ARRAY-CLOCK, using a start synchronisation circuit that also ensured that the START pulse enveloped only one positive transition of the ARRAY-CLOCK pulse.

5.2.2.5 Signal Extraction

The video output is a train of 1024 charge pulses flowing into the video recharge and dummy recharge line capacitances during each scan, with timing as shown in figure 5.2.10. The pulses on the dummy line contained switching transients only; those on the video line contained switching transients plus the video signal. The video and dummy lines were amplified differentially to extract a "noise-free" signal (figure 5.2.11)

Immediately after the multiplex switch is closed to sample the photodiode, the voltage change on the video line is sensed through the buffer amplifier, and sampled and held. The recharge gate is then pulsed negative to reset the video line before the next photodiode is sampled. This results in a sampled and held boxcar video signal (figure 5.2.12).

An output pulse (END-OF-SCAN) is provided by the photodiode array when the penultimate diode is sampled by the shift register scanning circuit.

5.2.2.6 Data Capture.

The END-OF-SCAN pulse from the photodiode array is used in conjunction with the START pulse to produce a BLANK-OUT pulse, which indicates the period during which the diodes are being scanned.

Each time a photodiode is sampled and held, the signal is digitised using a very fast (15MHz sampling rate, 66ns conversion) Analogue to Digital Converter (ADC), and stored in an Auxiliary Random Access Memory (RAM) chip. This was achieved by appropriately manipulating and applying the ARRAY-CLOCK and BLANK-OUT timing signals to the ADC and auxiliary RAM chips (figure 5.1.1 and 5.2.13).

When BLANK-OUT is LOW this indicates that the photodiodes are being sampled, so this signal was used to enable the ADC. When the ADC is enabled the ARRAY-CLOCK synchronizes its analogue-to-digital conversions;

the rising edge of the ARRAY-CLOCK latches the data sample while the falling edge shifts the digitised data to the ADC's output register, ready for storage in the Auxiliary RAM.

Both WRITE-ENABLE and OUTPUT-ENABLE pins on the Auxiliary RAM are ACTIVE-LOW. Thus, the BLANK-OUT signal is inverted and NANDed with the ARRAY-CLOCK before connecting to the WRITE-ENABLE pin of the Auxiliary RAM. This ensures that the Auxiliary RAM is written to and read from when appropriate. A ripple through UP-DOWN counter specifies which memory address is being read from or written to; the BLANK-OUT line is connected to the UP-DOWN pin so that when the memory is being written to, the address is incremented and when read from, the address is decremented.

5.2.2.7 Data Transfer

The UP-DOWN counter is triggered by either the ARRAY-CLOCK or the User Interrupt Service Routine ("BBC-CLOCK"). The ARRAY-CLOCK and the BBC-CLOCK are gated so as to be mutually exclusive; at any one time either the ARRAY-CLOCK, or the BBC-CLOCK is clocking the counter.

An algorithm (interrupt service routine, see appendix A5.3) in the BBC microcomputer monitored the BLANK-OUT signal which indicated the end of data capture. When the BLANK-OUT signal went LOW, the contents of the Auxiliary RAM were copied/transferred into the microcomputer's memory for future analysis. This analysis took the form of either, predicting an optimum photodiode integration period (Section 5.2.2.6 and 5.5.2), or,

converting of the captured data from the time domain to the frequency domain (Section 5.6).

5.3 Optical Hardware

5.3.1 Laser Beam Production

Details of the low-power, Helium-Neon laser used for timber illumination are given on the manufacturer's data sheets in Appendix B1. Appendix B2 explains the process of producing monochromatic (laser) light.

Monochromatic light was used, as opposed to white light, because it precludes the problem of chromatic aberrations which would otherwise be evident when the optical lenses are employed for beam expansion, image-gathering and focusing.

5.3.2 Beam Expansion.

The diameter of the beam emitted by the laser is only 1mm. This poses two potential problems; one relates to the post-process instrument, while the other concerns its in-process operation:

(1) With the post-process instrument, the 5:1 reduction (i.e. object to image) of the 1mm laser beam would necessitate critically precise sample-length-image and photodiode-array alignment (the image would be only 0.2mm wide). This implies sophisticated design of lens holders and adjustment mechanisms, and, accurate tolerancing of their component parts.

(2) With the in-process measurement, the amplitude of the vibration present could render such a small beam - directed at grazing incidence - inadequate for continuous and consistent surface illumination.

To alleviate both these potential problems a beam with a considerably larger diameter was required. This meant optically expanding the 1mm laser beam to an appropriate size. A 1:14 beam expander was designed, using thin lens theory, manufactured and fitted to the (1mm diameter beam) Helium-Neon laser (figure 5.3.1).

ASIDE:
Thin lens theory is based on the premise that the lens is of negligible thickness and can therefore be treated as two refracting surfaces, both of which act on the ray and both of which are at the same point in space. Based on these assumptions the following expression, known as the Lensmaker's Equation, can be derived which relate the focal length of a lens to corresponding object and image distances:

$$\frac{1}{f} = \frac{1}{S_o} + \frac{1}{S_i} \qquad \textbf{(5.3.1)}$$

where S_o = *object distance*
S_i = *image distance*
f = *focal length of lens*
(These are more clearly defined in figure 5.3.2*)*

The sign convention used is:-
All distances are measured to the optical centre, C.
Distances are positive if actually traversed by the light ray (distances to real objects and images).
Distances are negative if only apparently traversed by the light ray (distances to virtual objects and images).

Transverse magnification, **m**, *is defined by*

$$m = \frac{\textit{height of transverse image}}{\textit{height of transverse object}} \qquad \textbf{(5.3.2a)}$$

therefore

$$m = \frac{IM}{OB} \qquad \textbf{(5.3.2b)}$$

The two lenses were chosen in designing the beam expander; the first was a plano-convex lens, used to diverge the laser beam; the second was a double convex to converge the diverging rays onto a path which is parallel to the optic axis.

The focal length of the respective lenses were chosen as follows:

Refer to figure 5.3.3. The diverging lens is at point O and the converging lens is at point I. With reference to the diverging lens, the incoming laser beam, LB, is parallel (ie. object at infinity) causing a virtual image to be formed at its focal point, V, ie. at focal distance $\mathbf{f_d}$ in front of the diverging lens. In order that the converging lens emit rays which are parallel to the optic axis, the corresponding image has to be coincident with its focal point. The virtual image of the diverging lens (point V) is thus the object for the converging lens and is at focal distance $\mathbf{f_c}$ in front of the converging lens.

By similar triangles

$$\frac{\mathbf{f_d}}{\mathbf{OB}} = \frac{\mathbf{f_c}}{\mathbf{IM}}$$

Now **OB** = 1mm, and, **IM** = 14mm, so

$$\frac{\mathbf{f_d}}{\mathbf{1}} = \frac{\mathbf{f_c}}{\mathbf{14}}$$

giving

$$\mathbf{f_c = 14 f_d} \qquad \textbf{(5.3.3)}$$

Thus lenses were selected having appropriate diameters and focal lengths as specified above. A cylindrical mechanism was designed which held the two lenses in position and provided fine focusing (see figure 5.3.1).

5.3.3 Image Focusing and Sample Length.

Contacts within the woodworking industry (Goddard M, 1985) have indicated that a 125mm sample length would be adequate for the purpose of surface

analysis in terms of its frequency/harmonic content. This was supported by the following reasoning:

The distance, **L**, traversed by the timber travelling at constant linear velocity, **V**, during one revolution of the cutterhead that is rotating at angular velocity, **W**, is given by

$$\mathbf{L} = \frac{\mathbf{V}}{(2\pi/\mathbf{W})}$$

The maximum possible distance, $\mathbf{L_{max}}$, traversed during one revolution of the cutterhead then given by

$$\mathbf{L_{max}} = \frac{\mathbf{V_{max}}}{(2\pi/\mathbf{W_{min}})} \qquad \textbf{(5.3.4)}$$

Currently, $\mathbf{V_{max}}$ = 150m/min and $\mathbf{W_{min}}$ = 1500rpm, so

$$\mathbf{L_{max}} = \frac{(150/60)(2\pi)}{(15000.2\pi/60)} = 100\text{mm}$$

Thus, erring on the side of caution, 125mm was adopted as the fundamental sample length.

This necessitated the optical reduction of a 125mm-long object (the illuminated timber) to a 25mm long image, which must be focused onto the 25mm long glass window of the photodiode array. Figure 5.3.4 shows the optical arrangement.

The appropriate lens was chosen using the restrictions in the Lensmaker's Equation (equation **5.3.1**). Refer to figure 5.3.4: by similar triangles

$$\frac{\mathbf{IM}}{\mathbf{IC}} = \frac{\mathbf{OB}}{\mathbf{OC}}$$

therefore

$$\frac{IM}{OB} = \frac{IC}{OC} \qquad (5.3.5)$$

Hence from equation **5.3.2**

$$m = \frac{IC}{OC}$$

hence

$$m = \frac{S_i}{S_o} \qquad (5.3.6)$$

Now

$$IM = 25 \text{ mm}$$

and

$$OB = 125 \text{ mm},$$

therefore substituting in equation **5.3.2b** gives

$$m = \frac{1}{5} \qquad (5.3.7)$$

and substituting equation **5.3.7** in **5.3.6** gives

$$S_o = 5S_i \qquad (5.3.8)$$

which substituted in equation **5.3.1** gives

$$\frac{1}{f} = \frac{1}{5S_i} + \frac{1}{S_i} \qquad (5.3.9)$$

which gives

$$f = \frac{6S_i}{5} \qquad (5.3.10)$$

Using equation **5.3.10**, image distance S_i was plotted against lens focal length, f, (figure 5.3.5). Figure 5.3.5 was used as a guide in the selection of lens system with appropriate focal length and image coverage (25mm x 4mm). The system selected was a projector lens of focal length 50mm and corresponding image distance, S_i, of 41.7mm with 35mm x 23mm image coverage. The lens was mounted on a screw thread arrangement to facilitate adequate focusing of the image (figure 5.3.6).

5.4 Instrument Framework

5.4.1 Introduction

A framework had to be designed to accommodate and support the components which comprised the Laser Instrument. The major criterion was that of:

1) Correct alignment and positioning of the photodiode array, the image focusing lens and machined timber samples.

2) Arranging the datum face, against which the machined face of the timber samples located, so that it was perpendicular to the optical axis of the image focusing lens.

3) Positioning the laser light source so that the grazing angle of incidence, for timber illumination, could be varied, and, aligning the laser beam such that the illuminated surface formed an image which aligned itself to the photodiode array.

5.4.2 Framework

A T-shaped framework was designed which supported the timber samples and focusing lens, such that the timber surface and optical axis of the lens were orthogonal (figure 5.4.1).

A clamping device, designed to accommodate varying thicknesses of timber, was built into the framework to securely locate the timber samples during data capture (figure 5.4.2).

5.4.3 Adjustment Mechanisms

5.4.3.1 Angle of Incidence

A "floating" carriage, located on the left of the timber clamp, was designed to support the helium-neon laser light source. The carriage was free to rotate in the horizontal plane (figure 5.4.3), thus allowing variation in the angle of incidence of the laser beam. The angle of incidence was controlled by a micrometer-spring mechanism (figure 5.4.4); Table 1 shows a look-up chart of micrometer reading versus angle of incidence.

5.4.3.2 Object Position / Alignment

The vertical position of the laser light source could be controlled by adjusting the length of the three legs that supported it. This in effect governed the vertical position of the "horizontal" beam and hence the vertical position of timber illumination (ie. the Object of the focusing lens). The length of the single leg, relative to that of the other pair, was used to control the yaw of the beam.

5.4.3.3 Image Focusing

The image focusing lens was arranged to have a course and fine focus adjustment. The course focus was effected by slot and clamp arrangement; the lens support could be positioned and clamped anywhere along the slot (figure 5.3.6). The fine focus was achieved by use of a screw thread; the male screw thread on the lens holder was used to fine-adjust the horizontal position of the lens and hence the fine-focus of the image.

5.4.3.4 Image Alignment

The same slot used for the course focus of the image focusing lens was used to locate and clamp the support to which the photodiode array was attached. The vertical position (alignment) of the array could be adjusted by use of a screw thread arrangement (figure 5.4.5).

5.4.4 Dark-housing / Canopy

A dark-housing/canopy was designed to exclude ambient light and allow access for adjustments and changing of timber samples (figure 5.4.6).

5.5 Data Capture Software

To obtain a data set that represent the reflected light intensities from the planed timber, two start pulses must be sent to the photodiode array. The time interval between these start pulses (the integration period) determines the magnitude of the voltage signals received from each photodiode in the array (the total output from each cell being the product of the photo current and the integration period); for example, let a timber sample being assessed reflect a light intensity pattern which covers the full length of the photodiode array; let the maximum intensity of the reflected light falling on the photodiode array impinges, say, photodiode number 7, and the output voltage from photodiode 7, for an integration period of 5 ms, be 0.5 volts. A reduction in the integration period would result in a proportionally reduced voltage output on photodiode 7, whereas an increase in integration period would result in a proportionally increased voltage signal.

The integration period is controlled by the "Data Capture" algorithm (appendix A5.1). The design philosophy applied to this algorithm exploits automatic gain control; the criterion being, the maximising of the signal, with a view to optimising the resolution of the ADC. Thus every data set captured has the same maximum, however, the relative magnitude of the other points in the set, to this maximum, would differ from timber sample to timber sample. The process of data capture can be divided into two sections:-

a) Host computer's access to data stored in the Auxiliary RAM.
b) Computing the Optimum photodiode Integration Period.

5.5.1 Host Computer's Access to Auxiliary RAM

On receiving a start pulse the array is scanned, ie. all the photodiodes are sampled, the corresponding voltages digitised and stored in the Auxiliary RAM.

(Refer to schematic diagram and timing diagram, figures 5.1.1 and 5.2.13). During the scan period the BLANK-OUT line is HIGH. This line was connected to the BBC microcomputer's user port and caused an interrupt when a positive edge was detected.

The Interrupt Service Routine (Appendix A5.3) started at the label "int" and ended at the label "oldv" and its structure was as follows:-

WHILE** Interrupt Request Flag Set **DO
Save All Registers On Processor Stack
Check if Interrupt is from photodiode array Circuit
***IF** Array Circuit Interrupted*
THEN
Copy Data from Aux. RAM to Host micros RAM
ELSE
Recover Registers From stack
END IF
Hand back control to micros Operating System
(Or continue Interrupt Polling)

While the array is being scanned, the counter (used as a memory location pointer) counts UP under the influence of the array's clock. At the end of the scan BLANK-OUT goes HIGH putting the counter into the DOWN mode. Decrementing the counter is effected by the User Interrupt Service Routine, which sends pulses to the counter by writing ZEROs and ONEs to the

appropriate lines on the User Port; the contents of the Auxiliary RAM are copied into the host computer's memory.

5.5.2 Optimum Photodiode Integration Period.

As stated above, the desired integration period for the photodiode array should be such that the maximum magnitude output signal is obtained. This was achieved by monitoring the array element on which light of highest intensity was incident and adjusting the integration period until maximum (saturation) voltage was attained.

Improvement in the estimation of the integration period was accomplished using piecewise linear approximation. Refer to figure 5.5.1a. Remembering that, as stated in the Section 5.2.2.2, the charges on the capacitors of the photodiode array are removed by photocurrent and that photodiodes only operate under negative-bias conditions, the initial (maximum) voltage on the capacitors would be zero, and saturation would occur at some negative voltage, -V. Figure 5.5.1b shows the general case of figure 5.5.1a.

where

X_o is the initial voltage (capacitor fully charged)

X_i is the voltage after integration period (T_i - T_o).

Using similar triangles (see figure 5.5.1a), the integration period, C, for saturation can be estimated thus:-

$$\frac{AB}{BF} = \frac{FD}{DE} \qquad (5.3.11)$$

i.e.

$$\frac{X_o - X}{T_i - T_o} = \frac{X_i - V}{dt} \qquad (5.3.12)$$

therefore,

$$dt = \frac{(X_i - V)}{(X_o - X_i)} .(T_i - T_o) \qquad (5.3.13)$$

and

$$C = T_c - T_o \qquad (5.3.14)$$

therefore

$$C = T_i - T_o + dt \qquad (5.3.15)$$

Therefore the prediction is that an integration period of **C** (=T_i-T_o+**dt**) seconds will achieve saturation voltage, **V**.

The data capture algorithm which was written (see Appendix A5.1) utilises the above equations iteratively to calculate the optimum integration period. In the algorithm:-

Xi = max. negative sample in Aux. RAM after latest scan.
Xo = max. negative sample from penultimate scan
V = required maximum signal.
A **FOR - NEXT** loop timed out the integration period
The code labelled "start" is an assembly-code sub-routine which sends the start pulse to the array.

The structure of the computer algorithm which calculates the optimum integration period is as follows:-

```
START.
    REPEAT.
        Calculate new estimate of integration period.
        Send start pulse.
        Time out estimated integration period.
        Send start pulse.
        Wait for Aux. RAM to be filled with latest data.
    UNTIL peak signal is equal to maximum.
    Plot data on screen.
END.
```

The algorithm uses an iterative process (**REPEAT-UNTIL** loop) to improve the estimation of the optimum integration period until the signal is within a given tolerance of the required maximum.

5.6 Data Analysis Software

When captured the data was to be analyzed; other research (Mulvaney D.J, Newland D.E, 1986) has indicated that, of the orthogonal transforms commonly used in engineering, Fourier transforms (FT's) are admirably suitable for surface analysis because of their precision and their rapid rates of convergence. What follows outlines the theory, and derivation, of Discrete Fourier transforms (DFT's) and Fast Fourier transforms (FFT's); it shows the way in which an FFT algorithm was designed and tailored for the analysis of the data captured from the timber samples.

5.6.1 Fourier Transforms

5.6.1.1 Waveforms

To fully describe a waveform in time, values must be to assign at various points and there must be enough points of the waveform displayed in order to discern its shape or its type.

For example, if the sinusoid, shown in figure 5.6.1 (which was captured by a cathode ray oscilloscope with a time-base setting of 1ms) was captured using a setting of only 0.01ms per division, this would stretch the first tenth of the time division to cover the entire display; the waveform would thus appear to be a ramp instead of a sinusoid.

Once a waveform is completely described with respect to time, it is possible to construct a new description of it with respect to frequency. An example of this, for a sinusoid, is shown in figure 5.6.2, which depicts a

three-dimensional waveform space with amplitude as the vertical axis and time and frequency on the other two axes. The time-axis and amplitude-axis define a domain called the "time-plane", while the amplitude-axis and frequency-axis define the "frequency-plane"; the time and frequency planes (or domain) are orthogonal.

The time history of a sinusoid, such as that shown in figure 5.6.1, can be viewed as a projection on the time-plane. In concept, the sinusoid can be thought of as actually existing some distance from the time-plane; this distance is measured along the frequency axis and is equal to the reciprocal of the waveform's period. Similarly, the sinusoid also has a projection onto the frequency-plane; this projection takes the form of an impulse; the magnitude of this impulse is equal to the sinusoids amplitude. The position of the impulse coincides with the frequency of the sinusoid.

The single impulse in the magnitude diagram defines both the amplitude and frequency of the sinusoid. Although this information is sufficient to reconstruct the sinusoid in the time-domain, some additional information, phase, is needed in order to locate its position relative to the zero time reference.

This phase information is also represented in a phase diagram; this consists of an impulse located on a frequency axis, the amplitude of which is indicative of the phase associated with the sinusoid. The phase diagrams can be determined by locating the positive peak which is closest to time zero. Delay

is denoted by negative phase and advance by positive phase.

Using the type of description conventions developed above it is possible to build a variety of non-sinusoidal waveforms. For example, consider two sinusoids, one of frequency F_o and phase -90 degrees, the other of frequency $2F_o$ and phase -45 degrees; the amplitude of the first being twice that of the second. The first sinusoid is completely described (using the frequency description) in figure 5.6.3a, the second in figure 5.6.3b. The sum of the two sinusoids is shown in figure 5.6.3c.

For the complete picture figure 5.6.3 can be redrawn in three dimensions as shown in figure 5.6.4 where the concept of projecting onto the time plane and frequency plane is employed; here the idea of summing multiple or time-domain projections is introduced. The projections onto the time-domain is shown in dotted lines, their sum being indicated by a heavy solid line.

The technique of adding sinusoids can be continued so that various shaped projections onto the time-domain can be obtained. Each shape or waveform is characterised by a unique combination of sinusoids. If any one of the sinusoids is changed in frequency, amplitude or phase, the waveform's time-domain projection changes.

Most waveforms are measured in the time-domain; time-based measurements have historical precedence and are the most familiar data format. Time histories, however, only reveal limited information. Without a direct look at

the frequency-domain, waveshape changes are only an indication that some frequency component has been modified. There is a rule of thumb - that fast rise times indicate high frequencies - but this is a rather limited, non-specific tool for waveform analysis.

A more complete approach to getting frequency-domain information is to apply the rigorous mathematical technique known as Fourier analysis. This allows a time-domain waveform to be described in terms of both frequency-domain magnitude and phase. Fourier analysis also offers the option of results in rectangular form, which consists of real and imaginary parts of the complex frequency-domain.

However, the classical mathematical approach to Fourier analysis is frustrating for all but the simplest waveforms. If the waveform cannot be expressed as an equation, classic Fourier techniques cannot be applied. A waveform can, however, be sampled and digitized with a waveform digitizer; then discrete Fourier transforms (DFT) can be used to Fourier transform the digitized waveform.

FFT algorithms can be implemented through computer software, firmware or hardware. Their major advantage is the speed with which they analyzes large numbers of waveform samples. The following sections detail the background and theory behind the FFT algorithm; first, continuous Fourier theory for un-sampled waveforms is discussed, paving the way for the development of DFT and, subsequently, FFT.

5.6.1.2 Fourier Series

The general form of the Fourier series is

$$x(t) = a_0 + a_1.Cos(Wt) + a_2.Cos(2Wt) + ...+ a_n.Cos(nWt)$$
$$b_0 + b_1.Sin(Wt) + b_2.Sin(2Wt) + ...+ b_n.Sin(nWt) \quad (5.6.1)$$

where $W = 2\pi f$ and f is the fundamental frequency.

If a Fourier series can be written for a waveform then the components of the series completely describe the frequency content of the waveform. For this to be true certain conditions have to be met:

1) The waveform has to be periodic; ie. if the waveform is represented by $x(t)$ and there is a constant time, τ, that exists such that $x(t) = x(t+\tau)$ for all time, t, then $x(t)$ is periodic with period τ. That is to say, the waveform must repeat itself in time before a Fourier series can exist for it.

2) The Dirichlet conditions must prevail; they are:
   (a) If the function has discontinuities, their number must be finite in any period.
   (b) The function must contain a finite number of maxima and minima during any period.
   (c) The function must be absolutely integrable in any period; that is

$$\int_0^{\tau} |x(t)|\,dt < \infty$$

where $x(t)$ describes the function.

There are obviously some theoretical functions for which a Fourier series does

not exist. For all practical purposes, however, the Dirichlet conditions are met when a periodic function accurately describes a physical occurrence.

5.6.1.3 Discrete Spectra from Fourier Series.

The Fourier Series (equation **5.6.1**) can be written more concisely as

$$\mathbf{x(t) = a_o + \sum_{n=1}^{\infty} (a_n.Cos(nWt) + b_n.Sin(nWt))} \qquad \textbf{(5.6.2)}$$

The Fourier series for a specific waveform is written by using the salient features of the waveform to find specific values for the coefficients in equation **5.6.2.** The frequency, **W,** is found from the period of **x(t)** and is equal to $2\pi/\tau$ (also $W = 2\pi f$ where $f=1/\tau$). The coefficient, a_o, equal to the average value of **x(t)** over one period, is determined by

$$a_o = \frac{1}{\tau} \int_{\bullet}^{\tau} x(t)\, dt \qquad (5.6.3)$$

The remaining coefficients a_n and b_n are evaluated for

n=1,2,3,.. by

$$a_n = \frac{2}{\tau} \int_{0}^{\tau} x(t)\, Cos(nWt)\, dt \qquad (5.6.4)$$

and

$$b_n = \frac{2}{\tau} \int_{0}^{\tau} x(t)\, Sin(nWt)\, dt \qquad (5.6.5)$$

For example, the Fourier coefficient for the square wave shown in figure 5.6.5 has been evaluated to give the following series:

$$x(t) = \frac{4V}{\pi} [\text{Cos}(Wt) - 1/3\ \text{Cos}(3Wt) + 1/5\ \text{Cos}(5Wt) - .....] \qquad (5.6.6)$$

where $W = 2\pi f$.

The term $4/\pi$ is a constant resulting from the integration and V is the peak value of the square waveform.

The above series is a complete description of the frequency content in figure 5.6.5; from it diagrams of both the magnitude spectrum and phase spectrum can be constructed (figure 5.6.6) using the conventions discussed earlier (Section 5.6.1.1).

5.6.1.4 Spectral Diagrams.

The spectra of figure 5.6.6 are referred to as discrete spectra - each component being discretely located on a frequency axis and represented by a single line or impulse. The length of each spectral line indicates either magnitude or phase.

In the case of figure 5.6.6a the line spectrum of the magnitude is constructed from the Fourier series by first plotting the amplitude of the fundamental frequency. (The fundamental frequency is the reciprocal of the waveforms period ($f=W/2\pi$) and is indicated in the Fourier series by W). The magnitude of the fundamental is given by the first trigonometric term in the series ($n=1$)

For the square wave of figure 5.6.5 the magnitude of the fundamental is $4V/\pi$.

The diagram of figure 5.6.6 is constructed by first placing the fundamental spectral line at **f** and giving it an amplitude of $4V/\pi$. Subsequent Fourier terms are plotted in the same manner.

Each Fourier term is some integer multiple of the fundamental frequency and is referred to as a harmonic. The fundamental is often referred to as the first harmonic because f_0 is multiplied by one; integer multiples greater than one are always referred to as harmonics. In the case of figure 5.6.6a the square wave is made up of odd harmonics; these are shown with spectral lines of

$$3f_0,\ 5f_0,\ 7f_0,\ldots,\ nf_0$$

their magnitudes are, respectively,

$$1/3,\ 1/5,\ 1/7,\ldots,1/(2n-1)$$

of the fundamental magnitude.

The line spectrum for phase is constructed in a similar manner. There is a corresponding spectral line in the phase diagram for each line in the magnitude diagram and they are positioned on a frequency axis in the same manner; the length of these lines, however are indicative of the phase. In figure 5.6.6b the fundamental and the fifth harmonic are positive cosines and have zero phase; their spectral line length is zero; a heavy dot is used to indicate the presence of zero-phase components. The third and seventh harmonics are negative cosines and consequently have phases of 180°, this is indicated by the length of their spectral lines at **3f** and **7f**.

5.6.1.5 Non-periodic Waveforms.

The Fourier series is a useful tool for investigating the spectrum of periodic waveforms; unfortunately the signals in the real world are not composed exclusively of periodic waveforms.

The Fourier series and the Fourier integral, as analysis tools, are separate and distinct; the former is intended for use with periodic waveforms while the latter is reserved for non-periodic waveforms. Despite this clear distinction there is a subtle relationship which exists between the two; this relationship is helpful and useful in interpreting results.

5.6.1.6 Fourier Series to Fourier Integral.

Establishing the relationship between the Fourier series and the Fourier integral involves four major steps; these steps are briefly outlined below.

Step 1

The general form of the Fourier series is:

$$x(t) = a_o + \sum_{n=1}^{\infty} \{a_n \, Cos(nWt) + b_n \, sin(nWt)\} \qquad (5.6.7)$$

This can be expressed in exponential form, which is more appropriate for developing the integral, by substituting the exponential expression for **Cos(nWt)** and **Sin(nWt)**. The expressions are:

$$Cos(nWt) = \frac{\{e \, exp(jnWt) + e \, exp(-jnWt)\}}{2} \qquad (5.6.8)$$

$$\mathbf{Sin(nWt) = \frac{\{e\ exp(jnWt) - e\ exp(-jnWt)\}}{2j}} \qquad \mathbf{(5.6.9)}$$

where

e is the base of the natural logarithm

and

j is the imaginary unit in the complex number system {**j**=SQR(-1)}

Step 2

By substituting equations **5.6.8** and **5.6.9** in equation **5.6.7**, further manipulating and assigning new variables as appropriate, a more compact form of the Fourier series is obtained:

$$\mathbf{x(t) = \sum_{n=-\infty}^{\infty} C_n\ e\ exp(jnWt)} \qquad \mathbf{(5.6.10)}$$

where

$$\mathbf{C_n = \frac{1}{\tau} \int_{-\tau/2}^{\tau/2} x(t)\ e\ exp(-jnWt)\ dt} \qquad \mathbf{(5.6.11)}$$

and is evaluated for **n** = -∞,....-2,-1,0,1,2,....,+∞

For each **n**, $\mathbf{C_n}$ is evaluated to give the magnitude and phase of the harmonic component of **x(t)** having angular frequency **nW**.

The Fourier series is now in exponential form (equation **5.6.10**); the next step involves using the fact that each harmonic is separated by an amount **Δf**, where

$$\mathbf{\Delta f = \frac{\Delta W}{2\pi}} \qquad \mathbf{(5.6.12)}$$

Step 3

Substituting equation **5.6.12** in equation **5.6.10** and manipulating further, the series can be placed into the following form (which allows inspection of the limit as τ tends to infinity):

$$x(t) = \lim_{\tau \to \infty} \frac{1}{\tau} \sum_{n=-\infty}^{\infty} X(jnW)\, e\, \exp(jnWt) \qquad (5.6.13)$$

Since $\Delta f = \Delta W/2\pi$, equation **5.6.13** can be written as

$$x(t) = \lim_{\Delta W \to 0} \frac{1}{2\pi} \sum_{n=-\infty}^{\infty} X(jnW)\, e\, \exp(jnWt)\, \Delta W \qquad (5.6.14)$$

Step 4

Now, as ΔW tends to zero (period τ tends to infinity), the properties of the summation approaches those of an integral. This reduces the Fourier series to

$$x(t) = \frac{1}{2\pi} \int_{-\infty}^{+\infty} X(jW)\, e\, \exp(jWt)\, dW \qquad (5.6.15)$$

The Fourier coefficients have now become a function of a continuous frequency variable, **W**, and are given by

$$X(jW) = \int_{-\infty}^{+\infty} x(t)\, e\, \exp(-jWt)\, dt \qquad (5.6.16)$$

Equations **5.6.15** and **5.6.16** are together referred to as the Fourier transform pair. The former (equation **5.6.15**) is generally called the inverse Fourier transform and the latter (equation **5.6.16**) as the direct Fourier transform (or

simply Fourier transform).

The transform action of the Fourier integral is contrasted with that of the Fourier series in figure 5.6.7; each technique is applied to a different class of waveform and each provides different kind of frequency domain or spectral description. The Fourier series transforms time domain functions to frequency domain magnitudes and phases at specific, discrete frequencies. The Fourier integral, on the other hand, evaluates a continuous function of frequency.

Figure 5.6.8 shows graphically how the Fourier series (with discrete spectrum) is related to the Fourier integral (with continuous spectrum) by noting what happens to the spectrum as the period (of a pulse train), τ, tends to infinity.

5.6.1.7 Frequency Domain Diagrams

Both **X(jW)** and **x(t)** are defined over frequencies and times from minus infinity to plus infinity. The concept of negative time is intuitive; negative frequency is less so. To illustrate, figure 5.6.9 shows a sine wave, that is periodic in the time domain from minus infinity to plus infinity, and two pairs of spectral diagrams for this sine wave.

Figure 5.6.9b shows the magnitude and phase information that would be obtained by writing the Fourier series for the sine wave. Note that the time domain magnitude, V, is reflected exactly in the magnitude spectrum. The

time domain sine wave relative to time zero shows a phase of -90°(-π/2); this is shown on the phase diagram.

Figure 5.6.9c describe the sine wave in the frequency domain of the Fourier transform. Note, there are two spectral components - one at the positive frequency of the sine wave and one at its negative frequency. Each magnitude is half that of the time domain waveform (also, half the magnitude of the one in the Fourier series spectrum). The phase for the positive frequency is as for the Fourier series spectrum; -90° (-π/2) at 1/τ. Phase in the negative frequency domain is the inverted image of the positive domain; +90° (π/2) at -1/τ.

The frequency domain diagrams of figure 5.6.9 embody most of the conventions of magnitude and phase descriptions for the Fourier transform's frequency domain. These conventions are:

1) *The magnitudes in the positive and negative frequency domain exactly duplicate each other.*
   For every frequency indicated in the positive domain, one of equal magnitude is indicated at the same frequency in the negative domain; their sum being equal to the amplitude of the corresponding sinusoidal component in the time domain. In the case of DC, its frequency is zero and there is no division of magnitude.

2) *Phase in the positive frequency domain is duplicated in negative frequency, except the images are inverted.*
   This entails a sign change when passing between positive and negative frequencies.

With these conventions established, figure 5.6.8d can be redrawn for the Fourier integral's frequency domain; this is done in figure 5.6.10. The time domain pulse is a more generalised version with amplitude, V, and width, $2T_o$, centred about time zero (figure 5.6.10a). The frequency domain diagrams are shown in figure 5.6.10b and figure 5.6.10c.

ASIDE: ***Fourier Transform of a Pulse.***

The integral for transformation to the frequency domain is

$$\mathbf{X(jW) = \int_{-\infty}^{+\infty} x(t)\, e\, exp(-jWt)\, dt}$$

For the case of a pulse, $\mathbf{x(t)}$ *is zero everywhere except over the interval* $\mathbf{-T_0}$ *to* $\mathbf{T_0}$ *where it has a constant amplitude of* **V** *(figure 5.6.10). Since the Fourier transform of zero is zero, and the function (the pulse) has a constant value during the interval, the integral is reduced to*

$$\mathbf{X(jW) = V \int_{-T_o}^{T_o} e\, exp(-jWt)\, dt}$$

The integral evaluates to

$$\mathbf{X(jW) = 2VT_o \frac{sin(WT_o)}{WT_o} + j0}$$

which is the Fourier transform in rectangular coordinates. This is a classical frequency domain waveshape description, having a major lobe with decaying side lobes (see figure 5.6.10b), and can be generalised as (sin β*)/*β

5.6.1.8 Transforming Periodic Waveforms

Fourier transforms do not exist for periodic waveforms. To Fourier transform a periodic waveform, that waveform first has to be windowed ie. multiplied by a pulse (or rectangular window) of unit height.

The actual process of windowing a waveform is shown in figure 5.6.11. A cosine wave and a rectangular window is used. Each step is also shown in the frequency domain so that the effects can be illustrated. For simplicity

phase is ignored and only the frequency domain magnitude is shown.

In figure 5.6.11a an infinite extent cosine wave is shown in the time domain and two spectral components, at $\pm 1/\tau$, in the frequency domain. Figure 5.6.11b shows a rectangular window in the time domain and its "(sin β)/β" magnitude in the frequency domain. Multiplying the time domain window and the cosine wave together results in the product shown in figure 5.6.11c. This product is referred to as the rectangularly windowed cosine wave, and the magnitude of its Fourier transform is shown in figure 5.6.11d.

The transformed magnitude of the windowed cosine wave is not the product of the frequency domain functions for the cosine wave and the window (ie. multiplication in the time domain does not correspond to multiplication in the frequency domain).

It can be seen that figure 5.6.11d does exhibit some of the traits of both the cosine wave and the rectangular window:

> *The "(sin β)/β" magnitude of the window appears twice in figure 5.6.11d; once in positive frequency, once in negative frequency. The peaks of the double "(sinβ)/β" magnitude occur at the frequency (±1/τ) of the cosine wave.*

The frequency domain spectrum of the cosine wave and the rectangular window have undergone a mathematical process known as convolution (Schwartz M, Shaw L, 1975). Figure 5.6.11d is the result of convolving the cosine wave's frequency domain with the window's frequency domain.

5.6.1.9 Numerical Evaluation of Transform.

The Fourier transform a continuous signal, **x(t)**, is defined by:-

$$\mathbf{X(jW) = \int_{-\infty}^{+\infty} x(t)\, e\, exp(-jWt)dt} \qquad \mathbf{(5.6.17)}$$

The Fourier transform is an operation that creates from the time function, **x(t)**, a function, **X(jW)**, in the frequency domain. Then **X(jW)** displays the frequency content of the signal, **x(t)**, as a function of the continuous frequency variable, **W**.

To use numerical methods to evaluate Fourier transforms, a continuous signal **x(t)** has to be approximated by discrete sets of values. The zero-order approximation is to assume **x(t)** to be constant at **x(kT)** for

$$\mathbf{kT <= t <(k+1)T}$$

and the integral over this time interval is then approximated by the area of the rectangle (see figure 5.6.12), which is equal to

$$\mathbf{T\ x(kT)}$$

Hence equation **5.6.17** becomes under numerical approximation

$$\mathbf{X(jW) \approx \sum_{k=-\infty}^{+\infty} T\ x(t_k)\, e\, exp(-jWt_k)} \qquad \mathbf{(5.6.18)}$$

where $\mathbf{t_k = kT}$ and the summation is over an infinite range in general.

In practice the signal duration of, say, **NT** and can be assumed to start at **t=0.**

Then equation **5.6.18** becomes

$$X(jW) \approx \sum_{k=0}^{N-1} T\, x(t_k)\, e\, \exp(-jWt_k) \qquad (5.6.19)$$

This represents the approximate Fourier transform of a finite duration signal. The accuracy depends on the time step; the smaller **T** is the better the approximation.

In a similar manner, the inverse Fourier transform integral, defined by

$$x(t) = \frac{1}{2\pi} \int_{-\infty}^{+\infty} X(jW)\, e\, \exp(jWt)\, dW \qquad (5.6.20)$$

can be approximated by the summation

$$x(t) \approx \frac{\Delta W}{2\pi} \sum_{n=-M}^{M-1} X(jW)\, e\, \exp(jW_n t) \qquad (5.6.21)$$

where the signal is assumed to be band limited in frequency to $M\Delta W$, ΔW being the step size in frequency used in the approximation of the function $X(jW)$ and $W_n = n\Delta W$. Again $x(t)$ is a continuous function of the time variable, **t**, and is periodic in **t** with period

$$\frac{2\pi}{\Delta W}$$

The accuracy of the approximation depends on the frequency step size, ΔW. Suppose the two approximate functions, equations **5.6.19** and **5.6.21**, are

evaluated at N discrete points in frequency and time, respectively:

$$X(jW) = T \sum_{k=0}^{N-1} x(t_k)\, e\, \exp(-jW_n t_k) \qquad (5.6.22)$$

for $n = 0,1,2,\ldots,N-1$

and

$$x(t_k) = \frac{\Delta W}{2\pi} \sum_{n=-N/2}^{N/2} X(jW_n)\, e\, \exp(+jW_n t_k) \qquad (5.6.23a)$$

for $k = 0,1,2,\ldots,N-1$

where, for convenience, **M** was chosen to be **N/2**, so that there are the same number of data points in both time and frequency domains. It can be shown that, since the frequency function **X(jW)** in equation **5.6.22** is periodic with period **N**, the summation in equation **5.6.23a** can be written as

$$x(t_k) = \frac{\Delta W}{2\pi} \sum_{n=0}^{N-1} X(jW_n)\, e\, \exp(+jW_n t_k) \qquad (5.6.23b)$$

for $k = 0,1,2,\ldots,N-1$

The expression in equations **5.6.22** and **5.6.23** represents the approximate Fourier Transform Pair at the **N** discrete points in both the frequency and time domains.

5.6.2 Discrete Fourier Transform.

Consider a discrete signal **x(kT)**. If the signal has a finite number of points and its values are used in the approximate Fourier Transform derived above, then equation **5.6.22** yields the approximate frequency information about the signal at the **N** discrete frequency values.

ASIDE: ***Relationship between the time interval*** **T** ***and the frequency interval*** **ΔW.**

Assume that **x(kT)** *is obtained from a continuous signal* **x(t)** *by sampling it at a uniform rate of* **T** *seconds. Then, from the principle of sampling, the Fourier Transform of the sampled signal is periodic with period* **2π/T**. *Therefore, for the* **N** *frequency points to cover the entire frequency range, the following must be true:*

$$N.\Delta W = \frac{2\pi}{T} \quad thus \quad \Delta W = \frac{2\pi}{NT} \tag{5.6.24}$$

Then

$$\frac{\Delta W}{2\pi} = \frac{1}{NT} \quad and \quad W_n t_k = \frac{nk2\pi}{N} \tag{5.6.25}$$

(*NB.* $W_n = n\Delta W$, $t_k = kT$)

The **T** factor in equation **5.6.22** is often absorbed as part of the signal strength when sampled. Therefore, to define the discrete Fourier Transform, let

$$x_k = T\, x(t_k), \quad k = 0,1,..,N-1 \tag{5.6.26}$$

and

$$X_n = X(jW_n), \quad n = 0,1,..,N-1 \tag{5.6.27}$$

Then equations **5.6.22** and **5.6.23**, respectively, become

$$X_n = \sum_{k=0}^{N-1} x_k\, e\, \exp(-(j2\pi/N)nk) \tag{5.6.28}$$

$$n = 0,1,..,N-1$$

and

$$x_k = \frac{1}{N} \sum_{n=0}^{N-1} X_n\, e\, \exp((j2\pi/N)kn) \tag{5.6.29}$$

$$k = 0,1,..,N-1$$

and where use is made of the relations in equation **5.6.25**.

The two expressions in equations **5.6.28** and **5.6.29** are called the discrete Fourier transform (DFT) pair. The notation

$$\mathbf{X_n = DFT[x_k]} \qquad \textbf{(5.6.30)}$$

is used to denote the DIRECT Discrete Fourier Transform in equation **5.6.28** and

$$\mathbf{x_k = IDFT[X_n]} \qquad \textbf{(5.6.31)}$$

to denote the INVERSE Discrete Fourier Transform in equation **5.6.29**. The transform in equation **5.6.28** can be expressed in a more concise form. To do this let

$$\mathbf{W_N = e\ exp(-j2\pi/N)} \qquad \textbf{(5.6.32)}$$

Then equation **5.6.28** becomes

$$\mathbf{X_n = \sum_{k=0}^{N-1} x_k W_N^{nk}} \qquad \textbf{(5.6.33)}$$

for $\mathbf{n = 0,1,2,...,N-1}$

The transform in equation **5.6.29** can also be expressed in a more concise form. To do this let

$$\mathbf{W_N = e\ exp(j2\pi/N)} \qquad \textbf{(5.6.34)}$$

then equation **5.6.29** becomes

$$\mathbf{x_k = \frac{1}{N} \sum_{n=0}^{N-1} X_n W_N^{kn}} \qquad \textbf{(5.6.35)}$$

for $\mathbf{k = 0,1,...,N-1}$

.Note that W_N has the property

$$W_N^{nN+m} = W_N^m \qquad (5.6.36)$$

for any **m** and **n**

5.6.3 Fast Fourier Transform.

A considerable saving can be made, in computational time, if algorithms known as Fast Fourier Transforms (FFT) are employed. FFTs eliminate some redundant products in the original DFT by decomposing the data sample set into smaller subsets in an orderly manner. The total number in the data sample set must be an exact power of 2. One way of decomposing the data samples results in the "decimation in time" algorithm. The idea is to decompose the **N** point signal sequence, x_k, into two **N/2** point sub-sequences, one consisting of the even numbered samples and the other consisting of the odd numbered samples, as

$$a_k = x_{2k} \qquad \text{for } k = 0,1,2,\ldots,N/2-1 \qquad (5.6.37)$$

and

$$b_k = x_{2k+1} \qquad \text{for } k = 0,1,2,\ldots,N/2-1 \qquad (5.6.38)$$

and to write the DFT in equation **5.6.28** or **5.6.33** as

$$X_n = \sum_{k=0}^{N/2-1} x_{2k}\, W_N^{2nk} + \sum_{k=0}^{N/2-1} x_{2k+1}\, W_N^{n(2k+1)}$$

for $n = 0,1,\ldots,N-1$

where $W_N = e\ \exp(-j2\pi/N)$ as defined in equation **5.6.32.**

Since $W_N^2 = W_{N/2}$, the above two summations can be written as

$$X_n = \sum_{k=0}^{N/2-1} a_k \, W_{N/2}^{nk} + W_N^n \sum_{k=0}^{N/2-1} b_k \, W_{N/2}^{nk}$$

$$X_n = \quad A_n \quad + W_N^n \, B_n \qquad (5.6.39)$$

where

$$A_n = \sum_{k=0}^{N/2-1} a_k \, W_{N/2}^{nk} \qquad (5.6.40)$$

is the N/2 point DFT of a_k for $k = 0,1,...,N/2-1$ i.e. the even-numbered samples of the original signal sequence, and

$$B_n = \sum_{k=0}^{N/2-1} b_k \, W_{N/2}^{nk} \qquad (5.6.41)$$

is the N/2 point DFT of b_k for $k = 0,1,...,N/2-1$ i.e. the odd-numbered samples of the original signal sequence.

Being a N/2-point DFT, A_n and B_n each have only N/2 distinct elements with the property

$$A_{n+N/2} = A_n$$

and

$$B_{n+N/2} = B_n$$

for $n = 0,1,...,N/2-1$

Since $W_N^{n+N/2} = -W_N^n$, equation 5.6.39 can be written two parts as

$$X_n = A_n + W_N^n \, B_n \quad \text{for } n=0,1,....,N/2-1 \qquad (5.6.42)$$

$$X_{n+N/2} = A_n - W_N^n \, B_n \quad \text{for } n=0,1,....,N/2-1 \qquad (5.6.43)$$

Thus, an N-point DFT can be found from the N/2-point DFT of its even-numbered and the N/2-point DFT of its odd-numbered samples. The result of this first step in deriving the FFT algorithm for N=8 is depicted in figure 5.6.13.

The second step in the decimation-in-time derivation is to apply the same decomposition technique in the computation of the two N/2-point DFT's in order to obtain A_n and B_n for **n=0,1,.....N/2-1.** The two N/2-point sub-sequences a_k and b_k are each decomposed into the even-numbered samples and odd-numbered samples as

$$c_k = a_{2k} = x_{4k} \quad \text{for } k=0,1,..,N/4-1. \tag{5.6.44}$$

$$d_k = a_{2k+1} = x_{4k+2} \quad \text{for } k=0,1,..,N/4-1. \tag{5.6.45}$$

$$e_k = b_{2k} = x_{4k+1} \quad \text{for } k=0,1,..,N/4-1. \tag{5.6.46}$$

$$f_k = b_{2k+1} = x_{4k+3} \quad \text{for } k=0,1,..,N/4-1. \tag{5.6.47}$$

Following the same derivations leading to equation **5.6.42** and **5.6.43**, the following formulas are obtained to express the N/2-point DFT's A_n and B_n in terms of the N/4-point DFT's C_n, D_n, E_n, F_n:

$$A_n = C_n + W_N^{2n} D_n \quad \text{for } n=0,1,....,N/4-1 \tag{5.6.48}$$

$$A_{N/4+n} = C_n - W_N^{2n} D_n \quad \text{for } n=0,1,....,N/4-1 \tag{5.6.49}$$

$$B_n = E_n + W_N^{2n} F_n \quad \text{for } n=0,1,....,N/4-1 \tag{5.6.50}$$

$$B_{N/4+n} = E_n - W_N^{2n} F_n \quad \text{for } n=0,1,....,N/4-1 \tag{5.6.51}$$

where the property $W_{N/2} = W_N^2$ is used.

The result of the second step in the decimation-in-time decomposition process is shown in figure 5.6.14 for **N=8**

The process of computing a DFT by decomposition of the signal into two sub-sequences can be continued until a one point DFT is reached, which is just the sample point itself. Because **N** is some power of 2, let **r** be that power so that $N=2^r$. Thus, **r** steps are required in the above decomposition process to reach the one point DFT's.

The final result of the eight-point decimation-in-time FFT is shown in the flow graph of figure 5.6.15. The two-point DFT's require no multiplications. For example, the two-point DFT C_0 and C_1 can be obtained by combining the one-point DFT's of x_0 and x_4 which are just the signal samples themselves:

$$C_0 = x_0 + x_4 \qquad (5.6.52)$$

and

$$C_1 = x_0 - x_4 \qquad (5.6.53)$$

Also, since $W_8^2 = -j$, the four-point DFTs in equation **5.6.48** through to **5.6.51** for **N=8** do not actually require complex multiplication. Therefore, in general, in combining the one-point DFTs to form the two-point DFTs and the two-point DFTs to form the four-point DFTs, no complex multiplications are required, thus reducing the total number of multiplications for the FFT algorithm by **N**.

Note that in order for the DFT $[X_n]$, $n = 0,1,...,N-1$, to appear in its natural order, the original sequence x_k, $k=0,1,....,N-1$, must be rearranged as shown in figure 5.6.15. The subscripts in the rearranged order have an interesting relationship with those in the natural order. The relationship is the bit reversal of the subscript. If the subscript of the natural order are represented in binary form in r-bits (binary digits), where $r=\log_2 N$, then by reversing the bits in each binary representation and representing the reversed r-bits in the decimal system, the subscript for the rearranged input sequence is obtained. The bit-reversal result is illustrated in Table 2 for the case of N=8.

With the input sequence reordered properly by using the bit-reversal procedure, the computation of the FFT can be performed in-place. To show this refer to figure 5.6.15 for N=8. In every stage, pairs of variables are combined to form other pairs. For example, x_0 and x_4 are combined to form C_0 and C_1, but x_0 and x_4 are not used to form other values, and C_0 and C_1 do not require other values. Similarly, only C_0 and D_0 are used to calculate A_0 and A_2, and C_0 and D_0 are not used to calculate any other values. Therefore, after a pair of values is used to form a pair of new values, the old values are no longer needed. Hence, the calculated new values can be stored back in the same storage locations used for the old values. This in-place computation reduces the amount of storage required in the computer.

To start the decimation-in-time FFT algorithm, pairs of adjacent values in the bit-reversed sequence are first combined to form pairs of new values, starting from the top to the bottom using the in-place procedure as shown in the

extreme left of figure 5.6.15. The operations involved in the first stage are only complex additions (subtractions), as shown in equations **5.6.52** and **5.6.53**.

In the second stage, pairs of newly formed valves, two positions apart, are used to calculate pairs of new values in-place.

This process of calculating pairs of new values in-place from the "old" values is continued for **r** (=$\log_2 N$) stages, with the separation of the variables in the pairs increased from stage to stage by a factor of 2.

During any stage, the in-place calculation of a pair of values has the structure shown in figure 5.6.16 known as a butterfly. As stated previously, the term $W_N^m \, x_{k+L}^{(s)}$ is used in the calculation of both $x_k^{(s+1)}$ and $x_{k+L}^{(s+1)}$ in the butterfly-structure flow graph of figure 5.6.16, where, by the concept of in-place-calculation, the signal samples are denoted by the same variables, with the added superscripts indicating the stage number. The butterfly structure can therefore be modified to the one shown in figure 5.6.17, which stresses that only one complex multiplication is required.

By reordering the nodes in figure 5.6.15, alternative forms of decimation-in-time FFT algorithm can be obtained. For example, by exchanging the rows of nodes, while carrying the branches along in each exchange, so that the input samples are in natural order, the flow graph of figure 5.6.18 is obtained, where the resulting DFT is in bit-reversed order. In this version, in-place calculation is still possible; however, the DFT values must be reshuffled using the bit-reversal procedure. Because, in the proposed laser instrument, the photodiode array captures data in the natural order, this form of FFT algorithm was adopted for the data analysis.

The FFT algorithms derived in this section can also be used to compute the inverse DFT as defined in equation **5.6.29.** To do this, the complex exponential constant, W_N^m has to be modified as

$$W_N^m = e\ exp(+j2\pi m/N)$$

i.e. equation **5.6.34**, and the input will consist of X_n/N, **n=0,1,....,N-1.** The output of the algorithm is then the signal samples in the time domain.

5.6.4 The FFT Algorithm.

With the details outlined in Section 5.6.3 a BBC BASIC computer algorithm was developed to implemented the decimation-in-time FFT algorithm. The FFT algorithm was tailored to suit the requirements of the Laser Instrument as dictated by the Nyquist Sampling Theorem and Fast Fourier Transform Theory:

The basis of Sampling Theory (the Nyquist Theorem) is that: "a continuous-time signal can be completely recovered from its samples if, and only if, the sampling rate is greater than twice the signal bandwidth".

For the decimation-in-time FFT, however, the number of samples must be an integer power of 2.

The surface wave pitch currently produced by woodworking machines is greater than or equal to 1mm. For the 125mm sample length (see Section 5.3.3), the smallest sample size which satisfies both these criteria is 256. Thus, 256 equi-spaced data points (every fourth data point from the set of

1024 points captured using the photodiode array (see Section 5.2.2.5)) were to be used as the data set to be transformed in the BASIC FFT algorithm.

The BASIC FFT algorithm, shown in Appendix A6, starts with the input in natural order and results in bit-reversed order. As pointed out above (Section 5.6.1.9), the same algorithm can be used to compute the direct FFT and the inverse FFT, provided the complex exponential constant W_N is properly assigned, as shown in equations **5.6.32** and **5.6.34** for direct FFT and inverse FFT, respectively. This is accomplished in the BBC BASIC FFT computer algorithm by use of the variable SIGN (lines 760 and 960). SIGN equals 1 for the direct transform and -1 for the inverse transform.

The in-place calculations are implemented in lines 970 to 990. Note that $W_N^0=1$ requires no complex operations, so provision is made to eliminate the complex multiplication as implemented in lines 900 to 920.

With the aid of figure 5.6.18 it can be seen that the power **m** in W_N^m in each stage has a bit-reversal relationship with the position number, as shown in lines 880 to 890 of the algorithm. The bit-reversal sub-routine, FNrbitr (lines 490 to 700), is used here (line 890) for this purpose and later in line 1100 to bit-reverse the output samples. In order to reduce the execution time of the algorithm, the bit-reversal procedure was written in Assembly language. FNrbitr, accepts an 8-bit integer, A%, and returns a bit-reversed integer (still 8-bits).

The parameter DELTA (lines 760 and 1180) is used to multiply the samples so that the FFT algorithm can be used as an approximation to the continuous Fourier transform. According to equation **5.6.26**, this factor should be **T**, the step size in time used in the zero-order approximation of the Fourier integral. For the inverse Fourier transform, this factor is the step-size frequency used in the zero-order approximation of the inverse integral. For the implementation of a strict DFT, DELTA is set equal to 1 for the transform and equal to **1/N** for the inverse transform.

5.6.5 Validating the FFT Algorithm.

The BBC BASIC FFT algorithm, once written, had to be verified and its credibility appraised before it could be reliably employed in transforming captured data from the time domain to the frequency domain.

Verification was accomplished by synthesising data sets (using mathematical formulas) with known frequency content and observing whether the FFT algorithm produced the correct results. Figures 5.6.19 to 5.6.46 show the nature of the synthesised data and the resulting frequency spectrum obtained from the algorithm.

In the first instance (figures 5.6.19 to 5.6.25), the amplitude of a sine wave was kept constant and the frequency varied. (Note that the resolution of the computer screen proved inadequate for the display of frequencies higher than about 90Hz.)

Secondly, two sine waves of the same amplitude, but different frequencies, were summed; the frequency of one of the waves being varied (figures 5.6.26 to 5.6.29).

Further verification tests were conducted (figures 5.6.30 to 5.6.34) with the summation of two sine waves of different amplitudes and frequencies.

Finally appraisals were carried out (figures 5.6.35 to 5.6.46) with multiple summations of sine functions of differing amplitudes and phase relationships, and, pulse trains of differing amplitudes and mark-space-ratios.

6 TIMBER MACHINING INVESTIGATION

6.1 Introduction

6.2 The Planer - Moulder Machine

6.2.1 General Description

6.2.2 Final Top Head

6.2.2.1 Cutterhead

6.2.2.2 Cutterblock

6.2.3 Timber Control

6.2.3.1 Feedworks

6.2.3.2 Chipbreaker, Top and Side Pressure Rollers

6.2.4 Jointer

6.2.5 Extractor fan

6.3 Machining Variables and Parameters

6.4 Machine Preparation and Condition

6.4.1 Operating Conditions

6.4.2 Process Parameters

6.5 Timber Specification

6.6 Induced and Simulated Surface Finish Defects

6.6.1 Eccentric Cutterhead Rotation

6.6.1.1 Spindle Cylindricity

6.6.1.2 Cutterblock Concentricity

6.6.1.3 Spindle Concentricity/Dynamic Balance

6.6.2 Proud Knives

6.6.3 Workpiece Vibration

6.6.4 Single Knife finish

6.7 Surface Finish Analysis

6.7.1 Introduction

6.7.2 Laser Instrument Data Set

6.7.3 Talyrond 200 Data Set

6.7.4 Surface Simulation Data Set

6.7.5 Fast Fourier Transform of Data Sets

6.7.6 Defect Identification from FFT Spectrum

6.7.6.1 Ideal Timber Surface

6.7.6.2 Spindle Concentricity/Dynamic Balance

6.7.6.3 Proud Knives

6.7.6.4 Vibration: Timber, Spindle

6.7.6.5 Single Knife Finish

6.7.6.6 Fault Finding Algorithm

6.1 Introduction

Having constructed the laser instrument, it had to be tested, validated and commissioned. This was effected by machining timber samples with known and regulatable surface characteristics. The timber samples thus produced were assessed using the laser instrument and the results compared to that obtained using a conventional surface assessment instrument (Talyrond 200). In addition these results were compared with data generated using appropriate values for parameters in the surface simulation algorithm (SSA).

This chapter describes the techniques used in preparing the timber samples. A description is given of the planing machine used and the modular units of which it is comprised. The associated machining parameters are discussed and details of induced or simulated machining faults are described.

6.2 Planer - Moulder Machine

6.2.1 General Description

The planing machine used to generate all the timber samples during this investigation is known as the B-series 220 (abbreviated, 220B) and is shown in figure 6.1. The 220B is a modular, throughfeed planing and moulding machine having a choice of six or seven head configuration (figure 6.2) with the option of a four-position Universal head. The heads rotate at a maximum speed of 12,000 revs/min; the horizontal heads have a hydraulically pressurised outboard bearings with jointing at 6000 revs/min in order to provide multi-knife machining. The machine has a capacity of 220mm and was designed specifically for high productivity combined with high product

quality.

The throughfeed operation incorporates driven infeed and outfeed bedrollers which simplifies feeding, especially in handling mouldings of long length and in the control of timber during straightening operations. All the feed rollers are pneumatically loaded to provide positive and consistent feeding. All heads have vertical and horizontal adjustment and are provided with chipbreaker and pressure rollers.

The 200B has a highly efficient dust extraction system built with an integral sound enclosure, which makes it intrinsically safe and noise abated.

6.2.2 Final Top Head

The timber surfaces to be analyzed in this investigation, were in essence machined by the final top head (figure 6.3). In detail, this top head consists of a base unit with mounting faces provided for attaching the feedworks, bedplates and the cutterhead assembly. The drive motor is mounted on the rear or the base and a standard "V" belt drive transmits power to the main spindle.

6.2.2.1 Cutterhead

The cutterhead's spindle is 40mm in diameter; the spindle bearing assembly is as shown in figure 6.4. It comprises a back to back pair of angular contact bearings at the fenceside position; these are the datum bearing pair. A deep groove bearing supports the belt drive loads with another mounted in the

removable outboard bearing housing at the nearside of the cutterblock. The bearings are manufactured to EP7 standard and lubricated for life with ISOFLEX grease, KLUBER NB15. The head is driven by a 18kW electric motor.

6.2.2.2 Cutterblock

The type of tooling used to produce the timber samples during this investigation is known as a Hydrogrip Planing Cutterblock. This style of cutterblock, shown in figure 6.5, comprises two hydraulic expanding bushes fixed at either end of a high strength steel body in which six high-speed steel knives are mounted. The diameter of the cutterblock was 150mm, its length 180mm with a design rotational speed of 6000rpm.

The bushes are pressurised independently, to 450 bar (using a grease gun), which effectively centres the cutterblock on the spindle. This is done by hydrostatically collapsing the bore of the bush until it grips the spindle with sufficient force to enable the transmission of the power required. A fail-safe safety device is fitted such that the drive remains effective should the Hydrogrip function fail.

6.2.3 Timber Control

6.2.3.1 Feedworks

The heavy duty in-feedworks, which traverse the timber across the hard chrome machine table and pass the rotating cutterheads, is shaft driven by an infinitely-variable-speed, mechanical unit (figure 6.6). Feed speed range

from 6 to 180 metres per minute. The feedworks, which has a 22.5kW (30hp) electric drive motor with increment and reverse feed, also have a motor-powered (0.5kW) rise and fall facility. The in-feed system is pneumatically loaded and has serrated bed rollers which provide positive feeding (figure 6.6).

The out-feedworks comprise overhead, protective, polyurethane feedrollers, 140mm in diameter, and are pneumatically loaded to 4 bar to enable frictional feeding (figure 6.7).

6.2.3.2 Chipbreaker, Top and Side Pressure Rollers

The chipbreaker, top pressure roller and side pressure roller assemblies enable the timber to maintain contact with the reference surfaces - the machine table and fence.

The chipbreaker (figure 6.8) has a radial action which gives precise control, close to the cutting action, without the need to allow for timber thickness or width variation. Both the chipbreaker and top pressure rollers are pneumatically loaded to a pressure of 4 bar, generating a downward force on the traversing timber.

As the timber traverses across the bedplate, the side pressures rollers, which are spring loaded, push the timber hard against the fence (figure 6.9).

6.2.4 Jointer

The top head is fitted with a standard jointing device (figure 6.10). Jointing is effected by the hand rotation of the cross-feed-screw thus traversing the stone across the cutterblock; the jointing stone is fed into the cutterblock, in the radial direction, by means of the down-feed-screw; this is done at the end of each cross-traverse. Thus, the cutterhead is jointed without the need to remove it from its actual cutting position.

6.2.5 Extractor Fan

The top head (and other heads) is also fitted with a powerful extractor fan and appropriate ducting which removes the wood chips and dust particles produced during the planing process (figure 6.11).

6.3 Machining Variables and Parameters

There are numerous factors, parameters and variables associated with the rotary planing of timber. Typical examples are: age of the machine; depth of cut; type of tooling material; design of the machine tool; specifications of the workpiece material; ambient temperature; etc. Each parameter or variable, to some degree, contribute to the resultant surface finish. Previous researchers (Davis E.M, Nelson H. 1954; Koch P. 1956; Goodchild R. 1963 Jackson M.R. 1986) have isolated and identified the most significant parameters, variables and phenomena which have a marked effect on the aesthetic qualities (ie. the surface finish) of a spindle-machined, timber surface; they include:

1) Timber's linear feedspeed.
2) Cutterhead's rotational speed.
3) Number of knives on the cutterblock.
4) Depth of cut.
5) Concentricity of the main cutterhead spindle.
6) Cutterhead dynamic imbalance.
7) Machine vibration
8) Vibration between the workpiece and machine table.
9) Degree to which the cutterhead is correctly jointed (cutterhead cylindricity).
10) Knifes' resilience to wear.
11) Cutting velocities
12) Rake and clearance angles of knives
13) Quality and type of timber being machined.

etc.

During this investigation steps were taken and attempts made to control, or keep constant, the parameter and variables being manipulated during the machining process. This incurred some machine preparation before timber machining commenced.

6.4 Machine Preparation and Condition

In order to maintain consistency and ensure repeatability, each time the 220B planer-moulder was used to produce a batch of timber samples, certain basic operating conditions were established and specific process parameters measured during planing. These are discussed in the following section.

6.4.1 Operating Conditions

During or prior to using the 220B planer-moulder to machine timber samples the following machining conditions were established:

1) All components requiring lubrication on the 220B planer/moulder were adequately lubricated using the recommended lubricants.
2) The final top head spindle's static tracking error (eccentricity/run-out) was measured to confirm that it was less than 5µm at its fenceside end and less than 10µm at its nearside end, with the outboard bearing removed. This ensured tracking errors in the region of fractions of a micron when the outboard bearing was engaged.
3) The "V" belts which transmit power from the electric motor to the cutterhead were checked and belt tensions adjusted, as necessary, to comply with the manufacturers specifications.
4) The cutterblock used was dynamically balanced to within 30g.mm (see Section 6.6.1.3) using a two-plane balancing machine. The cutterblock was then mounted on the top head spindle such that it obtained a knife-to-knife tracking accuracy within 20µm, before jointing the cutterhead. The cutterblock was always located in the same angular position relative to the spindle by alignment to two reference marks.
5) The 220B planer-moulder drive motors were operated for one hour ("warm-up" period) with no load to establish optimum operating conditions.
6) The pressure of the feedrollers and chipbreaker were set to 4 bar.
7) All other machinery in the immediate vicinity of the 220B planer-moulder was switched off to prevent vibration being transmitted to, and affecting the action of, the final top head.
8) Vibration levels at the final top head (amplitude and frequency) were measured and recorded towards the end of the one hour "warm-up" period using a Bruel and Kjaer vibration meter (Type 2511) in conjunction with a Yokogawa Hokushin Electric Analysing recorder. (This piece of equipment was acquired late in the research period so that measurements

are not available for every timber sample).

6.4.2 Process Parameters

The parameters monitored during the machining of the timber samples were as follows.

1) The rotational speed of the final top head was registered during the planing of each sample.
2) When the equipment was available, vibration levels (frequency and amplitude), in the vicinity of the final top head were recorded during active planing.
3) The feedspeed of each timber sample (during the actual planing process) was noted and recorded.
4) Any induced or simulated machining faults (and associated parameters) were noted and recorded.

6.5 Timber Specification

The timber samples used through out this investigation were Swedish Redwood, this being commonly used in the woodworking industry in conjunction with the jointing process (Jackson M.R, 1986).

The dimensions of the workpieces were typically 50mm x 30mm x 1000mm having all four sides pre-machined, which effectively straightened the underside; the underside was used as a reference surface which made contact with the machine table.

Timber was selected such that its moisture content lay between 10% and 15%; this is the moisture content range recommended for ideal timber

machining (Jackson M.R, 1986).

6.6 Induced and Simulated Surface Finish Defects

This research concentrated on particular surface defects which were common and which could be induced by reproducing certain machining conditions or by simulating specific machine malfunctions or faults. There were three main areas:

i) Eccentric rotation of cutterhead
ii) Proud knives
iii) Workpiece support and control

6.6.1 Eccentric Cutterhead Rotation

Four major factors can cause a cutterhead to rotate eccentrically and hence affect the surface finish it generates. They are:

i) Spindle Cylindricity
ii) Cutterblock Concentricity
iii) Spindle Concentricity
iv) Cutterhead Dynamic Balance

6.6.1.1 Spindle Cylindricity

There have been immense advances in turning/grinding technology; the tight cylindricity tolerances to which spindles can now be manufactured ensures that lack of spindle cylindricity is no longer a major feature which affects the surface quality of planed timber (Goddard M,1985). Consequently, this phenomenon was not investigated during this research.

6.6.1.2 Cutterblock Concentricity

Similarly, lack of cutterblock concentricity as a cause of surface defects has been alleviated due to the development of hydraulically pressurised bearings; these Hydrogrip bearings are highly effective in centring the cutterblock on the spindle. Thus, cutterblock concentricity did not feature in this research. However, if the machine is operated with the hydrogrip bearings un-pressurised eccentric tracking will result.

6.6.1.3 Spindle Concentricity and Dynamic Balance

Spindle concentricity is still an active component in the quality of the surface which a cutterhead generates. The main reason for non-concentric rotation of spindles is bearing wear; this causes the spindle to orbit, rather than rotate, about its ideal axis.

When a cutterhead is used in an unbalance state there is a tendency for the spindle to bow under the influence of the unbalanced forces; this, depending on the magnitude and position of the unbalanced forces causes eccentric tracking. This is then transmitted to, and apparent in, the surface profile produced.

The effects of lack of spindle concentricity and dynamic imbalance on the surface profile is very similar; they both result in eccentric rotation of the cutterhead. Indeed, bearing wear is often a direct result of dynamic imbalance. (Balancing a cutterhhead is the process of attempting to improve the mass distribution of the cutterhead so that it rotates in its bearings

without unbalanced centrifugal forces. This aim can be attained only to a certain degree; even after applying the balancing process the cutterhead will possess residual imbalance.)

In this research cutterhead eccentricity was investigated. The high cost, to the collaborating establishment, of producing worn bearings proved prohibitive; that of generating out-of-balance forces was more feasible; this option was selected as the means of producing eccentric rotation of the cutterhead.

Initially, the cutterhead was balanced according to balance quality grade G2.5 (International Standard 1940/1 and British Standard 5750) which specifies a permissable residual imbalance of 93g.mm for the cutterhead size used (see Appendix D1). The balancing machine used was a series HK, Reutlinger two-plane balancing machine (K27.00 MC120E). (The cutterblock is dynamically balanced during manufacture to within 30g.mm. Once knives, which are weight matched to within 0.5g, are added, the inevitable variances in location mean that residual imbalance of the cutterhead, complete with wedges, is normally within 60g.mm. Allowance is made for a variation in imbalance due to the depressurising and re-pressuring of the hydraulic clamping sleeves (typically 10g.mm)).

Dynamic imbalance was induced in the cutterhead by the addition of extra masses to the periphery of the cutterblock in line with knife "number 1". (The cutterblock is designed so that the knives can be held in place using

socket screws; (some cutterblocks have serrations on the knife and cutterblock which allow the knife to be located in fixed radial positions.)) The degree of imbalance was varied incrementally by changing the length (and therefore the mass) of the socket screws which held knife "number 1" in position.

Two sets of socket screws were employed:

Set 1 were 12mm long and each one weighed 10.0g
Set 2 were 16mm long and each one weighed 13.0g

Initially, with **Set 1** socket screws in position, the cutterhead was dynamically balanced to within 30g.mm Then, the socket screws of **Set 1** were replaced in stages by those in **Set 2**, causing varying, but incremented values of cutterhead dynamic imbalance:

In figure 6.12 points A, B, C, D, and E represent the arrangement of the socket screws positions at knife "number 1".

First the socket screw in position C was replaced by a socket screw from **Set 2**, inducing the first increment of dynamic imbalance in the cutterhead. Timber samples were machined and records made of the associated machining conditions.

Dynamic imbalance was increased further by removing and replacing other socket screws in the set, but always maintaining mass symmetry about point C; further timber samples were machined with corresponding out-of-balance conditions recorded.

The surface waveform of the timber samples were assessed using the Laser Instrument and the Talyrond 200, as described in Section 6.7. The results of these investigations are presented in Section 7.3.2 and discussed in Section 8.4.2.2.

6.6.2 Proud Knives.

As with dynamic imbalance, proud knife is a phenomenon which can contribute to surface defects in machined timber. The major cause of proud knifes is poor machine tool setting. The fault usually occurs on cutterheads which use friction (as opposed to serrations) to locate the knives in their radial position. If it is not adequately secured by the holding screws there is a tendency for the knife to gradually slip under the influence of the centrifugal forces associated with the cutterheads rotation. They can also be jolted radially inwards (or loosened) by shock loads from knots, or other obstructions, in the timber.

In this investigation cutterheads with proud knives were created using two methods:

Method 1

The cutterhead was dynamically balanced to within 30g.mm and jointed. It was then used to machine timber samples to confirm that a "perfect" finish was being produced. Then without removing the cutterblock from the spindle, a knife was moved radially (in increments of approximately 4µm) towards the axis of rotation. The cutterhead was then used to

machine timber samples.

Method 2

As with method 1 the cutterhead was dynamically balanced to within 30g.mm, jointed and used to machine timber samples to confirm that a "perfect" finish was being produced. Then the cutterhead was removed and specific knives ground low (in increments of approximately 4µm) using an NX-grinder (figure 6.13). The cutterblock was then refitted to the spindle and used to machine timber samples.

The surface waveform of the timber samples were assessed using the Laser instrument and the Talyrond 200, as described in Section 6.7. The results of these investigations are presented in Section 7.3.3 and discussed in Section 8.4.3.2.

6.6.3 Vibration: Timber, Spindle

If it is not correctly supported and controlled the workpiece will vibrate as it is traversed across the machine bed. The vibration of the workpiece (in practice due to incorrect machine configuration) will contribute to the frequency content (defects) on the machined surface. The severity of workpiece vibration will depend on the extent of inadequate support and control. In seeking to produce timber samples with defects due to workpiece vibration, some attempt was made to regulate the amount of vibration which the traversing timber experienced because of unsatisfactory support and control.

The three machine components which, in conjunction with the machine table and fence, support and control the timber in the vicinity of the final tophead/cutterhead are:

1) the chipbreaker
2) top pressure roller
3) side pressure roller

The machine table and fence are fixed reference surfaces across, and against, which the workpiece slides; the top pressure roller and the chipbreaker provide downward forces which press the workpiece hard against the machine table; the side pressure roller presses the workpiece hard against the fence.

As the vibration-prone timber samples were produced the pressure, applied to the workpiece by the chipbreaker and top pressure roller, was varied; the side pressures being always fully operative. This theoretically limited any workpiece vibration to the vertical plane only.

Incorrect support of the cutterhead's spindle, at the outboard end, will also result in the cutterhead vibrating and adversely affecting the quality of the surface finish produced. Timber samples were machined with the outboard end of the spindle experiencing reducing degrees of support.

The surface waveform of the timber samples produced using reduced timber and spindle-outboard support were assessed using the Laser Instrument and the Talyrond 200, as described in Section 6.7. The results of these

investigations are presented in Section 7.3.4 and discussed in Section 8.4.2.4.

6.6.4 Single Knife Finish

The term "single-knife finish" is used to describe a mode of rotary timber machining in which only one knife (ie. the most proud knife), on a multi-knife, unjointed cutterhead, produces the finish surface profile. This mode is used in the industry as a dependable method of producing a high quality surface finish. The drawback, compared to a jointed multi-knife finish, is that, for a given cutterhead rotation speed (**W**), the timber feed speed for a required surface wave pitch (**p**) is much reduced: for single knife finish, the maximum timber feedspeed, V_{smax} , is given by:

$$V_{smax} = \frac{p.W}{2\pi} \qquad (6.1)$$

where **W** is in rad/s

This obviously reduces production rates, the advantage being a decrease in machine setting time and product consistency.

The surface waveform of the timber samples produced using single knife finish were assessed using the Laser instrument and the Talyrond 200, as described in Section 6.7. The results of these investigations are presented in Section 7.3.1 and discussed in Section 8.4.2.1.

6.7 Surface Finish Analysis

6.7.1 Introduction

Three surface waveform data sets were generated for each timber sample; the first set was produced using the Laser Instrument, the second using the Talyrond 200 and the third using the surface simulation algorithm (SSA). Each data set was transformed into the frequency domain using the FFT algorithm (Section 5.6.4). The FFT data was then analysed, with reference to the number of significant peaks present in the spectrum and their location in the harmonic scale range, thus ascertaining the type of faults present in the surface profile (see Section 6.7.6).

6.7.2 Laser Instrument Data Set

Each sample, in turn, was placed in the datum position of the Laser Instrument and illuminated with grazing incidence laser light (figure 6.14). Under software control (Section 5.5) a data set, which mirrored the frequency content of the surface waveform was captured and stored for future analysis using the FFT algorithm (Section 5.6.4)

6.7.3 Talyrond 200 Data Set

Each sample, in turn, was positioned on the Talyrond 200 Instrument (figure 6.15). Under software control (see appendix B4) a data set, which echoed the surface profile and hence the frequency content of the surface waveform, was captured and stored for future analysis using the FFT algorithm.

6.7.4 Surface Simulation Data Set

For each timber sample, a corresponding simulated data set was generated using appropriate parameter values (ie. timber feedspeed, cutterhead angular velocity, etc) in the surface simulation algorithm (SSA) (Section 4.6). The data set thus acquired was stored for future analysis using the FFT algorithm (Section 5.6.4)

6.7.5 Fast Fourier Transform of Data Sets

The three data sets generated for each timber sample were transformed into the frequency domain and each FFT spectrum displayed graphically. A typical result is shown in figure 7.G1.S1. For details on the full range of results see Section 7.3.

6.7.6 Defect Identification from FFT Spectrum

6.7.6.1 Ideal Timber Surface

The frequency domain description of an ideally machined timber surface should contain a single peak or local maxima (denoted, uni-modal); the pitch (ie. knife-mark or cusp distribution) of an ideal surface is uniform. The expected number of knife-marks, h_j, in a given sample length, L_s, is given by

$$h_j = \frac{WL_s}{2\pi V} N \qquad (6.2)$$

where

W = angular velocity of the cutterhead,

V = linear feed velocity of the timber,

N = number of knives (equi-spaced and jointed) on the cutterblock,

and where the suffix **j** indicates a jointed cutterhead or milti-knife finish.

Thus, for an ideally planed surface, harmonic $\mathbf{h_j}$ would be the only dominant (or principal) harmonic in the spectrum of the surface's profile. This was illustrated by using the SSA to generate models of ideally machined timber profiles (to varying specifications), and using the FFT algorithm to obtain their frequency or harmonic spectrum. A typical example is shown in figure 7.G0.S2c.

6.7.6.2 Spindle Concentricity / Dynamic Balance

Cutterheads with spindles that are not concentric, or cutterheads that are not dynamically balanced tend to produce planed surfaces which exhibit a "once per revolution" defect which is superposed onto an otherwise ideal surface profile. Such a profile will feature the expected number of knife marks, $\mathbf{h_j}$, superposed onto a surface which undulates sinusoidally, due to lack of spindle concentricity.

The frequency signature of a sample length of such a surface would contain two major peaks (denoted, bi-modal); one at principal harmonic $\mathbf{h_j}$ (see equation **6.2**)), the other at $\mathbf{h_1}$ (the principal harmonic which represents the surfaces undulation) given by

$$\mathbf{h_1 = \frac{WL_s}{2\pi V}} \qquad \textbf{(6.3)}$$

where

$\mathbf{W}$ = angular velocity of the cutterhead

$\mathbf{V}$ = linear feed velocity of the timber

$\mathbf{L_s}$ = length of the sample

and where the suffix **1** indicates a once per revolution effect

This was illustrated by using the SSA to generate surface models exhibiting this "once per revolution" defect, and using the FFT algorithm to obtain the corresponding frequency spectrum (see figures 7.G0.S4).

It should be noticed that as imbalance increases, the amplitude of spindle eccentricity (runout) also increases. The trajectory of the knife whose radial direction and sense coincides with, or is closest to, that of the imbalance force will cut deeper into the timber; that of the knife whose radial direction and sense is opposite to the imbalance force will cut less deeply. As imbalance is increased, a critical point will be reached when the amplitude of the eccentricity is such that the knife opposite to the imbalance force will not contribute a knife mark to the final surface profile. At this amplitude of eccentricity, $\mathbf{d_{crit}}$, the number of knife marks in a given sample length would be $(\mathbf{h_j}-\mathbf{h_1})$.

6.7.6.3 Proud Knives

As stated in Section 6.7.6.1, a perfectly functioning cutterhead would machine a surface profile whose FFT signature would contain a single peak at $\mathbf{h_j}$. Incorporating a single proud knife, into this otherwise ideal cutterhead, would cause it to produce surface profiles whose FFT signatures contain additional, peak harmonics.

The positions of the additional peak harmonics are dependent on the depth and width of the proud-knife knifemark, and, its rate of recurrence. The peak harmonics which characterises such a profile, is very similar to the frequency

signature for a pulse train of comparable width, amplitude and frequency to the proud-knife knifemarks); the harmonic number of the peaks following and arithmetically progressing series which start at $\mathbf{h_1}$ (see equation **6.3**); the amplitude of the peaks diminishing with increase in harmonic number.

This was illustrated by using the SSA to generate a "proud-knife" surface profile (of sample length, $\mathbf{L_s}$(=0.125m)) and using the FFT algorithm to obtain its frequency spectrum (see figure 6.16). A corresponding pulse train was also generated and transformed into the frequency domain for comparison (figure 6.17).

For a jointed, multi-knife finish, cutterheads with 4, 6, 8, and 10 knives are commonly used. With cutterheads possessing more than one proud knife, the degree of proudness of each individual knife and its possible angular position on the cutterblock are somewhat random functions but tend, in practice, to vary within certain limits:

The degree of proudness varies from zero to about 40μm (Goddard M, Garrett J, 1986)

The possible angular location of the proud knife is dependant on the total number of knives on the cutterblock, **N**, and the number of knives which are proud, **r**. There will be a number of possible arrangements (permutations) of the proud knives around the cutterhead. The number of possible ways of arranging the proud knives on the cutterhead is:

$$\frac{{}^{N}P_{r}}{N} = \frac{N!}{N(N-r)!} \qquad (6.4)$$

Thus:

Considering a 4-knife cutterblock, the number of ways of arranging:

2 proud knives is

$$\frac{{}^{4}P_{2}}{4} = \frac{4!}{4(4-2)!} = 3$$

3 proud knives is

$$\frac{{}^{4}P_{3}}{4} = \frac{4!}{4(4-3)!} = 6$$

Considering a 6-knife cutterblock, the number of ways of arranging:

2 proud knives is

$$\frac{{}^{6}P_{2}}{6} = \frac{6!}{6(6-2)!} = 5$$

3 proud knives is

$$\frac{{}^{6}P_{3}}{6} = \frac{6!}{6(6-3)!} = 20$$

4 proud knives is

$$\frac{{}^{6}P_{4}}{6} = \frac{6!}{6(6-4)!} = 60$$

5 proud knives is

$$\frac{{}^{6}P_{5}}{6} = \frac{6!}{6(6-5)!} = 120$$

Similar permutations can be calculated for the arrangement of proud knives on 8-knife and 10-knife cutterblocks.

As the number of knives on the cutterhead increases, the task of modelling the surface profiles produced by all the possible arrangements of proud knives becomes more tedious and complicated. The model experiences an even higher degree of tedium and complexity if the exact extent of the proudness of each knife is considered. Examples of "proud knife" surface models which were generated by the SSA and their corresponding frequency signatures are shown in figures 7.G0.S5a to 7.G0.S5f; here, each proud knife protrudes the nominal cutting circle diameter by exactly the same amount, +8μm.

The frequency signature of the surface profiles show a distinct pattern or trend; as the number of proud knives is increased, the harmonic interval between $\mathbf{h_i}$ and $\mathbf{h_j}$ becomes congested with dispersed local peaks (denoted, multi-modal), indicating a fault within the machining process.

6.7.6.4 Timber Vibration

There are no apparent patterns or rules which readily and clearly predict the frequency and amplitude of vibration of a workpiece which is machined while inadequately supported. Therefore the profile and frequency signature of a timber sample so machined can be somewhat unpredictable or random.

This fault requires further analytical investigation. The number of possible variables involved is considerable and if they are successfully identified many of their numerical values will be unknown. It is apparent that incorrectly supported timber will vibrate at some frequency (as its traversed across the machine table); this will be dependant on the forcing frequency, the mode of

workpiece support (ie. simply supported, cantilever, etc.), the dimensions, the elasticity/rigidity, characteristic damping factor of the timber and the masses and forces associated with the restraining components.

6.7.6.5 Single Knife Finish

The frequency domain description of a timber surface machined in single-knife-finish mode should contain a single peak or local maxima (similar to ideal, multi-knife mode machining) because the wave pitch should be uniform. The expected number of knife-marks, $\mathbf{h_{sgl}}$, in a given sample length, $\mathbf{L_s}$, is given by

$$\mathbf{h_{sgl}} = \frac{\mathbf{WL_s}}{\mathbf{2\pi V}} \qquad \textbf{(6.5)}$$

where

$\mathbf{W}$ = angular velocity of the cutterhead
$\mathbf{V}$ = linear feed velocity of the timber
$\mathbf{L_s}$ = length of the sample

The value of $\mathbf{h_{sgl}}$ is the same as principal harmonic $\mathbf{h_1}$ (see equation **6.3**)

6.7.6.6 Fault Finding Algorithm

Based on the above discussion a fault finding algorithm (FFA) was written, which, analyses the frequency signature (ie. the FFT), and attempts to detect any inherent "defects" in the surface's waveform. The FFA first scans the FFT to identify the harmonic with the maximum magnitude. The algorithm then searches through the FFT data for local maxima which are compared with an "arbitrary" threshold value, which is some fraction of the detected

maximum. Harmonics with amplitudes equal to, or greater than, this threshold are considered significant. The significant harmonics are then compared to a number of criteria (ie. the principal harmonics) which are dependent on the machining parameters used to produce the sample. Eventually, through a process of elimination, the nature or "cause" of the "fault" is identified. The structure of the FFA is as follows (see next page) and is listed in appendix A8:

Structure of the Fault Finding Algorithm

```
Find maximum magnitude harmonic, h_peak
Scan FFT data
FOR harmonic = zero TO highest harmonic
  Check for local maxima
  IF1 local maxima
    THEN1
      IF2 maxima >= threshold
        THEN2
          IF3 harmonic = h1
            THEN3
              Check for local maxima between h1 and hj
              Keep record of any found
IF4 none found
  THEN4
   "Fault" must be Ob1 or Sk
    Check for Ob1 ie look for hj
    IF5 hj found
      THEN5
        record Ob1 and hj:to endif5
      ELSE5
        record Sk:to endif5
    ENDIF5
    to endif4
  ELSE4
    Could be proud knife
    Check for proud knife
    IF6 proud knife
      THEN6
       Keep record of proud knife:to endif6
      ELSE6
       Keep record of Ob1:to endif6
    ENDIF6
ENDIF4
          to endif3
        ELSE3
        Must be some other fault
         Try principal harmonics
         IF7
          IF harmonic = h2 THEN fault must be Ob2
          IF harmonic = hsgl THEN single knife finish
          IF harmonic > hj THEN high frequency vib.
                                digital noise
         to endif7
        ELSE7
        Must be some other fault
        eg. combination of number of faults
        Call this a "Unknown fault":
        So store harmonic :to endif7
      ENDIF7
      to endif3
   ENDIF3
   to endif2
ELSE2
    ENDIF2
  ELSE1 to endif1
 ENDIF1
NEXT harmonic

where h1 = once-per-revolution harmonic
      h2 = twice-per-revolution harmonic
      hj = multi-knife finish harmonic
    hsgl= single-knife finish harmonic
    Ob1 = once-per-revolution out-of-balance
    Ob2 = twice-per-revolution out-of-balance
```

See Appendix A8 for a listing of the FFA

7 RESULTS

7.1 Introduction

7.2 Theoretical Results

7.2.1 Single-knife Finish

7.2.2 Multi-knife finish

7.2.2.1 Ideal Machining

7.2.2.2 Machining Faults

7.2.2.3 Fault Parameter Variation

7.3 Machined Timber Sample Results

7.3.1 Single Knife Finish

7.3.2 Cutterhead Imbalance

7.3.3 Proud Knives

7.3.4 Vibration: Timber, Spindle

7.3.5 Fault Combination

7.1 Introduction

In this chapter results from the machining investigations are presented. The theoretical results, based purely on the mathematical model (ie. the SSA (Chapter 4)), are presented in Section 7.2; those from the machined timber samples (see Section 6.6) are presented in Section 7.3.

7.2 Theoretical Results

The surface simulation algorithm (SSA) was used to generate a variety of theoretical profiles. These generated profiles, prefixed G0, are shown in figures 7.G0.S1 to 7.G0.S6 together with their corresponding FFT. Each figure also contains a record of the pertinent variables and parameters used in the SSA to produce the profile and the results of the analysis of the FFT spectrums using the Fault Finding Algorithm (FFA).

7.2.1 Single-knife Finish

Simulated, single-knife finish, profiles are presented in figures 7.G0.S1a. through to figure 7.G0.S1d

7.2.2 Multi-knife finish

Figures 7.G0.S2 to 7.G0.S6 illustrated simulated milti-knife finish surface profiles.

7.2.2.1 Ideal Machining

Simulated ideal machining finish profiles are presented in figures 7.G0.S2a through to figure 7.G0.S3a.

7.2.2.2 Machining Faults

Figure 7.G0.S3b to 7.G0.S3j introduced the simulated timber machining faults; they were eccentricity (out-of-balance cutterhead), proud knives and timber vibration.

7.2.2.3 Fault Parameter Variation

Figures 7.G0.S4, 7.G0.S5 and 7.G0.S6 illustrated the effect of varying the value of the machining fault parameters.

7.3 Machined Timber Sample Results

Each timber sample produced was categorised and numbered according to the type of fault induced on its surface profile. The captured data from each timber sample was presented graphically (figures 7.G1.S1 to 7.G5.S5). Each figure contains three data sets:

1) That captured by the laser instrument (**LAS**)
2) That captured by the Talyround 200 (**TAL**)
3) That generated by the surface simulation algorithm (**SSA**)

Directly beneath the graph of each captured data set is a histogram of its FFT spectrum or frequency signature. Underneath the three pairs of graphs are the machining parameters used to produce the timber sample and the results from assessing each FFT data set using the FFA.

The results presented here are a selection from many timber samples produced, and are divided into 5 main groups or categories:

(a) single-knife finish **(category G1)**

(b) multi-knife finish

i) cutterhead imbalance **(category G2)**

ii) proud knives **(category G3)**

iii) timber vibration **(category G4)**

(c) fault combinations **(category G5)**

7.3.1 Single Knife Finish.

The first category of samples, G1, were generated using a single knife finish machining mode (see Section 6.6.4). The values of machining parameters and variables used are recorded in Table G1. The captured data corresponding to each timber sample is shown graphically in figures 7.G1.S1 to 7.G1.S8.

7.3.2 Cutterhead Imbalance

The second category of samples, prefixed G2, were machined using cutterheads with varying degrees of out-of-balance (see Section 6.6.1.3). The machining parameters and variables were as recorded in Table G2 while figures 7.G2.S1 to 7.G2.S12 contain the graphical representation of the captured data with their respective frequency signatures (FFT).

7.3.3 Proud Knives

The third category of samples, G3, investigated the proud knife fault (see Section 6.6.2). Table G3 shows a record of the machining variables and parameters used in the machining of the samples, while figures 7.G3.S1 to 7.G3.S15 show graphically the corresponding results obtained using the laser

instrument, talyrond 200 and surface simulation algorithm (SSA).

7.3.4 Vibration: Timber, Spindle

The forth category of timber samples, prefixed G4, were composed of those machined while the workpiece was inadequately supported or controlled (see Section 6.6.3). Table G4 shows the variables and parameters used, while figures 7.G4.S1a to 7.G4.S6c show, graphically, the associated captured data sets and their frequency spectra.

7.3.5 Fault Combinations.

The fifth category of timber samples, prefixed G5, were machined using process parameters and machining conditions which created surface profiles that combined the various process faults. The parameters and conditions were recorded in Table G5 an the results shown in figures 7.G5.S1 to 7.G5.S5.

8 DISCUSSION

8.1 Introduction

8.2 Hardware

8.2.1 Electronics

8.2.1.1 Host Computer

8.2.1.2 Photodiode Array

8.2.1.3 Data Acquisition

8.2.2 Optics

8.2.2.1 Helium-Neon Laser

8.2.2.2 Beam Expansion

8.2.3 Instrument Structure/Adjustment Mechanism

8.3 Software

8.3.1 Data Capture

8.3.1.1 Laser Instrument Data Capture

8.3.1.2 Talyrond 200 Data Capture

8.3.1.3 SSA Data "Capture"

8.3.2 Data Analysis

8.3.2.1 Fast Fourier Transform Algorithm

8.3.2.2 Fault Finding Algorithm

8.4 Machining Investigations

8.4.1 Theoretical Results

8.4.1.1 Single-knife Finish

8.4.1.2 Multi-knife finish

8.4.1.3 Superposed Machining Faults

8.4.1.4 Fault Parameter Variation

8.4.2 Timber Machining Results

8.4.2.1 Single Knife Finish

8.4.2.2 Spindle Eccentricity / Dynamic Balance

8.4.2.3 Proud Knives

8.4.2.4 Timber and Spindle Vibration

8.4.2.5 Fault Combinations

8.5 General Comments

8.1 Introduction

This chapter discusses the various aspects associated with, and the performance of the laser instrument for assessing the surface waviness of planed timber. Firstly the hardware is considered under three main sub-divisions:

1) Electronics
2) Optics
3) Mechanics

Then the software associated with the instrument is addressed. This is dealt with under two main headings

1) Data Capture
2) Data Analysis

Finally the results of the investigation are examined. Here, theoretical results from the mathematical model (ie. SSA) are discusses followed by an examination of the results from the timber machining investigations.

8.2 Hardware

8.2.1 Electronics

8.2.1.1 Host Computer

The use of a BBC micro-computer as the Host proved useful as a development tool. It was a very versatile, programmable device with screen resolution germane to the application. However, there were inadequacies (such as its comparative low computing speed and its limited 8-bit capacity) which

became frustratingly apparent as the research progressed. So much so that in order to reduce computing time attempts were being made to convert the FFT algorithm to machine code version (Appendix A7). Before this was completed funding was secured to purchase a faster, higher capacity microcomputer. A 32-bit, RISC chip, BBC-Achimedes computer was acquired about two-thirds of the way through the research period which dramatically reduced computing time.

The physical size and cost of the computer and its many "redundant" components and functions, implies that it does not lend itself for incorporation into a feasible, compact instrument. What is required is a dedicated, chip level, system capable of performing the specific computing and logical tasks required. The system can be individually developed or it can be construct using a "building block" approach. The building blocks can be selected and interfaced into the system. For example, there are commercially available, DSP chips capable of preforming FFT on very large data sets in milliseconds (Gomez S, Gonzalez S, Hsu D, Kuo A. 1988) and numerous single chip microprocessors many of which have on board memory.

8.2.1.2 Photodiode Array

The photodiode array used in this research project performed the task required. The drive requirements were satisfied by a combination of commercially available drive cards and specifically designed interfacing. The spectral response characteristics of the array corresponded with the spectral frequency of the source of timber illumination thus effecting maximised signal

output.

The array produced a "noise free" signal despite it sometimes being used outside the linear region of its characteristic curve. This meant that the calculation of optimum photodiode integration period, estimated by the host computer, required more iterations than would otherwise be necessary. This obviously increased the data acquisition time.

The photodiode array's linear resolution (25µm) proved amply suitable for the application, allowing for a possible two-fold (100%) increase (in resolution) should this be required.

The current application of the laser instrument is post-process; the desirable goal was to realise an in-process device. Thus the photodiode array will eventually be replaced by a single photodiode. This will, of course, imply different drive and timing requirements for data acquisition.

8.2.1.3 Data Acquisition - Auxiliary RAM and ADC

The interface between the photodiode array and the host computer performed the digitizing and temporary storage of the captured data as conceived. The conversion speed of the ADC and the access times of the RAM proved appropriate for the application.

The rising edge of the ARRAY-CLOCK was used to clock the auxiliary RAM while the HIGH period of the ARRAY-CLOCK was used to write data to the

auxiliary RAM. The ARRAY-SAMPLE pulse is also triggered by the rising edge of the ARRAY-CLOCK. This inevitably meant that the data stored in memory location 0 was erroneous (that in locations 1 to 1023 were correct). Though this was not a serious loss, this quandary was catered for by copying into location 0 the contents of location 1023 (see line 3100 of the Interrupt Service Routine algorithm - Appendix A5.3). This served to reduce any rapid change in amplitudes between the last data sample and the first, which may give rise to high frequency noise when the FFT is applied.

8.2.2 Optics

8.2.2.1 Helium-Neon Laser

The low-power (5mW), helium-neon laser was used as a source of illumination because monochromatic light precludes aberration problems and presents a beam of uniform and constant density. The major disadvantage with the illumination source in its present form is its bulkiness. It is too large to be incorporated into a compact instrument. There are more compact semiconductor lasers which may be investigated with a view to possible replacement.

Another possible source of concern is the 15 minute warm-up period required by the current laser (see laser specification: Appendix B1). This may present unacceptable time delays in the commercial use of the instrument.

8.2.2.2 Beam Expansion

As detailed in Section 5.3.2, the cross section of the beam was expanded using a "home made" collimator. This component was designed and manufactured using rather limited optics expertise. It was certainly less sophisticated than commercially available collimators, but cost substantially less.

The performance of the home made collimator, however, did not seem to adversely affect the effectiveness of the instrument, although its consistency in producing a uniform density broad beam was a cause for concern. This inconsistency seemed to be caused by the use of incorrect fixing screws used to hold the collimator to the laser. The tapped screw threads in the laser became damaged and the collimator was not always securely held in the correct position (ie. collimator axis did not always align with the laser's axis).

The enlarged diameter of the illuminating laser beam was appropriate, thus alleviating the need for elaborate image and object alignment mechanisms.

8.2.3 Instrument Mechanism/Adjustment Mechanism

Although the adjusting mechanisms and locking mechanism performed the tasks for which they were designed some difficulty was experienced in aligning the image with the photodiode array and in insuring that only 125mm of the timber surface was sampled. This was in part due to the primitive nature of the designs and lack of optical tools. The design tolerances were not realized in the manufacture, so that some intended sliding fits turned out to be very loose or erratic.

The fine and coarse focusing mechanisms of the imaging lens functioned according to plan and the spring loaded timber clamp was efficient in holding the timber samples against the datum face of the T-shaped framework. The hinged doors of the dark-housing allowed access to the various components of the instrument and was effective in excluding ambient light from the photodiode array.

The angle of incidence of the illuminating beam was accurately controlled by the micrometer/spring arrangement.

8.3 Software

8.3.1 Data Capture

8.3.1.1 Laser Instrument Data Capture

The capture of data from the timber samples using the Laser instrument (Section 5.5 and 6.7.2) was successful and consistent. The use of "automatic gain control" in acquiring the data set meant that the resolution of the ADC was always fully exploited and the best signal to noise ratio guaranteed.

Being iterative, the data capture algorithm (Appendix A5.1) required an initial start point or estimate of the integration period in order to approximate an optimum period. The closer the initial guess was to the required value the shorter would be the time required to calculate the optimum integration period.

In the algorithm the value of C% was used to represent the estimated integration period and was given an empirically derived, initial value of 2000 (the final value of C% being used as representative of the optimum integration period). There were occasions when this initial value of C% was so much in error that the algorithm failed (or took an unacceptably long period) to converge to the optimum integration period. When this happened the data-capture attempt was abandoned and the initial estimate of C% revised manually.

This problem requires a more sophisticated solution. For example, the algorithm could be altered to monitor the value of C% so that if its value crosses a certain threshold the algorithm is re-initiated with a more appropriate initial value for C%.

The integration periods for the photodiode array could have been more accurately timed; instead of using a **FOR-NEXT** loop, one of the counters/timers in the PIA could have been employed. This will increase the repeatability and constancy of the instrument.

8.3.1.2 Talyrond 200 Data Capture

The capture of data from the timber samples using the talyrond 200 was successful and consistent. The method relied a ten-bit analogue to digital converter (ADC) with synchronising and control signals from a BBC microcomputer for the capture of data.

The Talyrond 200 is a well established, reliable instrument, with high resolution and accuracy, and was used during this research as a credible reference.

8.3.1.3 SSA Data "Capture"

The mathematical model on which the SSA is based is very rigorous and caters for a wide range of timber machining parameters and conditions. The conditions that it does not presently accommodate are timber slippage and sudden variation in timber feedspeed. It also needs to be modified to deal more appropriately with the various modes of timber vibration / regimes of timber support. The SSA is very accurate, versatile and has proved to be a useful tool, giving insight into machined timber profiles.

The resolution of the profile can be varied by changing the number of data points generated in a given sample length. This, of course, has the disadvantage of requiring more time to generate the profile and analysis.

8.3.2 Data Analysis

8.3.2.1 Fast Fourier Transform Algorithm

The FFT algorithm performed well the task of converting the captured data into the frequency domain. There was, however, much frustration with the time taken to complete the transform of 1024 data points. Various techniques were employed to reduce the execution time.

The first was as follows; rather than calculating the sine and cosine values

during FFT execution, a data look-up table of the sine and cosine coefficients was generated prior to run-time and referenced, at various stages, during execution. This provided a significant speed advantage over run-time computation, the only drawback being the memory requirement to store the data in the look-up table.

The second technique was to arrange so that the number of data points to be transformed was as close as possible to, but above, the Nyquist limit of 250 (ie. 256, which also satisfies the decimation-in-time FFT criteria that the number of data point to be transformed must be some power of 2). Although this greatly reduced the computing time, in a number of instances aliasing resulted, due to foldover of sidelobes (Rabiner L.R, Gold B, 1975b) whose frequencies were greater than the Nyquist limit. This was remedied by increasing the number of data points in the sample length to 512.

The third technique was to convert the algorithm from BBC BASIC to machine code (Appendix A6). As mentioned above this was abandoned due to the limited capacity of the BBC-Master computer and the purchase of a 32-bit BBC Archimedes computer which implemented the algorithm in approximately 7.38 seconds (compared to the original 4.75 minutes). Also, mentioned above, there are dedicated DSP chips available (Gomez S, Gonzalez S, Hsu D, Kuo A, 1988) that can perform the FFT (in a few milliseconds), which can be used to supersede the present algorithm.

8.3.2.2 Fault Finding Algorithm (FFA)

The FFA analysed the FFT data by initially searching through the harmonics for local maxima and deciding if they were of significance by comparing the peaks with a specified threshold value. Then, the number of the significant harmonics were compared with the number of the principle-harmonics. Hence by a prioritised process of elimination the cause of the surface quality was identified (see Section 6.7.6.6).

The FFA is presently in a primitive/embryonic form. The algorithm is proficient at detecting machining faults such as cutterhead eccentricity (out-of-balance and runout) and proud-knives provided that the FFA threshold used is not too low. The threshold value currently used (0.4) was arrived at by an empirical, trial and error approach. With ideally machined surfaces, multi-knife or single-knife finish, the FFA proved effective.

The FFA failed to record totally accurate results when analysing frequency signatures from samples produced by cutterheads whose degree of imbalance was such that the magnitude of the eccentricity induced meant that there was a tendency for only N-1 knife-marks to be left on the machine surface for every one revolution of the cutterhead (see Section 6.7.6.2). This was because the FFA was not contrived to investigate this "secondary" phenomenon; the FFA can of course be modified to incorporate this.

8.4 Machining Investigations

8.4.1 Theoretical Results

A selected set of results, generated using the SSA, are shown in figures 7.G0.S1 to 7.G0.S6. The variables used in producing the examples were chosen so as to keep their graphical display within the screen's resolution. The results in this section were generated to demonstrate the versatility of the mathematical model and the SSA and to highlight the features of the FFA.

8.4.1.1 Single-knife Finish

Figure 7.G0.S1 presents surface profiles produced using single-knife finish (Section 6.6.4). The one proud knife in position 1 "satisfied" the un-jointed nature of the single-knife method. A 6-knife cutterhead with rotational speed of 5000 rpm was used and only the value of the timber speed was varied in figure 7.G0.S1.

In figure 7.G0.S1a a timber feedspeed of 7.5 m/min resulted in a surface wave pitch of 1.5mm (see equation **6.1**). This gave a dominant peak at harmonic 83 in the FFT, as expected; there are diminishing side lobes associated with harmonic 83 (ie. harmonics 167,250 and 179) which are due to the effects of windowing (Rabiner L.R, Gold B, 1975a), see figure 5.6.11, Section 5.6.1.8. It should be noted that aliasing of the one of the side lobes has occurred in figure 7.G0.S1a. Harmonic 179 is actually harmonic 333 which has been "folded back" down the spectrum about the Nyquist frequency (256), ie.179=256-(333-256).

The analysis of the FFT by the FFA (threshold=0.4) concluded that the finish was that produced by the single-knife cutting mode, giving a dominant peak at harmonic 83.

Similarly, in figure 7.G0.S1b a timber feedspeed of 10 m/min resulted in a surface wave pitch of 2mm. This gave a dominant peak at harmonic 62 in the FFT. Again, there were diminishing side lobes at harmonics 125, 189, 250, 200 and 137 of which harmonic 200 and 137 were aliases of harmonics 311 and 373, respectively. The FFA analysis concluded that the finish was that produced by the single-knife cutting mode, with the dominant harmonic at 62.

In figures 7.G0.S1c and 7.G0.S1d the timber feedspeed was increased to 12.5 m/min and 15 m/min, respectively. Resulting in corresponding dominant harmonics at 50 and 42. In each figure there are the usual side lobes but no aliasing has occurred since the side lobes decayed to "zero" within the specified bandwidth.

The respective FFA analysis of each FFT data set concluded that the profile was consistent with that of single-knife finish. However, in figure 7.G0.S1d the stated value of $\mathbf{h_1}$ (=41) varied by 1 compared to actual dominant peak value (=42) in the FFT. This was because the value of $\mathbf{h_1}$ was quoted in integer form and thus had a tolerance of ±1.

8.4.1.2 Multi-knife finish

Figures 7.G0.S2 to 7.G0.S6 presents simulated surface profiles produced using multi-knife finish, under ideal conditions (Section 6.6), and demonstrates the effects of variation in parameters and their superposition.

Figure 7.G0.S2 deals with the variation of the basic parameters:

1) Number of Knives per cutterhead
2) Timber feedspeed
3) Cutterhead rotational speed

In figure 7.G0.S2a the number of knives on the cutterhead was 6, the timber feedspeed was 90 m/min and the rotational speed was 5000 rpm (these can be considered as the "nominal" values of variables for figure 7.G0.S2). The relationship between the feedspeed and rotational speed was such that each knife leaves a finish mark. There were no proud knives, hence the cutterhead is considered to be jointed (h_j=41±1). This resulted in an ideal, simulated surface profile whose frequency spectrum had a peak at harmonic 42 and diminishing side lobes, approximately every 42 harmonics thereafter. This multi-knife, finish was detected in the FFT spectrum by the FFA, using a threshold of 0.4.

In figure 7.G0.S2b the feedspeed was increased to 100 m/min, with number of knives and rotational speed unchanged, increasing the wave pitch (h_j=37±1), and giving a spectrum with a peak at 38. The FFA again detected this.

In figure 7.G0.S2c the feedspeed was reduced to 80 m/min, with number of knives and rotational speed unchanged, decreasing the wave pitch (h_j=46±1), and giving a spectrum with a peak at 47. Again, the FFA detected this.

Figure G0.S2d and G0.S2e shows the profile and spectrum of a simulated surface generated using the nominal values except that the rotational speed was varied; in the first instance it was increased to 6000 rpm, in the second it was reduced to 4000 rpm. The quicker rotational speed resulted in a smaller wave pitch (h_j=50±1), with harmonic 50 being dominant; the slower speed gave a courser wave pitch (h_j=33±1), with dominant harmonic at 33. In each case the FFA accurately detects the multi-knife nature of the profile.

In figures 7.G0.S2f and 7.G0.S2g the number of knives are varied from the nominal value; firstly it is increased to 8 (h_j=55±1), and then reduced to 4 (h_j=27±1), giving respective peak at 56 and 28. In each case the FFA detected the multi-knife nature and dominant harmonic of the simulated profile.

8.4.1.3 Superposed Machining Faults

Figure 7.G0.S3 introduced the machining faults; eccentricity (called here out-of-balance), proud knives and timber vibration. They were each introduced in turn and superposed onto the ideal finish; later these same faults were combined, permutated and superposed, again onto an ideal surface.

Figure 7.G0.S3a started with the nominal values, giving the ideal machined

surface as before.

Then, in figure 7.G0.S3b, a once per revolution eccentricity (out-of-balance) with amplitude of 8μm was featured ($\mathbf{h_1}$=6±1, $\mathbf{h_j}$=41±1). The undulating nature of the knife-marks can be clearly seen in the generated profile; the FFT peaking at harmonics 7 and 42 and the FFA (threshold=0.4) detected the two peaks.

In figure 7.G0.S3c the out-of-balance was removed and replaced with a proud knife (10μm) in position number 4. The proud knife marks can be seen on the profile as can the proud-knife, characteristic peaks at harmonics 7, 14, 21 and 28 of the FFT spectrum. The multi-knife finish of the profile transformed to a peak at harmonic 42. The FFA (threshold=0.4) detected both proud-knife and multi-knife conditions.

Figure G0.S3d introduced timber vibration to the ideal surface ($\mathbf{h_j}$=41±1). The timber vibration (four cycles during the period of knife engagement with the timber) was specified and superposed onto the ideal surface. For each knife, only two (of the four) vibration cycles contributed to the final surface finish. Hence the peak at harmonic 83. The FFA analysis verified this.

Figure 7.G0.S3e combined two of the simulated faults, the proud knife (position 4) and out-of-balance ($\mathbf{h_1}$=6±1), and superposed them onto the ideal surface ($\mathbf{h_j}$=41±1). This resulted in a frequency signature that peaks at 42 (multi-knife finish) and the "pulse train" peak harmonics at 7, 14, 21 and 28.

The effect of the out-of-balance is masked by the proud-knife component at harmonic 7. However, comparing harmonic 7 in figure 7.G0.S3e with harmonic 7 in figure 7.G0.S3c, it is evident that harmonic 7 in figure 7.G0.S3e is of greater magnitude than that in figure 7.G0.S3c. This is because the out-of-balance component ($\mathbf{h_1}$) has reinforced the amplitude of harmonic 7. This, however, is not detected by the FFA in its present configuration; all it "sees" is the proud-knife effect. So some modification or "fine-tuning" of the FFA may be required.

Figure 7.G0.S3f combined the proud knife (in position 4) and out-of-balance ($\mathbf{h_1}$=6±1) faults, and superposed them onto the ideal surface ($\mathbf{h_j}$=41±1). This resulted in a frequency signature that peaked at harmonics 7 (out-of-balance), 42 (multi-knife finish) and 83 (timber vibration). The FFA accurately detected these.

Figure 7.G0.S3g combined the proud knife (in position 4) and timber vibration (4 cycles per knife cut) faults, and superposed them onto the ideal surface ($\mathbf{h_j}$=41±1). This resulted in a frequency signature with peaked at harmonic 42 (multi-knife finish) and 83 (timber vibration), and "pulse-trains", starting at harmonic 7. The FFA accurately detected these features.

All three faults were combined in figure 7.G0.S3h resulting in the expected frequency spectrum and FFA analysis. Figure 7.G0.S3i and 7.G0.S3j reflected the same conditions but the FFA employed reduced thresholds of 0.1 and 0.05 respectively. Notice the extension to the number of peak which constitutes

a proud-knife fault and to the number of harmonics attributed to timber vibration or noise. This, to some extent, illustrates that caution must be applied in selecting the threshold value when using the FFA in its present form.

8.4.1.4 Fault Parameter Variation

Figures 7.G0.S4, 7.G0.S5 and 7.G0.S6 illustrated the effect of varying the value of the fault parameters:

Figure 7.G0.S4a to 7.G0.S4d showed variations in the amplitude of the eccentricity (out-of-balance). The amplitudes varied from 2 microns through to 12 microns. In each case the shape of the FFT is as predicted. (In the case of figure 7.G0.S4a, where the eccentric amplitude was 2 microns, the FFA failed to detect the unbalance because the threshold of 0.4 was too high.)

In figure 7.G0.S4d there were "additional" peaks at harmonics 28 and 39. These "extra" harmonics can be accounted for as follows:

As the cutterhead spindle undulates due to eccentricity, the depth of cut of each knife will vary depending on its angular position; those cutting when the spindle is at a trough will cut deeper than those cutting when it at a crest. Hence the width (and depth) of the knife-mark will vary from a maximum through to a minimum and back to maximum, as cutting continues. The frequencies of

the sine waves in the FFT that synthesise the surface waveform will also account for this variation in the depth and width of the knife-mark. This is accounted for in the FFT by the emergence of the "extra" peaks at harmonics 28 and 39. The "lower" harmonic, $\mathbf{h_{jlo}}$ (=28), accounts for the widening and deepening of the knife-marks at the troughs; the "higher" harmonic, $\mathbf{h_{jhi}}$ (=39), is associated with the shallowing and narrowing of the knife-marks at the crests. This effect can be seen in other examples such as figures 7.G0.S4b and 7.G0.S4c.

As the magnitude of the eccentricity increases its value will approach $\mathbf{d_{crit}}$ (Section 6.7.6.2). At this stage the knife that cuts at the crest of the undulation does not contribute a knife-mark to the final surface finish. So effectively, there are only N-1 knives cutting (hence one less knife-mark per revolution of the cutterhead) giving rise to an FFT signature with a peak at harmonic $\mathbf{h_{dcrit}}$. The value of $\mathbf{h_{dcrit}}$ is given by

$$\mathbf{h_{dcrit} = h_j - h_1} \qquad \textbf{(8.1)}$$

As the magnitude of the eccentricity increased from zero to $\mathbf{d_{crit}}$, so the amplitude of the "shallowing" harmonic, $\mathbf{h_{jhi}}$, reduces while that of $\mathbf{h_{jlo}}$ increases (see figures 7.G0.S4e and 7.G0.S4f). Note that

$$\mathbf{h_{jhi} = h_j + h_1} \qquad \textbf{(8.2)}$$

and

$$h_{jlo}=h_j- h_1 \qquad (8.3)$$

Figure 7.G0.S5a to 7.G0.S5f show variations in the number, and position, of proud knives. The total number of knives on the cutterhead was increased to 8 and each proud knife protruded by the same amount, 8 microns.

Figures 7.G0.S5a and 7.G0.S5b shows the surface due to one proud knife, placed in position 1 and 5, respectively. The FFT's exhibits the typical "pulse-train" effect and the FFA successfully determined the faults which caused the surface.

Figures 7.G0.S5c and 7.G0.S5d features 2 proud knives. The first had the proud knives in cutterhead positions 1 and 3 the other in positions 1 and 6. The FFT signatures generated differ from those characteristic of a single, proud-knife finish. The peaks that appear between h_1 and h_j are not regularly spaced or necessarily positioned in order of descending magnitude. Although in figure 7.G0.S5d the FFA was "successful" in detecting "the proud knife", in figure 7.G0.S5c it failed.

Similarly, in figures 7.G0.S5e and 7.G0.S5f where 3 proud knives are featured in positions as specified, the FFTs of the surface profile take on yet different "shapes", with unsuccessful results

when the current FFA was applied.

The FFA in its present form does not contend well with detection of more than one proud knife. It presently searches only for the "pulse-train" type effect in the FFT signature. In figure 7.G0.S5c the pulse train (ie. peaks at harmonics 6, 12, 18, 24, ...) is missing, resulting in an incorrect diagnosis. However, the FFA did report "unknown faults" at harmonics 17, 22 and 28. The algorithm obviously needs modifying. One possibility would be to study these "unknowns" and establish the pattern or trend in the FFT which emanates from these types of faults and incorporate this into the detection process of the FFA. Another would be to create FFT "templates" of known faults and cross-correlate them with the unknown FFT signatures. Yet another would be to infer that if more than one peak is found between $\mathbf{h}_1$ and $\mathbf{h}_j$, this would constitute some form of proud-knife fault and allow the FFA to conclude as such, without specifying further details.

Figure 7.G0.S6a to G0.S6d shows variations in timber vibration rate. The rate was changed from 6 through to 12 in increments of 2. (To prevent loss of discrimination, due to the host computer's screen resolution, during the variation of timber vibration rate the nominal rotational speed was reduced from 5000 rpm to 4000 rpm).

In figure 7.G0.S6a the peak at harmonic 33 (=$\mathbf{h}_j$) indicated a

multi-knife finish while the peak at harmonic 100 corresponded to timber vibration, $\mathbf{h_v}$. The effect of vibration is very similar in result to that of spindle eccentricity; the consequence of the vibration is more marked at the trough of the knife-mark than at either flank. Hence, associated with vibration harmonic, $\mathbf{h_v}$ (=100), is a lower, "deepening" harmonic, $\mathbf{h_{vd}}$ (=67) and a higher, "shallowing" harmonic, $\mathbf{h_{vs}}$ (=133), where

$$\mathbf{h_{vd} = h_v - h_j} \qquad \textbf{(8.4)}$$

and

$$\mathbf{h_{vs} = h_v + h_j} \qquad \textbf{(8.5)}$$

Similar results are shown in figures 7.G0.S6b to 7.G0.S6d. At present in the actual machining of timber the value of $\mathbf{h_v}$ is unpredictable, due to the lack of a governing mathematical relationship and large number of unknown variables that govern it.

(It should be noticed that in figure 7.G0.S6b the FFA detected a peak at harmonic 133 because its amplitude was above the threshold of 0.4. (due to reinforcement). This failing is partly due to the vagueness of the criterion used for detecting timber vibration (because of its current unpredictability) and the arbitrary choice of threshold).

8.4.2 Timber Machining Results

Figures 7.G1.S1 to 7.G1.S5 show examples of data captured from timber samples using the laser instrument and the talyrond 200, and, profiles generated using apposite variable values in the SSA. Each figure has boxes which feature:

1) the captured (or generated) data and its FFT,
2) the machining parameters used,
3) the associated principle peak harmonics

and 4) the result of analysing each FFT using the FFA.

The samples from the machining investigation were subdivided into 2 main groups:

1) Single-knife finish
2) Multi-knife finish

which broadly classified the type of "fault" or the condition of the machine at the time of machining. Multi-knife finish was further sub-divided into four groups:

1) Spindle Eccentricity/Cutterhead Imbalance
2) Proud knives
3) Vibration
4) Fault combinations

Figures 7.G1.S1 to 7.G1.S8 present data from samples produced using single-knife finish; figures 7.G2.S1 to 7.G2.S12 deal with spindle eccentricity;

figures 7.G3.S1 to 7.G3.S15 is concerned with proud-knives; figures 7.G4.S1 to 7.G4.S6 addresses samples subjected to timber vibration; finally figures 7.G5.S1 to 7.G5.S5 present data captured from timber samples featuring combinations of machining faults.

8.4.2.1 Single Knife Finish

(Refer to Table G1)

In figure 7.G1.S1 a significant peak can be seen at harmonic $\mathbf{h_1}$ (=37±1) on the spectrum of each data set. This was as expected for the machining parameters used, and, the FFA analysis detected a single-knife finish in each case.

There is also a significant peak at harmonic 1 in the FFT of the laser data, which is absent in the data captured using the talyrond and that generated by the SSA. This difference can be explained as follows:

The amplitude of the reflected light from sample G1.S1 showed considerable variation throughout the particular sample length considered. This was because the timber sample was resinous; the sites where the resins was high in concentration reflect light less efficiently and corresponded to regions where the reflected light intensity was relatively low; the areas of low resin concentration more effectively reflected light and corresponded to regions where the reflected light intensity was relatively high. This variation accounted for the comparatively large amplitude of

the very low harmonics (harmonics 1 and 2) in the spectrum. The idea that the significant peaks at very low harmonics were not due to a machining fault is substantiated by the fact that the amplitude of the very low harmonics in the FFT of data captured (from the same region of the same sample) using the Talyrond were comparatively small.

This phenomenon - resin significantly affecting the amplitude of the reflected light - was witnessed to varying degrees throughout the research; typical examples, in the investigation of single-knife finish, are figures 7.G1.S3, 7.G1.S4, 7.G1.S5 and 7.G1.S7. This is not a major drawback to the surface-form-analysis technique, however, because, in timber the resinous grains are always "very-long-wavelength" in nature, compared with the surface waves produced by the machining operation. For this reason, in developing the philosophy of the FFA, the very low harmonics of the FFT were ignored.

Timber sample number G1.S6, (see figure 7.G1.S6) had peaks at harmonic 42 when one was expected at harmonic $\mathbf{h_1}$ (=37±1). This large discrepancy can be explained in terms of timber slippage:

> At the time of machining the efficiency of the timber feed mechanism was less than 100%. This meant that the timber was travelling slower (due to slippage) than the reading indicated by the drive unit, hence inducing a finer machined surface wave pitch than anticipated (an error of some +16%).

In its present form the FFA cannot detect the fact that slippage has occurred and can only report "unknown fault". When this was discovered hand timing, with a stop watch, was employed to double check the readings indicated by the drive unit.

It is anticipated that great difficulty will be encountered in effecting an algorithm which readily detect timber slippage using the FFT data. One method of circumventing the problem is to use a rolling contact encoder which accurately monitors the timbers feed speed; instead of relying on erroneous data obtained from the drive unit's gearbox.

The other timber samples in the "single-knife" category show consistent results and good correlation between the data sets.

8.4.2.2 Spindle Eccentricity (Dynamic Balance)

(Refer to Table G2)

Samples G2.S1, G2.S2 and G2.S3 were produced using ideal machining conditions (see figures 7.G2.S1, 7.G2.S2 and 7.G2.S3). The samples which followed these, G2.S4a to G2.S4c were produced the same cutterhead, but, having induced it with varying degrees of imbalance (1 screw, 2 screws, 3 screws or 5 screws) (see figures 7.G2.S4a, 7.G2.S4b and 7.G2.S4c). (In the SSA each screw is deemed to induce a eccentricity of 1µm)

In figure 7.G2.S4a the frequency signature resulting from the laser instrument and the talyrond 200 both have a peak at harmonic 40, compared

to a peak at harmonic 38 in the SSA generated data set. The difference in can be explained in terms of timber slippage during machining. However, the harmonic value falls within the tolerance band of $h_j \pm 2$ specified in the FFA. Hence, analysis of the FFT signature produced the favourable verdict of "multi-knife" finish. The induced out-of-balance, though present and visible (at harmonic 10), its amplitude was below the FFA threshold value used, hence the fault was not detected.

In sample G2.S4b, during the production of which the cutterhead imbalance was increased by one increment, showed, as expected, a more pronounced peak at h_1 (=9±1) than in sample G2.S4a. Harmonic h_j (=38±1) showed comparable relative amplitude. Similarly in sample G2.S4c where before machining the value of cutterhead balance was increased by a further increment, the frequency spectrum peaked, as expected, at the principle harmonics, h_1 and h_j.

It is further noticed that as the value of cutterhead imbalance increased the amplitude of h_{jlo} (=28) and h_{jhi} (=47) - the "deepening" and "shallowing" harmonics - were significantly enhanced. Again (probably due to slippage) there was some variation in the theoretical peak harmonics and those associated with the timber sample.

Sample G2.S5 was produced using a jointed, six-knife cutterhead rotating at 6000rpm with a timber feedspeed of 80 m/min. Analysis of the captured data (from laser instrument and talyrond) revealed two major peak in the FFT

signature; one, as expected, at harmonic h_j (=56±1), the other (unexpected) at harmonic 17. The SSA generated data had just the one expected peak at harmonic h_j. The FFA analysis revealed that harmonic 17 corresponded to a twice-per-revolution, out-of-balance defect. However there were other "peaks" in the vicinity of harmonic 17 (such as harmonics 13 and 22) and neighbouring harmonics of considerable amplitude. Visual examination of the sample confirmed a poor surface finish. The cutterhead was again jointed and sample G2.S6 machined. This proved to be a much improved surface with only one peak (harmonic h_j) in the FFT.

Samples G2.S7a and G2.S7b were also machined using the same machining parameters as G2.S6 but with progressively induced, incremented imbalance. Figure 7.G2.S7a and 7.G2.S7b show the data obtained. Here, again, the faults are highlighted by the significant peaks in the FFT signatures, and are correctly diagnosed by the FFA. In figure G2.S7b the peaks at approximately harmonics 47 and 66 (ie. h_{jlo} and h_{jhi}) are very prominent.

Similar results were obtained with other timber samples that were machined with out-of-balanced cutterheads. Figures 7.G2.S8 to 7.G2.S12 catalogue the results.

Sample number G2.S9b is note worthy (see figure 7.G2.S9b); here the process of replacing the 5 fixing screws to induce cutterhead imbalance seem to have dislodged the knife, thus producing an out-of-balance, proud-knife condition. This is detected in the FFT signature by the FFA.

8.4.2.3 Proud Knives

(Refer to Table G3)

The timber samples with the prefix G3, were produced to investigate the proud-knife phenomenon. Samples number G3.S1 and G3.S8 were produced using ideal machining conditions (see figures 7.G3.S1 and 7.G3.S8). The other samples in the group were produced using cutterheads with various arrangements of proud knives.

Figures 7.G3.S2 to 7.G3.S4 present the results for samples machined with the cutterhead having one knife proud of the nominal cutting circle. The amount of proudness was varied in increments (of about 4µm) starting at about 4µm.

The results were as predicted, showing the characteristic "pulse-train" effect associated with a single proud-knife, the magnitude of the harmonics due to the proud knife increasing as the proudness was incremented. The FFA successfully detected the proud knife fault from the FFT signatures.

Before machining sample number G3.S6, two adjacent knives on the cutterhead were caused to be proud. The subsequent results are shown in figure 7.G3.S6 which revealed a slightly different FFT signature to that produced by the single proud-knife. Similarly, with sample number G3.S7 where knife numbers 1 and 3 were caused to be proud before machining, the FFT signatures show a "proud-knife" fault (figure 7.G3.S7).

Sample G3.S8, machined under ideal conditions, was used as a reference for comparing the other "proud-knife" samples in its family (samples G3.S8 to G3.S11). The second member of the family was sample G3.S9 in which one knife was proud of the nominal cutting radius by about 4µm. The degree of proudness was increased to about 8µm and 12µm for samples G3.S10 and G3.S11, respectively. The corresponding figures show the results for each sample. The FFT signatures (and FFA results) show the expected outcomes for samples G3.S9 and G3.S10.

However, the results for G3.S11 showed some inconsistency; the FFT of the laser data did not show the characteristic "pulse-train" effect - there were significant harmonics between $\mathbf{h}_1$ and $\mathbf{h}_j$ which did not correspond to any of the principal or expected harmonics - whereas the talyrond 200 results revealed the anticipated FFT signature. This difference could not be readily explained. It is suspected that the two data sets did not originate form the same timber sample - a mistake may have been made in the labelling of one of the data sets.

Sample number G3.S12 (see figure G3.S12) was machined using a 8-knife cutterhead under ideal conditions. The same machining parameters were used to produce samples G3.S13 and G3.S14 (figures 7.G3.S13 and 7.G3.S14) except that one knife was ground so its cutting edge was below the cutting radius of the jointed knives. The proudness values were approximately -4µm and -8µm respectively. In each sample the proud-knife, pulse-train effect was apparent, and was detected by the FFA.

Figure 7.G3.S15 shows the result for sample number G3.S15, which was machined using a cutterhead with two knives (in positions, diametrically opposed), having proudness values of approximately -8µm. The FFT signatures for this sample show a distinct difference to the others machined using proud knives. Because the arrangement of the knives is symmetrical, the frequency of knifemarks due to the proud-knifes is doubled. Hence the first peak or significant harmonic in the FFT signature is 16±1 and not 8±1. The FFA did not cope with this, and concluded that the fault was a twice-per-revolution fault (O.balance2) with significant "unknown" faults at harmonics 33 and 50.

8.4.2.4 Timber and Spindle Vibration

(Refer to Table G4)

Samples in group G4 deal with vibration. Figures 7.G4.S1 to 7.G4.S6 shows the results from investigations into the effect of timber support (or timber control) and spindle support on the surface waviness/quality produced. The mathematical modelling of the various modes of timber vibration is so deficient that the SSA cannot be reliably used as a predictive tool. Hence, ideal machining parameters were used to generate the SSA data which corresponded to each timber sample.

The first two timber samples (G4.S1a and G4.S1b) were produced under "single-knife" cutting conditions. The first (see figure 7.G4.S1a) had an ideally machined surface (machine fully set), while the second (see figure 7.G4.S1b) was machined without the use of the chipbreaker. There is a

difference between the FFTs obtained from the two samples; the ideal has only one significant peak (harmonic 37±1(=$\mathbf{h}_1$)) in its FFT signature; that machined without the chipbreaker has two significant peaks, one at $\mathbf{h}_1$ the other at harmonic 27. The FFA failed to detect the peak at the 27th harmonic because of the strategy adopted by the algorithm - that of essentially searching for the principal peaks, $\mathbf{h}_1$ and $\mathbf{h}_j$, and when found looking for other significant peaks in between them. Hence, harmonics lower than $\mathbf{h}_1$ were ignored. The FFA needs to be amended to contend with this situation.

Sample G4.S2a and G4.S2b were produced under multi-knife-finish machining conditions; G4.S2a was ideally machined while G4.S2b was planed without the use of the top pressure roller or the chipbreaker. The difference between the FFT signatures for the two samples was marked (see figures 7.G4.S2a and 7.G4.S2b). The quality of the surface of G4.S2b was very poor; visual inspection of the sample revealed that the waviness pitch for the first one-third of its length has some resemblance to what was expected, while the other two-thirds had a much larger pitch and considerably greater amplitude (see figure 7.G4.S2b; talyrond trace - TAL). The FFA incorrectly flagged up a "proud-knife" fault for this sample.

For machining samples G4.S3a, G4.S3b, G4.S3c and G4.S4, the number of knives on the cutterhead was increased to 6, the timber feedspeed to 80m/min and rotational speed of the cutterhead to 6000 rpm. These samples investigated spindle vibration by gradually reducing the degree of spindle

support at its outboard end.

Gradual deterioration of the surface quality was seen as the spindle's outboard end was freed (see figures 7.G4.S3a through to 7.G4.S3c). When the outboard bearing was completely removed for the machining of sample number G4.S4 the results on the surface finish was catastrophic (see figure 7.G4.S4). The FFA returned a "proud-knife" verdict in each case above. This verdict while being incorrect, due to the primitive nature of the FFA, indicated, however, that there was a problem with the machining process.

Samples number G4.S5a through to G4.S6c illustrated the effect of reducing the downward force applied by the chipbreaker, to the timber being machined. The first two samples (G4.S5a and G4.S5b) were machined using a timber feedspeed of 65m/min while the for other three (G4.S6a, G4.S6b and G4.S6c) it was increased to 75m/min.

The results (see figure 7.G4.S5a and 7.G4.S5b) show that a machining fault was present when sample G4.S5b was produced; the FFA "failed" to accurately identify the fault but gave indications (Unknown Faults) that all was not well with the machining process.

Similarly (see figure 7.G4.S6a, 7.G4.S6b and 7.G4.S6c) with the other three samples, as the chipbreaker force was reduced, the quality of the surface finish diminished. Again the FFA indicated, without accurately specifying, that there were problems with the machining process.

8.4.2.5 Fault Combinations

(Refer to Table G5)

The timber samples in Group G5 were machined with the purpose of producing surface profiles on which there were a combination of process faults. The first sample, G5.S1 (see figure 7.G5.S1) was produced under ideal conditions and used as the reference profile for in the group.

Sample number G5.S2, machined with the cutterhead in a state of out-of-balance; the results (see figure 7.G5.S2) were as expected, with major peaks at harmonic 10 (=$\mathbf{h}_1 \pm 1$) and 60 (=$\mathbf{h}_j \pm 1$).

Sample G5.S3 was produced under the same conditions as G5.S2 but with one additional fault - a proud knife. The result (see figure 7.G5.S3) were again as expected, with the "pulse-train" effect evident in the harmonic signature.

With sample G5.S4 another fault was added to those of G5.S3 - the downward pressure of the chipbreaker was reduced. This caused further deterioration in the quality of the surface finish; (see figure 7.G5.S4) the principle harmonic $\mathbf{h}_j$ (=60) although "visible" on the frequency signature, was not of significantly magnitude to be detected by the FFA (threshold=0.4).

In sample G5.S5 yet another fault was added to the conditions under which G5.S4 was machined - the outboard bearing was untied before machining commenced. Surprisingly, this seemed to caused a slight improvement in the machined surface quality, as assessed by visual inspection. However, the

FFA "saw" a similar result to that for sample number G5.S4.

8.5 General Comments

Noise, leakage and aliasing are related to the implementation of the FFT because of the way the analogue waveform is acquired and sampled. Apart from these general types of errors, there are others related to the specific hardware and techniques used to acquire the data. For example, optical errors may have become part of the data - the lens optics system may have added geometric distortion to the acquired waveform. This distortion may have become part of the data that the FFT worked on and may have significant effect on the frequency spectrum.

9 CONCLUSIONS

9.1 Objectives Realised

9.2 Future Work

9.1 Objectives Realised

The objectives of the research were realised in that the design and manufacture of a non-contact transducer, with signal conditioning, for the assessment of the surface form of machined timber was investigated. The investigation of an appropriate parameter which can be used to indicate the quality of machined surface profiles was also undertaken. The timber planing-moulding process was studied with the aim of producing a mathematical model that represented a range of prevalent machining conditions and machined surface profiles.

The work carried out had a significant measure of success; a non-contact laser instrument was developed, which analysed the frequency content of planed timber surfaces; the frequency content being the parameter which indicates the aesthetic qualities of the surface, as established by isolated and identifiable machine faults. The technique was validated by comparing results with that obtained using a Talyrond 200 system, a widely accepted measurement standard in engineering.

The research also yielded a rigorous mathematical model that formed the foundation of a computer surface simulation algorithm (SSA) that simulated planed and spindle moulded surface profiles. The model and algorithm proved to be very accurate and versatile tool, giving insight into the nature of surface profile faults, and their origins.

9.2 Future Work

The laser instrument requires further improvements, refinements and modifications. This will include making the device more compact; the use of a single-chip microprocessor with on board RAM/ROM instead of a mini-computer; the replacing of the existing laser with a compact semi-conductor laser; the redesign of the beam expander to reduce its size and accuracy.

The software which analyses the captured data needs some refinement; the FFT algorithm can be replaced with an application specific FFT processor chip; the FFA needs to be further developed to cater for process faults such as timber slippage, poor timber support, and, combinations of separate faults. The mathematical model and the SSA can be used to assist in the improvement of the FFA.

The mathematical model and SSA, though sound, also needs to be refined; the timber slippage fault needs to be incorporated; poor support of workpiece and the associated parameters should also be researched with a view to modifying the mathematical model. The model can be further used to pioneer research into the type of frequency signature that results from certain machining conditions. These signatures can be retained for use as templates for cross correlation with data capture from actual planed surfaces. The results of the cross correlation can then be employed to determine the fault origin.

There are other types of faults that need to be investigated (such as the beating effect that occurs when two adjacent cutterheads are rotating at

almost the same frequency or the vibratory effects of drive belt on the cutterhead) and incorporated into the mathematical model, SSA and FFA. The surface assessment technique can form the basis for developing quantifiable parameters which can indicate the degree to which the surface varies from the ideal.

The laser instrument was appropriate for post-process use, but designed using the principles of in process assessment. Further to these modifications, therefore, the instrument need to be adapted for in process use; the photodiode array can be replaced by a single photodiode, with suitable signal conditioning, and, a rotary encoder added to the instrument as a means of defining data sampling points. There would obviously be a need for field trials to establish the validity of the in process instrument.

When the in process instrument is realised, it can be incorporated into a quality control strategy, facilitating adaptive control which can optimise the machining process based on prevailing machining conditions.

REFERENCES

Arecchi F.T, Bertani D, Ciliberto S. 1979
A Fast Versatile Optical Profilometer
Optics Communications
December, 1979, Vol 31, part 3, pp.263-266

Babus'Haq R F, Probert S D,
O'Callaghan P W, Evans G N 1988
Peaks and Troughs of Surface Measurement
Professional Engineering
June, 1988, pp.52-53.

Bolzing D, Liu F. 1987
CIM - Integrated Engineering Concepts
Industrial and Production Engineering
1987, Vol 11, part 3, pp.28-44

Broadmann R. 1986
Roughness Form and Waviness Measurement by means of Light Scattering
Precision Engineering
October, 1986, Vol 8, No 4, pp.221-226

Brown H.P, Panshin A.J, Forsaith C.C. 1952
Textbook of Wood Technology
Volume II
McGraw-Hill Book Co inc New York

Brown I.D. 1960
Visual and Tactual Judgments of Surface Roughness
Ergonomics, Vol 3, Part 1, pp.51-61.

Burnner H.E. 1929
Ball Bearings as Applied to Woodworking Machinery
American Society of Mechanical Engineers' Transactions
1929

Cooley J.W, Tukey J.W. 1965
An Algorithm for the Machine Computation of Complex Fourier Series.
Math. Comp., 19, pp.297-301
April 1965

Cowdery M.J. 1990
The "Intelligent" Sawmill
Mechatronics: Designing Intelligent Machines
Proceedings of the Institution of Mechanical Engineers
pp.5-15
International Conference
Robinson College
University of Cambridge
12th - 13th September, 1990

Crookall J.R. and Sherwood K.F, 1968
Surface Finish Assessment by an Electrical Capacitance Technique
Proceedings of the Institute of Mechanical Engineers
1968, Vol 182, p.344

Cummings J.D. and Peters C.C 1970
Measuring Wood Surface Smoothness
Forest Product Journal
December, 1970, Vol 20, part 12, pp.40-43

Davis E.M, Nelson H. 1954
Machining Tests of Wood with the Moulder
Journal of Forest Products Research Society
October, 1954, Vol 4, part 5, pp.227-245

Deal R.C. 1951
Standardization of Surface Quality of Wood Products
Woodworking Digest
February, 1951, Vol 4, part 5, pp.227-245

Dobosz M. 1984
Accuracy of Profile Measurements by means of a Focused Laser Beam
Wear
November, 1984, Vol 98, pp.117-126

Drews W.E 1987
Surface Measurement; An Advanced Technology
Quality Progress
April 1987, Vol 20, Part 4, pp.43-46.

Dupuy M.O. 1967
High Precision Optical Profilometer for the Study of Micro-Geometrical Surface Defects
Proc. Inst. Mech. Engrs.
1967, Vol 182, Part 3k, pp.255-259

Elmendorf A and Vaughan T.W 1958
A Survey of Methods of Measuring Smoothness of Wood
Forest Products Journal, Vol 8
1958

Goddard M. 1985
Business Development Seminar/Technical Discussion
Woodworking Division, Wadkin Plc, Green Lane Rd, Leicester
August, 1985

Goddard M, Garrett J. 1986
Business Development Seminar/Technical Discussion
Woodworking Division, Wadkin Plc, Green Lane Rd, Leicester
January, 1986

Gomez S, Gonzalez S, Hsu D, Kuo A. 1988
An Application Specific FFT Processor
Electronic Engineering Supplement
June 1988, pp.99-106

Gonzalez R.C, Wintz P. 1977
Digital Image Processing
Addison-Wesley Publishing Company, Inc.
1977

Goodchild R. 1963
Investigating Finish in Rotary Planing
Engineering
January 25th 1963, pp.172-173

Greenwood J.A. 1968
Surface Measurement
Institute of Mechanical Engineers Symposium: Experimental Methods in Tribology, Paper 1
13th-14th March, 1968

Harris P.G, Trigg A.D 1987
Surface Analysis Techniques and their Application to Material and Device Characterization
G.E.C. Journal of Research
1987, Vol 5. part 2, pp.88-98

Han R.A. 1957
A Method of Quantitative Topographic Analysis of Wood Surfaces
Forest Products Journal
December, 1957, Vol 7, part 12, pp.448-452

Hattori M. 1981
Development of In-Process Sensor for Surface and Roundness Profiles
Bulletin of Mechanical Engineering Laboratory 35(6)
1981

Hingle H. 1986
Tool Wear Monitoring by the Component
Modern Production and Metrology Seminar
Technische Universitat, Vienna paper 147.3
1986

Inasaki I. 1982
Development of In-Process Sensor for Surface Roughness Measurement
Proc. 23 Int. MTDR
1982

Jackson M.R. 1986
Some effects of Machine Characteristics of the Surface Quality of Planed and Spindle Moulded Wooden Products
PhD Thesis, 1986

Kivimaa E. 1950
Cutting Forces in Woodworking
PhD Thesis
Finland Institute of Technology
1950

Knudsen V.O. 1928
"Hearing" with a Sense of Touch
Journal of General Psychology, Vol 1
1928, pp. 320-352.

Koch P. 1955
An Analysis of the Lumber Planing Process: Part I
Forest Products Journal
August, 1955, pp.255-263.

Koch P. 1956
An Analysis of the Lumber Planing Process: Part II
Forest Products Journal
October, 1956, pp.393-401.

Koch P. 1964
Woodmachining Processes
Roland Press Company
New York
1964

Mansfield J.H. 1952
Woodworking Machinery, History and Development 1852-1952
Journal of American Society of Mechanical Engineers
1952, Vol 74

Maycock K.M, Parkin R.M, Buttery T. 1987
Measurement and Control Techniques for Timber Production Processes
Proc. of 3rd Conference on Sensors and their Applications
Cambridge, September, 1987

Mitsui K. 1986
In-Process Sensor for Surface Roughness and their Applications
Precision Engineering, Vol 8, No. 4
October 1986

Mori M and Hoshi T 1964
Studies of Surfacing of Wood with Planers (II)
Bulletin of the Government Forest Experimental Station No.163
Tokyo, Japan
February 1964.

Mulvaney D.J, Newland D.E. 1986
A Comparison of orthogonal transforms in their Application to Surface Texture Analysis
Proceedings of Institute of Mechanical Engineers
1986, Vol 200, No. C6.

Parkin R.M. 1988
The Application of CIM to Planing and Moulding Machines in the Woodworking Industry
COMODEM 88: The First UK Seminar on Condition Monitoring and Diagnostic Engineering Management
City of Birmingham Polytechnic, Birmingham
19th- 21st September, 1988

Peklenik J. 1968
New Developments in Surface Characterisation and Measurements by means of Random Process Analysis
Mechanical Engineering Conference: Properties and Metrology of Surfaces, paper 24, Oxford
April, 1968

Pernick B.J. 1979
Surface Roughness Measurements with an Optical Fourier Spectrum Analyzer
Applied Optics
15 March, 1979, Vol 18, No. 6

Petter C. 1954
Development Work on Wood Planers
Journal of Forest Product Research Society
1954, Vol 561, pp. 134-136

Phillips M.J, Whitehouse D.J. 1977
Some Theoretical Aspects of the Measurement of Curved Surfaces
Journal of Physics E: Scientific Instruments
1977, Vol 10, p.164

Pryor T.R, Hagemoers O.L, North W.P.T. 1972
Diffractographic Dimensional Measurement.
Part 1: Displacement Measurement
Part 2: Profile Measurement
Applied Optics
February, 1972, Vol 11, No. 2, pp.308-318

Quality Today - Measurement and Inspection Technology 1986
Roughness in the Palm of Your Hands
March, 1986, p.37

Rabiner L.R, Gold B. 1975a
Theory and Application of Digital Signal Processing
Prentice-Hall inc. pp.89-90
1975

Rabiner L.R, Gold B. 1975b
Theory and Application of Digital Signal Processing
Prentice-Hall inc. pp.26-28
1975

Rakels J.H. 1986
Diffraction - an old optical phenomenon used as an advanced metrology tool
Modern Production and Metrology Seminar
Technische Universitat
Vienna paper 79.3

Schmaltz G. 1936
Techinsche Oberflachenkunde
Springer, Berlin
1936

Schwartz M, Shaw L 1975
Signal Processing: Discrete spectral analysis, detection and Estimation
McGraw-Hill Book Company
1975 pp. 162-168

Sherrington I, Smith E.H. 1988
Modern Measurement Techniques in Surface Metrology
Wear
1988, Vol 125, part 3, pp.271-288

Smith P.F, Player M.A, Collie D.L.A. 1988
The Determination of Surface Topology by the Signal Processing of Ultrasonic Pulses
J. Phys. E: Sci. Instrum.
1988, Vol 21, pp.397-402

Sommargren G.E. 1981
Optical Heterodyne Profilometry
Appl. Opt. Vol 20 p.610

Stevens D.M.G. 1989
An Investigation into the use of a Wide Range Interferometric Transducer for Roundness Measurement
M Phil Thesis
Leicester Polytechnic
August 1989.

Stumbo D.A. 1960
Surface Texture Measurement for Quality of Production Control
Forest Product Journal
February, 1960, pp.122-124

Stumbo D.A. 1963
Surface Texture Measurement Methods
Forest Product Journal
July, 1963, pp.299-303

Thomlinson J. 1987
CIM - Bringing the Islands Together
Chartered Mechanical Engineer
March, 1987, pp.49-51

Thomlinson R, Harrington J.S. 1960
Rotary Cutting
Forest Products Journal
October, 1960, pp.419-421

Timber Trades Journal 1986a
Weinig Launch a New CNC System
October, 1986, pp.43-44

Timber Trades Journal 1986b
High-speed Spindles come of age in the new XR130 Moulder from Wadkin
22 November, 1986, pp.25-26

Timber Trades Journal 1987
SCM The Dynamic Giant
9th May, 1987, pp.30-32

Timber Trades Journal 1990a
Thumbs Up for Woodmex
November, 1990, pp.16-20

Timber Trades Journal 1990b
The Clock Watcher
October, 1990, pp.21-22

Toshimitsu A. and Hitoshi F 1977
Roughness Measurements of metal Surfaces using Laser Speckle
J. Opt. Soc. Am.,
September, 1977, Vol 67, No. 9

Whitehouse D.J 1972
Modern Methods of Assessing the Quality and Functions of Surfaces
Proc. Soc. Manufacturing Engineers
Chicago
1972

Whitehouse D.J. 1985
Instrumentation for Measuring Finish Defects and Gloss
SPIE, Vol 525, p.106

Whitehouse D.J, Bowen D.K, Chetwynd et al 1987
Nano-Calibration for Stylus Based Surface Measurement
Physics Engineering, Vol 21, Part 1, pp.46-51.

Wyant J.C. 1985
Optical Profilometers for Surface Roughness
SPIE Vol 525, p.174

FIGURES

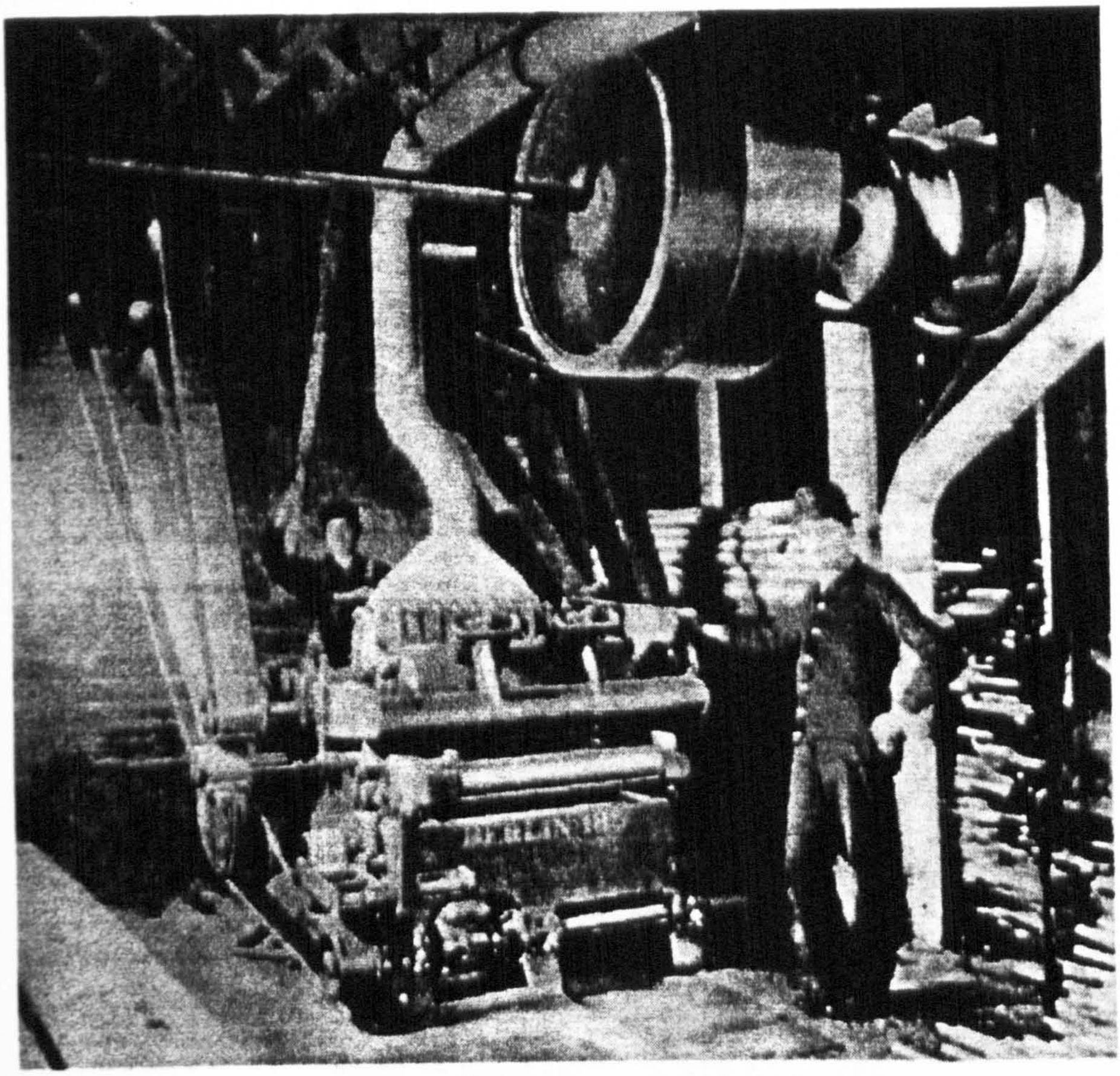

Figure 1.1: Early power-operated machinery was belt driven from lineshafts

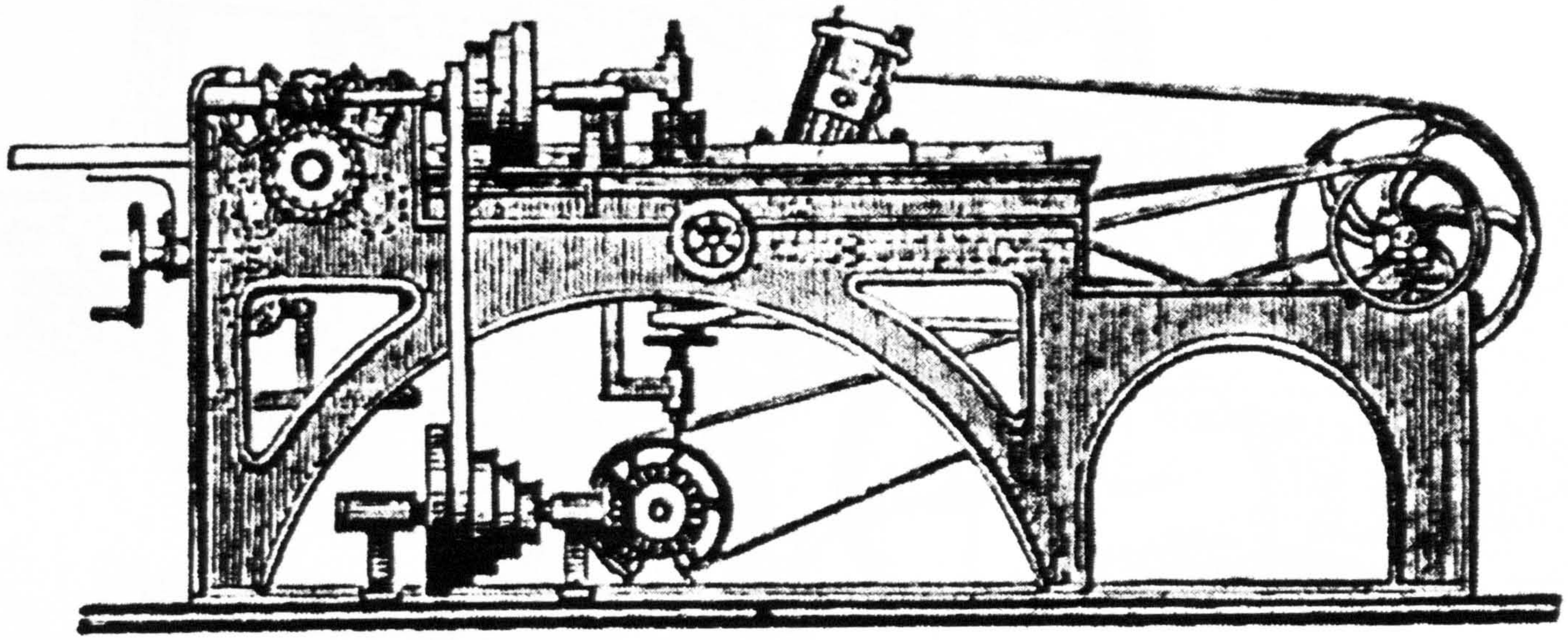

Figure 1.2: Malcolm Muir's Planer, 1827

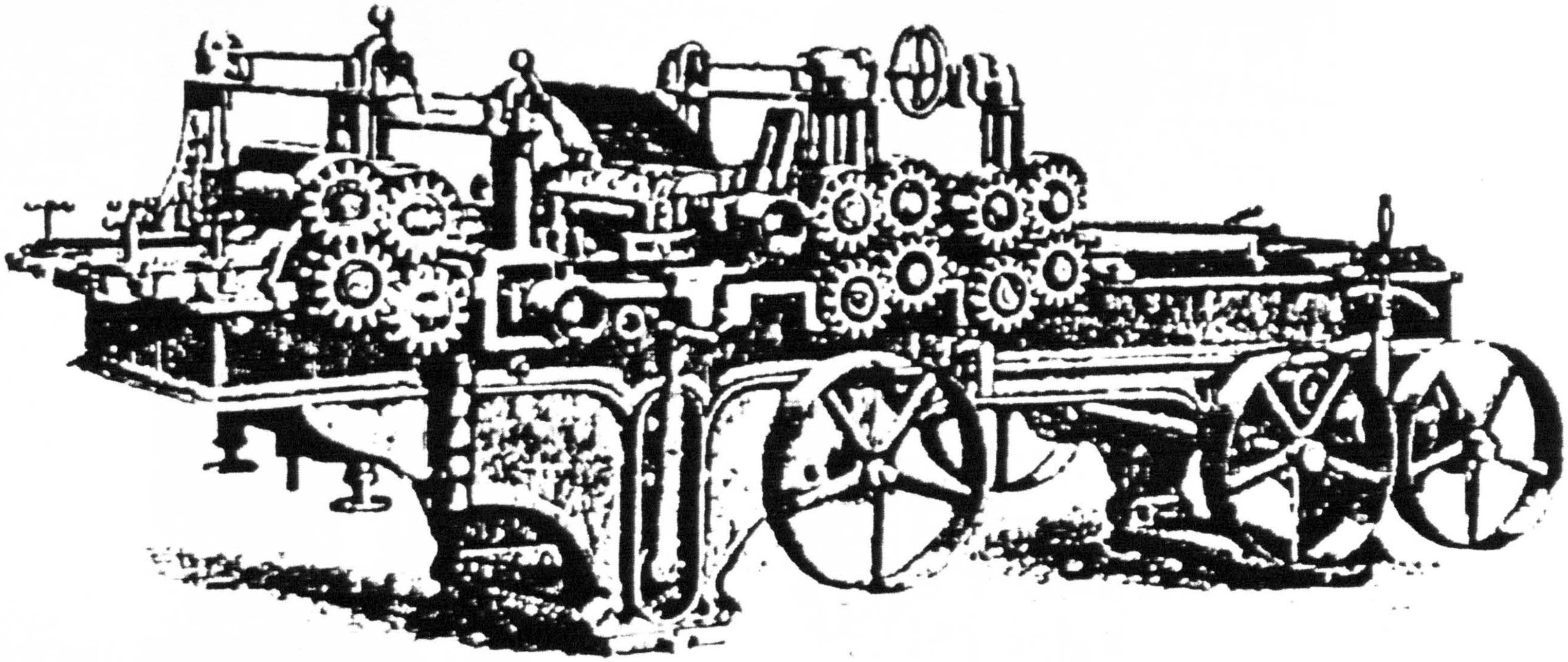

Figure 1.3: John McDowall's Planer, 1836

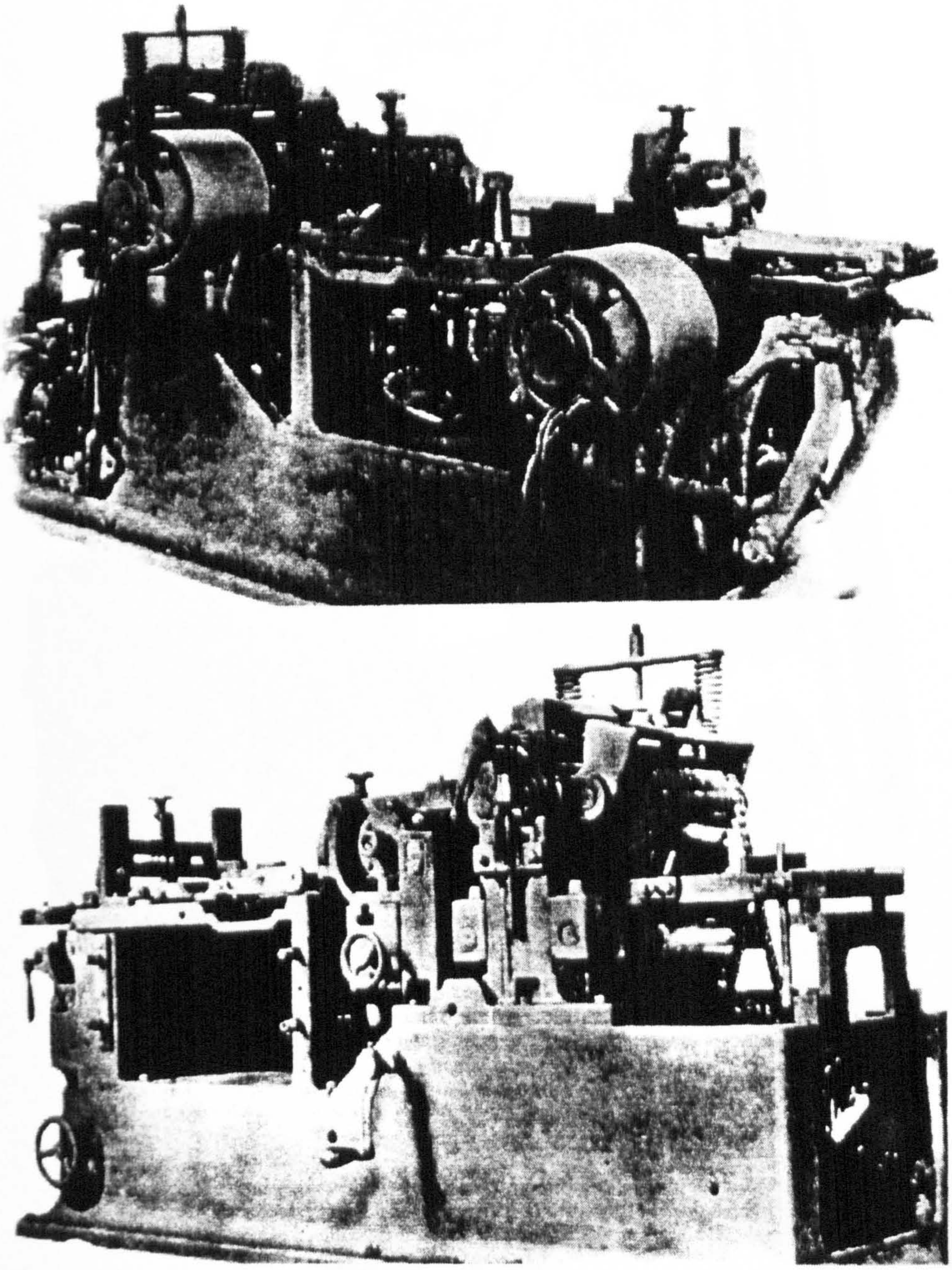

Figure 1.4: First Moulder with Integral Electric Motors, 1916

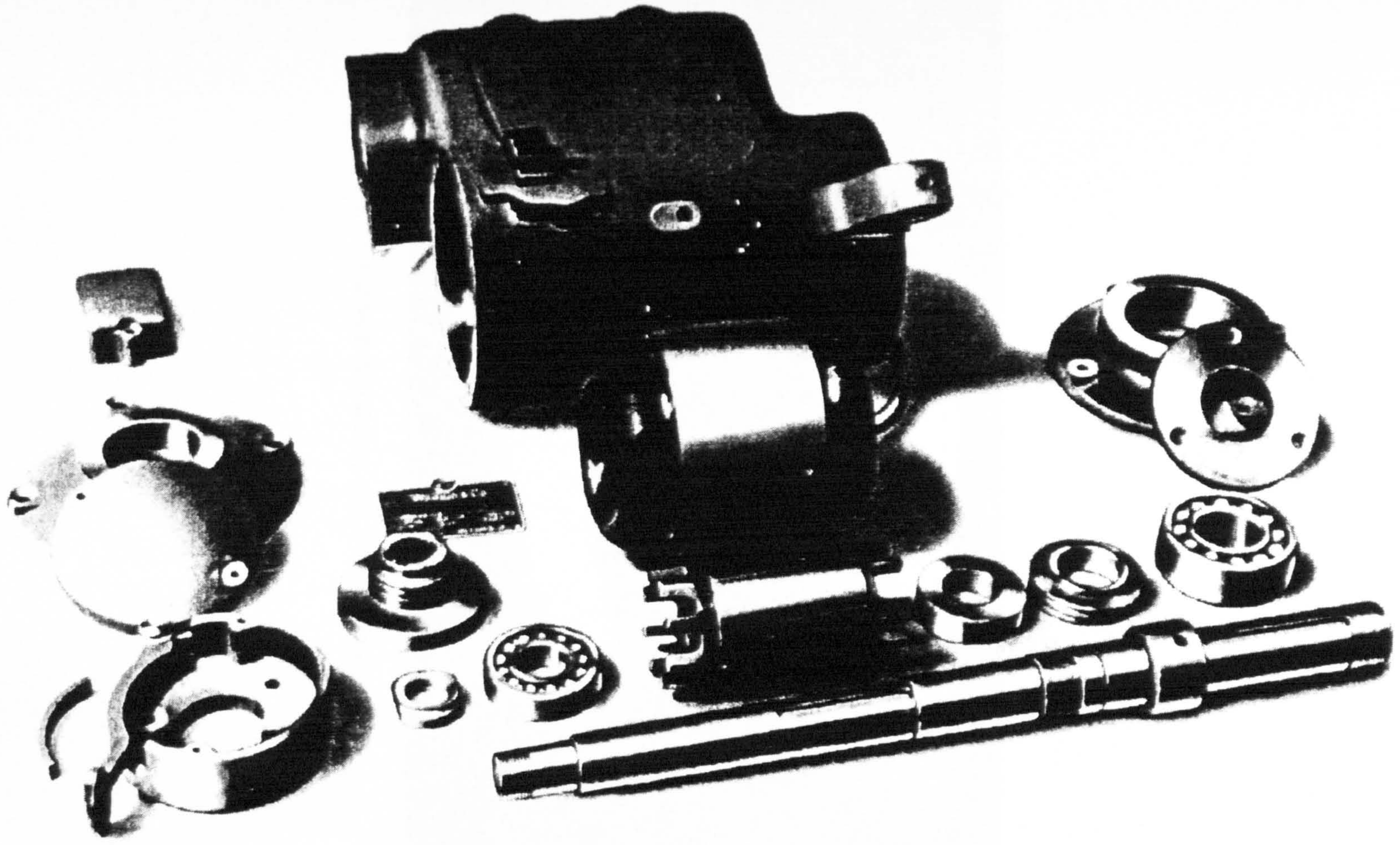

Figure 1.5: Elements of a Motorised Cutterhead with Spindle and Bearings

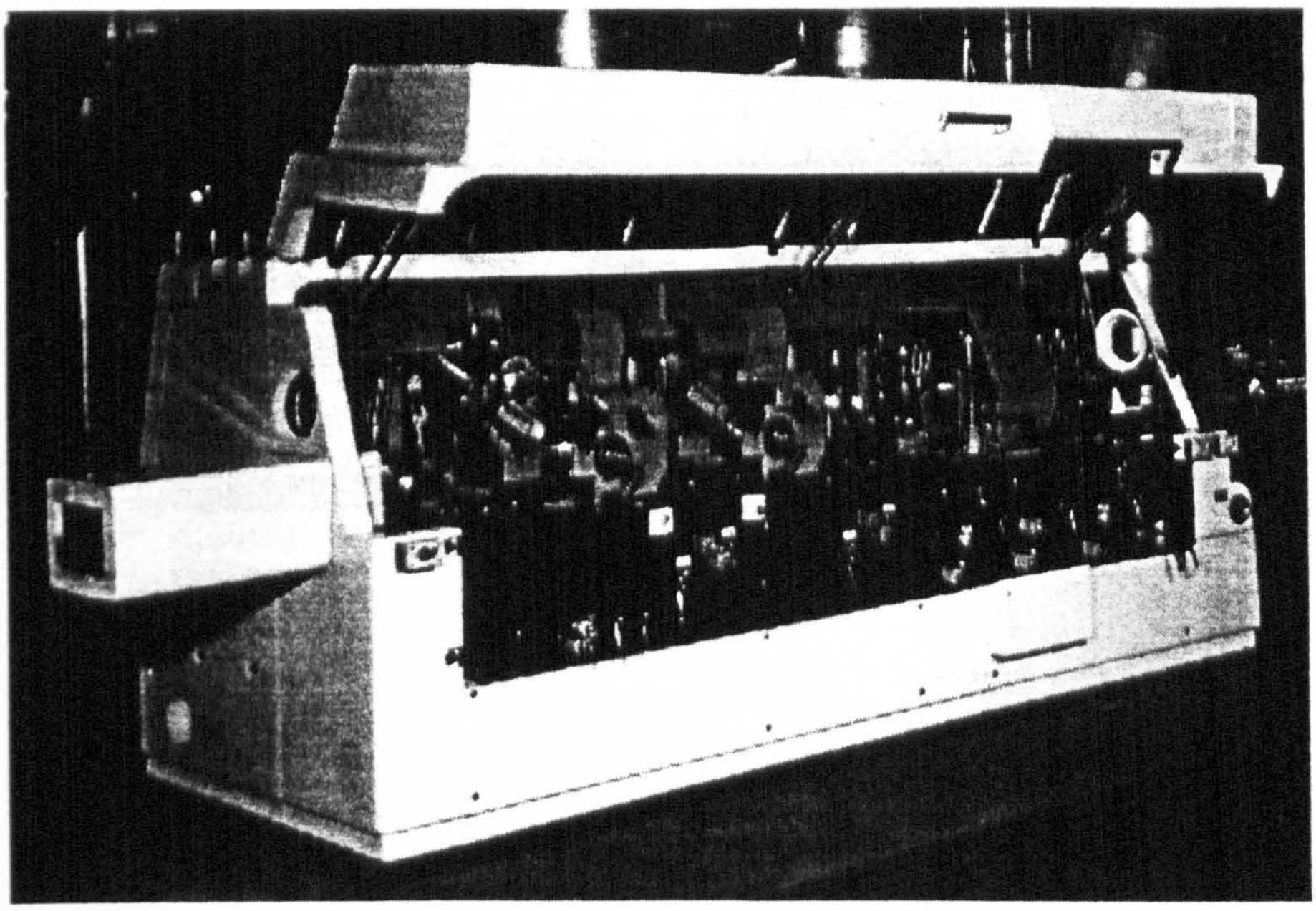

Figure 1.6: A Modern Moulding and Planing Machine

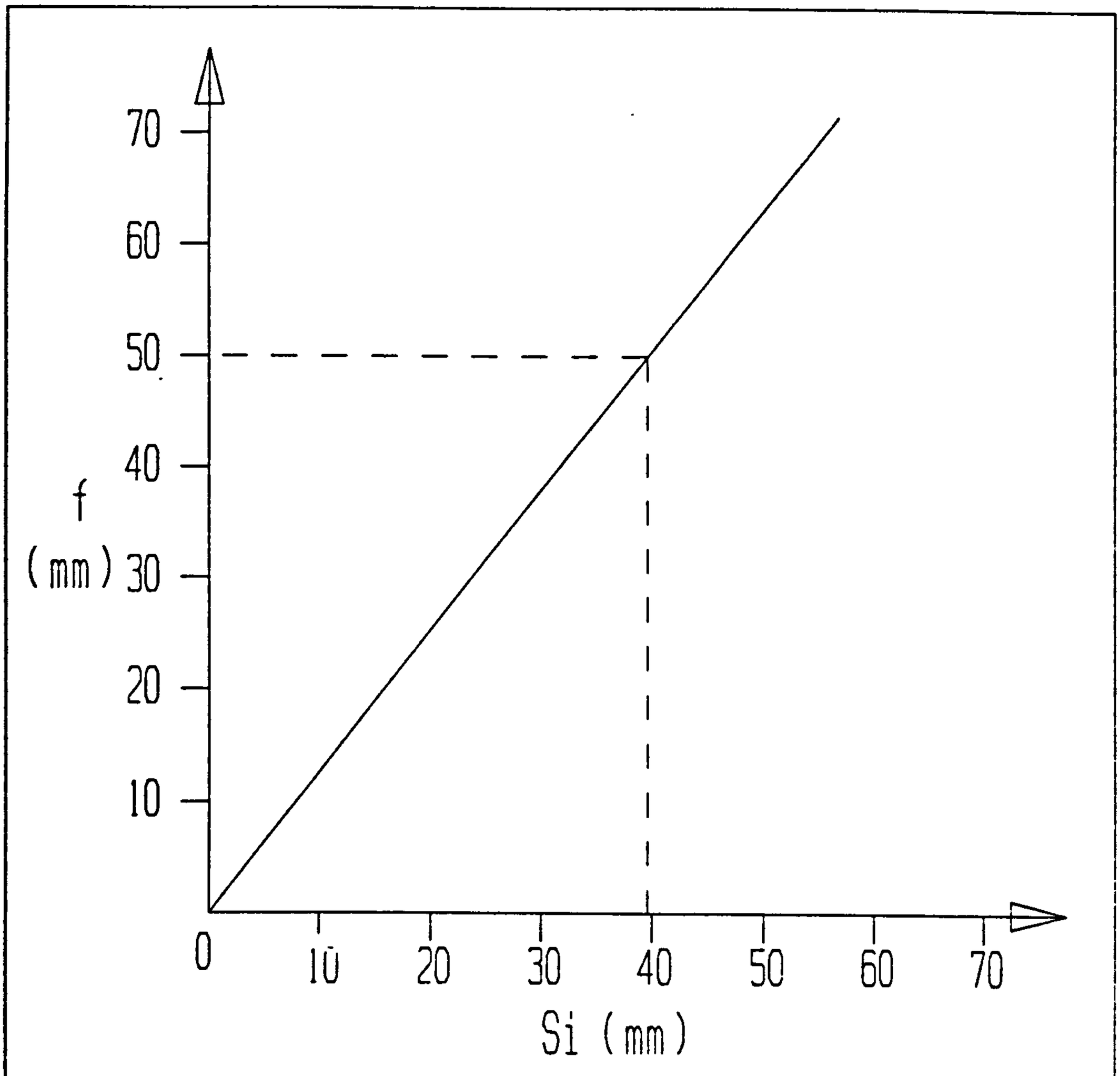

GRAPH OF FOCAL LENGTH against IMAGE DISTANCE

Figure 5.3.5

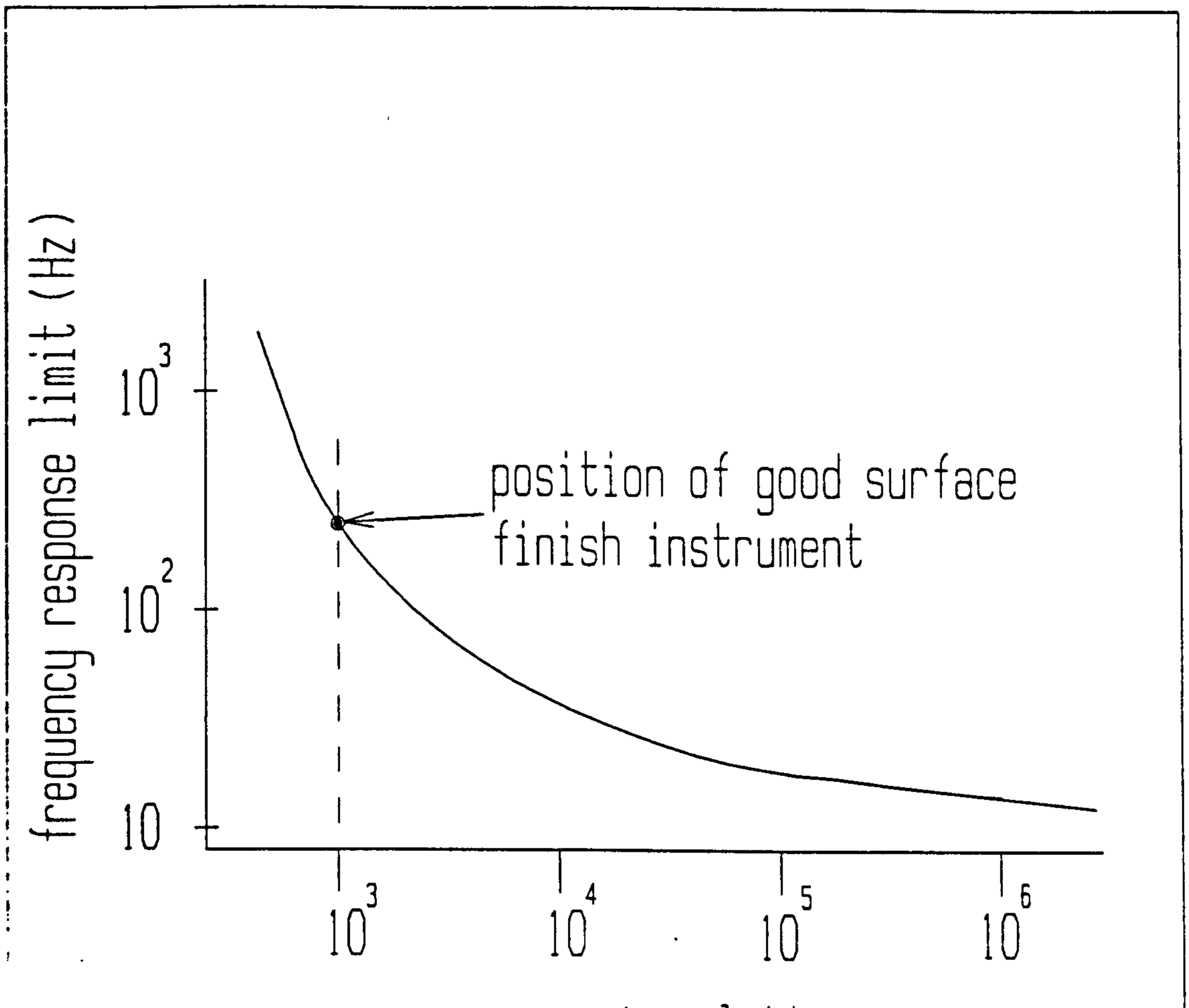

A METHOD OF ASSESSING SURFACE MEASURING INSTRUMENTATION

Figure 2.1

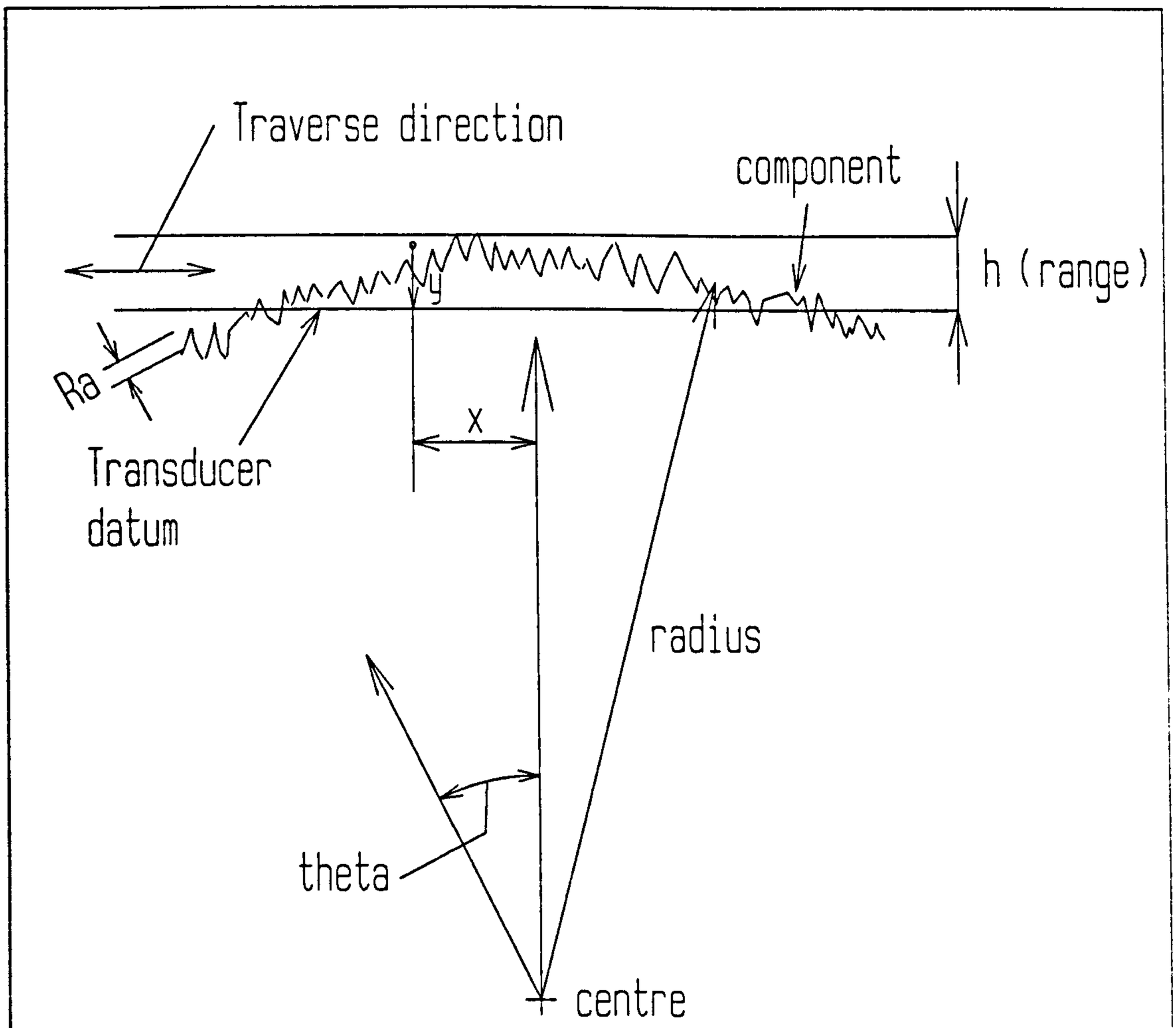

MULTI-FEATURE MEASUREMENT

Digital Methods combined with High-sensitivity wide-range transducers

Figure 2.2

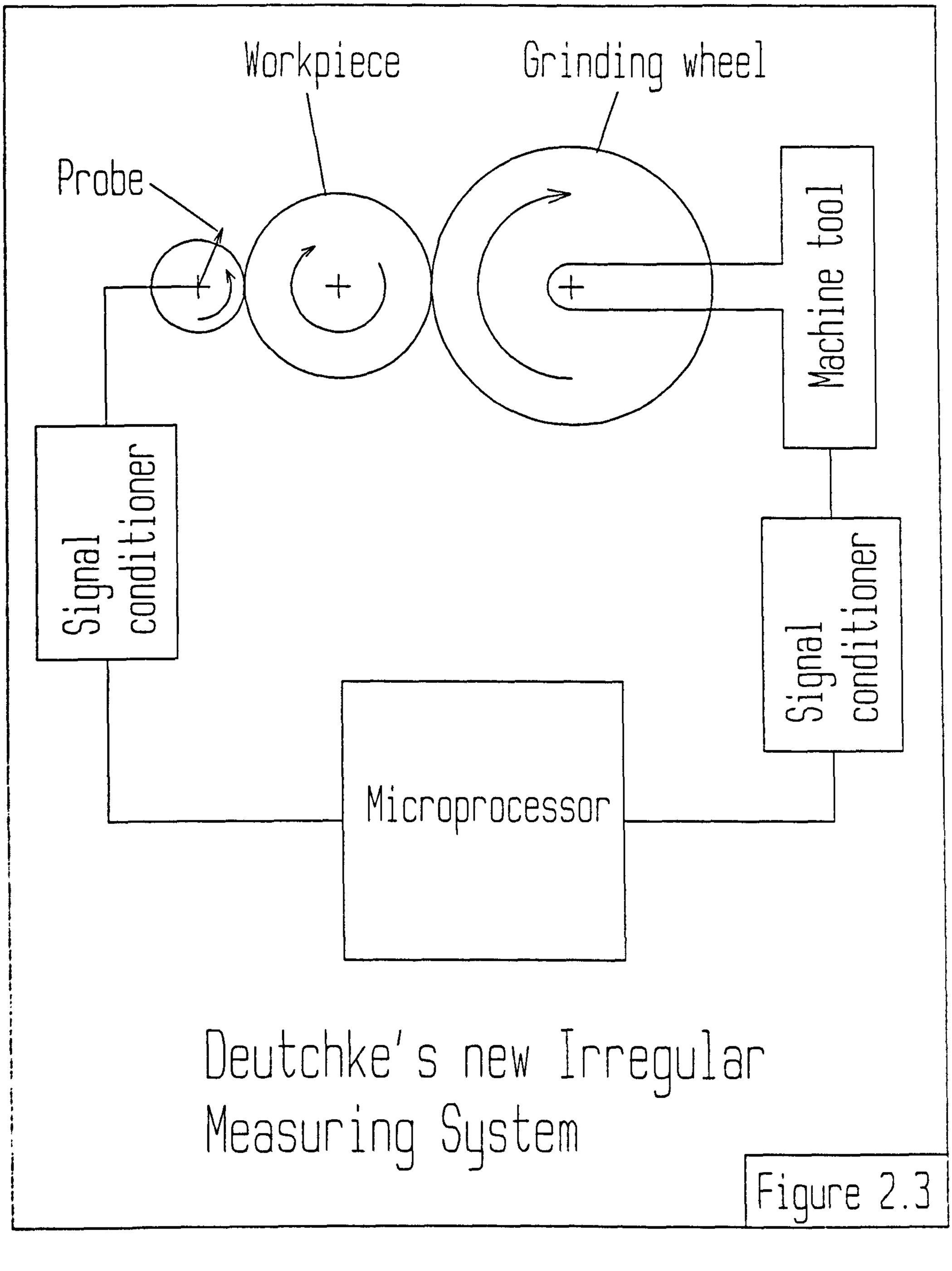
Workpiece
Grinding wheel
Probe
Machine tool
Signal conditioner
Signal conditioner
Microprocessor
Deutchke's new Irregular Measuring System

Figure 2.3

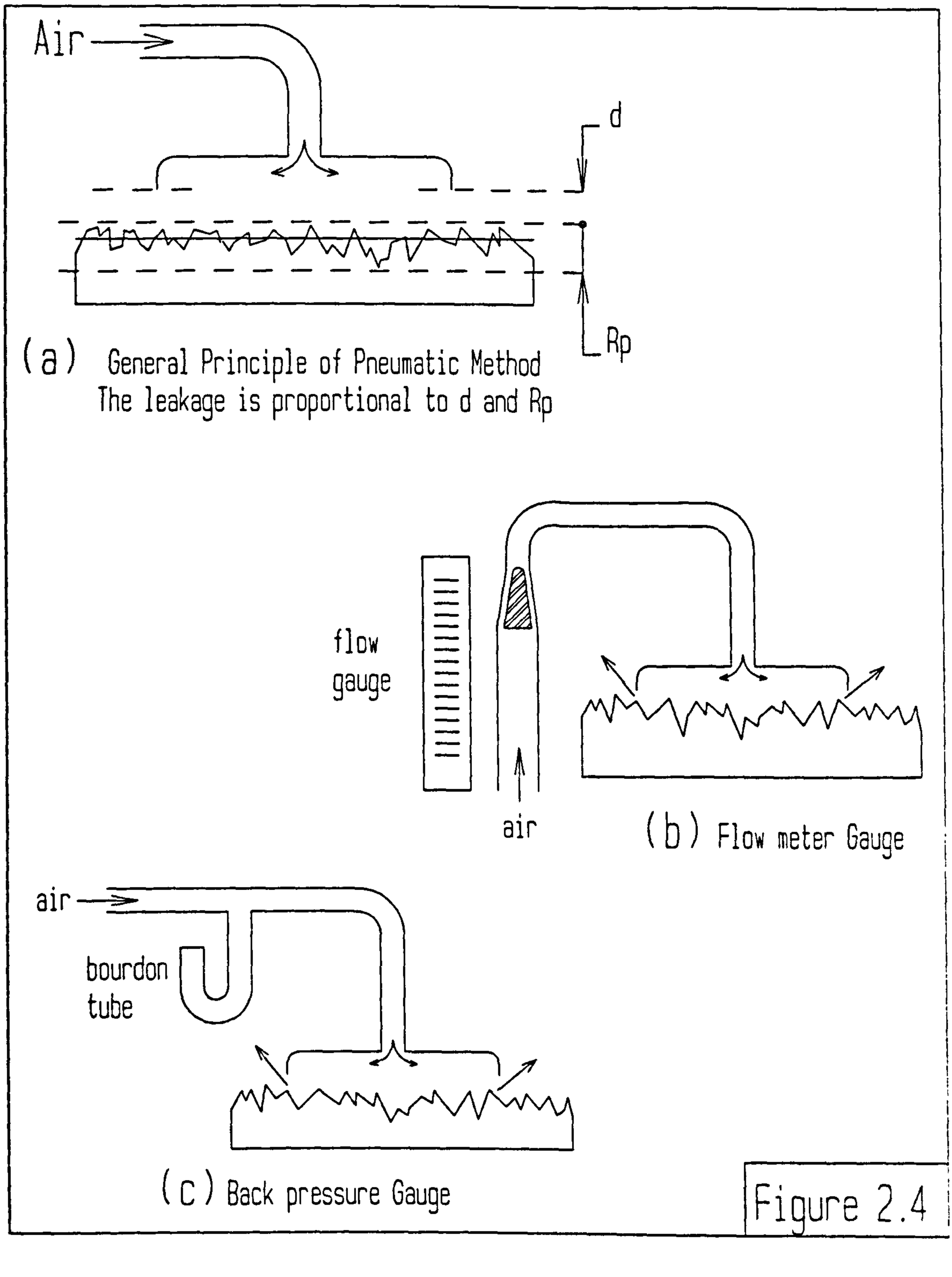
Air
d
Rp
(a) General Principle of Pneumatic Method
The leakage is proportional to d and Rp
flow
gauge
air
(b) Flow meter Gauge
air
bourdon
tube
(c) Back pressure Gauge

Figure 2.4

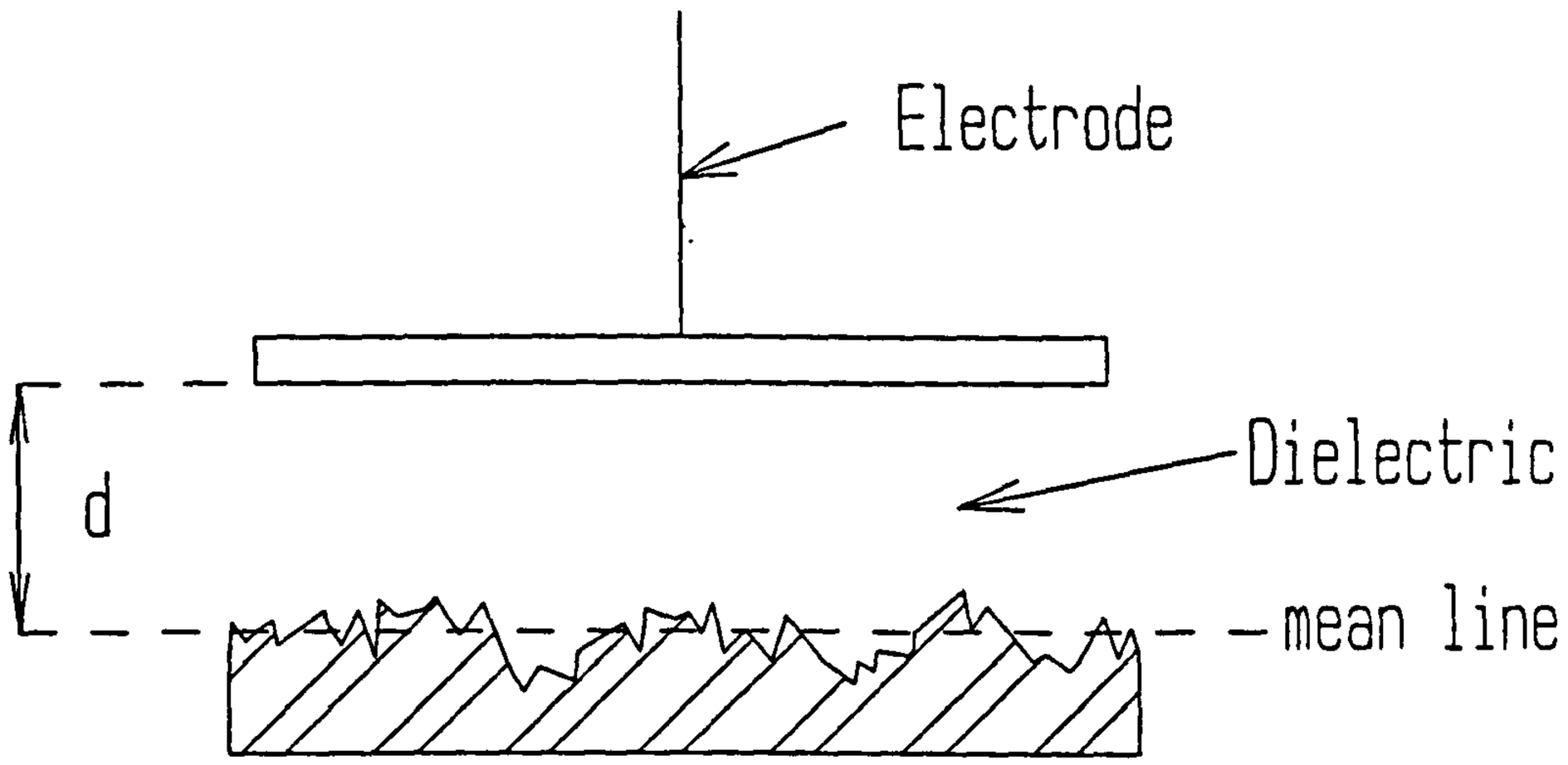

PRINCIPLE OF CAPACITIVE METHOD

Figure 2.5

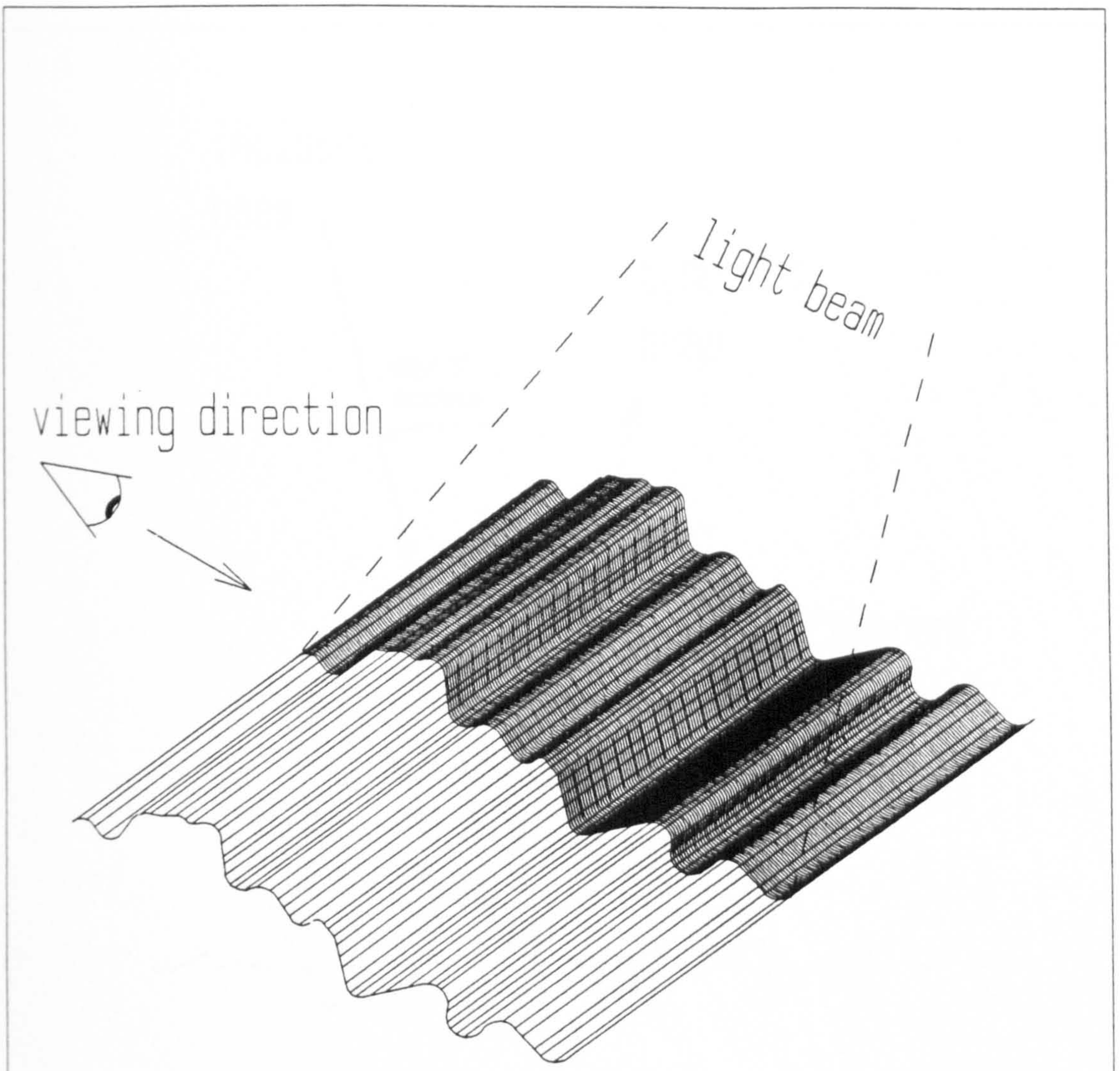

SCHMALTZ'S FIRST METHOD OF ASSESSING SURFACE FINISH

Figure 2.6

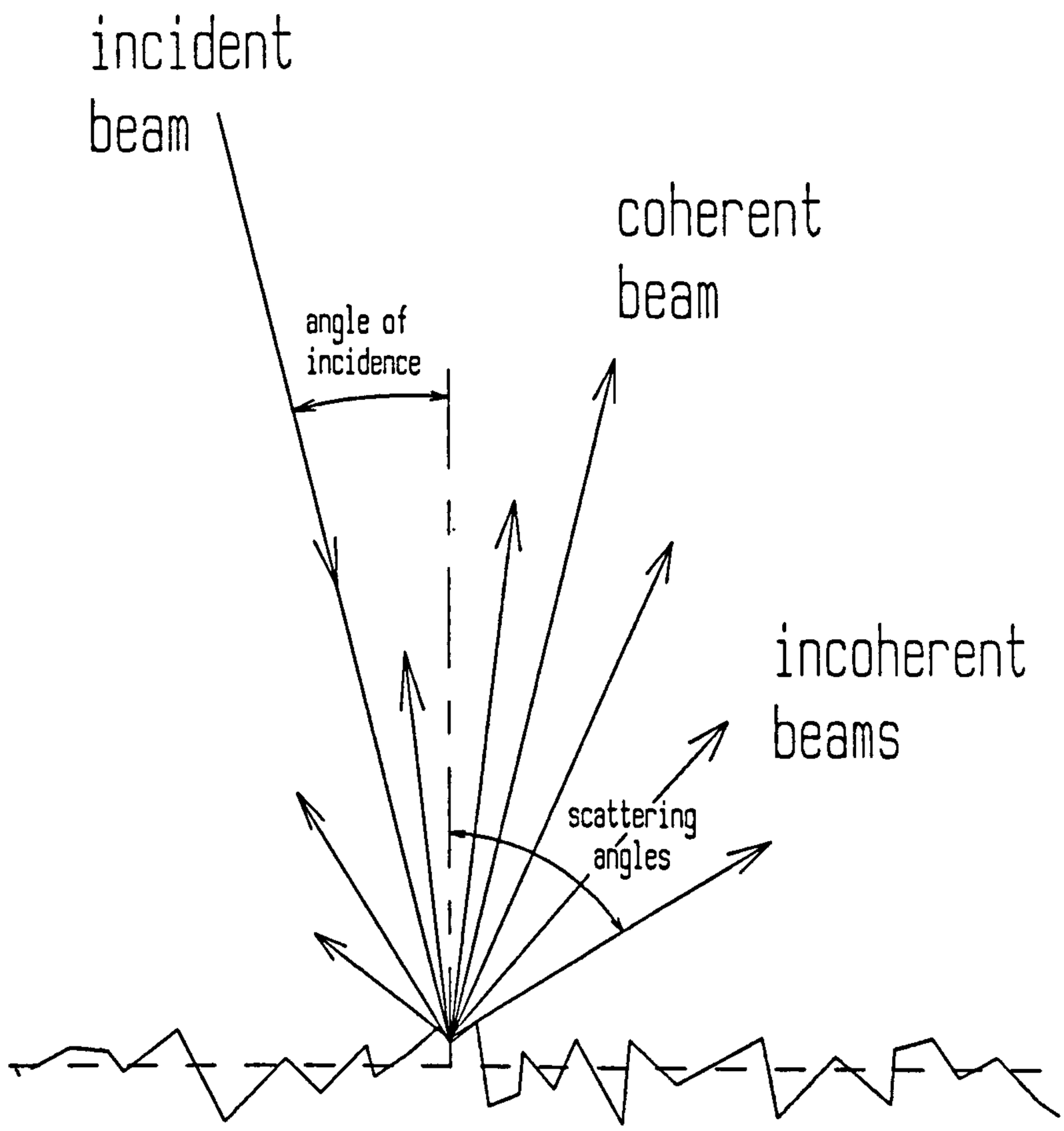

THE BASIC PRINCIPLES OF MOST OPTICAL TECHNIQUES

Figure 2.7

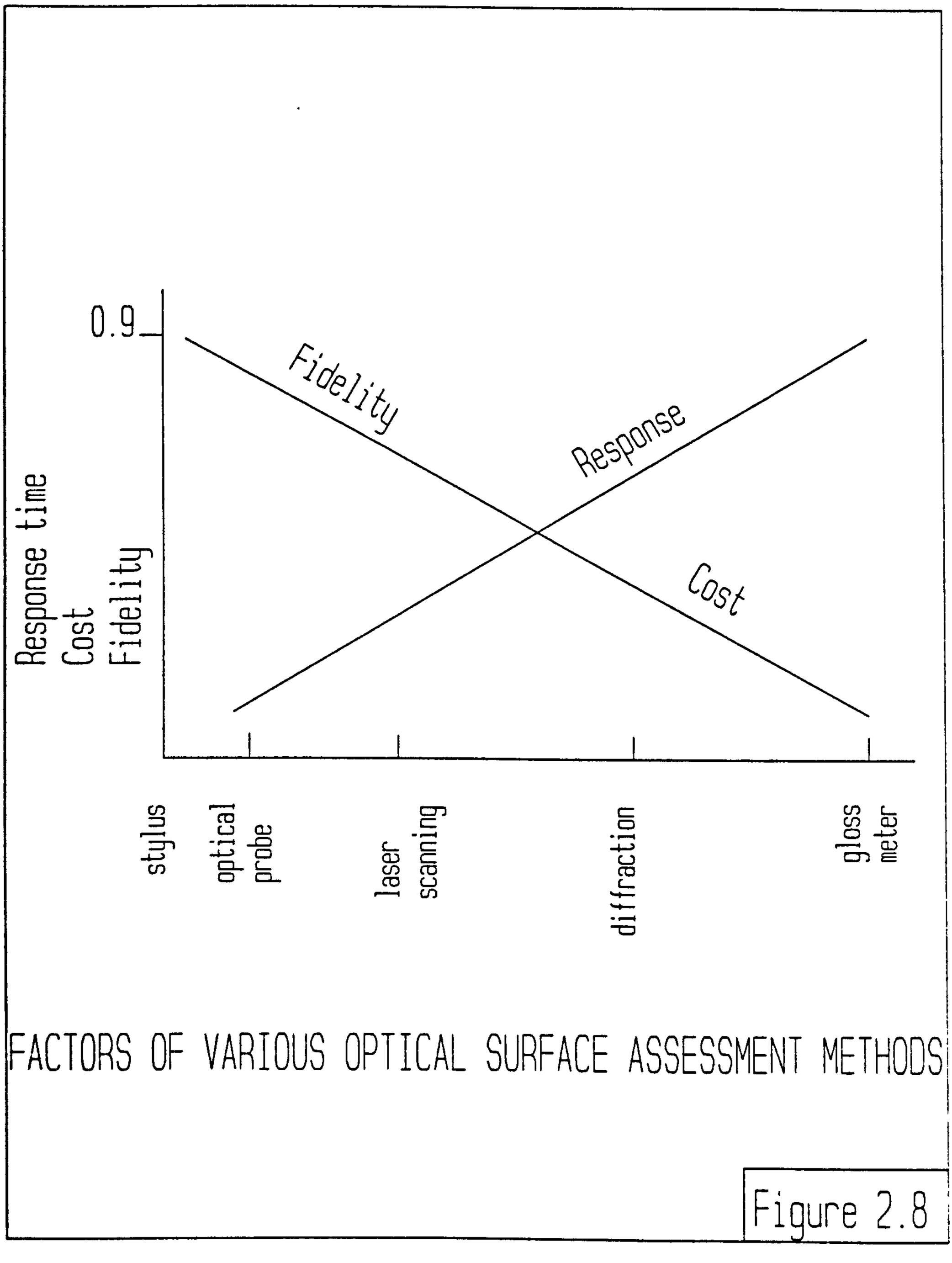

FACTORS OF VARIOUS OPTICAL SURFACE ASSESSMENT METHODS

Figure 2.8

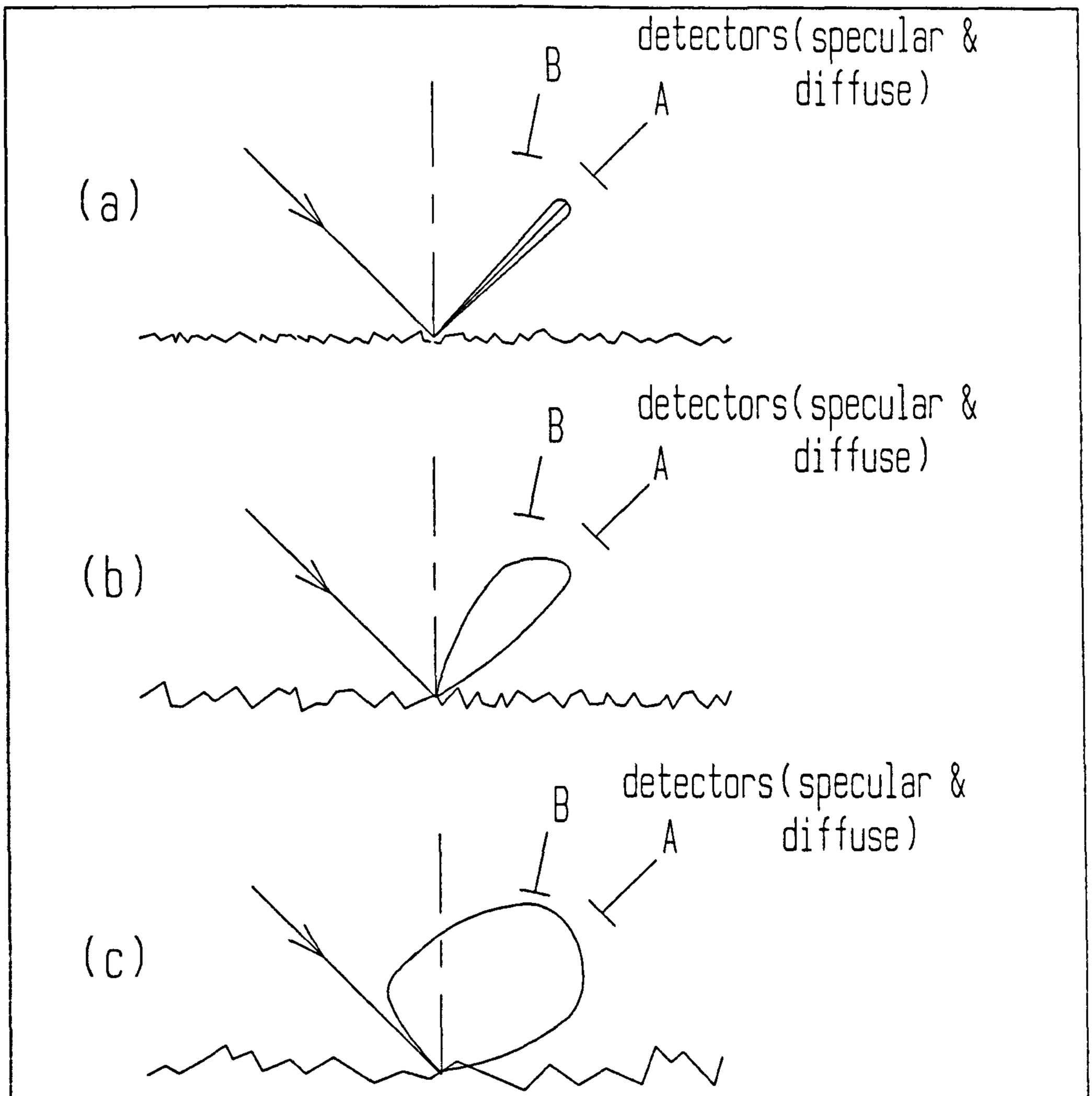

The Glossmeter Principle

The pattern of scattered light for various degrees of roughness
(a) Fine surface
(b) Medium surface
(c) Rough surface

Figure 2.9

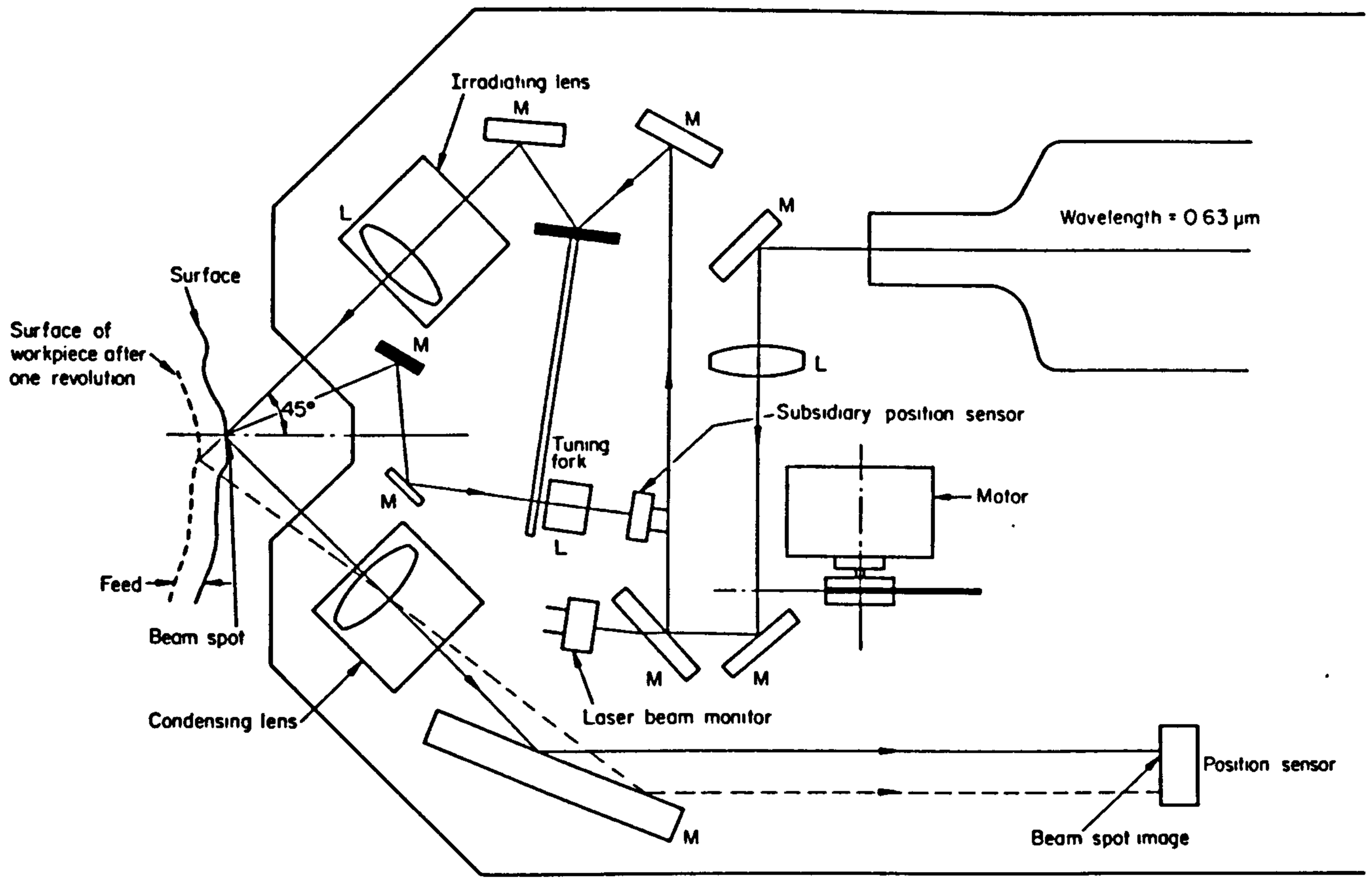

Optical system layout of a surface roughness sensor. L = lens and M = mirror

Figure 2.10: Mitsui's Instrument

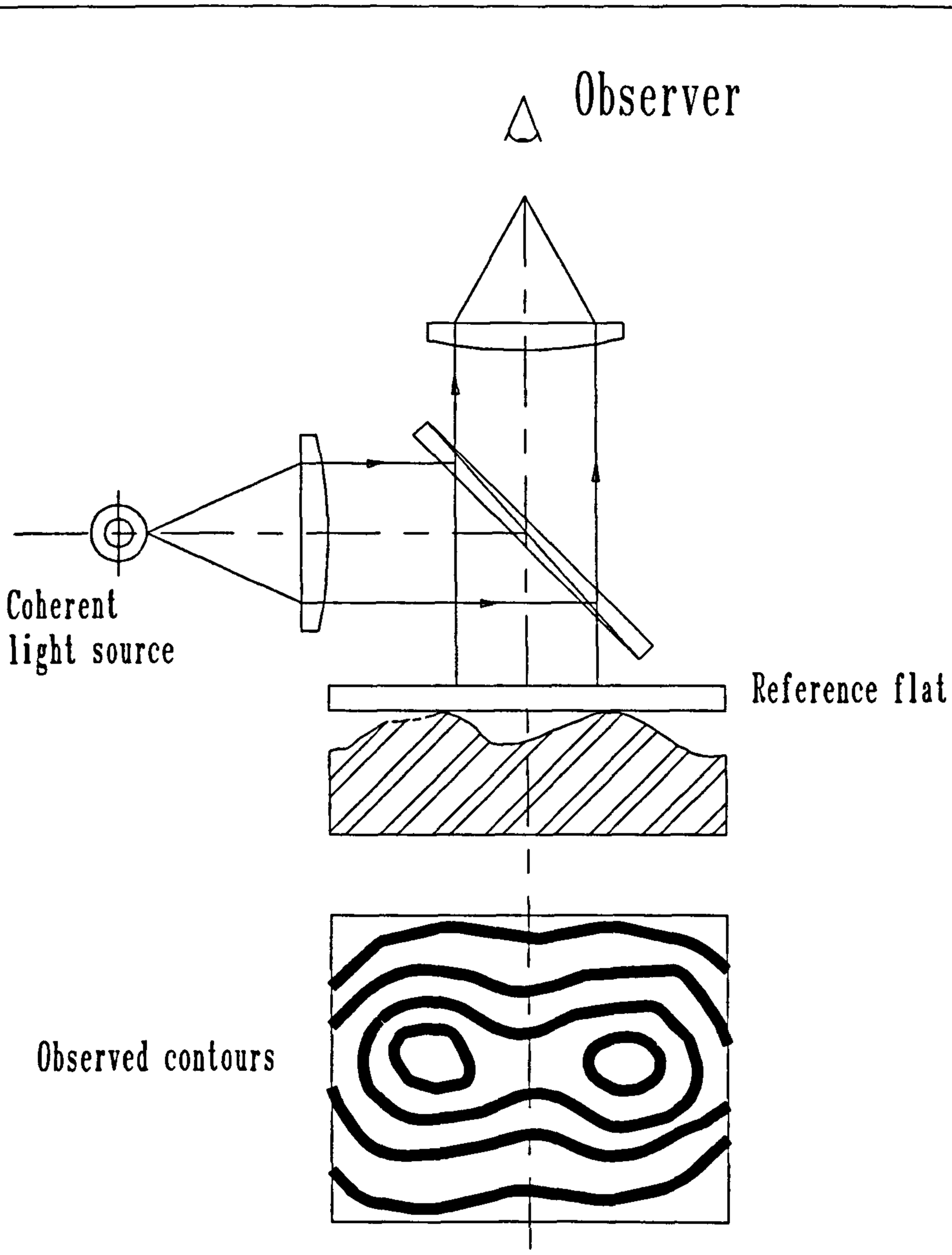

Interference Method for examining surface form

Figure 2.11

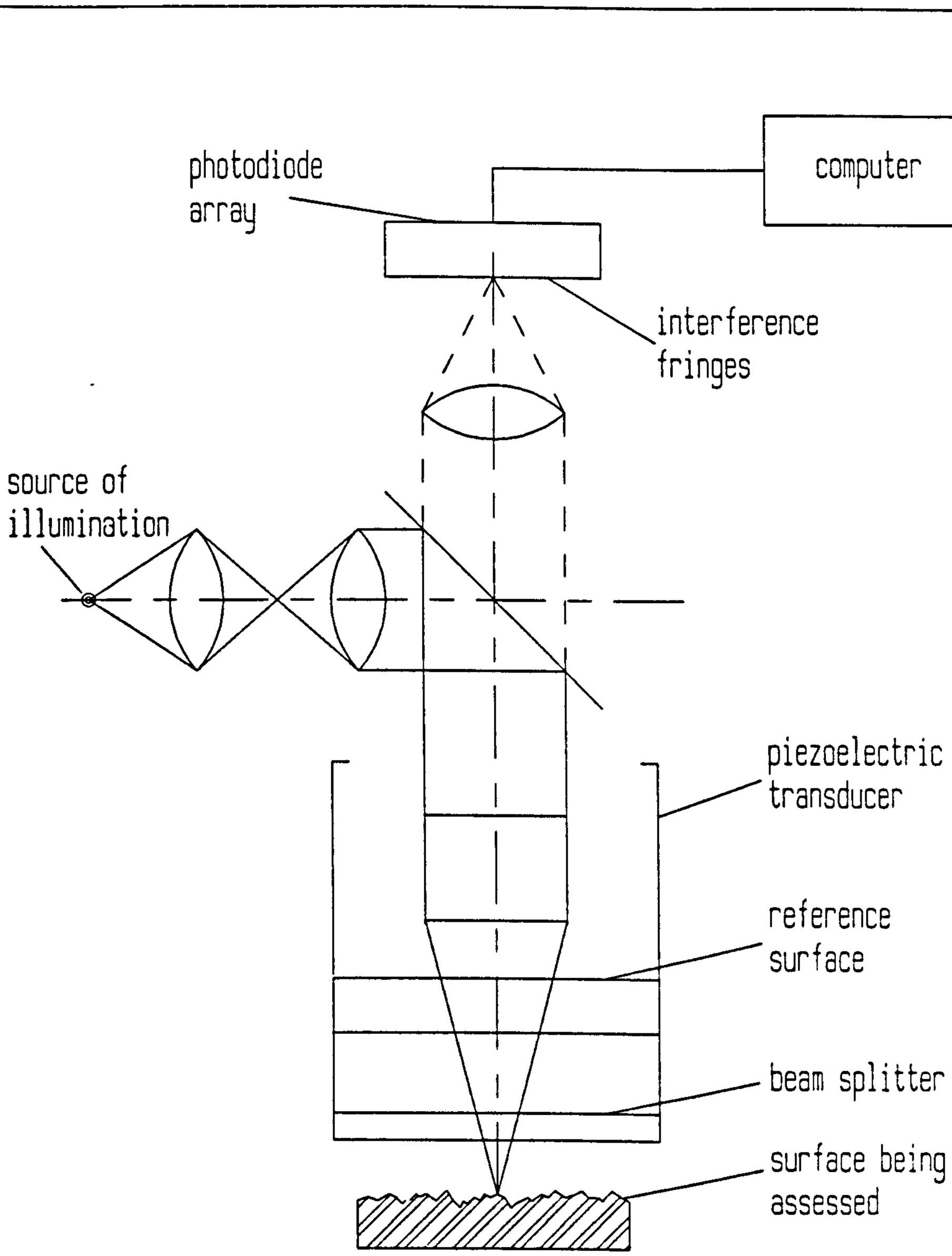

INTERFEROMETER PRINCIPLE

Figure 2.12

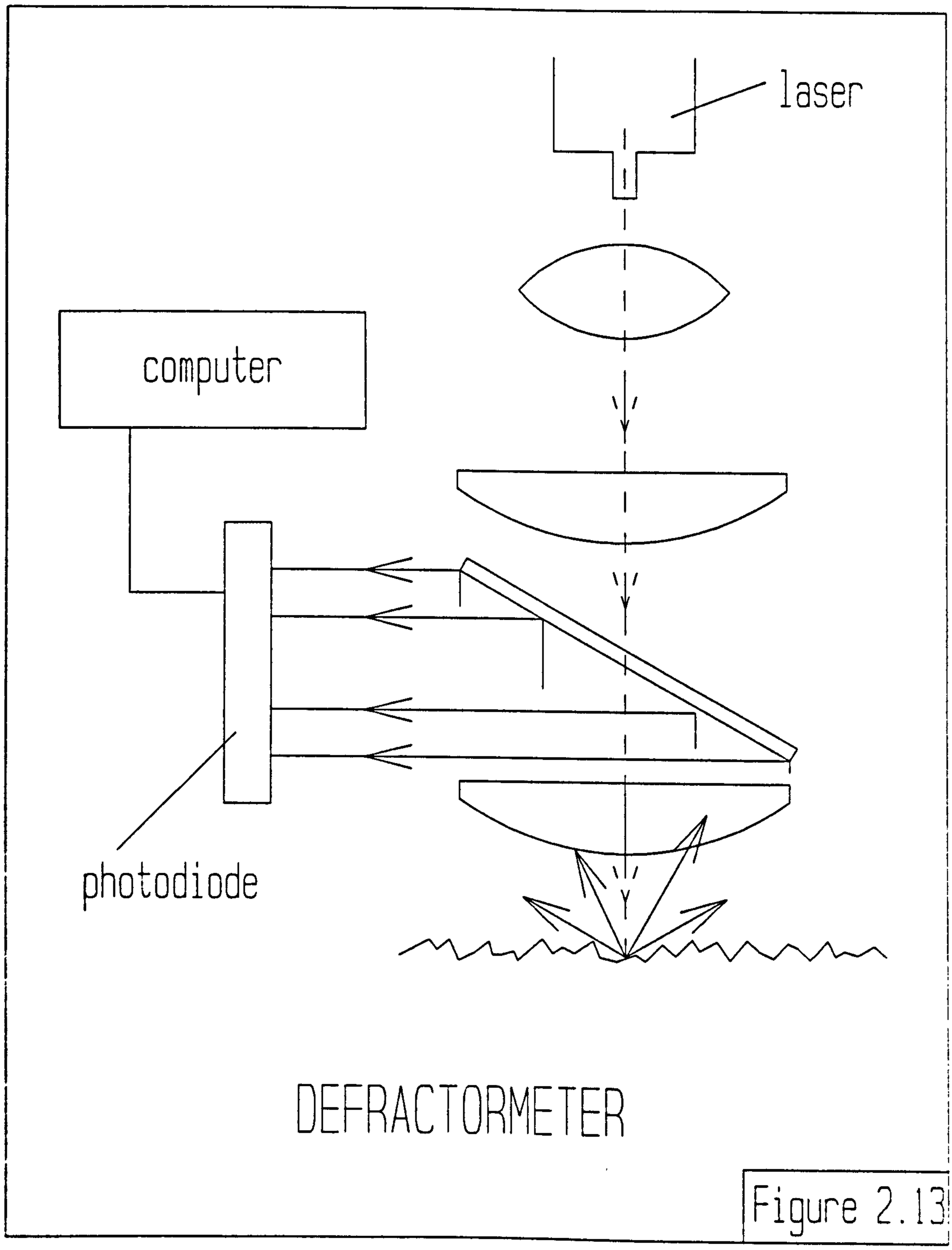

Figure 2.13

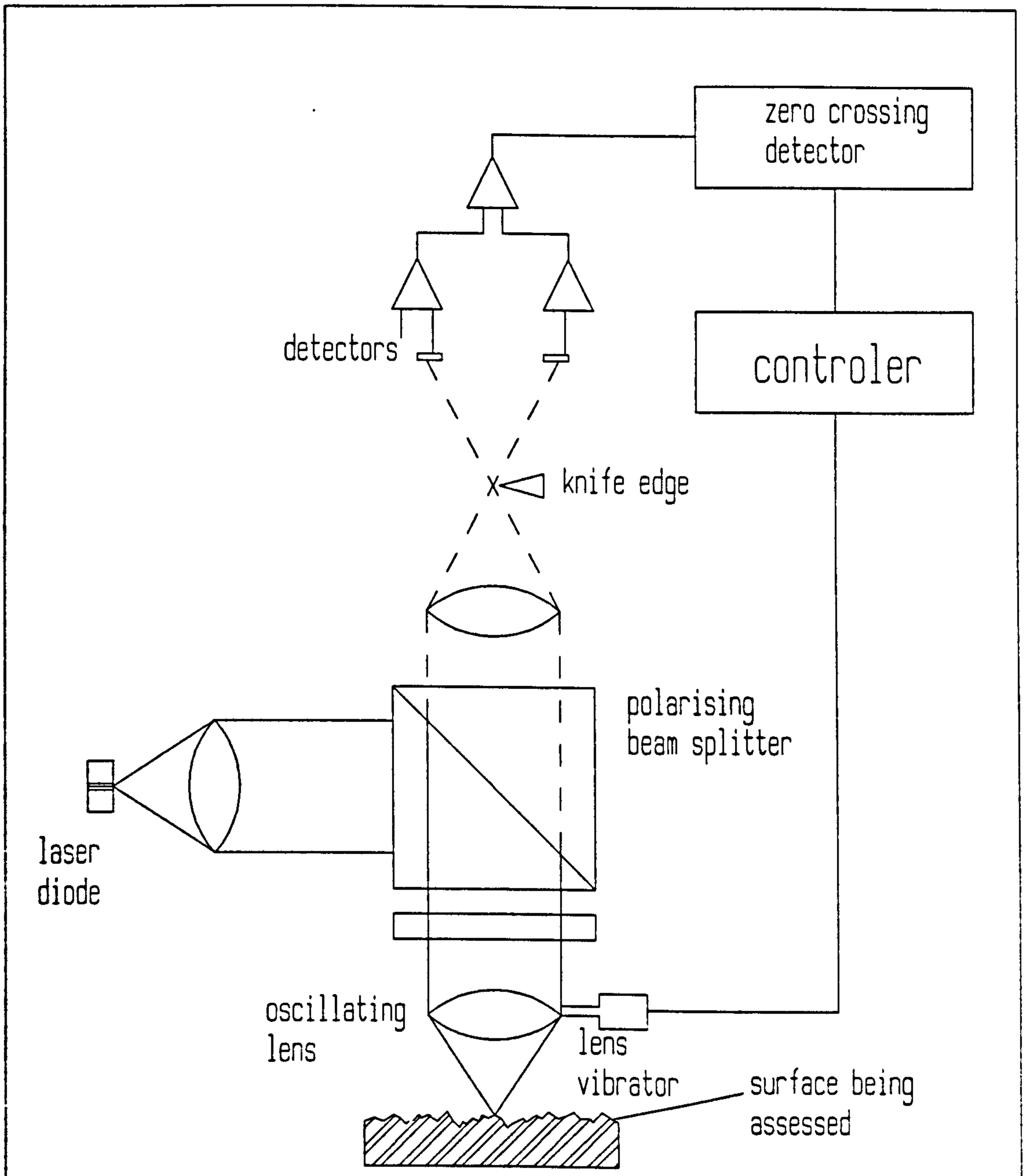

FOUCAULT KNIFE-EDGE METHOD

Figure 2.14

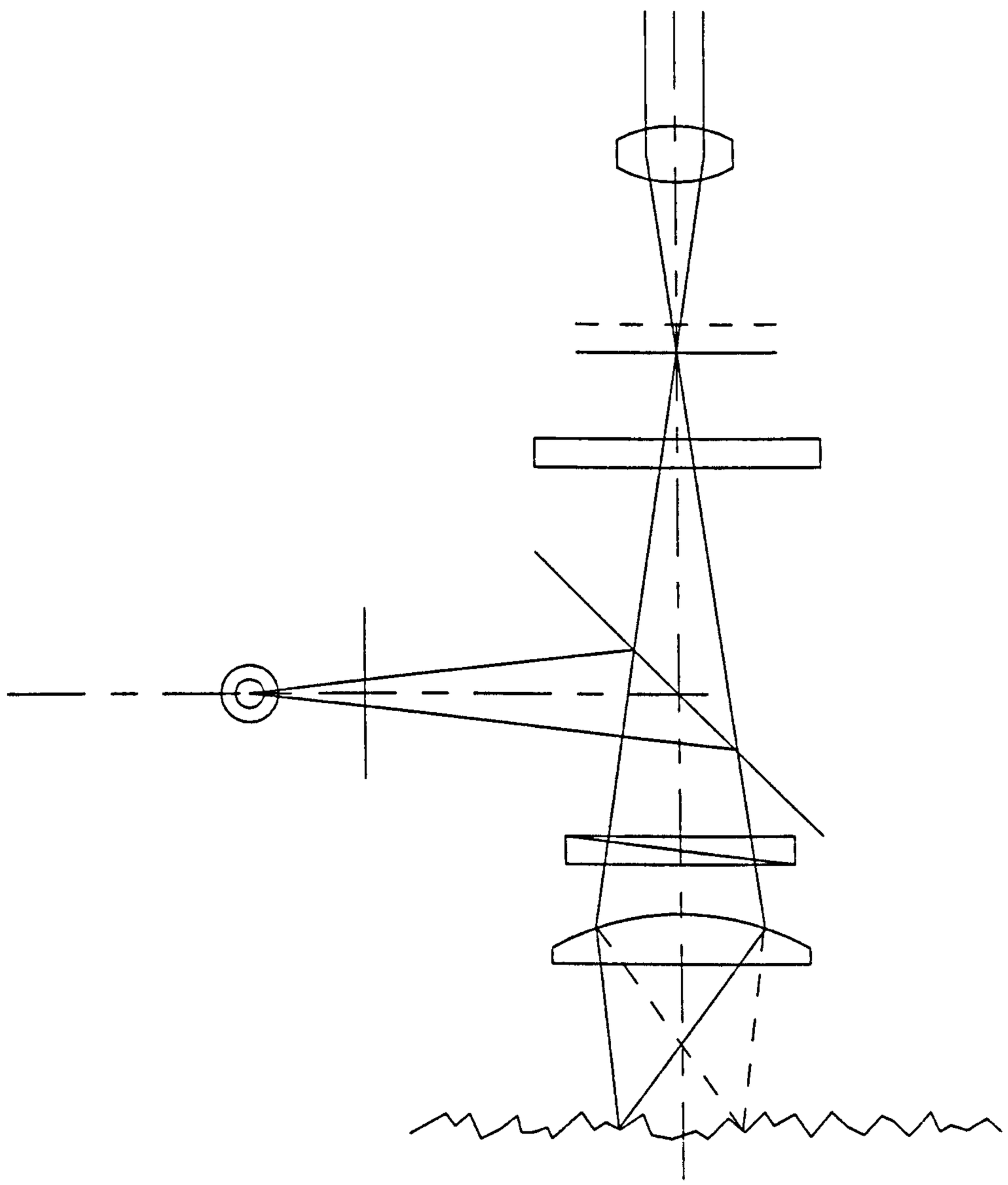

SCHEMETIC DIAGRAM OF A HETERODYNE METHOD

Figure 2.15

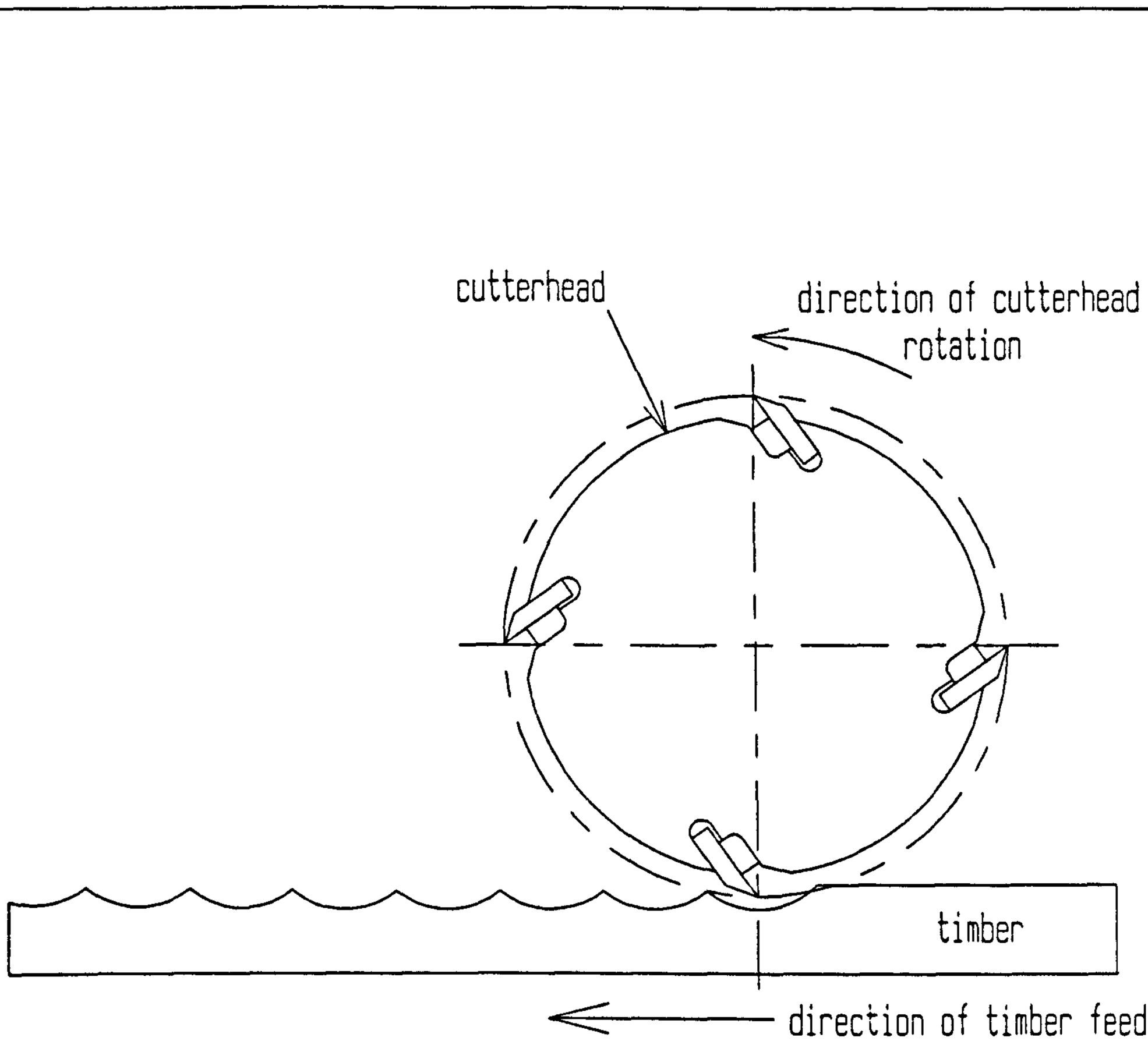

UP-CUTTING MODE USED IN WOODWORKING INDUSTRY

Figure 3.1

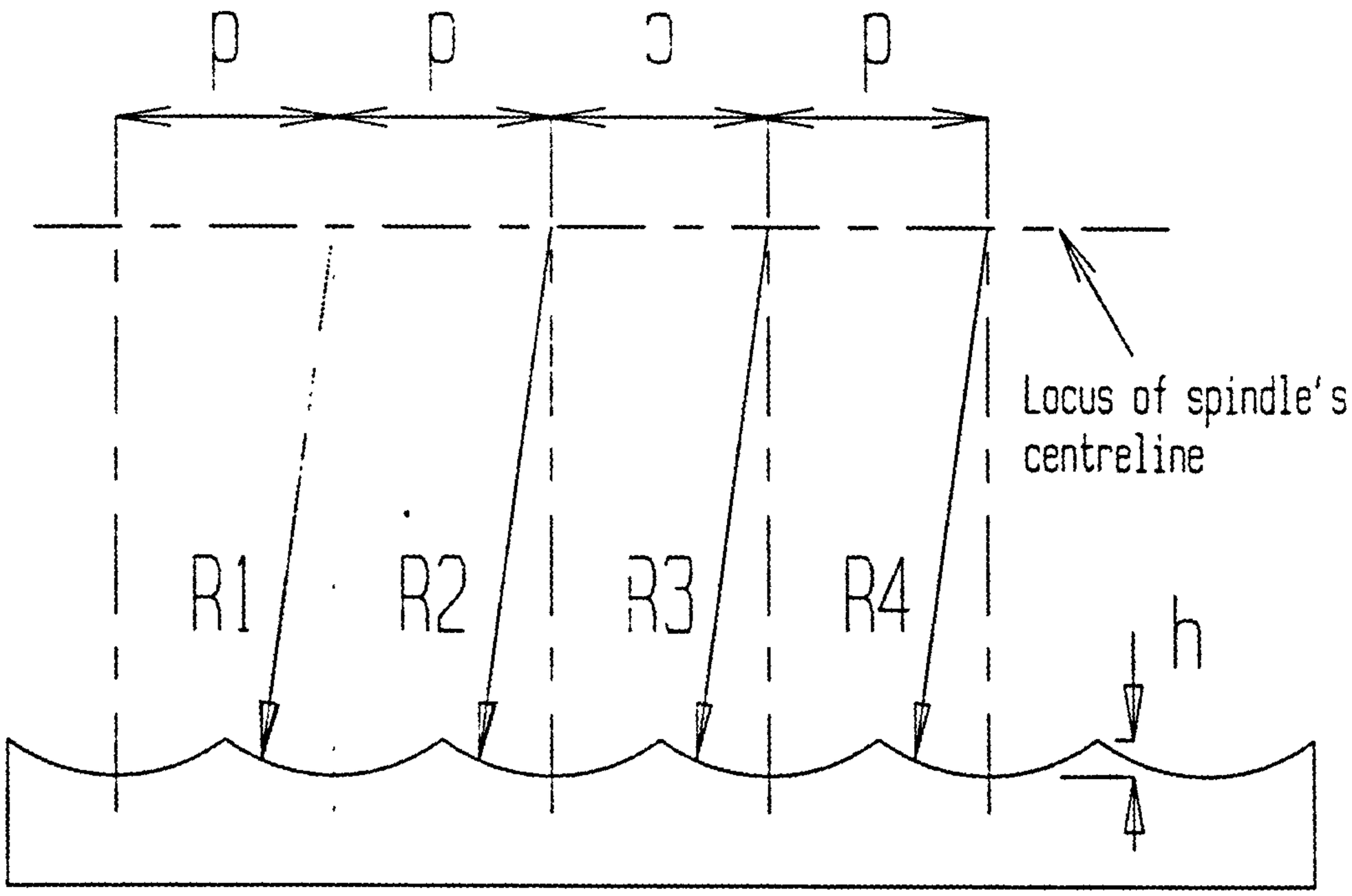

IDEALLY PLANED SURFACE

Figure 3.2

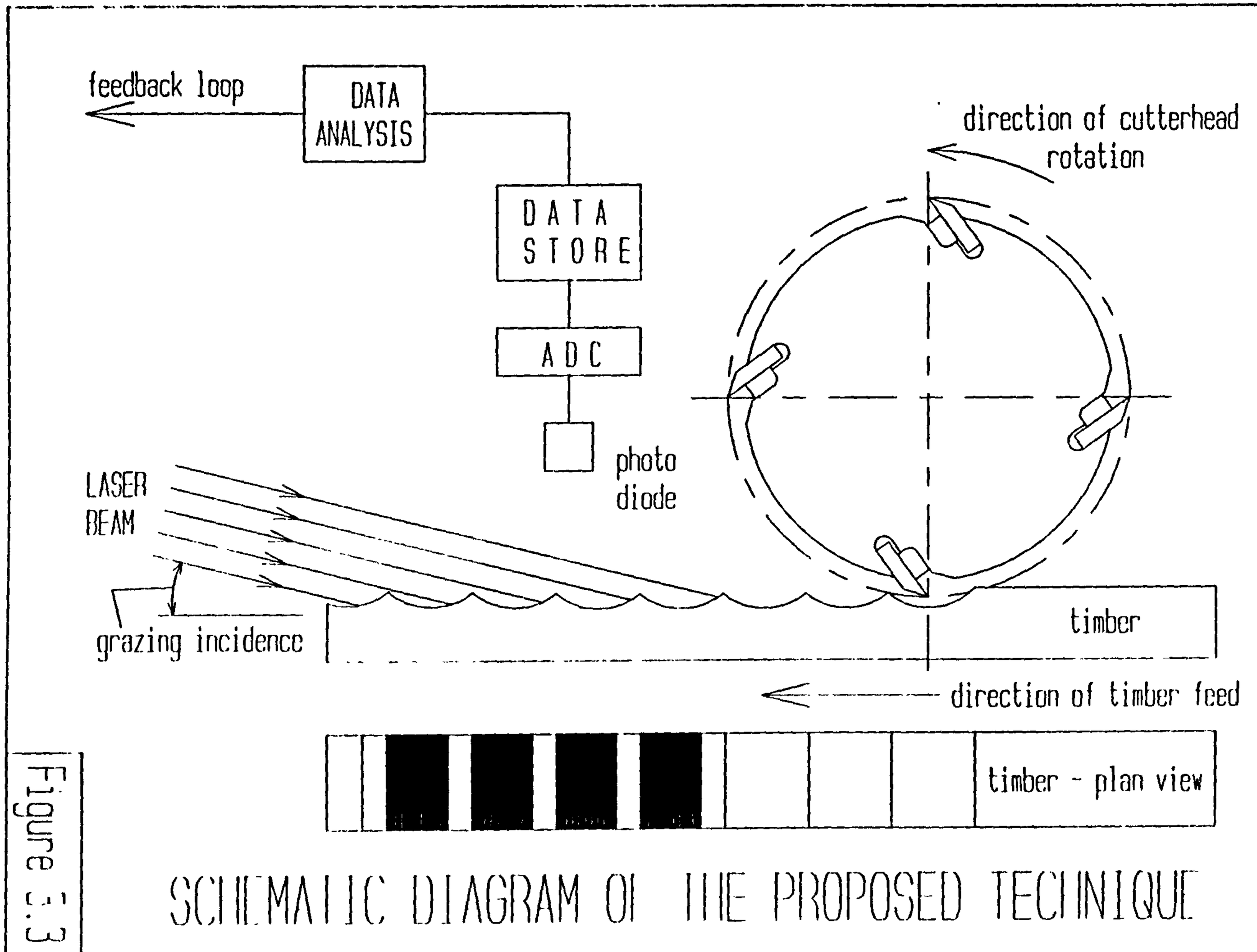

Figure 3.3

SCHEMATIC DIAGRAM OF THE PROPOSED TECHNIQUE

SCHEMATIC DIAGRAM OF INSTRUMENT DEVELOPMENT SCHEME

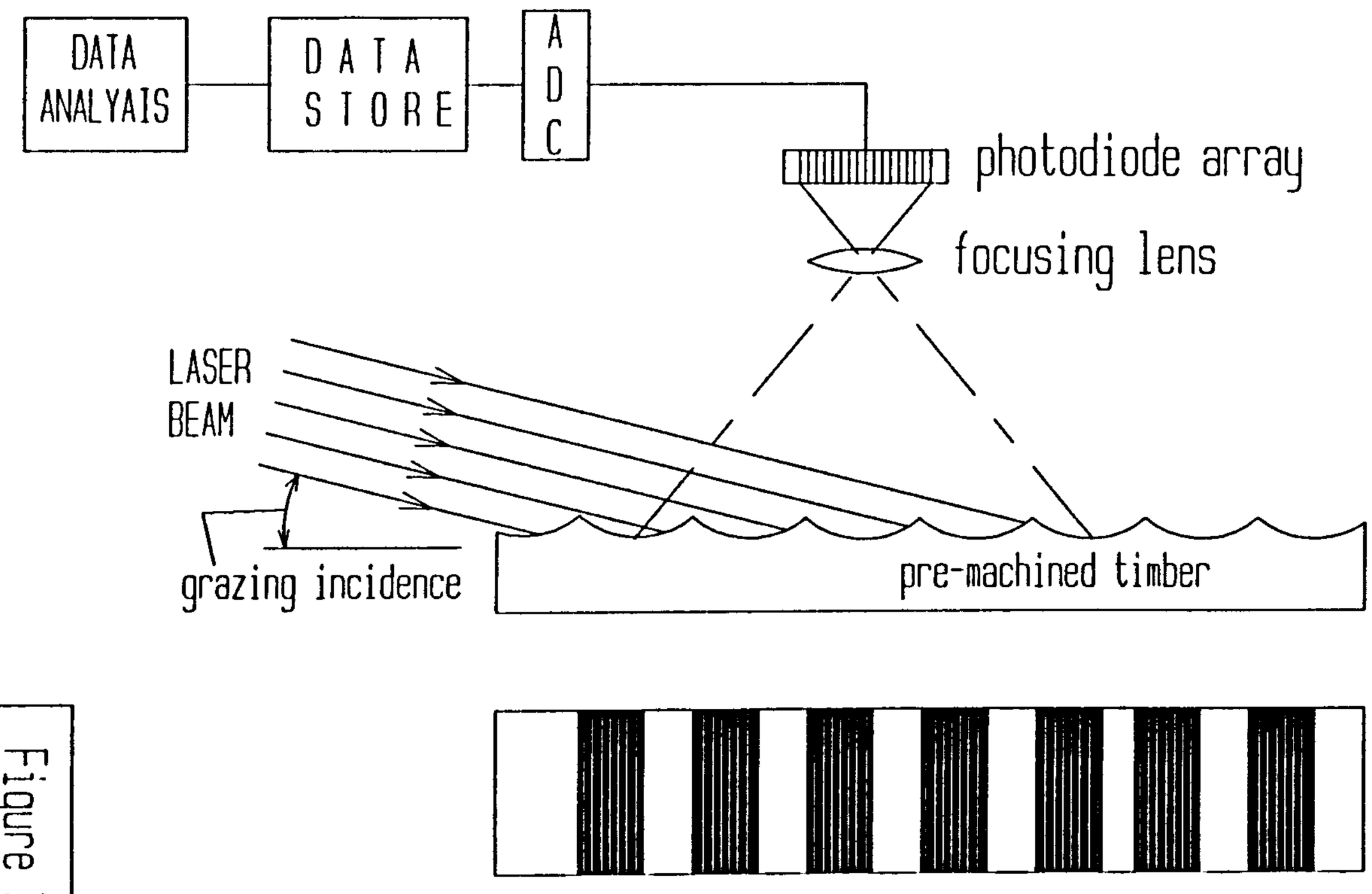

Figure 3.4

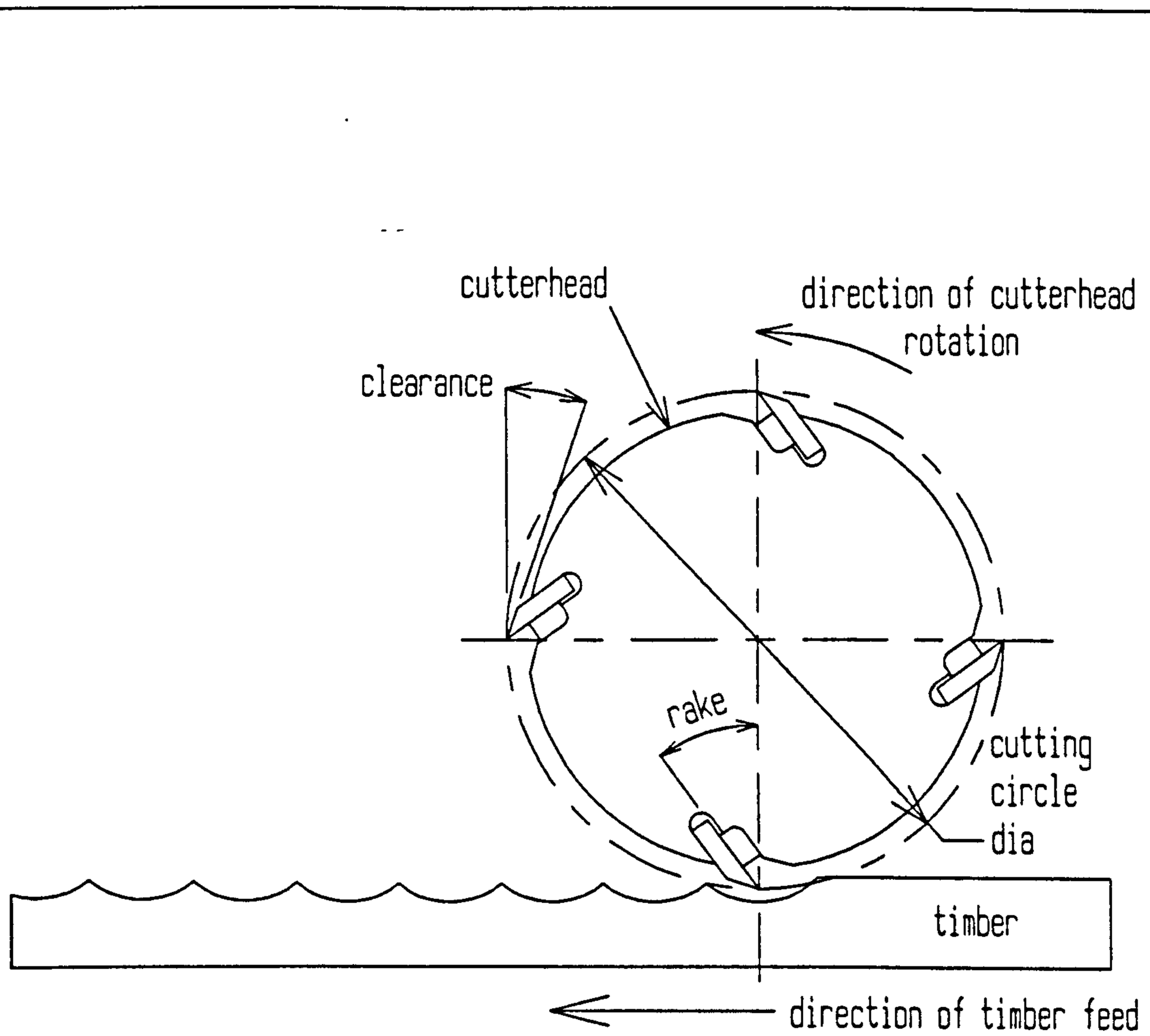

UP-CUTTING MODE USED IN WOODWORKING INDUSTRY

Figure 4.1

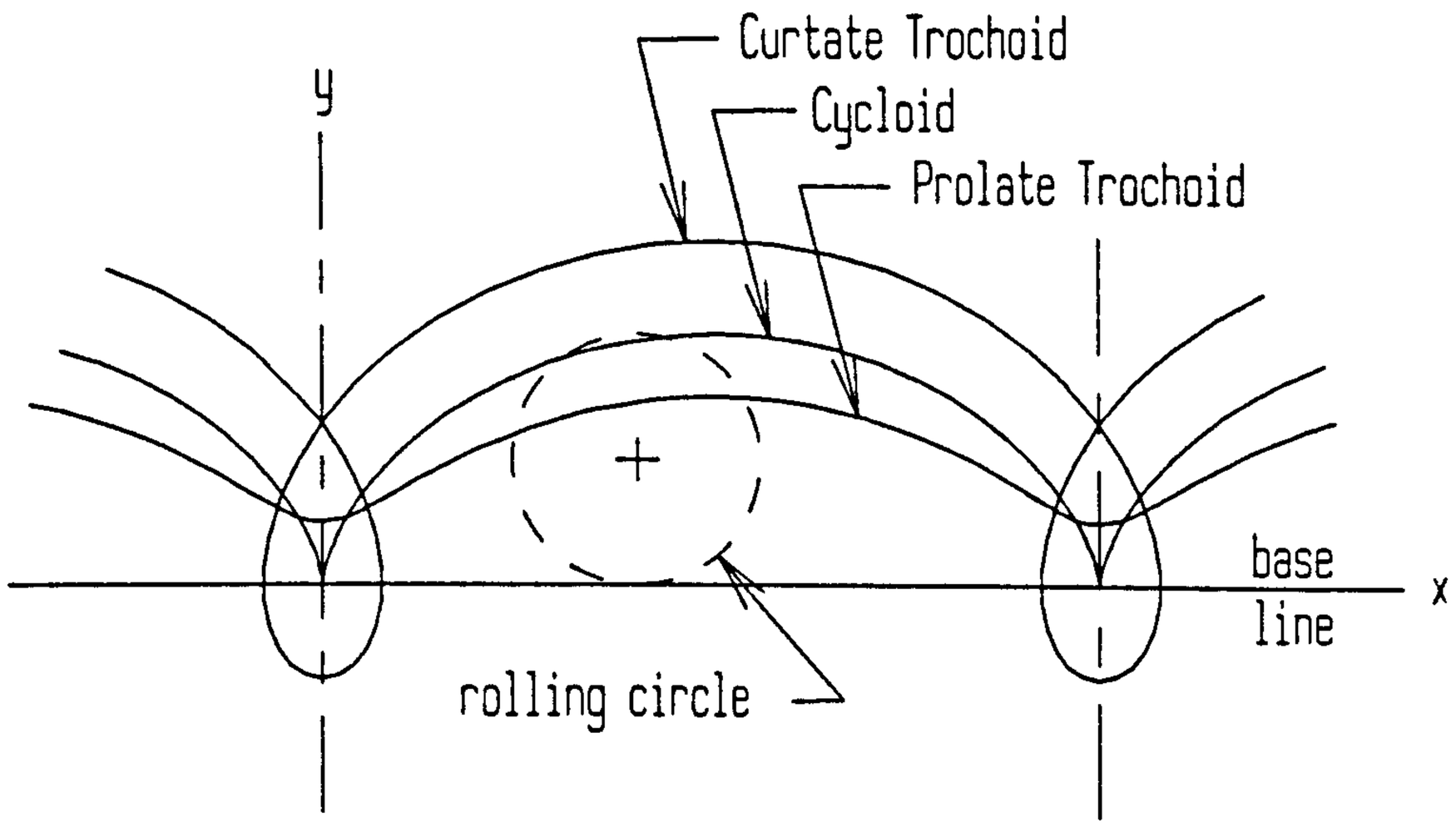

TROCHOID FAMILY

Figure 4.2

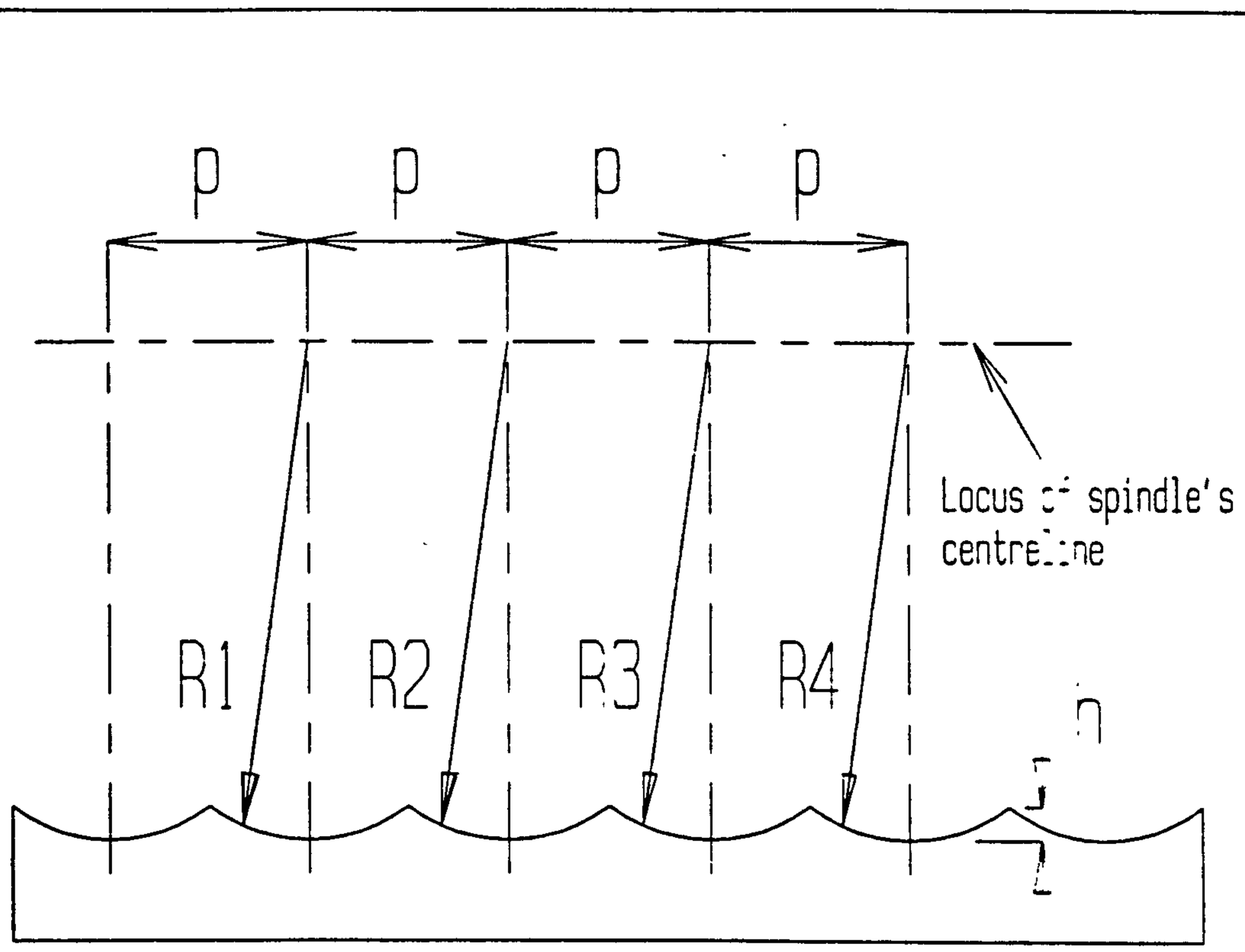

IDEALLY PLANED SURFACE

R1 = R2 = R3 = R4

Figure 4.3

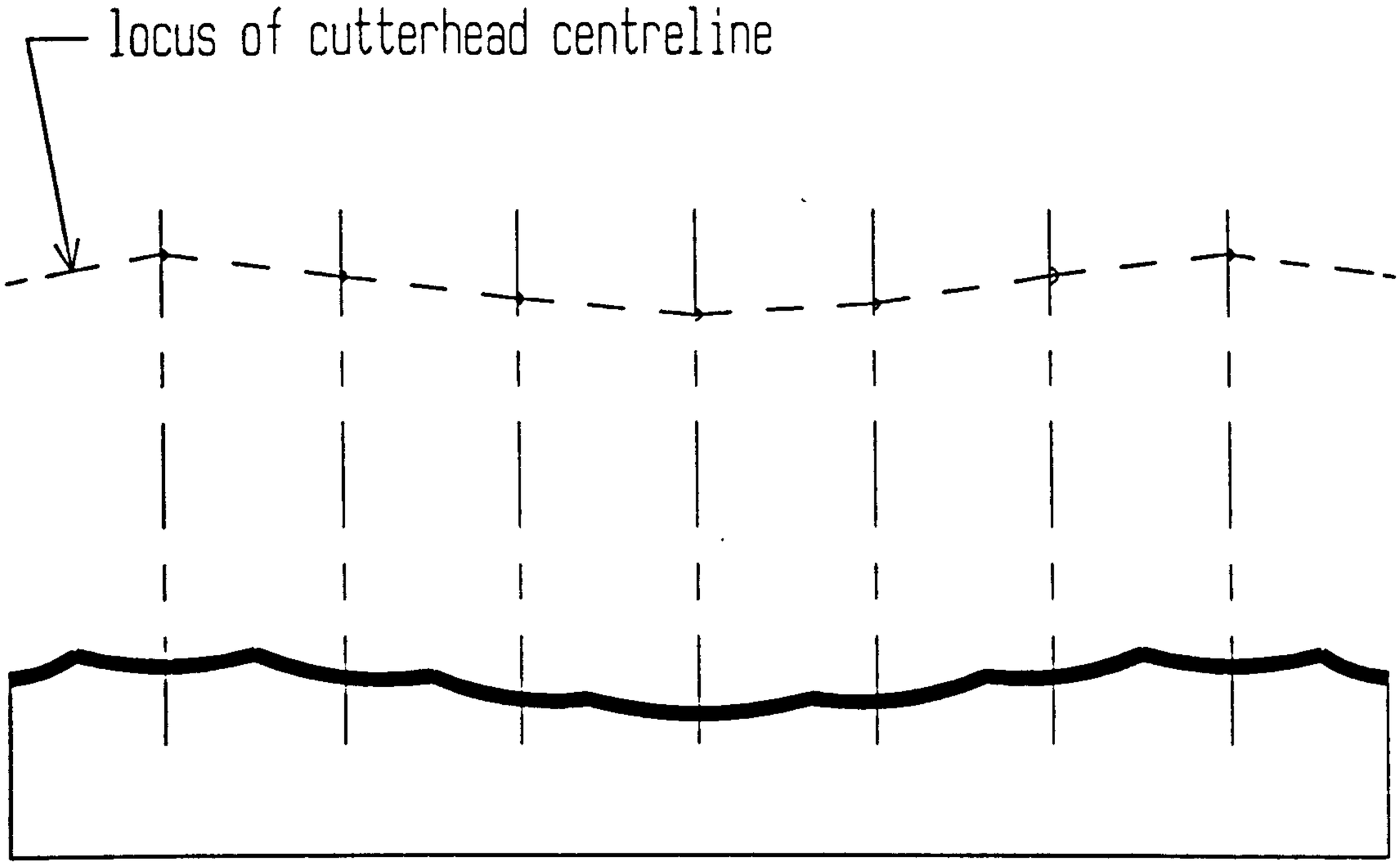

TYPICAL SURFACE PROFILE OF PLANED TIMBER

Figure 4.4

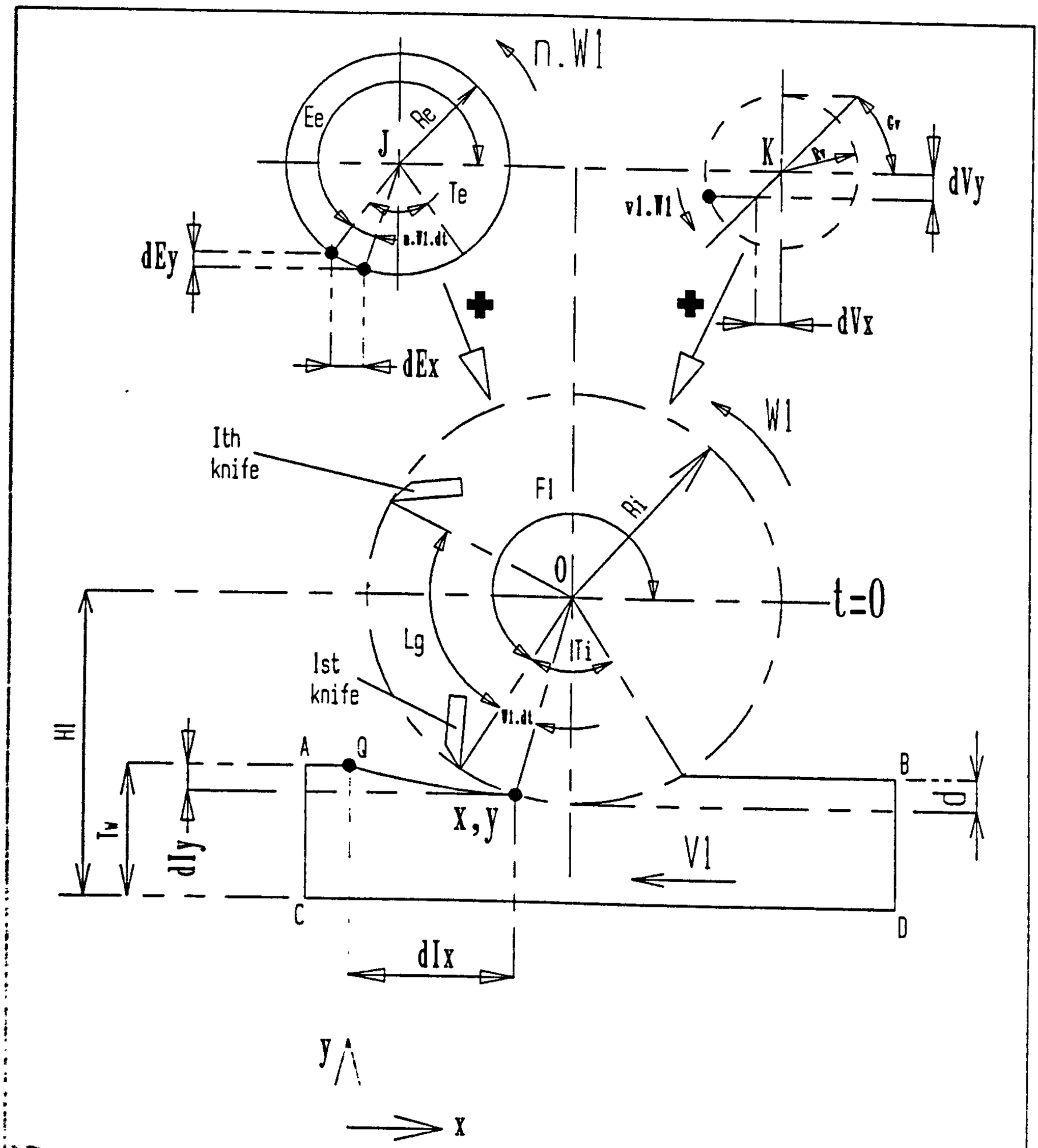

SCHEMATIC OF GENERAL CUTTERHEAD ACTION

Figure 4.5

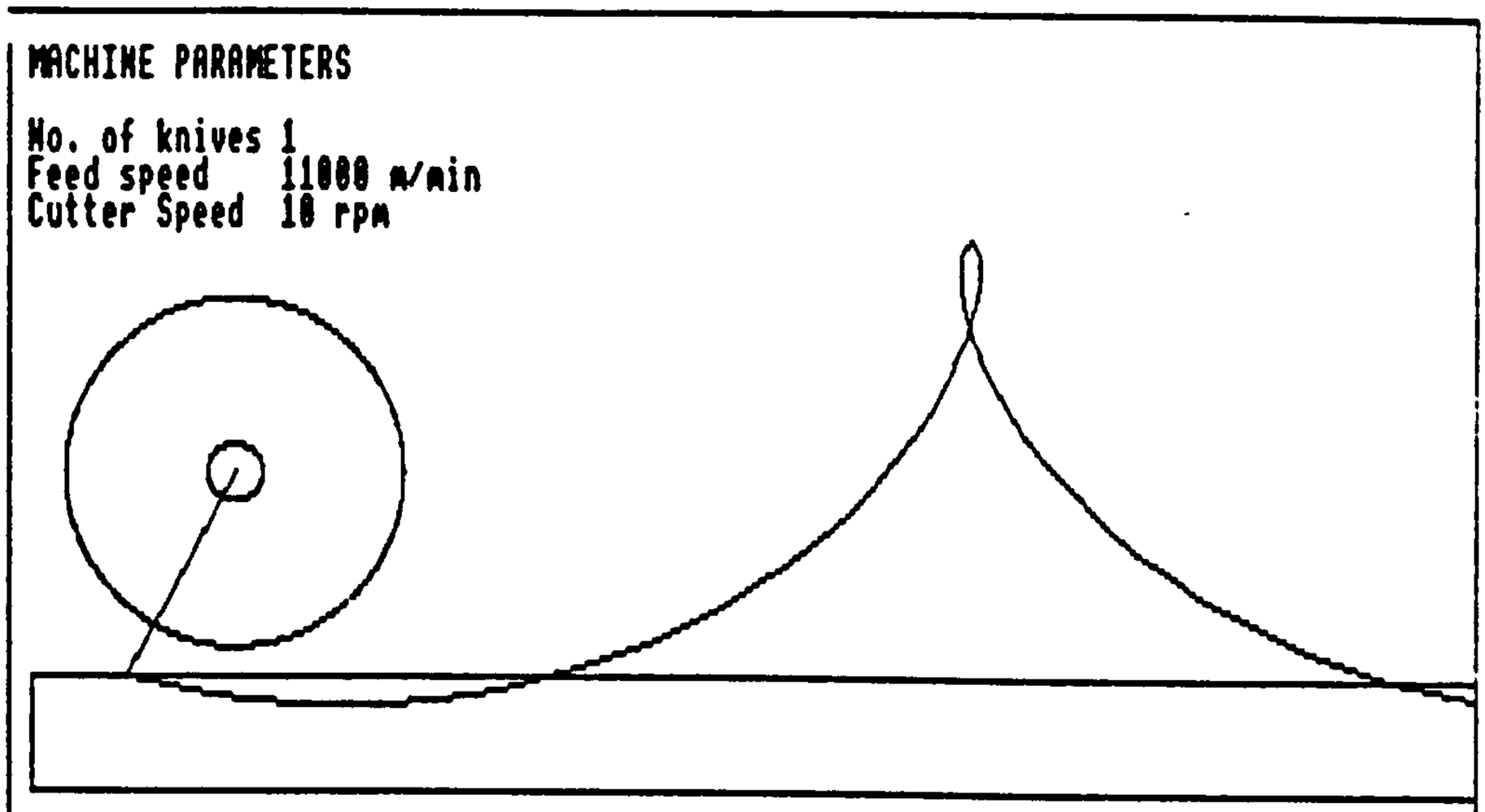

Figure 4.6a: Typical Knife-tip Loci from Algorithm LOCI-0 (SSA - Stage 1)

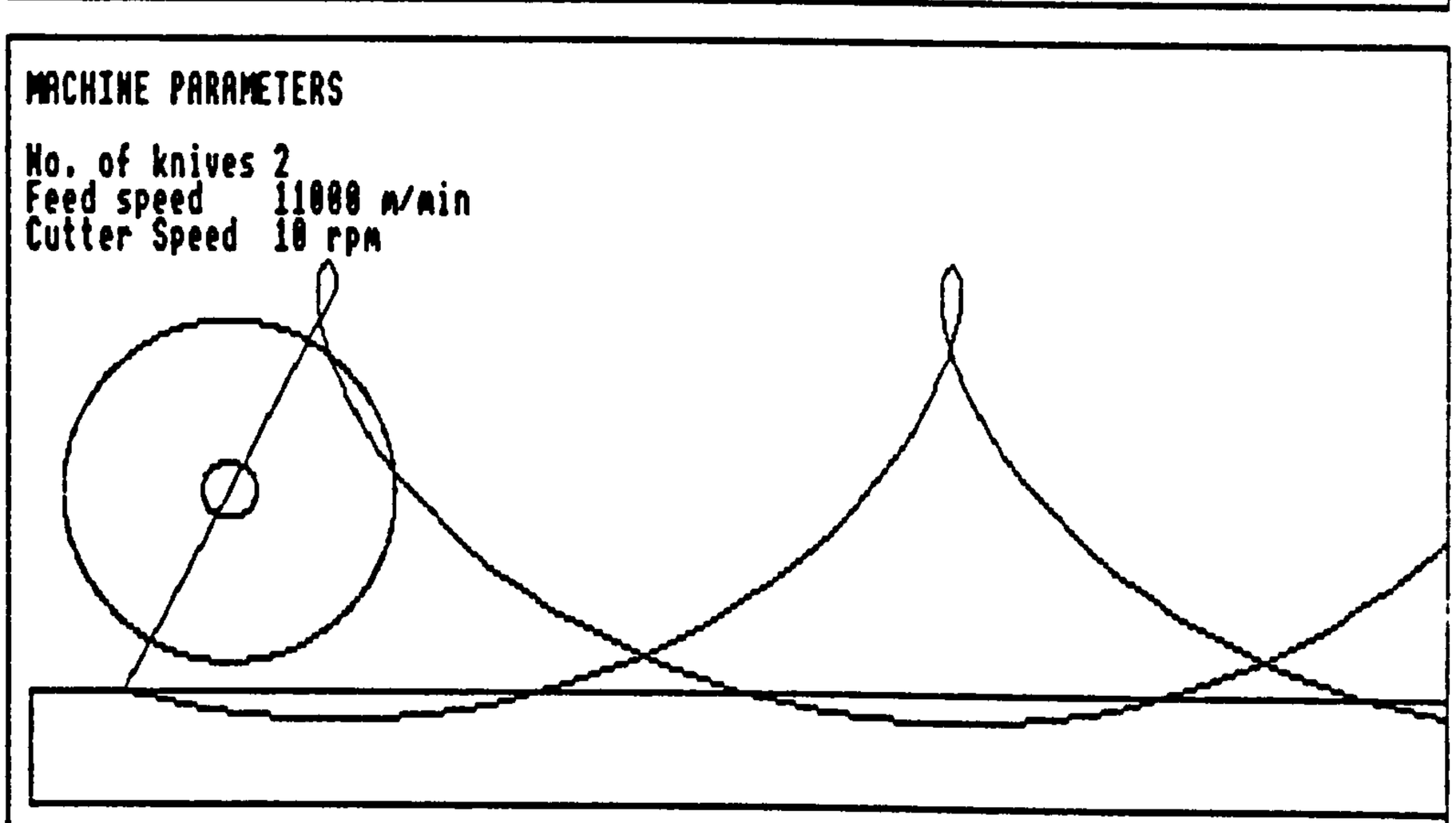

Figure 4.6b: Typical Knife-tip Loci from Algorithm LOCI-0 (SSA - Stage 1)

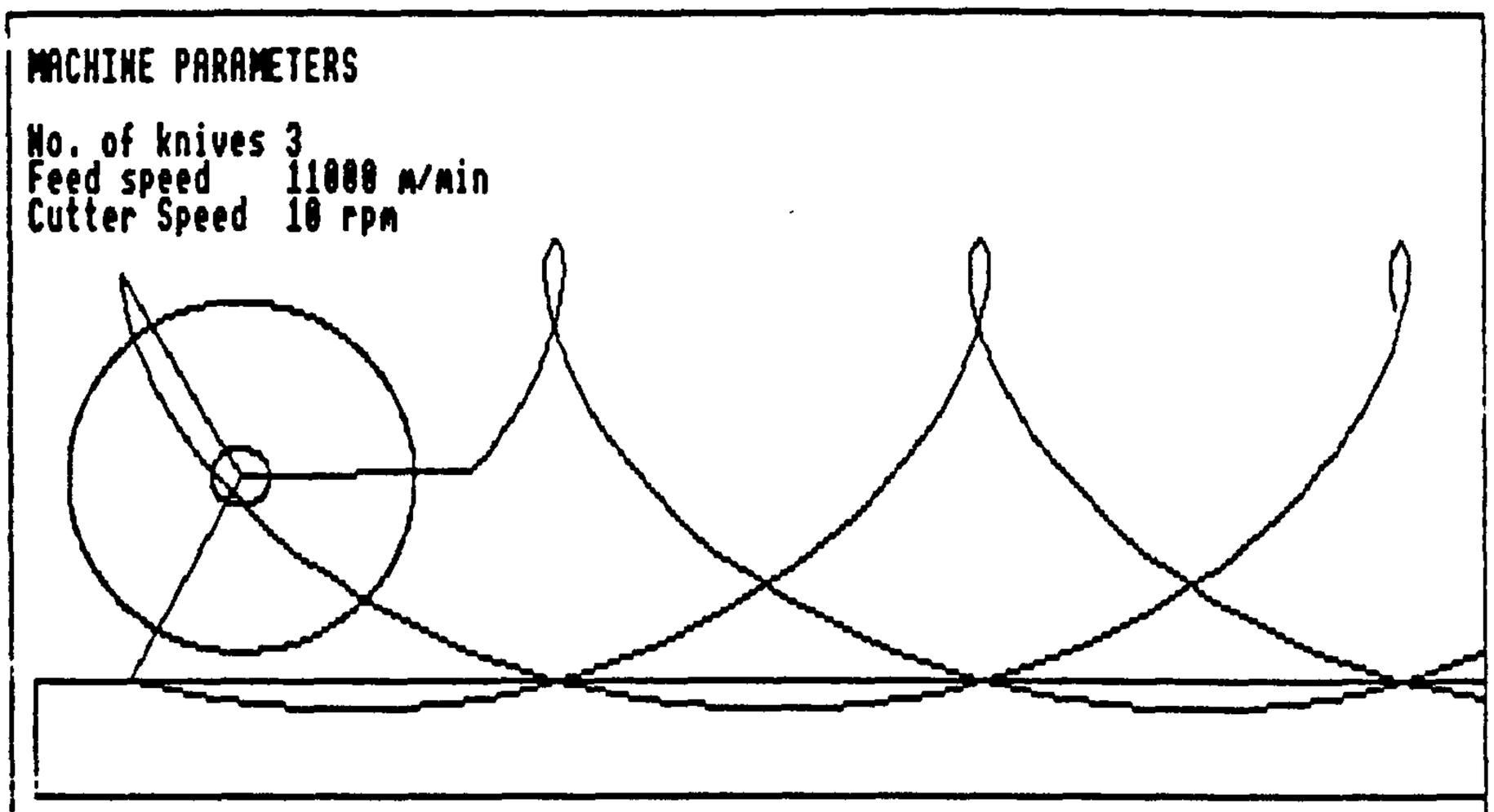

Figure 4.6c: Typical Knife-tip Loci from Algorithm LOCI-0 (SSA - Stage 1)

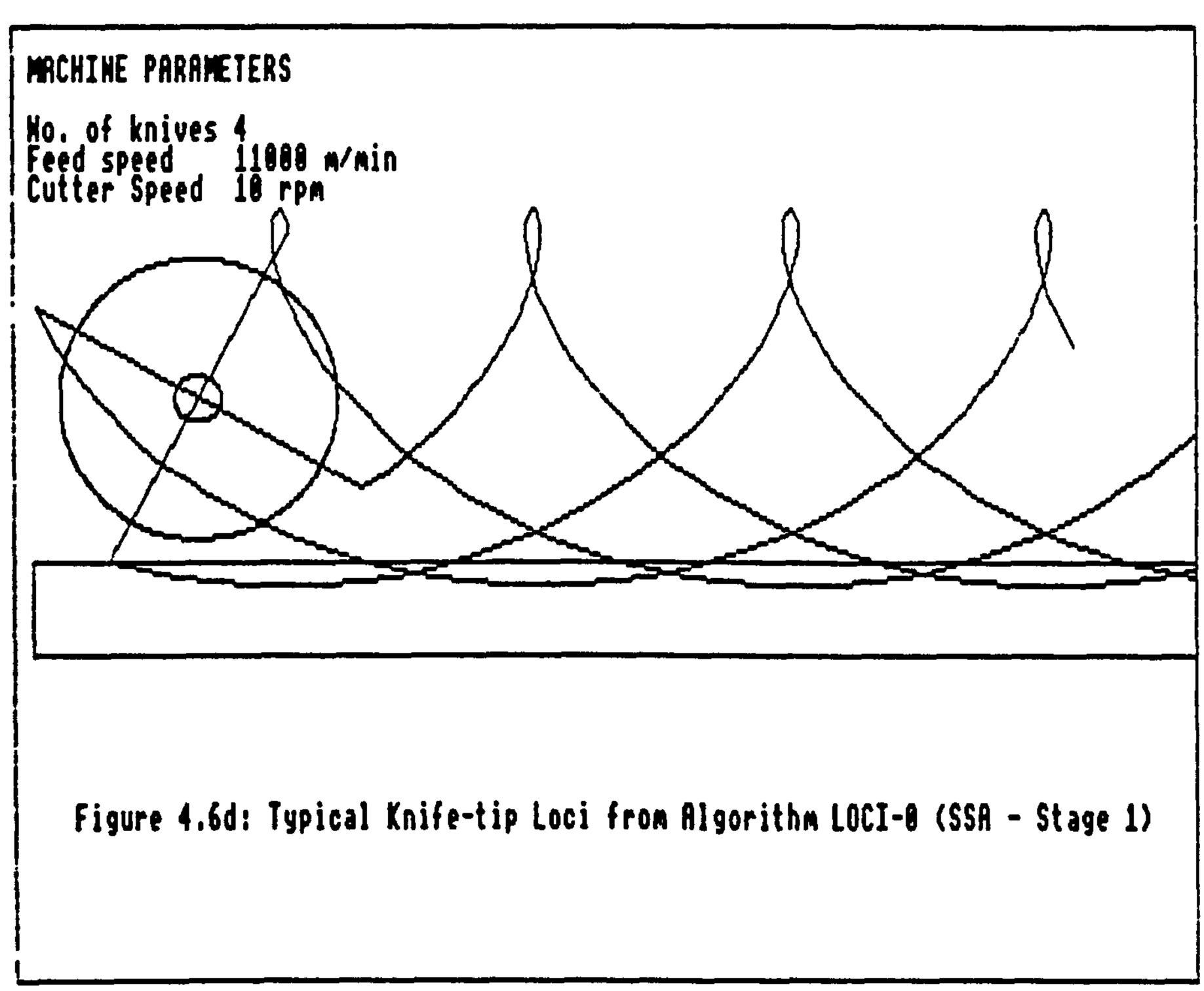

Figure 4.6d: Typical Knife-tip Loci from Algorithm LOCI-0 (SSA - Stage 1)

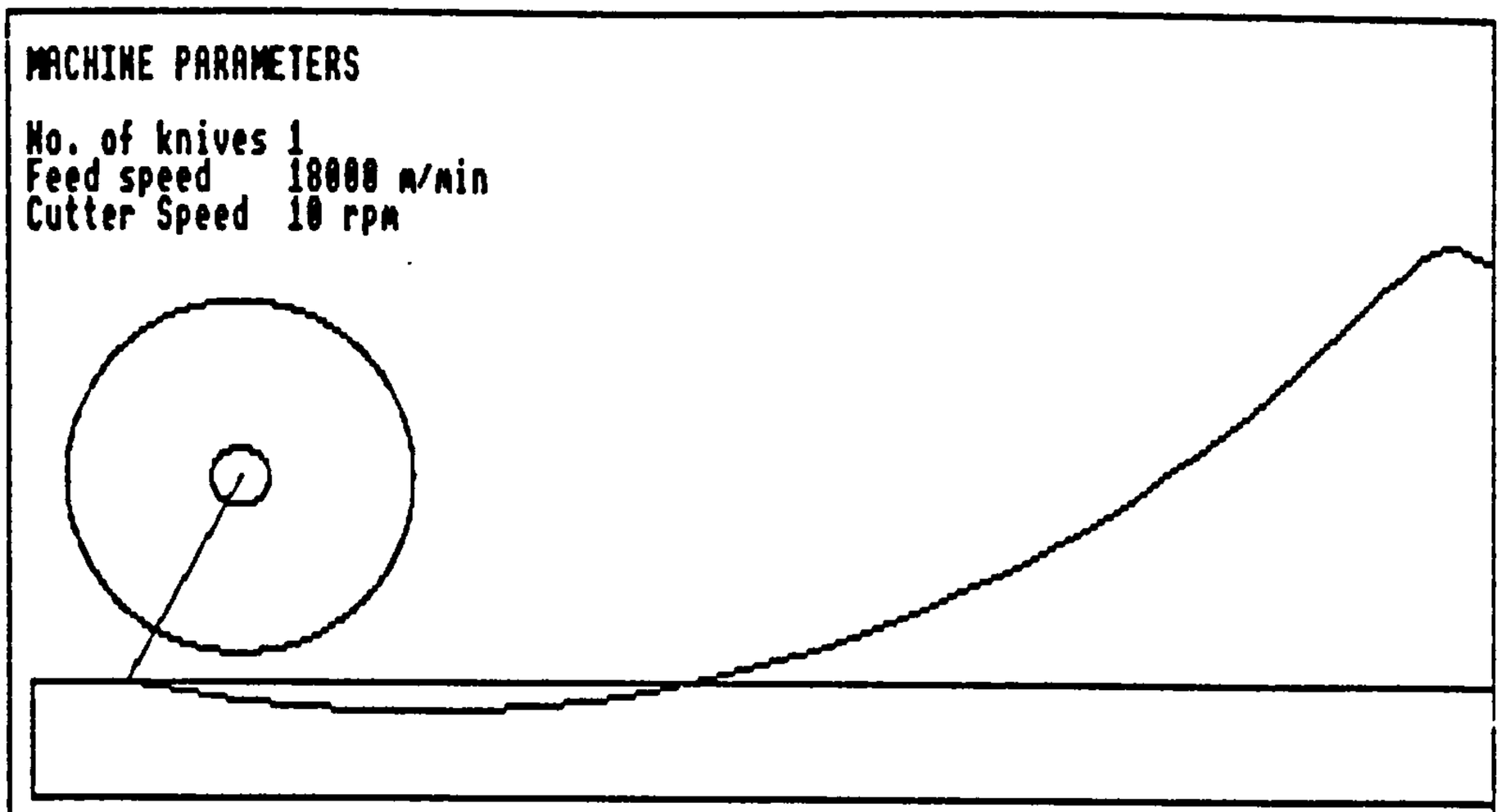

Figure 4.6e: Typical Knife-tip Loci from Algorithm LOCI-0 (SSA - Stage 1)

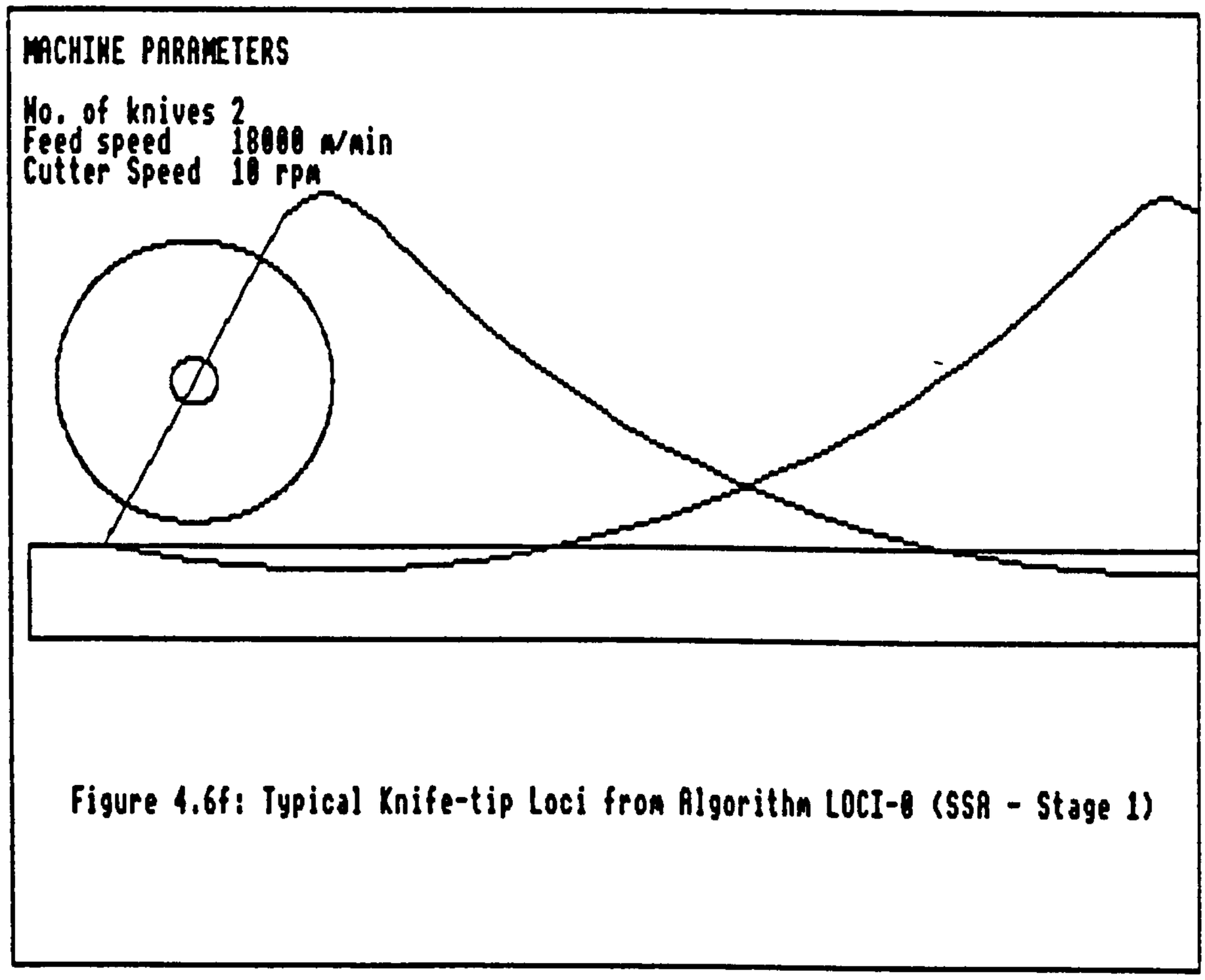

Figure 4.6f: Typical Knife-tip Loci from Algorithm LOCI-0 (SSA - Stage 1)

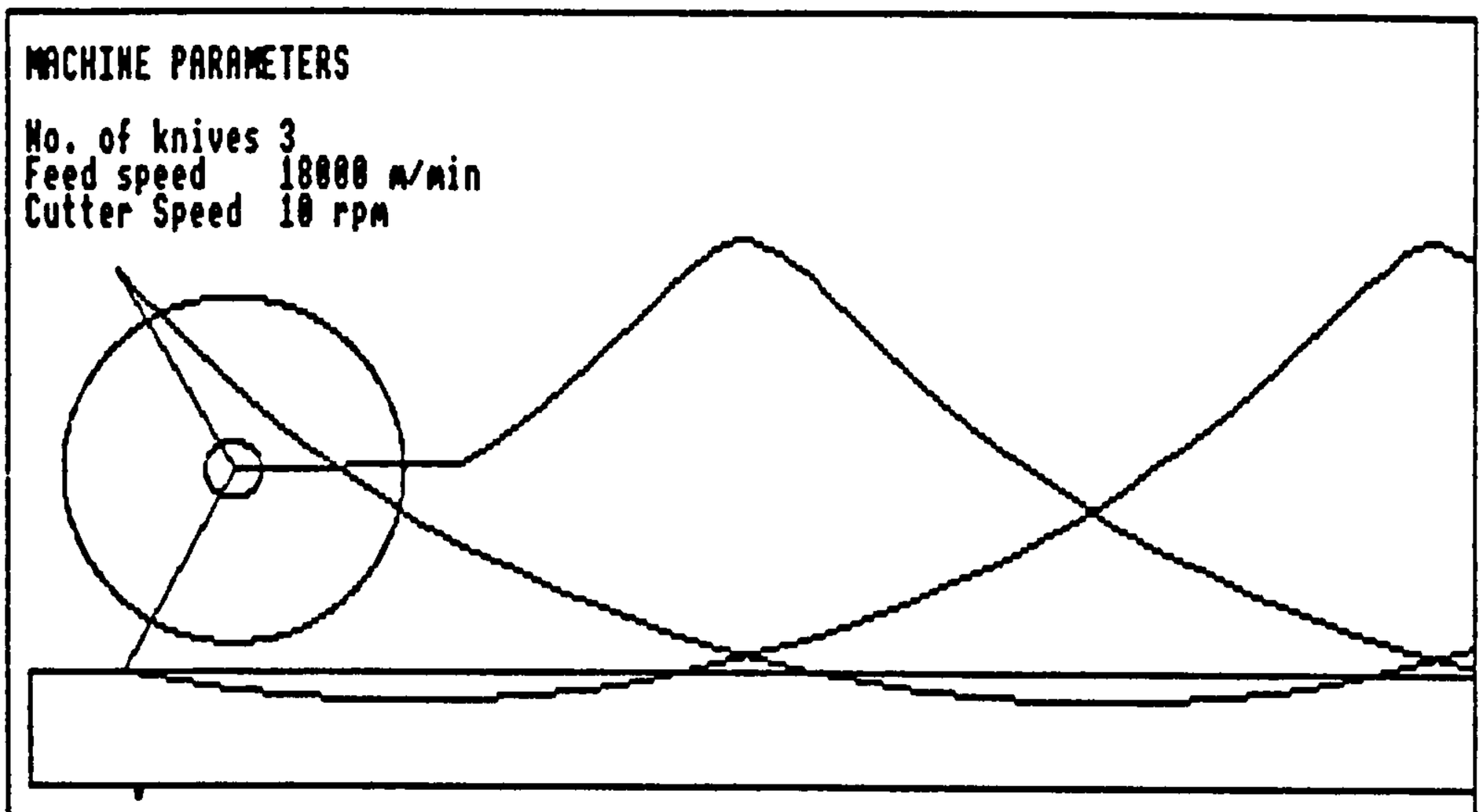

Figure 4.6g: Typical Knife-tip Loci from Algorithm LOCI-0 (SSA - Stage 1)

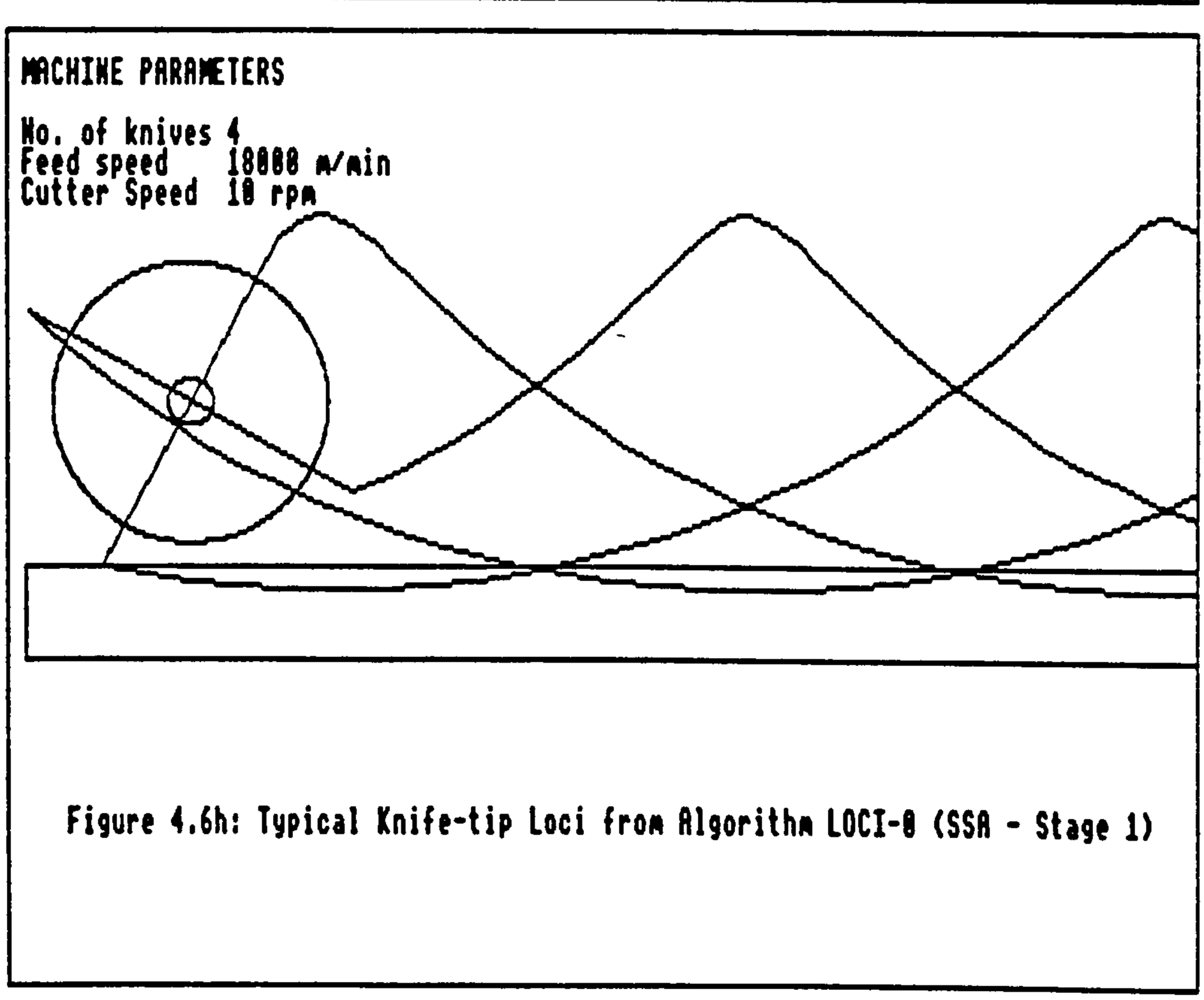

Figure 4.6h: Typical Knife-tip Loci from Algorithm LOCI-0 (SSA - Stage 1)

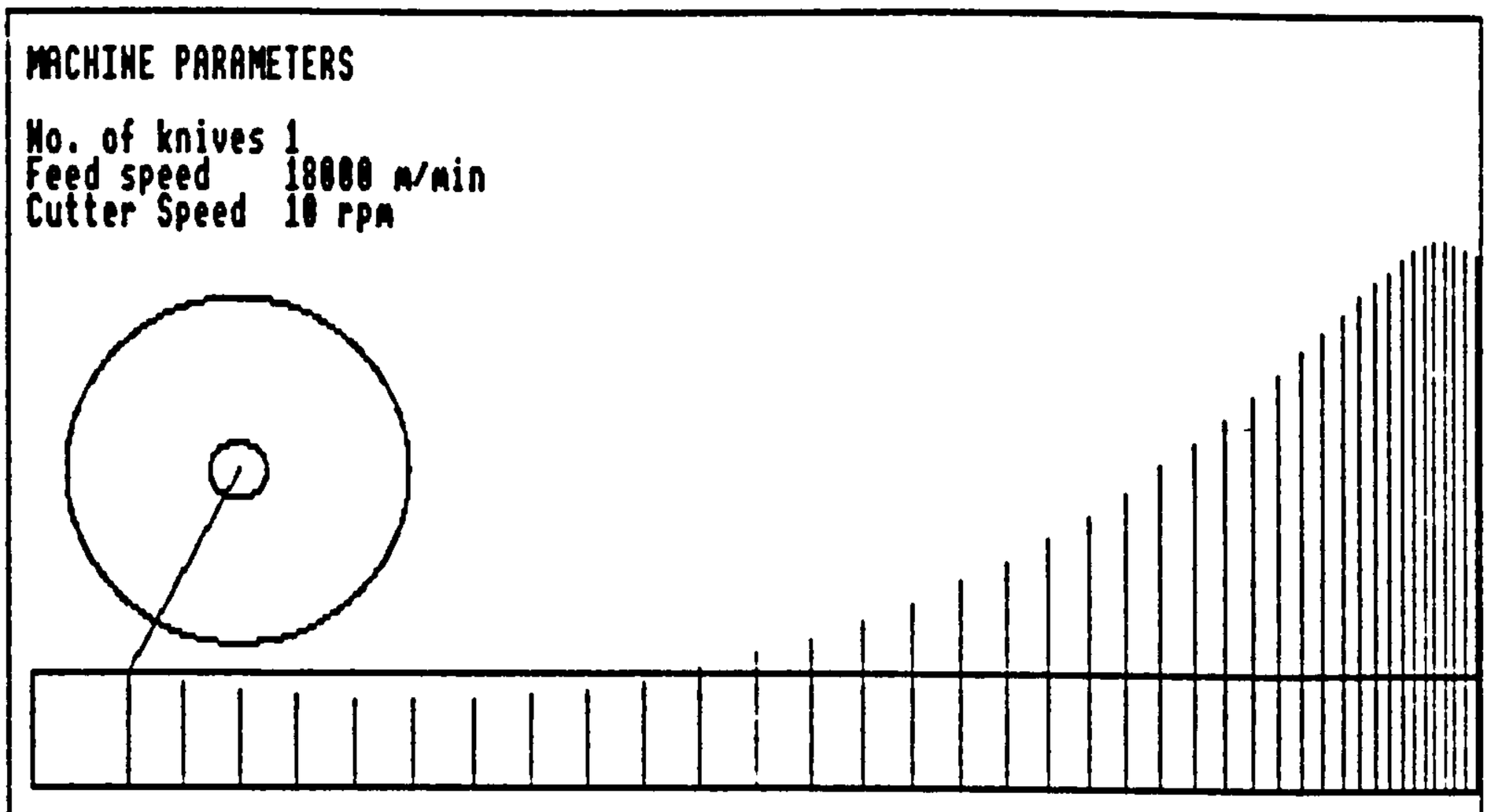

Figure 4.7a: Typical Knife-tip Loci from Algorithm LOCI-1 (SSA - Stage 1)

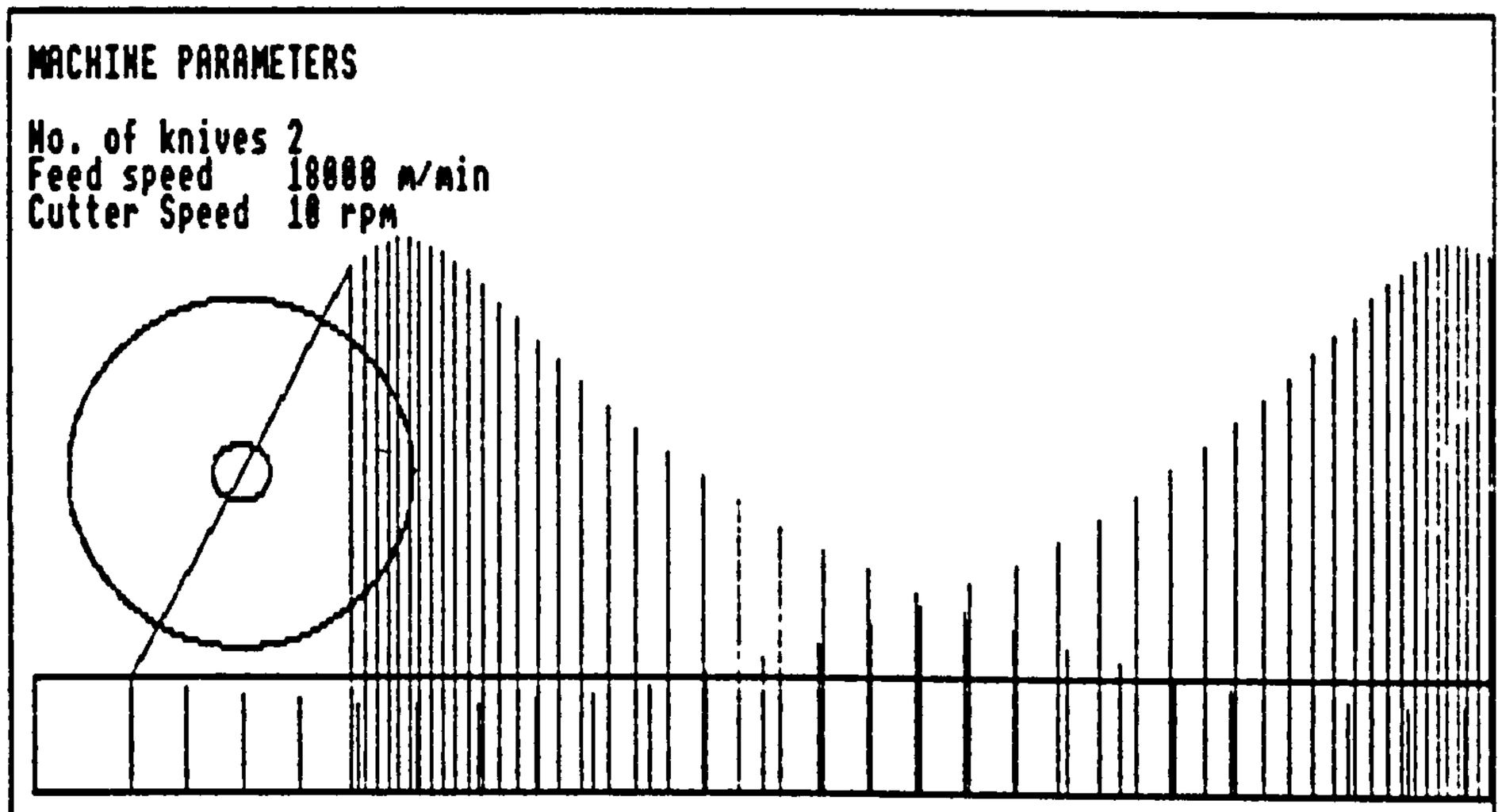

Figure 4.7b: Typical Knife-tip Loci from Algorithm LOCI-1 (SSA - Stage 1)

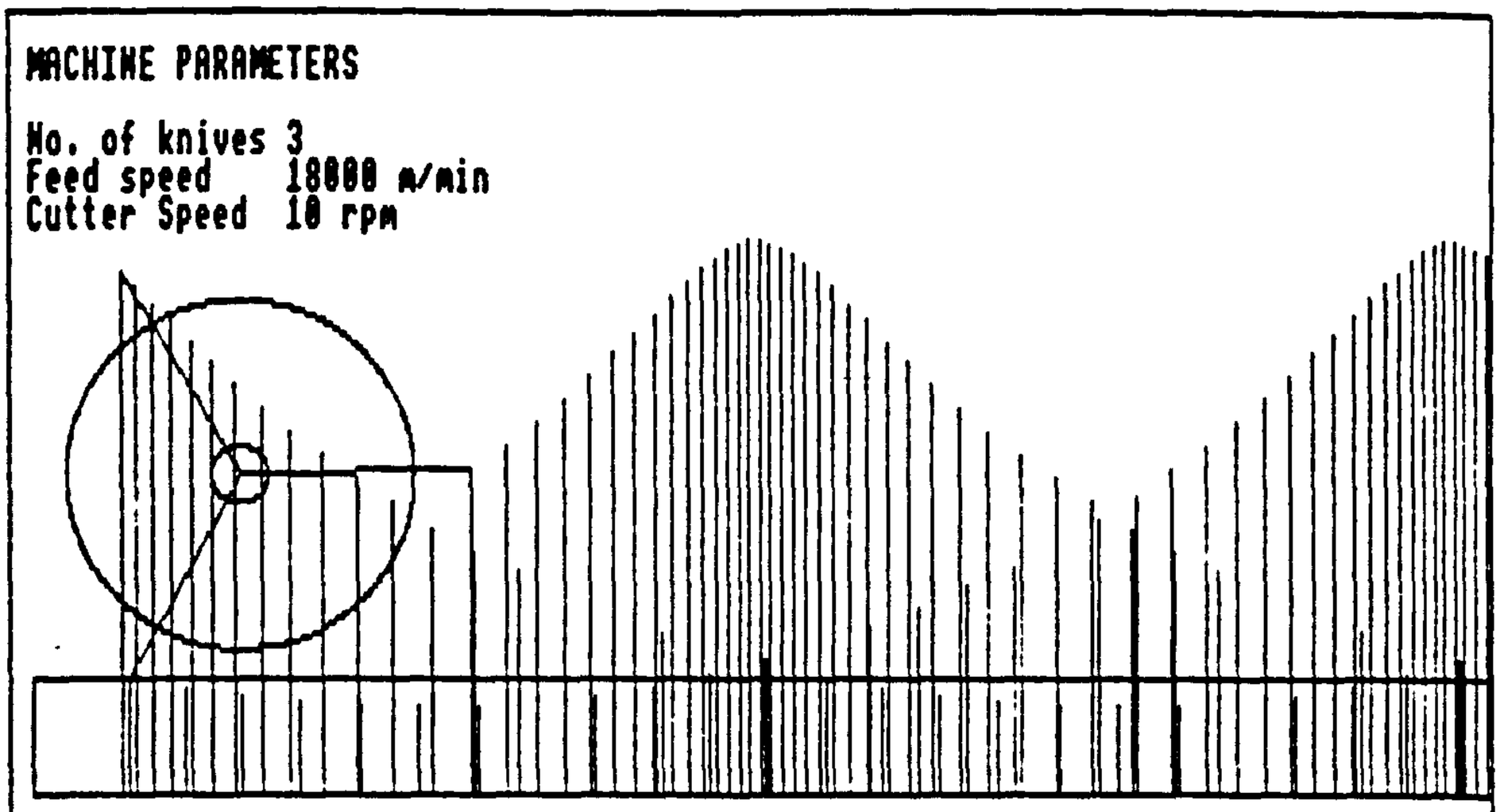

Figure 4.7c: Typical Knife-tip Loci from Algorithm LOCI-1 (SSA - Stage 1)

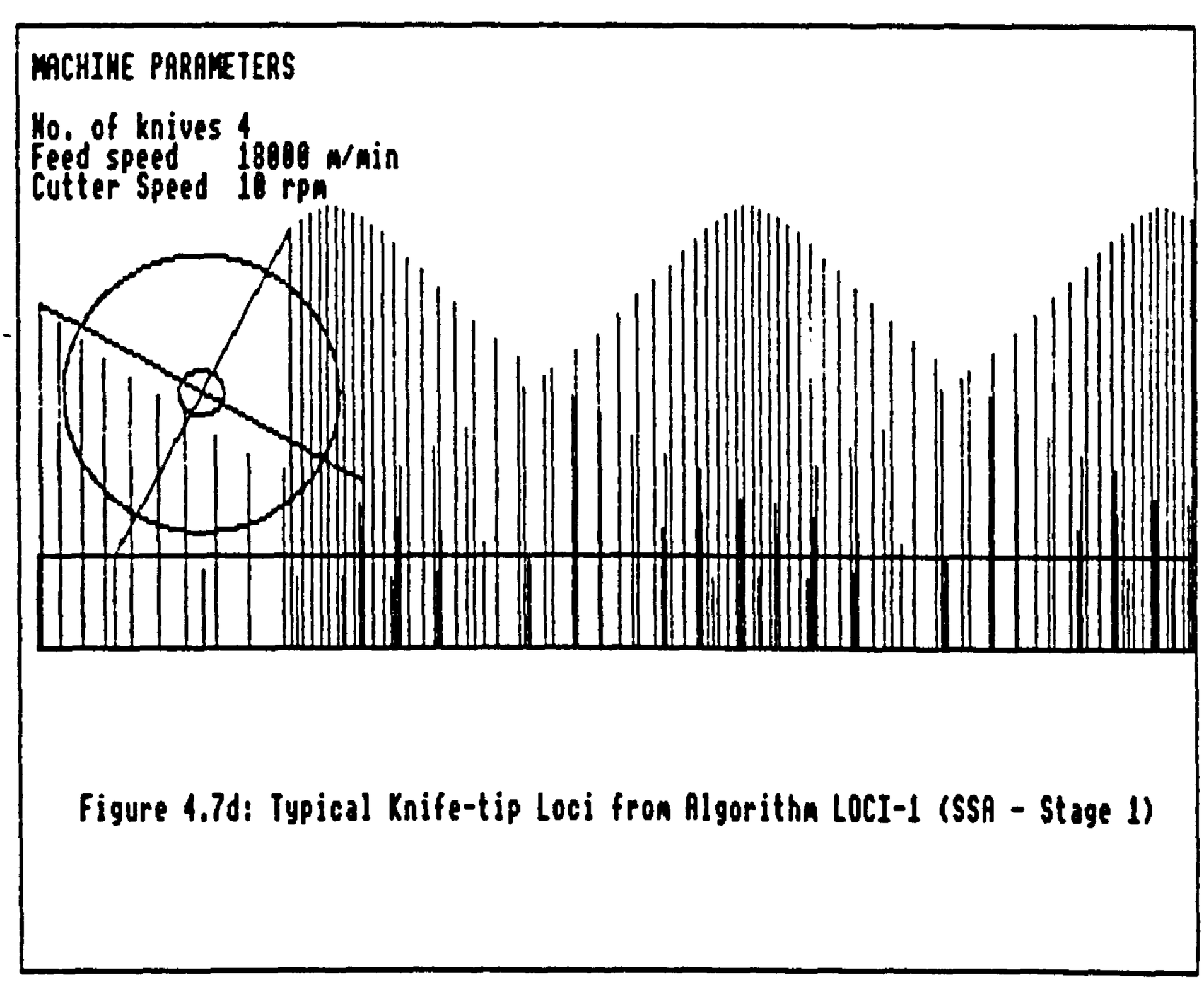

Figure 4.7d: Typical Knife-tip Loci from Algorithm LOCI-1 (SSA - Stage 1)

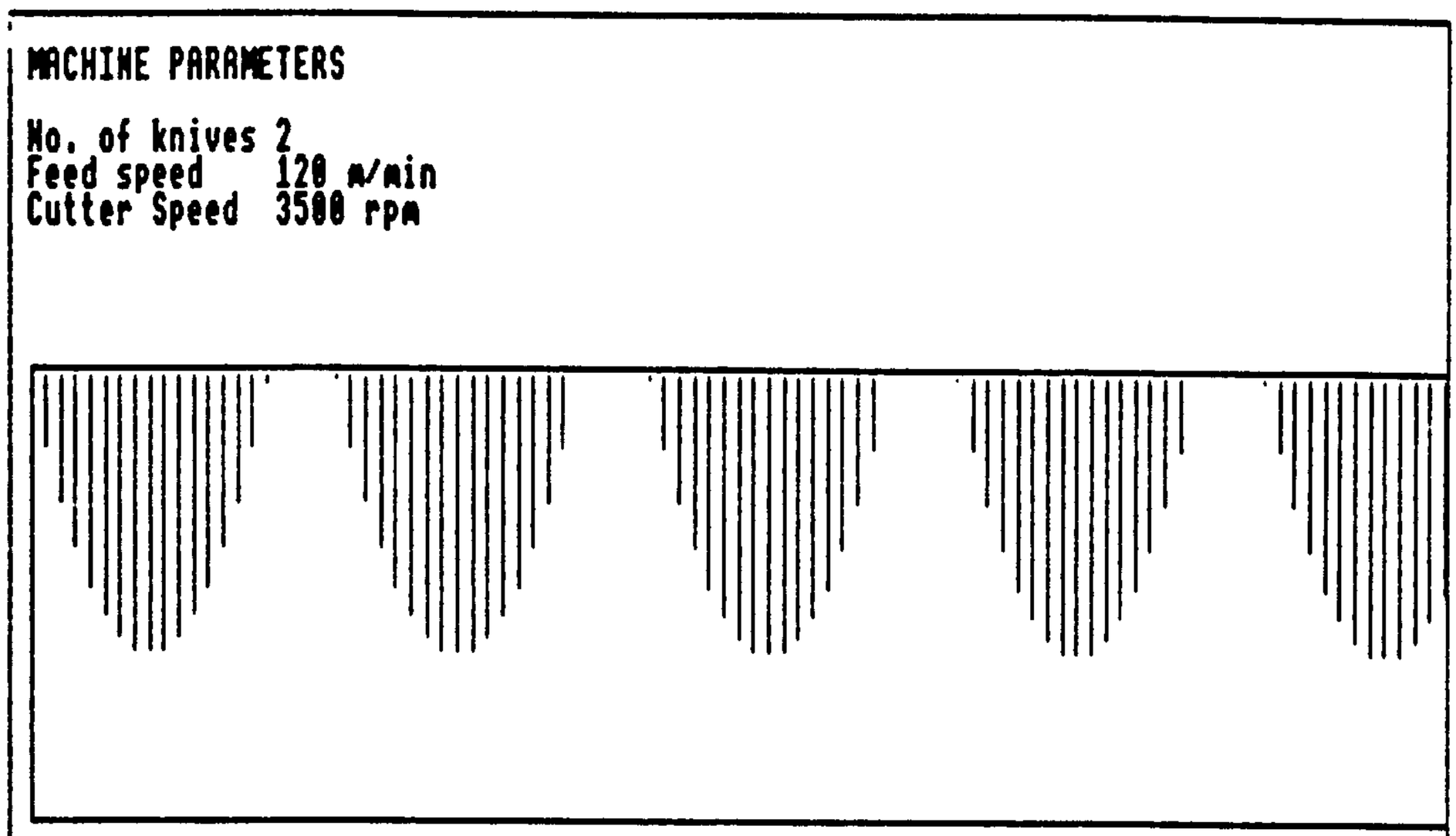

Figure 4.8a: Typical Knife-mark Loci from Algorithm LOCI-2 (SSA - Stage II)

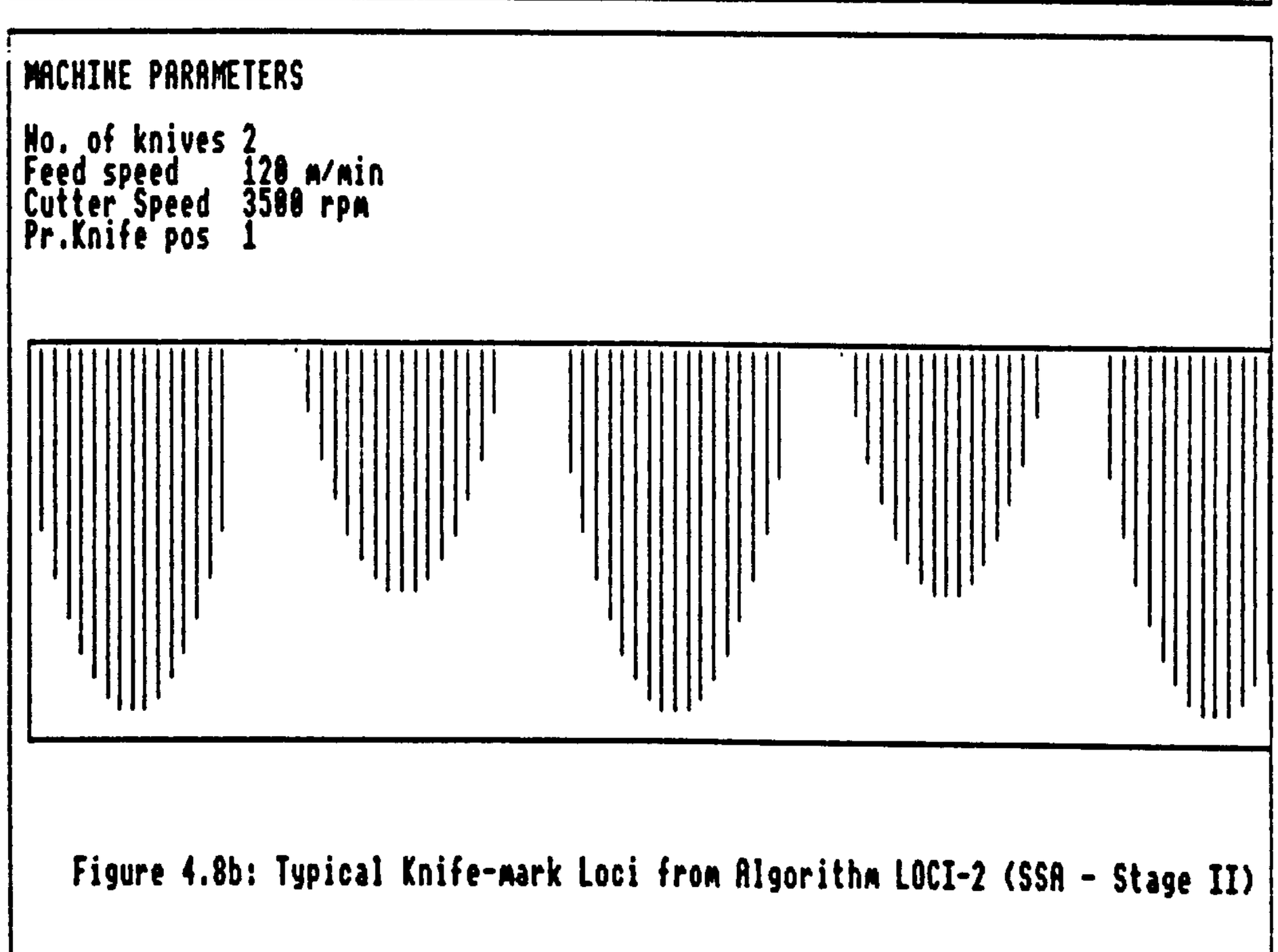

Figure 4.8b: Typical Knife-mark Loci from Algorithm LOCI-2 (SSA - Stage II)

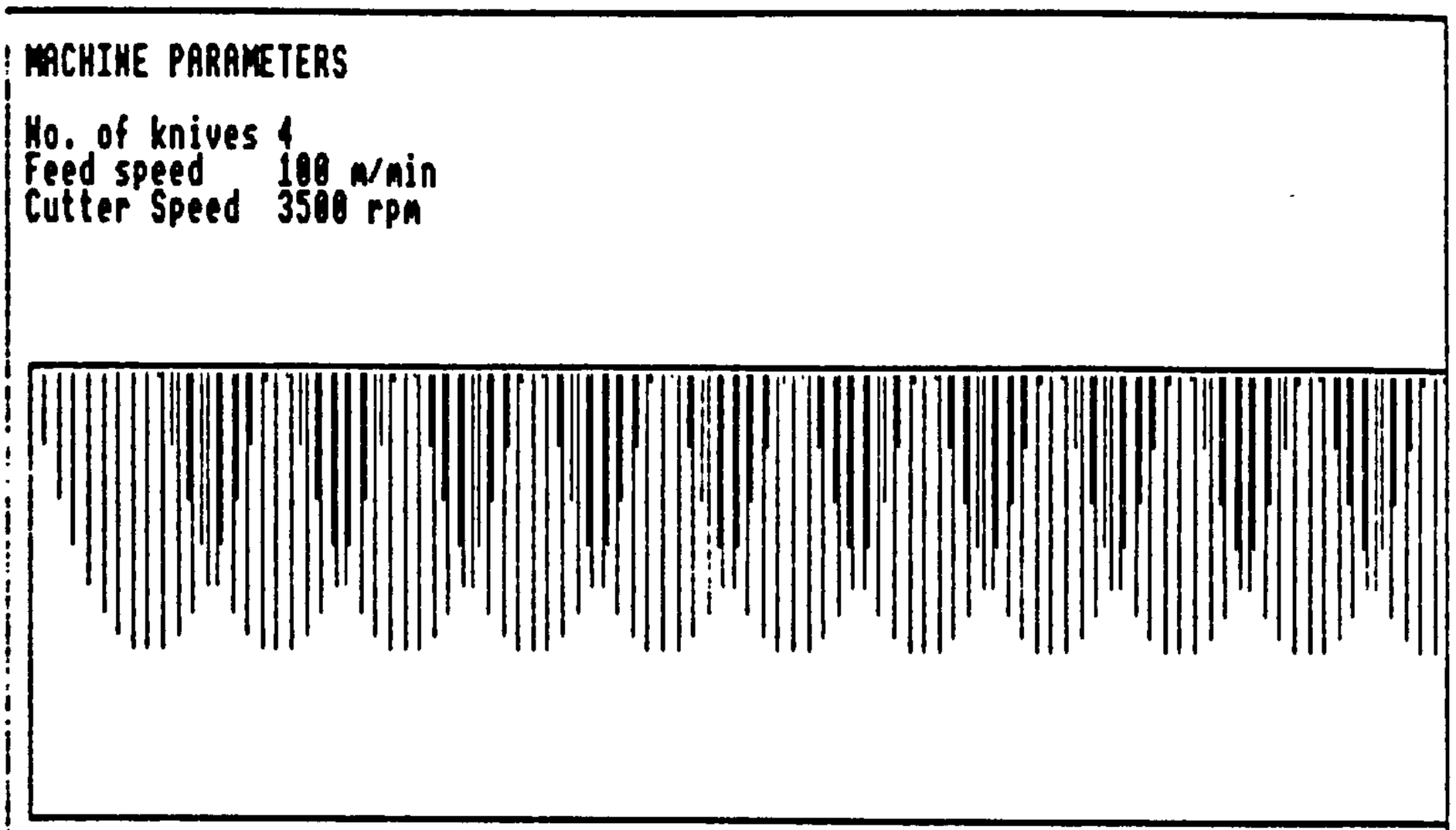

Figure 4.8c: Typical Knife-mark Loci from Algorithm LOCI-2 (SSA - Stage II)

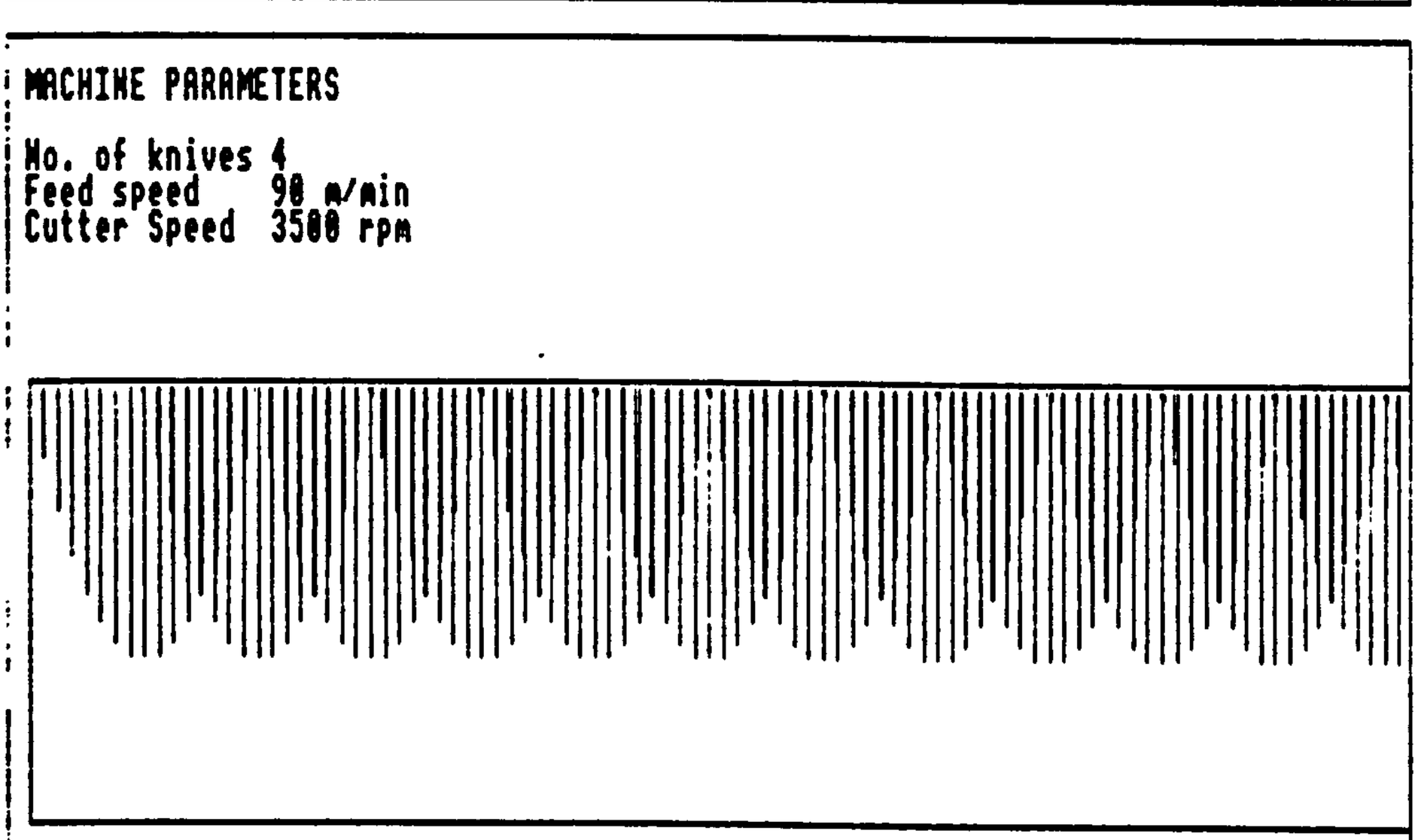

Figure 4.8d: Typical Knife-mark Loci from Algorithm LOCI-2 (SSA - Stage II)

MACHINE PARAMETERS

No. of knives 4
Feed speed 100 m/min
Cutter Speed 3500 rpm

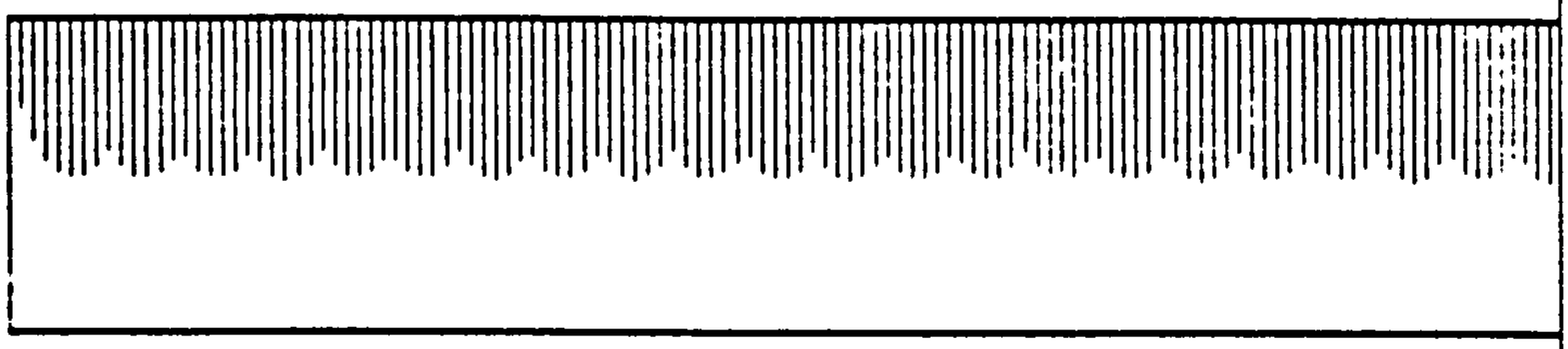

Figure 4.9a: Typical Knife-mark Loci from Algorithm LOCI-3 (SSA - Stage III)

MACHINE PARAMETERS

No. of knives 4
Feed speed 90 m/min
Cutter Speed 3500 rpm

Ecc.rate/rev 1

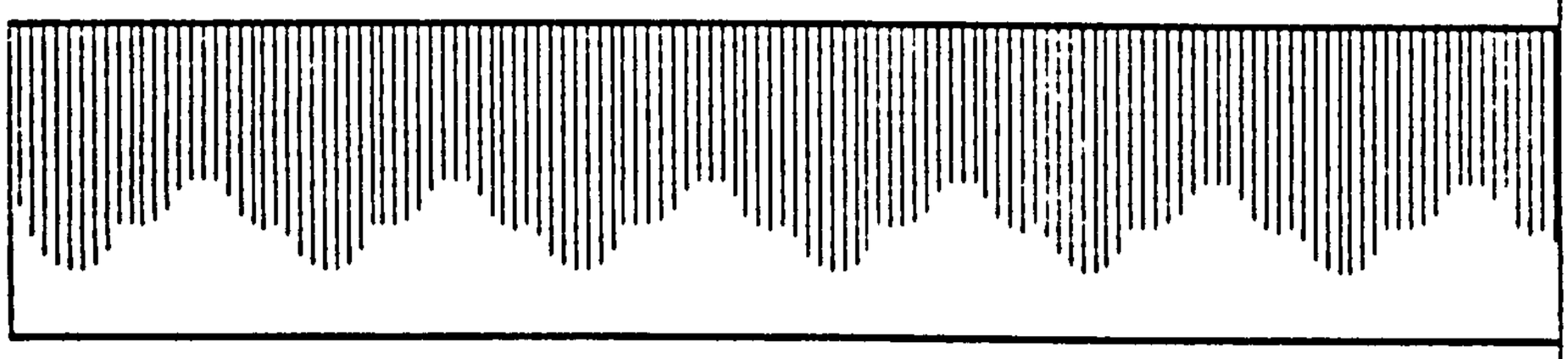

Figure 4.9b: Typical Knife-mark Loci from Algorithm LOCI-3 (SSA - Stage III)

SIMULATION PARAMETERS	
No. of knives	4
Feed speed	100 m/min
Cutter Speed	3500 rpm
Vib. rate	0
Proud Knives	0
Ecc.rate/rev	0
Spindle Runout	0 microns

Figure 4.10a: Typical Surface Profile from Surface Simulation Algorithm

SIMULATION PARAMETERS	
No. of knives	4
Feed speed	90 m/min
Cutter Speed	3500 rpm
Vib. rate	0
Proud Knives	0
Ecc.rate/rev	1
Spindle Runout	20 microns

Figure 4.10b: Typical Surface Profile from Surface Simulation Algorithm

SIMULATION PARAMETERS	
No. of knives	4
Feed speed	90 m/min
Cutter Speed	3500 rpm
Vib. rate	0
Proud Knives	1 >>> 2
Ecc.rate/rev	0
Spindle Runout	0 microns

Figure 4.10c: Typical Surface Profile from Surface Simulation Algorithm

SIMULATION PARAMETERS	
No. of knives	6
Feed speed	90 m/min
Cutter Speed	3500 rpm
Vib. rate	0
Proud Knives	2 >>> 1 5
Ecc.rate/rev	0
Spindle Runout	0 microns

Figure 4.10d: Typical Surface Profile from Surface Simulation Algorithm

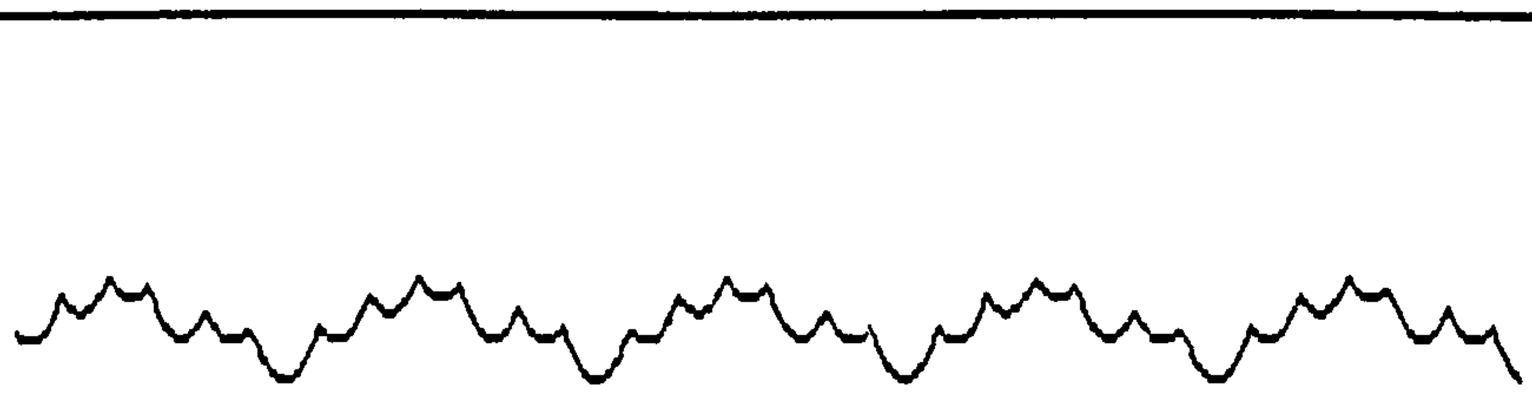

SIMULATION PARAMETERS

No. of knives	6
Feed speed	90 m/min
Cutter Speed	3500 rpm
Vib. rate	0
Proud Knives	2 >>> 1 5
Ecc.rate/rev	1
Spindle Runout	20 microns

Figure 4.10e: Typical Surface Profile from Surface Simulation Algorithm

SIMULATION PARAMETERS

No. of knives	6
Feed speed	90 m/min
Cutter Speed	3500 rpm
Vib. rate	300
Proud Knives	2 >>> 1 5
Ecc.rate/rev	1
Spindle Runout	15 microns

Figure 4.10f: Typical Surface Profile from Surface Simulation Algorithm

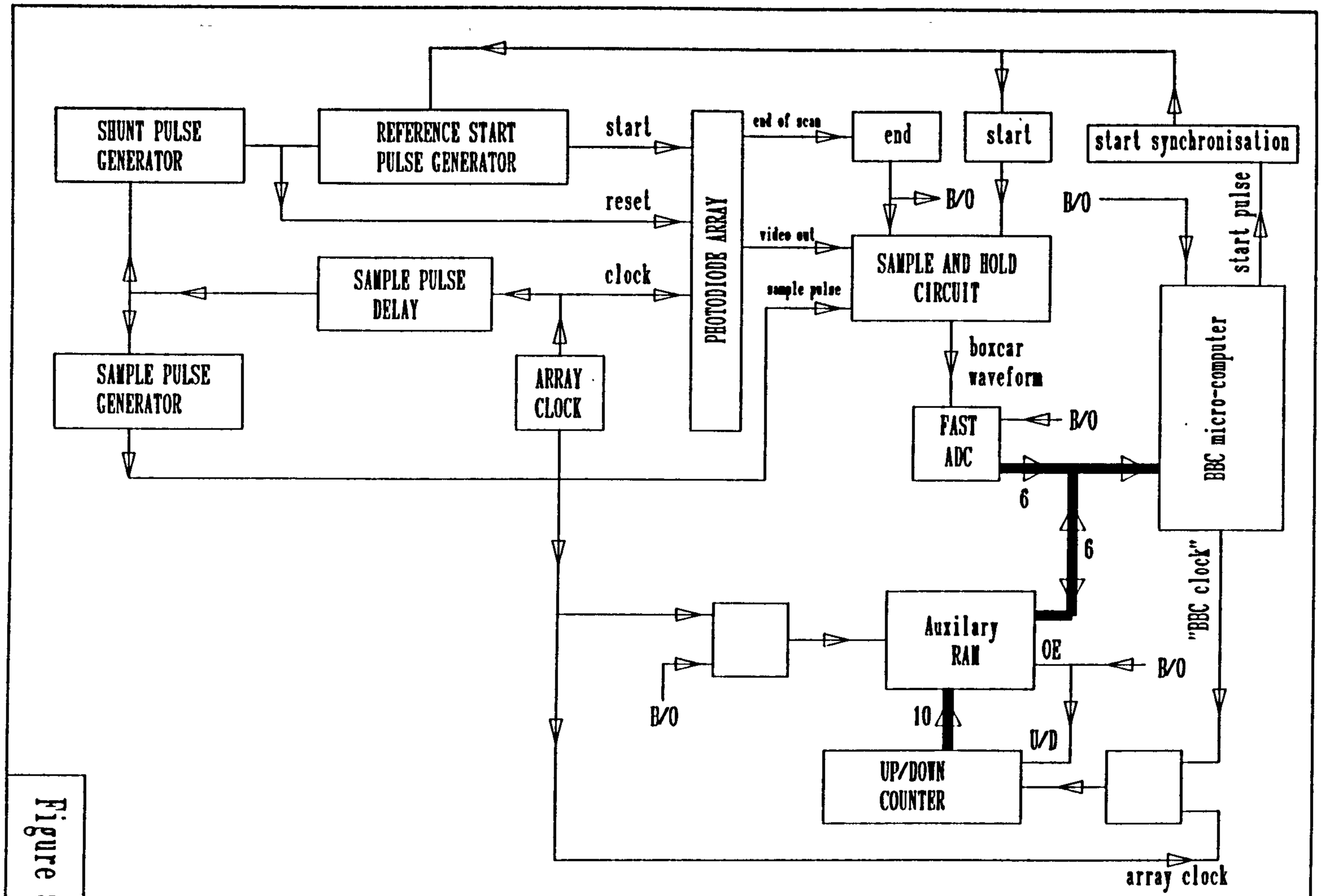

Figure 5.1.1

SCHEMATIC OF POST PROCESS SYSTEM

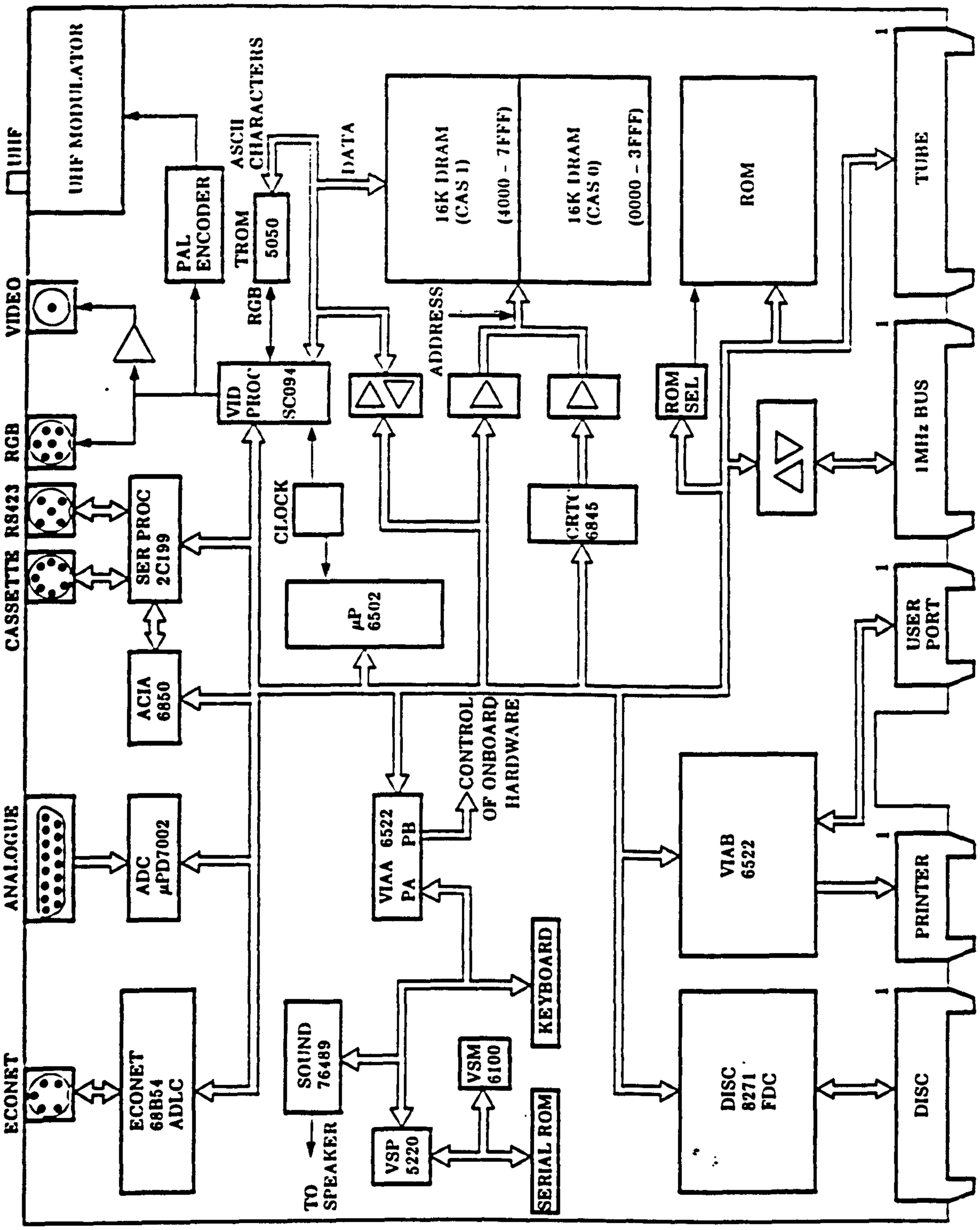

Figure 5.2.1: Schematic of the BBC microcomputer

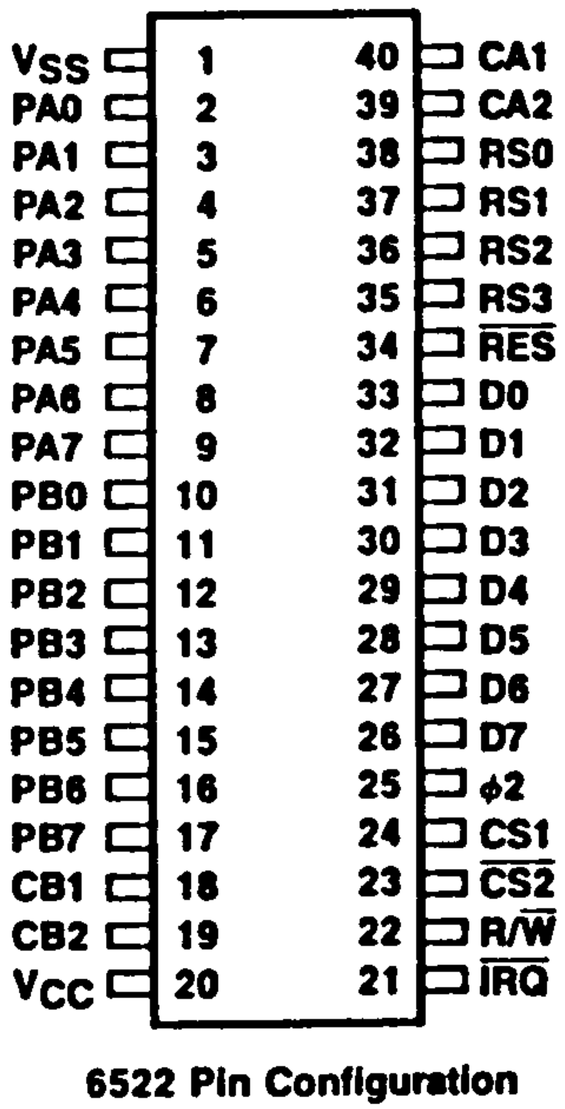

6522 Pin Configuration

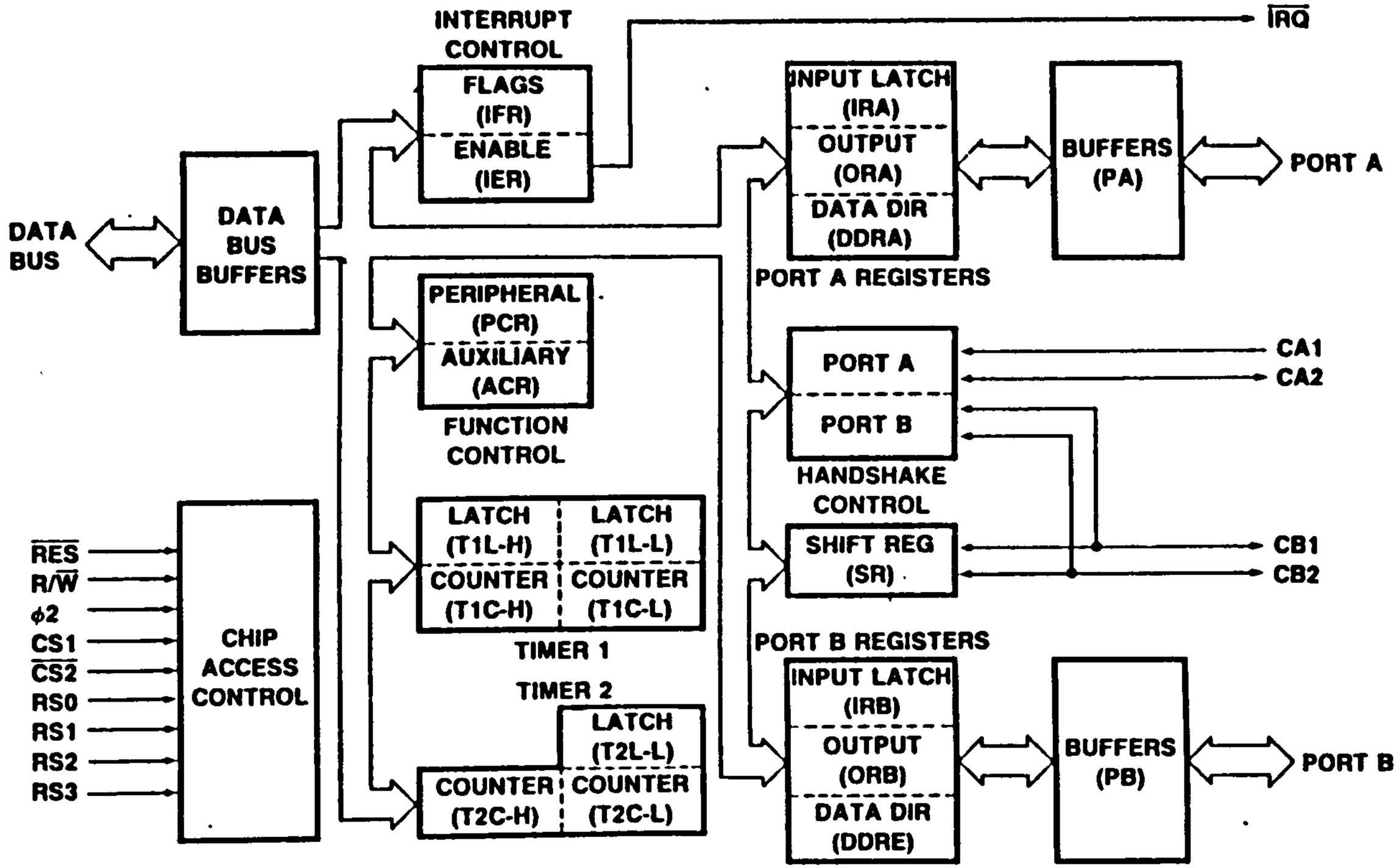

Figure 5.2.2: Schematic of the 6522 VIA

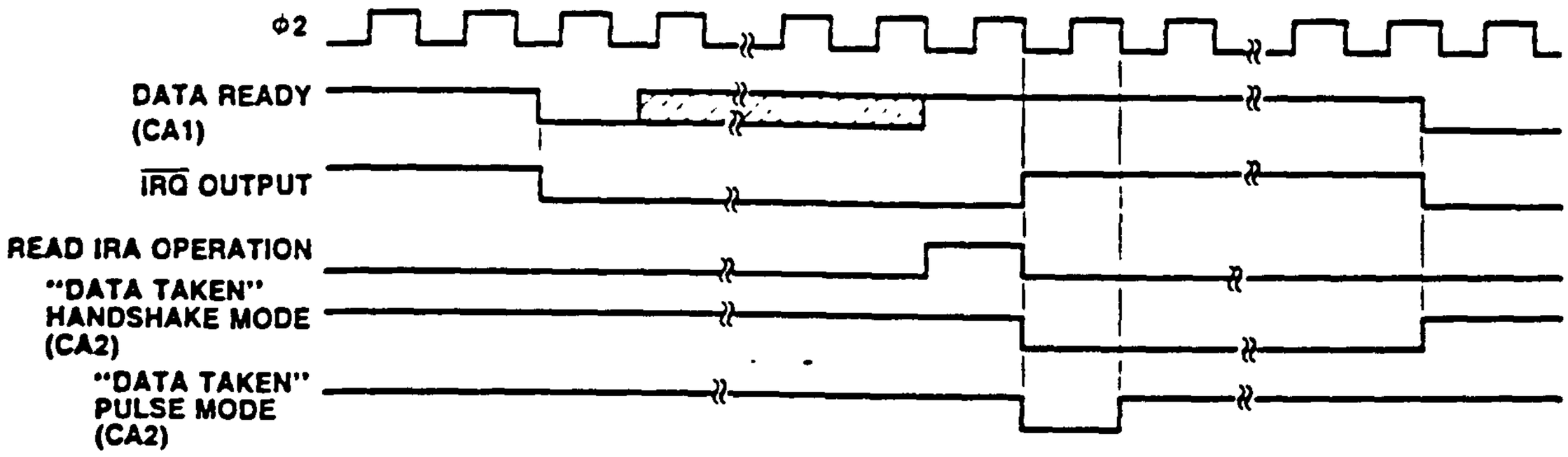

Figure 5.2.3: Read Handshake Timing Diagram for Port A Only

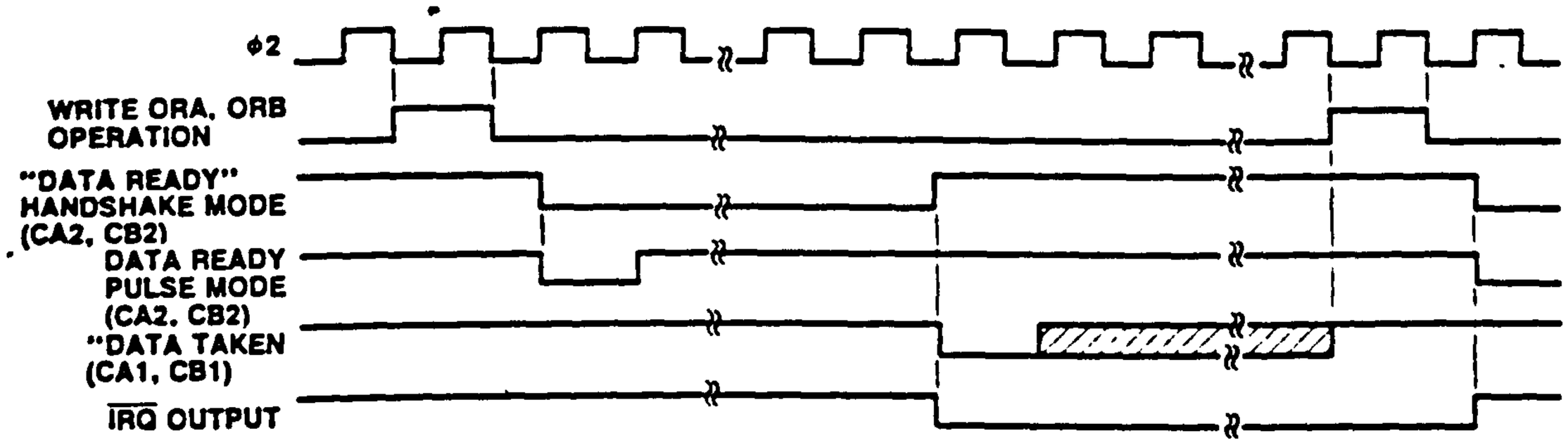

Figure 5.2.4: Write Handshake Timing Diagram

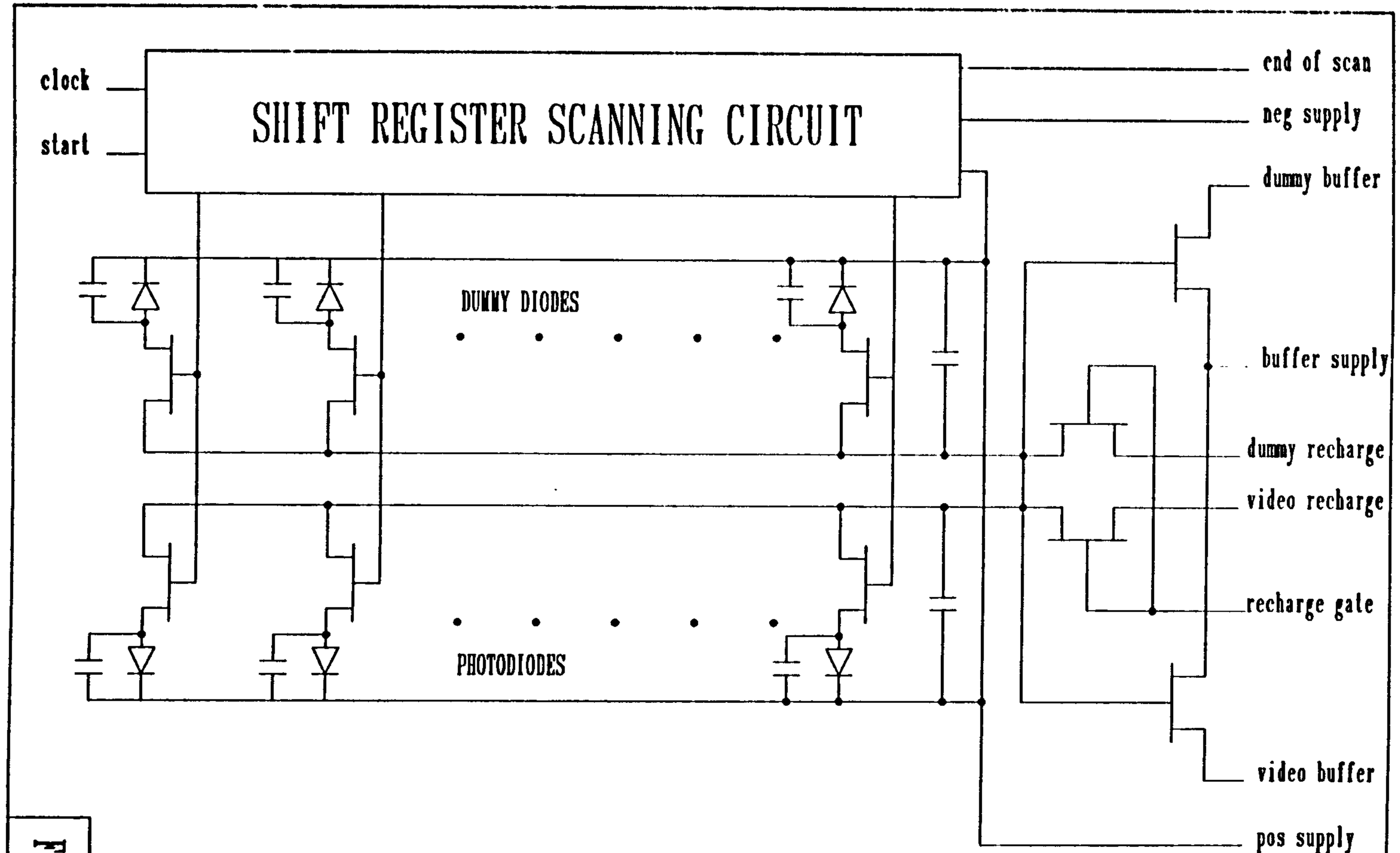

Figure 5.2.5

SCHEMATIC CIRCUIT OF PHOTODIODE ARRAY

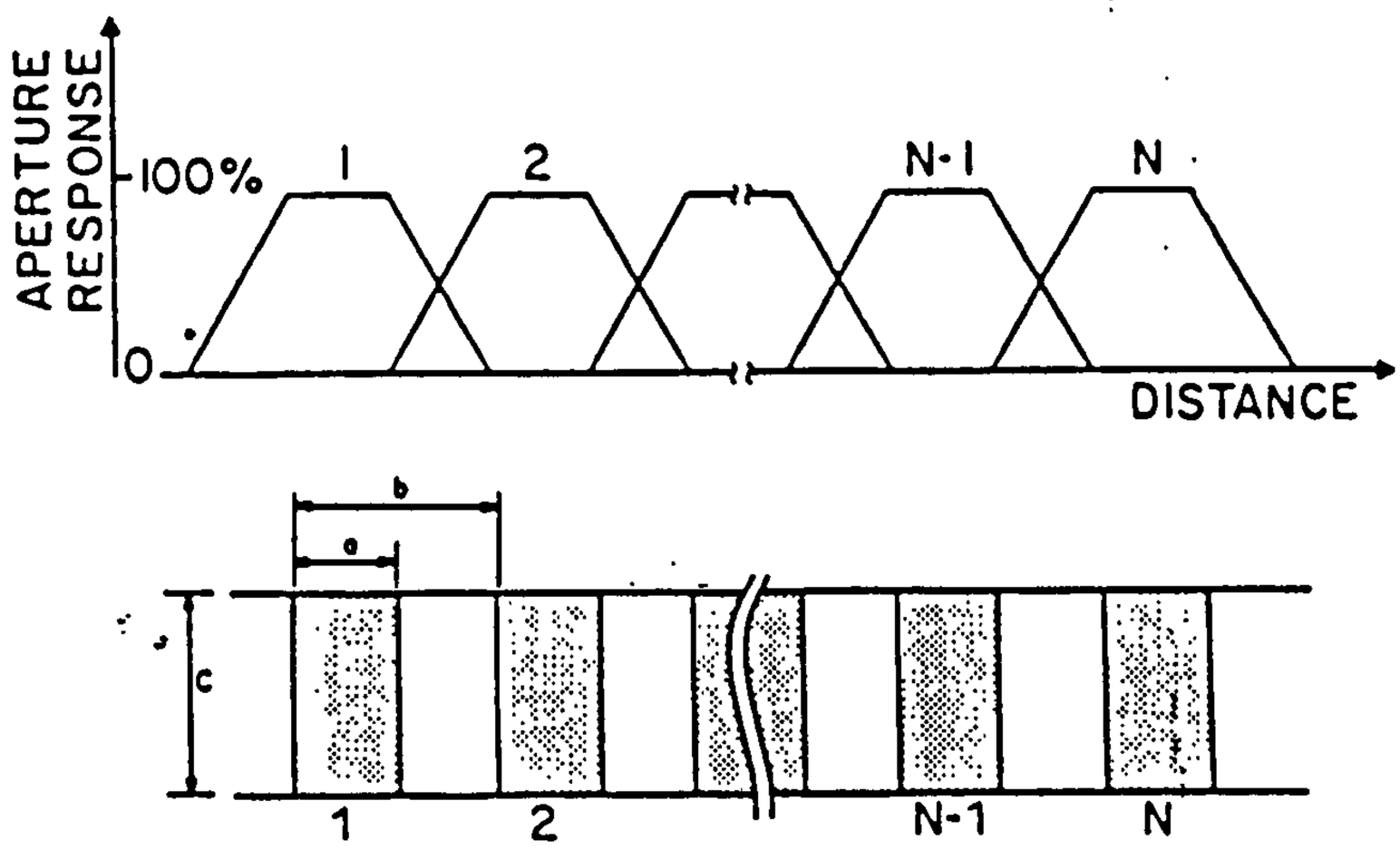

Figure 5.2.6: Sensor Geometry and Idealised apperture Response Function
a=15µm: b=25µm: c=26µm

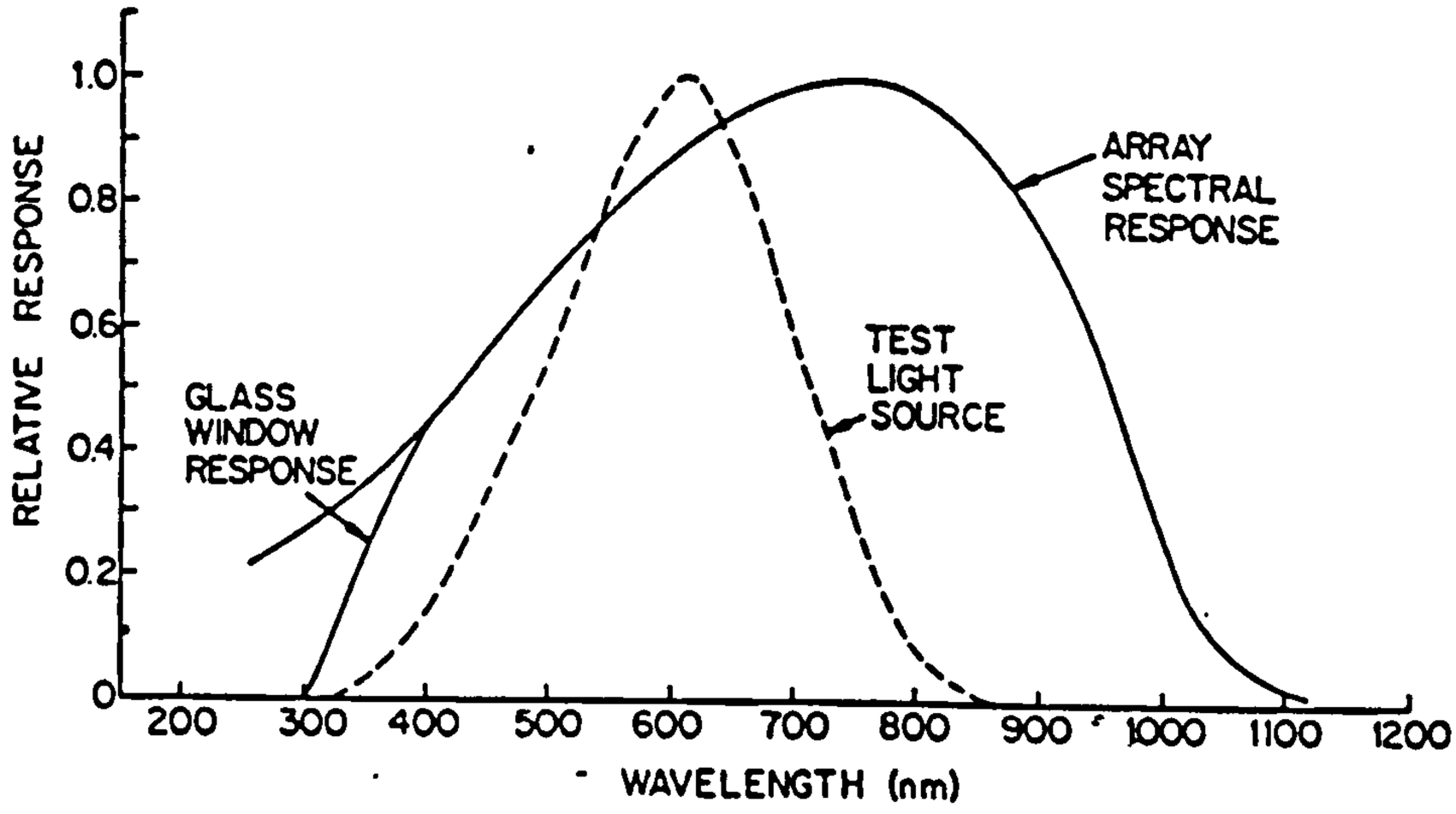

Figure 5.2.7: Photodiode Relative Spectral Response as Function of Wavelength

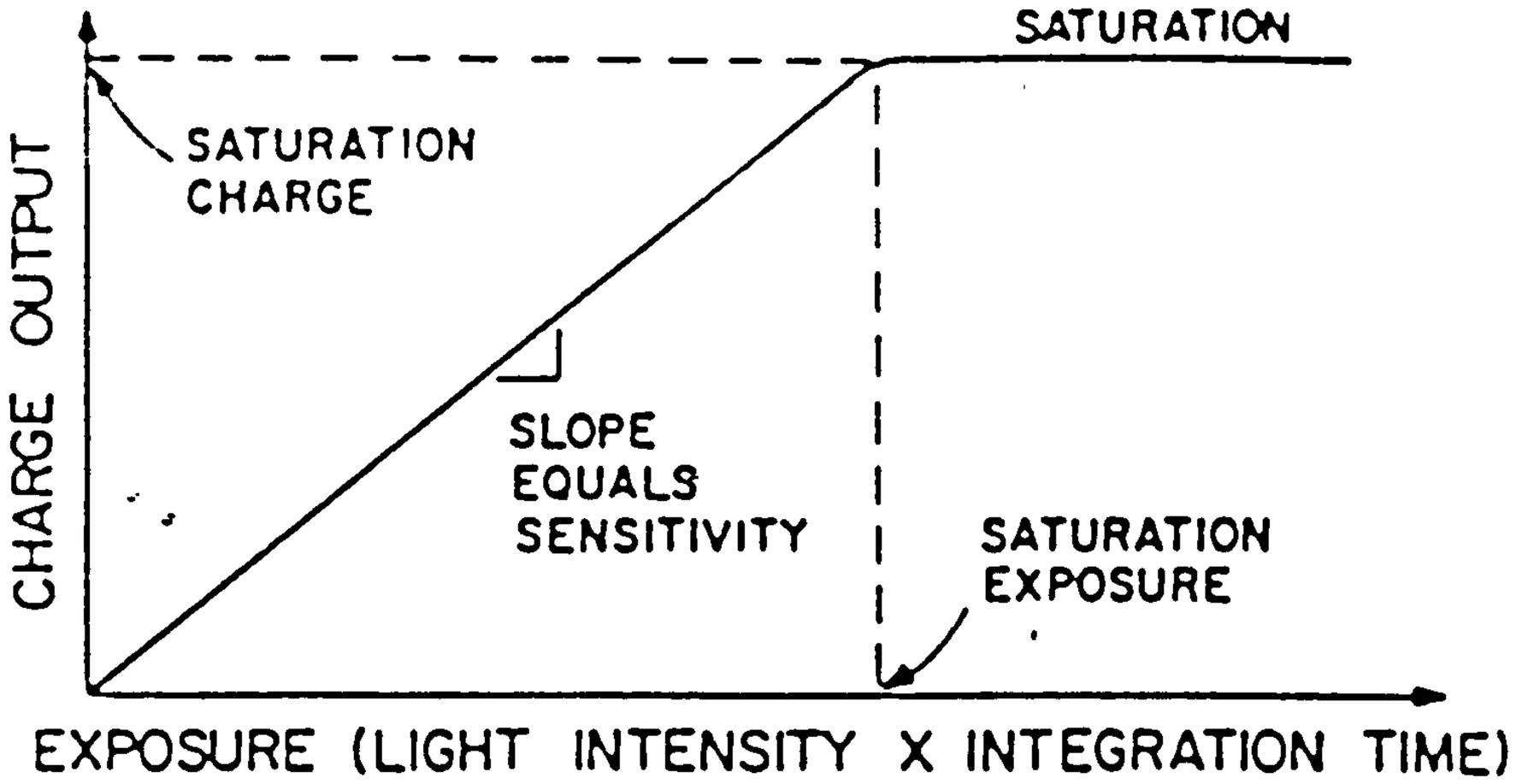

Figure 5.2.8: Photodiode Output Charges verses Exposure Characteristic

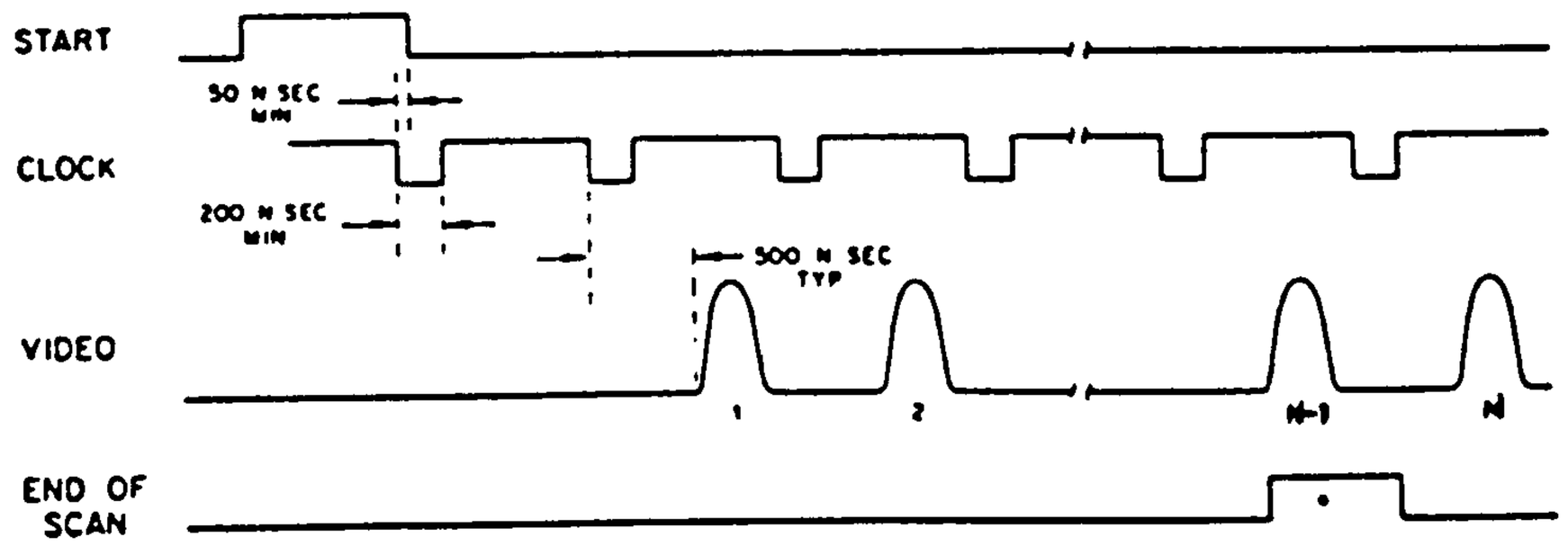

Figure 5.2.10: Timing Diagram for Array clock and Start input in realation to Video and End-of-Scan Outputs

NOTE: All capacitances are in microfarads

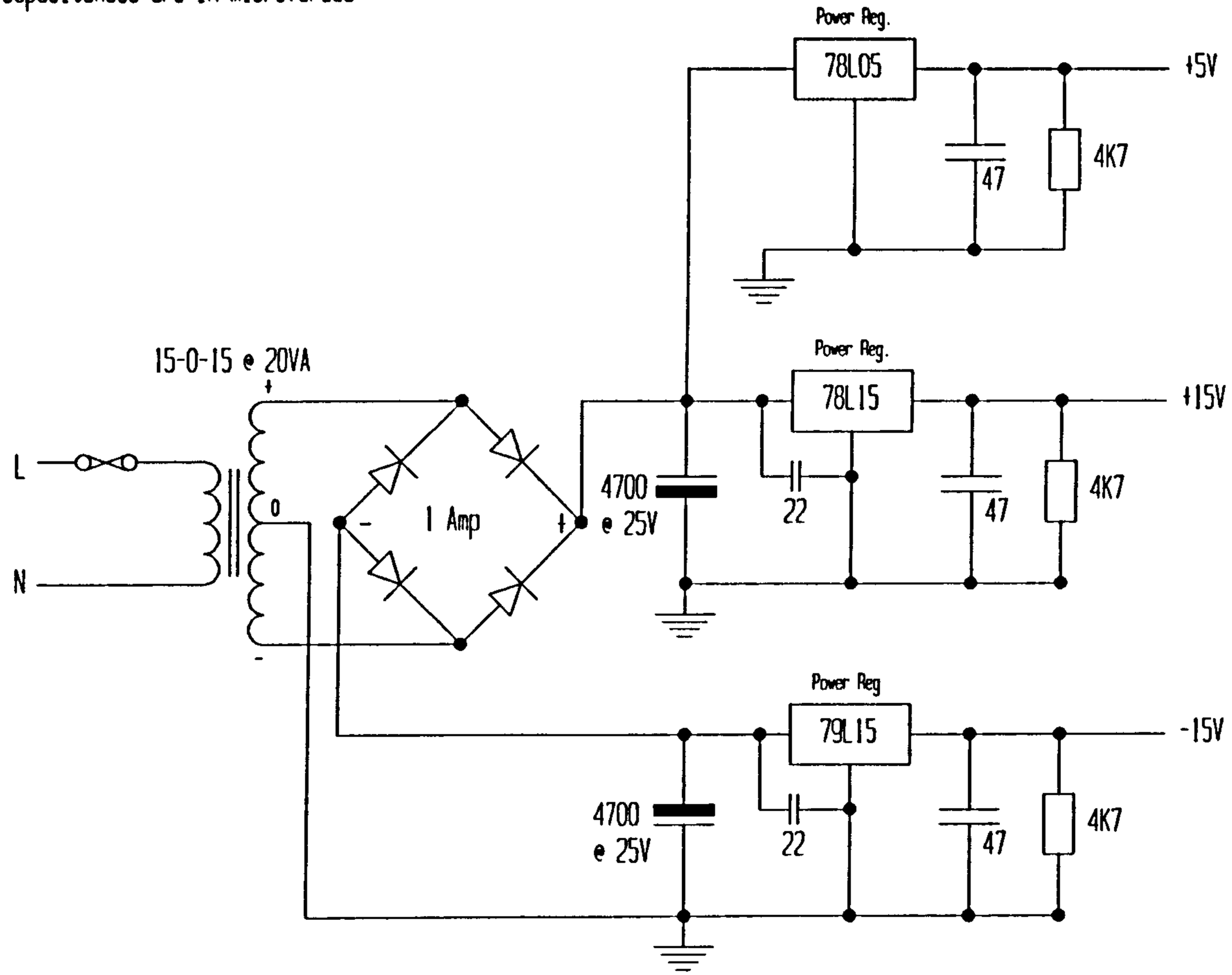

Figure 5.2.9

POWER SUPPLY CIRCUIT DAIGRAM

NOTE:
Resistors are in Ohms
Capacitors are in microfarads

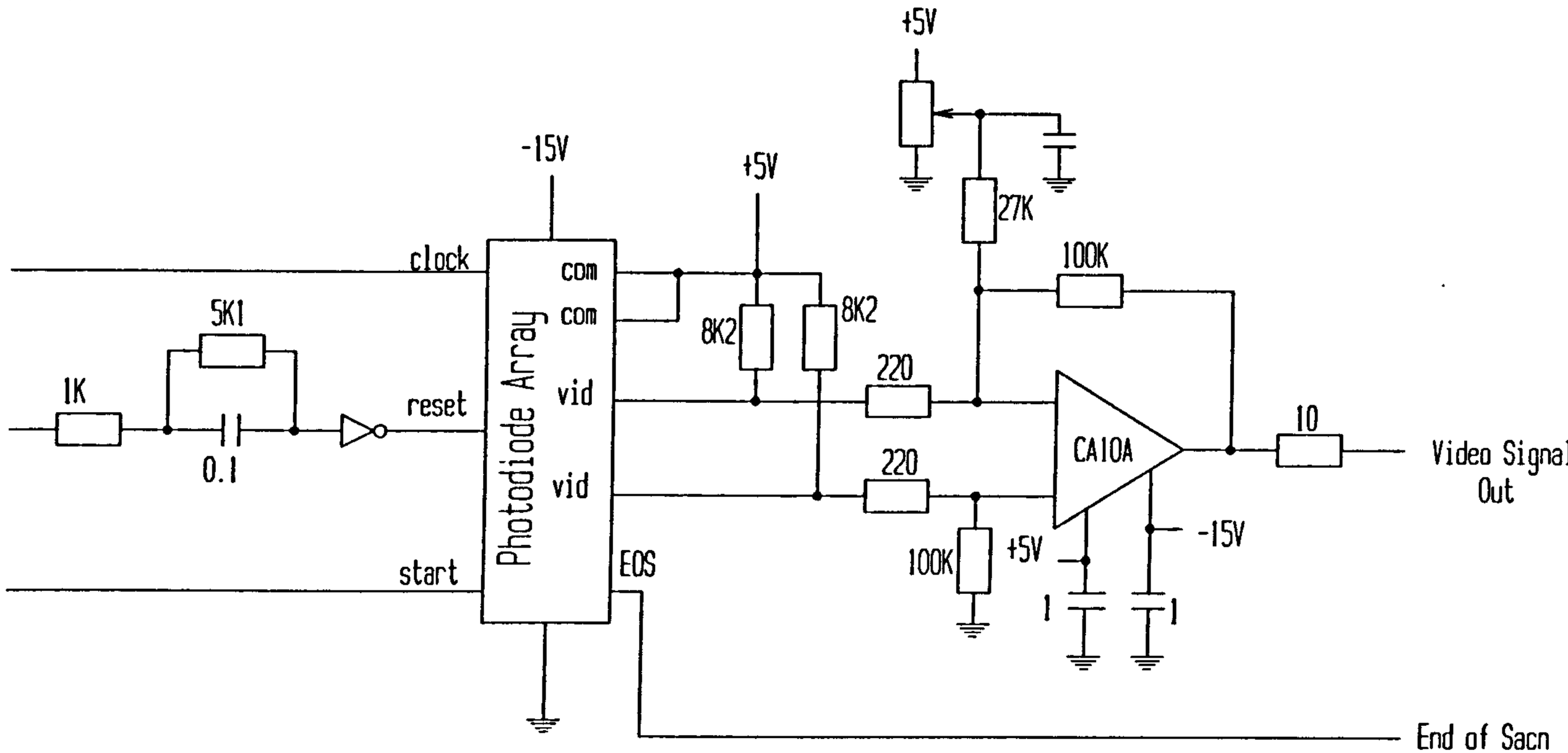

Figure 5.2.11

DIFFERENTIAL AMPLIFICATION OF VIDEO AND DUMMY LINES

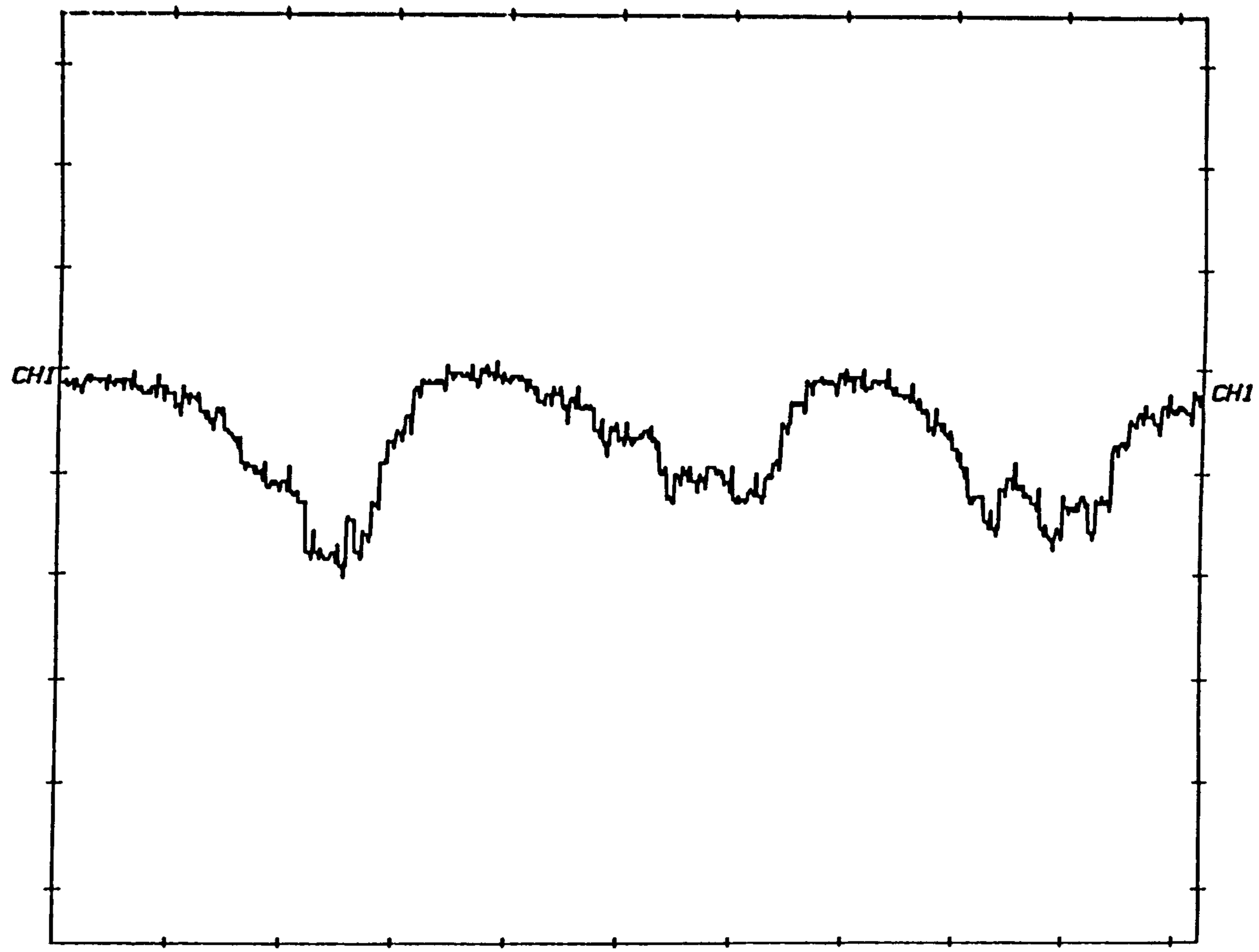

Figure 5.2.12: Sample and Hold Boxcar Video Signal

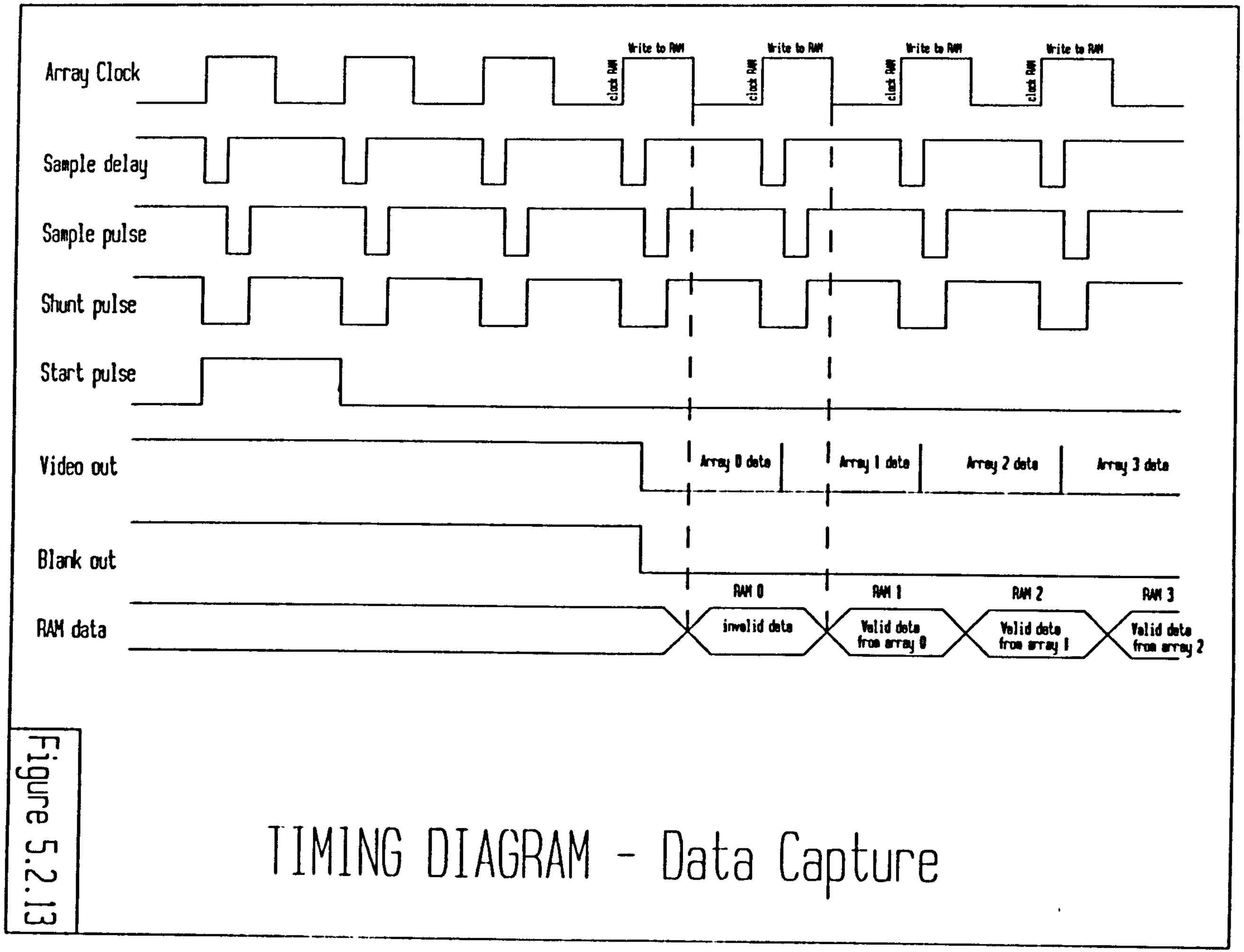

Figure 5.2.13

TIMING DIAGRAM - Data Capture

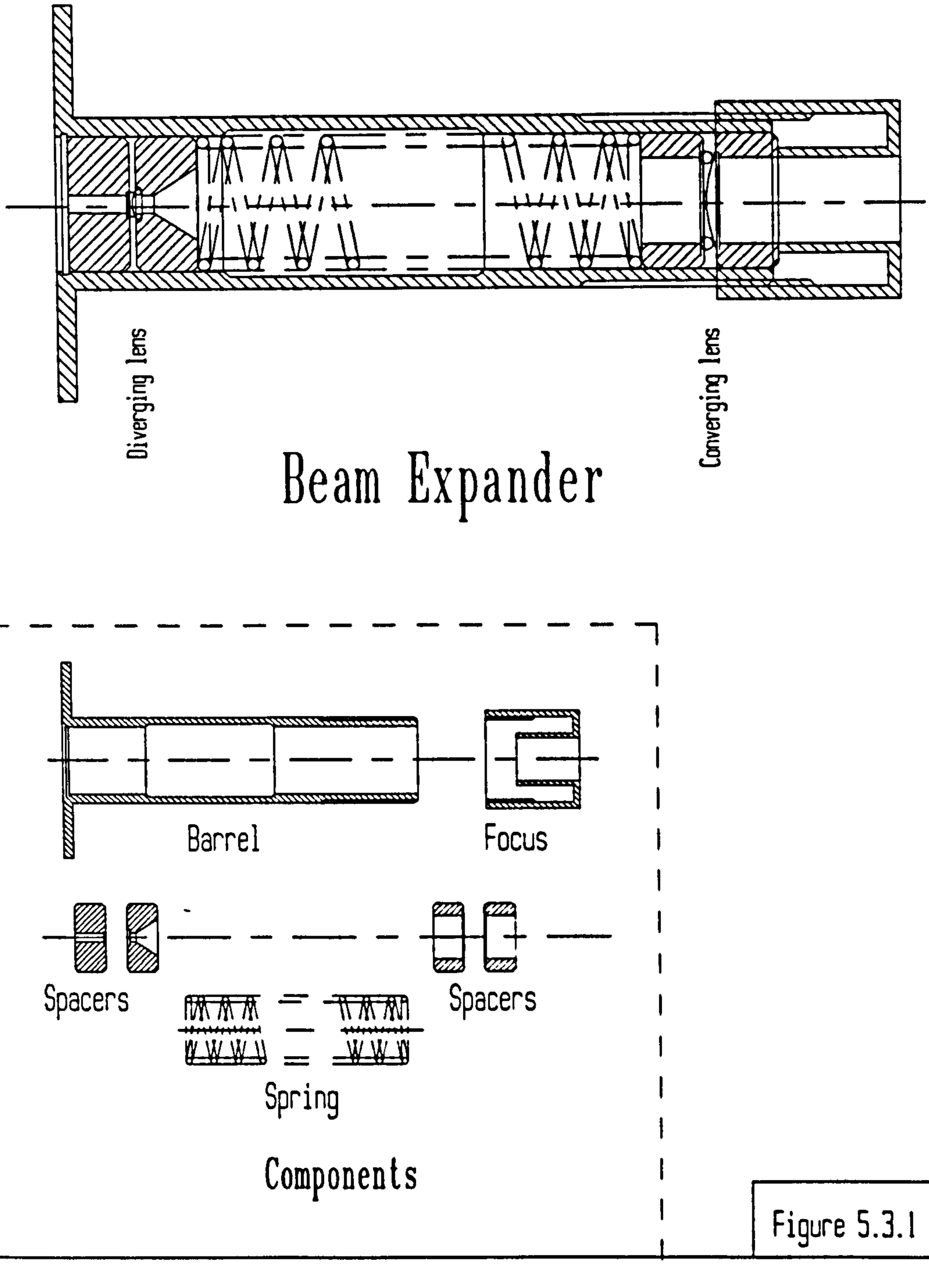
Diverging lens
Converging lens
Beam Expander
Barrel
Focus
Spacers
Spacers
Spring
Components

Figure 5.3.1

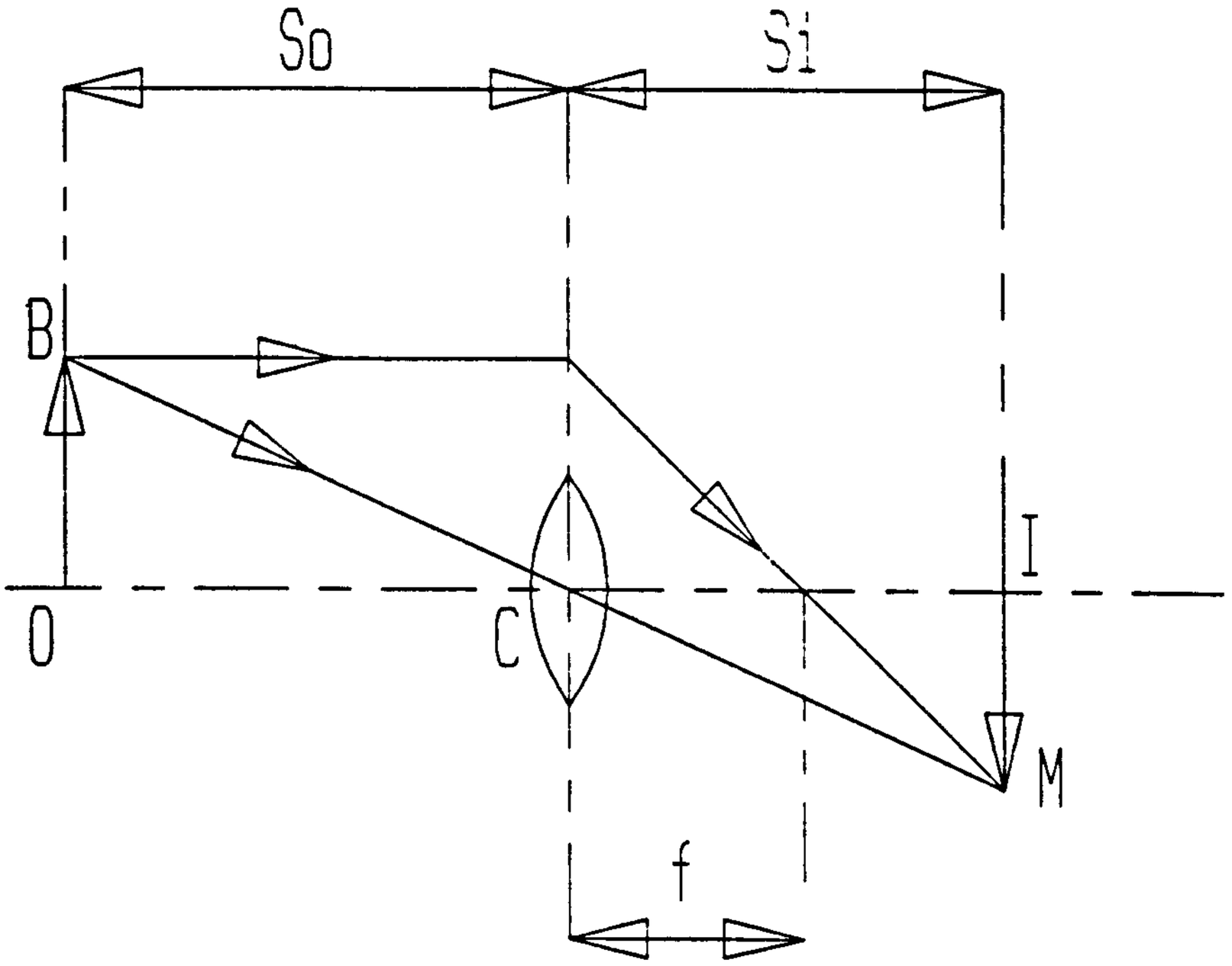

LENS MAKER'S FORMULA: Symbol Definition

Figure 5.3.2

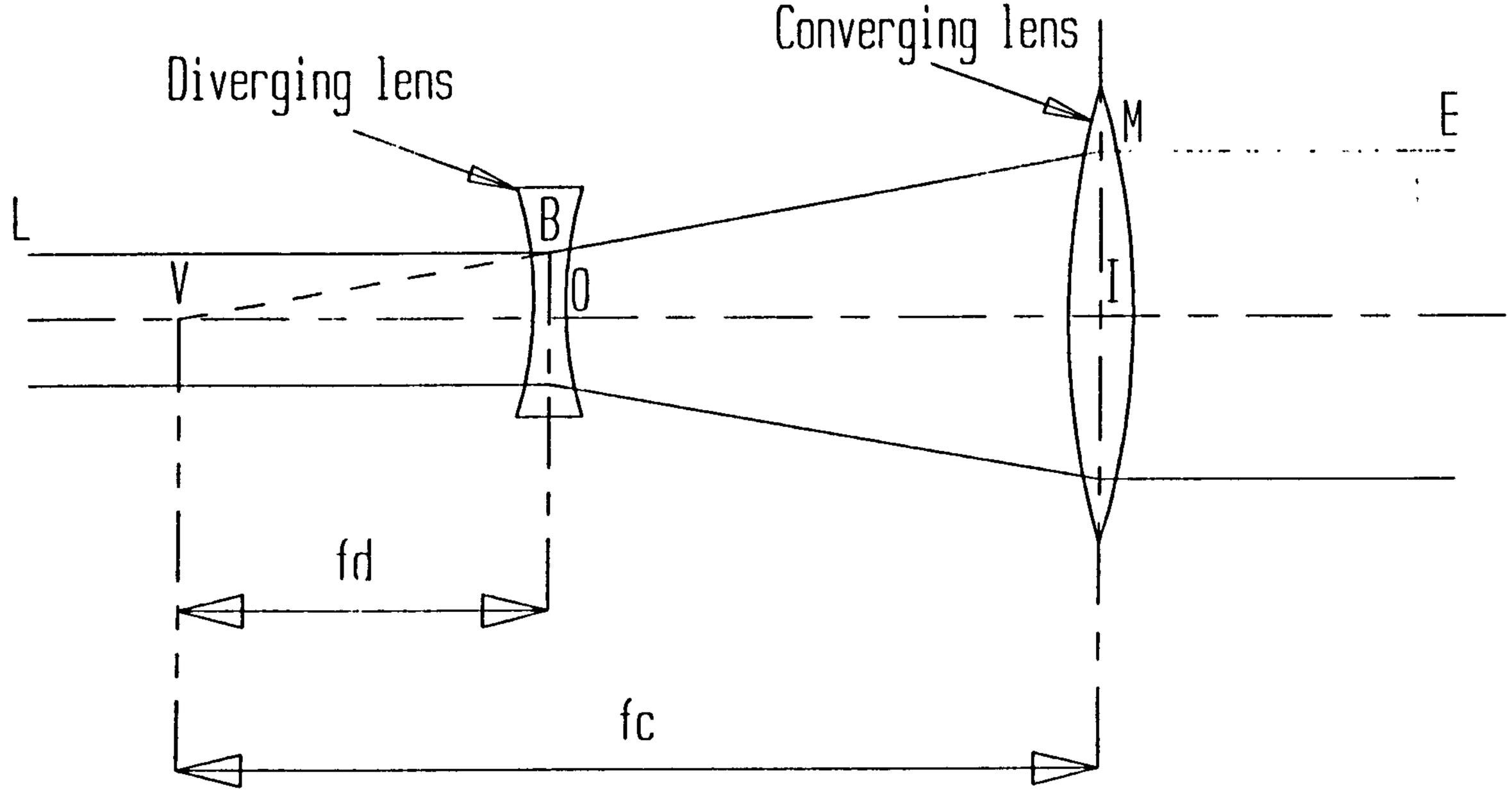

Figure 5.3.3

BEAM EXPANDER - The optical arrangement

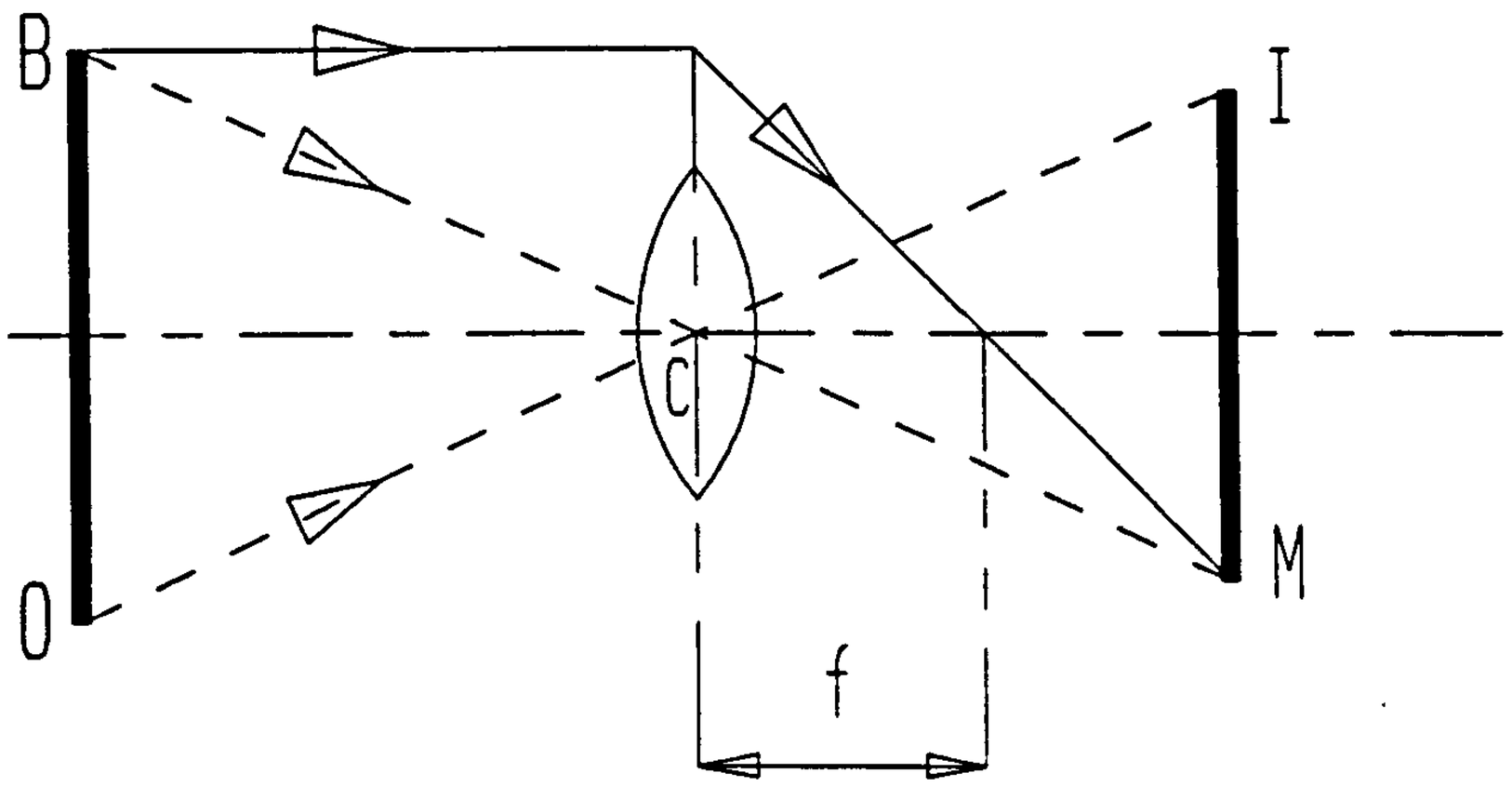

OB = sample length
= 125mm
IM = image length
= 25mm
f = lens focal length
= 50mm

IMAGE FOCUSING - The Optical Arrangement

Figure 5.3.4

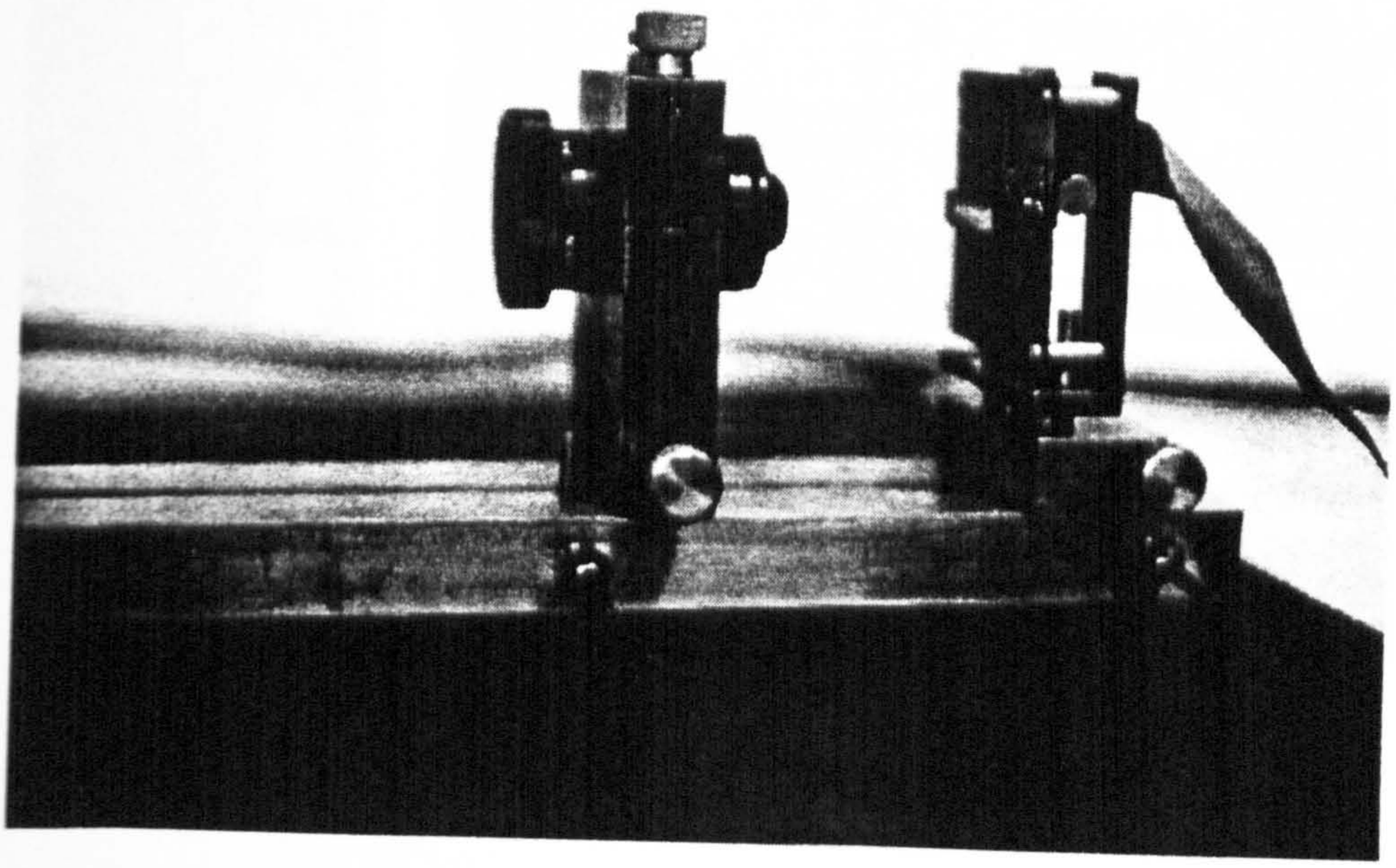

Figure 5.3.6: Lens Mount

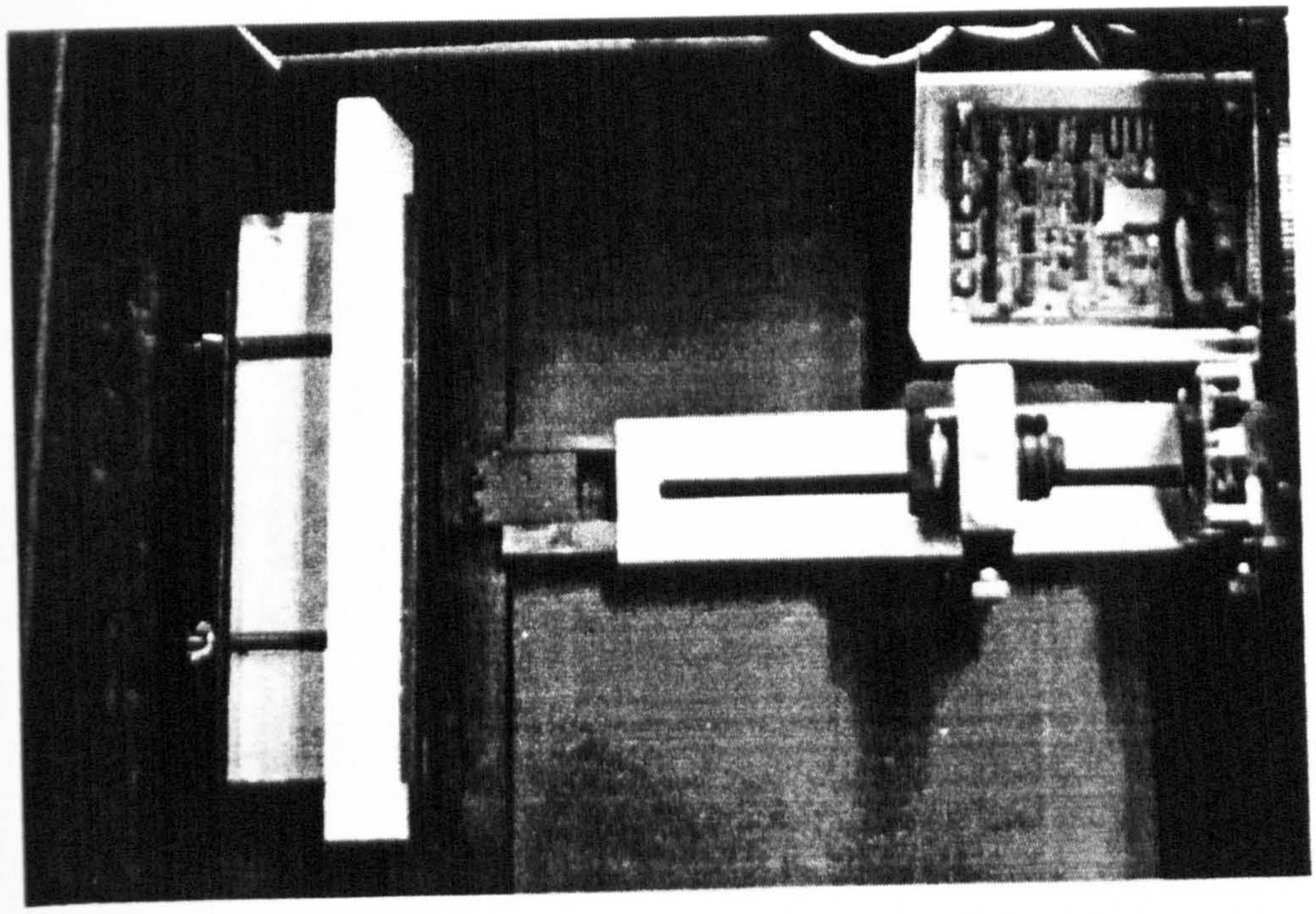

Figure 5.4.1: Framework

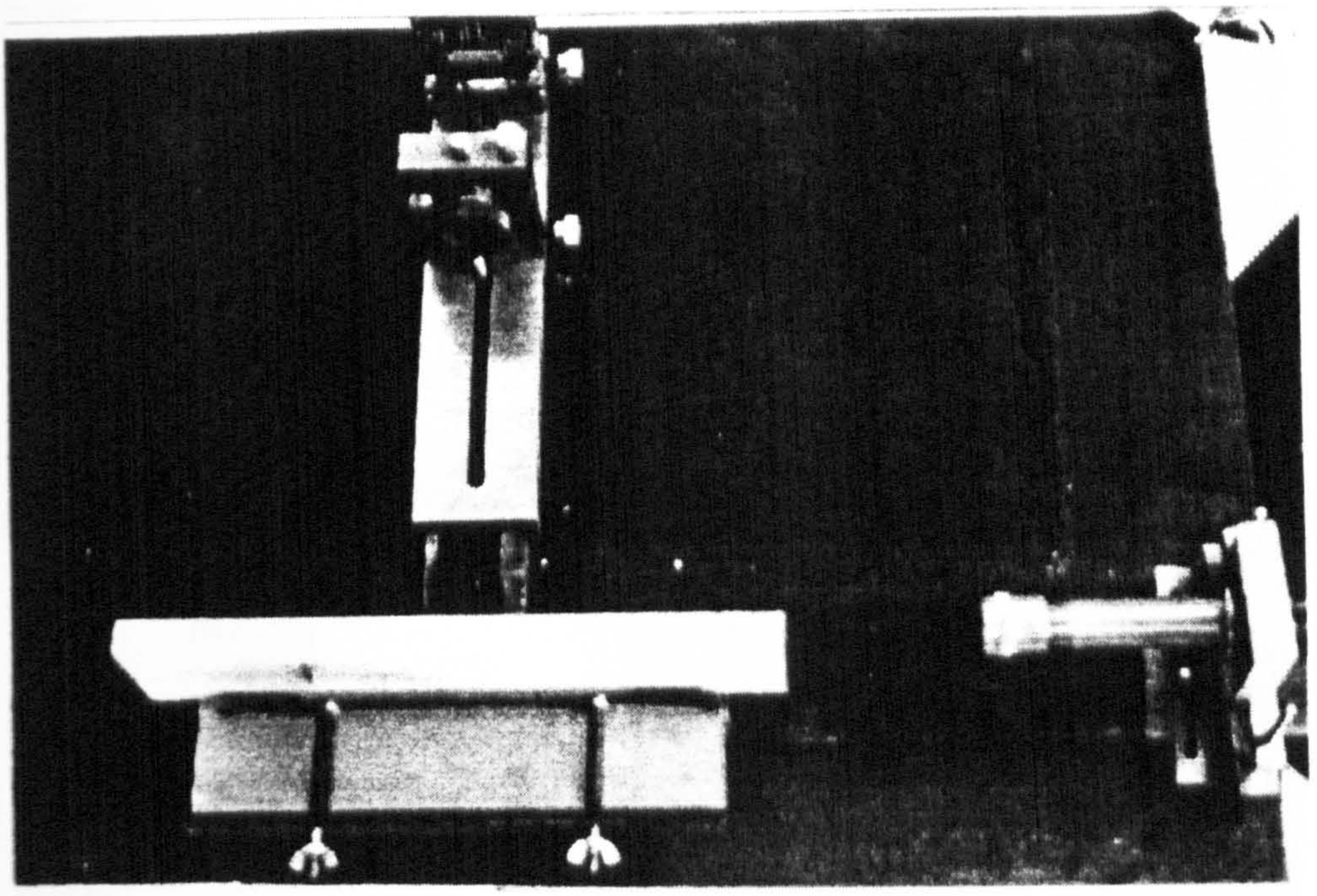

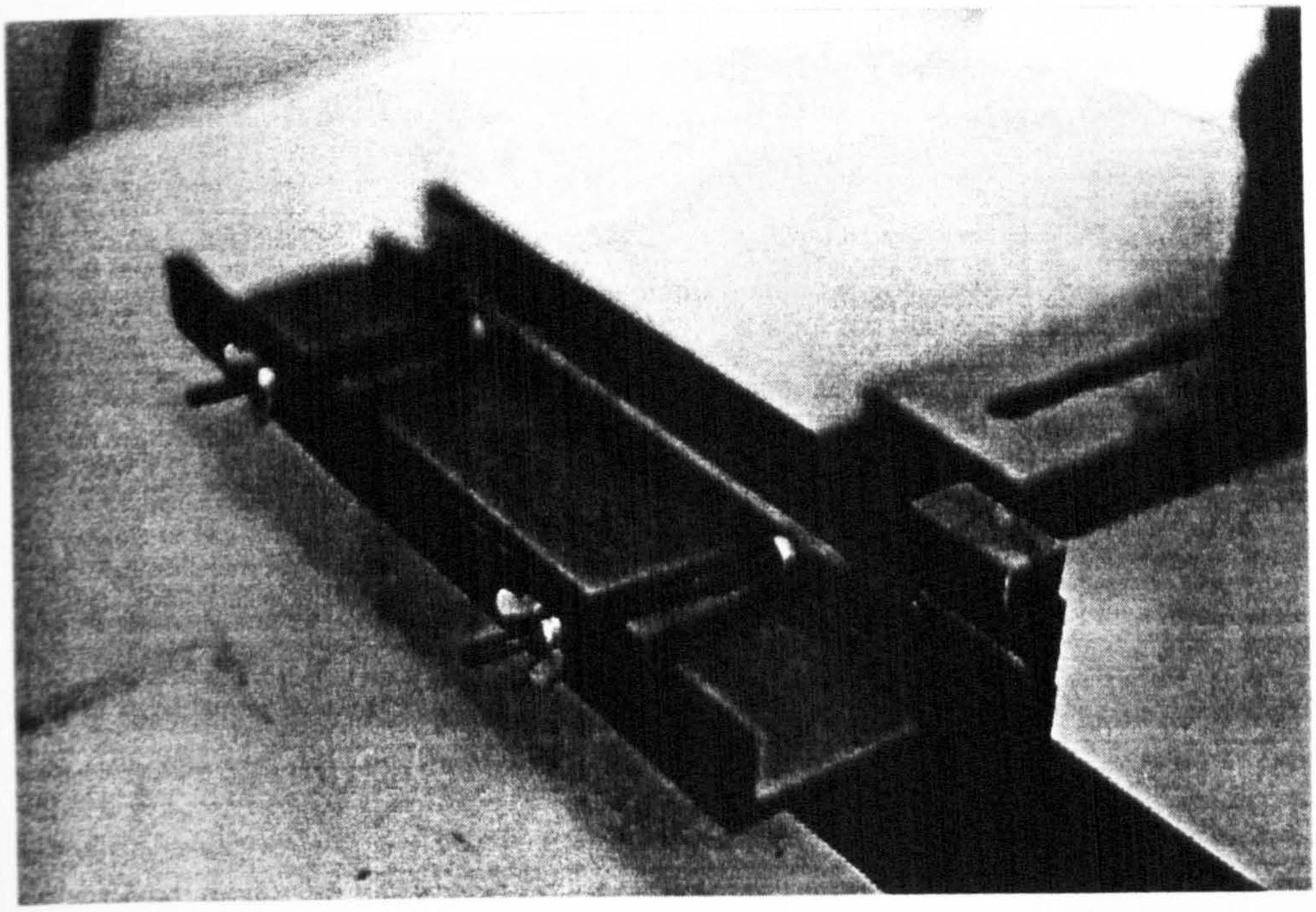

Figure 5.4.2: Timber-Sample Clamping Device

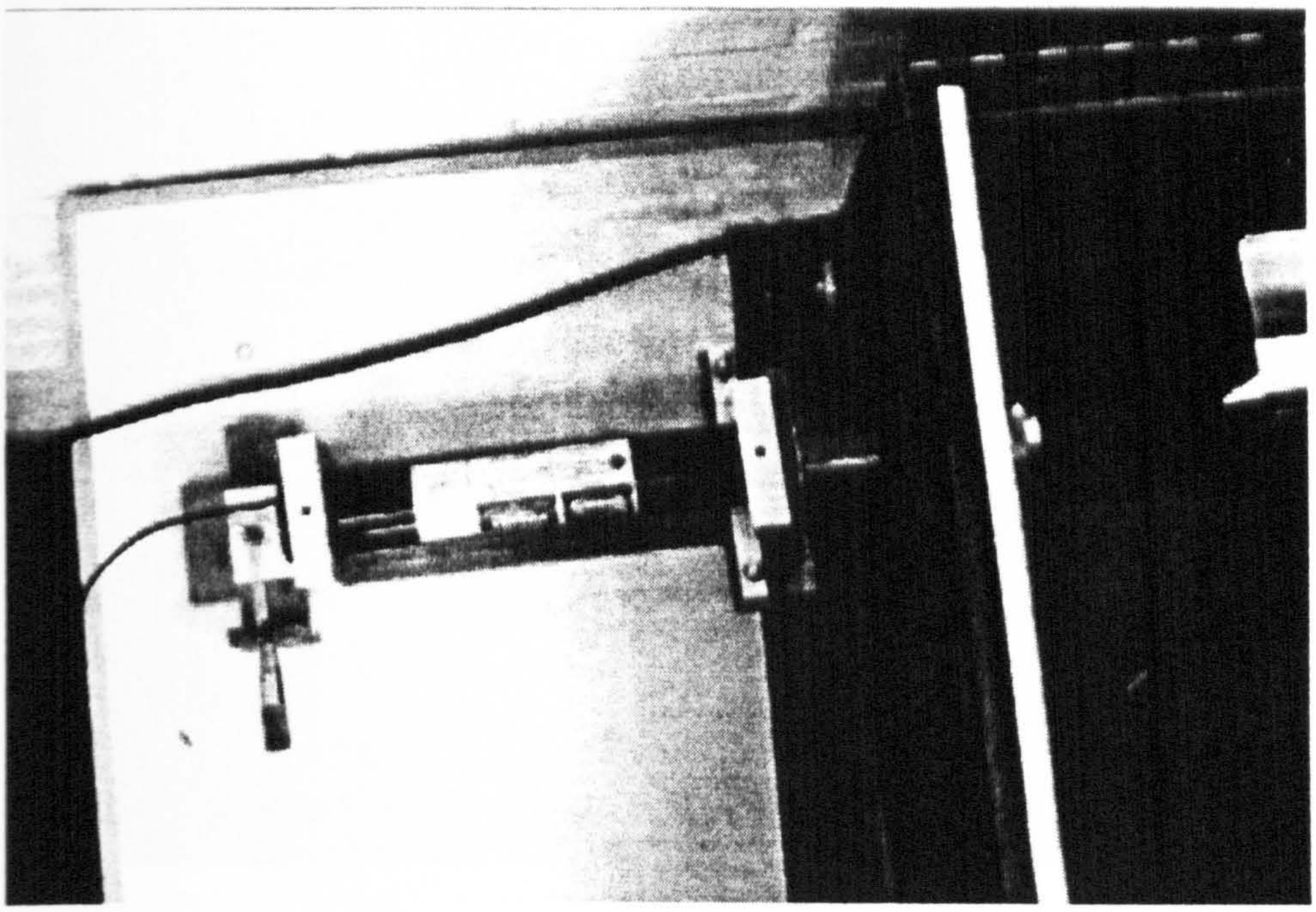

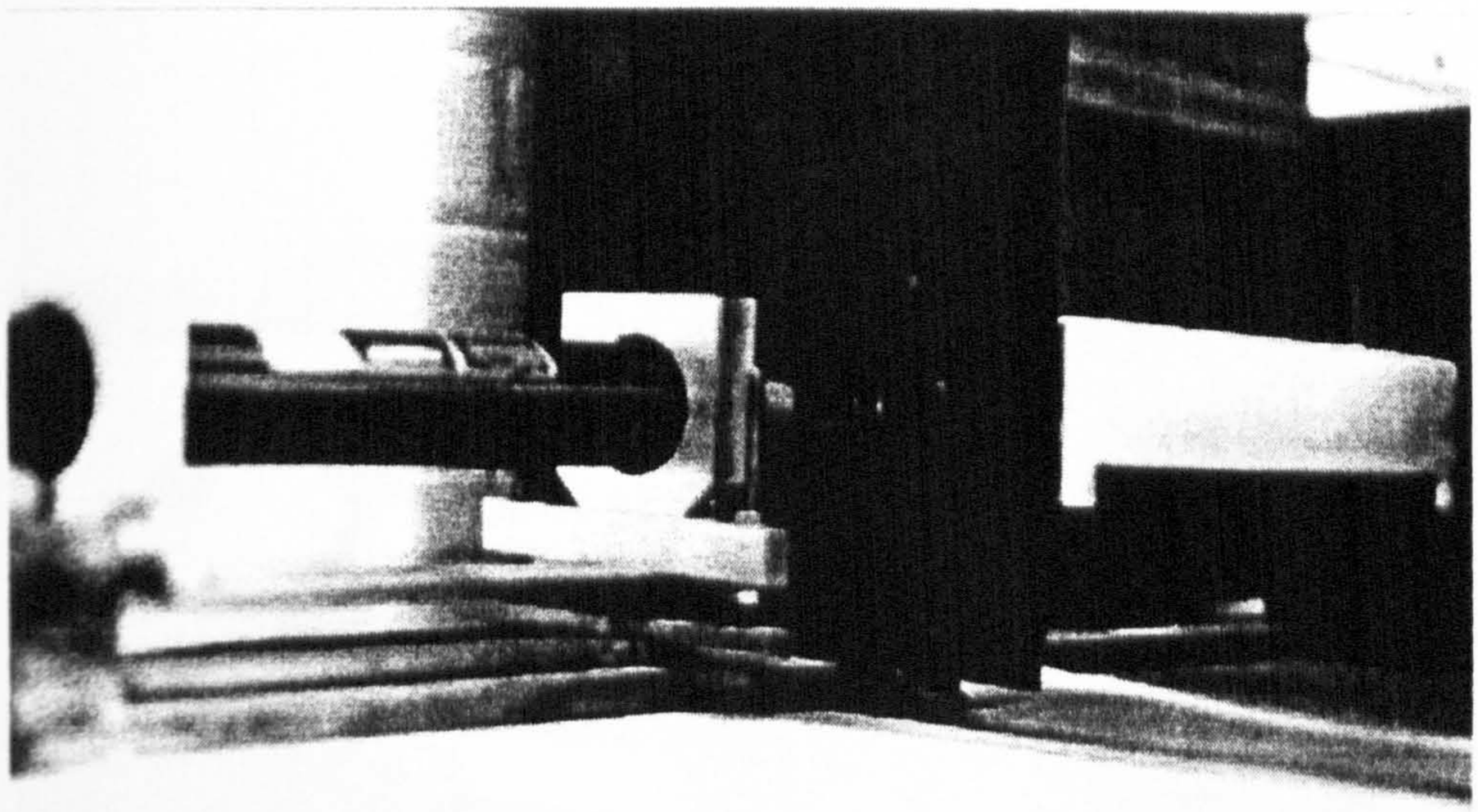

Figure 5.4.3: Helium-neon Laser and "Floating" Carrage

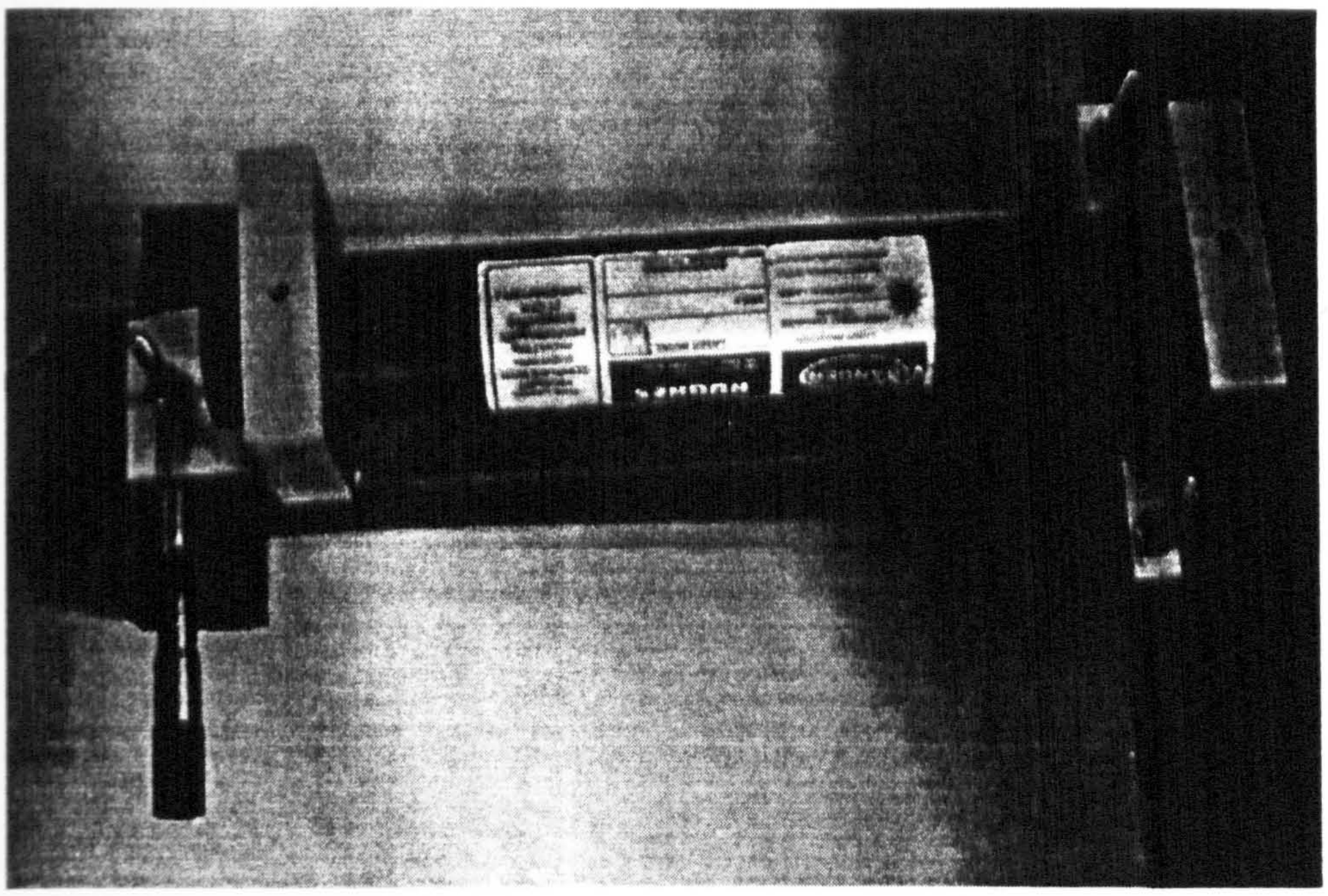

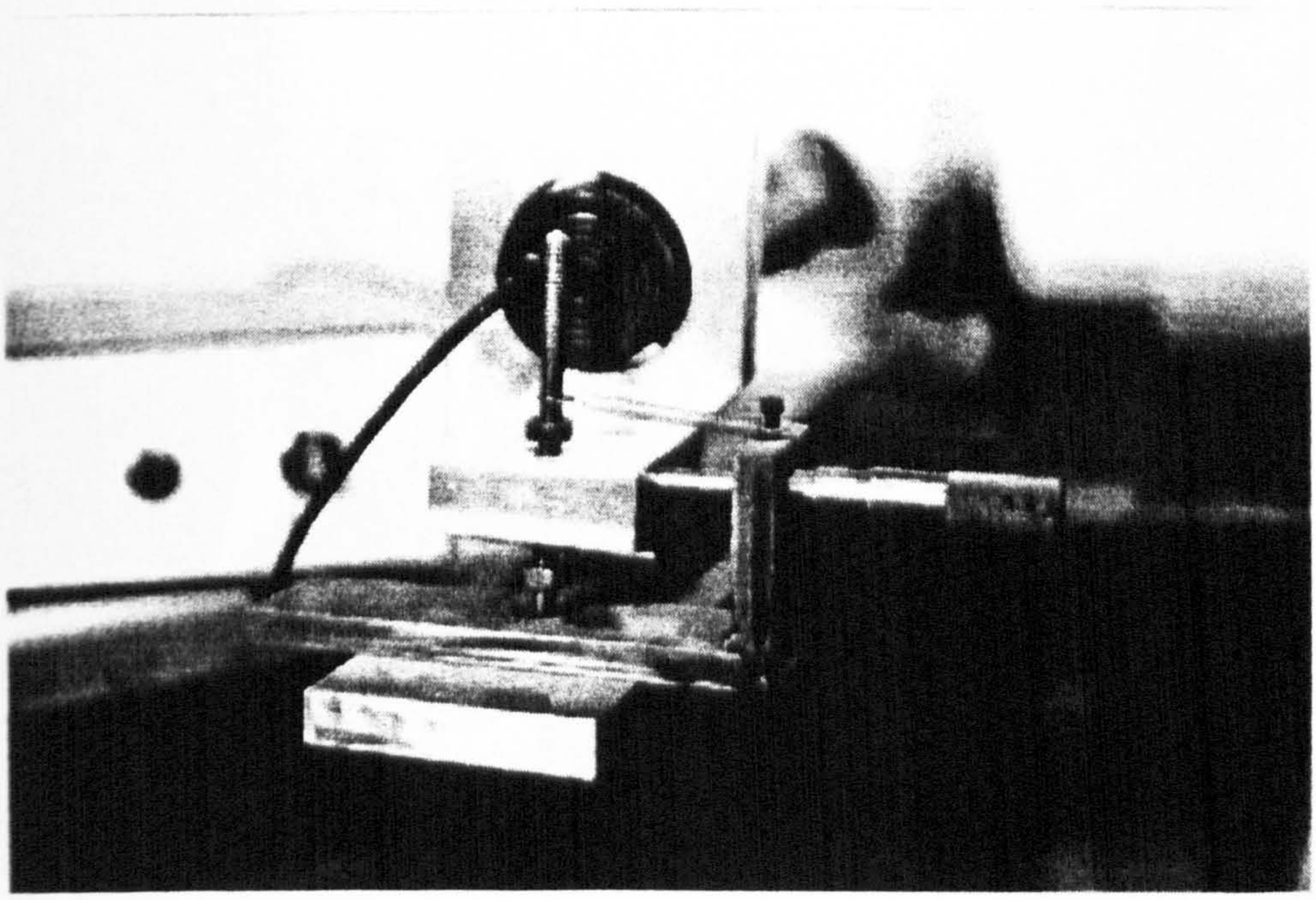

Figure 5.4.4: Laser beam incidence angle adjustment using Micrometer - Spring mechanism

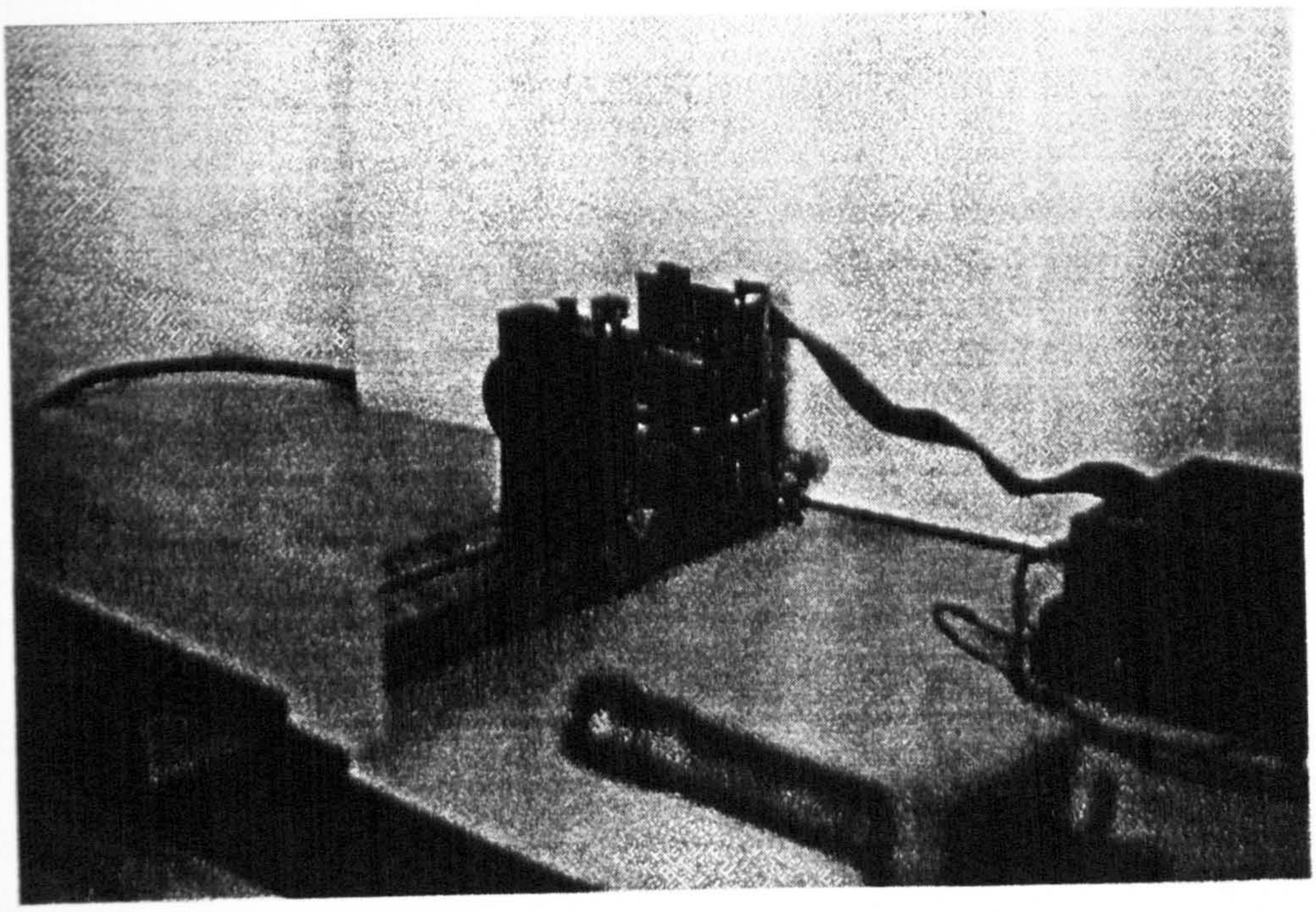

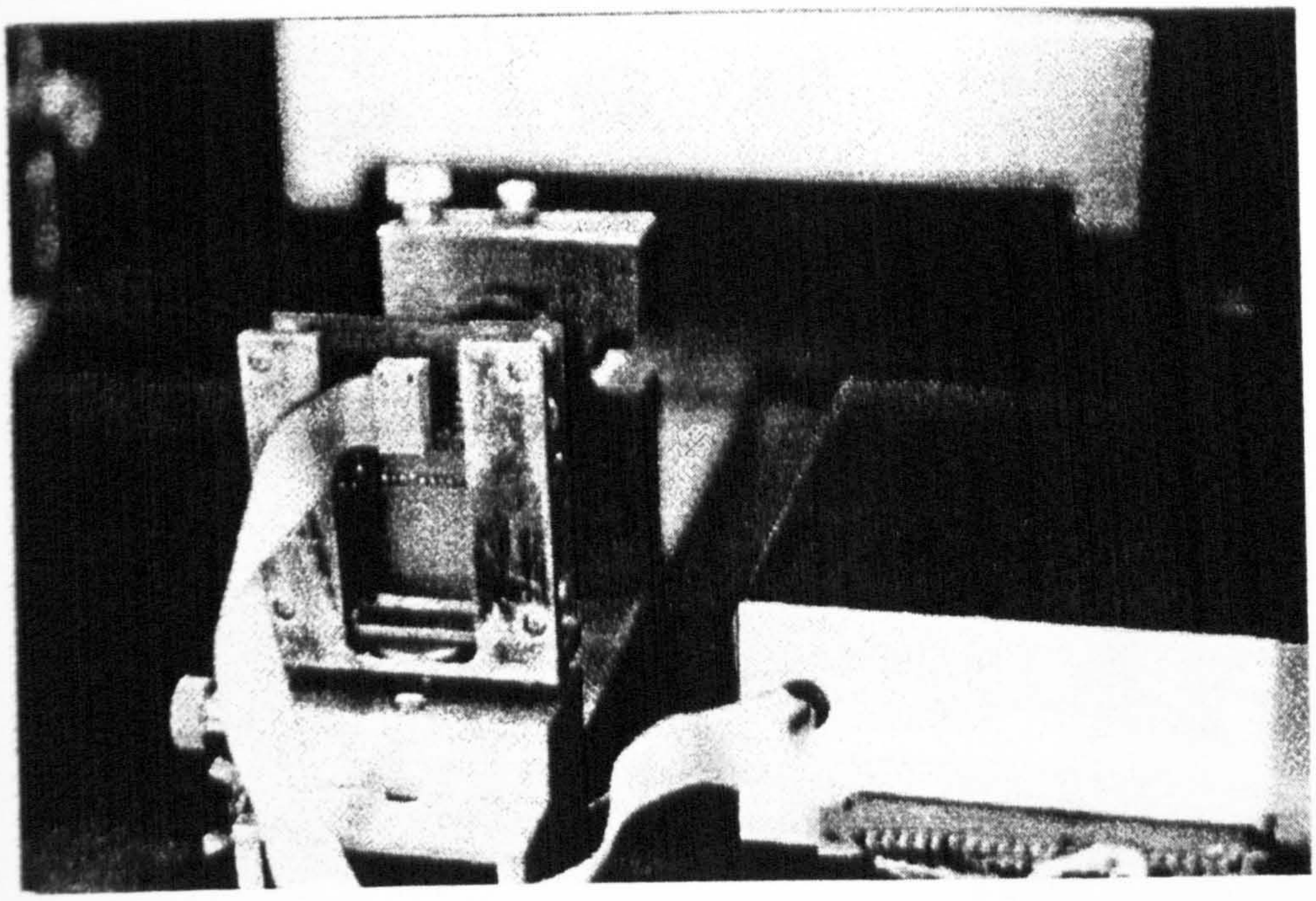

Figure 5.4.5: Image Alignment Mechinism

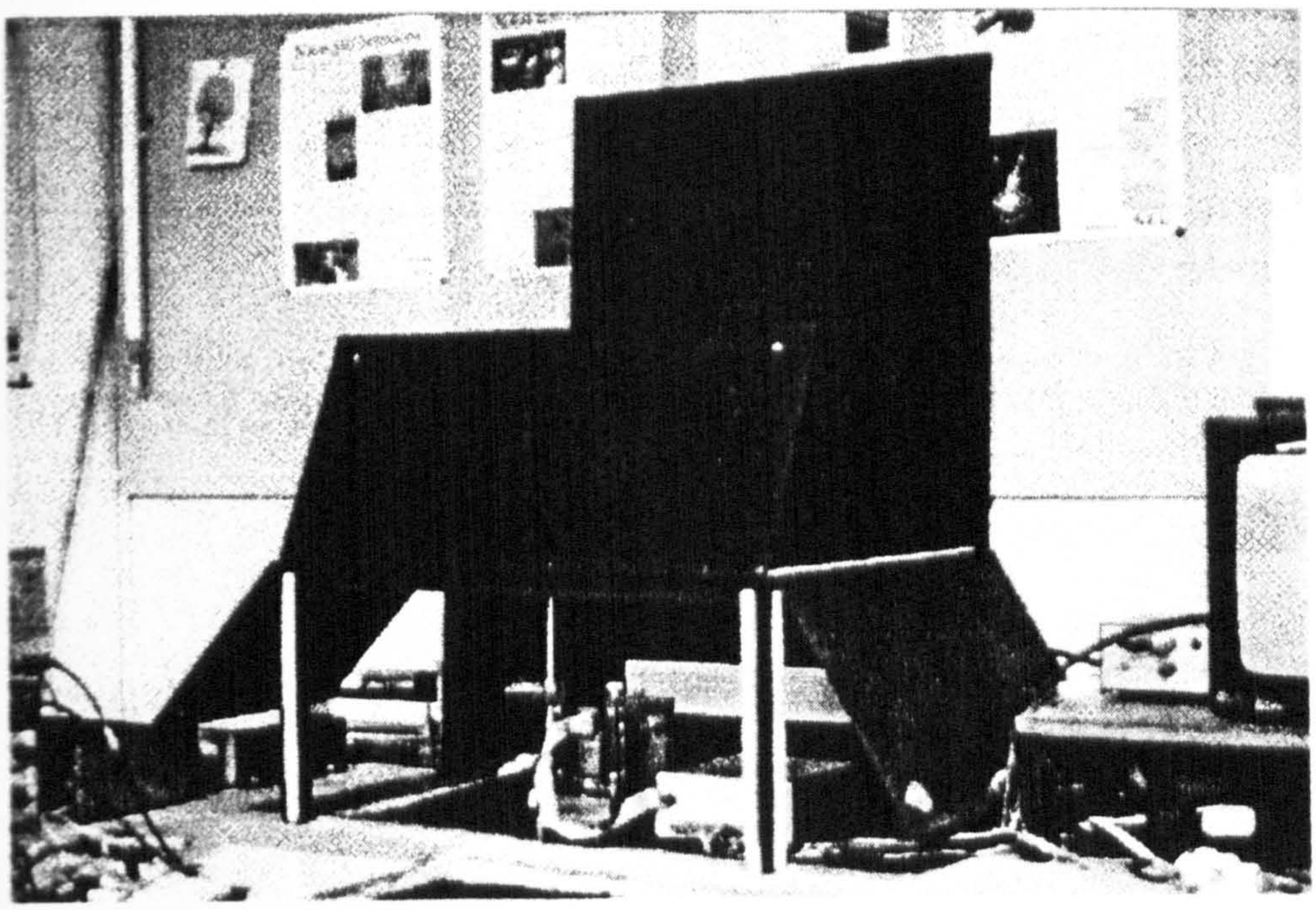

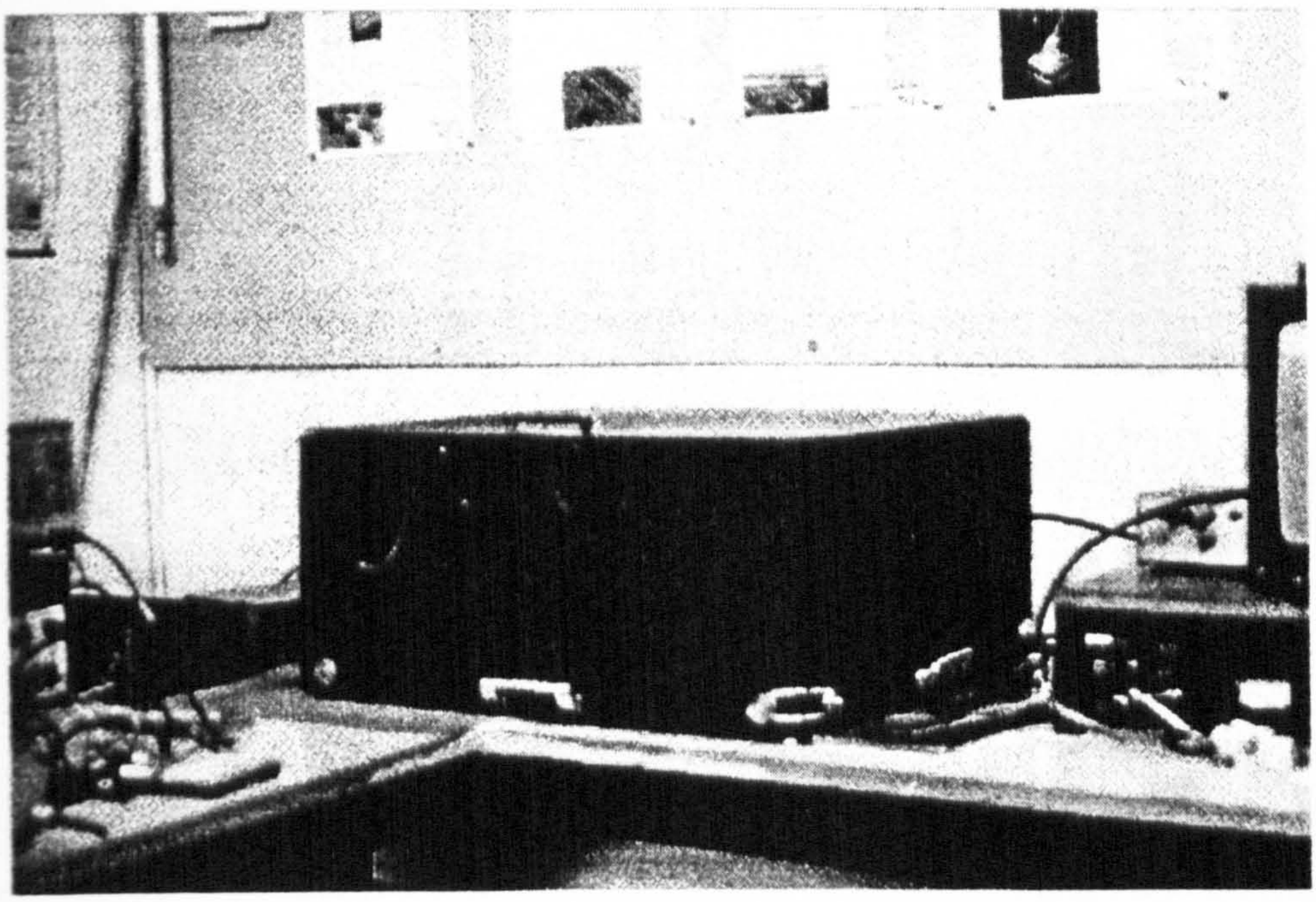

Figure 5.4.6: Dark-housing to exclude Ambient light

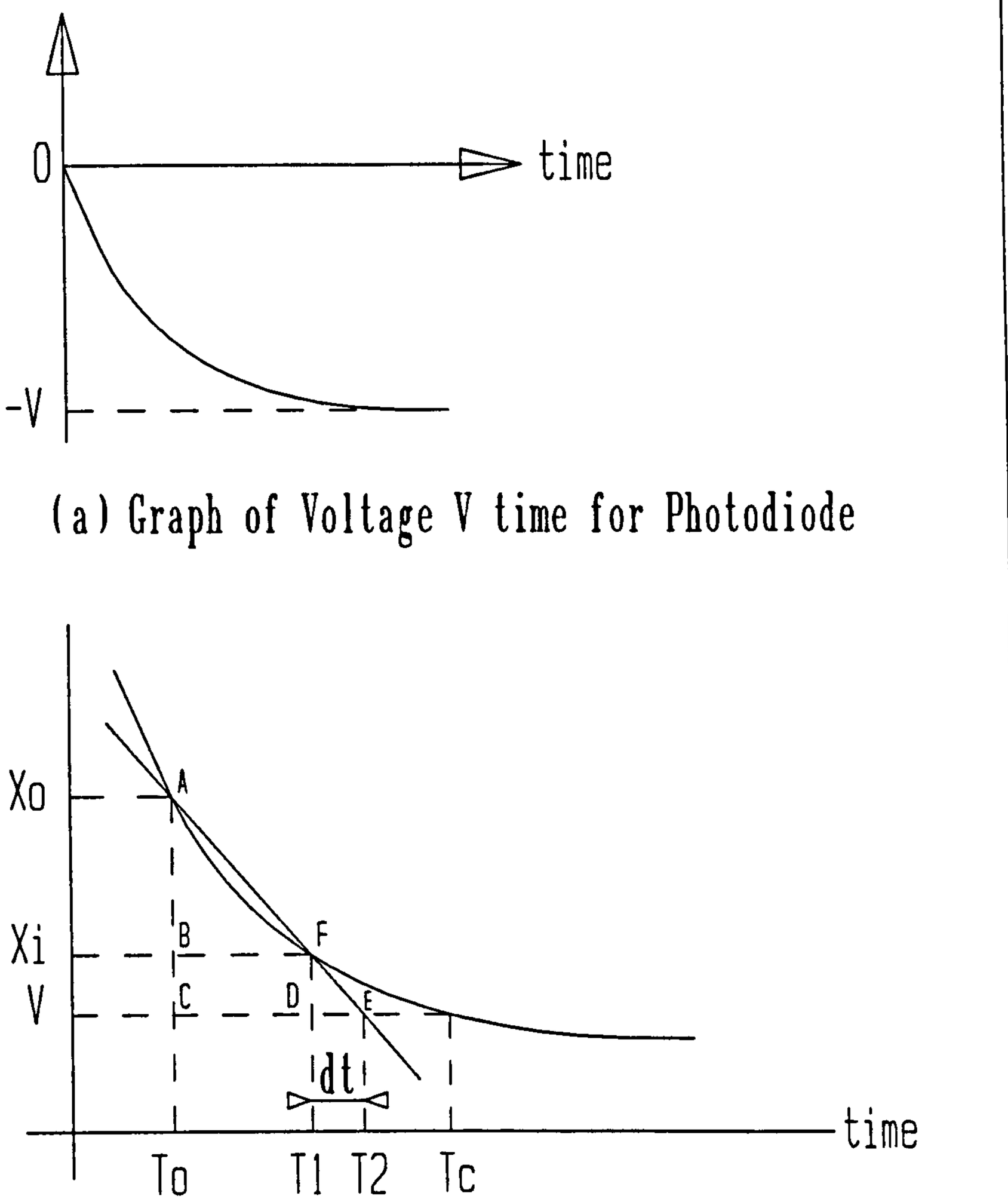

(a) Graph of Voltage V time for Photodiode

(b) General Case of figure (a)

DETERMINING OPTIMUM PHOTODIODE INTEGRATION PERIOD

Figure 5.5.1

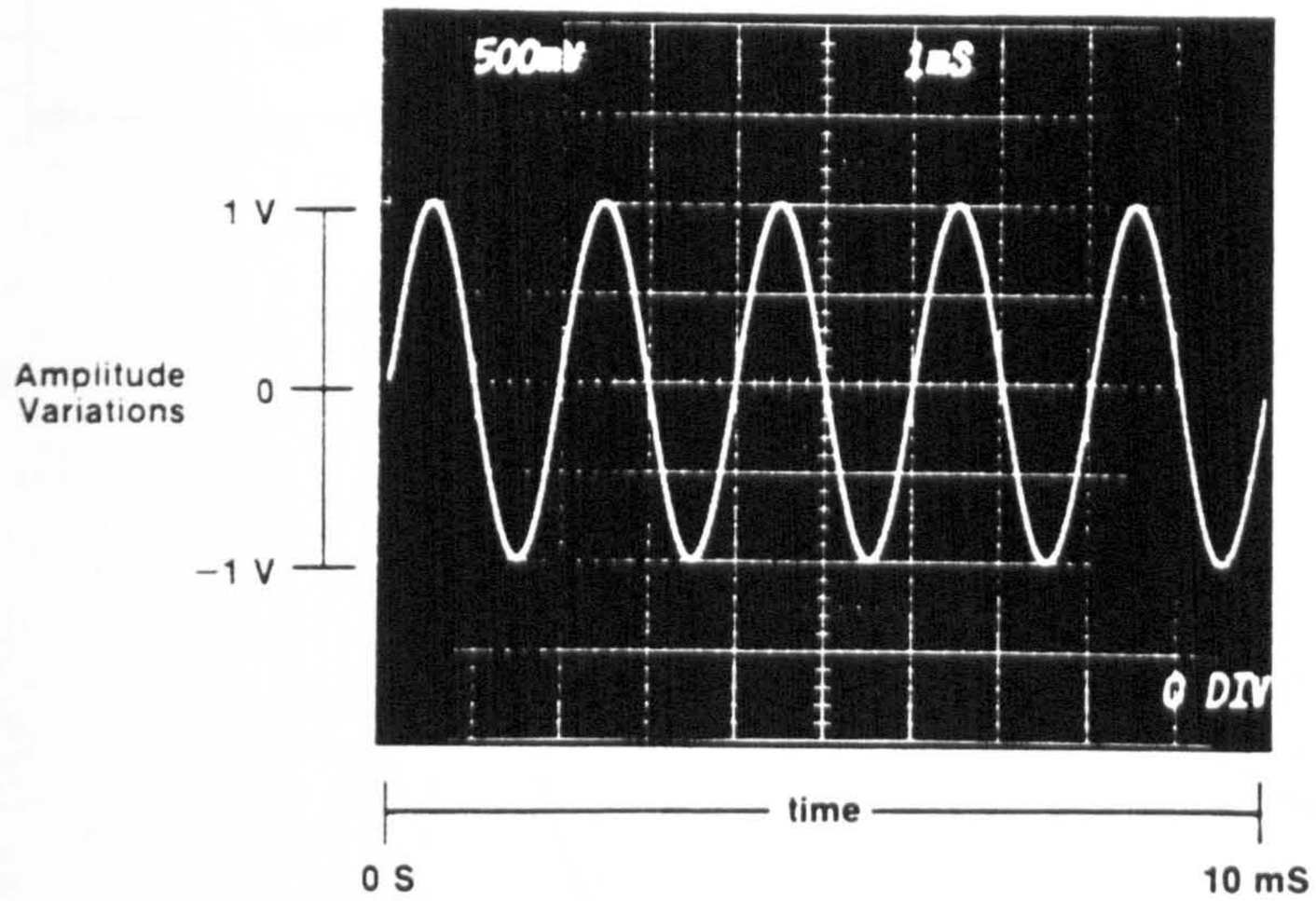

Figure 5.6.1: Time History of Sinusoid obtained with Oscilloscope

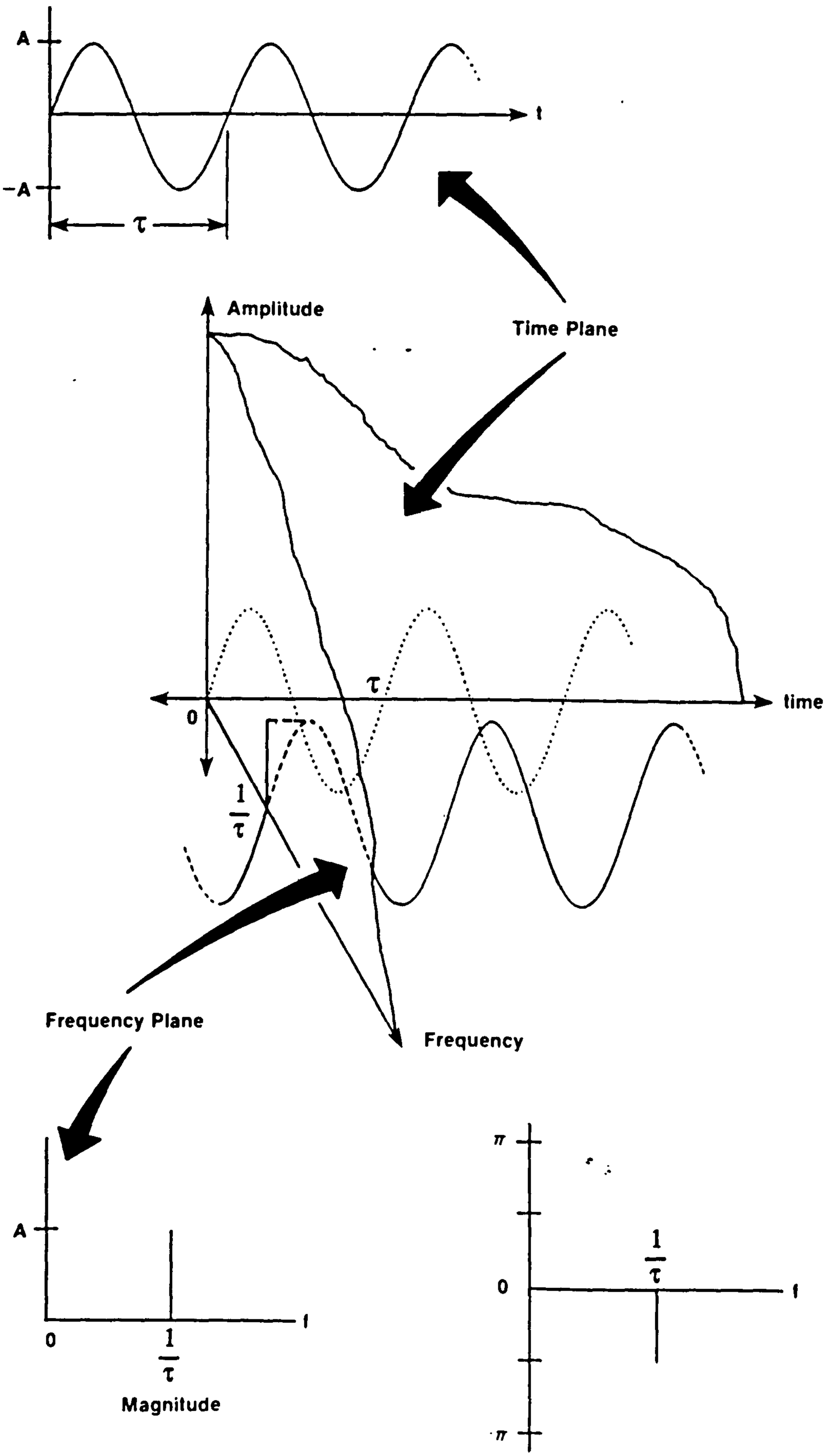

Figure 5.6.2: Time and Frequency Description of a Sine Wave

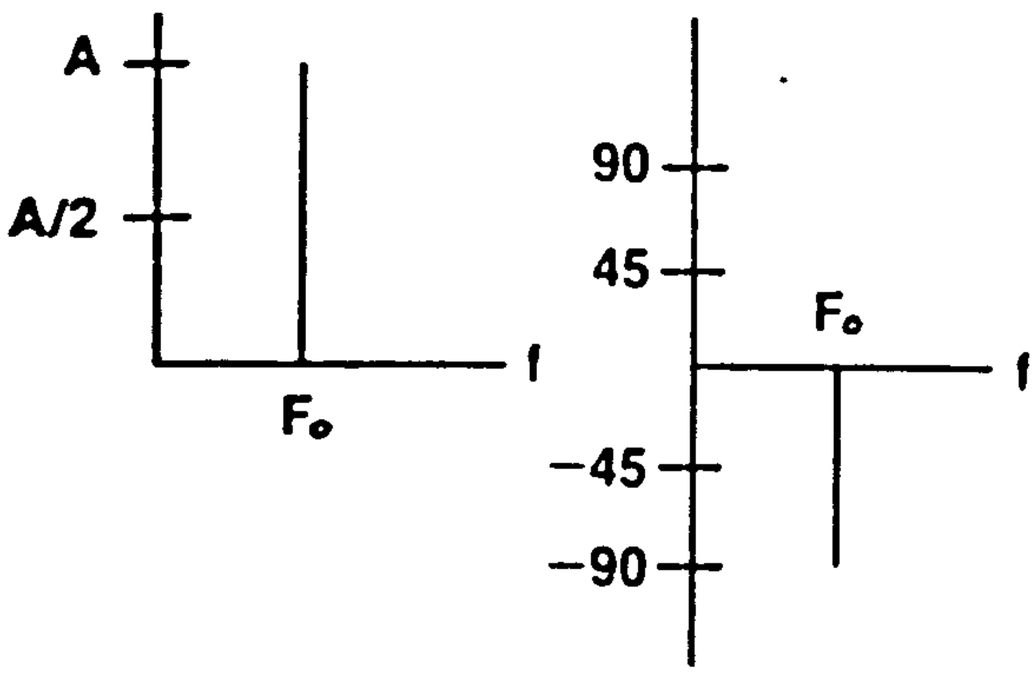

a. Sinusoid of frequency F_o, amplitude A, -90° phase

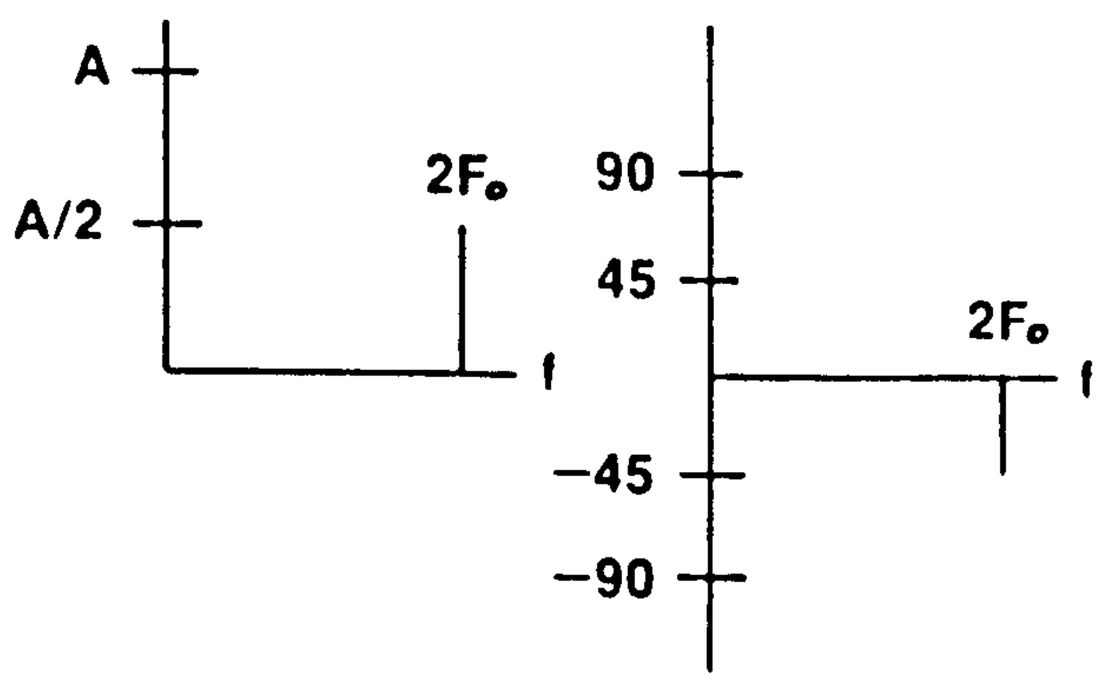

b. Sinusoid of frequency $2F_o$, amplitude A/2, phase -45°

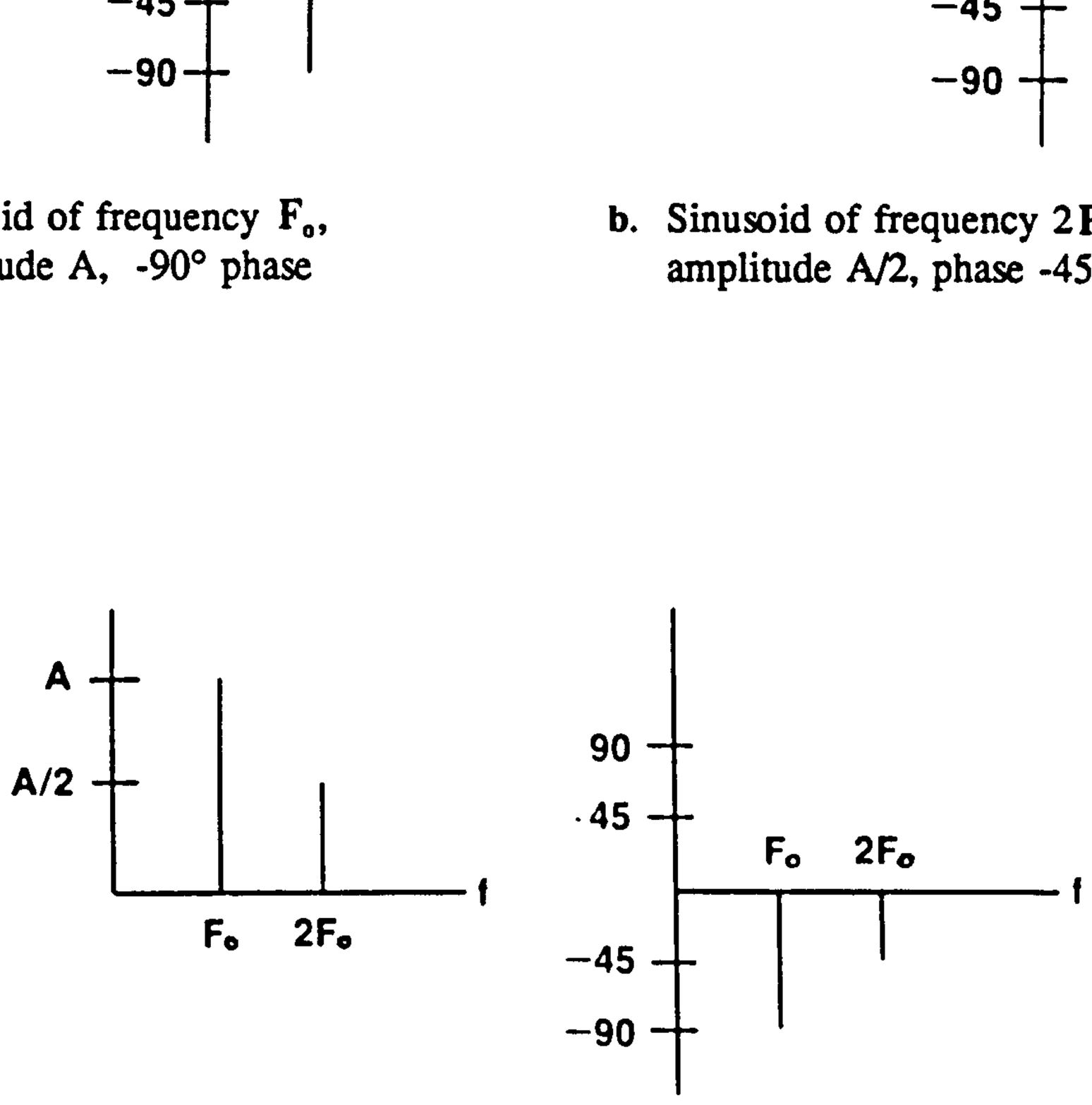

c. Nonsinusoidal waveform composed of a and b

Figure 5.6.3: Summing Frequency Description of Sinusoids

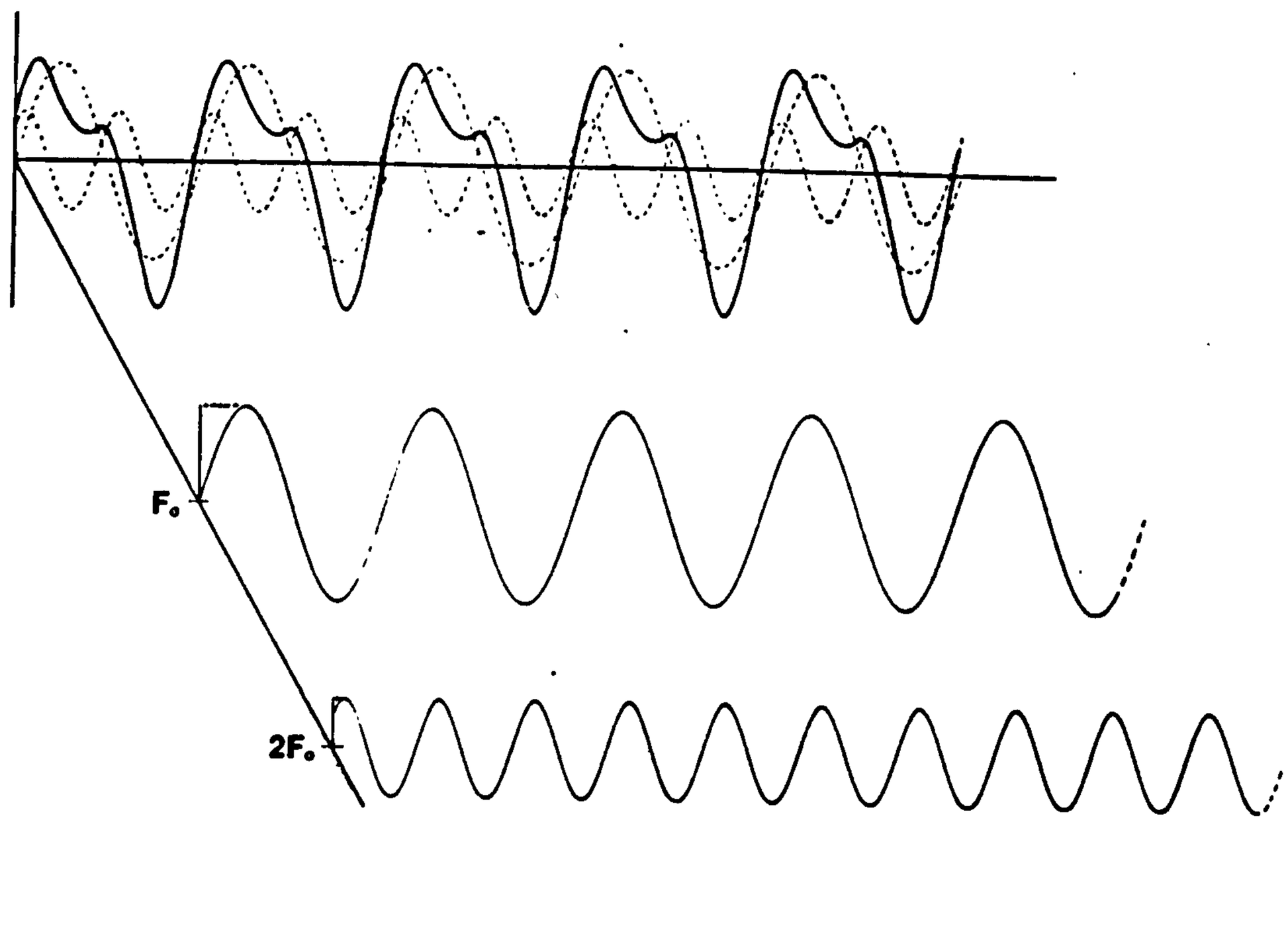

Figure 5.6.4: Composing a Non-sinusoidal Waveform by Summing Sinusoids

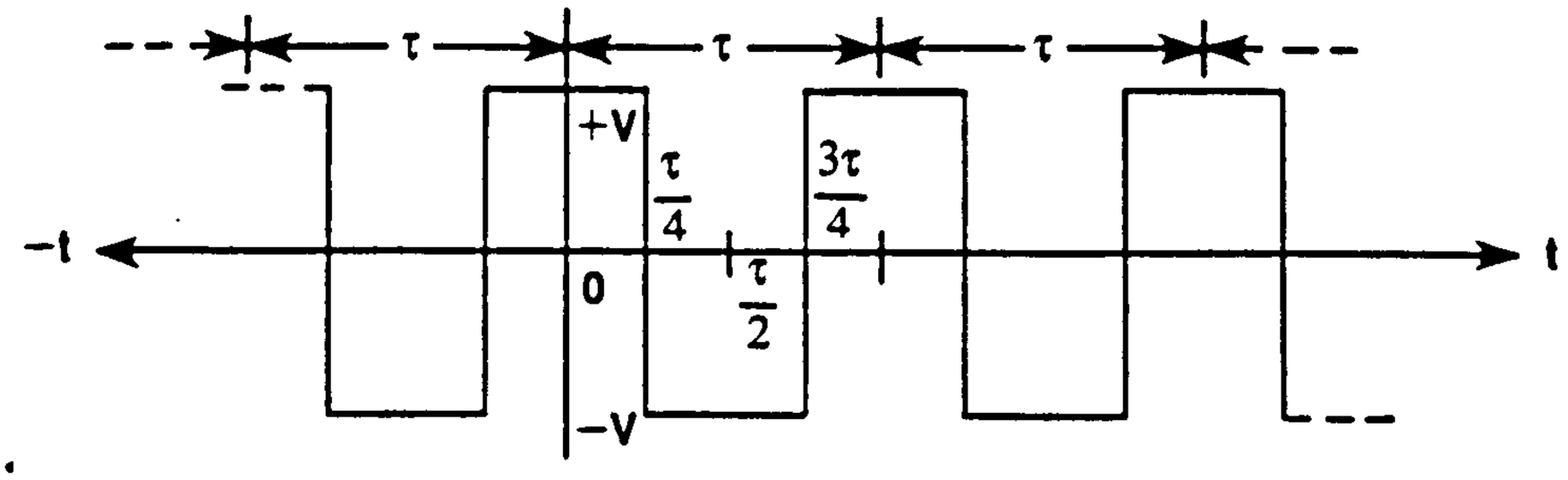

a. Periodicity--x(t) = x(t + τ).

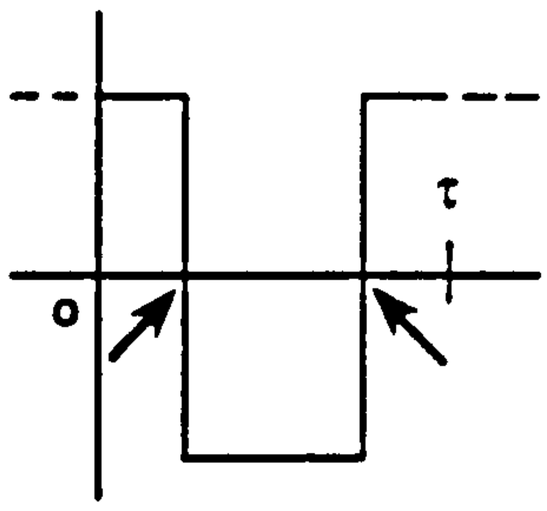

b. Finite number of discontinuities.

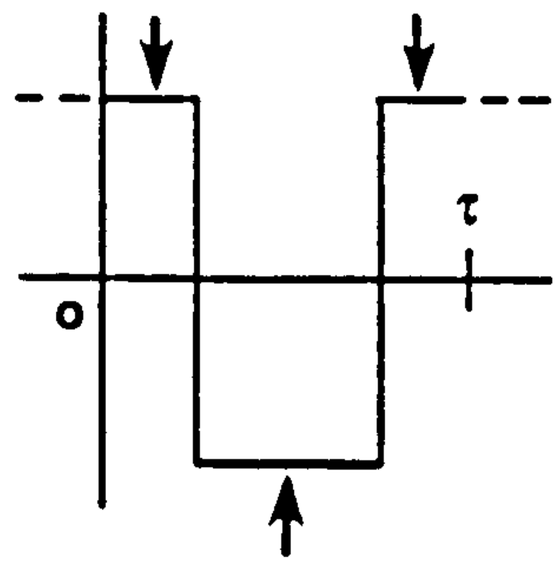

c. Finite number of maxima and minima.

d. Integrable-- $\int_0^\tau |x(t)|\,dt < \infty$.

Figure 5.6.5: Square Wave satisfies conditions for its Foueier Series to exist

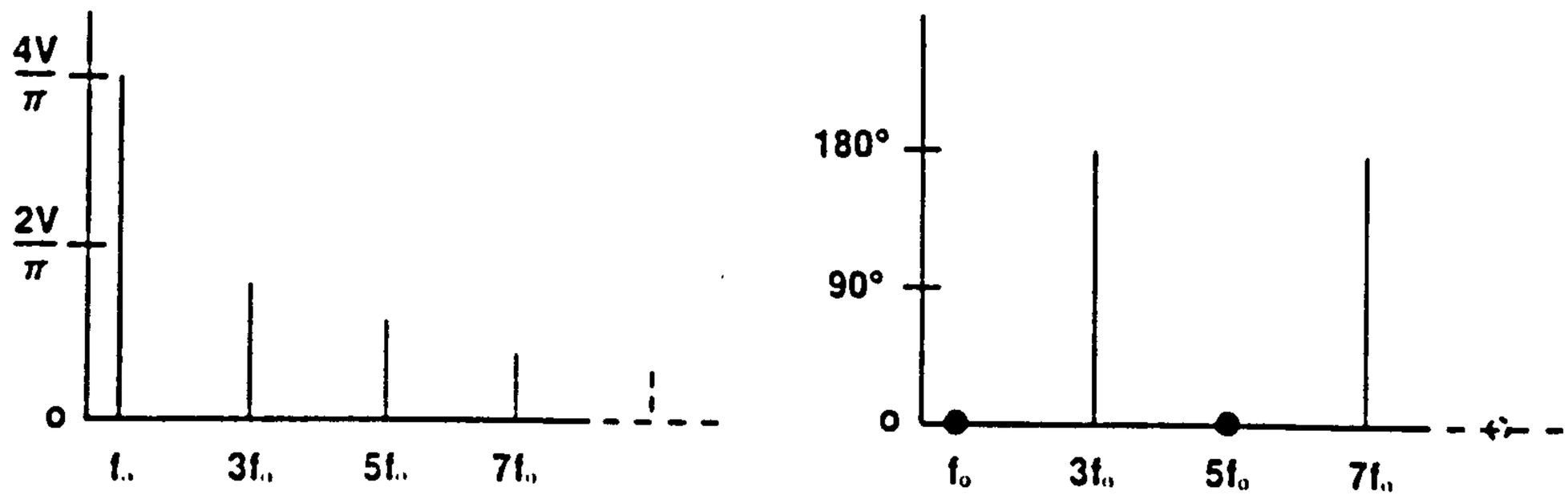

a. Magnitude

b. Phase

Figure 5.6.6: Magnitude and Phase Spectra for Square Wave in figure 5.6.5a

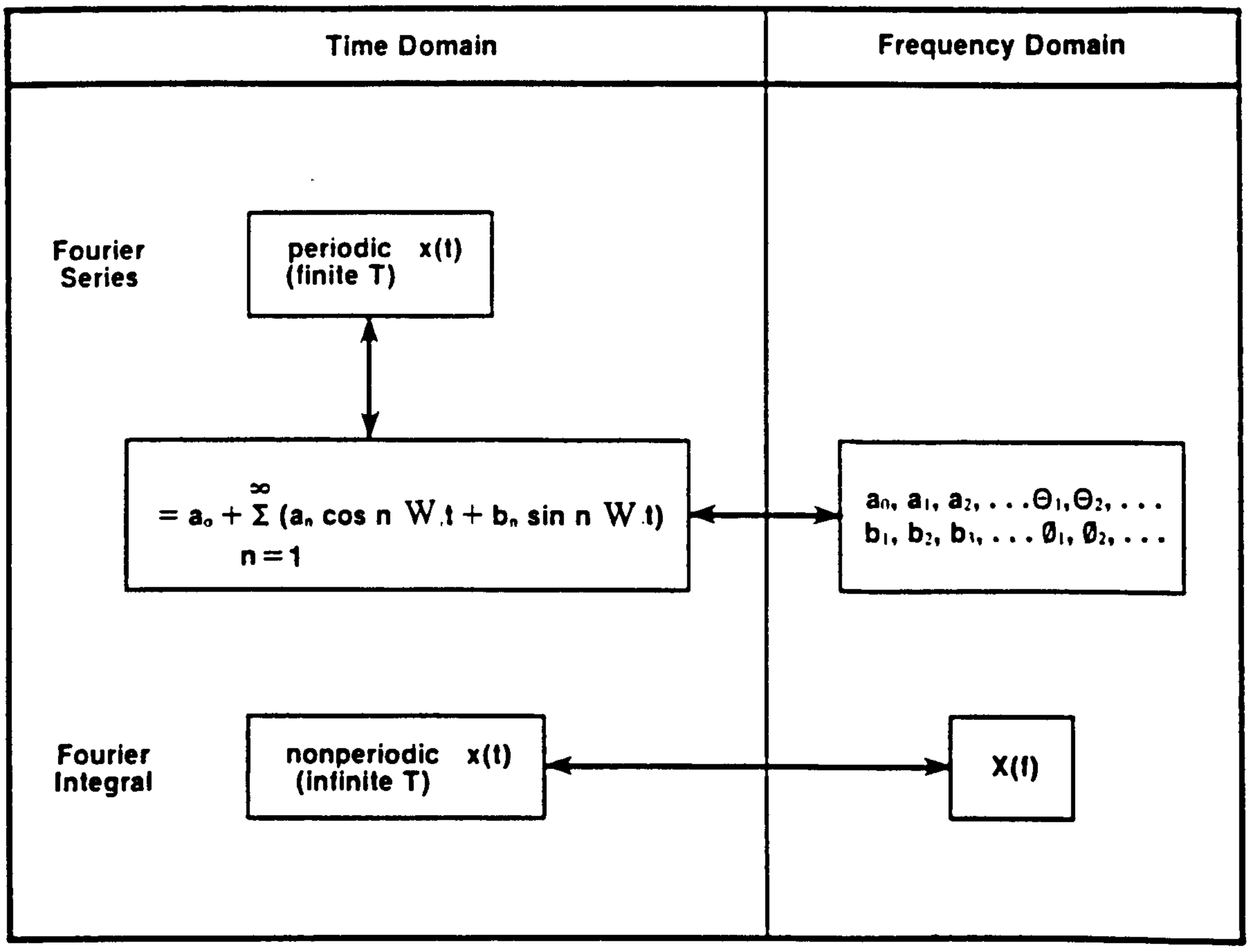

Figure 5.6.7: Fourier Series and Fourier Intergral - different paths between time and frequency

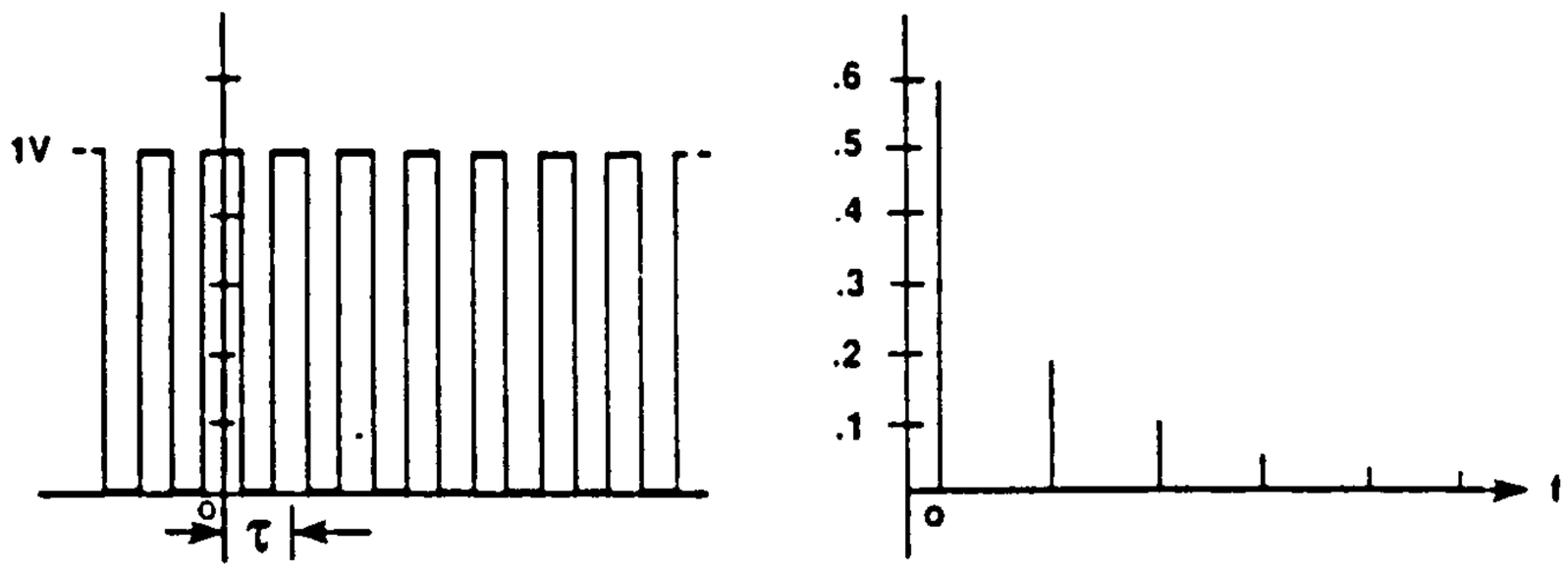

a. Pulse width--a=0.025; period--τ=0.05.

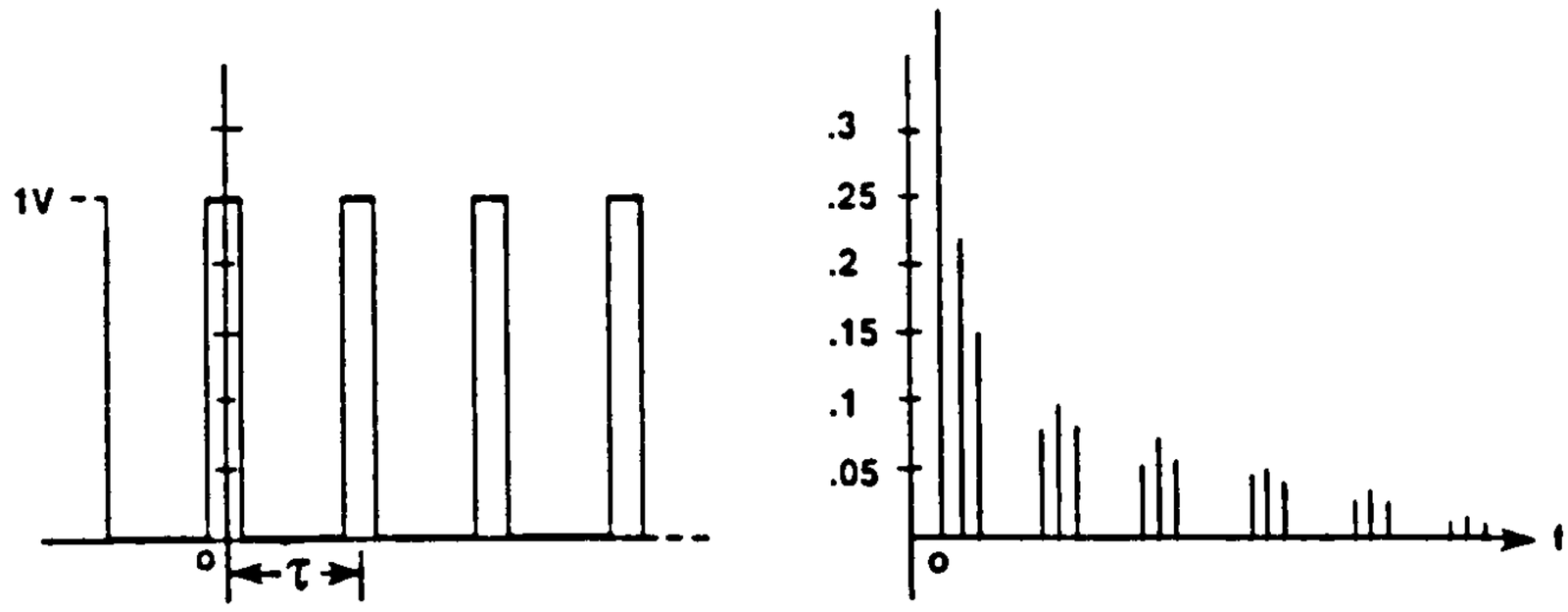

b. a=0.025; τ=0.1

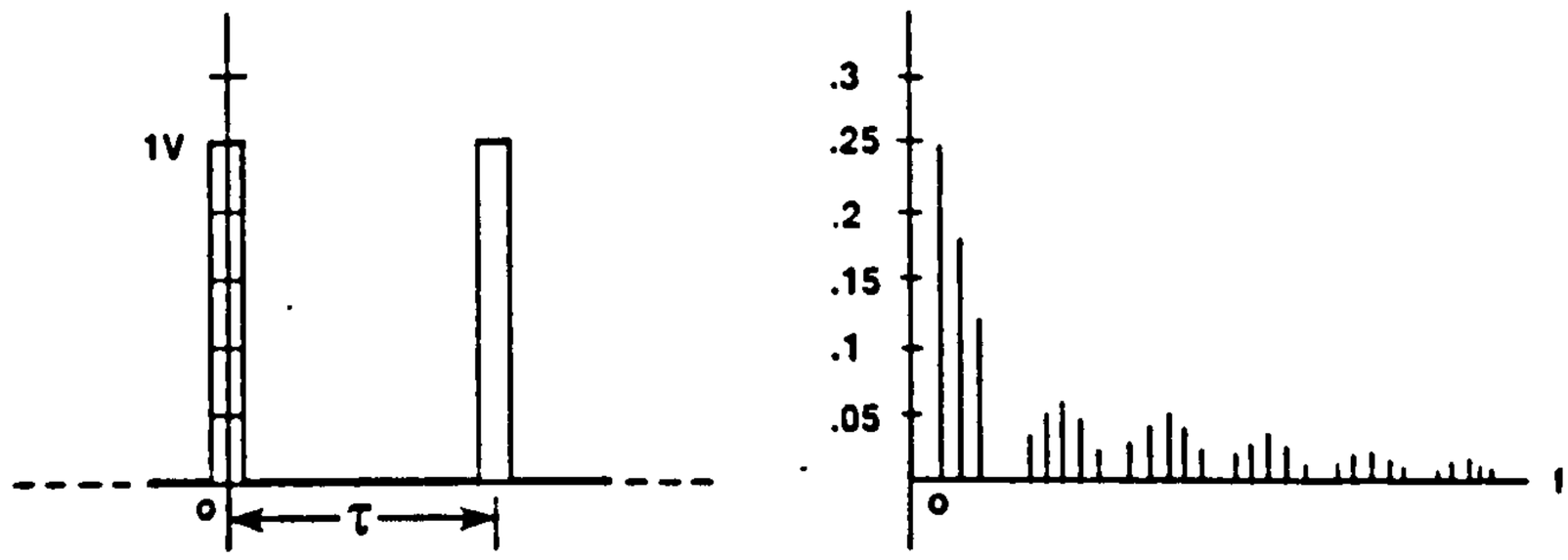

c. a=0.025; τ=0.2

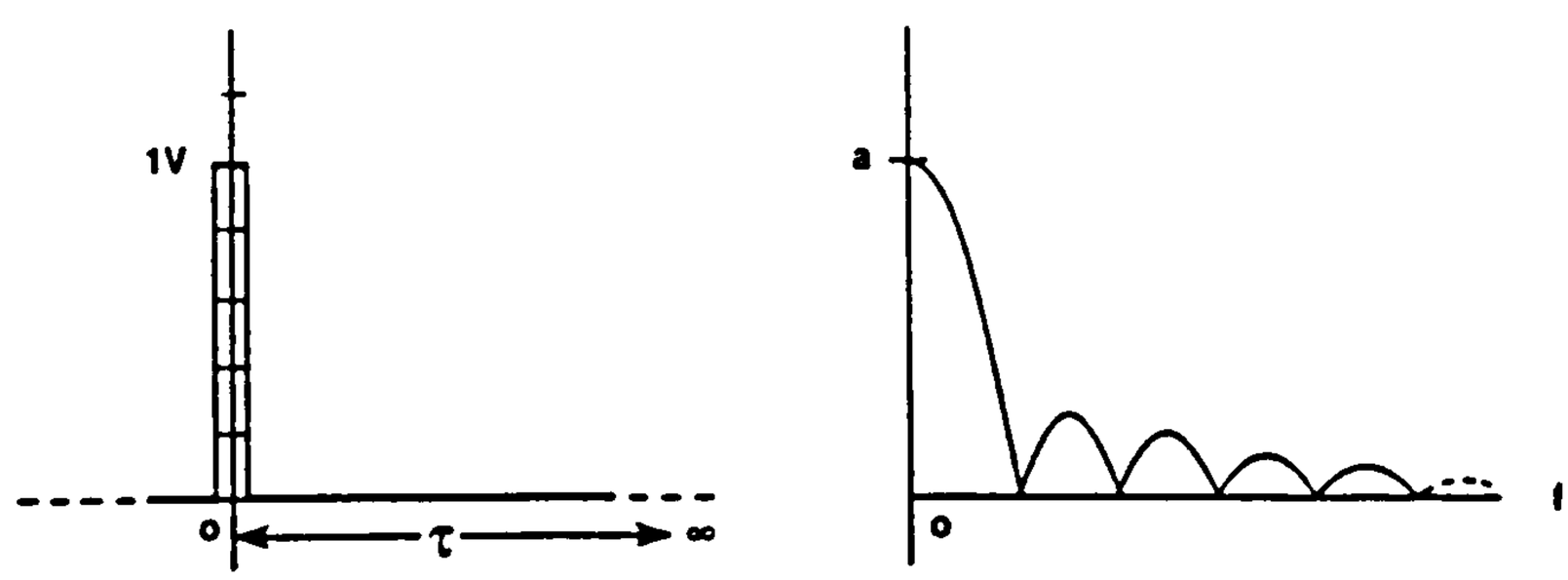

d. a=0.025; τ→∞

Figure 5.6.8: Relationship between Fourier Series and Fourier Intergral
As $\tau \to \infty$ the spectral lines become closer, when $\tau = \infty$ the spacing between lines is zero

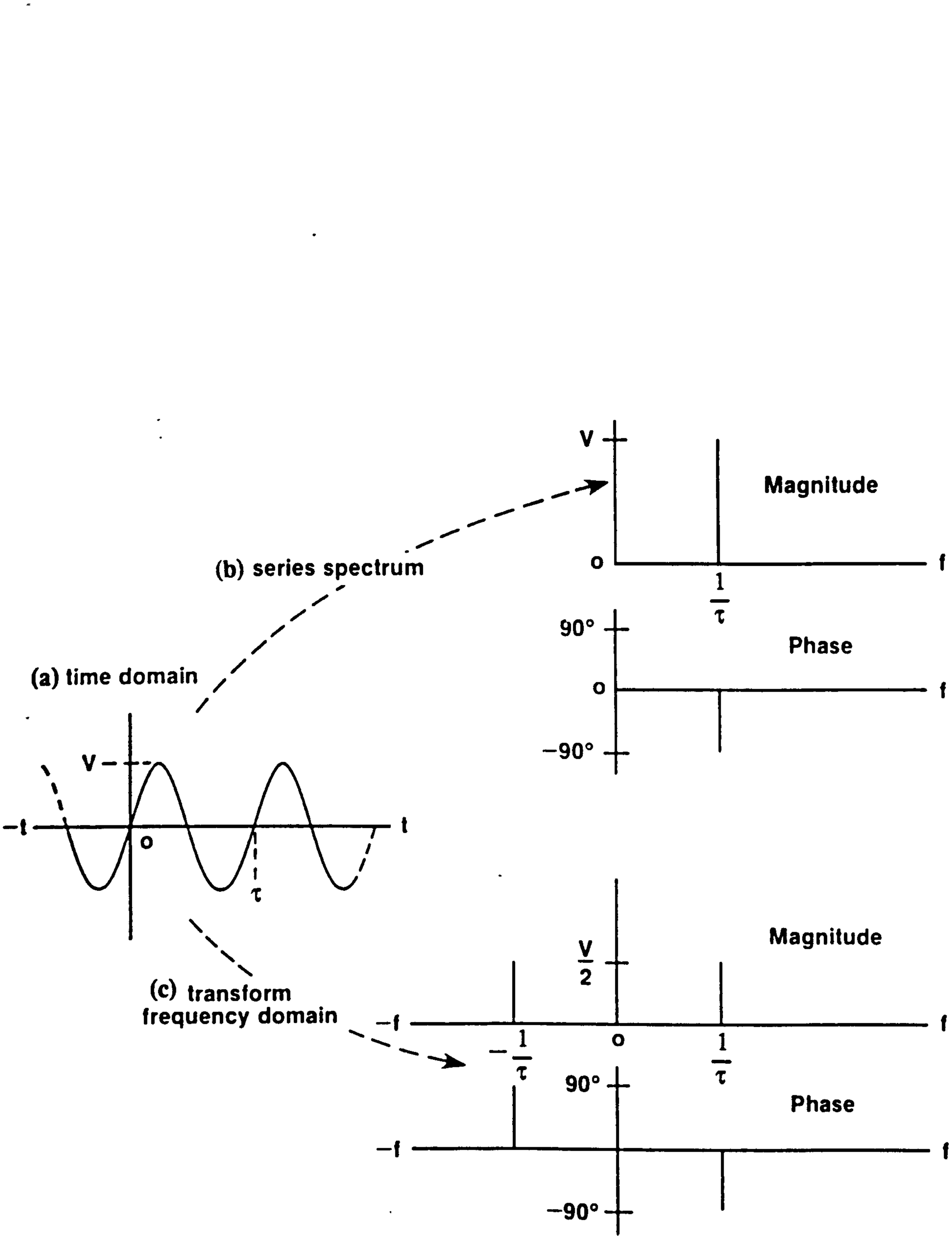

Figure 5.6.9: Comparison of daigram conventions in the Series Spectrum and Transform Frequency domain

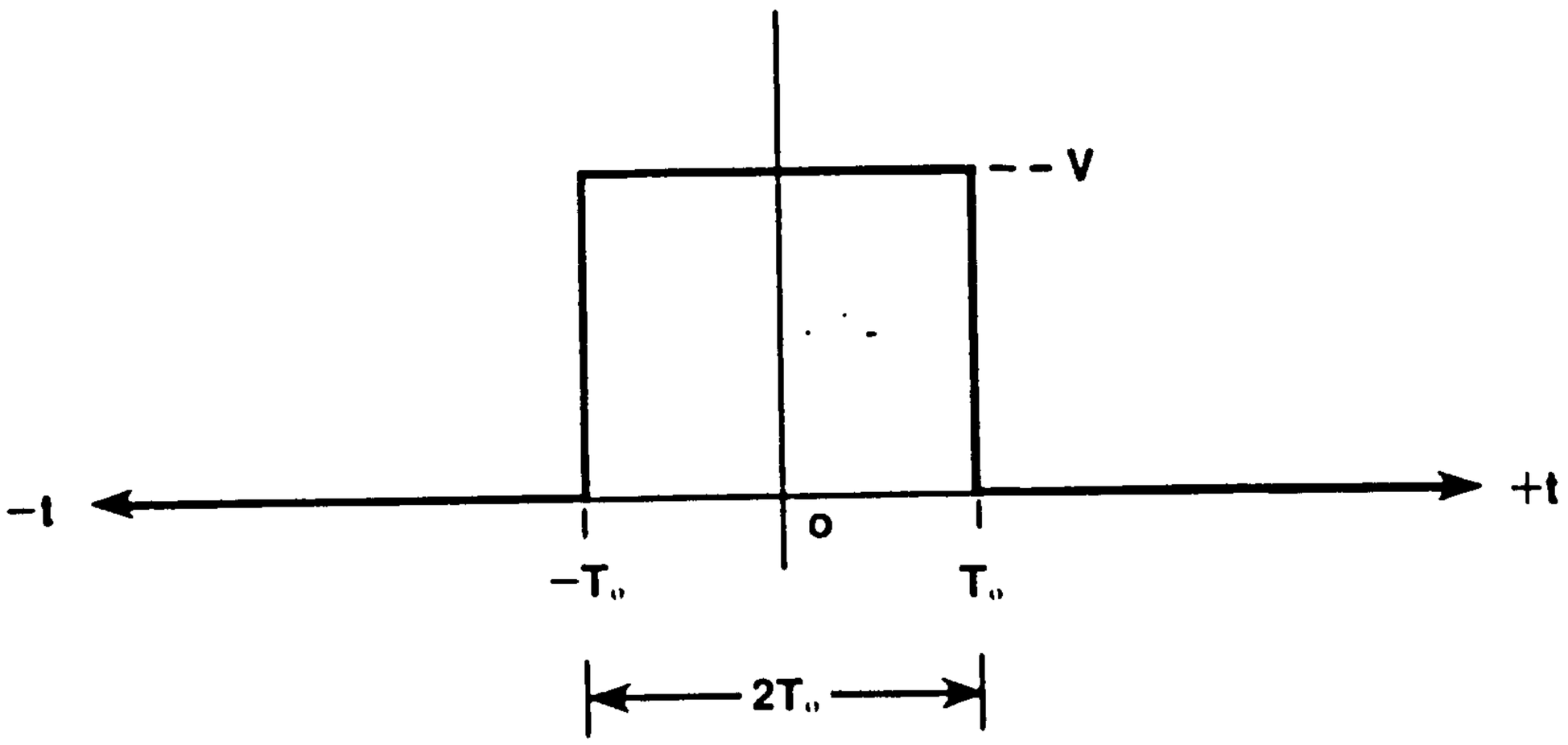

a. Square pulse.

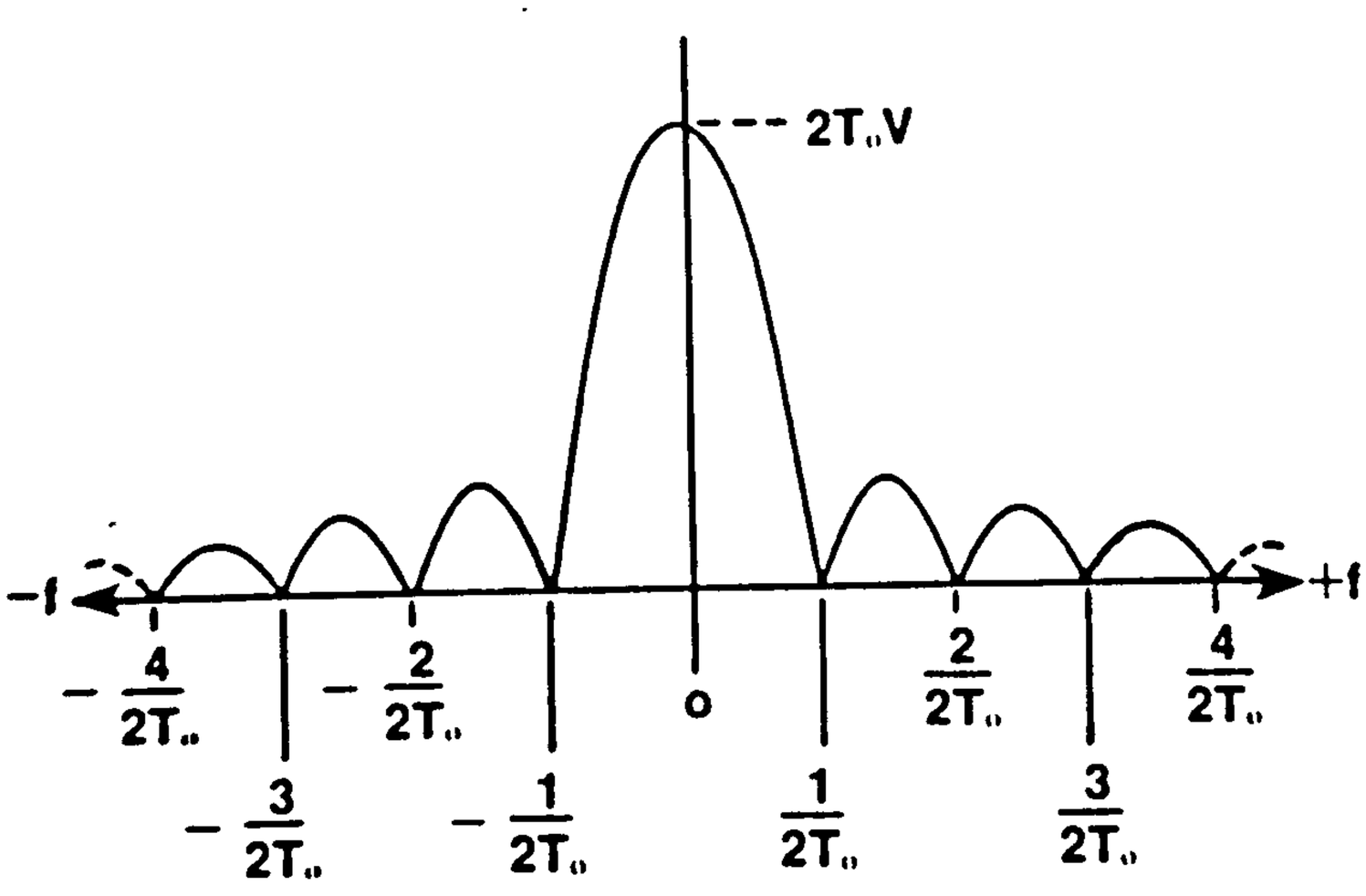

$$|X(f)| = |2VT_o \frac{\sin WT_o}{WT_o}|$$

b. Frequency-domain magnitude.

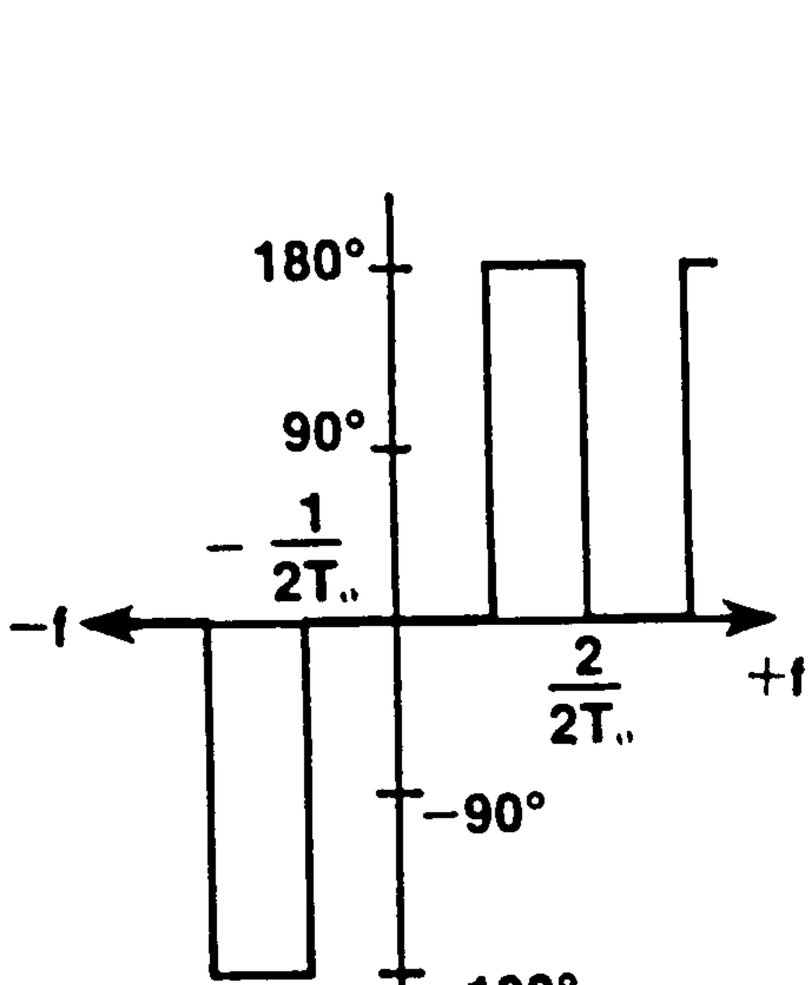

c. Frequency-domain phase.

Figure 5.6.10: A Generalised Square Pulse and its Frequency-domain Magnitude and Phase

Time Domain Function	Frequency Domain Magnitude
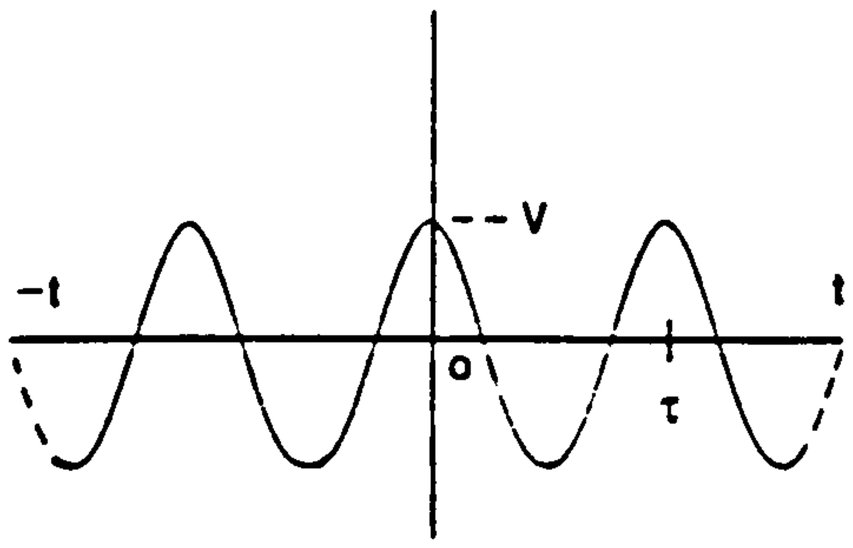	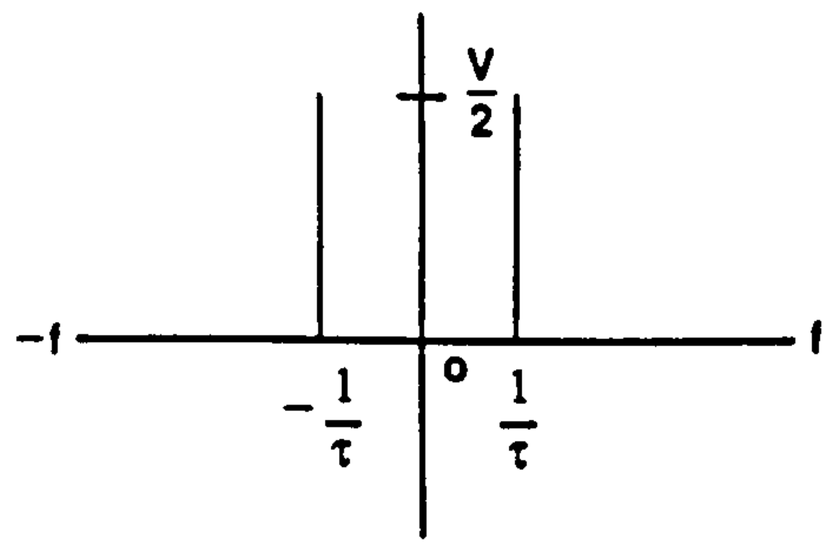
a. Cosine wave.	
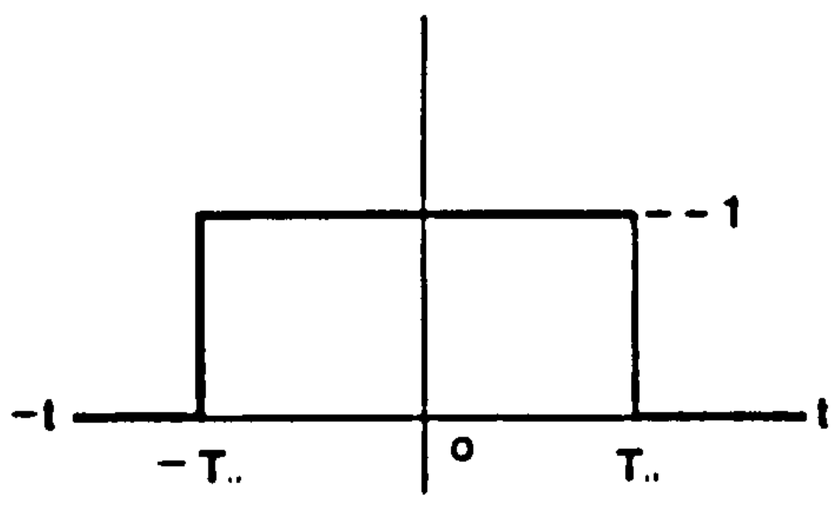	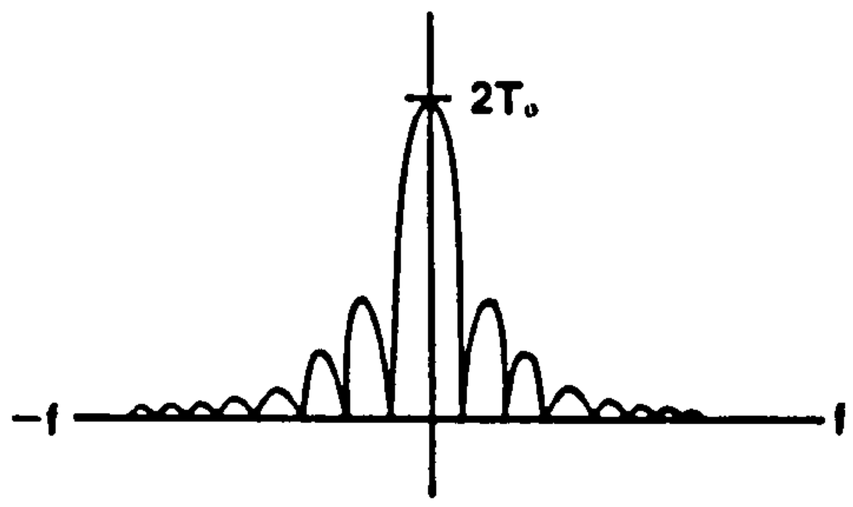
b. Rectangular window.	
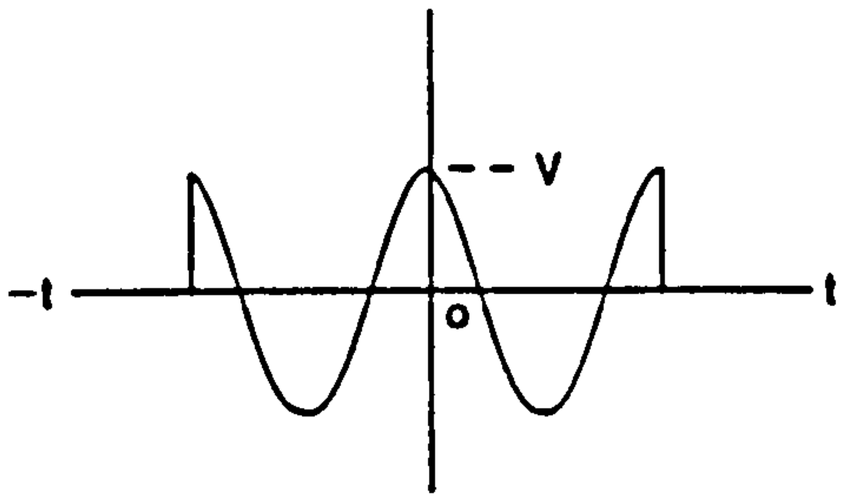	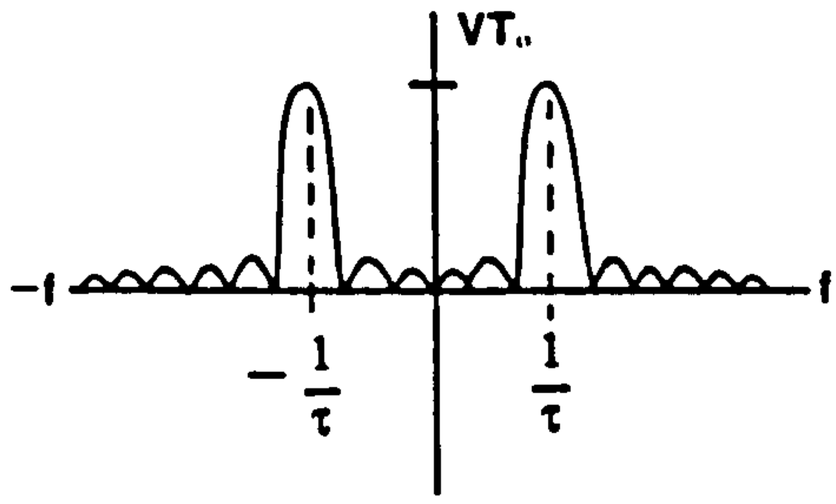
c. Rectangularly windowed cosine wave obtained by time-domain multiplication of a and b.	d. Magnitude of rectangularly windowed cosine wave obtained by frequency-domain convolution of a and b.

Figure 5.6.11: The Process of Rectangular Windowing

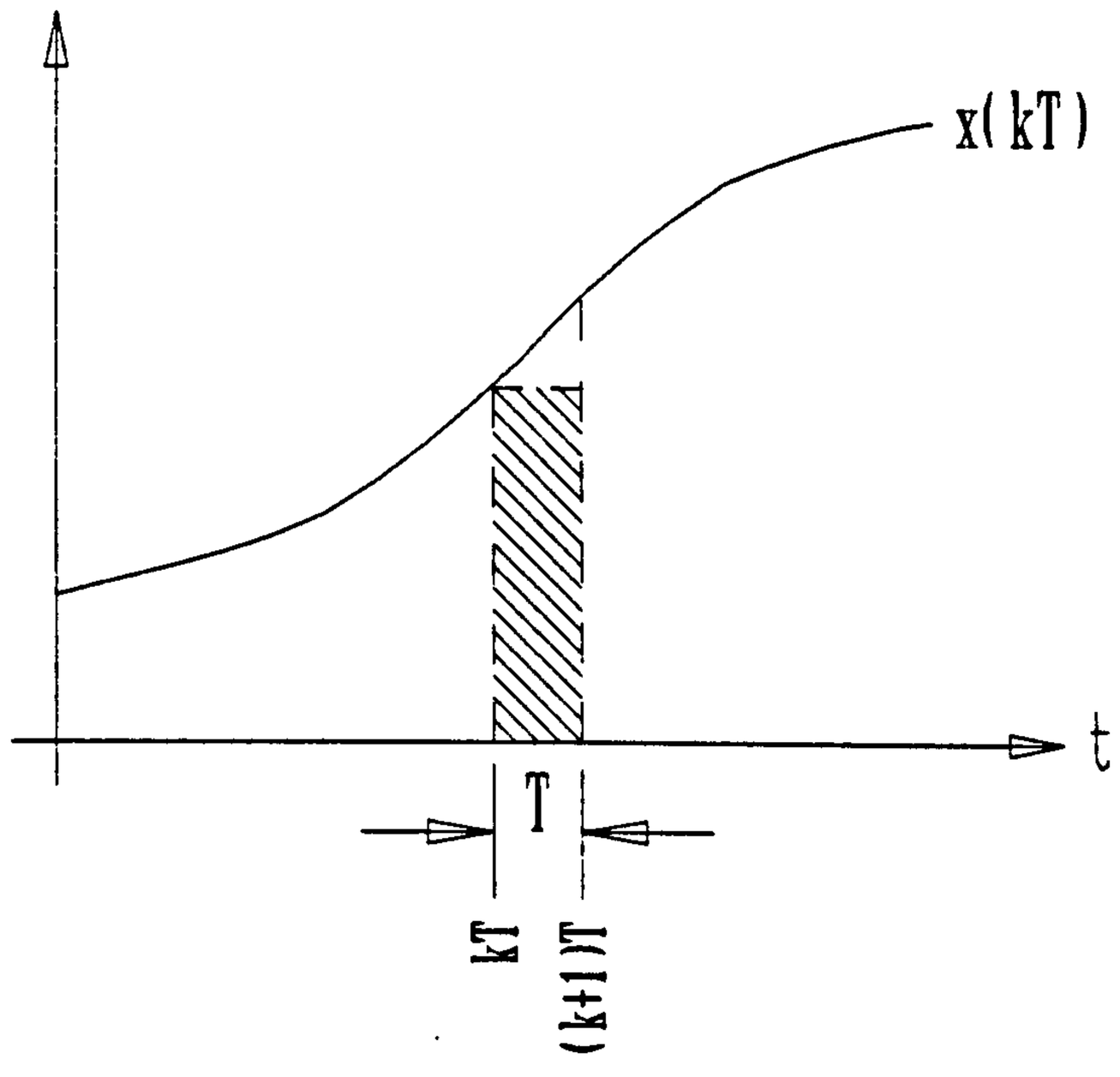

ZERO-ORDER APPROXIMATION

Figure 5.6.12

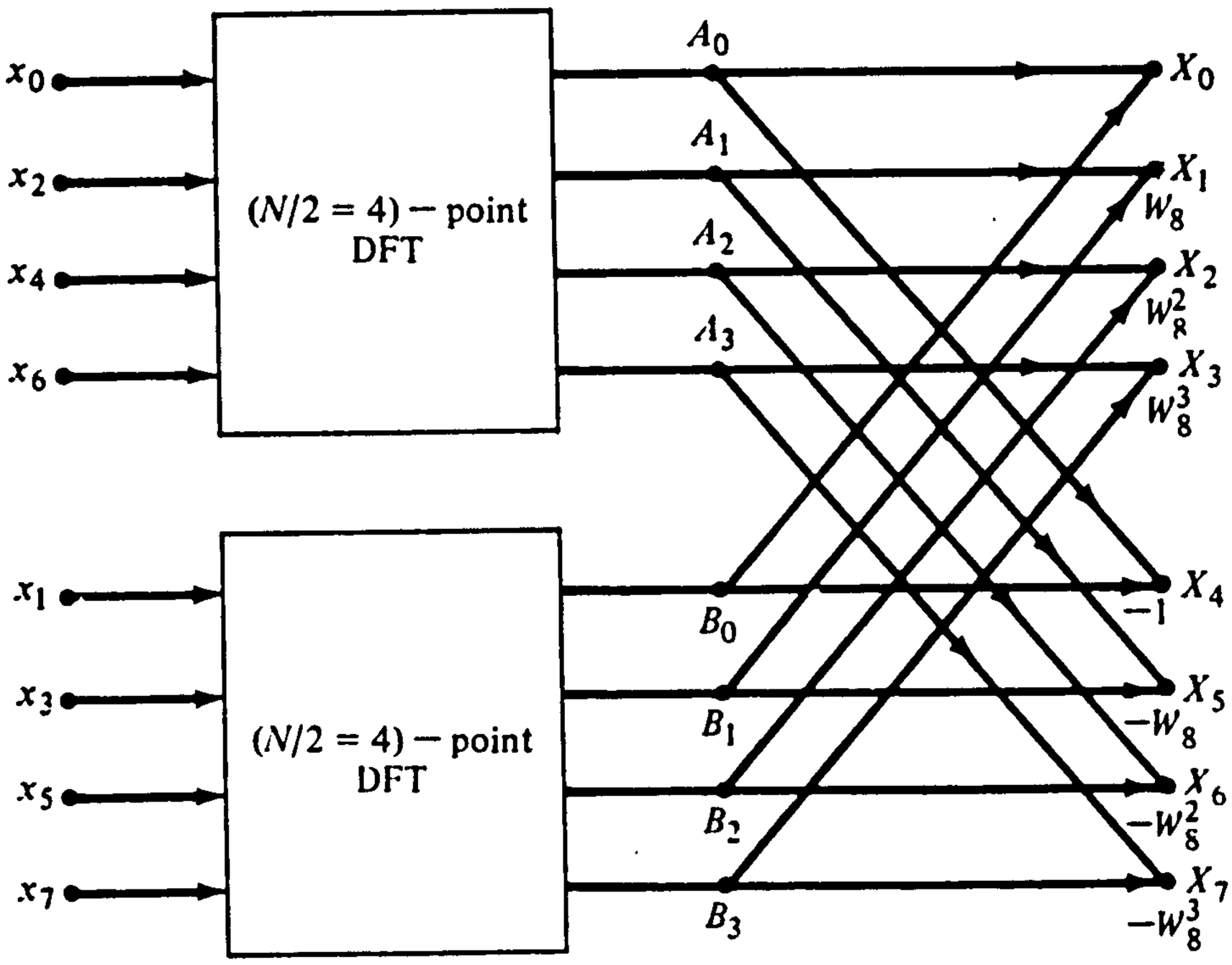

Figure 5.6.13: Result of the first step for an N=8 point decimation-in-time FFT

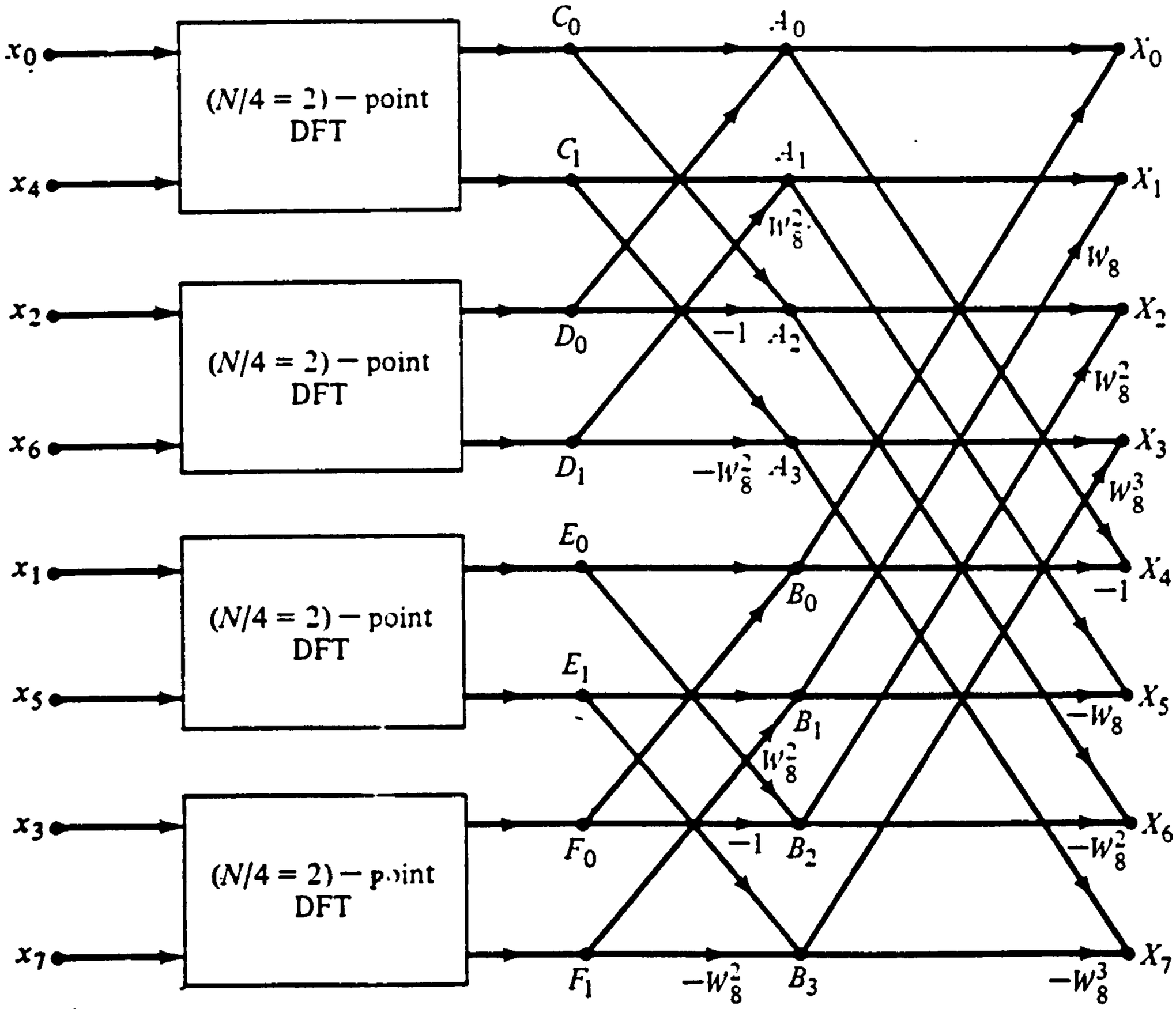

Figure 5.6.14: Result of the second step for an N=8 point decimation-in-time FFT

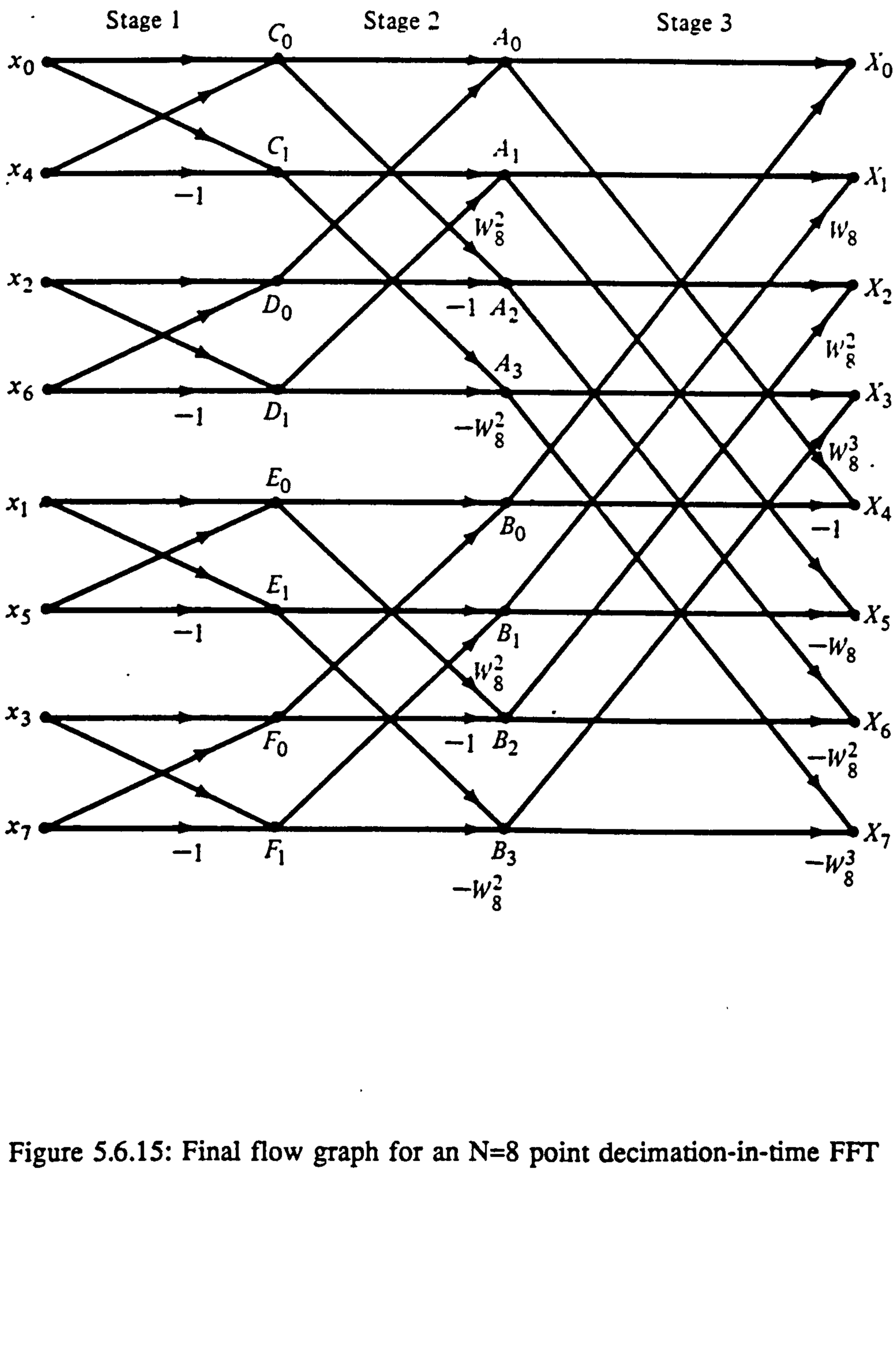

Figure 5.6.15: Final flow graph for an N=8 point decimation-in-time FFT

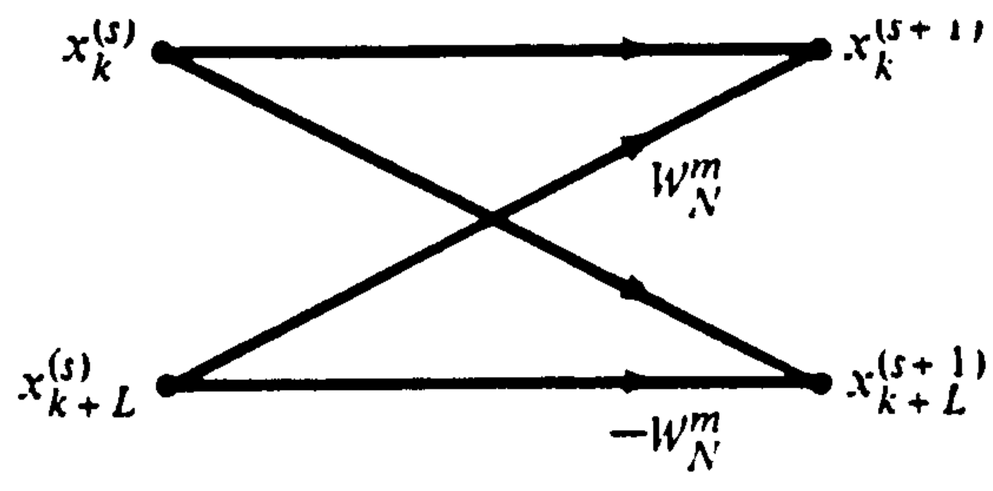

Figure 5.6.16: The Butterfly structure in the various stages of a decimation-in-time FFT

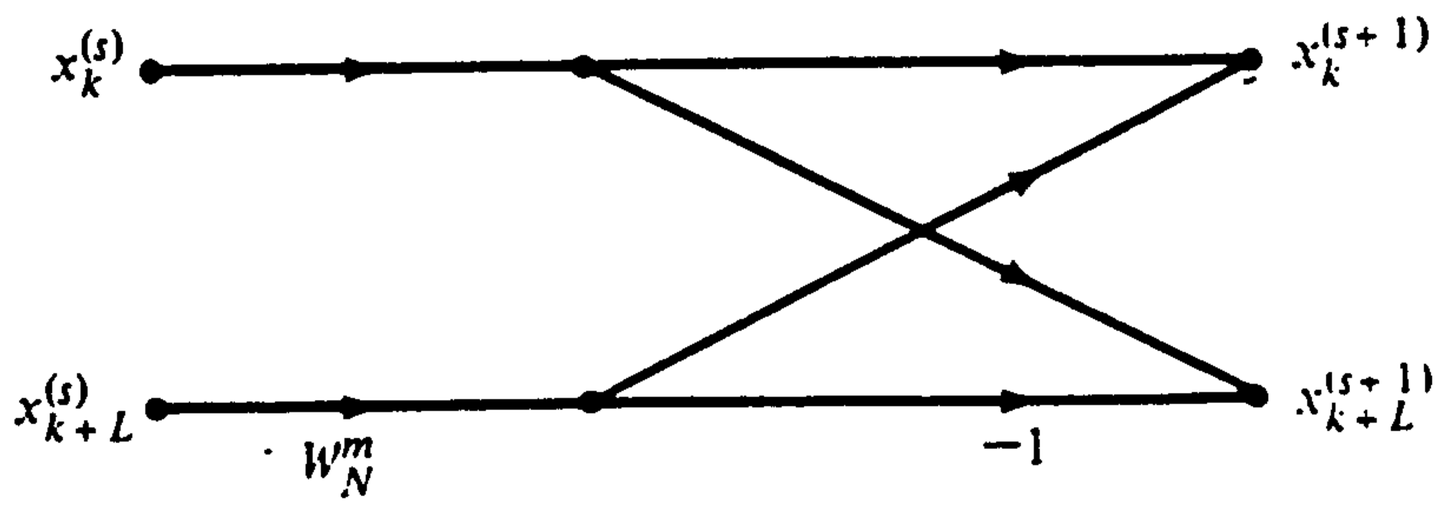

Figure 5.6.17: Modified Butterfly structure requiring only one complex multplication

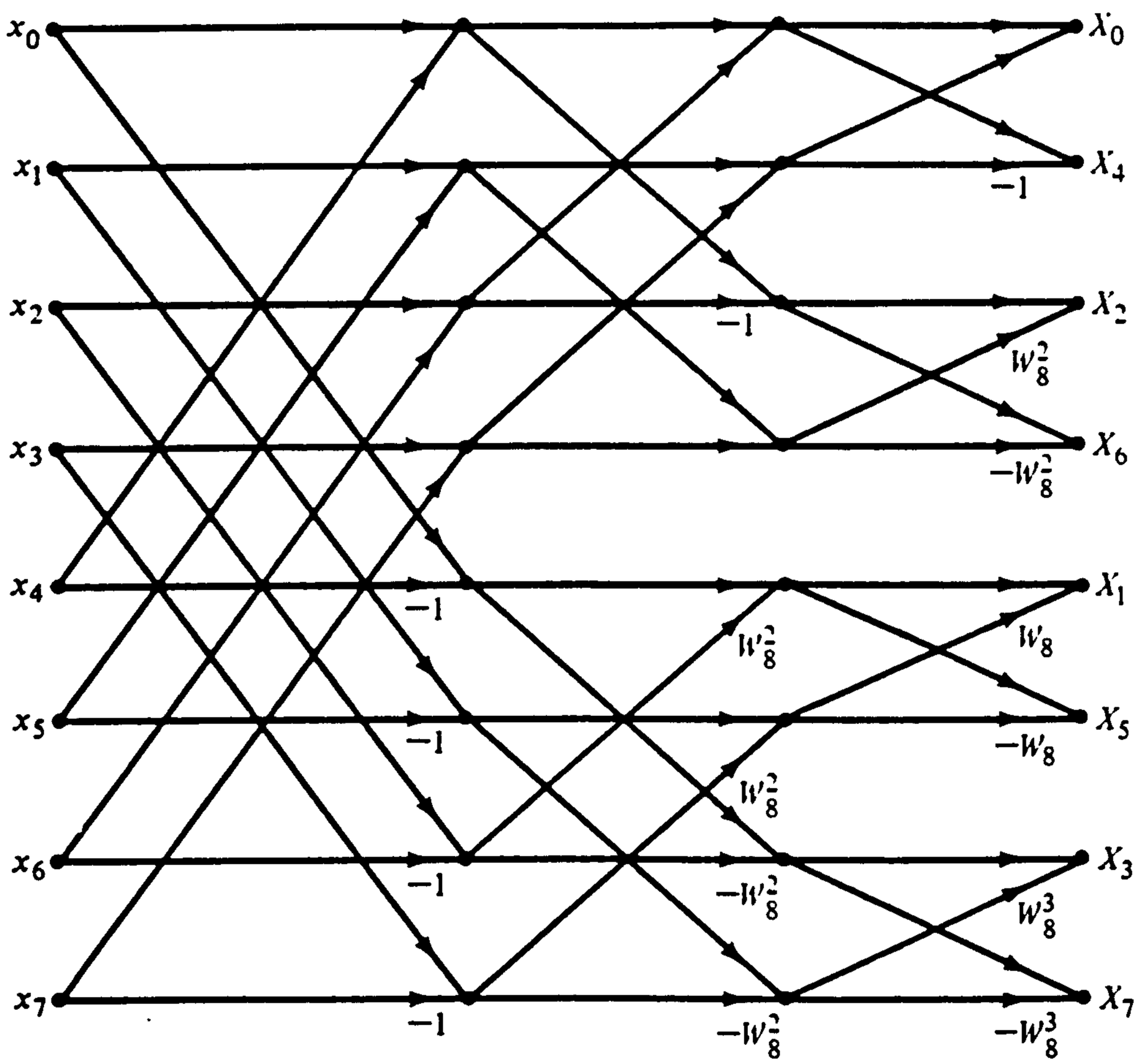

Figure 5.6.18: Rearangement of figure 5.6.15 with input in natural order and output in bit-reversed order

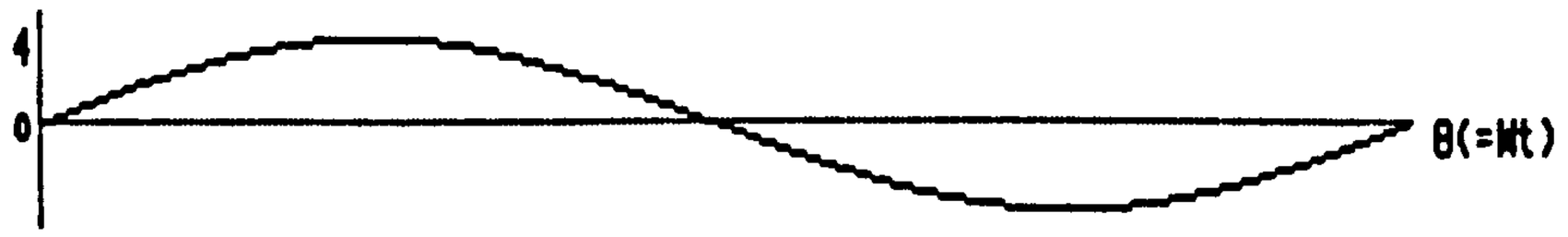

FUNCTION:

f(Wt) = 4.SIN(2π.1.t)

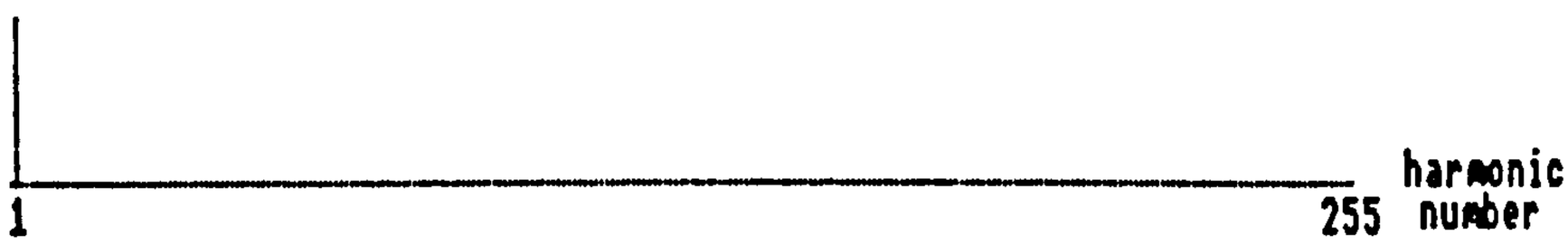

FFT OF FUNCTION

Figure 5.6.19: Typical Results from FFT Algorithm Vaildation

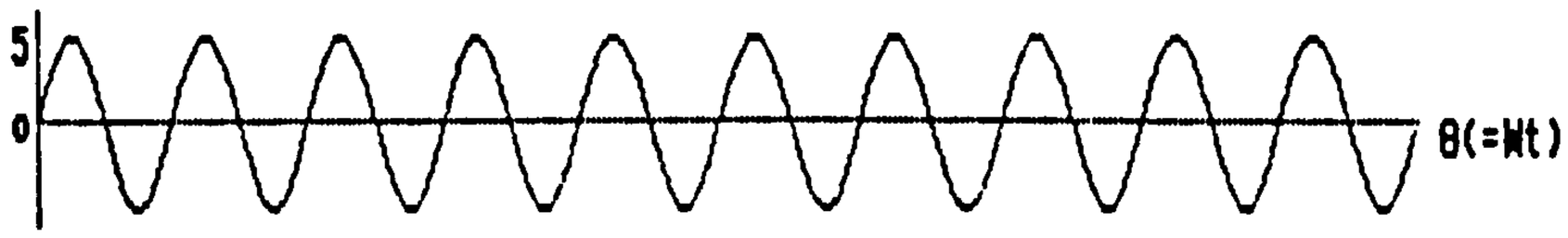

FUNCTION:

f(Wt) = 4.SIN(2π.10.t)

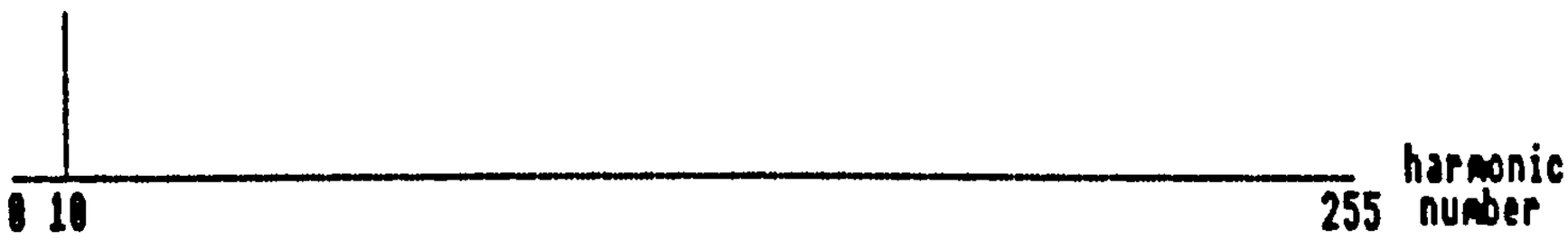

FFT OF FUNCTION

Figure 5.6.20: Typical Results from FFT Algorithm Vaildation

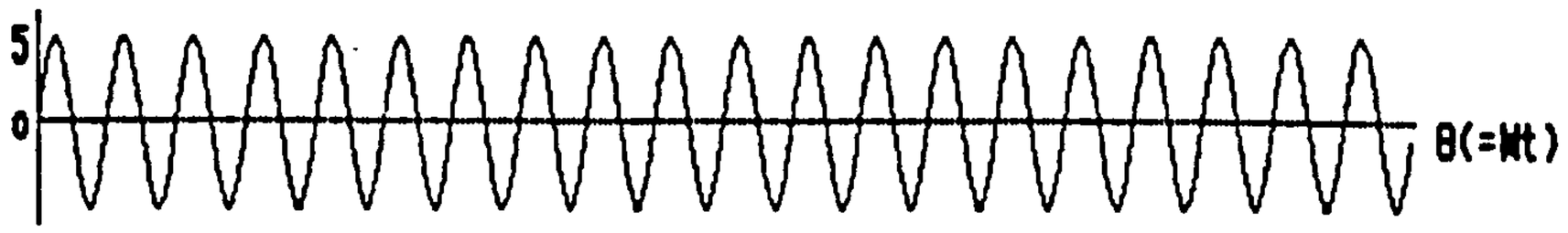

FUNCTION:

f(Wt) = 4.SIN(2π.20.t)

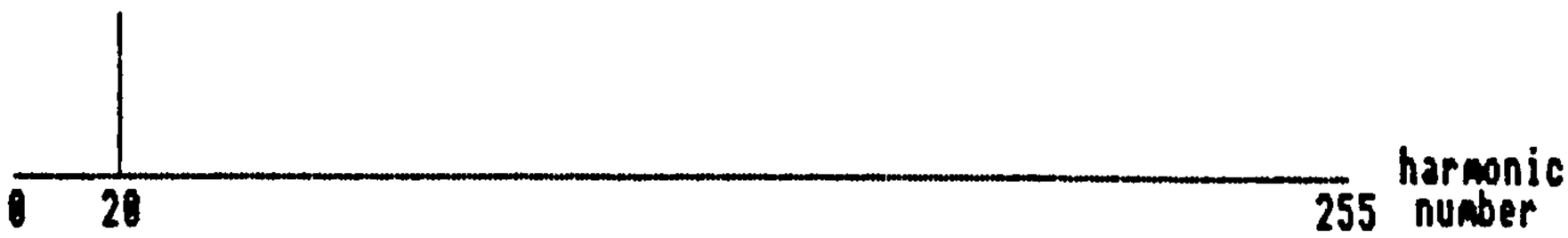

FFT OF FUNCTION

Figure 5.6.21: Typical Results from FFT Algorithm Vaildation

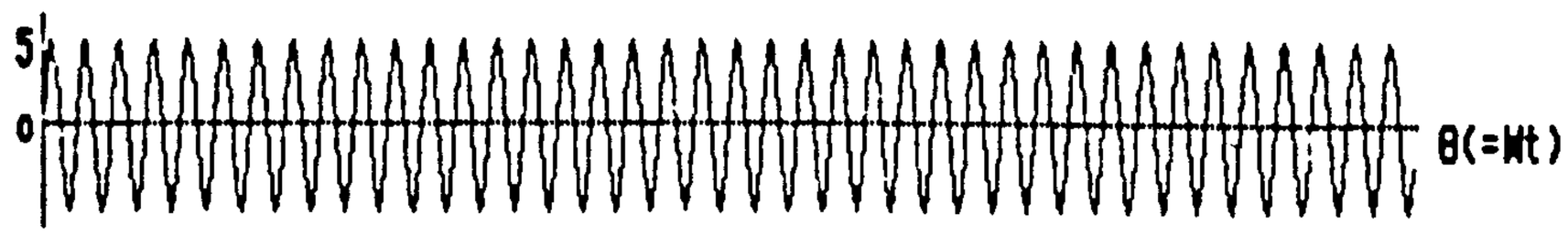

FUNCTION:

f(Wt) = 4.SIN(2π.40.t)

FFT OF FUNCTION

Figure 5.6.22: Typical Results from FFT Algorithm Vaildation

FUNCTION:

f(Wt) = 4.SIN(2π.80.t)

FFT OF FUNCTION

Figure 5.6.23: Typical Results from FFT Algorithm Vaildation

FUNCTION:

f(Wt) = 4.SIN(2π.100.t)

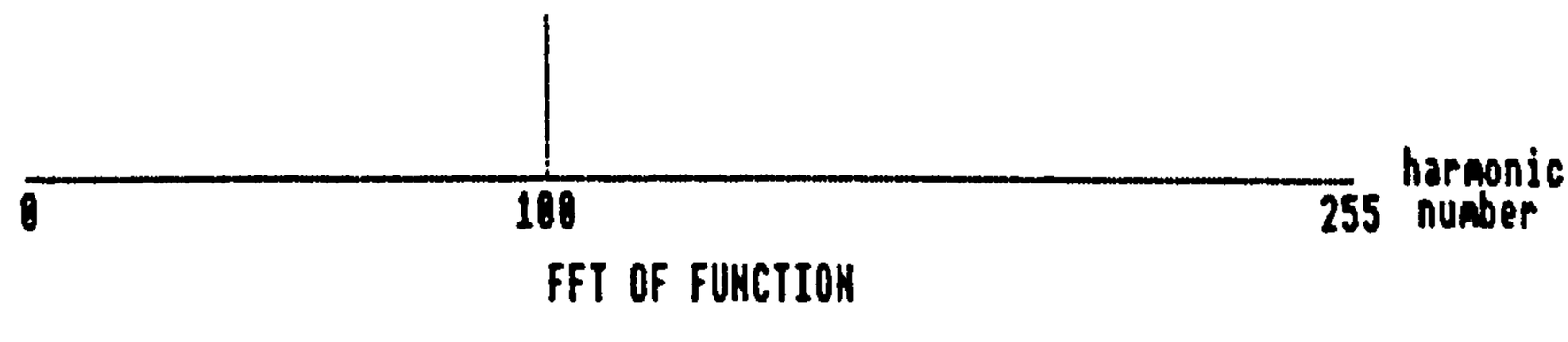

FFT OF FUNCTION

Figure 5.6.24: Typical Results from FFT Algorithm Vaildation

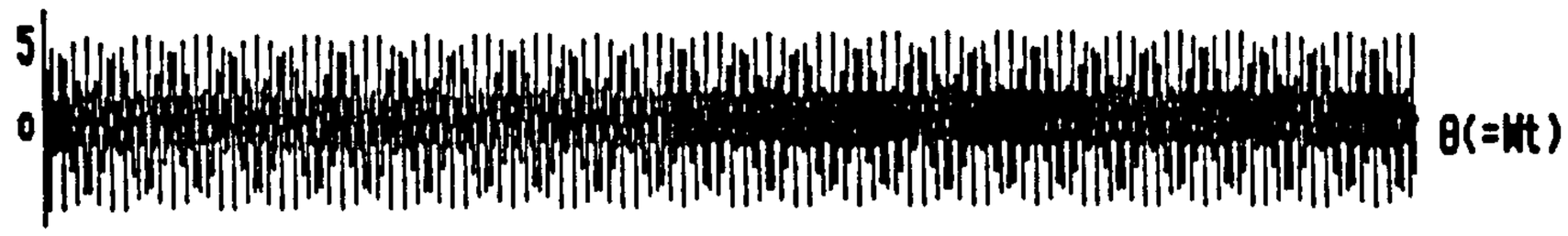

FUNCTION:

f(Wt) = 4.SIN(2π.200.t)

FFT OF FUNCTION

Figure 5.6.25: Typical Results from FFT Algorithm Vaildation

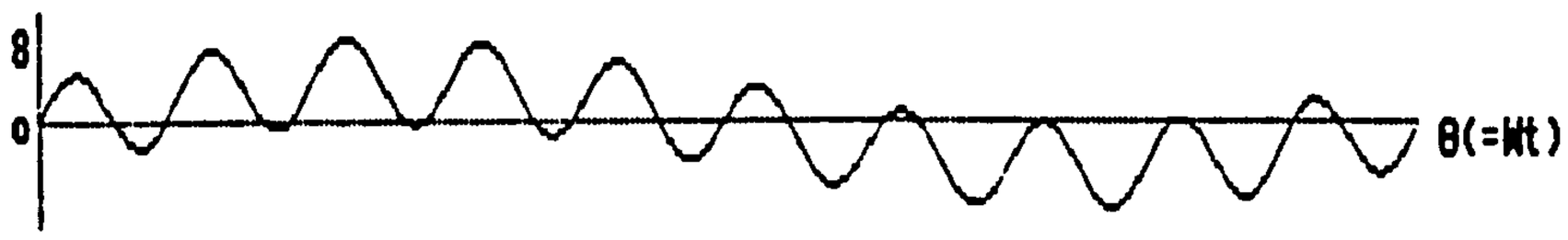

FUNCTION:

f(Wt) = 4.SIN(2π.1.t) + 4.SIN(2π.10.t)

FFT OF FUNCTION

Figure 5.6.26: Typical Results from FFT Algorithm Vaildation

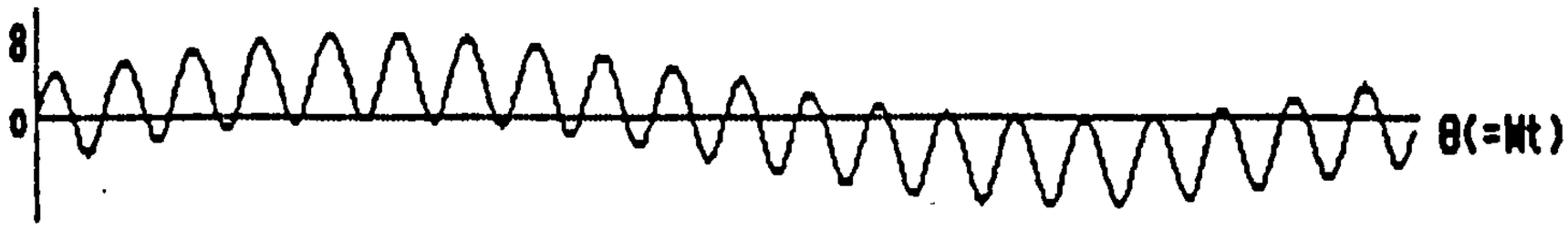

FUNCTION:

$$f(Wt) = 4.SIN(2\pi.1.t) + 4.SIN(2\pi.20.t)$$

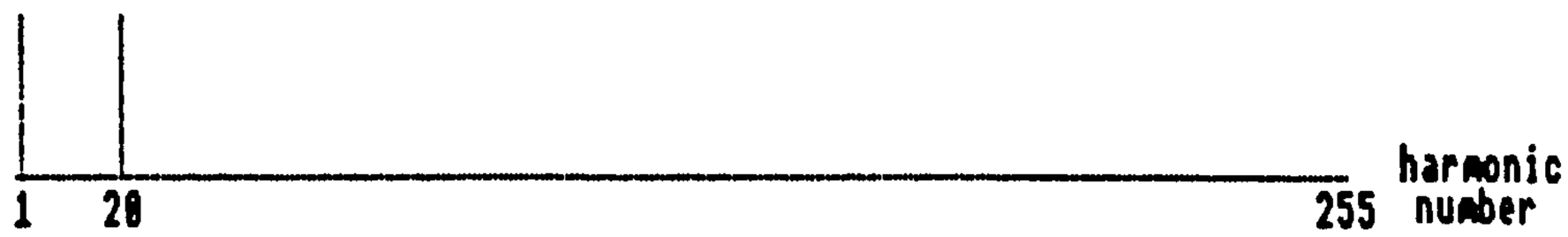

FFT OF FUNCTION

Figure 5.6.27: Typical Results from FFT Algorithm Vaildation

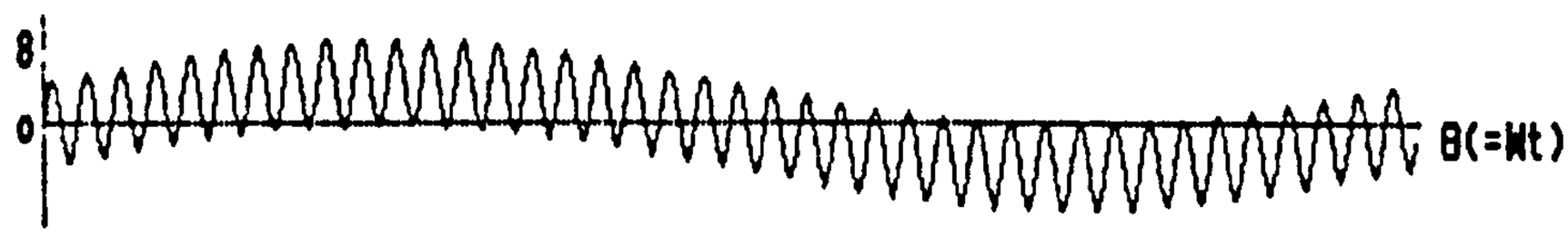

FUNCTION:

$$f(Wt) = 4.SIN(2\pi.1.t) + 4.SIN(2\pi.40.t)$$

FFT OF FUNCTION

Figure 5.6.28: Typical Results from FFT Algorithm Vaildation

FUNCTION:

f(Wt) = 4.SIN(2π.1.t) + 4.SIN(2π.80.t)

FFT OF FUNCTION

Figure 5.6.29: Typical Results from FFT Algorithm Vaildation

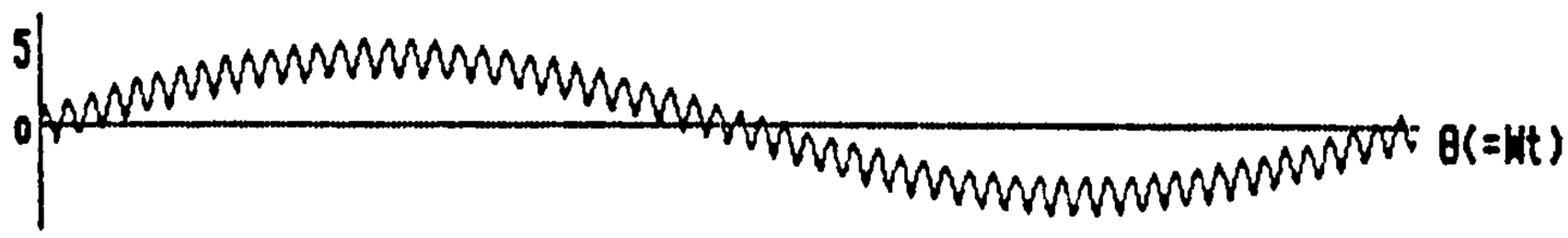

FUNCTION:

f(Wt) = 4.SIN(2π.1.t) + 1.SIN(2π.60.t)

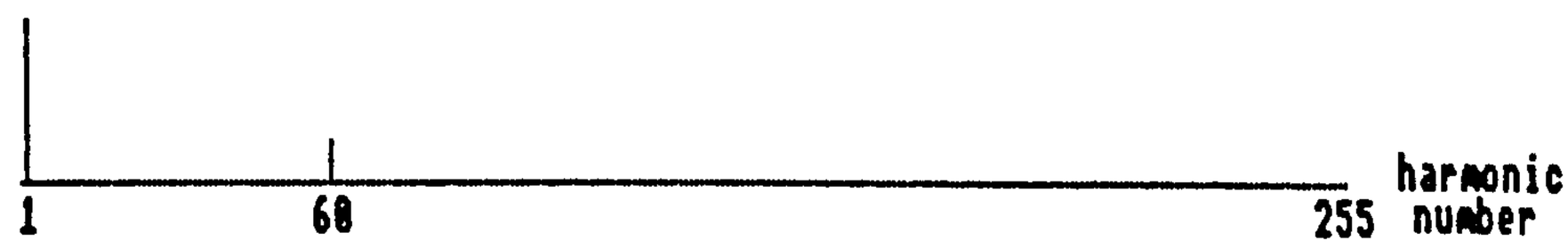

FFT OF FUNCTION

Figure 5.6.30: Typical Results from FFT Algorithm Vaildation

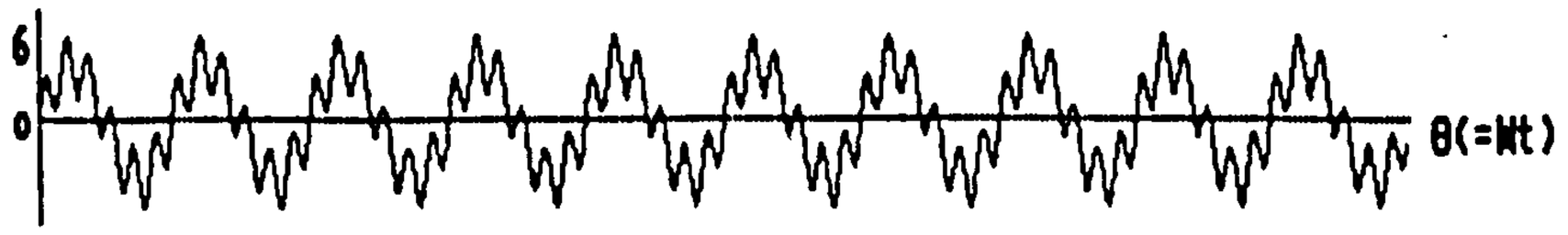

FUNCTION:

f(Wt) = 4.SIN(2π.10.t) + 2.SIN(2π.60.t)

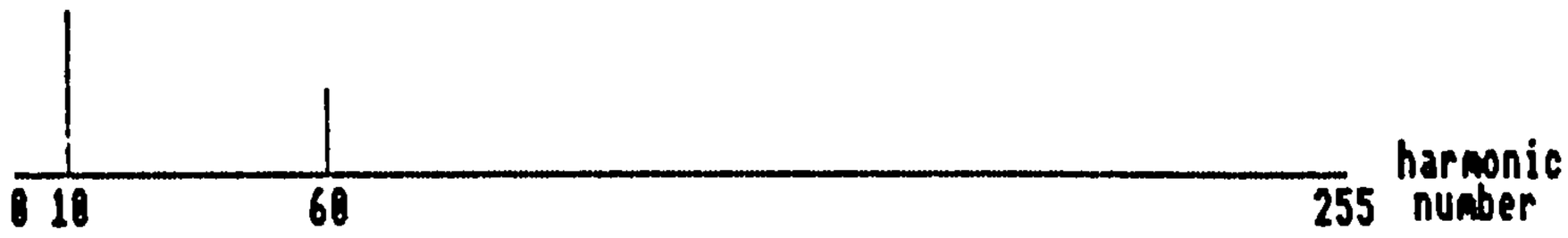

FFT OF FUNCTION

Figure 5.6.31: Typical Results from FFT Algorithm Vaildation

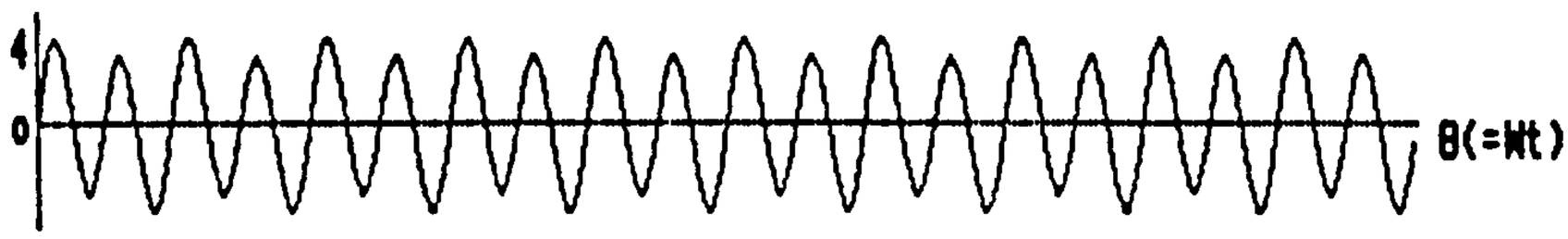

FUNCTION:

f(Wt) = 3.SIN(2π.20.t) + 0.5.SIN(2π.10.t)

FFT OF FUNCTION

Figure 5.6.32: Typical Results from FFT Algorithm Vaildation

FUNCTION:

$$f(Wt) = 5.SIN(2\pi.70.t) + 4.5.SIN(2\pi.25.t)$$

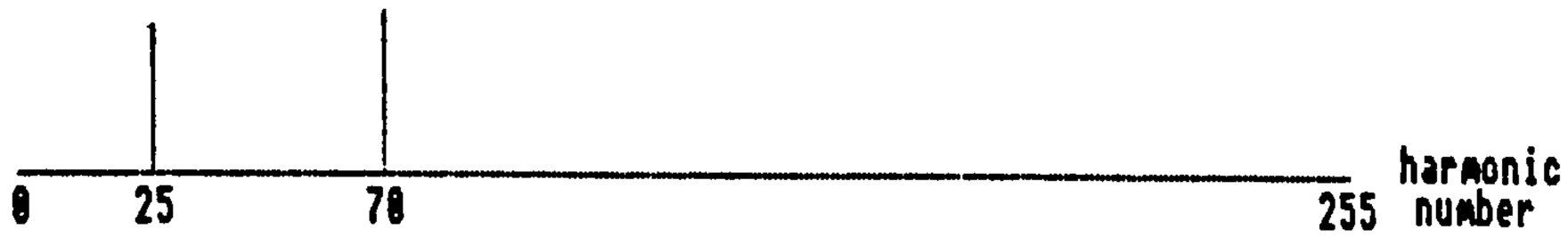

FFT OF FUNCTION

Figure 5.6.33: Typical Results from FFT Algorithm Vaildation

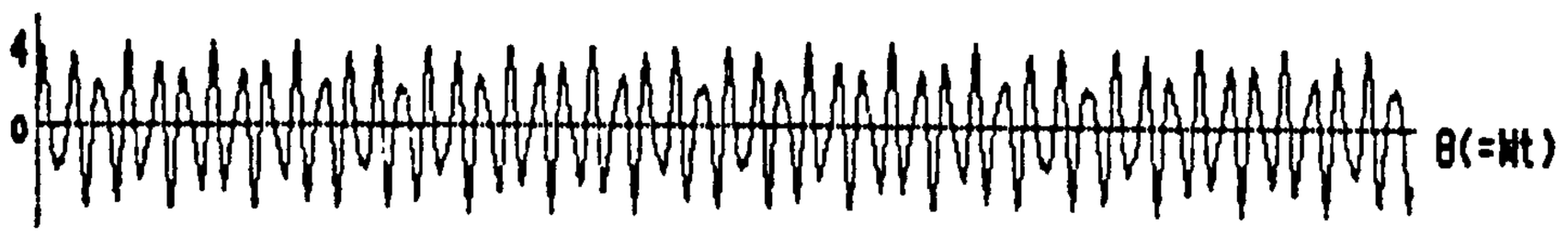

FUNCTION:

$$f(Wt) = 2.5.SIN(2\pi.50.t) + 1.SIN(2\pi.82.t)$$

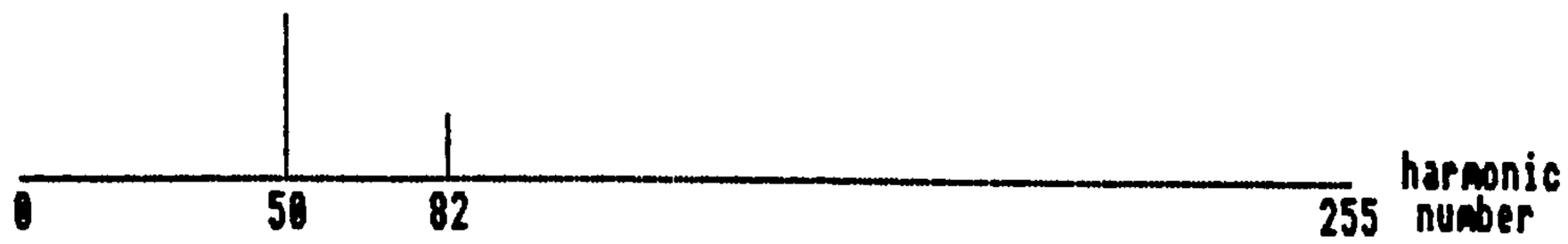

FFT OF FUNCTION

Figure 5.6.34: Typical Results from FFT Algorithm Vaildation

FUNCTION:

f(Wt) = 2.SIN(2π.50.5.t) + 1.SIN(2π.82.5.t) + 0.5.SIN(2π.5.t)
+ 0.1.SIN(2π.80.t)

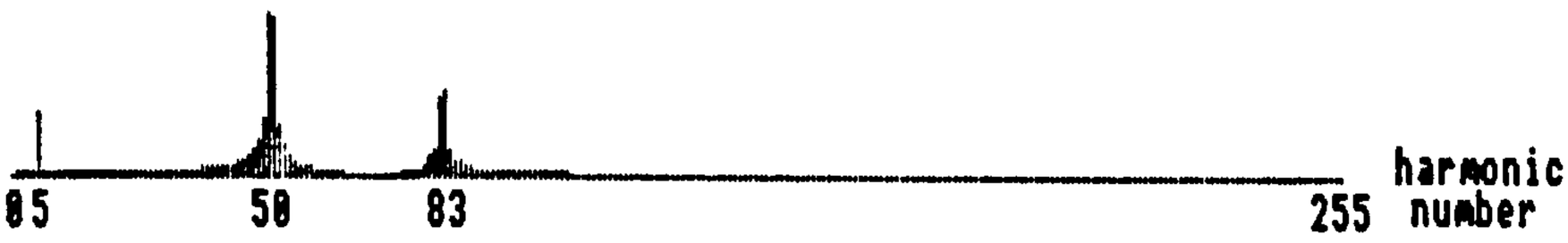

FFT OF FUNCTION

Figure 5.6.35: Typical Results from FFT Algorithm Vaildation

FUNCTION:

f(Wt) = 1.SIN(2π.18.3.t) + 0.5.SIN(2π.7.t) + 2.SIN(2π.60.48.t)
+ 0.75.SIN(2π.86.364.t)

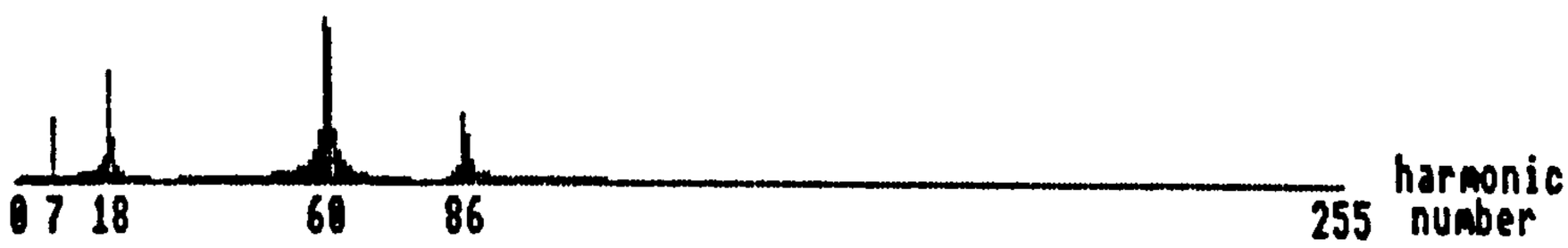

FFT OF FUNCTION

Figure 5.6.36: Typical Results from FFT Algorithm Vaildation

FUNCTION:

f(Wt) = 0.5.SIN(2π.20.t) + 0.5.SIN(2π.50.3.t) + 0.5.SIN(2π.80.2.t)
+ 0.5.SIN(2π.90.1.t) + 0.5.SIN(2π.120.4.t)

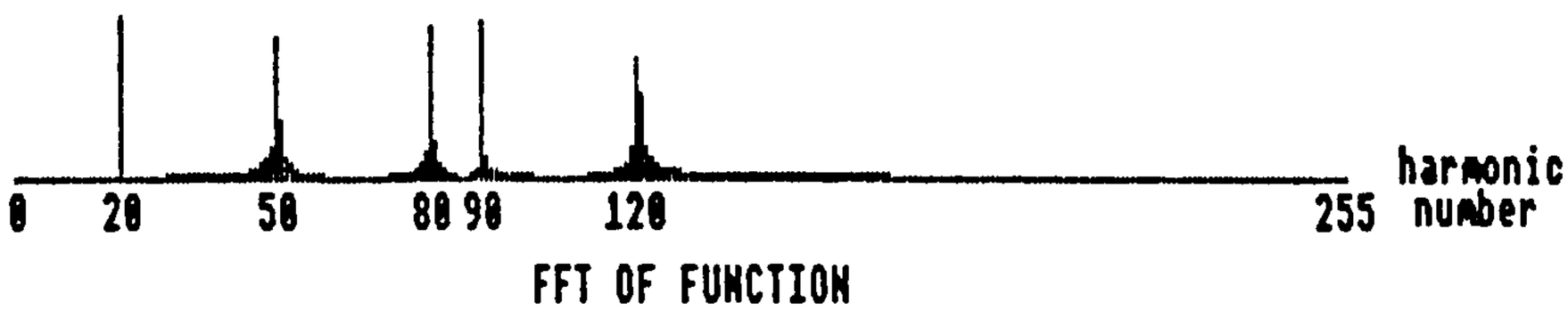

FFT OF FUNCTION

Figure 5.6.37: Typical Results from FFT Algorithm Vaildation

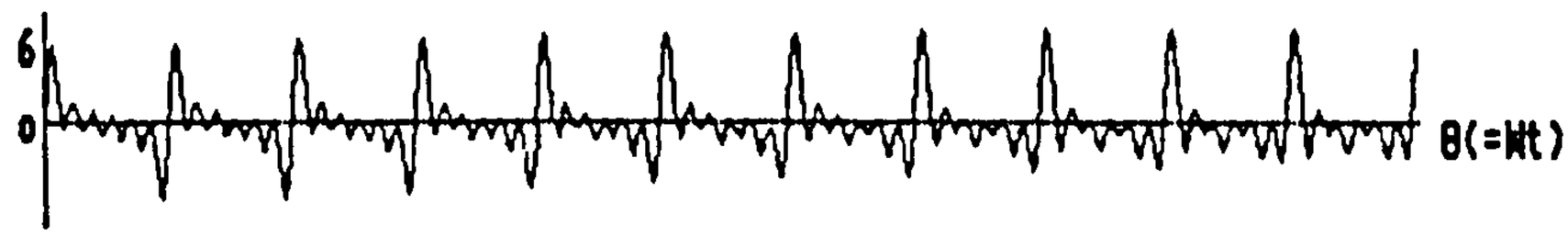

FUNCTION:

f(Wt) = 1.SIN(2π.11.2.t) + 1.SIN(2π.22.2.t) + 1.SIN(2π.33.3.t)
+ 1.SIN(2π.44.2.t) + 1.SIN(2π.55.2.t) + 1.SIN(2π.66.2.t)

FFT OF FUNCTION

Figure 5.6.38: Typical Results from FFT Algorithm Vaildation

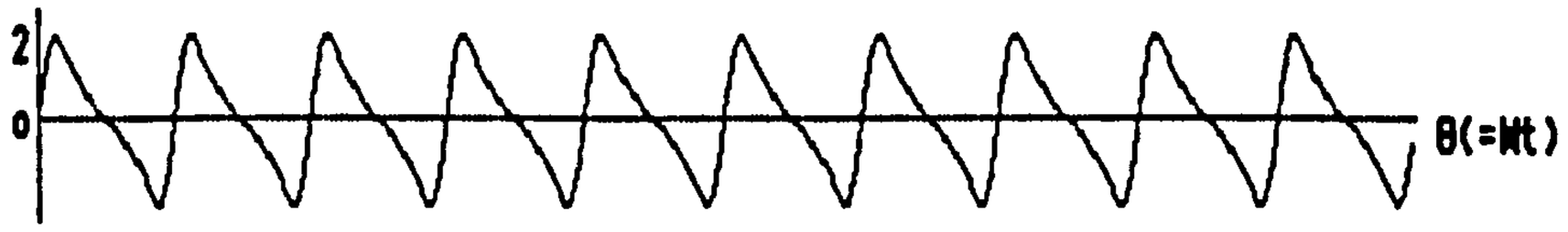

FUNCTION:

f(Wt) = 1.SIN(2π.10.t) + 0.5.SIN(2π.20.t) + 0.2.SIN(2π.30.t)
+ 0.07.SIN(2π.40.t) + 2E-3.SIN(2π.50.t)

FFT OF FUNCTION

Figure 5.6.39: Typical Results from FFT Algorithm Vaildation

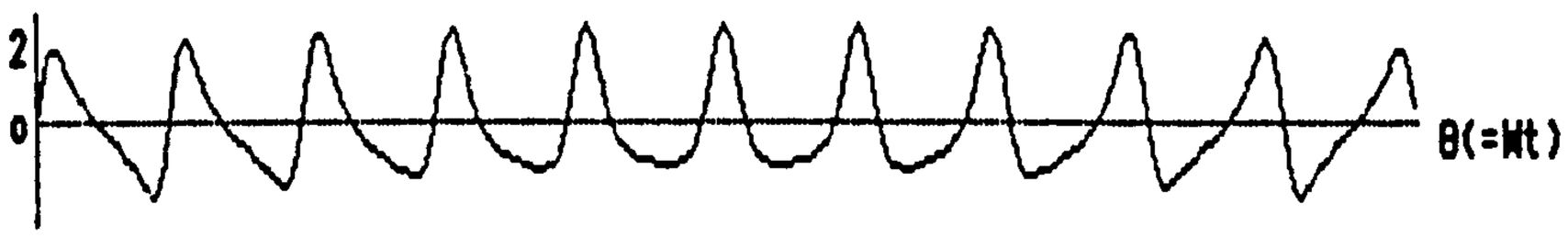

FUNCTION:

f(Wt) = 1.SIN(2π.10.5.t) + 0.5.SIN(2π.20.5.t) + 0.2.SIN(2π.30.5.t)
+ 0.07.SIN(2π.40.5.t) + 2E-3.SIN(2π.50.5.t)

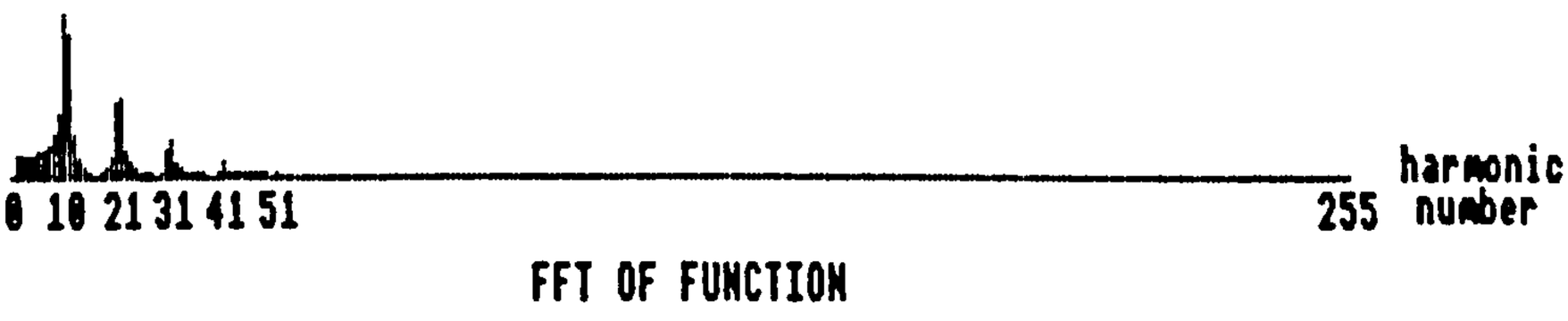

FFT OF FUNCTION

Figure 5.6.40: Typical Results from FFT Algorithm Vaildation

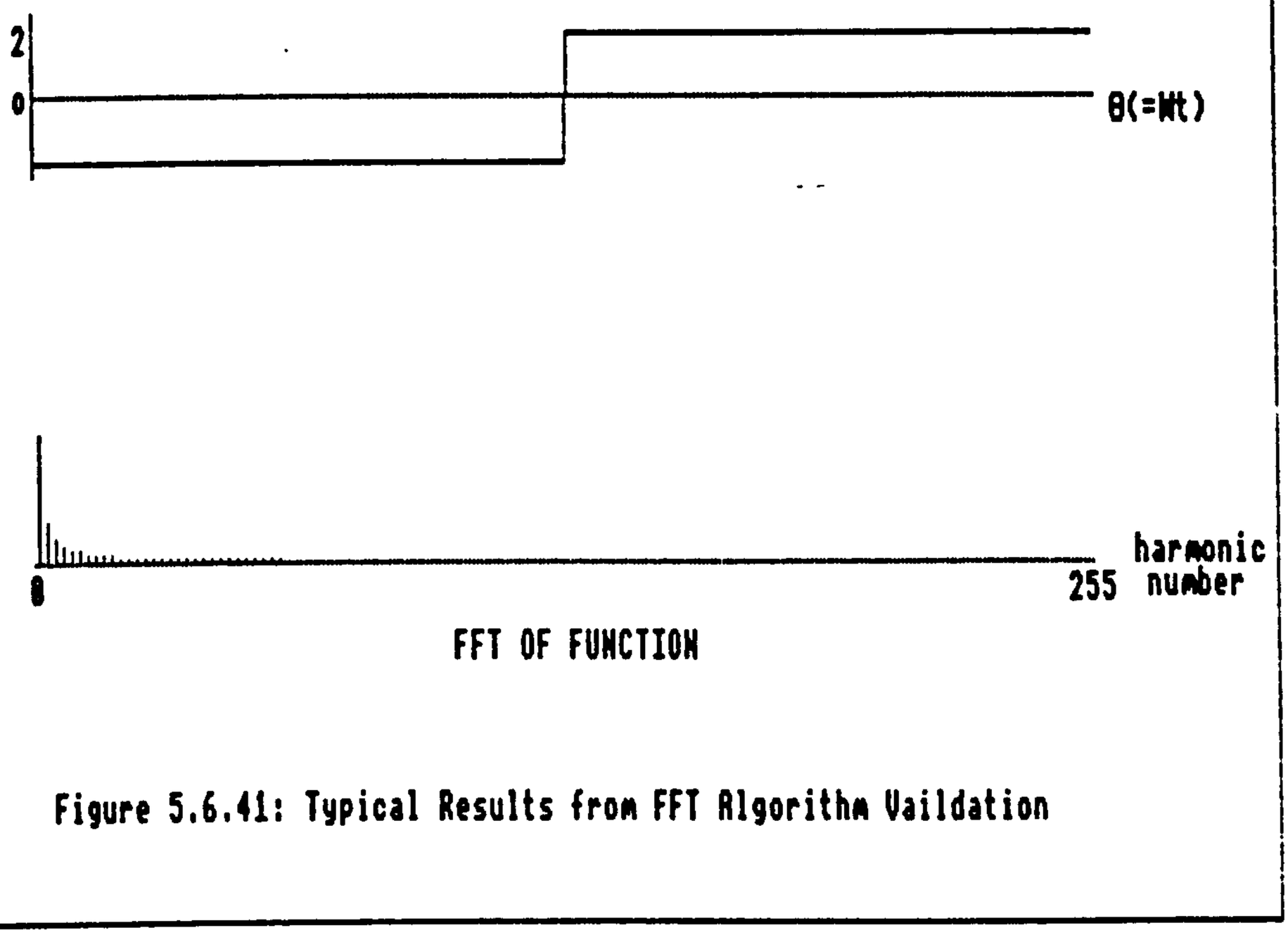

Figure 5.6.41: Typical Results from FFT Algorithm Vaildation

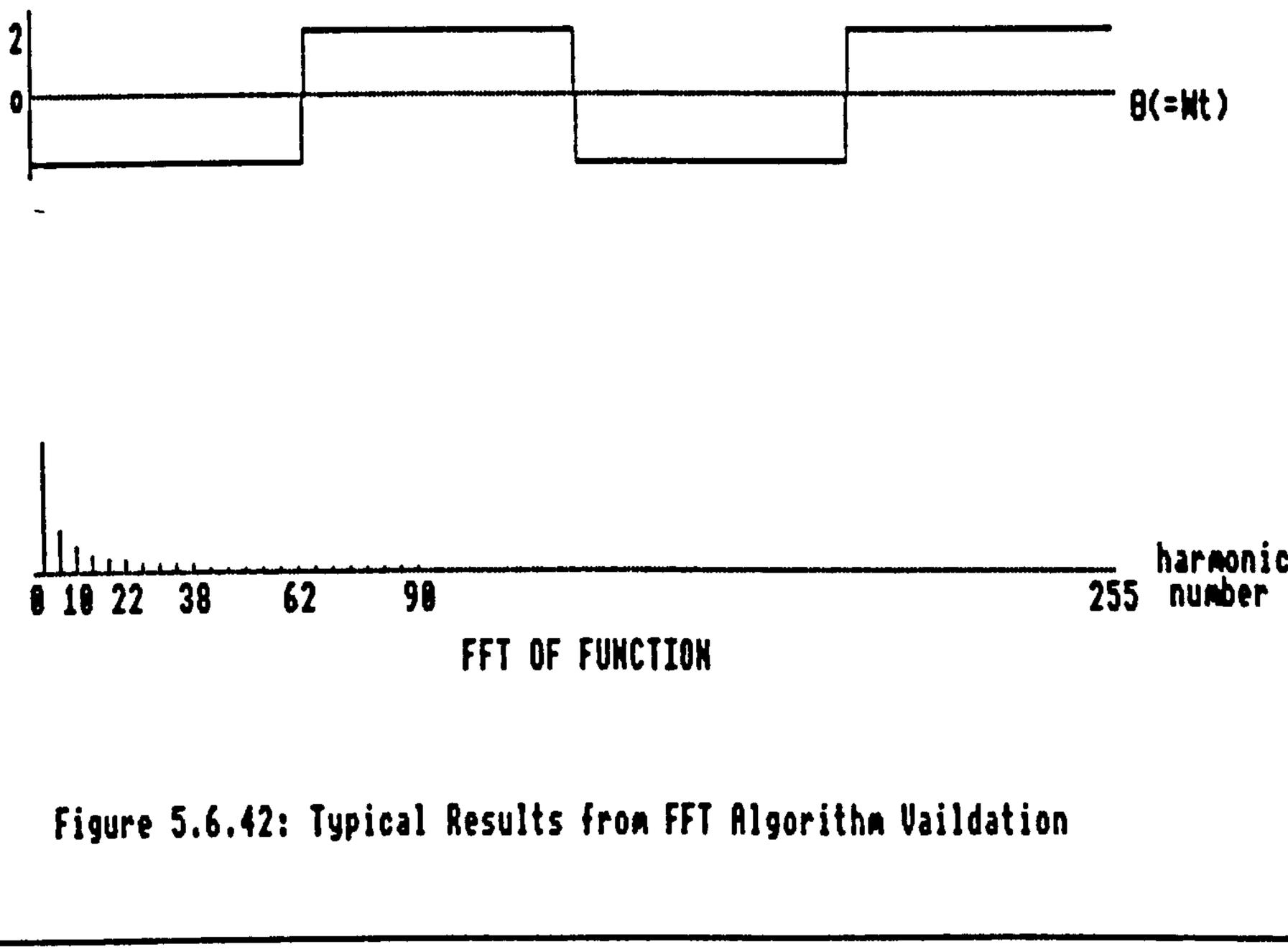

Figure 5.6.42: Typical Results from FFT Algorithm Vaildation

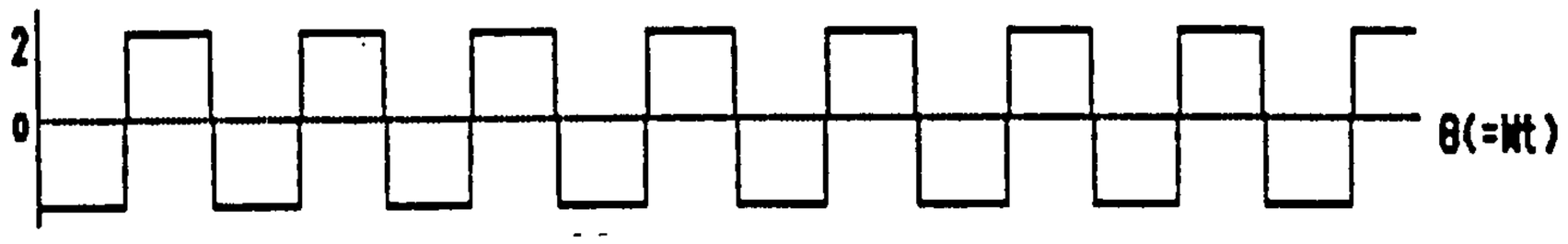

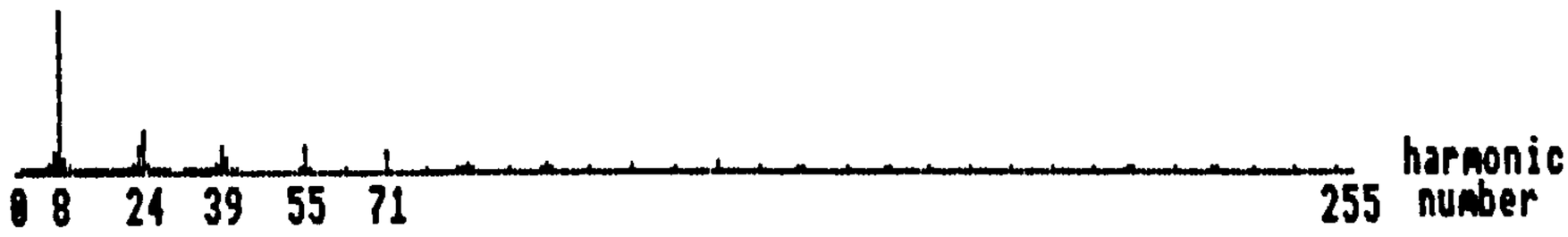

FFT OF FUNCTION

Figure 5.6.43: Typical Results from FFT Algorithm Vaildation

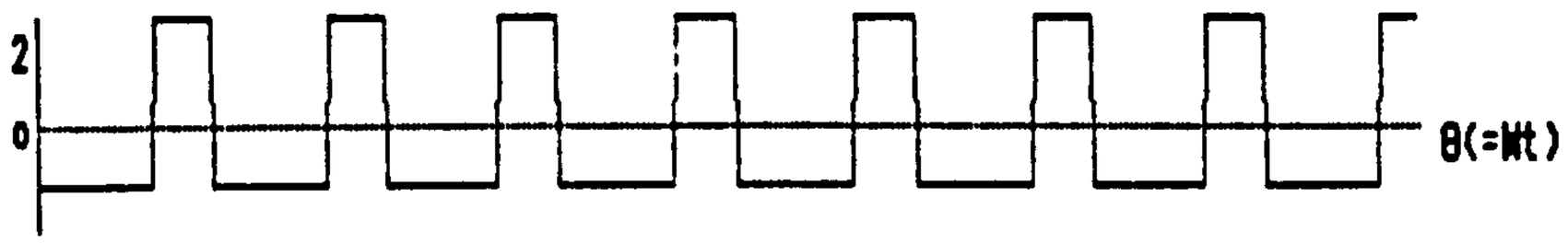

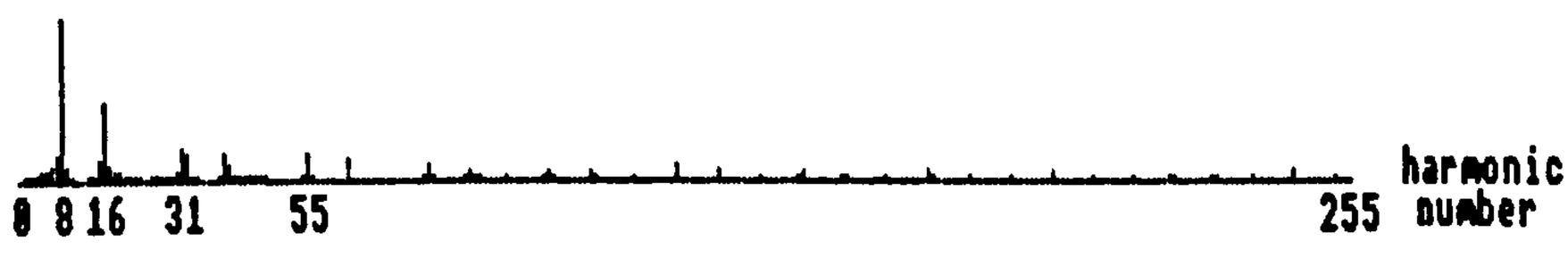

FFT OF FUNCTION

Figure 5.6.44: Typical Results from FFT Algorithm Vaildation

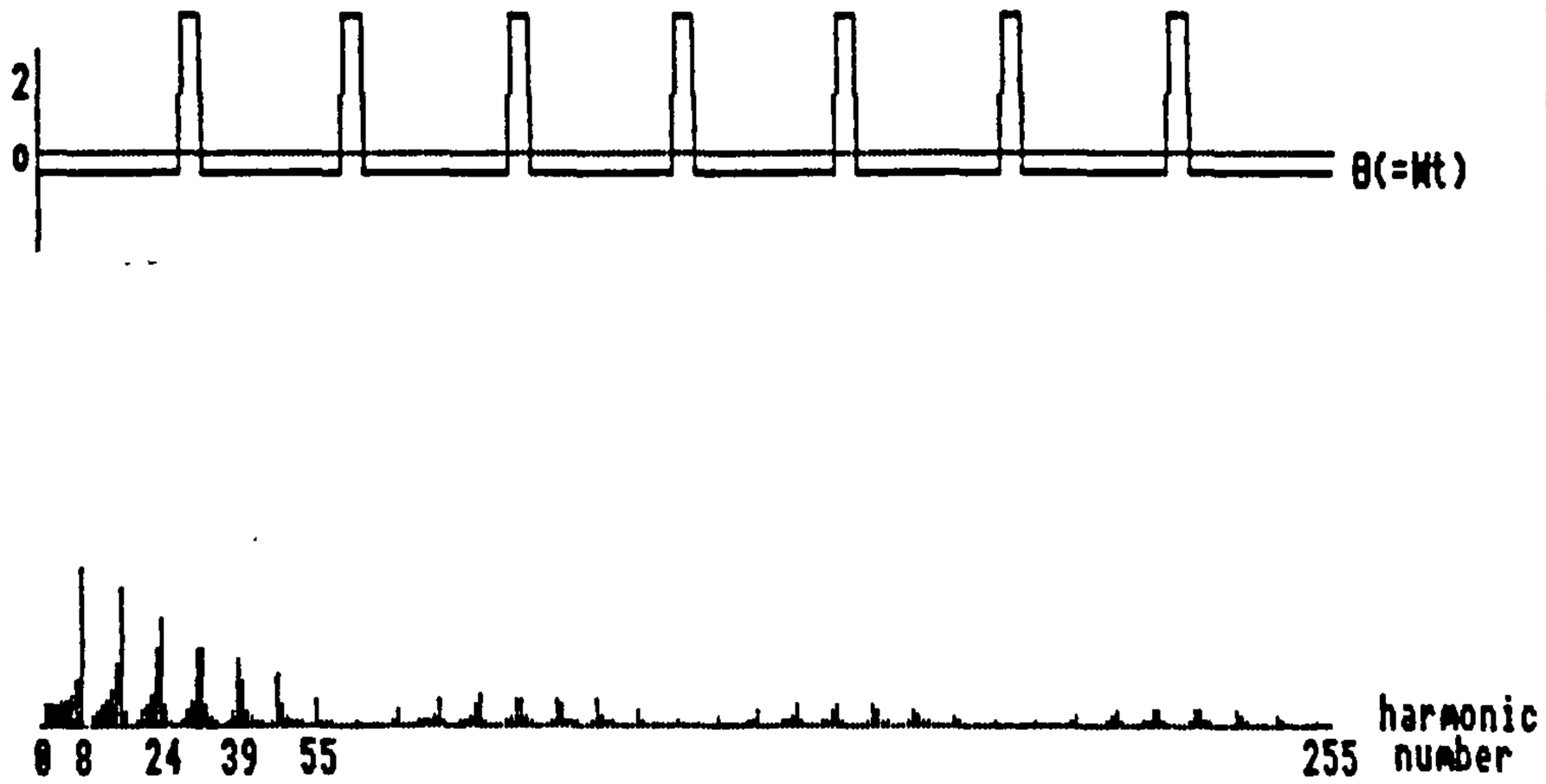

FFT OF FUNCTION

Figure 5.6.45: Typical Results from FFT Algorithm Vaildation

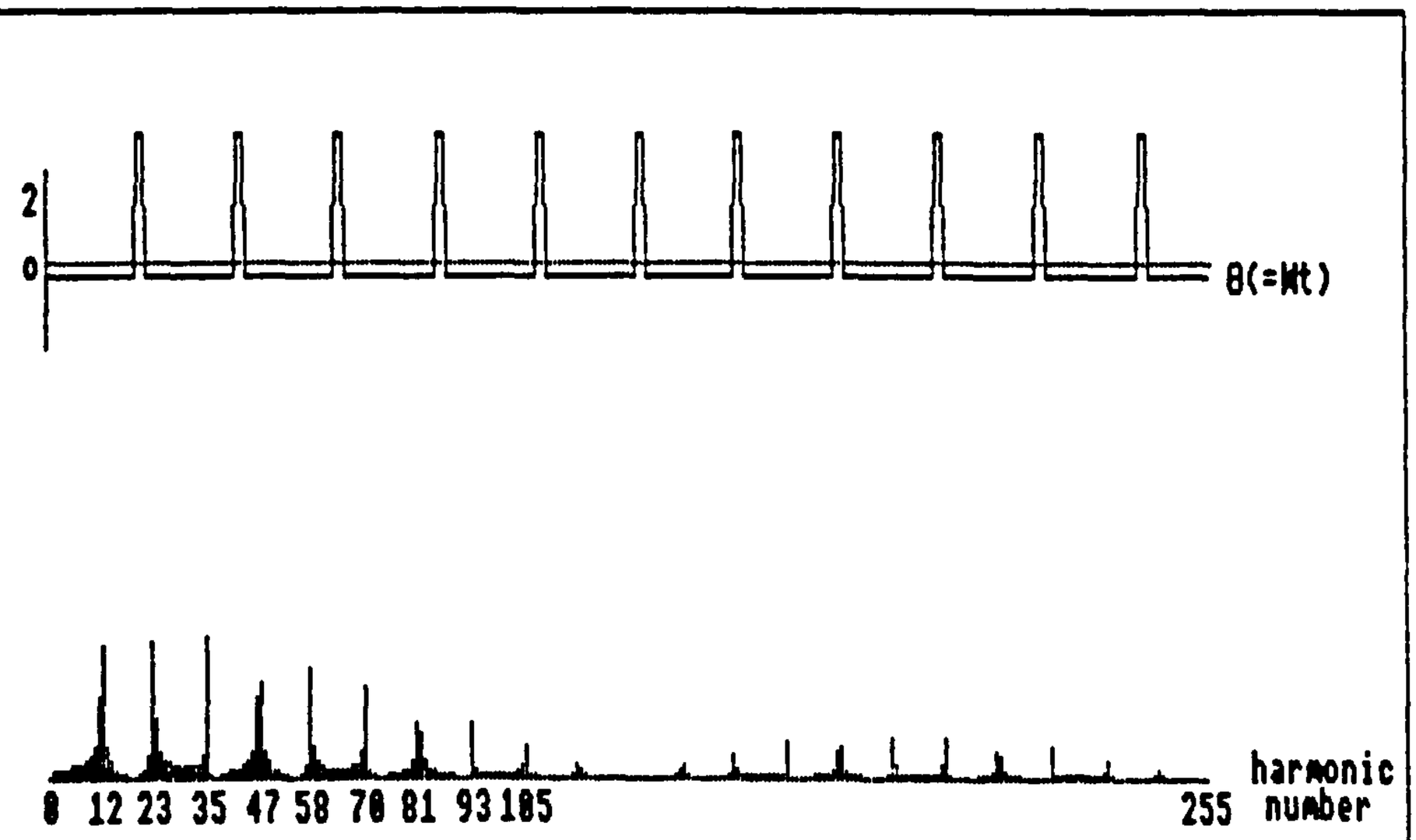

FFT OF FUNCTION

Figure 5.6.46: Typical Results from FFT Algorithm Vaildation

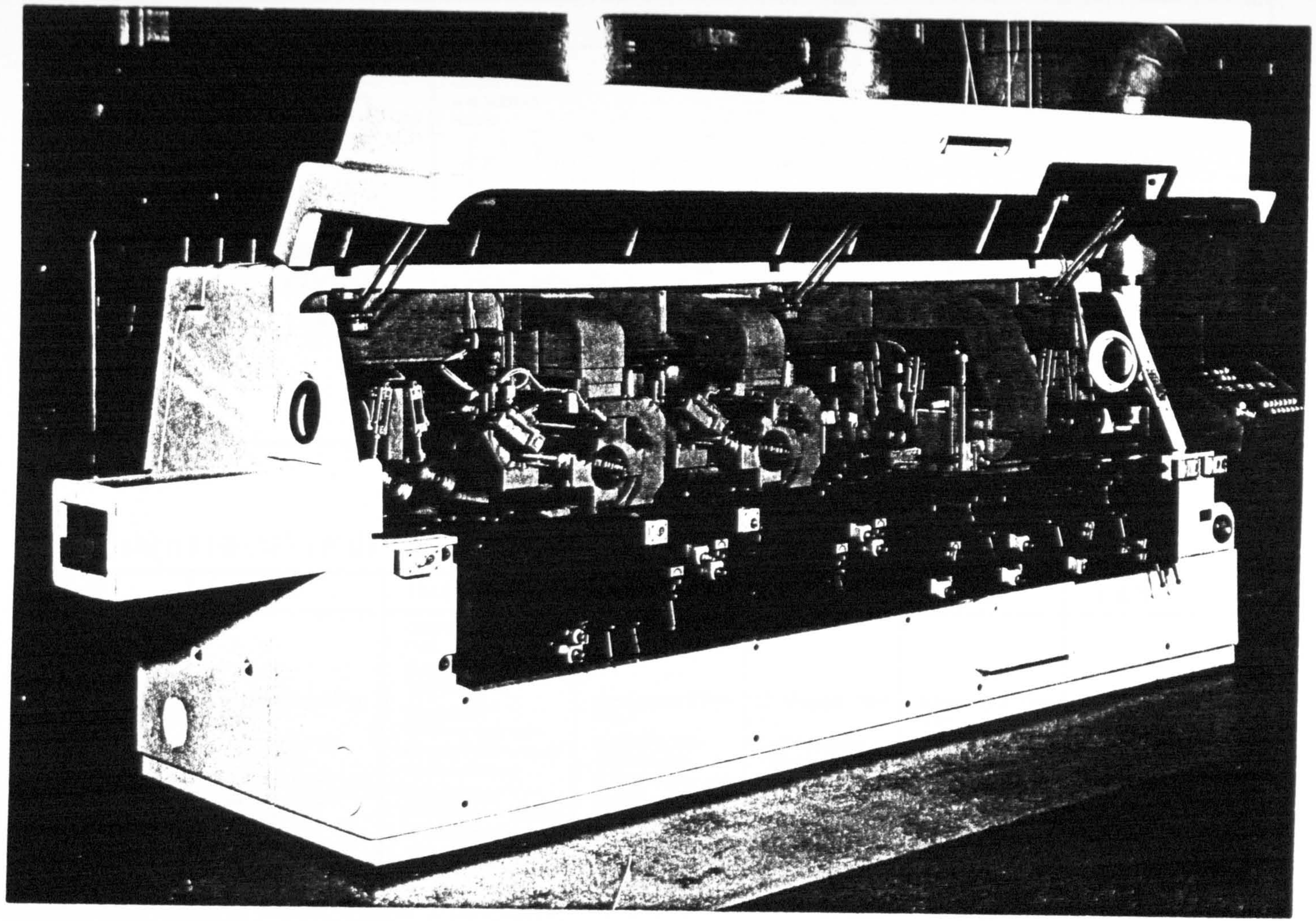

Figure 6.1: The B-series 220 Planer - Moulder Machine

MODEL 4S

OPTIONAL UNIVERSAL HEAD

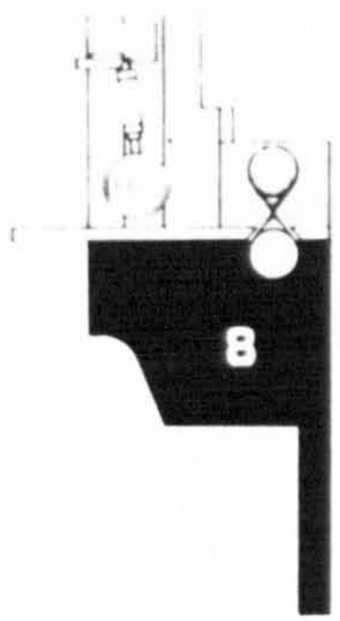

STANDARD HEAD SEQUENCE

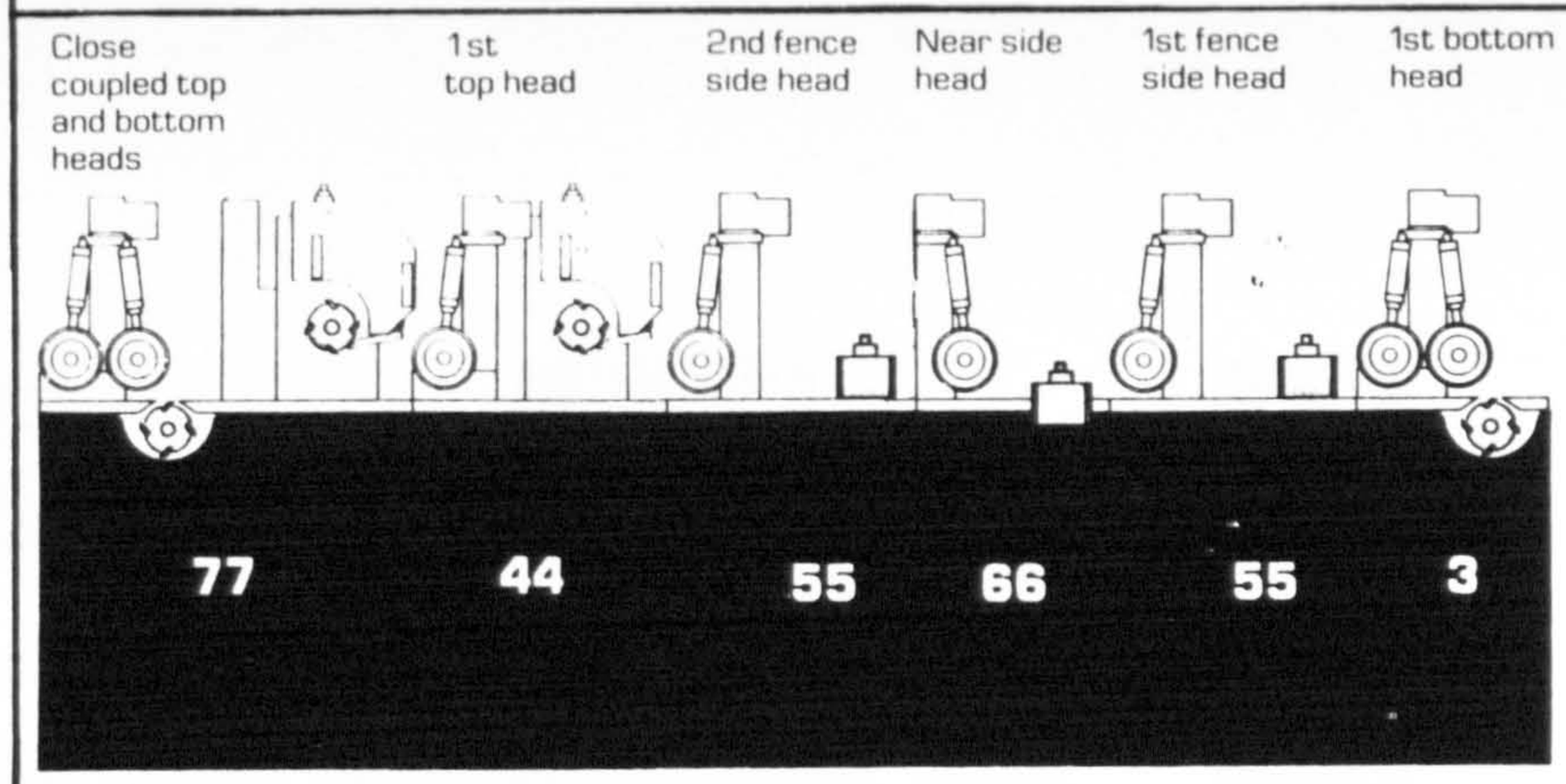

STANDARD HEAD UNIT SPECIFICATIONS

Unit 8	Unit 33	Unit 77	Unit 44	Unit 66	Unit 55	Unit 3
Top or bottom horizontal or intermediates and vertical nearside. Head motor 15 hp max. Cutting circles 125 mm min. 200mm max.	Head motor 25hp max. Cutting circles 125mm min. 230mm max. with or without jointing	Head motor 25hp max. Cutting circles 125mm min. Top head 230mm max. with jointing 250mm max. without jointing Bottom head 230mm max. with or without jointing	Head motor 25hp max. Cutting circles 125mm min. 230mm max. with jointing 250mm max. without jointing	Head motor 15hp max. Cutting circles 125mm min. 200mm max. with or without jointing	Head motor 15hp max. Cutting circles 125mm min. 200mm max. with or without jointing	Head motor 15hp max. Cutting circles 125mm min. 185mm max. with or without jointing

Figure 6.2: Head unit Specifications of the Modular "200B"

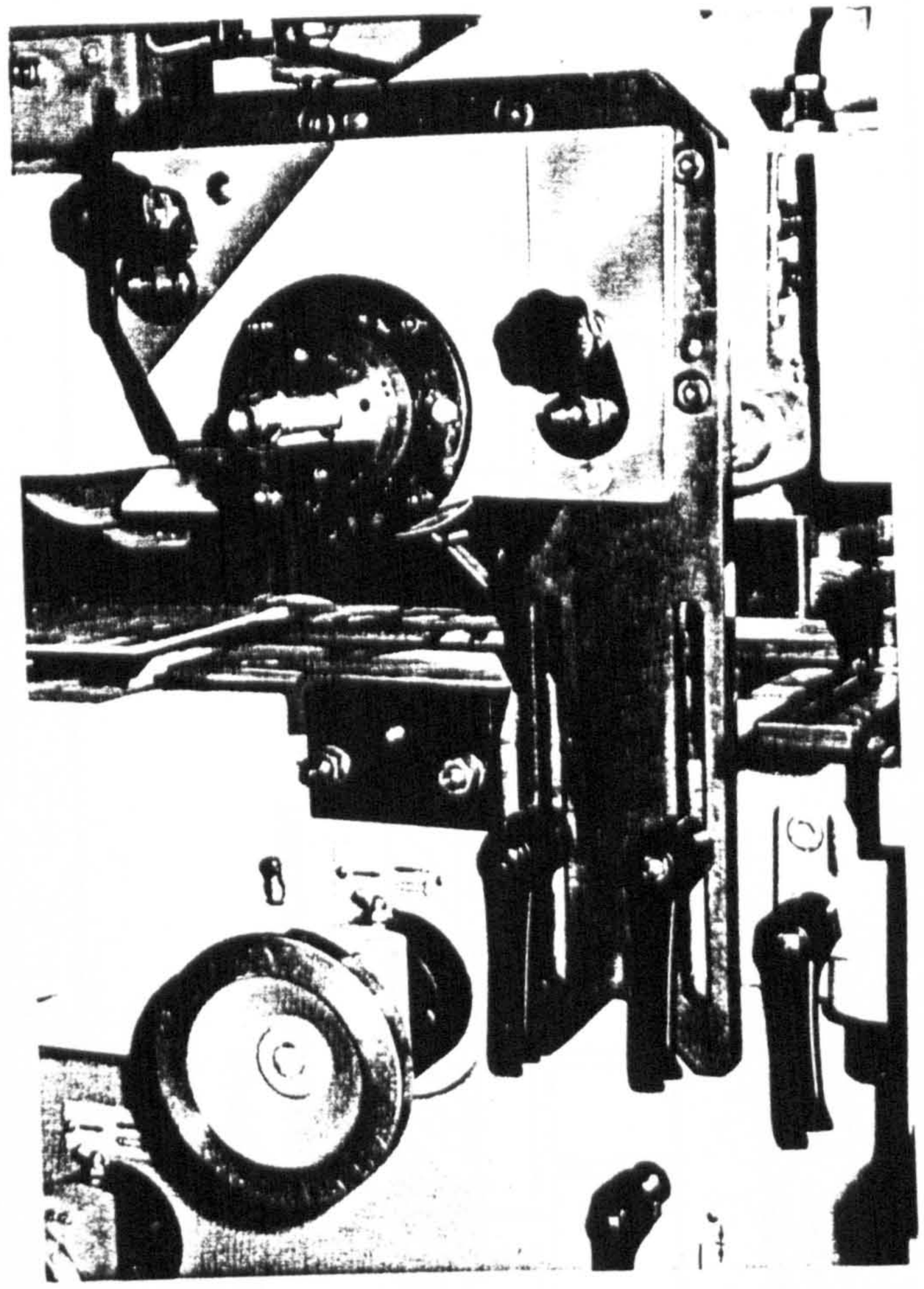

Figure 6.3: Final Top Head

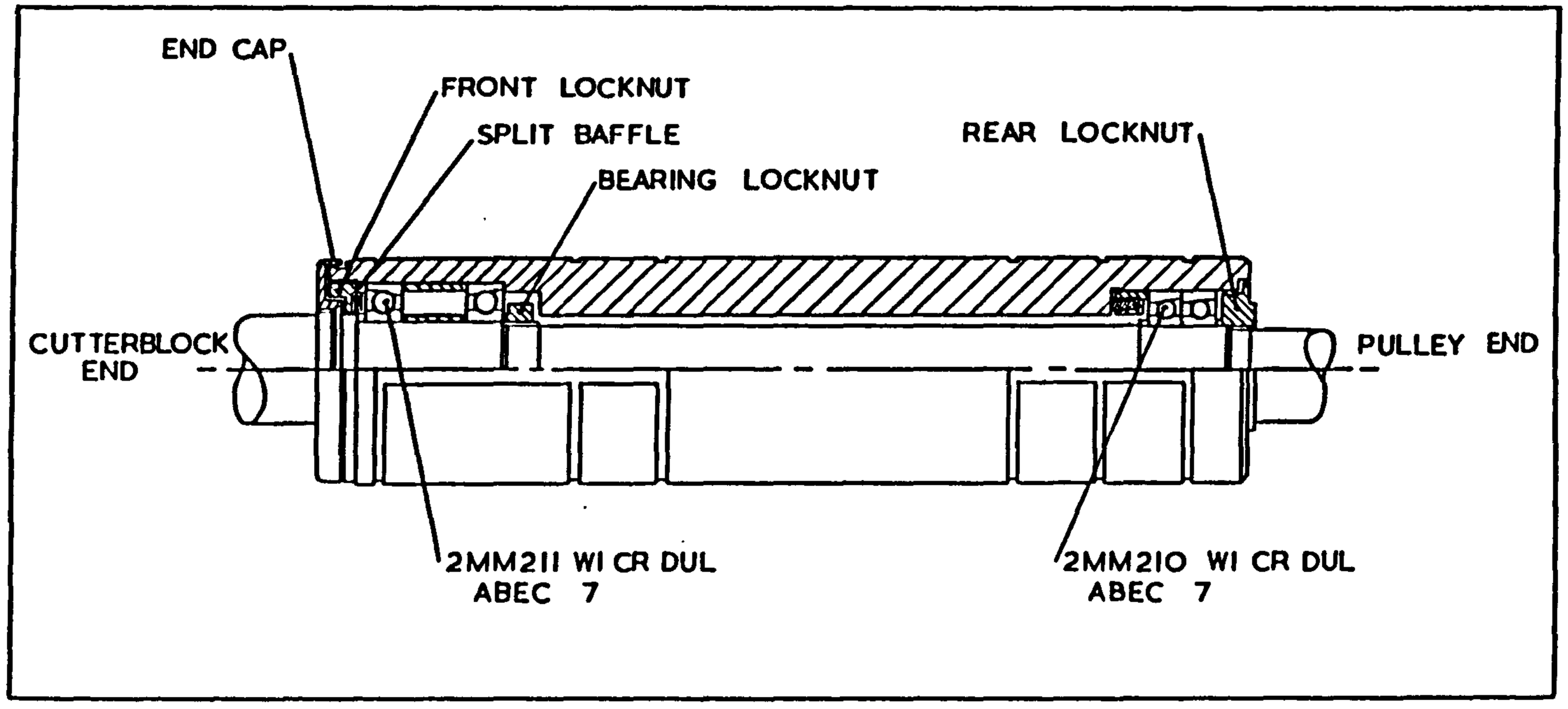

Figure 6.4: Spindle Unit Bearing Assembly

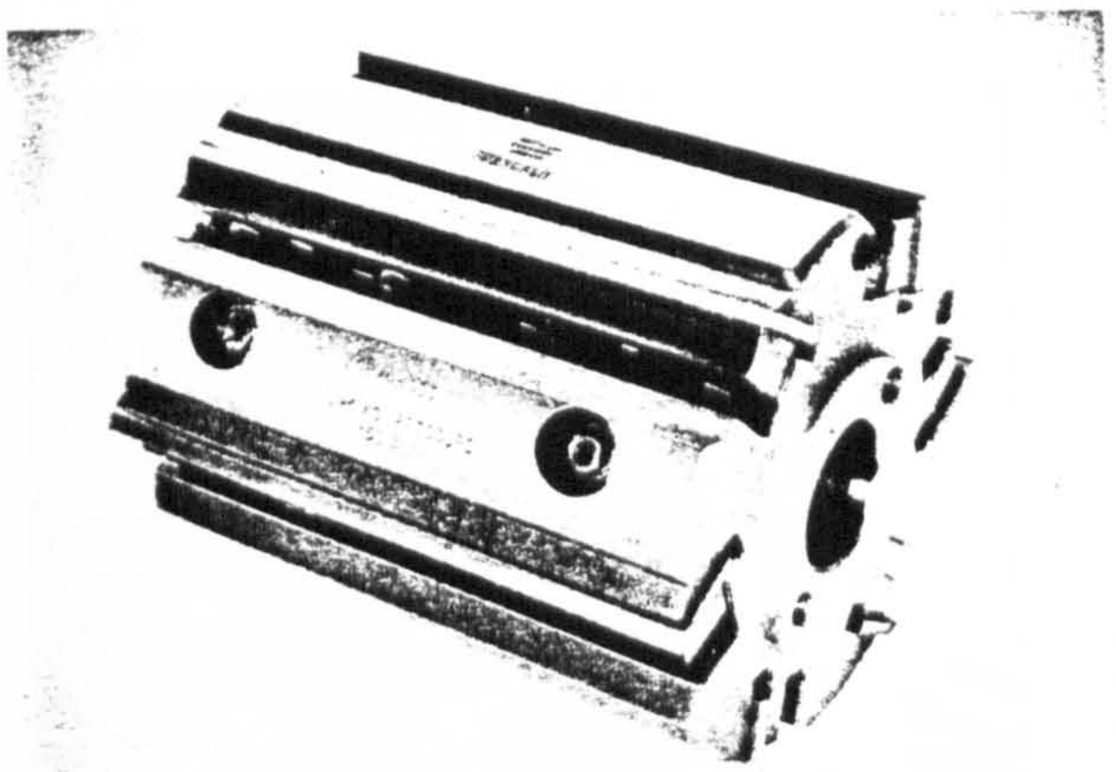

Hydrogrip Planing Cutterblock

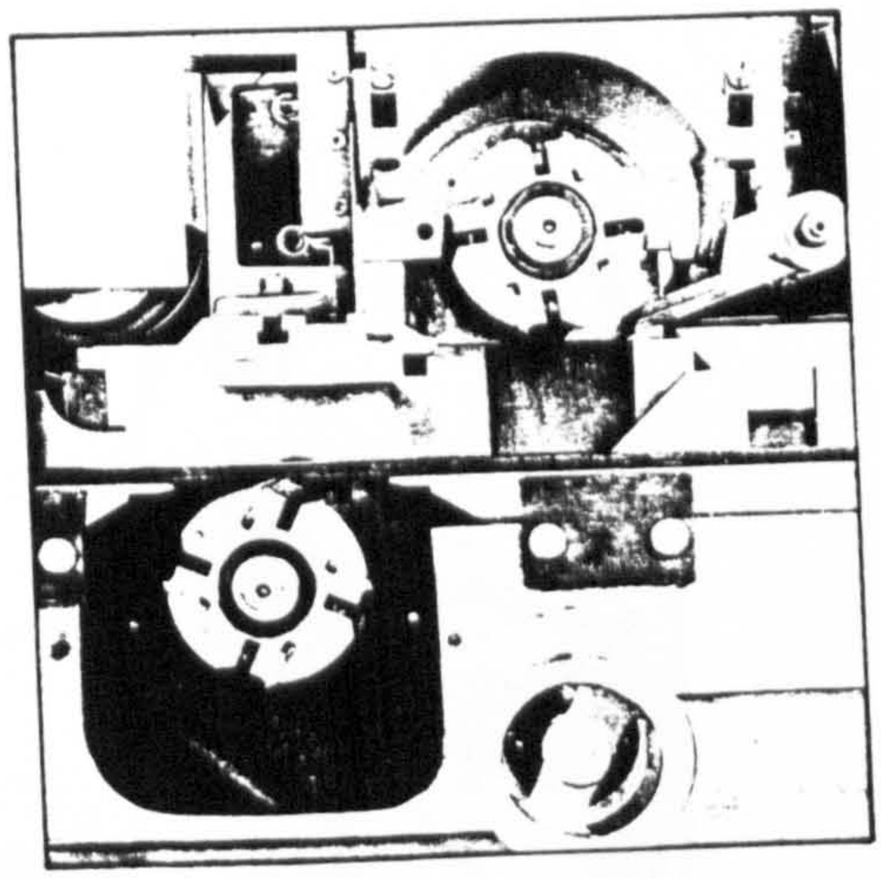

Hydrogrip Planing Cutterheads in situ

Figure 6.5: Hydrogrip Planing Cutterblock and Cutterheads

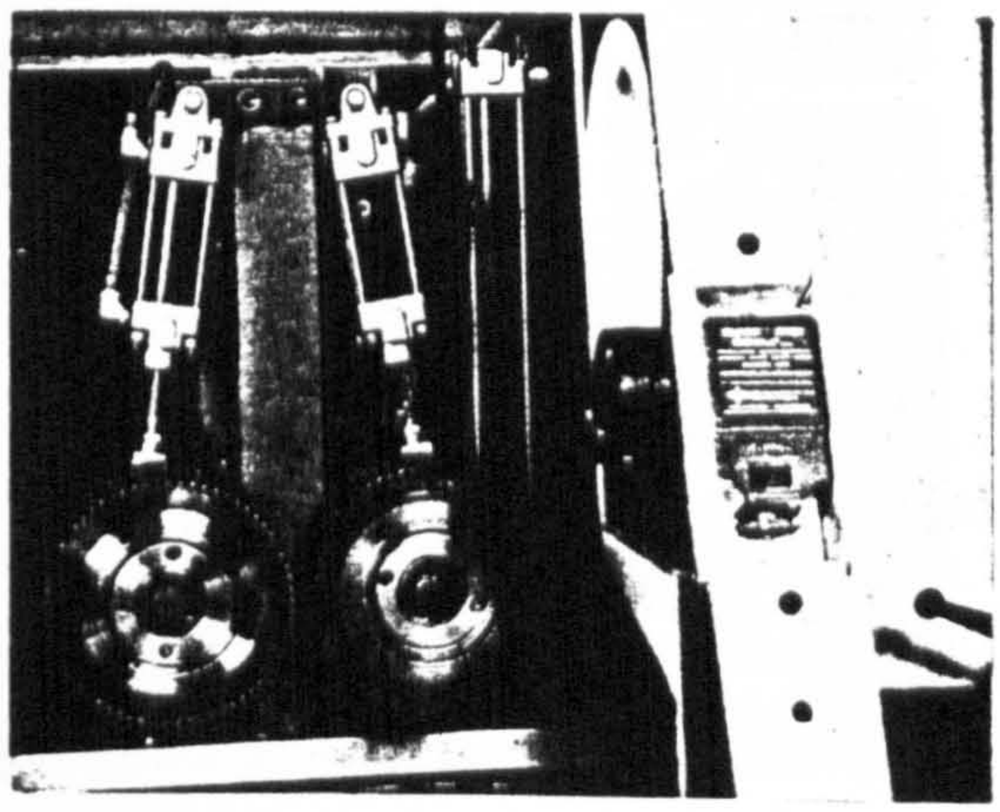

Heavy Duty In-feedworks

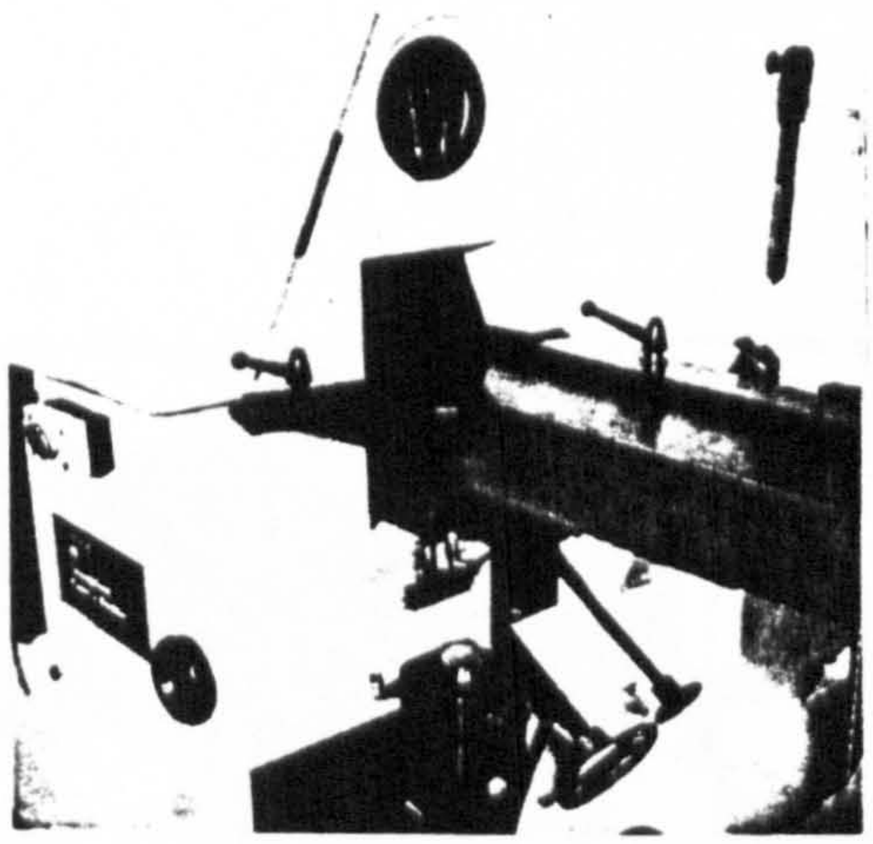

In-feed Table

Figure 6.6: Heavy Duty In-feedworks and In-feed Table

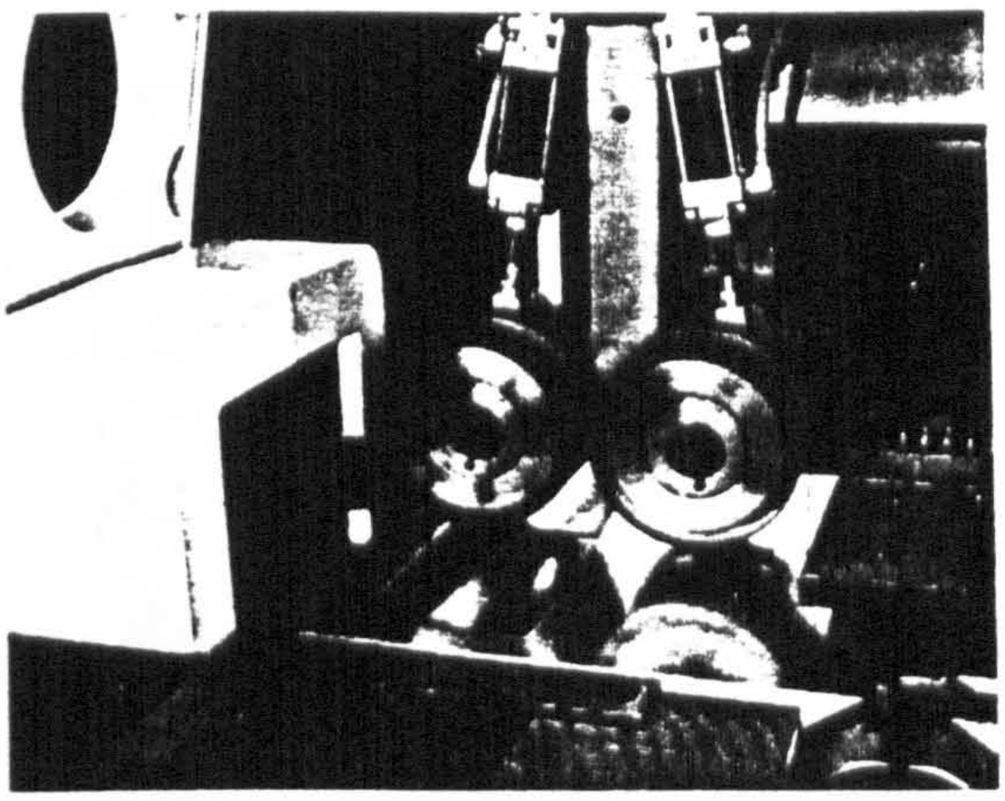

Figure 6.7: Out-feedworks

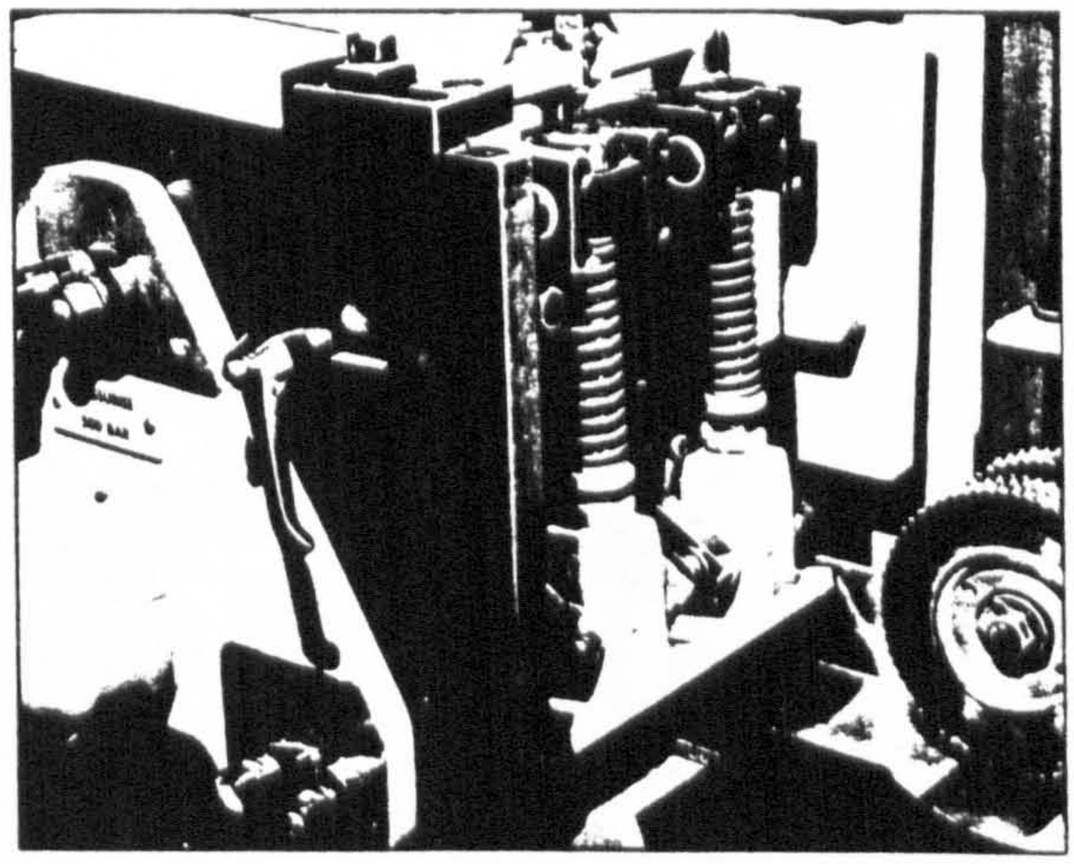

Figure 6.8: Chipbreaker

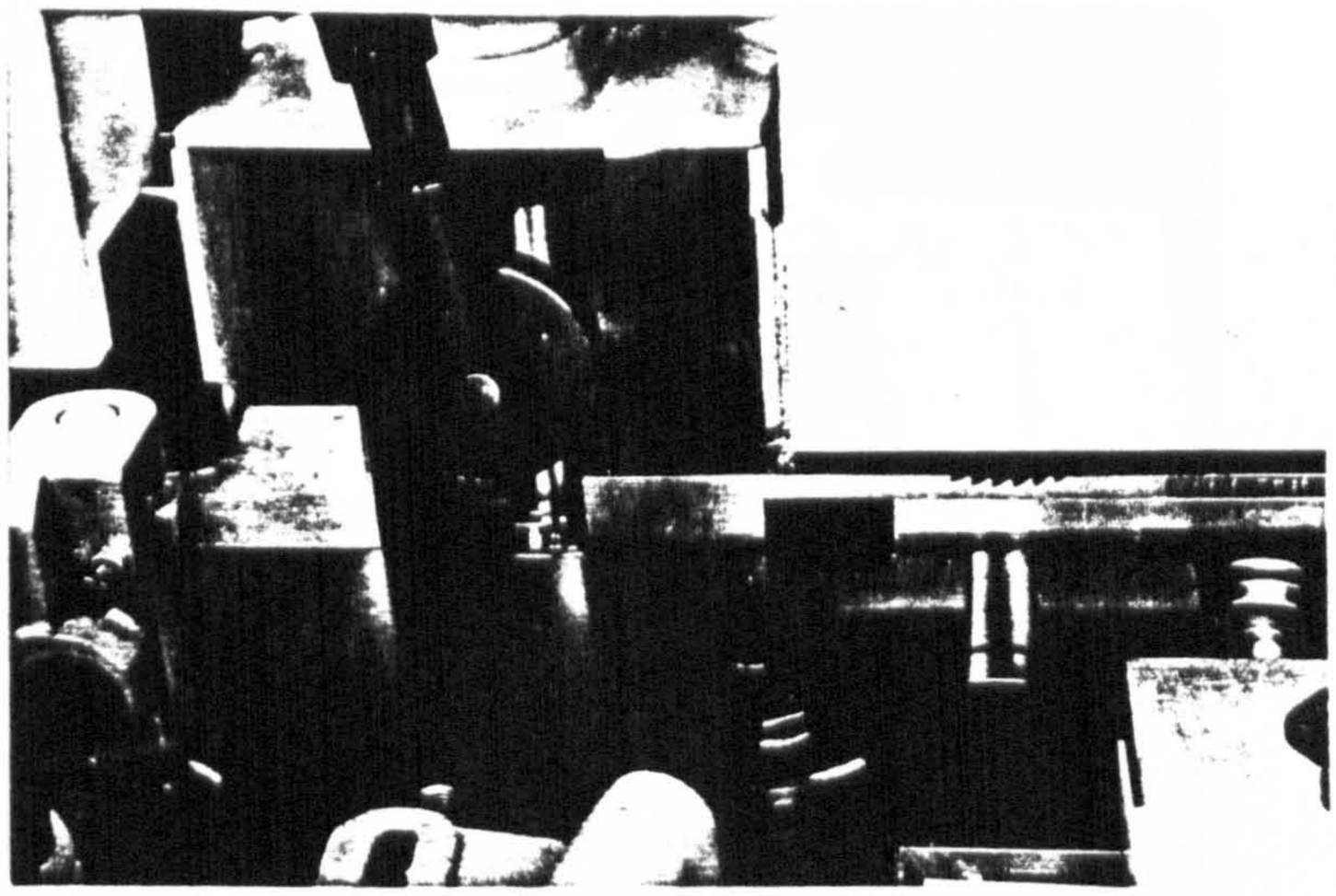

Figure 6.9: Side Pressure Rollers

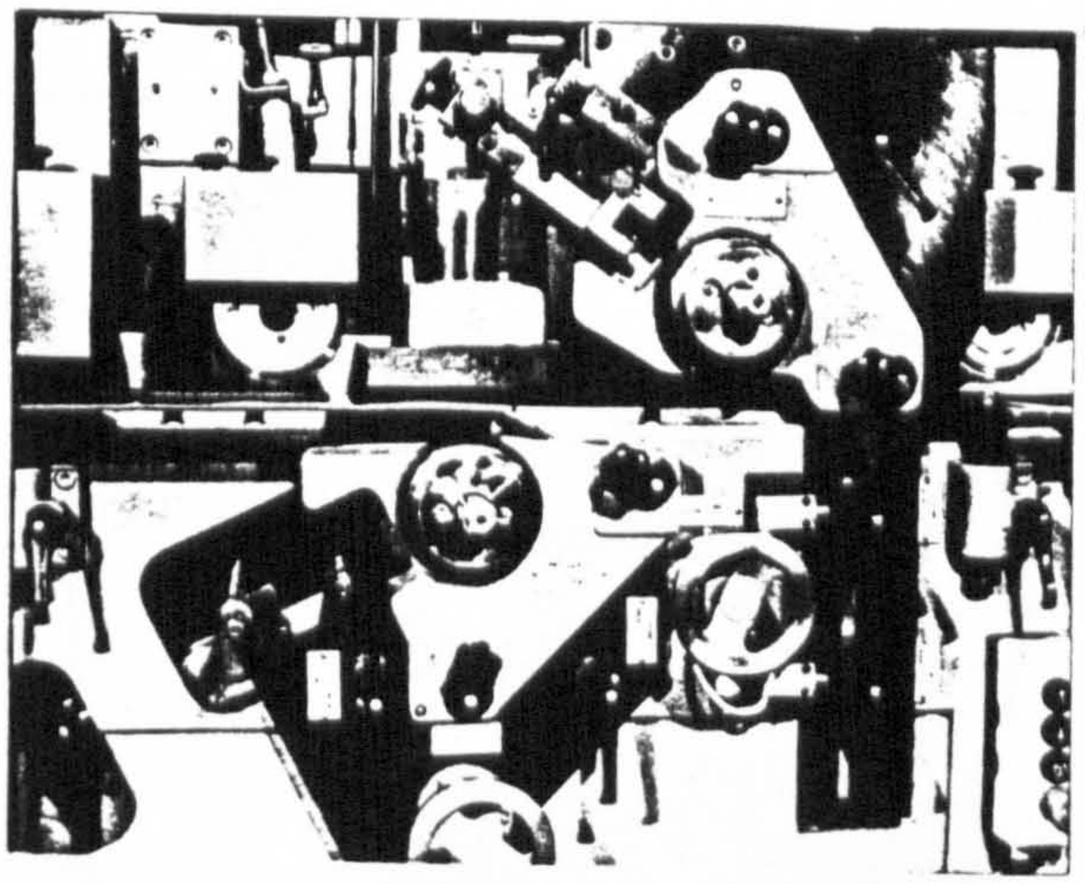

Figure 6.10: Standard Jointer fitted to Top and Bottom Cutterheads

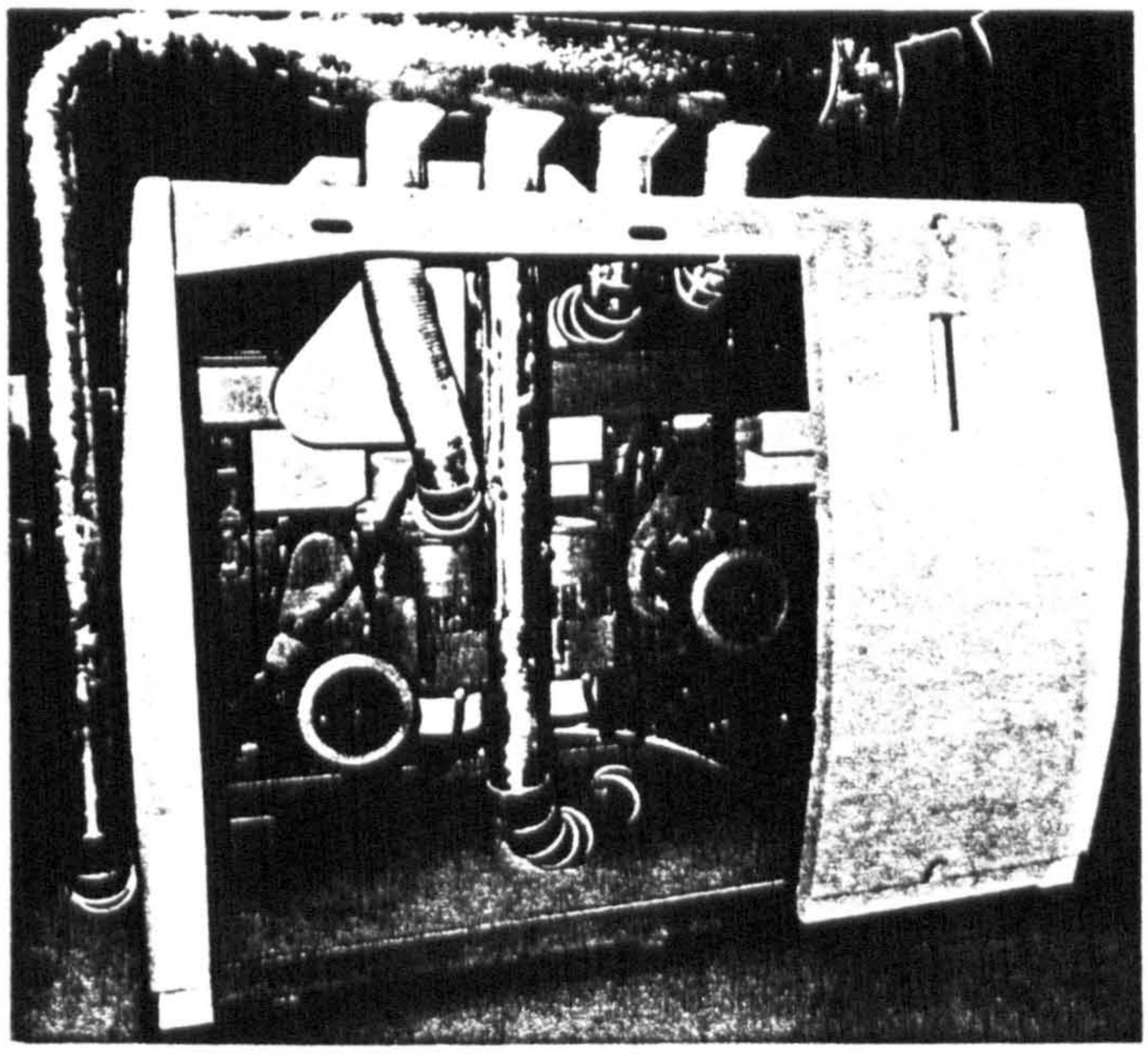

Figure 6.11: Dust Extractor System

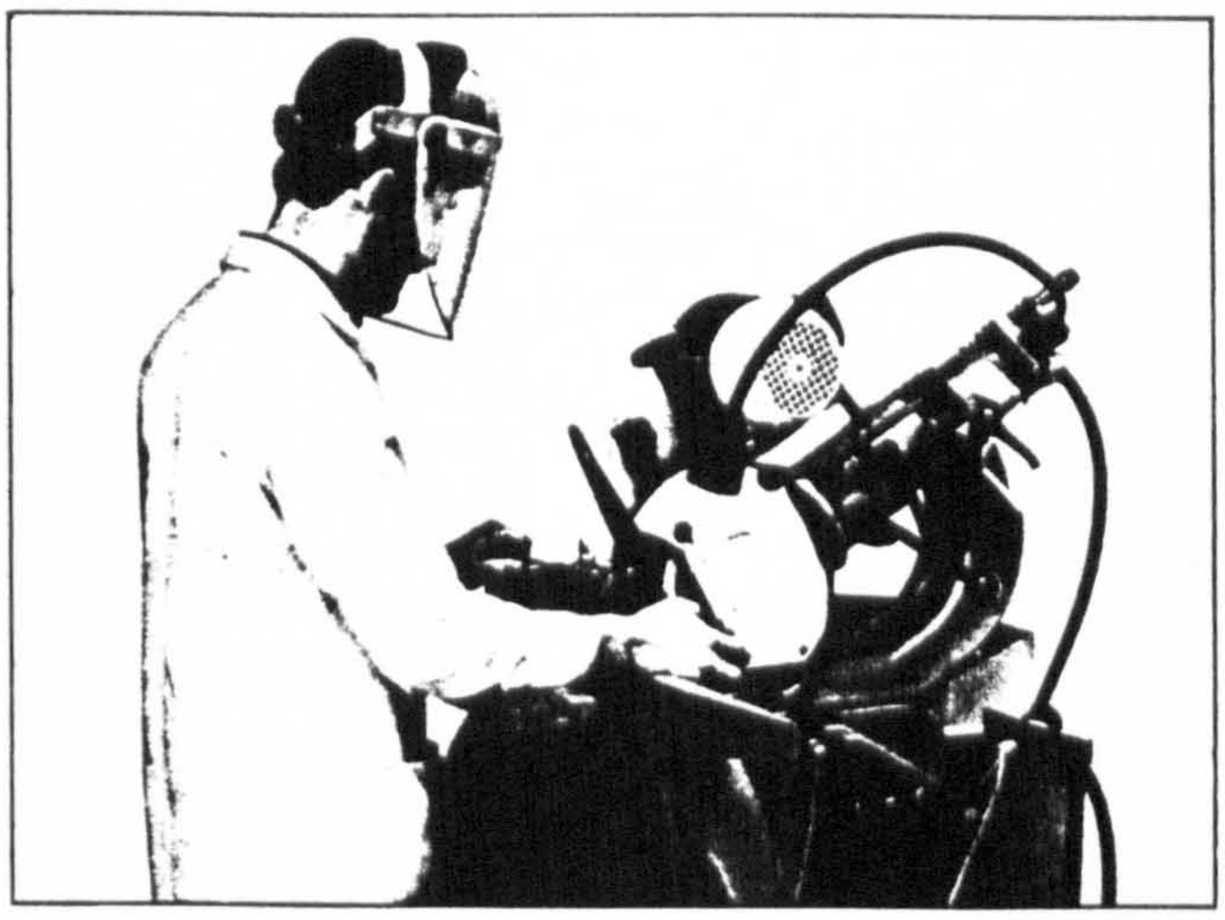

Figure 6.13: An NX-grinder used for producing Proud-knives

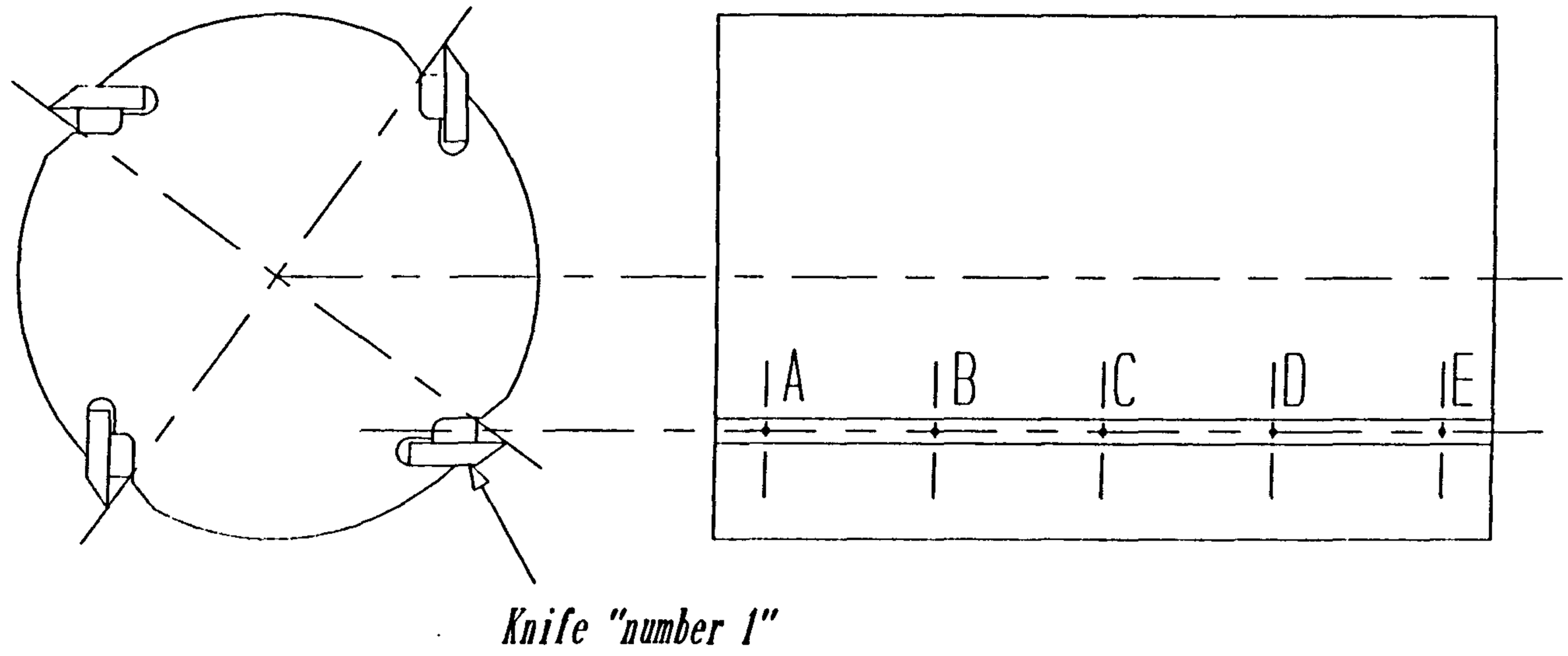

Figure 6.12

SOCKET SCREW POSITIONS USED TO INDUCE CUTTERHEAD IMBALANCE

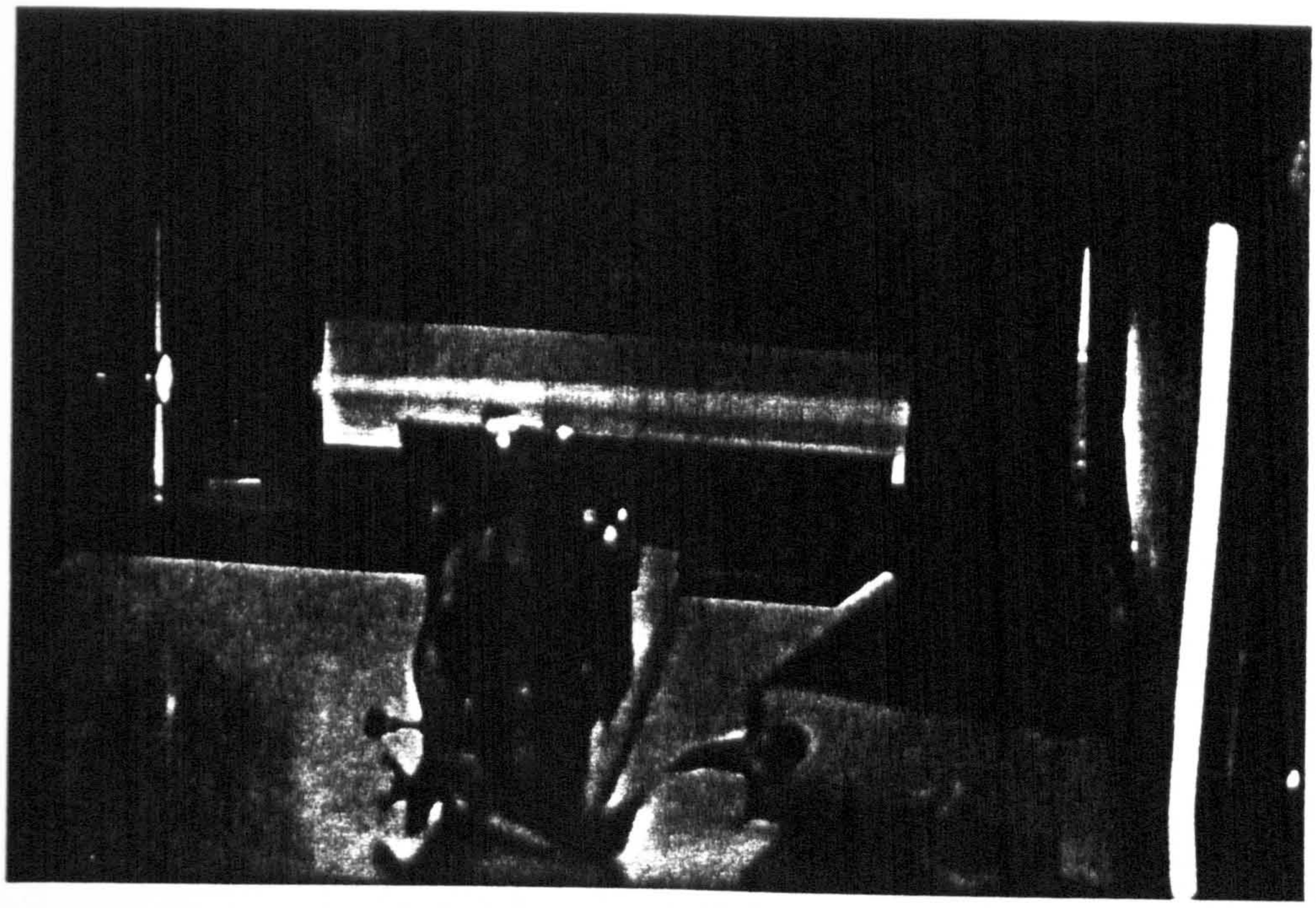

Figure 6.14: Timber Sample Analysis by Laser Instrument

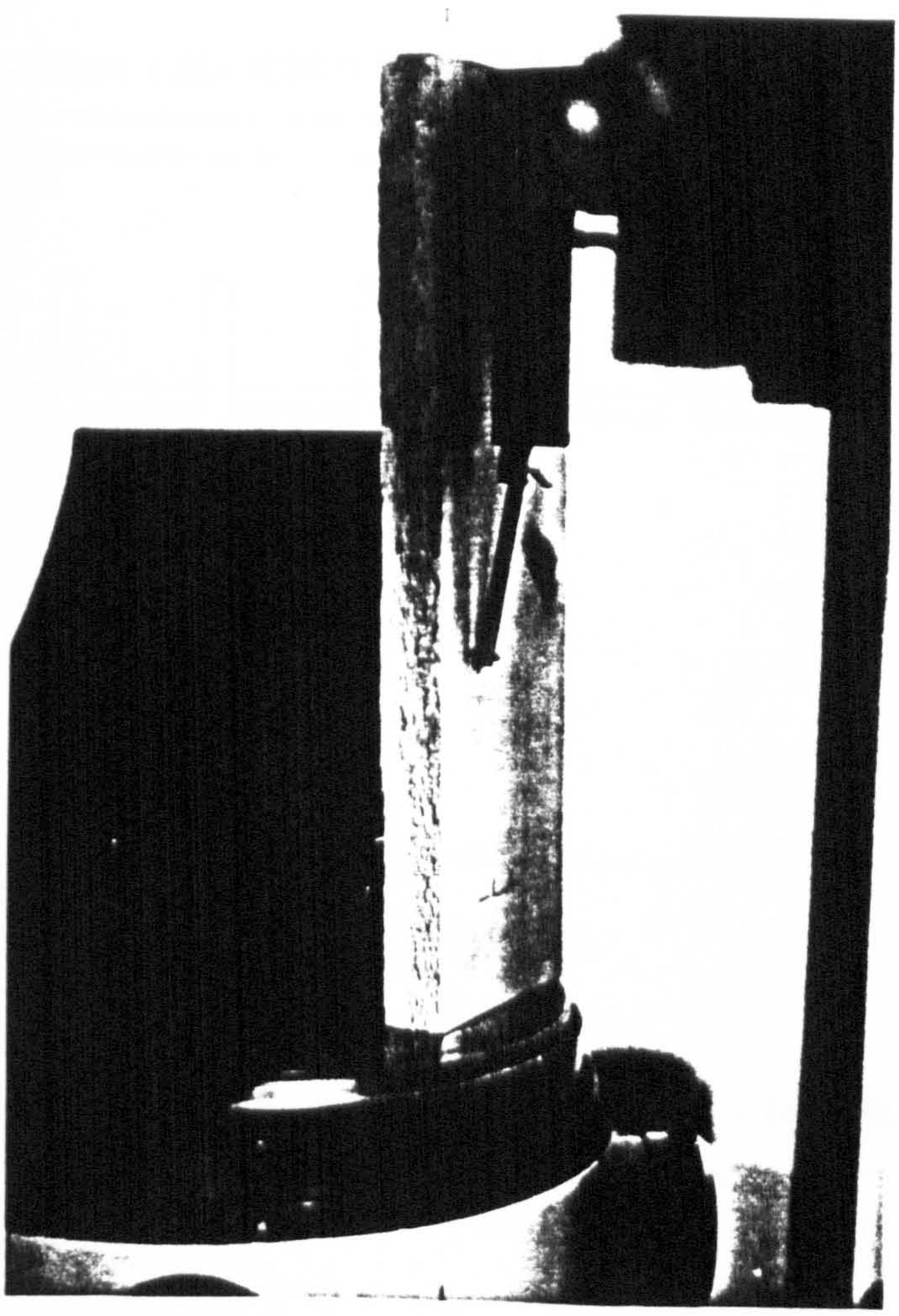

Figure 6.15: Timber Sample Analysis by Talyrond 200

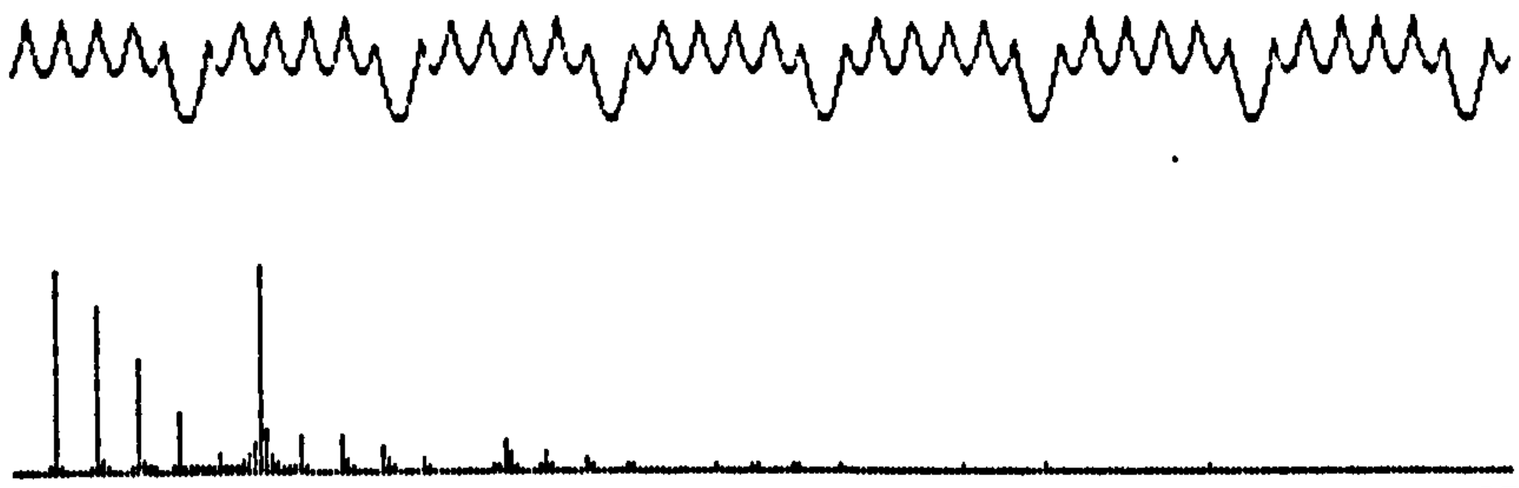

SIMULATION PARAMETERS	
No. of knives	6
Feed speed	80 m/min
Cutter Speed	4500 rpm
Vib. rate	0
Proud Knives	1 >>> 1
Ecc.rate/rev	0
Spindle Runout	0 microns

Figure 6.16: RESULTS OF PROFILE SIMULATION - PROUD-KNIFE

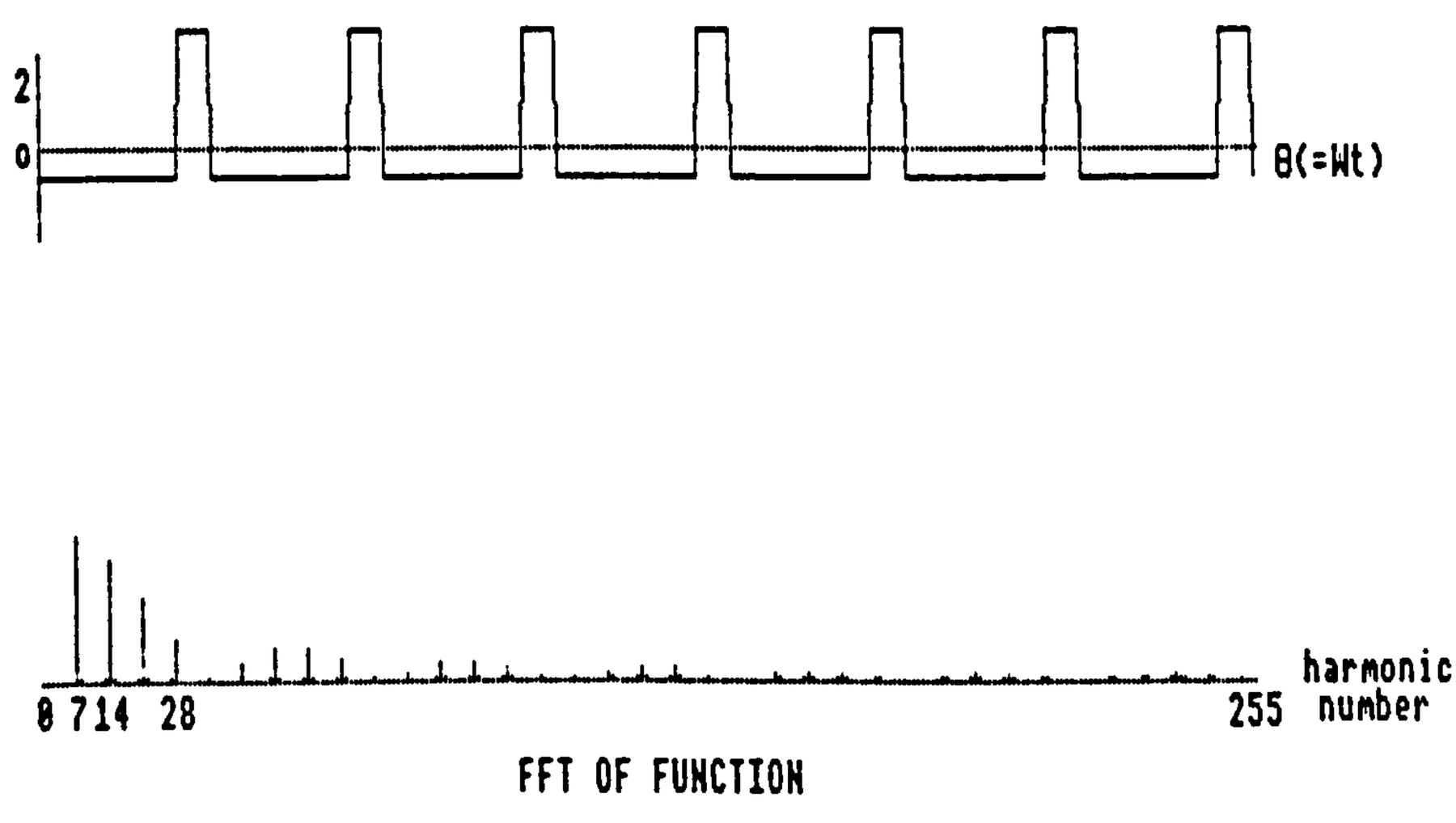

Figure 6.17: RESULTS OF PULSE-TRAIN SIMULATION - PROUD-KNIFE

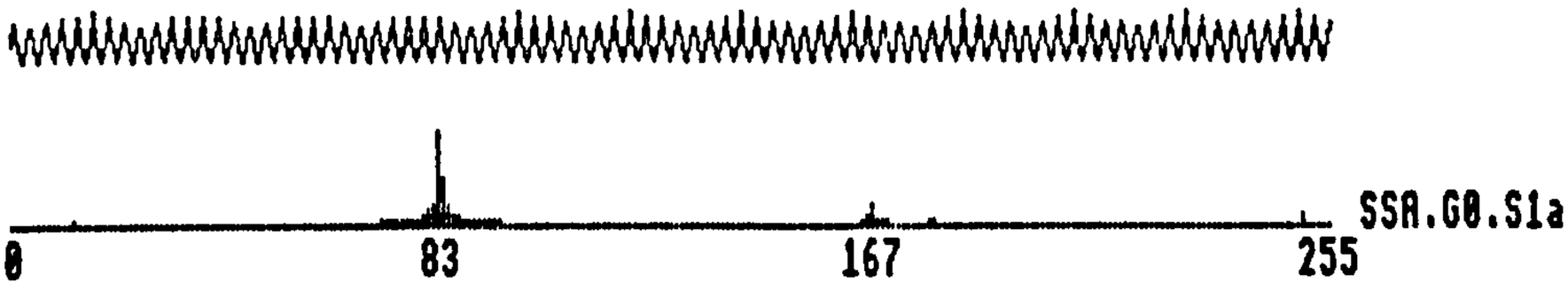

SIMULATION PARAMETERS	
No. of knives	6
Feed speed	7.5 m/min
Cutter Speed	5000 rpm
Vib. rate	0
Proud Knives	1 >>> 1
Ecc.rate/rev	0
Spindle Runout	0 microns

ANALYSIS OF FFT USING FFA
THRESHOLD=0.4
(Single knife) Harmonic 83

PRINCIPAL PEAK HARMONICS
h1 = 83 h2 = 166 hj = 500

Figure 7.60.S1a: RESULTS FOR PROFILE SIMULATION NUMBER 60.S1a

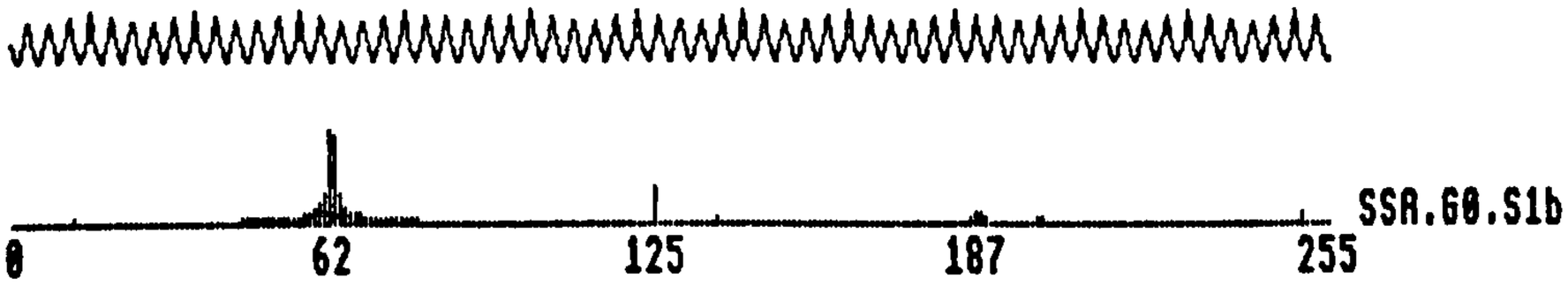

SIMULATION PARAMETERS	
No. of knives	6
Feed speed	10 m/min
Cutter Speed	5000 rpm
Vib. rate	0
Proud Knives	1 >>> 1
Ecc.rate/rev	0
Spindle Runout	0 microns

ANALYSIS OF FFT USING FFA
THRESHOLD=0.4
(Single knife) Harmonic 62

PRINCIPAL PEAK HARMONICS
h1 = 62 h2 = 124 hj = 375

Figure 7.60.S1b: RESULTS FOR PROFILE SIMULATION NUMBER 60.S1b

SIMULATION PARAMETERS	
No. of knives	6
Feed speed	12.5 m/min
Cutter Speed	5000 rpm
Vib. rate	0
Proud Knives	1 >>> 1
Ecc.rate/rev	0
Spindle Runout	0 microns

ANALYSIS OF FFT USING FFA
THRESHOLD=0.4
(Single knife) Harmonic 50

PRINCIPAL PEAK HARMONICS
h1 = 50 h2 = 100 hj = 300

Figure 7.G0.S1c: RESULTS FOR PROFILE SIMULATION NUMBER G0.S1c

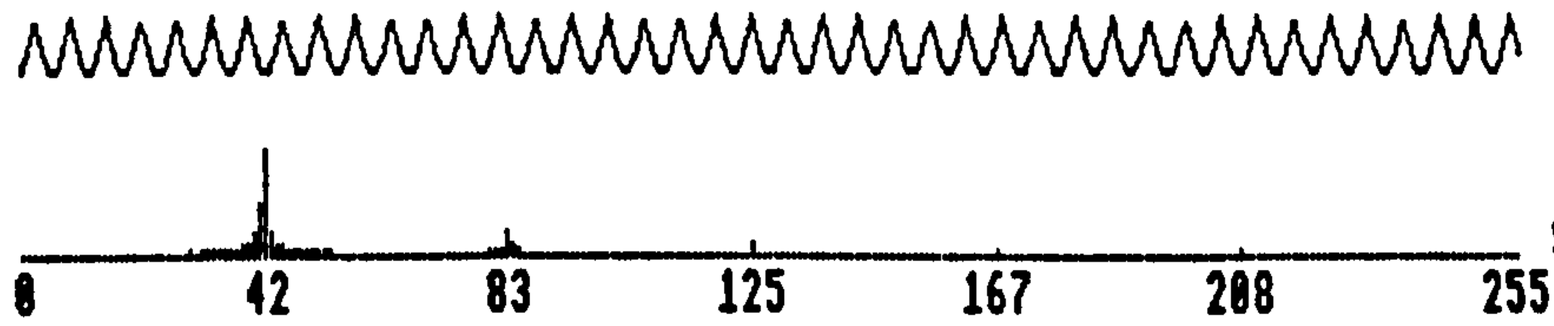

SIMULATION PARAMETERS	
No. of knives	6
Feed speed	15 m/min
Cutter Speed	5000 rpm
Vib. rate	0
Proud Knives	1 >>> 1
Ecc.rate/rev	0
Spindle Runout	0 microns

ANALYSIS OF FFT USING FFA
THRESHOLD=0.4
(Single knife) Harmonic 42

PRINCIPAL PEAK HARMONICS
h1 = 41 h2 = 82 hj = 250

Figure 7.G0.S1d: RESULTS FOR PROFILE SIMULATION NUMBER G0.S1d

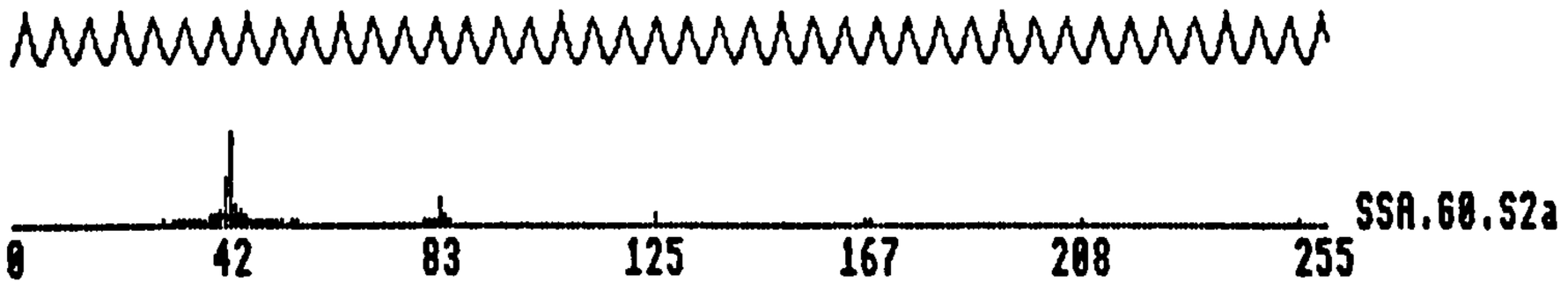

SIMULATION PARAMETERS	
No. of knives	6
Feed speed	90 m/min
Cutter Speed	5000 rpm
Vib. rate	0
Proud Knives	0
Ecc.rate/rev	0
Spindle Runout	0 microns

ANALYSIS OF FFT USING FFA
THRESHOLD=0.4
(Multi-knife) Harmonic 42

PRINCIPAL PEAK HARMONICS
h1 = 6
h2 = 12
hj = 41

Figure 7.60.S2a: RESULTS FOR PROFILE SIMULATION NUMBER 60.S2a

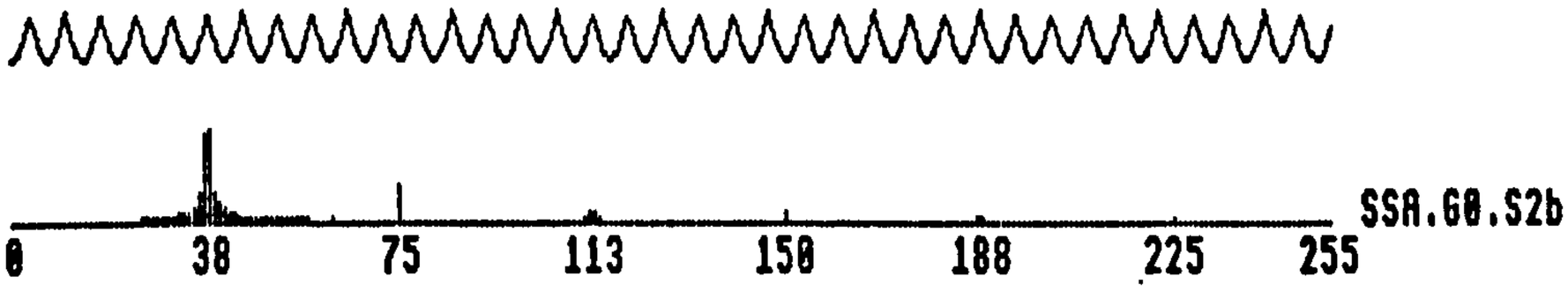

SIMULATION PARAMETERS	
No. of knives	6
Feed speed	100 m/min
Cutter Speed	5000 rpm
Vib. rate	0
Proud Knives	0
Ecc.rate/rev	0
Spindle Runout	0 microns

ANALYSIS OF FFT USING FFA
THRESHOLD=0.4
(Multi-knife) Harmonic 38

PRINCIPAL PEAK HARMONICS
h1 = 6
h2 = 12
hj = 37

Figure 7.60.S2b: RESULTS FOR PROFILE SIMULATION NUMBER 60.S2b

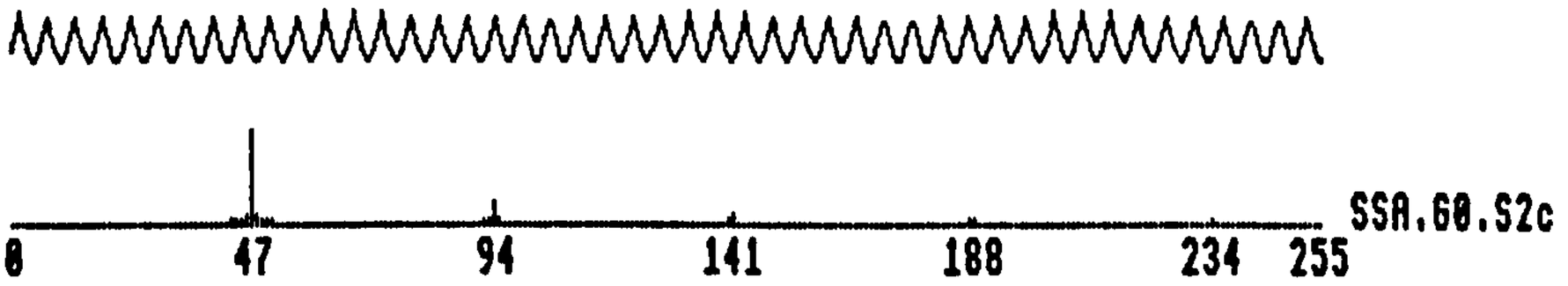

SIMULATION PARAMETERS	
No. of knives	6
Feed speed	80 m/min
Cutter Speed	5000 rpm
Vib. rate	0
Proud Knives	0
Ecc.rate/rev	0
Spindle Runout	0 microns

ANALYSIS OF FFT USING FFA
THRESHOLD=0.4
(Multi-knife) Harmonic 47

PRINCIPAL PEAK HARMONICS
h1 = 7
h2 = 14
hj = 46

Figure 7.60.S2c: RESULTS FOR PROFILE SIMULATION NUMBER 60.S2c

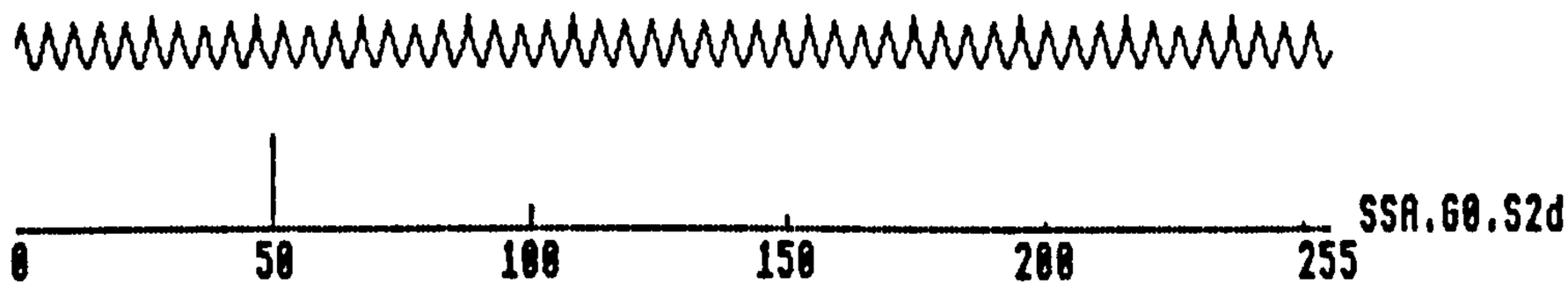

SIMULATION PARAMETERS	
No. of knives	6
Feed speed	90 m/min
Cutter Speed	6000 rpm
Vib. rate	0
Proud Knives	0
Ecc.rate/rev	0
Spindle Runout	0 microns

ANALYSIS OF FFT USING FFA
THRESHOLD=0.4
(Multi-knife) Harmonic 50

PRINCIPAL PEAK HARMONICS
h1 = 8
h2 = 16
hj = 50

Figure 7.60.S2d: RESULTS FOR PROFILE SIMULATION NUMBER 60.S2d

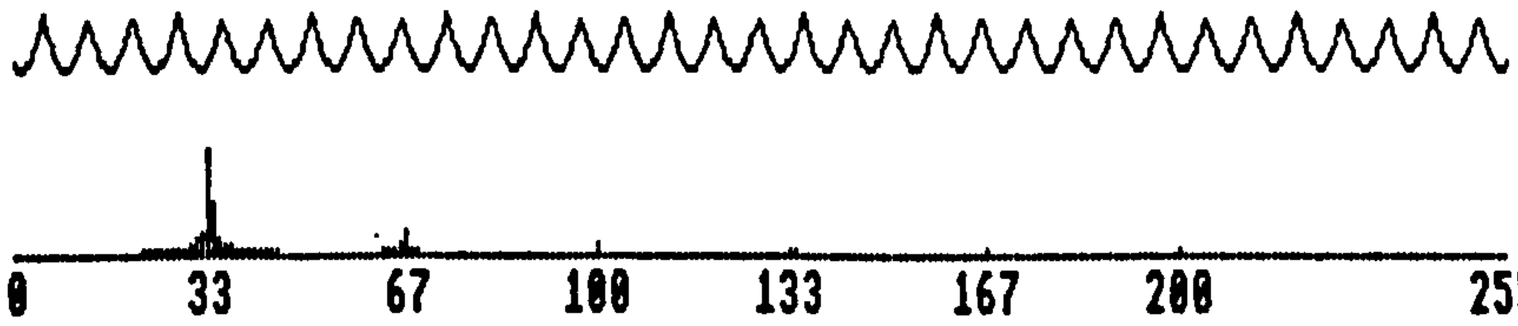

SIMULATION PARAMETERS	
No. of knives	6
Feed speed	90 m/min
Cutter Speed	4000 rpm
Vib. rate	0
Proud Knives	0
Ecc.rate/rev	0
Spindle Runout	0 microns

ANALYSIS OF FFT USING FFA
THRESHOLD=0.4
(Multi-knife) Harmonic 33

PRINCIPAL PEAK HARMONICS
h1 = 5 h2 = 10 hj = 33

Figure 7.G0.S2e: RESULTS FOR PROFILE SIMULATION NUMBER G0.S2e

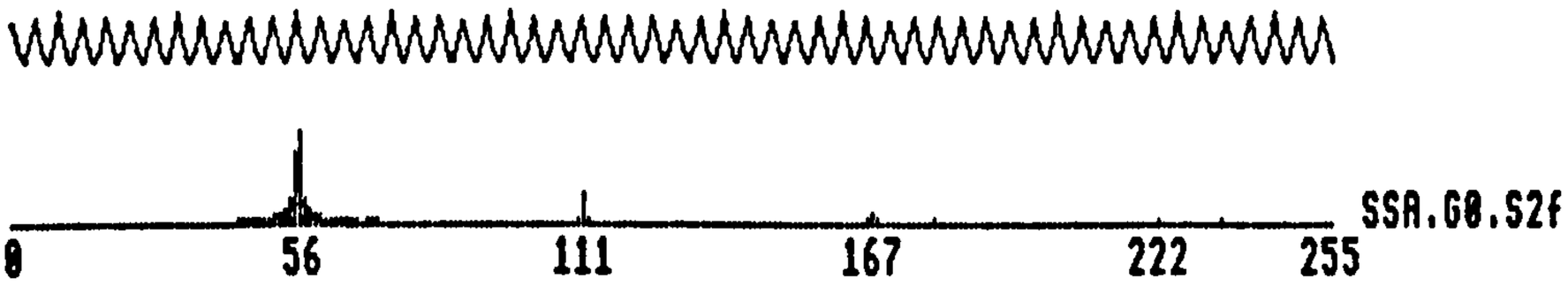

SIMULATION PARAMETERS	
No. of knives	8
Feed speed	90 m/min
Cutter Speed	5000 rpm
Vib. rate	0
Proud Knives	0
Ecc.rate/rev	0
Spindle Runout	0 microns

ANALYSIS OF FFT USING FFA
THRESHOLD=0.4
(Multi-knife) Harmonic 56

PRINCIPAL PEAK HARMONICS
h1 = 6 h2 = 12 hj = 55

Figure 7.G0.S2f: RESULTS FOR PROFILE SIMULATION NUMBER G0.S2f

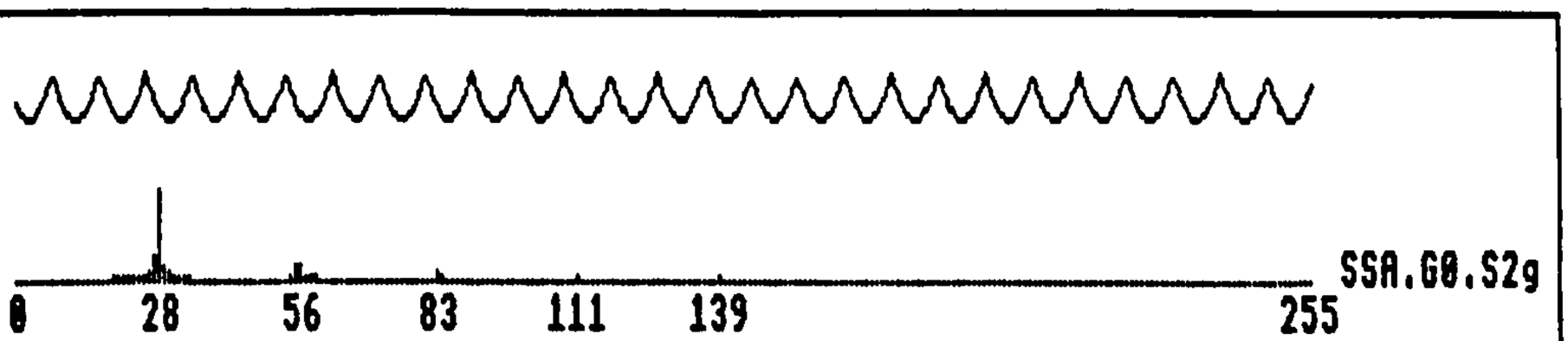

SIMULATION PARAMETERS	
No. of knives	4
Feed speed	90 m/min
Cutter Speed	5000 rpm
Vib. rate	0
Proud Knives	0
Ecc.rate/rev	0
Spindle Runout	0 microns

PRINCIPAL PEAK HARMONICS
h1 = 6 h2 = 12 hj = 27

ANALYSIS OF FFT USING FFA
THRESHOLD=0.4
(Multi-knife) Harmonic 28

Figure 7.G0.S2g: RESULTS FOR PROFILE SIMULATION NUMBER G0.S2g

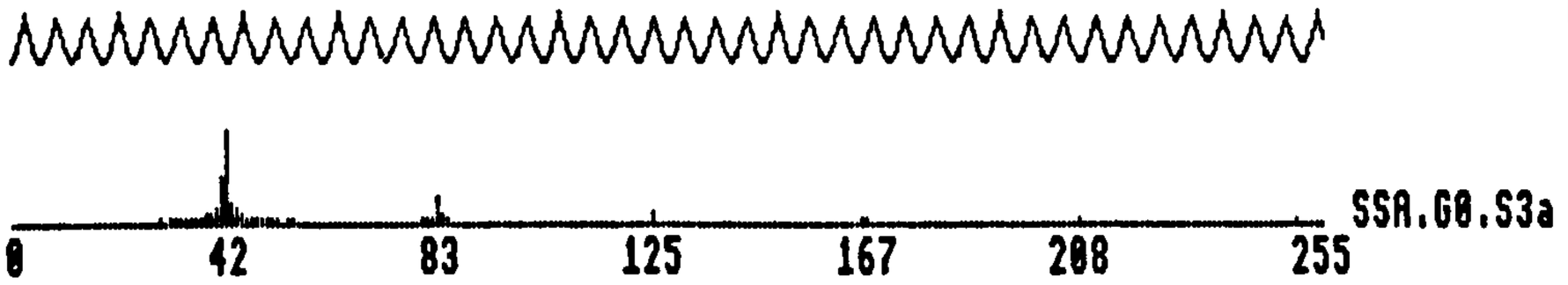

SIMULATION PARAMETERS	
No. of knives	6
Feed speed	90 m/min
Cutter Speed	5000 rpm
Vib. rate	0
Proud Knives	0
Ecc.rate/rev	0
Spindle Runout	0 microns

ANALYSIS OF FFT USING FFA
THRESHOLD=0.4
(Multi-knife) Harmonic 42

PRINCIPAL PEAK HARMONICS
h1 = 6 h2 = 12 hj = 41

Figure 7.G0.S3a: RESULTS FOR PROFILE SIMULATION NUMBER G0.S3a

SIMULATION PARAMETERS	
No. of knives	6
Feed speed	90 m/min
Cutter Speed	5000 rpm
Vib. rate	0
Proud Knives	0
Ecc.rate/rev	1
Spindle Runout	8 microns

ANALYSIS OF FFT USING FFA
THRESHOLD=0.4
(0.balance 1) Harmonic 7 (Multi-knife) Harmonic 42

PRINCIPAL PEAK HARMONICS
h1 = 6 h2 = 12 hj = 41

Figure 7.G0.S3b: RESULTS FOR PROFILE SIMULATION NUMBER G0.S3b

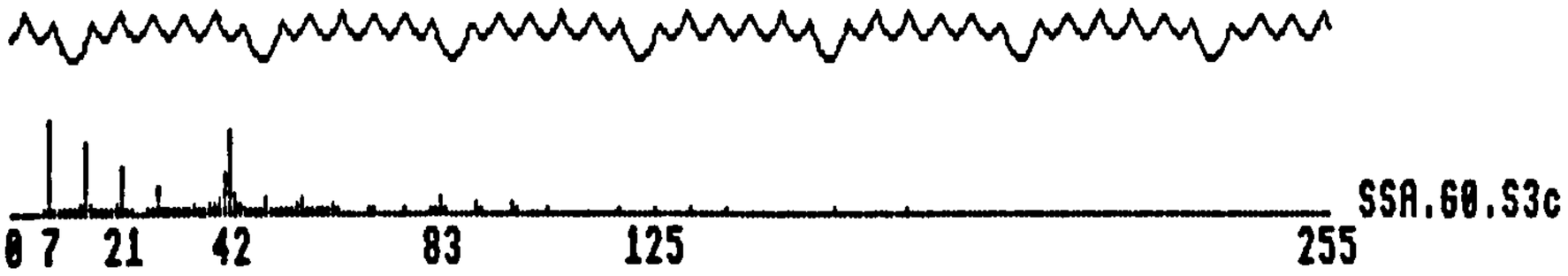

SIMULATION PARAMETERS	
No. of knives	6
Feed speed	90 m/min
Cutter Speed	5000 rpm
Vib. rate	0
Proud Knives	1 >>> 4
Ecc.rate/rev	0
Spindle Runout	0 microns

PRINCIPAL PEAK HARMONICS
h1 = 6 h2 = 12 hj = 41

ANALYSIS OF FFT USING FFA
THRESHOLD=0.4
(Proud Knife) Harmonic 7 Harmonic 14 Harmonic 21 (Multi-knife) Harmonic 42

Figure 7.60.S3c: RESULTS FOR PROFILE SIMULATION NUMBER 60.S3c

SIMULATION PARAMETERS	
No. of knives	6
Feed speed	90 m/min
Cutter Speed	5000 rpm
Vib. rate	4 >>> Amp=5 microns
Proud Knives	0
Ecc.rate/rev	0
Spindle Runout	0 microns

PRINCIPAL PEAK HARMONICS
h1 = 6 h2 = 12 hj = 41

ANALYSIS OF FFT USING FFA
THRESHOLD=0.4
(Multi-knife) Harmonic 42 (Vibs or Noise) Harmonic 83

Figure 7.60.S3d: RESULTS FOR PROFILE SIMULATION NUMBER 60.S3d

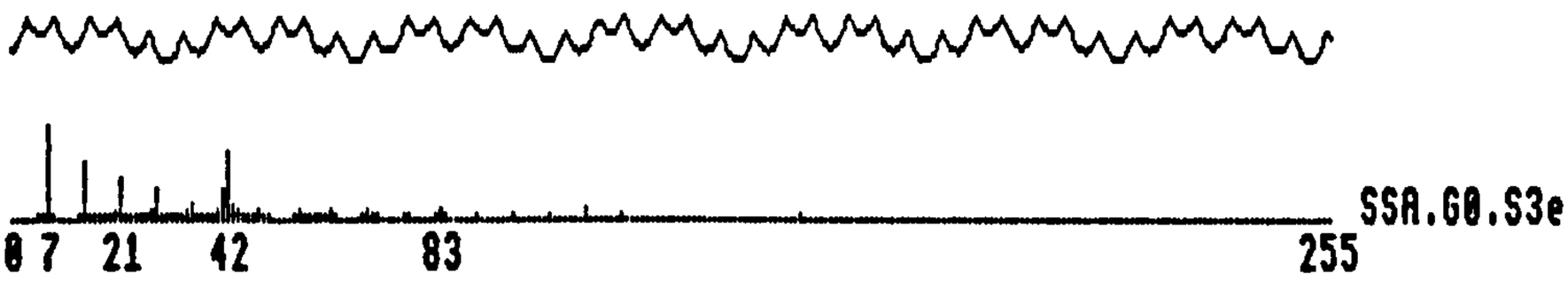

SIMULATION PARAMETERS	
No. of knives	6
Feed speed	90 m/min
Cutter Speed	5000 rpm
Vib. rate	0
Proud Knives	1 >>> 4
Ecc.rate/rev	1
Spindle Runout	8 microns

PRINCIPAL PEAK HARMONICS
h1 = 6
h2 = 12
hj = 41

ANALYSIS OF FFT USING FFA
THRESHOLD=0.4
(Proud Knife)
Harmonic 7
Harmonic 14
Harmonic 21
(Multi-knife)
Harmonic 42

Figure 7.G0.S3e: RESULTS FOR PROFILE SIMULATION NUMBER G0.S3e

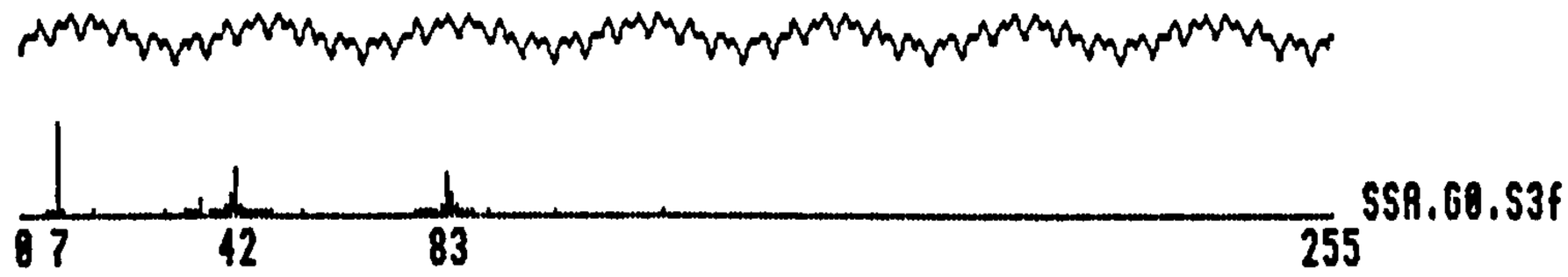

SIMULATION PARAMETERS	
No. of knives	6
Feed speed	90 m/min
Cutter Speed	5000 rpm
Vib. rate	4 >>> Amp=5 microns
Proud Knives	0
Ecc.rate/rev	1
Spindle Runout	8 microns

PRINCIPAL PEAK HARMONICS
h1 = 6
h2 = 12
hj = 41

ANALYSIS OF FFT USING FFA
THRESHOLD=0.4
(O.balance 1)
Harmonic 7
(Multi-knife)
Harmonic 42
(Vibs or Noise)
Harmonic 83

Figure 7.G0.S3f: RESULTS FOR PROFILE SIMULATION NUMBER G0.S3f

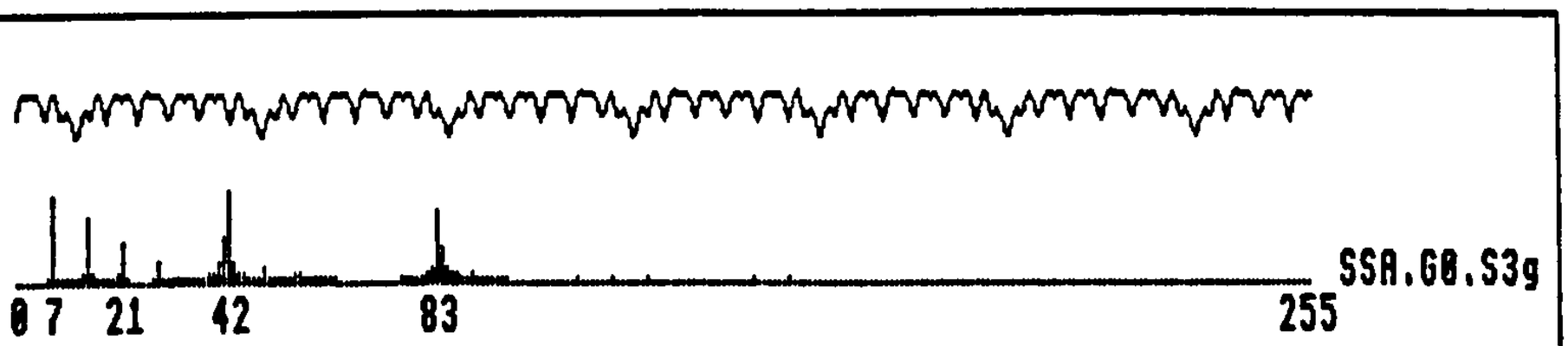

SIMULATION PARAMETERS	
No. of knives	6
Feed speed	90 m/min
Cutter Speed	5000 rpm
Vib. rate	4 >>> Amp=5 microns
Proud Knives	1 >>> 4
Ecc.rate/rev	0
Spindle Runout	0 microns

PRINCIPAL PEAK HARMONICS
h1 = 6
h2 = 12
hj = 41

ANALYSIS OF FFT USING FFA
THRESHOLD=0.4
(Proud Knife)
Harmonic 7
Harmonic 14
Harmonic 21
(Multi-knife)
Harmonic 42
(Vibs or Noise)
Harmonic 83

Figure 7.G0.S3g: RESULTS FOR PROFILE SIMULATION NUMBER G0.S3g

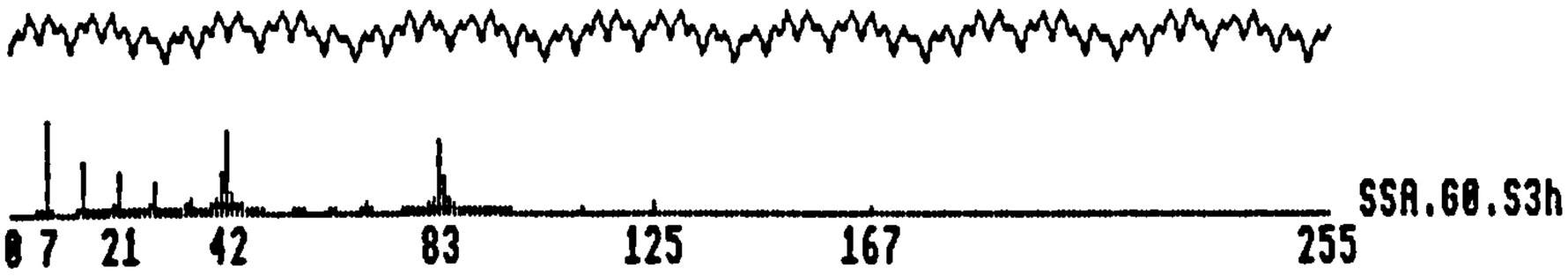

SIMULATION PARAMETERS	
No. of knives	6
Feed speed	90 m/min
Cutter Speed	5000 rpm
Vib. rate	4 >>> Amp=5 microns
Proud Knives	1 >>> 4
Ecc.rate/rev	1
Spindle Runout	8 microns

PRINCIPAL PEAK HARMONICS
h1 = 6
h2 = 12
hj = 41

ANALYSIS OF FFT USING FFA
THRESHOLD=0.4
(Proud Knife)
Harmonic 7
Harmonic 14
Harmonic 21
(Multi-knife)
Harmonic 42
(Vibs or Noise)
Harmonic 83

Figure 7.60.S3h: RESULTS FOR PROFILE SIMULATION NUMBER 60.S3h

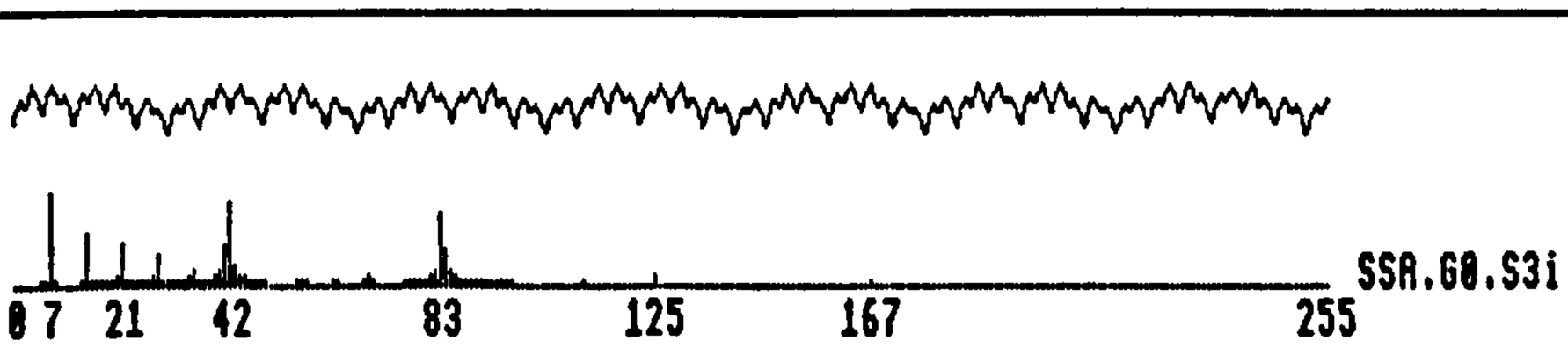

SIMULATION PARAMETERS	
No. of knives	6
Feed speed	90 m/min
Cutter Speed	5000 rpm
Vib. rate	4 >>> Amp=5 microns
Proud Knives	1 >>> 4
Ecc.rate/rev	1
Spindle Runout	8 microns

PRINCIPAL PEAK HARMONICS
h1 = 6
h2 = 12
hj = 41

ANALYSIS OF FFT USING FFA
THRESHOLD=0.1
(Proud Knife)
Harmonic 7
Harmonic 14
Harmonic 21
Harmonic 28
Harmonic 35
(Multi-knife)
Harmonic 42
(Vibs or Noise)
Harmonic 83
Harmonic 125

Figure 7.G0.S3i: RESULTS FOR PROFILE SIMULATION NUMBER G0.S3i

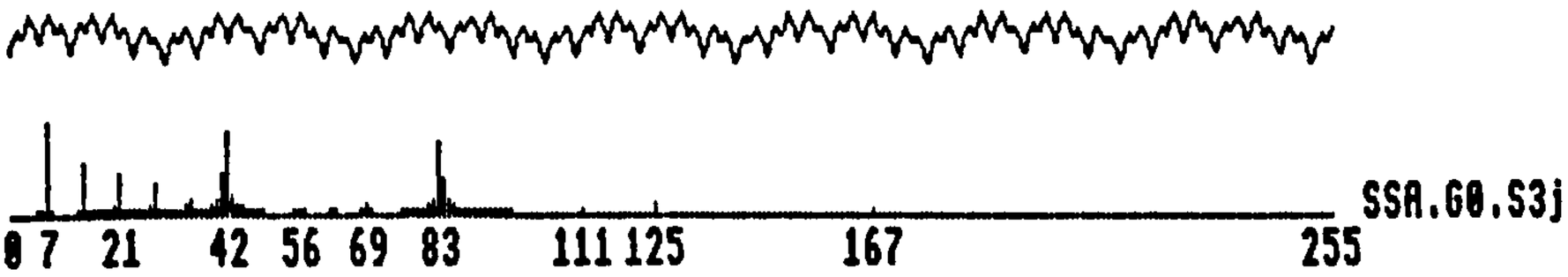

SIMULATION PARAMETERS	
No. of knives	6
Feed speed	90 m/min
Cutter Speed	5000 rpm
Vib. rate	4 >>> Amp=5 microns
Proud Knives	1 >>> 4
Ecc.rate/rev	1
Spindle Runout	8 microns

PRINCIPAL PEAK HARMONICS
h1 = 6
h2 = 12
hj = 41

ANALYSIS OF FFT USING FFA
THRESHOLD=0.05
(Proud Knife)
Harmonic 7
Harmonic 14
Harmonic 21
Harmonic 28
Harmonic 35
(Multi-knife)
Harmonic 42
(Vibs or Noise)
Harmonic 56
Harmonic 62
Harmonic 69
Harmonic 83
Harmonic 111
Harmonic 125

Figure 7.G0.S3j: RESULTS FOR PROFILE SIMULATION NUMBER G0.S3j

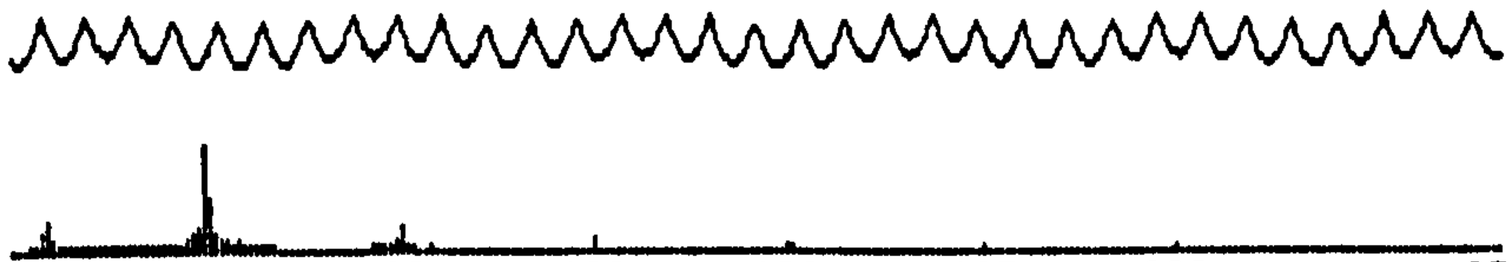

SIMULATION PARAMETERS	
No. of knives	6
Feed speed	90 m/min
Cutter Speed	4000 rpm
Vib. rate	0
Proud Knives	0
Ecc.rate/rev	1
Spindle Runout	2 microns

ANALYSIS OF FFT USING FFA
THRESHOLD=0.4
(Multi-knife) Harmonic 33

PRINCIPAL PEAK HARMONICS
h1 = 5
h2 = 10
hj = 33

Figure 7.60.S4a: RESULTS FOR PROFILE SIMULATION NUMBER 60.S4a

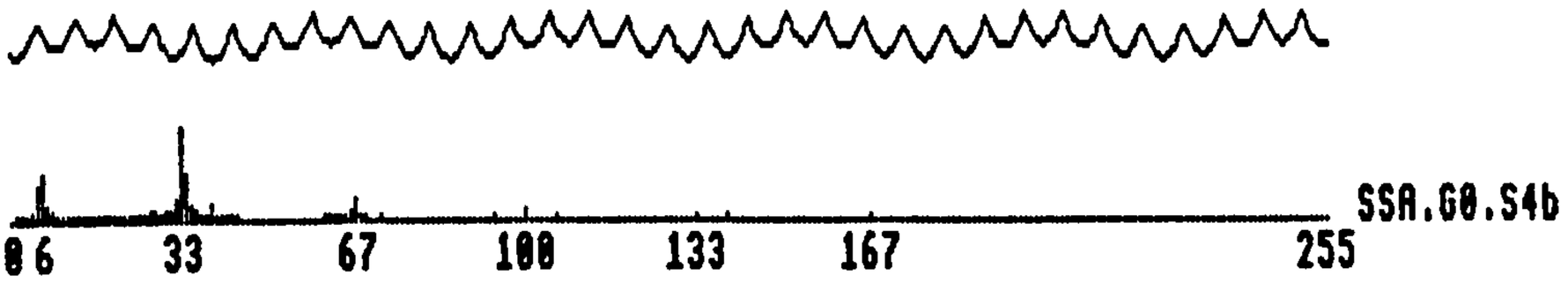

SIMULATION PARAMETERS	
No. of knives	6
Feed speed	90 m/min
Cutter Speed	4000 rpm
Vib. rate	0
Proud Knives	0
Ecc.rate/rev	1
Spindle Runout	4 microns

ANALYSIS OF FFT USING FFA
THRESHOLD=0.4
(0.balance 1) Harmonic 6 (Multi-knife) Harmonic 33

PRINCIPAL PEAK HARMONICS
h1 = 5
h2 = 10
hj = 33

Figure 7.60.S4b: RESULTS FOR PROFILE SIMULATION NUMBER 60.S4b

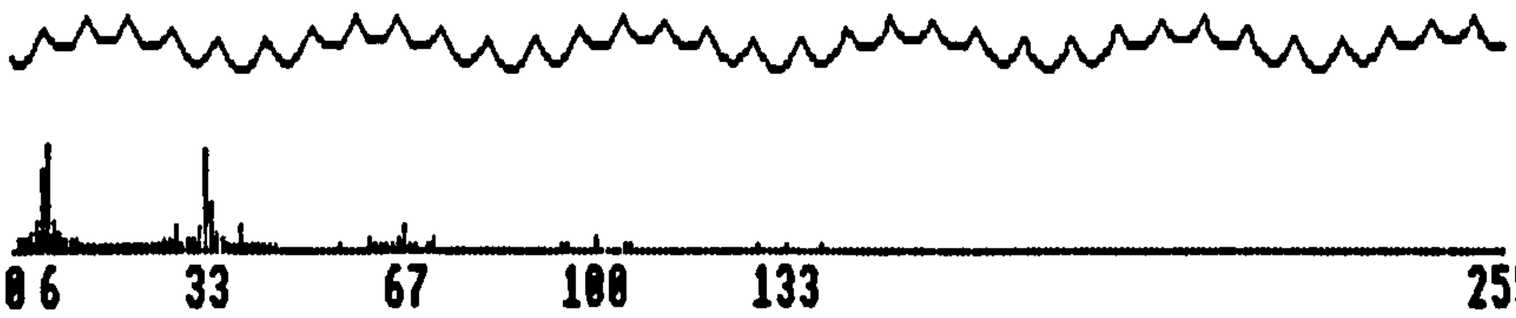

SIMULATION PARAMETERS	
No. of knives	6
Feed speed	90 m/min
Cutter Speed	4000 rpm
Vib. rate	0
Proud Knives	0
Ecc.rate/rev	1
Spindle Runout	8 microns

ANALYSIS OF FFT USING FFA
THRESHOLD=0.4
(0.balance 1) Harmonic 6 (Multi-knife) Harmonic 33

PRINCIPAL PEAK HARMONICS
h1 = 5 h2 = 10 hj = 33

Figure 7.60.S4c: RESULTS FOR PROFILE SIMULATION NUMBER 60.S4c

SIMULATION PARAMETERS	
No. of knives	6
Feed speed	90 m/min
Cutter Speed	4000 rpm
Vib. rate	0
Proud Knives	0
Ecc.rate/rev	1
Spindle Runout	12 microns

ANALYSIS OF FFT USING FFA
THRESHOLD=0.4
(0.balance 1) Harmonic 6 (Multi-knife) Harmonic 33

PRINCIPAL PEAK HARMONICS
h1 = 5 h2 = 10 hj = 33

Figure 7.60.S4d: RESULTS FOR PROFILE SIMULATION NUMBER 60.S4d

SIMULATION PARAMETERS	
No. of knives	6
Feed speed	90 m/min
Cutter Speed	4000 rpm
Vib. rate	0
Proud Knives	0
Ecc.rate/rev	1
Spindle Runout	24 microns

PRINCIPAL PEAK HARMONICS
h1 = 5
h2 = 10
hj = 33

ANALYSIS OF FFT USING FFR
THRESHOLD=0.2
(0.balance 1)
Harmonic 6
(Multi-knife)
Harmonic 33
(Unknown Faults)
Harmonic 28

Figure 7.G0.S4e: RESULTS FOR PROFILE SIMULATION NUMBER G0.S4e

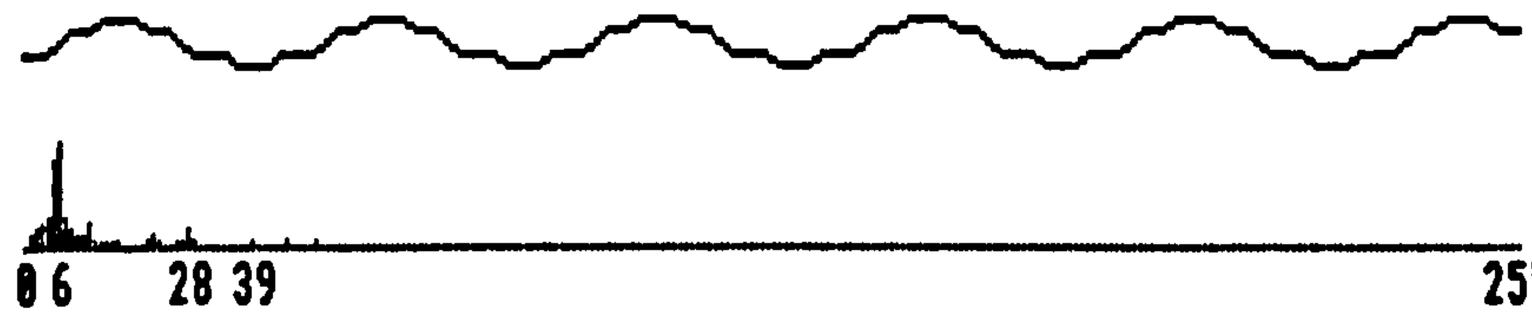

SIMULATION PARAMETERS	
No. of knives	6
Feed speed	90 m/min
Cutter Speed	4000 rpm
Vib. rate	0
Proud Knives	0
Ecc.rate/rev	1
Spindle Runout	48 microns

PRINCIPAL PEAK HARMONICS
h1 = 5
h2 = 10
hj = 33

ANALYSIS OF FFT USING FFR
THRESHOLD=0.2
(Proud Knife)
Harmonic 6
Harmonic 11

Figure 7.G0.S4f: RESULTS FOR PROFILE SIMULATION NUMBER G0.S4f

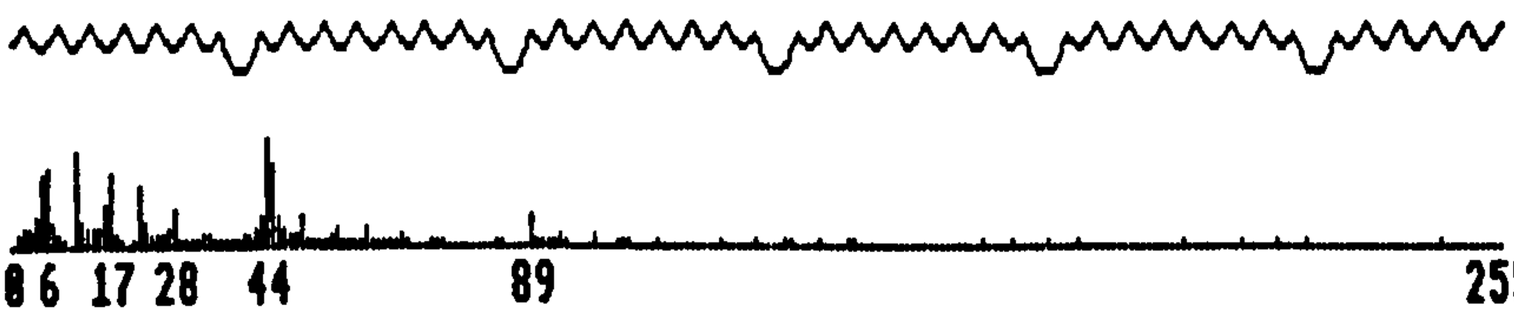

SIMULATION PARAMETERS	
No. of knives	8
Feed speed	90 m/min
Cutter Speed	4000 rpm
Vib. rate	0
Proud Knives	1)))) 1
Ecc.rate/rev	0
Spindle Runout	0 microns

PRINCIPAL PEAK HARMONICS
h1 = 5
h2 = 10
hj = 44

ANALYSIS OF FFT USING FFA
THRESHOLD=0.4
(Proud Knife)
Harmonic 6
Harmonic 11
Harmonic 17
Harmonic 22
(Multi-knife)
Harmonic 44

Figure 7.G0.S5a: RESULTS FOR PROFILE SIMULATION NUMBER G0.S5a

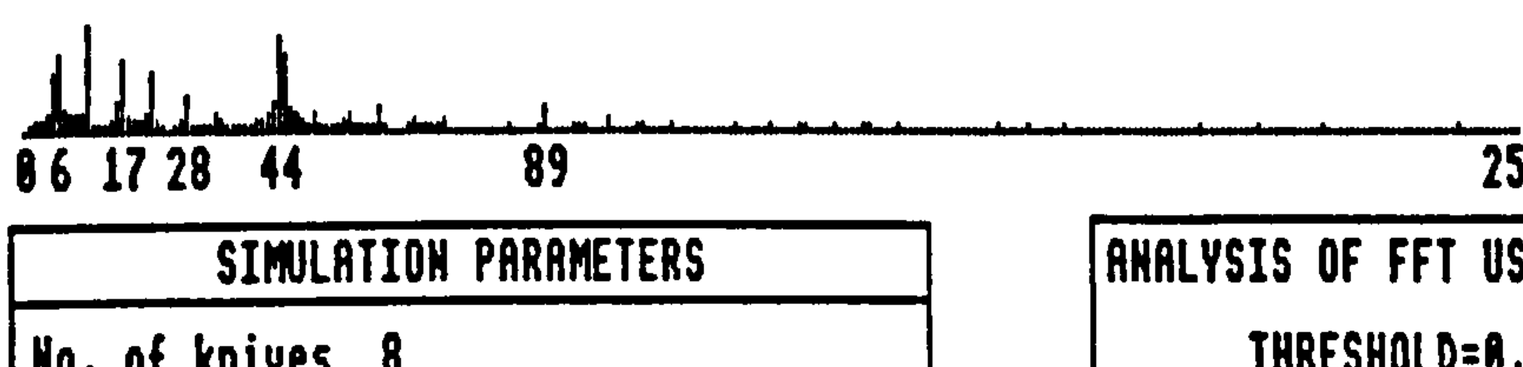

SIMULATION PARAMETERS	
No. of knives	8
Feed speed	90 m/min
Cutter Speed	4000 rpm
Vib. rate	0
Proud Knives	1)))) 5
Ecc.rate/rev	0
Spindle Runout	0 microns

PRINCIPAL PEAK HARMONICS
h1 = 5
h2 = 10
hj = 44

ANALYSIS OF FFT USING FFA
THRESHOLD=0.4
(Proud Knife)
Harmonic 6
Harmonic 11
Harmonic 17
Harmonic 22
(Multi-knife)
Harmonic 44

Figure 7.G0.S5b: RESULTS FOR PROFILE SIMULATION NUMBER G0.S5b

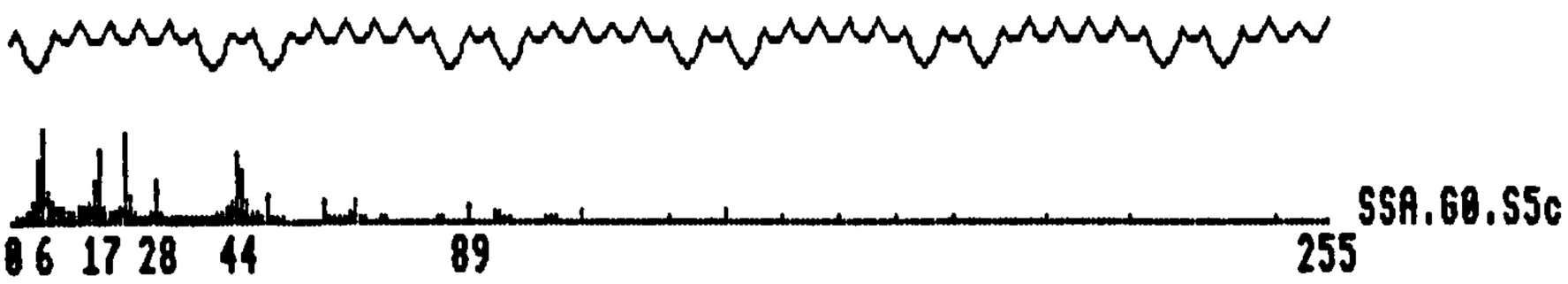

SIMULATION PARAMETERS	
No. of knives	8
Feed speed	90 m/min
Cutter Speed	4000 rpm
Vib. rate	0
Proud Knives	2 >>> 1 3
Ecc.rate/rev	0
Spindle Runout	0 microns

PRINCIPAL PEAK HARMONICS
h1 = 5
h2 = 10
hj = 44

ANALYSIS OF FFT USING FFA
THRESHOLD=0.4
(0.balance 1)
Harmonic 6
(Multi-knife)
Harmonic 44
(Unknown Faults)
Harmonic 17
Harmonic 22
Harmonic 28

Figure 7.60.S5c: RESULTS FOR PROFILE SIMULATION NUMBER 60.S5c

SIMULATION PARAMETERS	
No. of knives	8
Feed speed	90 m/min
Cutter Speed	4000 rpm
Vib. rate	0
Proud Knives	2 >>> 1 6
Ecc.rate/rev	0
Spindle Runout	0 microns

PRINCIPAL PEAK HARMONICS
h1 = 5
h2 = 10
hj = 44

ANALYSIS OF FFT USING FFA
THRESHOLD=0.4
(Proud Knife)
Harmonic 6
Harmonic 11
Harmonic 17
(Multi-knife)
Harmonic 44
(Unknown Faults)
Harmonic 28

Figure 7.60.S5d: RESULTS FOR PROFILE SIMULATION NUMBER 60.S5d

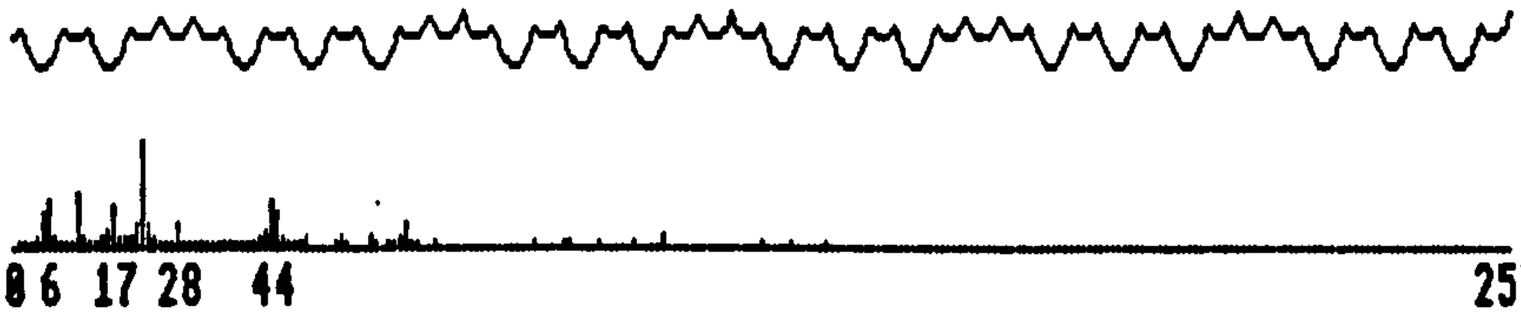

SIMULATION PARAMETERS	
No. of knives	8
Feed speed	90 m/min
Cutter Speed	4000 rpm
Vib. rate	0
Proud Knives	3)))) 1 3 5
Ecc.rate/rev	0
Spindle Runout	0 microns

PRINCIPAL PEAK HARMONICS
h1 = 5
h2 = 10
hj = 44

ANALYSIS OF FFT USING FFA
THRESHOLD=0.4
(Proud Knife)
Harmonic 6
Harmonic 11
Harmonic 17
Harmonic 22
(Multi-knife)
Harmonic 44

Figure 7.G0.S5e: RESULTS FOR PROFILE SIMULATION NUMBER G0.S5e

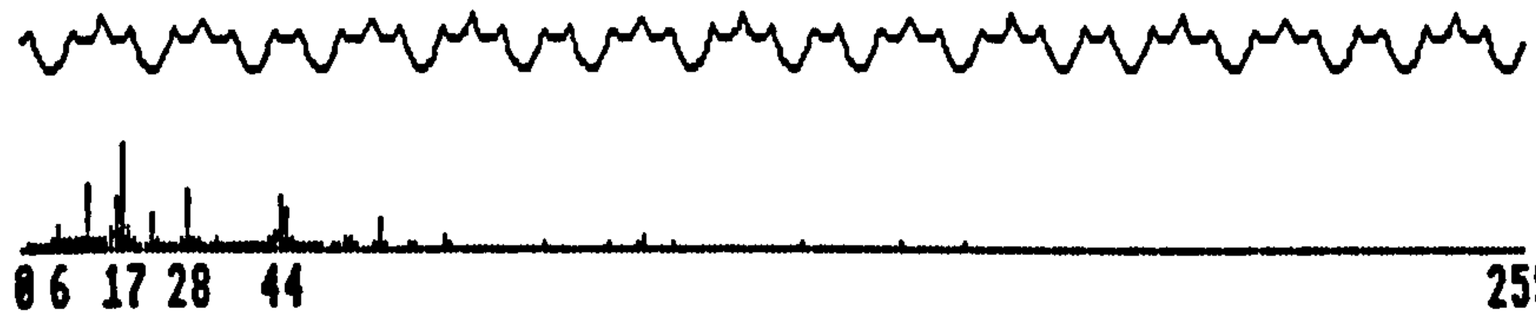

SIMULATION PARAMETERS	
No. of knives	8
Feed speed	90 m/min
Cutter Speed	4000 rpm
Vib. rate	0
Proud Knives	3)))) 1 3 6
Ecc.rate/rev	0
Spindle Runout	0 microns

PRINCIPAL PEAK HARMONICS
h1 = 5
h2 = 10
hj = 44

ANALYSIS OF FFT USING FFA
THRESHOLD=0.4
(O.balance 2)
Harmonic 11
(Multi-knife)
Harmonic 44
(Unknown Faults)
Harmonic 17
Harmonic 28

Figure 7.G0.S5f: RESULTS FOR PROFILE SIMULATION NUMBER G0.S5f

SIMULATION PARAMETERS	
No. of knives	6
Feed speed	90 m/min
Cutter Speed	4000 rpm
Vib. rate	6)))) Amp=5 microns
Proud Knives	0
Ecc.rate/rev	0
Spindle Runout	0 microns

ANALYSIS OF FFT USING FFA
THRESHOLD=0.4
(Multi-knife) Harmonic 33 (Vibs or Noise) Harmonic 100

PRINCIPAL PEAK HARMONICS
h1 = 5 h2 = 10 hj = 33

Figure 7.60.S6a: RESULTS FOR PROFILE SIMULATION NUMBER 60.S6a

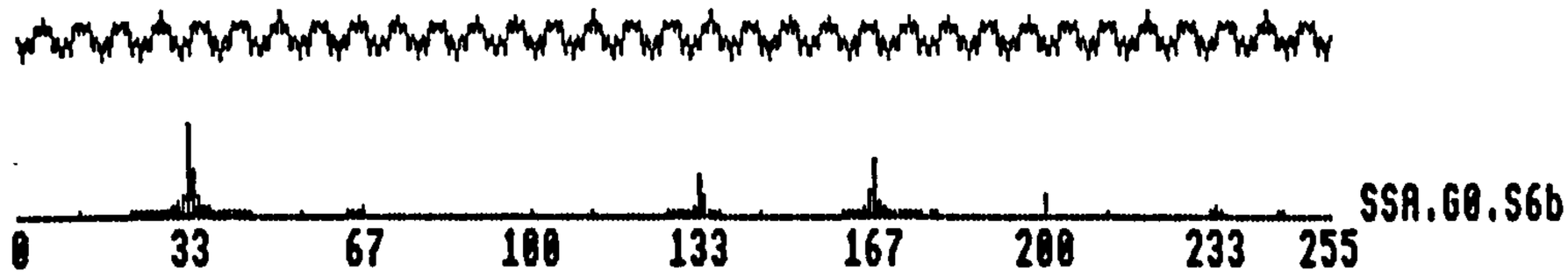

SIMULATION PARAMETERS	
No. of knives	6
Feed speed	90 m/min
Cutter Speed	4000 rpm
Vib. rate	8)))) Amp=5 microns
Proud Knives	0
Ecc.rate/rev	0
Spindle Runout	0 microns

ANALYSIS OF FFT USING FFA
THRESHOLD=0.4
(Multi-knife) Harmonic 33 (Vibs or Noise) Harmonic 133 Harmonic 167

PRINCIPAL PEAK HARMONICS
h1 = 5 h2 = 10 hj = 33

Figure 7.60.S6b: RESULTS FOR PROFILE SIMULATION NUMBER 60.S6b

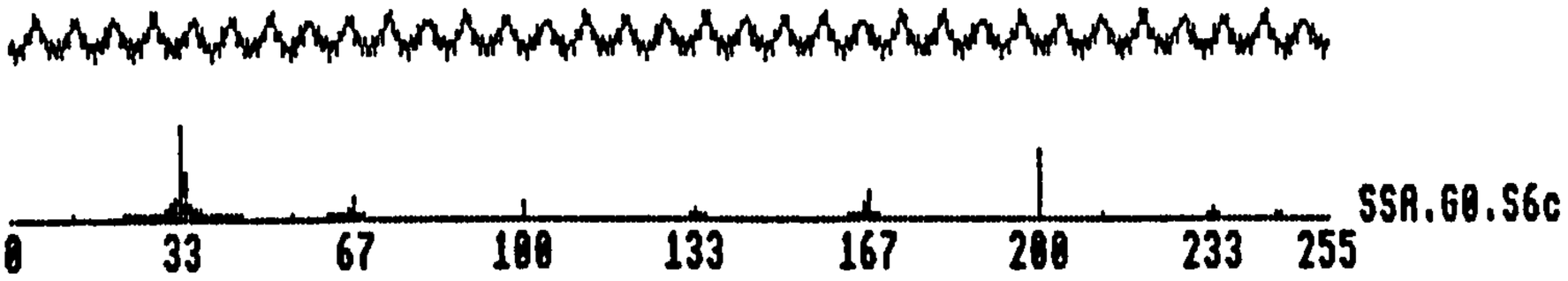

SIMULATION PARAMETERS	
No. of knives	6
Feed speed	90 m/min
Cutter Speed	4000 rpm
Vib. rate	10 >>> Amp=5 microns
Proud Knives	0
Ecc.rate/rev	0
Spindle Runout	0 microns

ANALYSIS OF FFT USING FFA
THRESHOLD=0.4
(Multi-knife) Harmonic 33 (Vibs or Noise) Harmonic 200

PRINCIPAL PEAK HARMONICS
h1 = 5 h2 = 10 hj = 33

Figure 7.60.S6c: RESULTS FOR PROFILE SIMULATION NUMBER 60.S6c

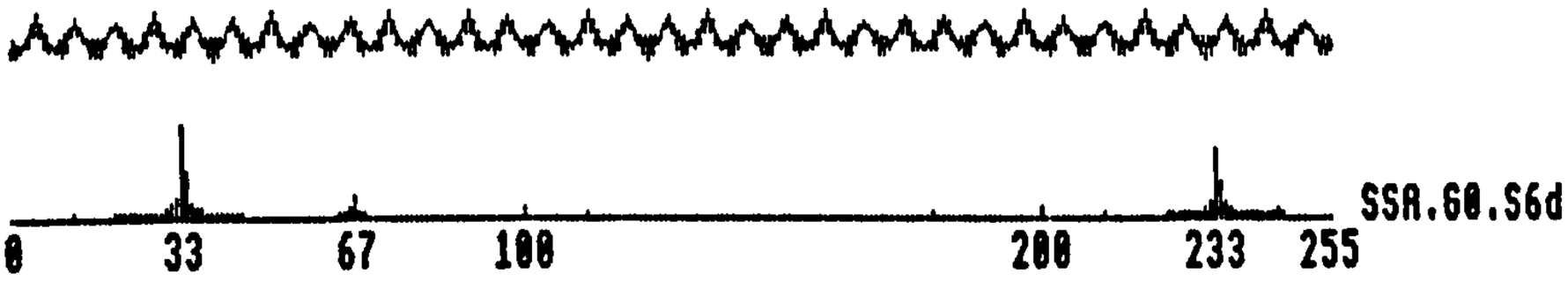

SIMULATION PARAMETERS	
No. of knives	6
Feed speed	90 m/min
Cutter Speed	4000 rpm
Vib. rate	12 >>> Amp=5 microns
Proud Knives	0
Ecc.rate/rev	0
Spindle Runout	0 microns

ANALYSIS OF FFT USING FFA
THRESHOLD=0.4
(Multi-knife) Harmonic 33 (Vibs or Noise) Harmonic 233

PRINCIPAL PEAK HARMONICS
h1 = 5 h2 = 10 hj = 33

Figure 7.60.S6d: RESULTS FOR PROFILE SIMULATION NUMBER 60.S6d

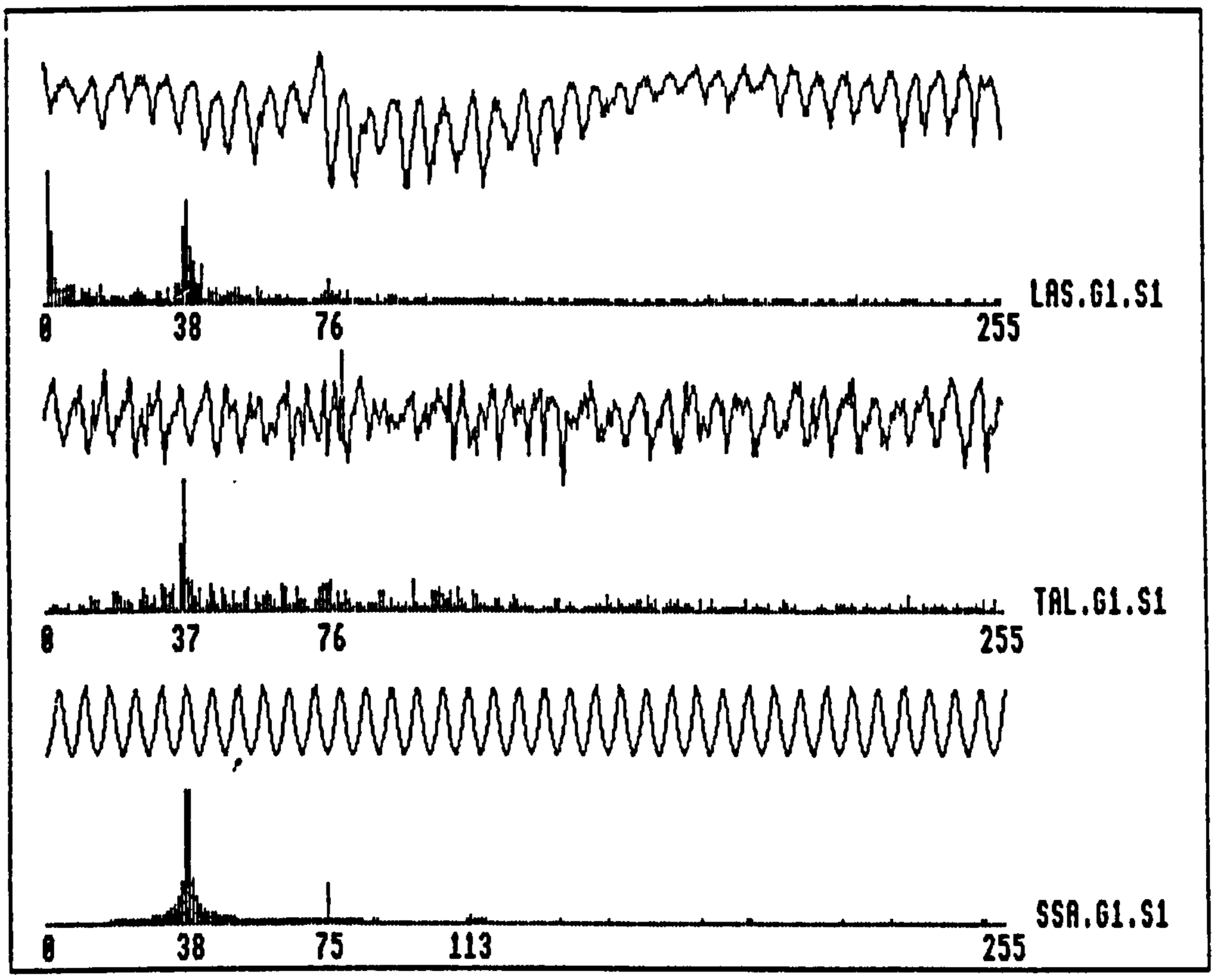

MACHINING PARAMETERS	PRINCIPAL PEAK HARMONICS
No. of knives 4 Feed speed 15 m/min Cutter Speed 4500 rpm Vib. rate 0 Proud Knives 1 >>> 1 Ecc.rate/rev 0 Spindle Runout 0 microns	h1 = 37 h2 = 74 hj = 149

ANALYSIS OF FFT's USING FAULT FINDING ALGORITHM (FFA)		
FFA ON LASER DATA THRESHOLD=0.4	FFA ON TALY DATA THRESHOLD=0.4	FFA ON SSA DATA THRESHOLD=0.4
(Single knife) Harmonic 38	(Single knife) Harmonic 37	(Single knife) Harmonic 38

Figure 7.G1.S1: RESULTS FOR TIMBER SAMPLE NUMBER G1.S1

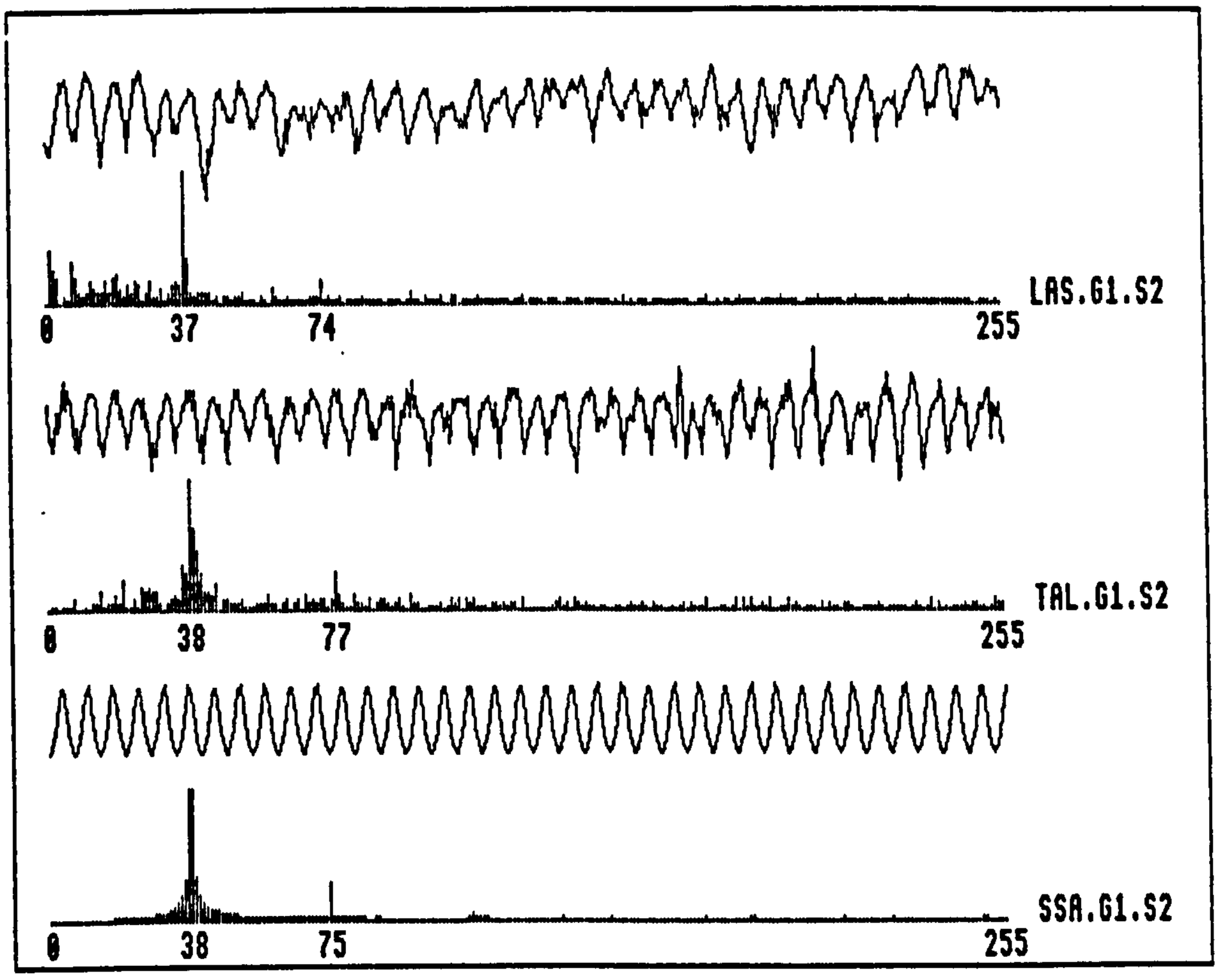

MACHINING PARAMETERS	PRINCIPAL PEAK HARMONICS
No. of knives 4 Feed speed 15 m/min Cutter Speed 4500 rpm Vib. rate 0 Proud Knives 1 >>> 1 Ecc.rate/rev 0 Spindle Runout 0 microns	h1 = 37 h2 = 74 hj = 149

ANALYSIS OF FFT's USING FAULT FINDING ALGORITHM (FFA)		
FFA ON LASER DATA THRESHOLD=0.4	FFA ON TALY DATA THRESHOLD=0.4	FFA ON SSA DATA THRESHOLD=0.4
(Single knife) Harmonic 37	(Single knife) Harmonic 38	(Single knife) Harmonic 38

Figure 7.G1.S2: RESULTS FOR TIMBER SAMPLE NUMBER G1.S2

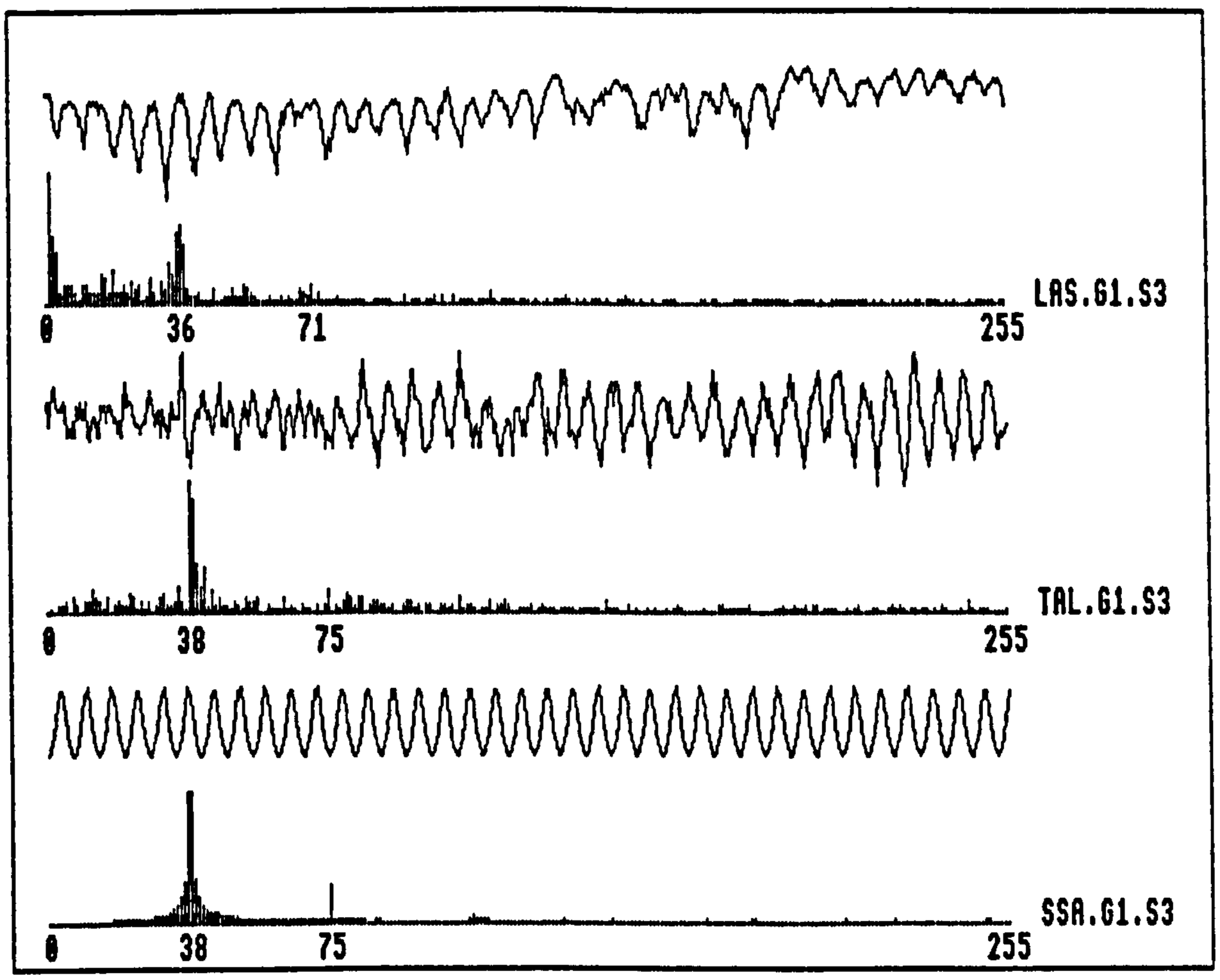

MACHINING PARAMETERS		PRINCIPAL PEAK HARMONICS
No. of knives	4	h1 = 37 h2 = 74 hj = 149
Feed speed	15 m/min	
Cutter Speed	4500 rpm	
Vib. rate	0	
Proud Knives	1 >>> 1	
Ecc.rate/rev	0	
Spindle Runout	0 microns	

ANALYSIS OF FFT's USING FAULT FINDING ALGORITHM (FFA)		
FFA ON LASER DATA THRESHOLD=0.4	FFA ON TALY DATA THRESHOLD=0.4	FFA ON SSA DATA THRESHOLD=0.4
(Single knife) Harmonic 36	(Single knife) Harmonic 38	(Single knife) Harmonic 38

Figure 7.G1.S3: RESULTS FOR TIMBER SAMPLE NUMBER G1.S3

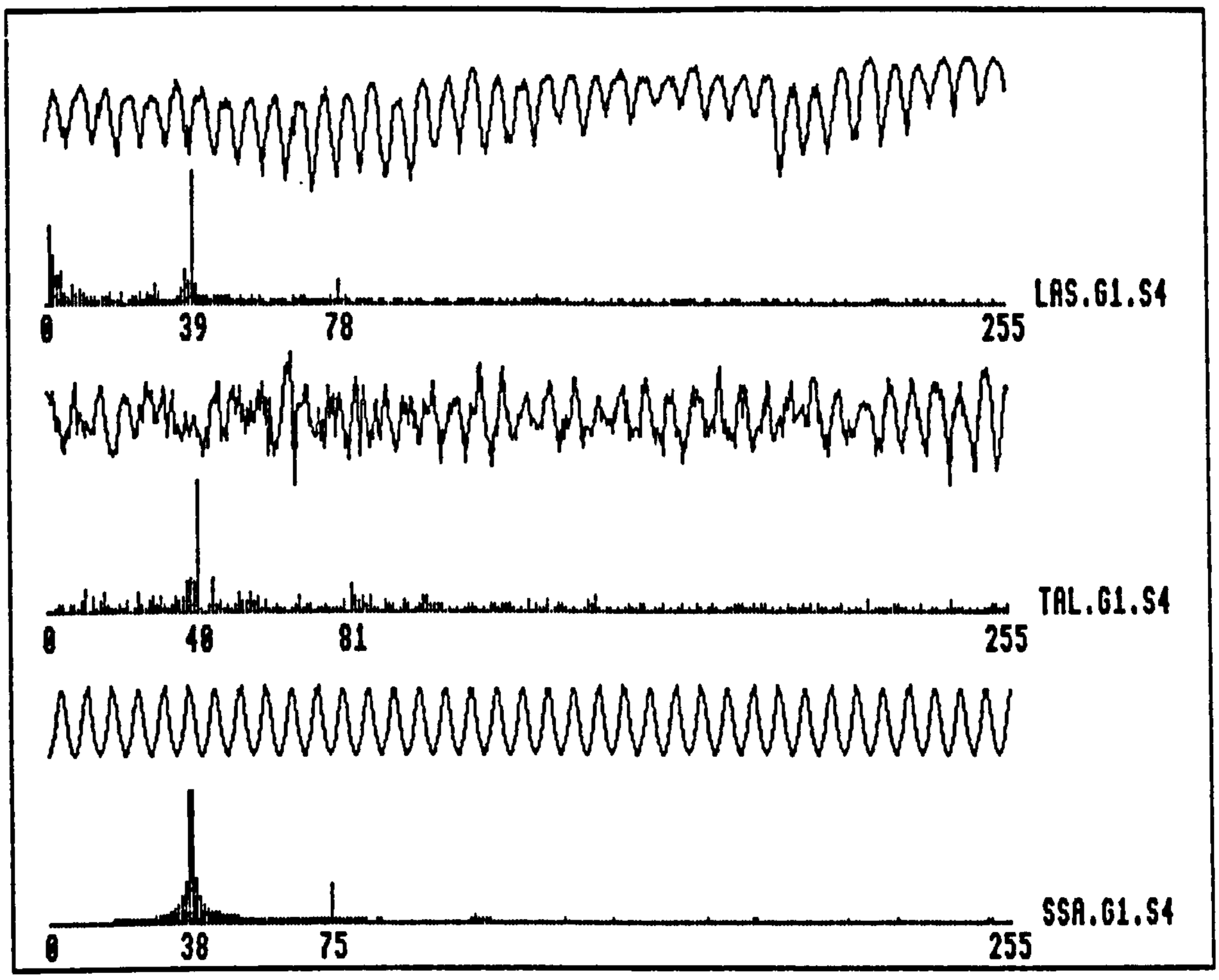

MACHINING PARAMETERS	PRINCIPAL PEAK HARMONICS
No. of knives 4 Feed speed 15 m/min Cutter Speed 4500 rpm Vib. rate 0 Proud Knives 1 >>> 1 Ecc.rate/rev 0 Spindle Runout 0 microns	h1 = 37 h2 = 74 hj = 149

ANALYSIS OF FFT's USING FAULT FINDING ALGORITHM (FFA)		
FFA ON LASER DATA THRESHOLD=0.4	FFA ON TALY DATA THRESHOLD=0.4	FFA ON SSA DATA THRESHOLD=0.4
(Single knife) Harmonic 39	(Single Knife) Harmonic 40	(Single knife) Harmonic 38

Figure 7.61.S4: RESULTS FOR TIMBER SAMPLE NUMBER G1.S4

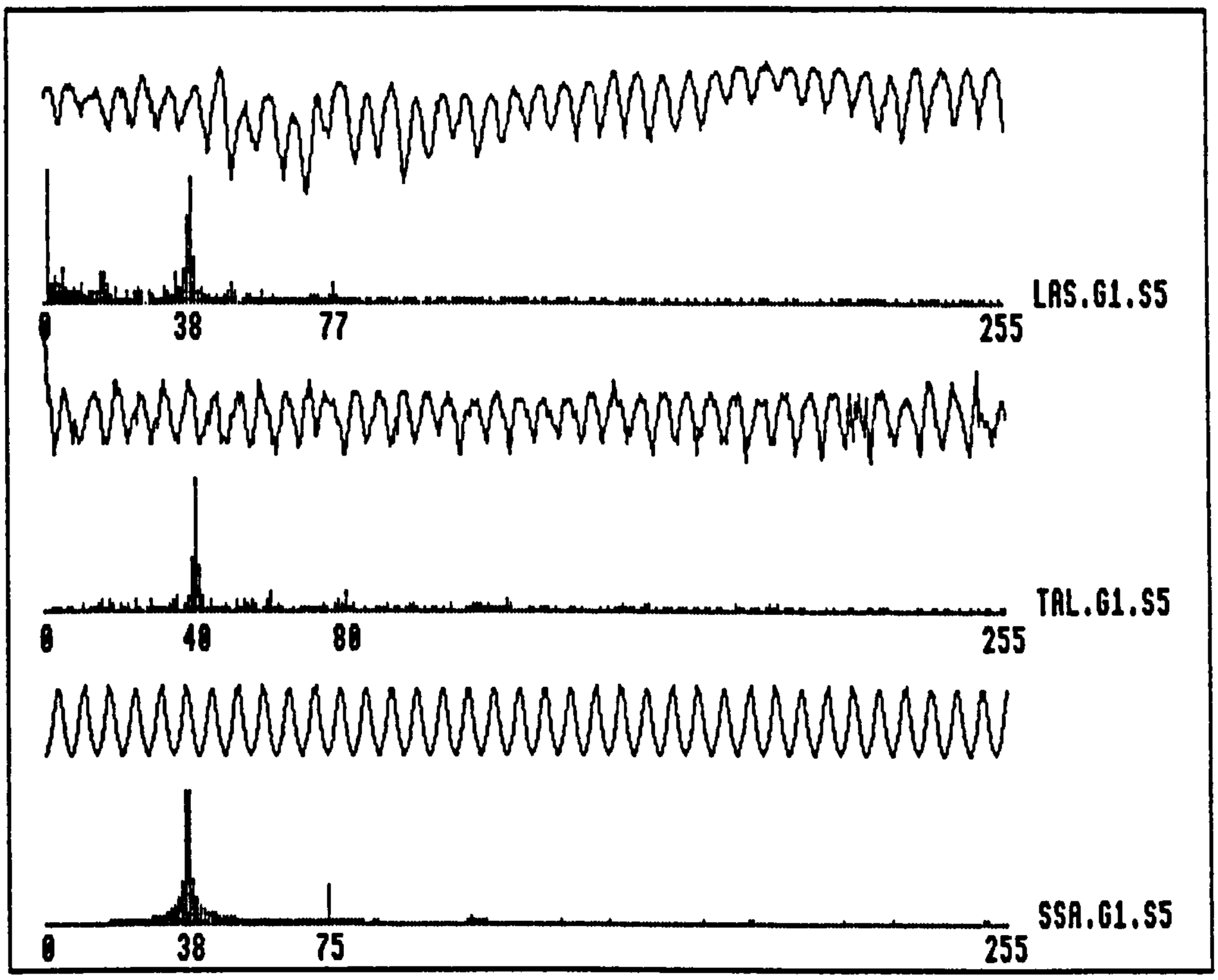

MACHINING PARAMETERS	PRINCIPAL PEAK HARMONICS
No. of knives 4 Feed speed 15 m/min Cutter Speed 4500 rpm Vib. rate 0 Proud Knives 1))) 1 Ecc.rate/rev 0 Spindle Runout 0 microns	h1 = 37 h2 = 74 hj = 149

ANALYSIS OF FFT's USING FAULT FINDING ALGORITHM (FFA)		
FFA ON LASER DATA THRESHOLD=0.4	FFA ON TALY DATA THRESHOLD=0.4	FFA ON SSA DATA THRESHOLD=0.4
(Single knife) Harmonic 39	(Single Knife) Harmonic 40	(Single knife) Harmonic 38

Figure 7.G1.S5: RESULTS FOR TIMBER SAMPLE NUMBER G1.S5

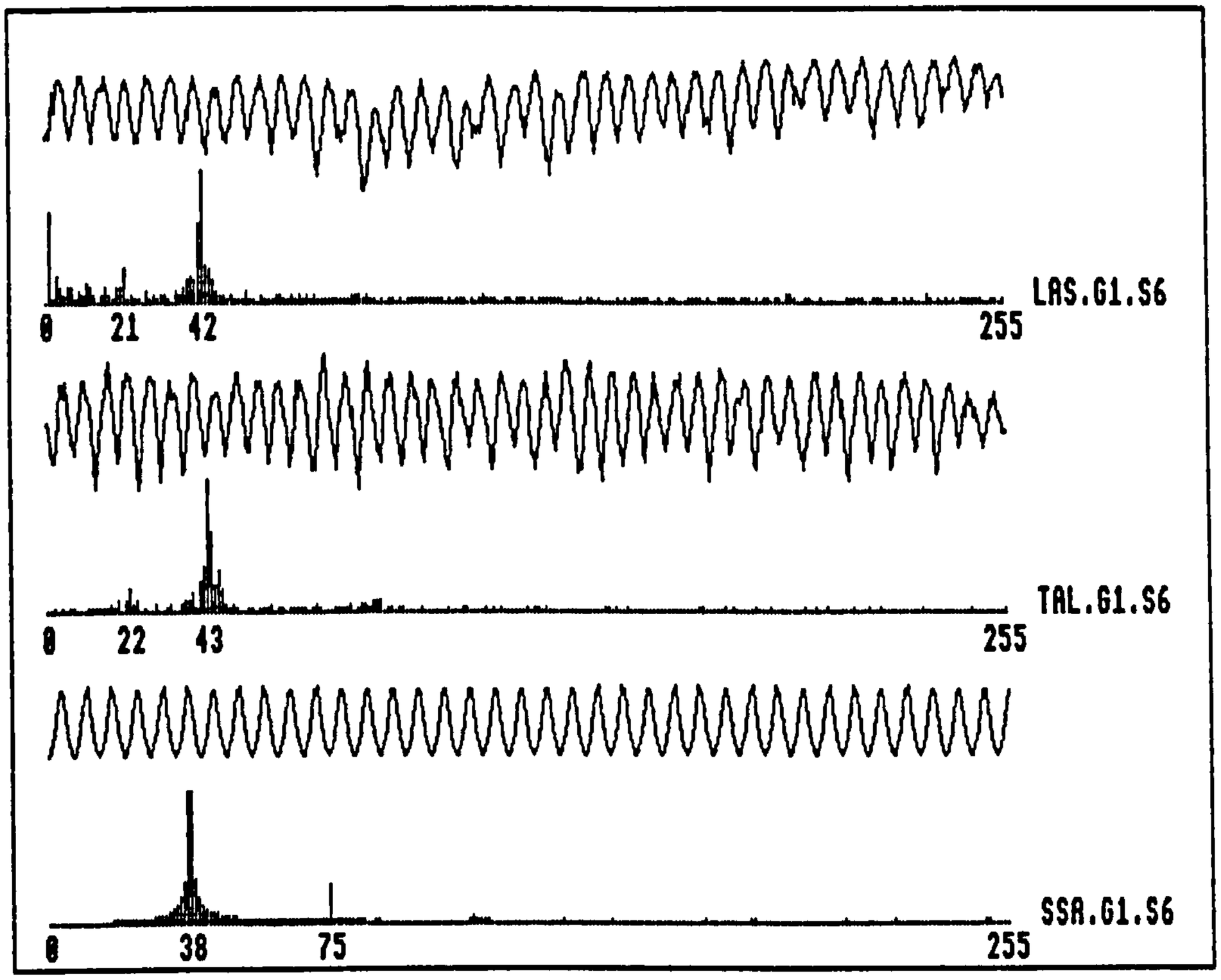

MACHINING PARAMETERS	PRINCIPAL PEAK HARMONICS
No. of knives 4 Feed speed 15 m/min Cutter Speed 4500 rpm Vib. rate 0 Proud Knives 1 >>> 1 Ecc.rate/rev 0 Spindle Runout 0 microns	h1 = 37 h2 = 74 hj = 149

ANALYSIS OF FFT's USING FAULT FINDING ALGORITHM (FFA)		
FFA ON LASER DATA THRESHOLD=0.4	FFA ON TALY DATA THRESHOLD=0.4	FFA ON SSA DATA THRESHOLD=0.4
(Unknown Faults) Harmonic 42	(Unknown Faults) Harmonic 43	(Single knife) Harmonic 38

Figure 7.61.S6: RESULTS FOR TIMBER SAMPLE NUMBER G1.S6

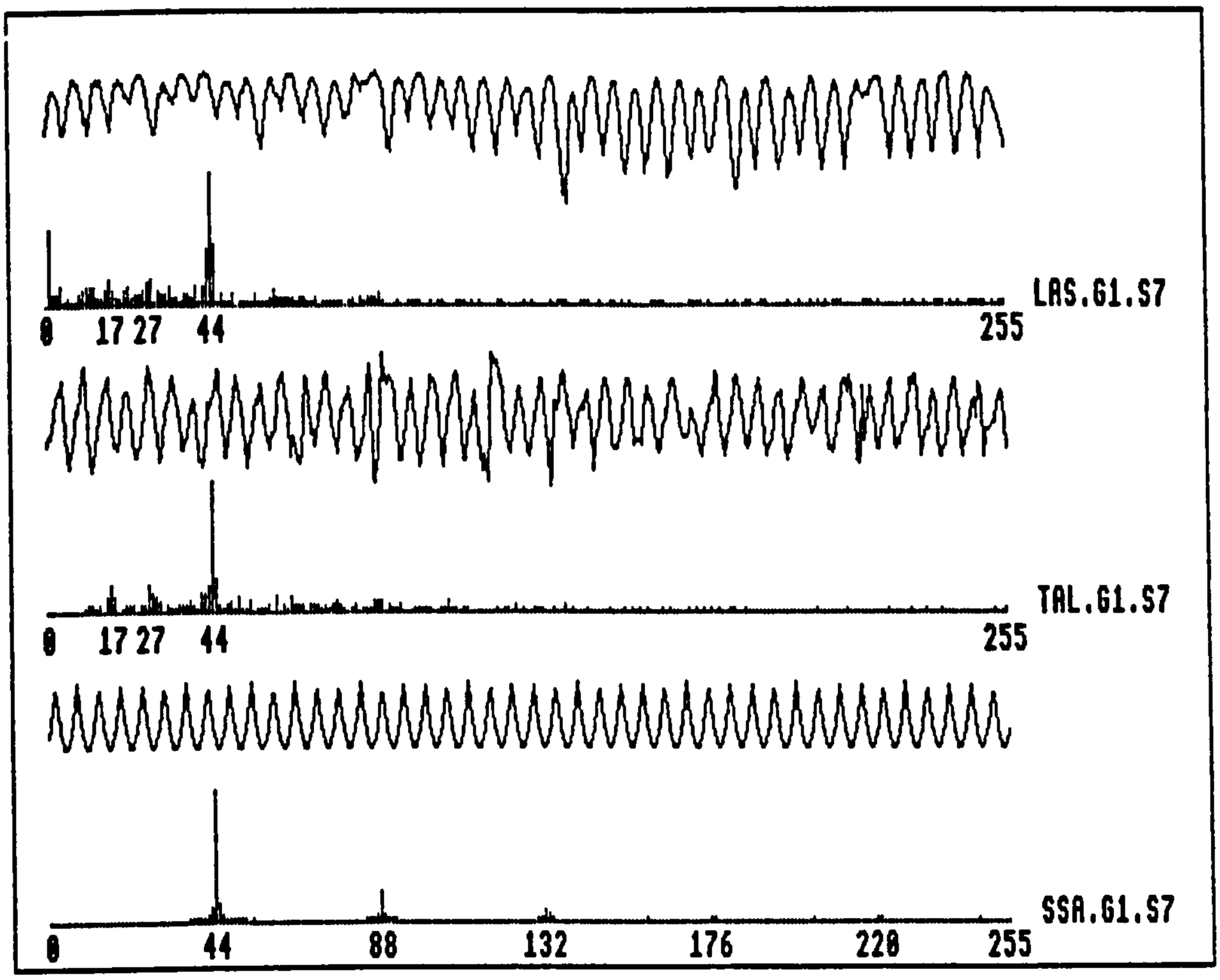

MACHINING PARAMETERS		PRINCIPAL PEAK HARMONICS
No. of knives	4	h1 = 44 h2 = 88 hj = 176
Feed speed	17 m/min	
Cutter Speed	6000 rpm	
Vib. rate	0	
Proud Knives	1))) 1	
Ecc.rate/rev	0	
Spindle Runout	0 microns	

ANALYSIS OF FFT's USING FAULT FINDING ALGORITHM (FFA)		
FFA ON LASER DATA THRESHOLD=0.4	FFA ON TALY DATA THRESHOLD=0.4	FFA ON SSA DATA THRESHOLD=0.4
(Single knife) Harmonic 44	(Single knife) Harmonic 44	(Single knife) Harmonic 44

Figure 7.61.S7: RESULTS FOR TIMBER SAMPLE NUMBER G1.S7

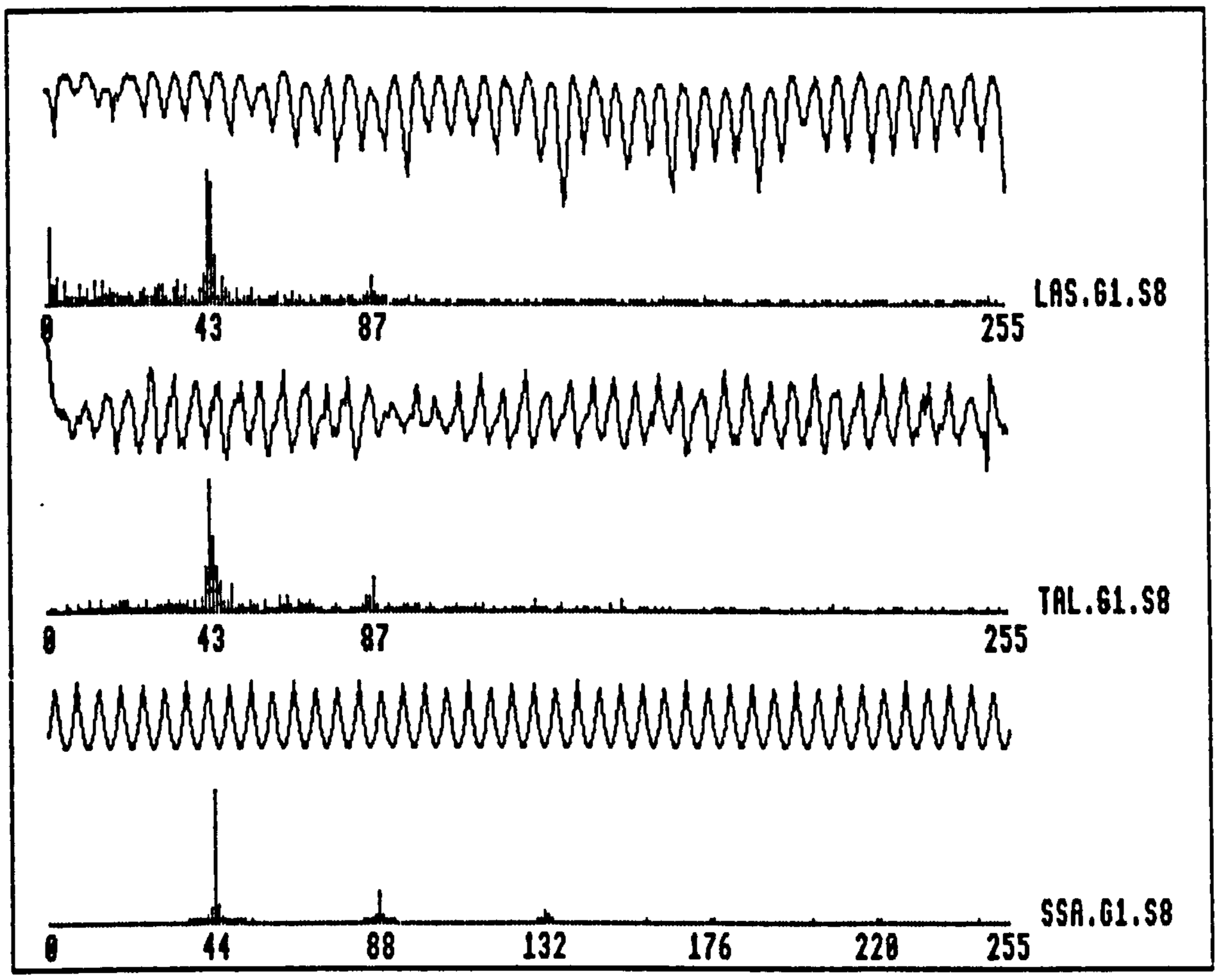

MACHINING PARAMETERS	PRINCIPAL PEAK HARMONICS
No. of knives 4 Feed speed 17 m/min Cutter Speed 6000 rpm Vib. rate 0 Proud Knives 1 >>> 1 Ecc.rate/rev 0 Spindle Runout 0 microns	h1 = 44 h2 = 88 hj = 176

ANALYSIS OF FFT's USING FAULT FINDING ALGORITHM (FFA)		
FFA ON LASER DATA THRESHOLD=0.4	FFA ON TALY DATA THRESHOLD=0.4	FFA ON SSA DATA THRESHOLD=0.4
(Single knife) Harmonic 43	(Single knife) Harmonic 43	(Single knife) Harmonic 44

Figure 7.G1.S8: RESULTS FOR TIMBER SAMPLE NUMBER G1.S8

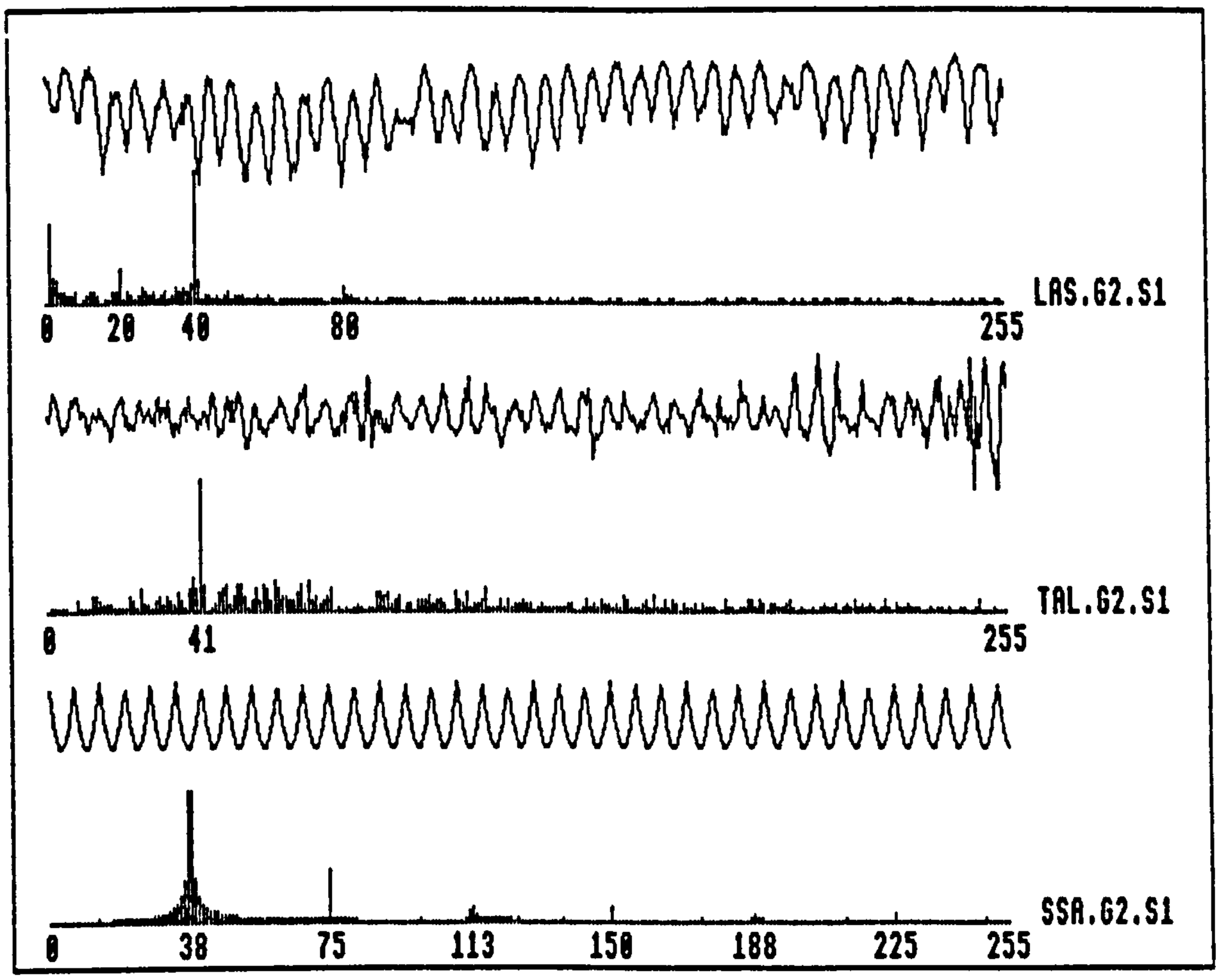

MACHINING PARAMETERS	PRINCIPAL PEAK HARMONICS
No. of knives 4 Feed speed 60 m/min Cutter Speed 4500 rpm Vib. rate 0 Proud Knives 0 Ecc.rate/rev 0 Spindle Runout 0 microns	h1 = 9 h2 = 18 hj = 37

ANALYSIS OF FFT's USING FAULT FINDING ALGORITHM (FFA)		
FFA ON LASER DATA THRESHOLD=0.5	FFA ON TALY DATA THRESHOLD=0.5	FFA ON SSA DATA THRESHOLD=0.5
(Multi-knife) Harmonic 40	(Unknown Faults) Harmonic 41	(Multi-knife) Harmonic 38

Figure 7.G2.S1: RESULTS FOR TIMBER SAMPLE NUMBER G2.S1

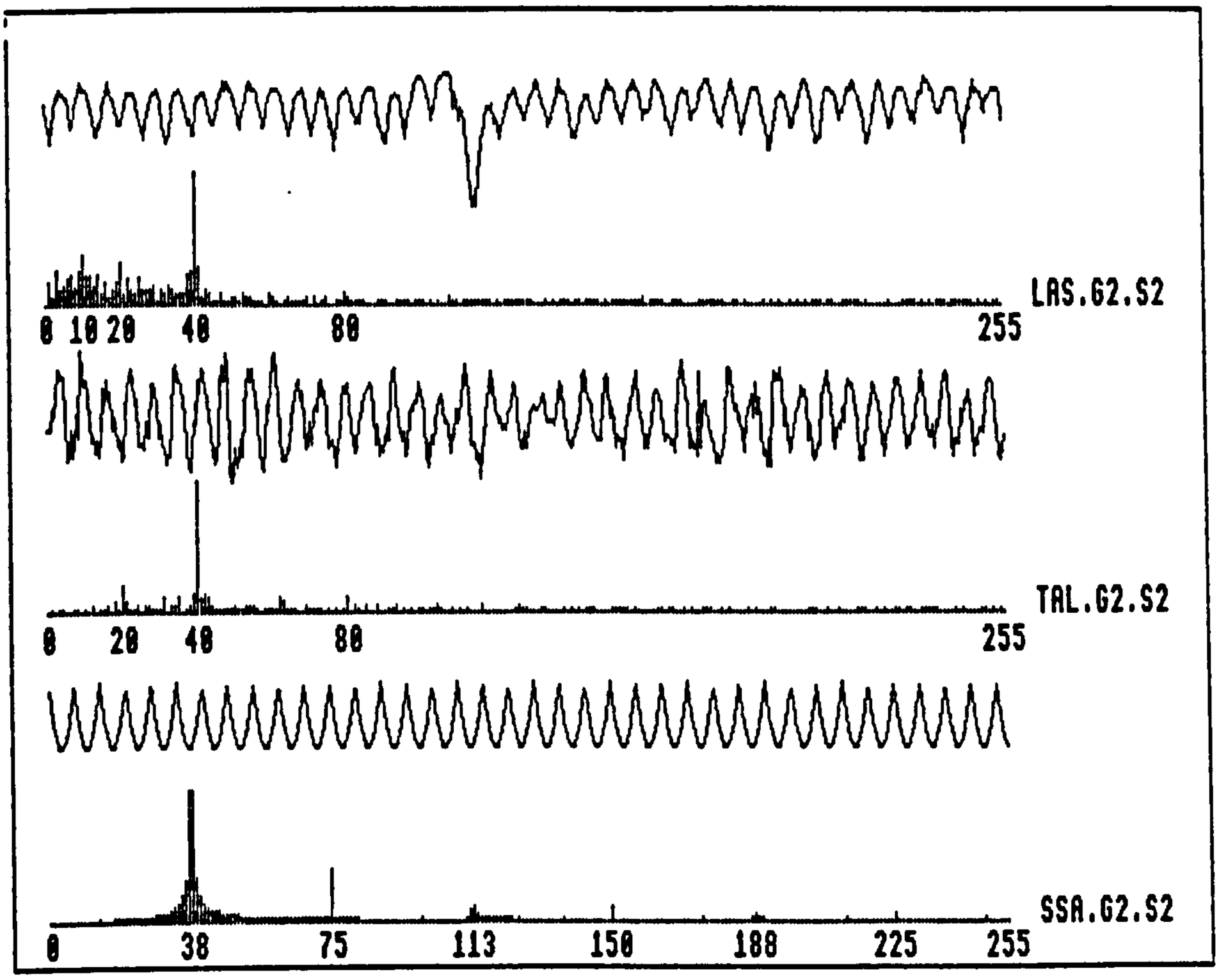

MACHINING PARAMETERS	PRINCIPAL PEAK HARMONICS
No. of knives 4 Feed speed 60 m/min Cutter Speed 4500 rpm Vib. rate 0 Proud Knives 0 Ecc.rate/rev 0 Spindle Runout 0 microns	h1 = 9 h2 = 18 hj = 37

ANALYSIS OF FFT's USING FAULT FINDING ALGORITHM (FFA)		
FFA ON LASER DATA THRESHOLD=0.4	FFA ON TALY DATA THRESHOLD=0.4	FFA ON SSA DATA THRESHOLD=0.4
(Multi-knife) Harmonic 40	(Multi-knife) Harmonic 40	(Multi-knife) Harmonic 38

Figure 7.G2.S2: RESULTS FOR TIMBER SAMPLE NUMBER G2.S2

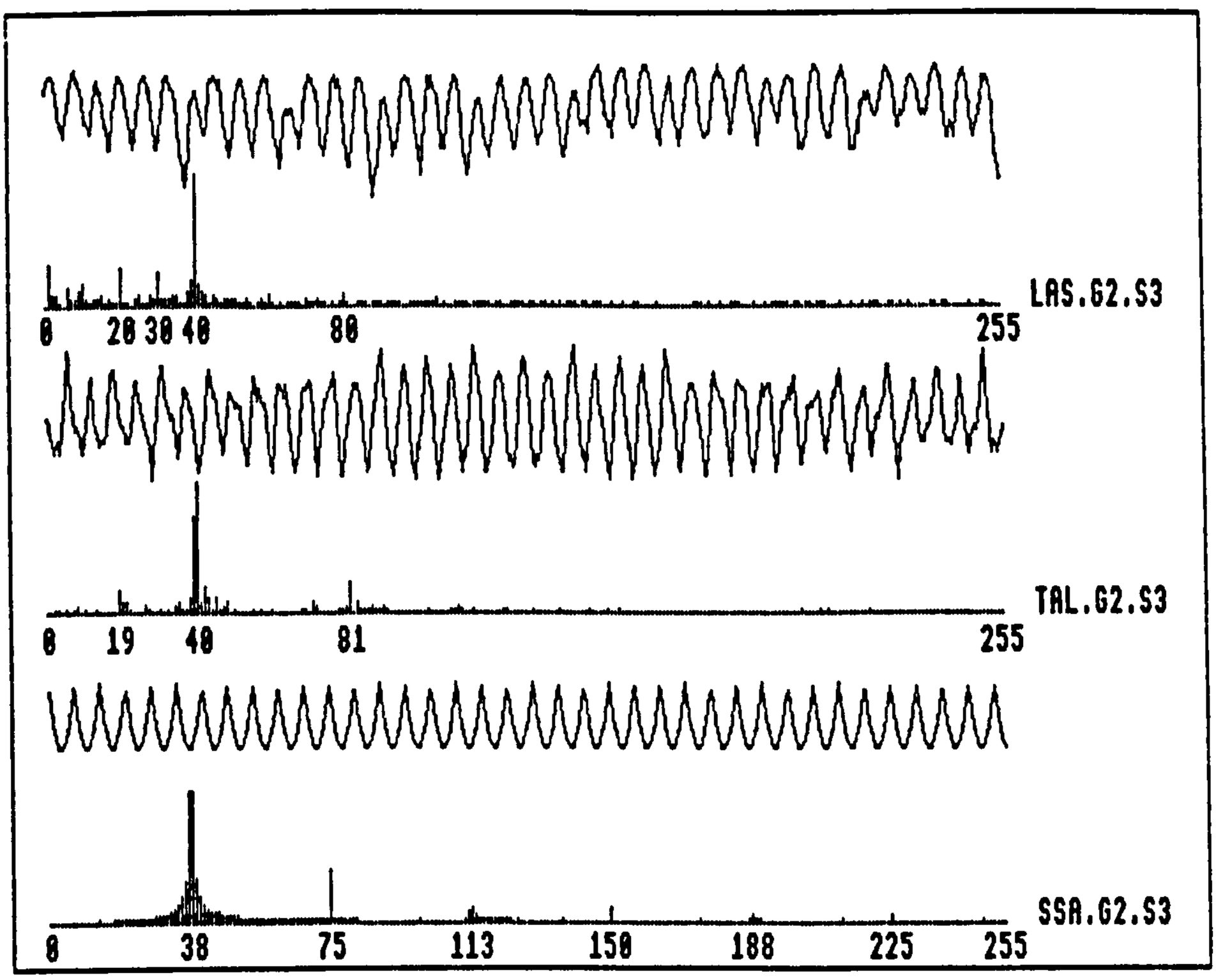

MACHINING PARAMETERS	PRINCIPAL PEAK HARMONICS
No. of knives 4 Feed speed 60 m/min Cutter Speed 4500 rpm Vib. rate 0 Proud Knives 0 Ecc.rate/rev 0 Spindle Runout 0 microns	h1 = 9 h2 = 18 hj = 37

ANALYSIS OF FFT's USING FAULT FINDING ALGORITHM (FFA)		
FFA ON LASER DATA THRESHOLD=0.4	FFA ON TALY DATA THRESHOLD=0.4	FFA ON SSA DATA THRESHOLD=0.4
(Multi-knife) Harmonic 40	(Multi-knife) Harmonic 40	(Multi-knife) Harmonic 38

Figure 7.G2.S3: RESULTS FOR TIMBER SAMPLE NUMBER G2.S3

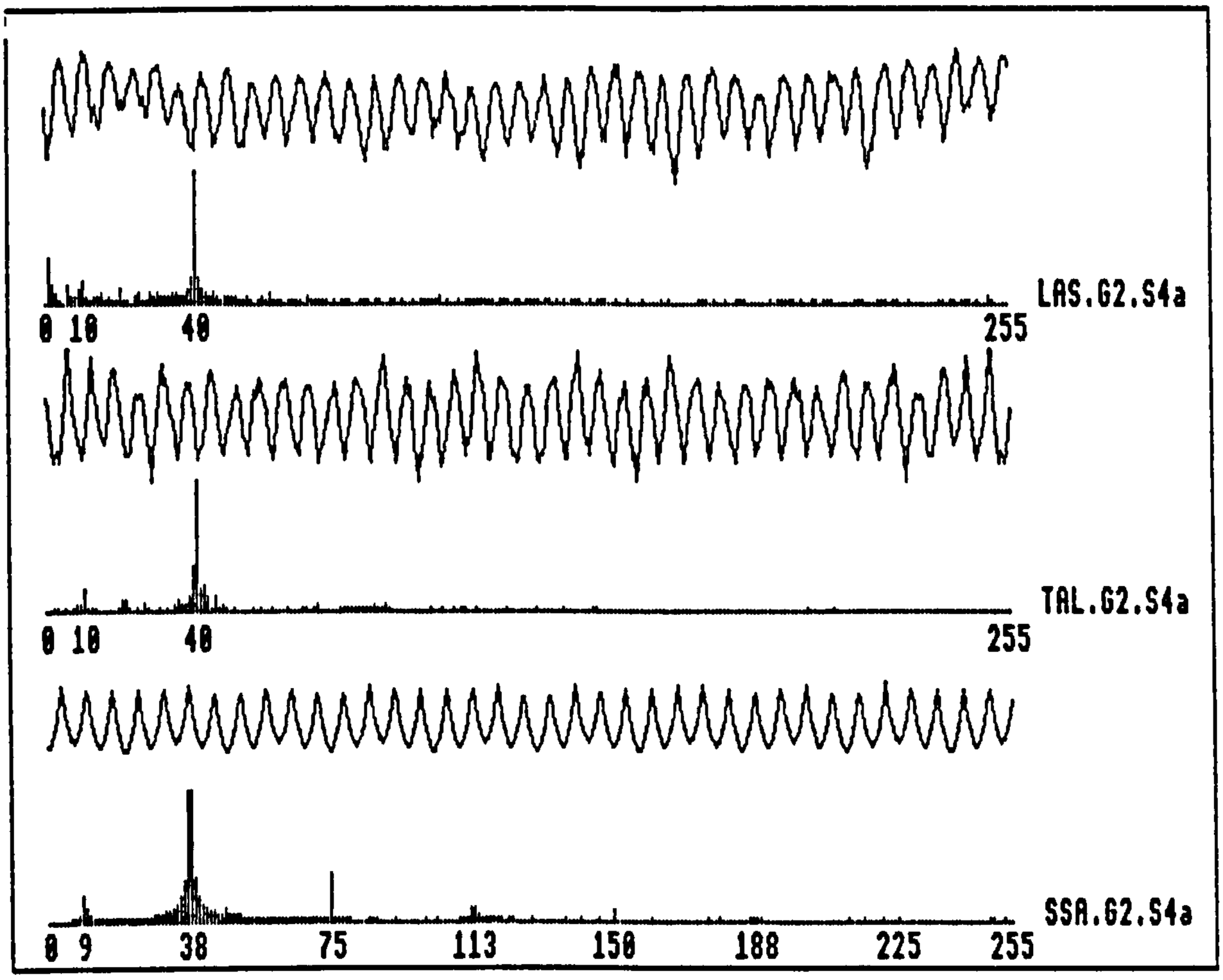

MACHINING PARAMETERS	PRINCIPAL PEAK HARMONICS
No. of knives 4 Feed speed 60 m/min Cutter Speed 4500 rpm Vib. rate 0 Proud Knives 0 Ecc.rate/rev 1 Spindle Runout 1 microns	h1 = 9 h2 = 18 hj = 37

ANALYSIS OF FFT's USING FAULT FINDING ALGORITHM (FFA)		
FFA ON LASER DATA THRESHOLD=0.4	FFA ON TALY DATA THRESHOLD=0.4	FFA ON SSA DATA THRESHOLD=0.4
(Multi-knife) Harmonic 40	(Multi-knife) Harmonic 40	(Multi-knife) Harmonic 38

Figure 7.62.S4a: RESULTS FOR TIMBER SAMPLE NUMBER 62.S4a

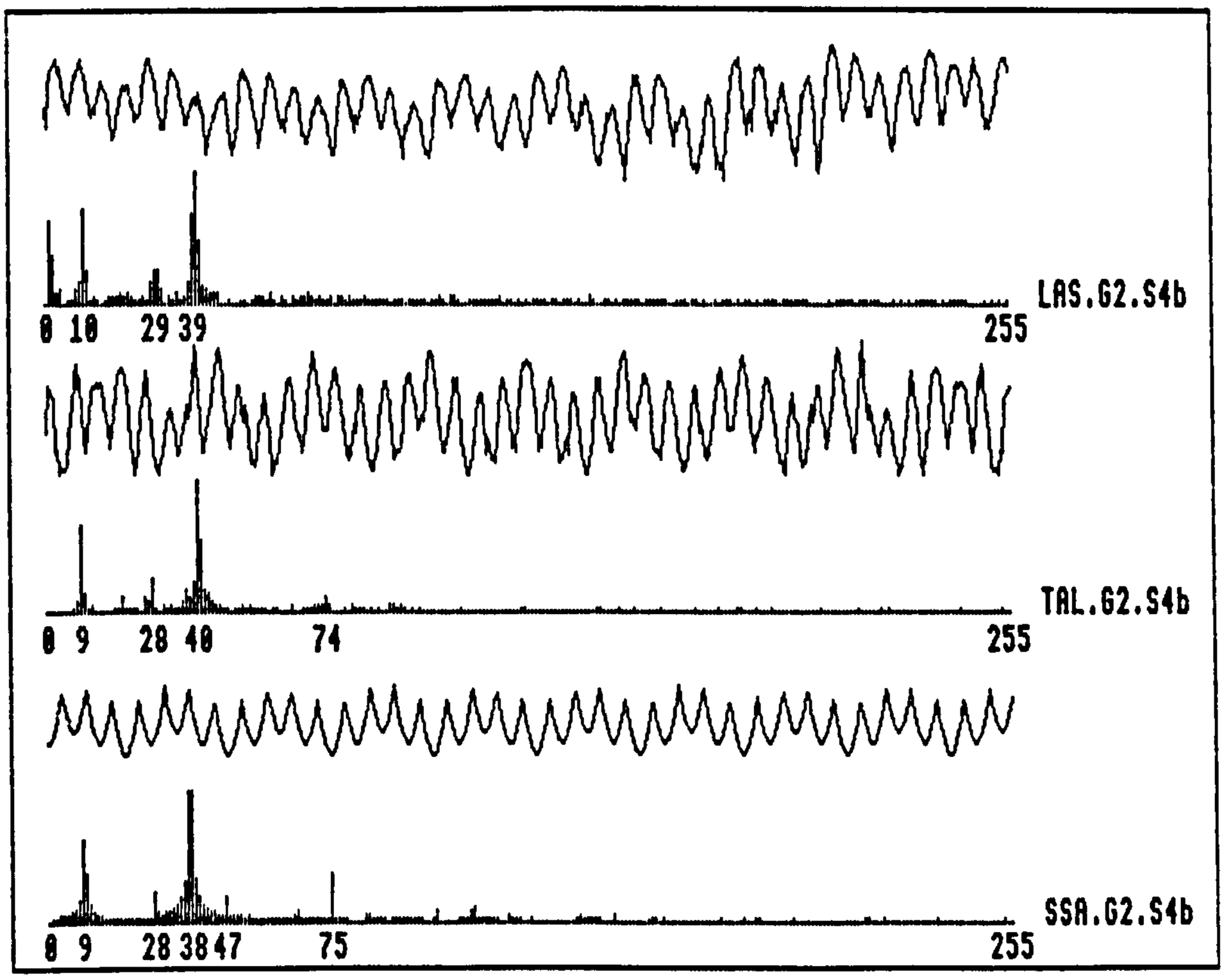

MACHINING PARAMETERS	PRINCIPAL PEAK HARMONICS
No. of knives 4 Feed speed 60 m/min Cutter Speed 4500 rpm Vib. rate 0 Proud Knives 0 Ecc.rate/rev 1 Spindle Runout 3 microns	h1 = 9 h2 = 18 hj = 37

ANALYSIS OF FFT's USING FAULT FINDING ALGORITHM (FFA)		
FFA ON LASER DATA THRESHOLD=0.4	FFA ON TALY DATA THRESHOLD=0.4	FFA ON SSA DATA THRESHOLD=0.4
(0.balance 1) Harmonic 10 (Multi-knife) Harmonic 40	(0.balance 1) Harmonic 9 (Multi-knife) Harmonic 40	(0.balance 1) Harmonic 9 (Multi-knife) Harmonic 38

Figure 7.G2.S4b: RESULTS FOR TIMBER SAMPLE NUMBER G2.S4b

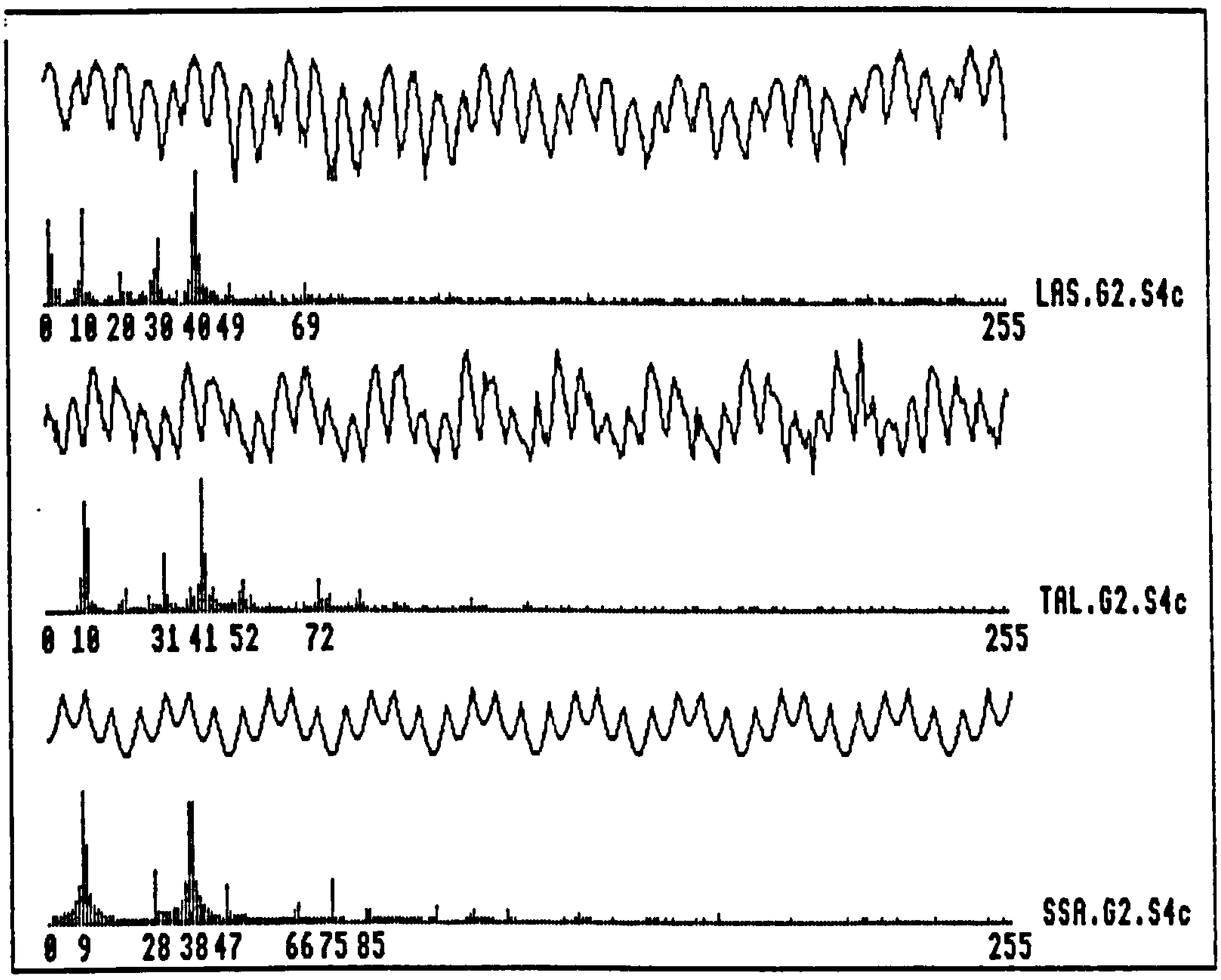

MACHINING PARAMETERS	PRINCIPAL PEAK HARMONICS
No. of knives 4 Feed speed 60 m/min Cutter Speed 4500 rpm Vib. rate 0 Proud Knives 0 Ecc.rate/rev 1 Spindle Runout 5 microns	h1 = 9 h2 = 18 hj = 37

ANALYSIS OF FFT's USING FAULT FINDING ALGORITHM (FFA)		
FFA ON LASER DATA THRESHOLD=0.4	FFA ON TALY DATA THRESHOLD=0.4	FFA ON SSA DATA THRESHOLD=0.4
(0.balance 1) Harmonic 10 (Multi-knife) Harmonic 40 (Unknown Faults) Harmonic 30	(0.balance 1) Harmonic 10 (Unknown Faults) Harmonic 31 Harmonic 41	(0.balance 1) Harmonic 9 (Multi-knife) Harmonic 38

Figure 7.G2.S4c: RESULTS FOR TIMBER SAMPLE NUMBER G2.S4c

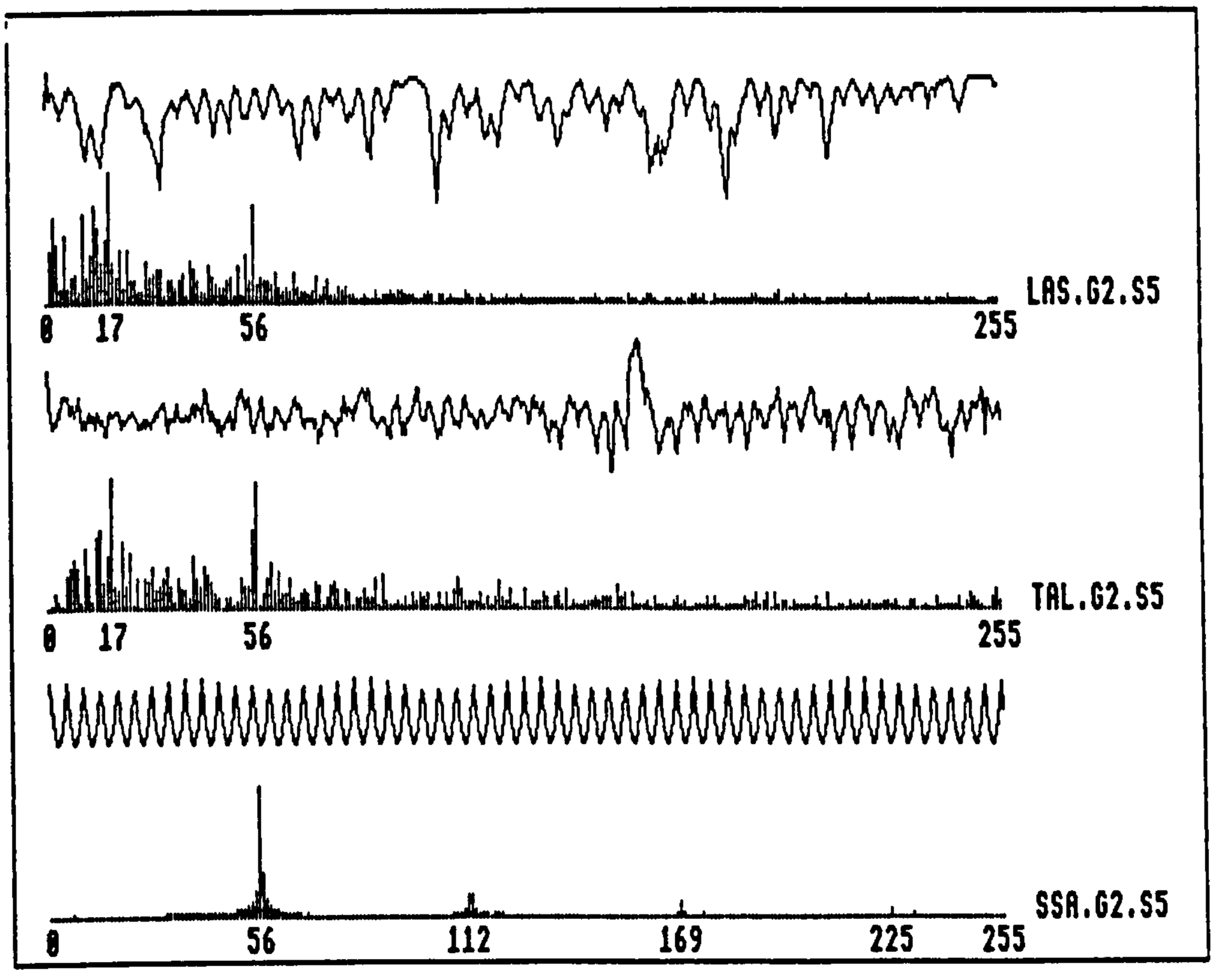

MACHINING PARAMETERS		PRINCIPAL PEAK HARMONICS
No. of knives	6	h1 = 9
Feed speed	80 m/min	h2 = 18
Cutter Speed	6000 rpm	hj = 56
Vib. rate	0	
Proud Knives	0	
Ecc.rate/rev	0	
Spindle Runout	0 microns	

ANALYSIS OF FFT's USING FAULT FINDING ALGORITHM (FFA)		
FFA ON LASER DATA THRESHOLD=0.4	FFA ON TALY DATA THRESHOLD=0.4	FFA ON SSA DATA THRESHOLD=0.4
(O.balance 2) Harmonic 17 (Multi-knife) Harmonic 56 (Unknown Faults) Harmonic 13 Harmonic 22	(O.balance 2) Harmonic 17 (Multi-knife) Harmonic 56 (Unknown Faults) Harmonic 39	(Multi-knife) Harmonic 56

Figure 7.G2.S5: RESULTS FOR TIMBER SAMPLE NUMBER G2.S5

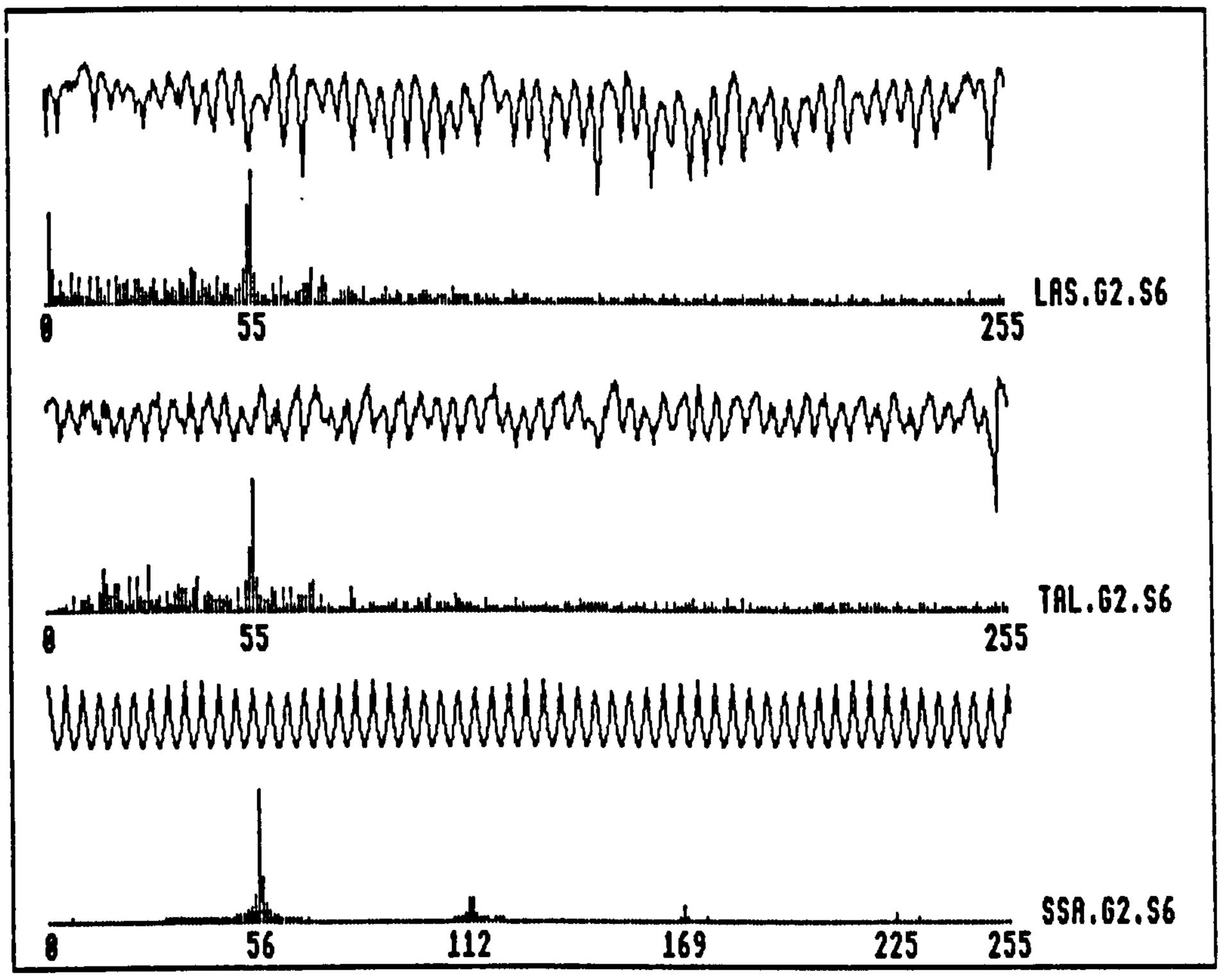

MACHINING PARAMETERS	PRINCIPAL PEAK HARMONICS
No. of knives 6 Feed speed 80 m/min Cutter Speed 6000 rpm Vib. rate 0 Proud Knives 0 Ecc.rate/rev 0 Spindle Runout 0 microns	h1 = 9 h2 = 18 hj = 56

ANALYSIS OF FFT's USING FAULT FINDING ALGORITHM (FFA)		
FFA ON LASER DATA THRESHOLD=0.4	FFA ON TALY DATA THRESHOLD=0.4	FFA ON SSA DATA THRESHOLD=0.4
(Multi-knife) Harmonic 55	(Multi-knife) Harmonic 55	(Multi-knife) Harmonic 56

Figure 7.G2.S6: RESULTS FOR TIMBER SAMPLE NUMBER G2.S6

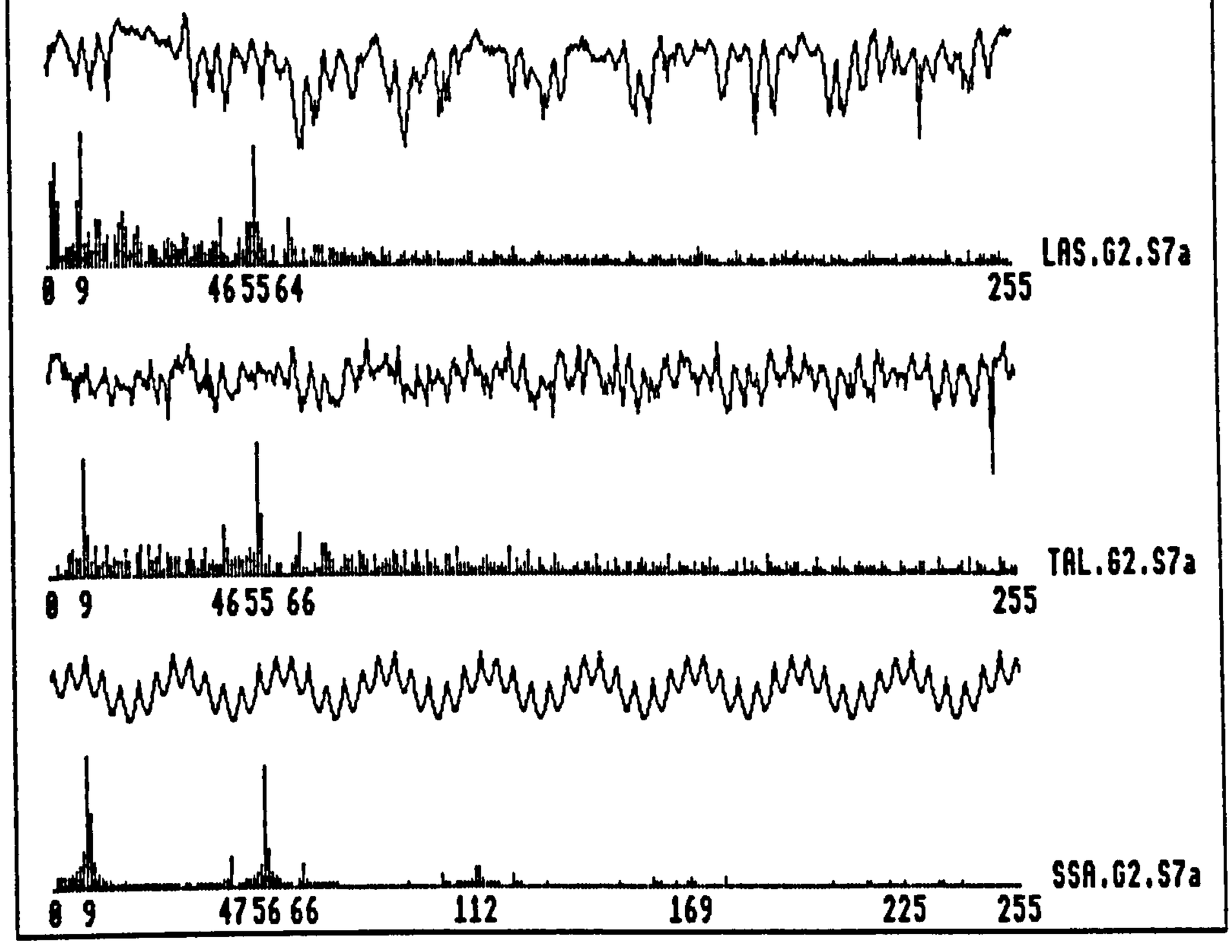

MACHINING PARAMETERS	PRINCIPAL PEAK HARMONICS
No. of knives 6 Feed speed 80 m/min Cutter Speed 6000 rpm Vib. rate 0 Proud Knives 0 Ecc.rate/rev 1 Spindle Runout 3 microns	h1 = 9 h2 = 18 hj = 56

ANALYSIS OF FFT's USING FAULT FINDING ALGORITHM (FFA)		
FFA ON LASER DATA THRESHOLD=0.4	FFA ON TALY DATA THRESHOLD=0.4	FFA ON SSA DATA THRESHOLD=0.4
(0.balance 1) Harmonic 9 (Multi-knife) Harmonic 55	(0.balance 1) Harmonic 9 (Multi-knife) Harmonic 55	(0.balance 1) Harmonic 9 (Multi-knife) Harmonic 56

Figure 7.G2.S7a: RESULTS FOR TIMBER SAMPLE NUMBER G2.S7a

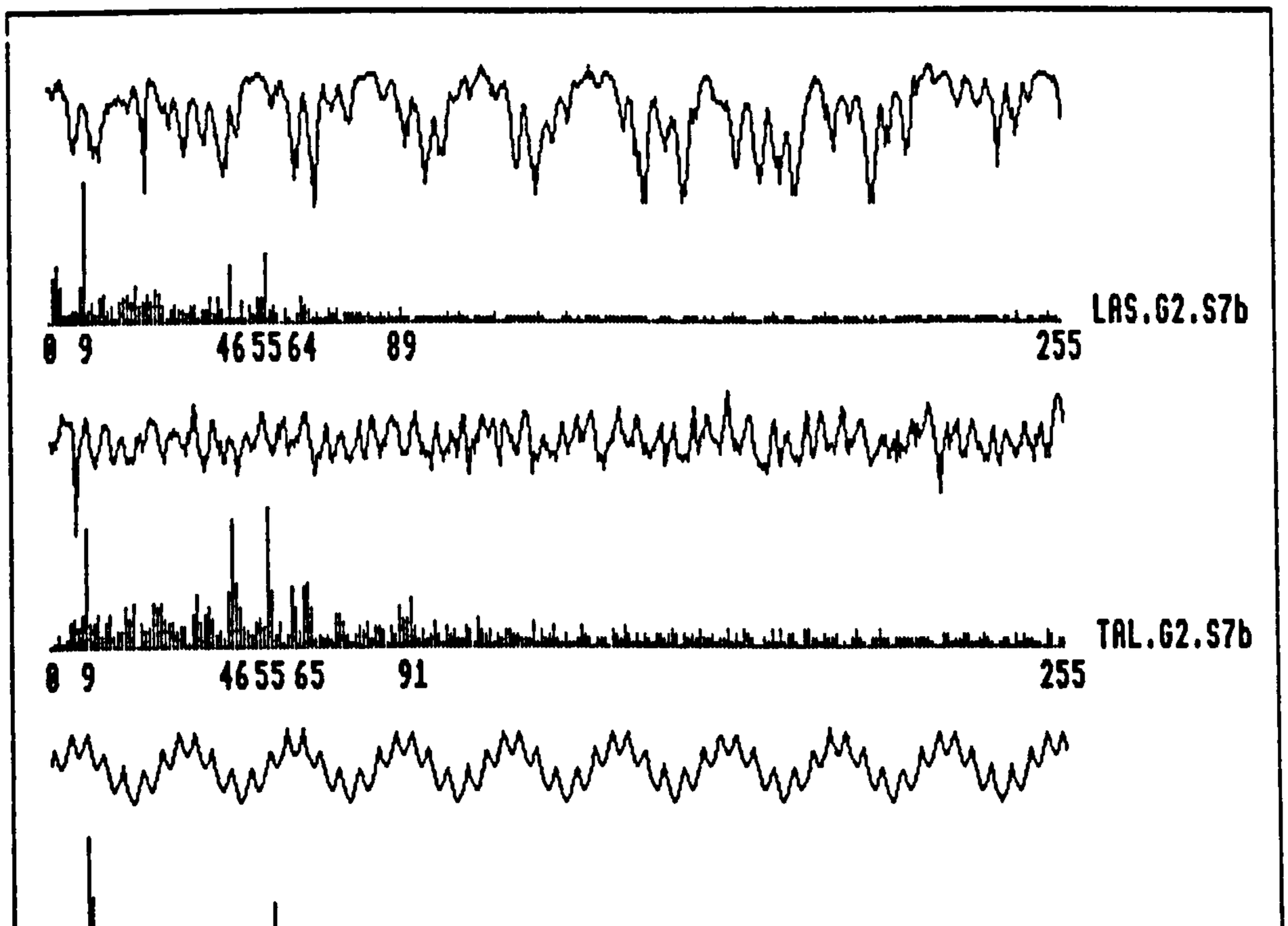

MACHINING PARAMETERS	PRINCIPAL PEAK HARMONICS
No. of knives 6 Feed speed 80 m/min Cutter Speed 6000 rpm Vib. rate 0 Proud Knives 0 Ecc.rate/rev 1 Spindle Runout 5 microns	h1 = 9 h2 = 18 hj = 56

ANALYSIS OF FFT's USING FAULT FINDING ALGORITHM (FFA)		
FFA ON LASER DATA THRESHOLD=0.4	FFA ON TALY DATA THRESHOLD=0.4	FFA ON SSA DATA THRESHOLD=0.4
(0.balance 1) Harmonic 9 (Multi-knife) Harmonic 55 (Unknown Faults) Harmonic 46	(0.balance 1) Harmonic 9 (Multi-knife) Harmonic 55 (Unknown Faults) Harmonic 46 Harmonic 65	(0.balance 1) Harmonic 9 (Multi-knife) Harmonic 56

Figure 7.G2.S7b: RESULTS FOR TIMBER SAMPLE NUMBER G2.S7b

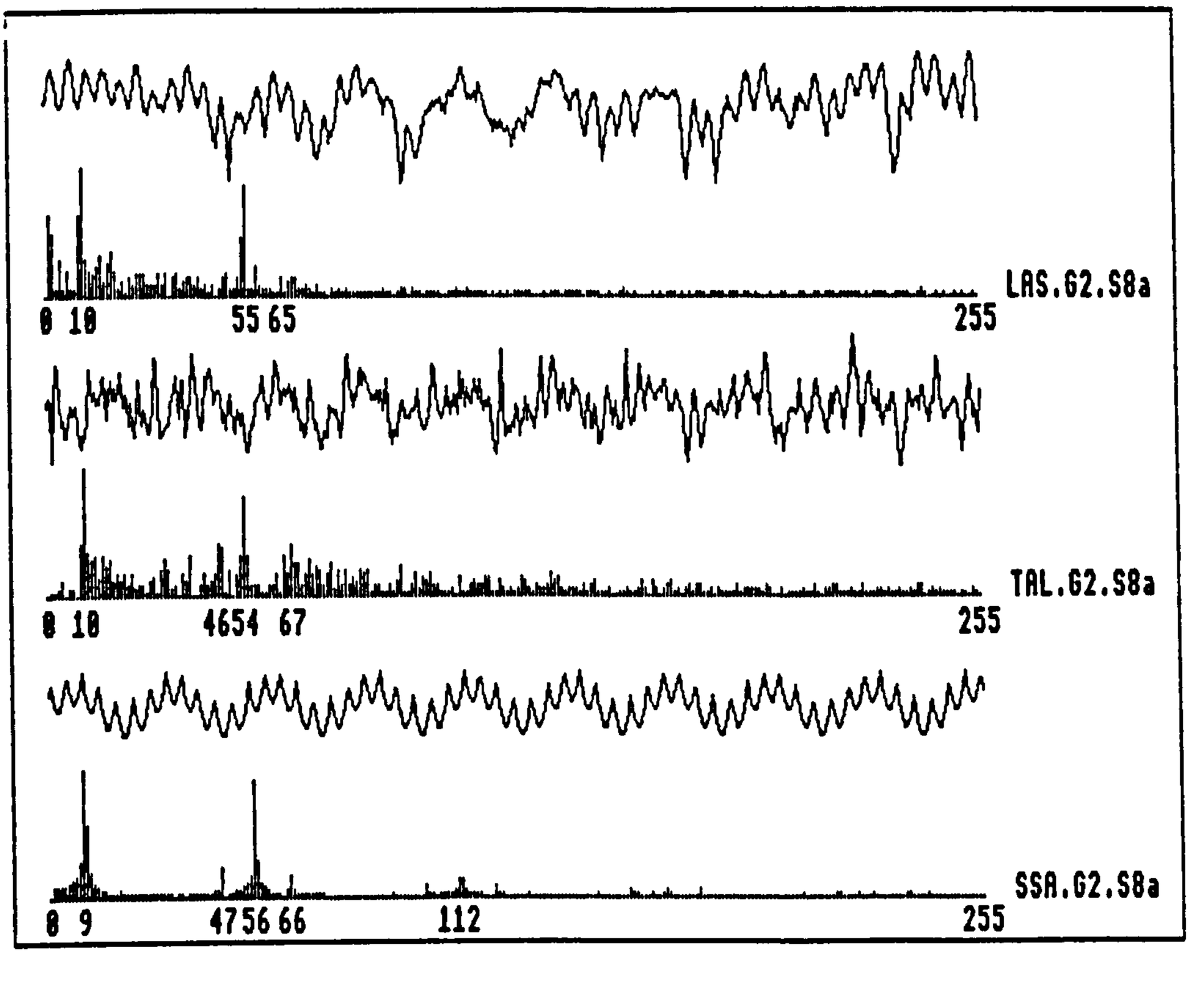

MACHINING PARAMETERS	PRINCIPAL PEAK HARMONICS
No. of knives 6 Feed speed 80 m/min Cutter Speed 6000 rpm Vib. rate 0 Proud Knives 0 Ecc.rate/rev 1 Spindle Runout 3 microns	h1 = 9 h2 = 18 hj = 56

ANALYSIS OF FFT's USING FAULT FINDING ALGORITHM (FFA)		
FFA ON LASER DATA THRESHOLD=0.4	FFA ON TALY DATA THRESHOLD=0.4	FFA ON SSA DATA THRESHOLD=0.4
(O.balance 1) Harmonic 10 (Multi-knife) Harmonic 55	(O.balance 1) Harmonic 10 (Multi-knife) Harmonic 54 (Unknown Faults) Harmonic 47 Harmonic 67	(O.balance 1) Harmonic 9 (Multi-knife) Harmonic 56

Figure 7.G2.S8a: RESULTS FOR TIMBER SAMPLE NUMBER G2.S8a

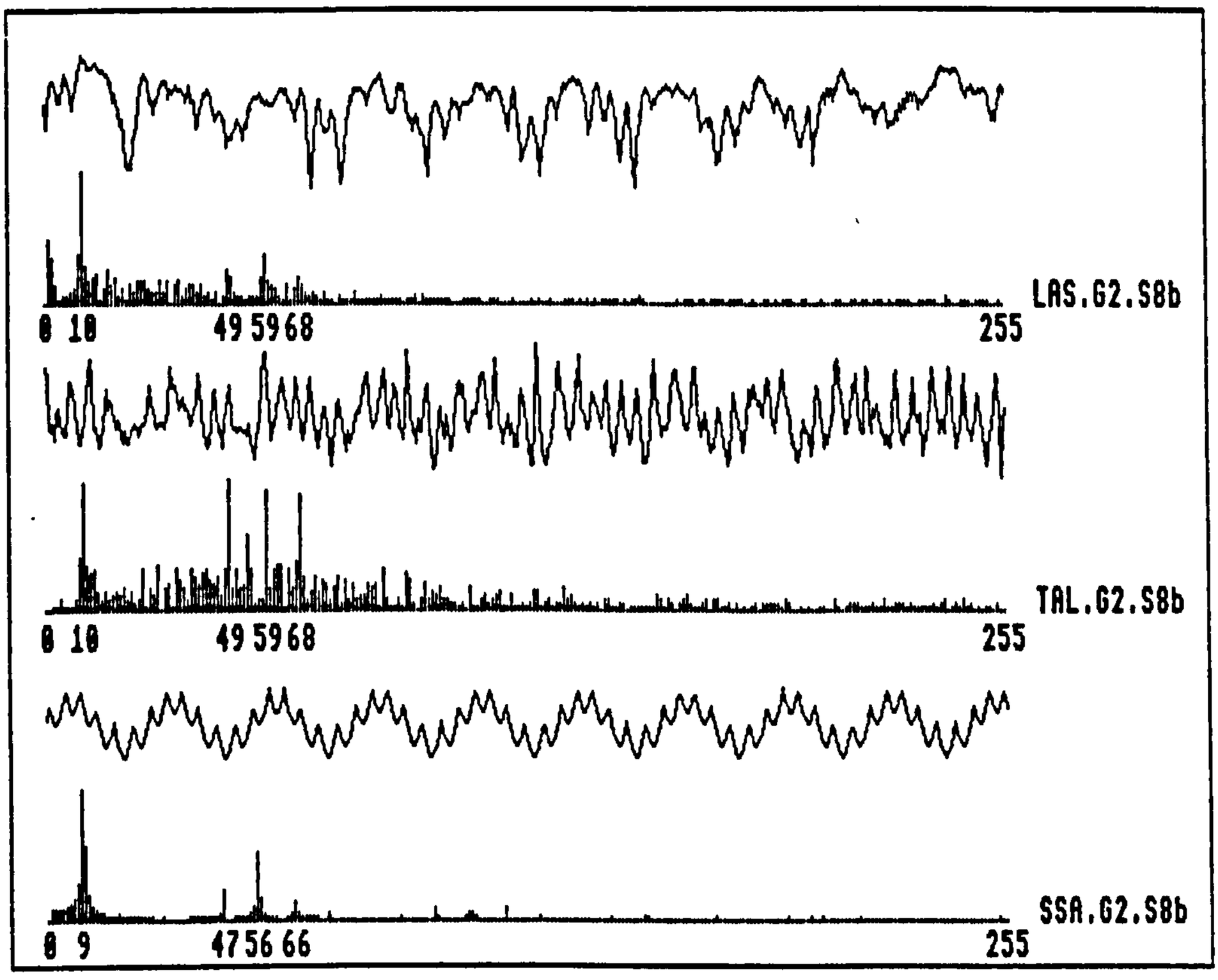

MACHINING PARAMETERS		PRINCIPAL PEAK HARMONICS
No. of knives	6	h1 = 9 h2 = 18 hj = 56
Feed speed	80 m/min	
Cutter Speed	6000 rpm	
Vib. rate	0	
Proud Knives	0	
Ecc.rate/rev	1	
Spindle Runout	5 microns	

ANALYSIS OF FFT's USING FAULT FINDING ALGORITHM (FFA)		
FFA ON LASER DATA THRESHOLD=0.4	FFA ON TALY DATA THRESHOLD=0.4	FFA ON SSA DATA THRESHOLD=0.4
(0.balance 1) Harmonic 10 (Multi-knife) Harmonic 59	(0.balance 1) Harmonic 10 (Multi-knife) Harmonic 54 (Unknown Faults) Harmonic 49 Harmonic 68	(0.balance 1) Harmonic 9 (Multi-knife) Harmonic 56

Figure 7.G2.S8b: RESULTS FOR TIMBER SAMPLE NUMBER G2.S8b

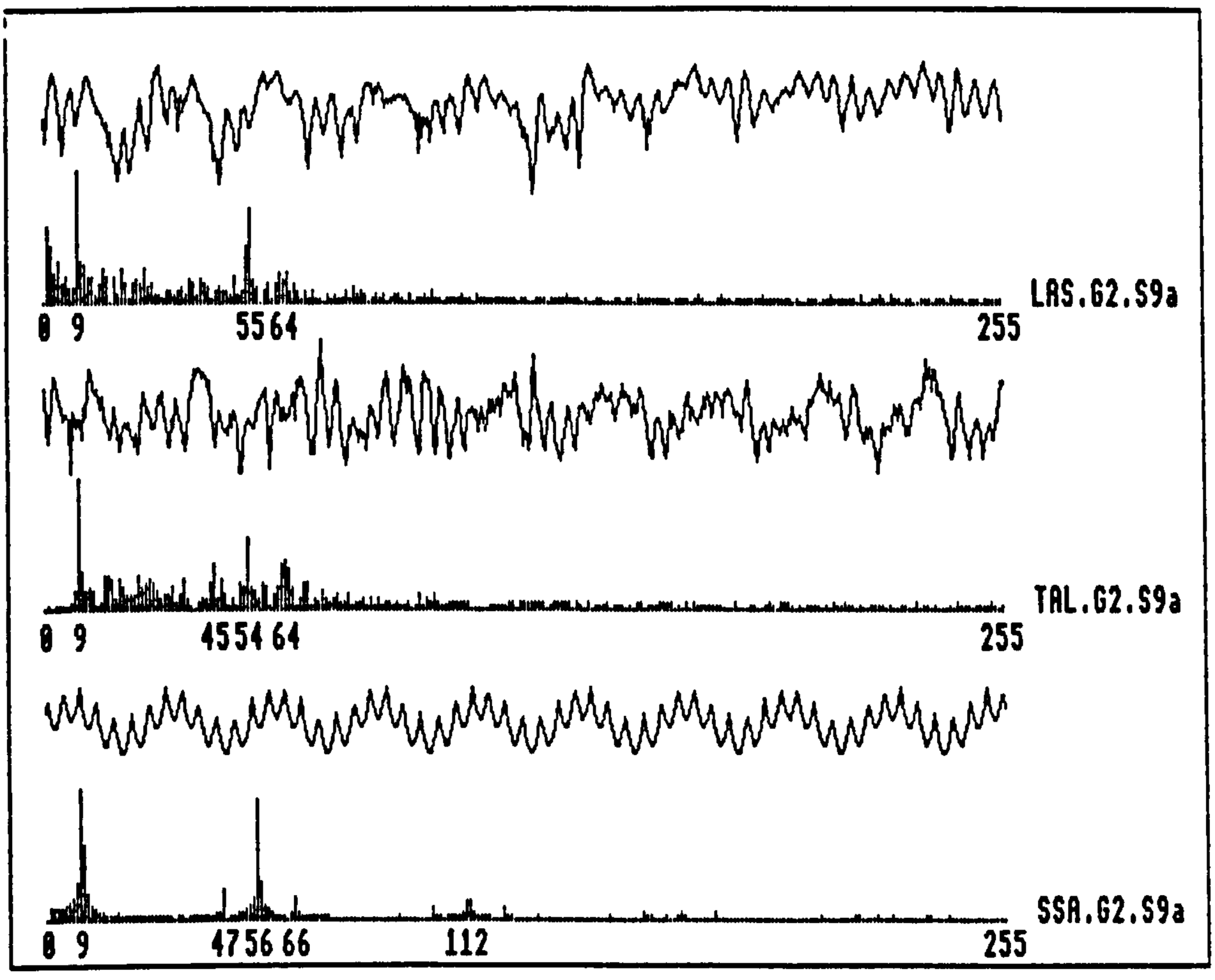

MACHINING PARAMETERS	PRINCIPAL PEAK HARMONICS
No. of knives 6 Feed speed 80 m/min Cutter Speed 6000 rpm Vib. rate 0 Proud Knives 0 Ecc.rate/rev 1 Spindle Runout 3 microns	h1 = 9 h2 = 18 hj = 56

ANALYSIS OF FFT's USING FAULT FINDING ALGORITHM (FFA)		
FFA ON LASER DATA THRESHOLD=0.4	FFA ON TALY DATA THRESHOLD=0.4	FFA ON SSA DATA THRESHOLD=0.4
(0.balance 1) Harmonic 9 (Multi-knife) Harmonic 55	(0.balance 1) Harmonic 9 (Multi-knife) Harmonic 54	(0.balance 1) Harmonic 9 (Multi-knife) Harmonic 56

Figure 7.G2.S9a: RESULTS FOR TIMBER SAMPLE NUMBER G2.S9a

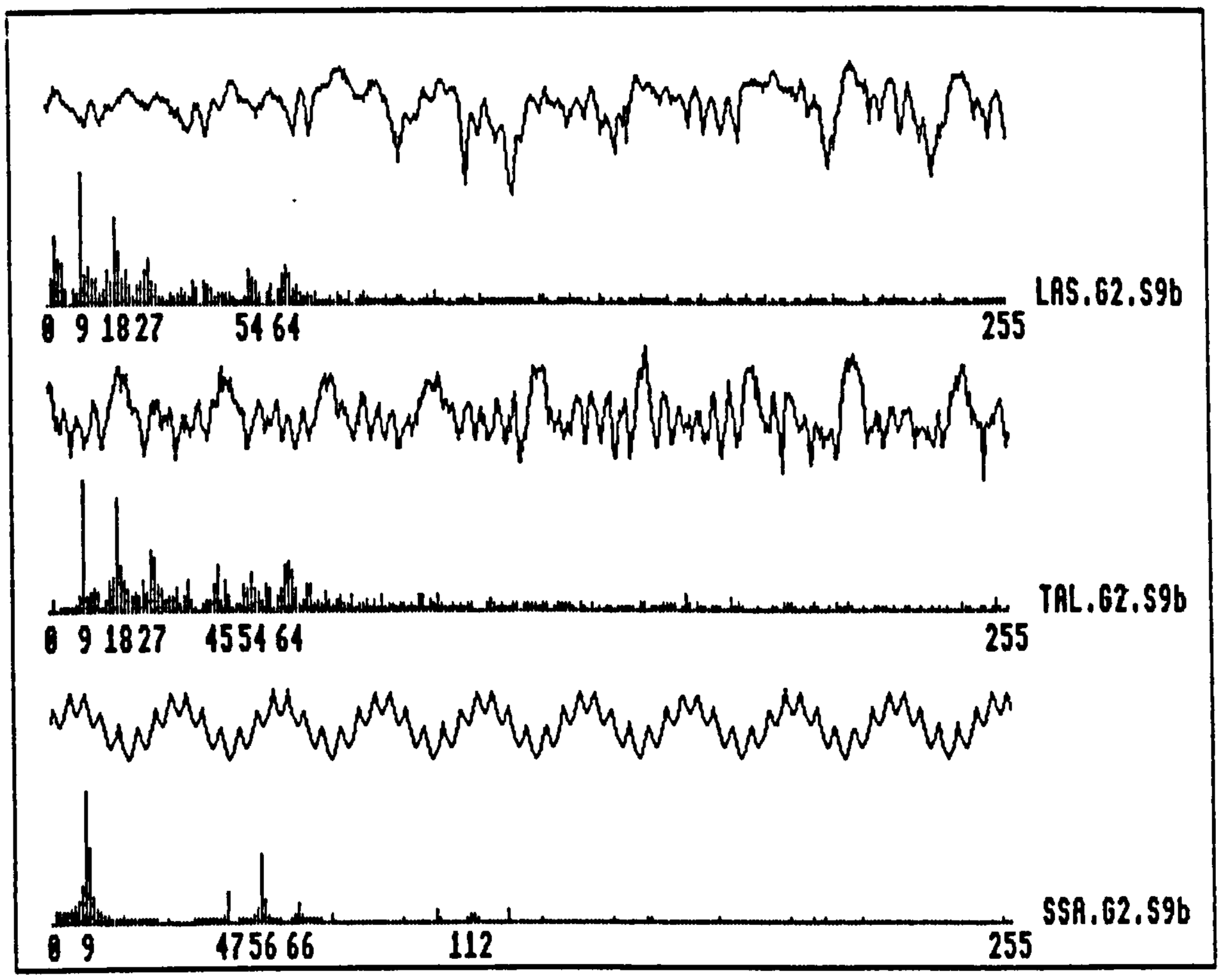

MACHINING PARAMETERS	PRINCIPAL PEAK HARMONICS
No. of knives 6 Feed speed 80 m/min Cutter Speed 6000 rpm Vib. rate 0 Proud Knives 0 Ecc.rate/rev 1 Spindle Runout 5 microns	h1 = 9 h2 = 18 hj = 56

ANALYSIS OF FFT's USING FAULT FINDING ALGORITHM (FFA)		
FFA ON LASER DATA THRESHOLD=0.4	FFA ON TALY DATA THRESHOLD=0.4	FFA ON SSA DATA THRESHOLD=0.4
(Proud Knife) Harmonic 9 Harmonic 18	(Proud Knife) Harmonic 9 Harmonic 18 Harmonic 27	(O.balance 1) Harmonic 9 (Multi-knife) Harmonic 56

Figure 7.G2.S9b: RESULTS FOR TIMBER SAMPLE NUMBER G2.S9b

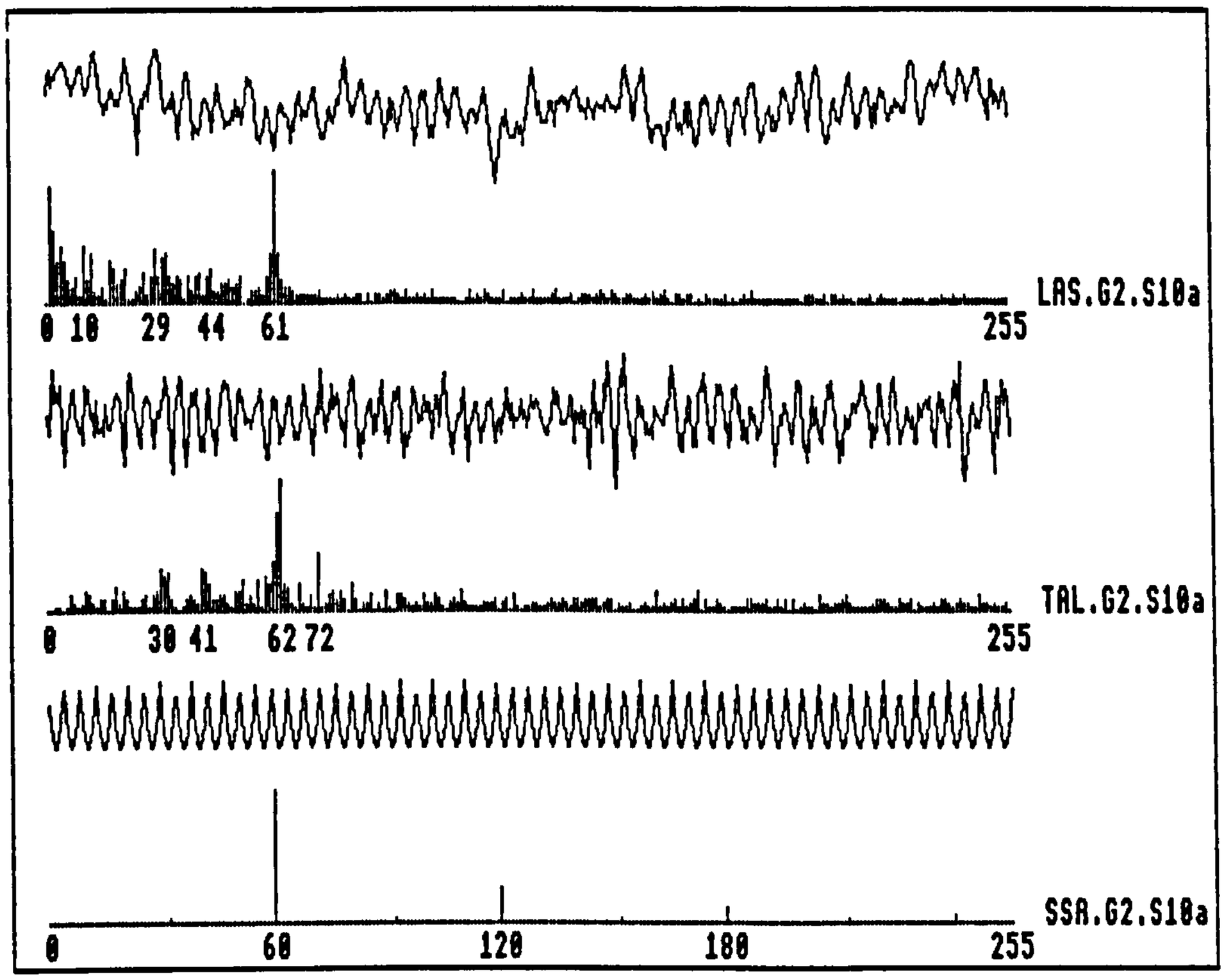

MACHINING PARAMETERS	PRINCIPAL PEAK HARMONICS
No. of knives 6 Feed speed 75 m/min Cutter Speed 6000 rpm Vib. rate 0 Proud Knives 0 Ecc.rate/rev 0 Spindle Runout 0 microns	h1 = 10 h2 = 20 hj = 60

ANALYSIS OF FFT's USING FAULT FINDING ALGORITHM (FFA)		
FFA ON LASER DATA THRESHOLD=0.4	FFA ON TALY DATA THRESHOLD=0.4	FFA ON SSA DATA THRESHOLD=0.4
(O.balance 1) Harmonic 10 (Multi-knife) Harmonic 61 (Unknown Faults) Harmonic 29	(Multi-knife) Harmonic 62 (Unknown Faults) Harmonic 72	(Multi-knife) Harmonic 60

Figure 7.G2.S10a: RESULTS FOR TIMBER SAMPLE NUMBER G2.S10a

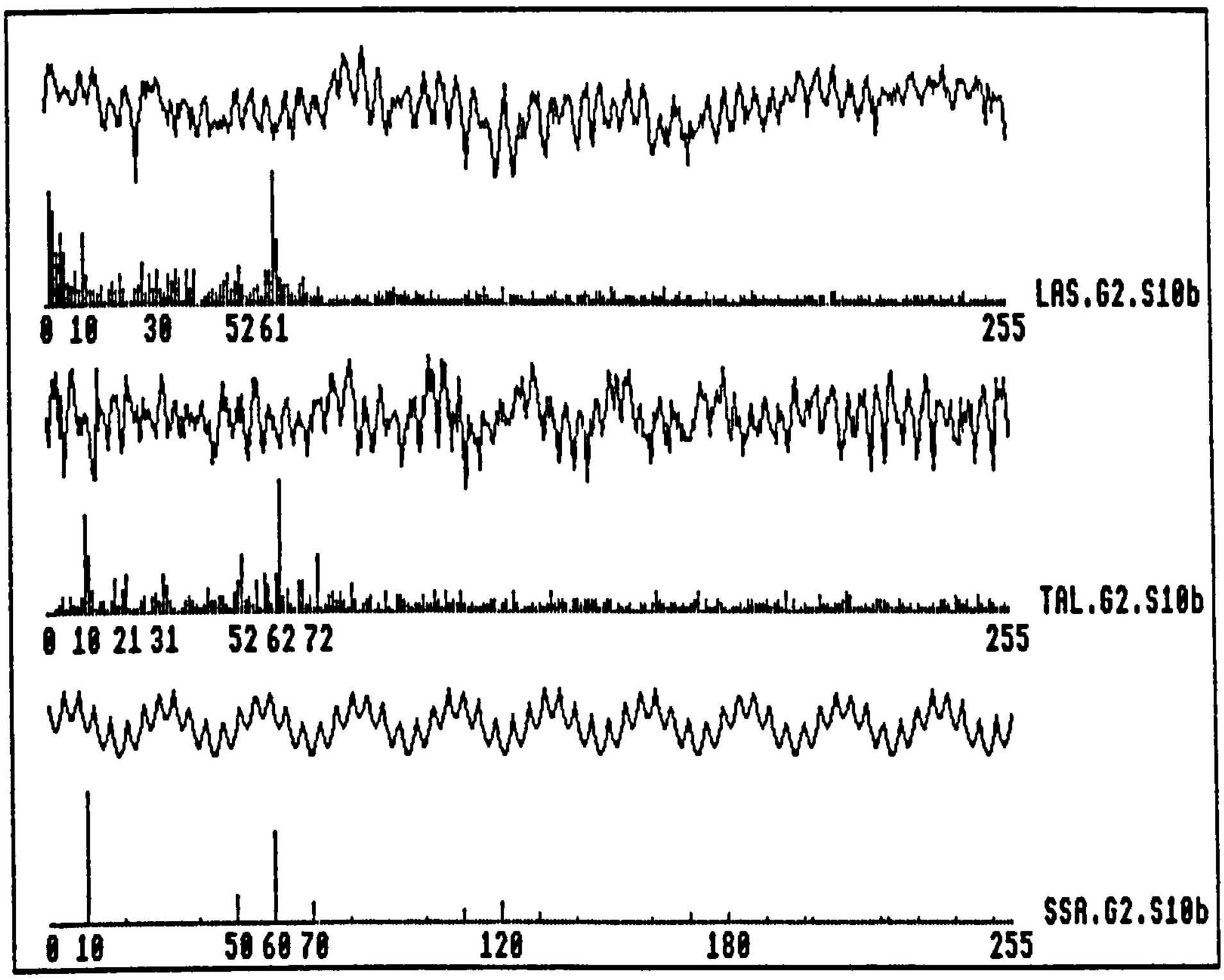

MACHINING PARAMETERS	PRINCIPAL PEAK HARMONICS
No. of knives 6 Feed speed 75 m/min Cutter Speed 6000 rpm Vib. rate 0 Proud Knives 0 Ecc.rate/rev 1 Spindle Runout 3 microns	h1 = 10 h2 = 20 hj = 60

ANALYSIS OF FFT's USING FAULT FINDING ALGORITHM (FFA)		
FFA ON LASER DATA THRESHOLD=0.4	FFA ON TALY DATA THRESHOLD=0.4	FFA ON SSA DATA THRESHOLD=0.4
(0.balance 1) Harmonic 10 (Multi-knife) Harmonic 61	(0.balance 1) Harmonic 10 (Multi-knife) Harmonic 62 (Unknown Faults) Harmonic 52 Harmonic 72	(0.balance 1) Harmonic 10 (Multi-knife) Harmonic 60

Figure 7.62.S10b: RESULTS FOR TIMBER SAMPLE NUMBER 62.S10b

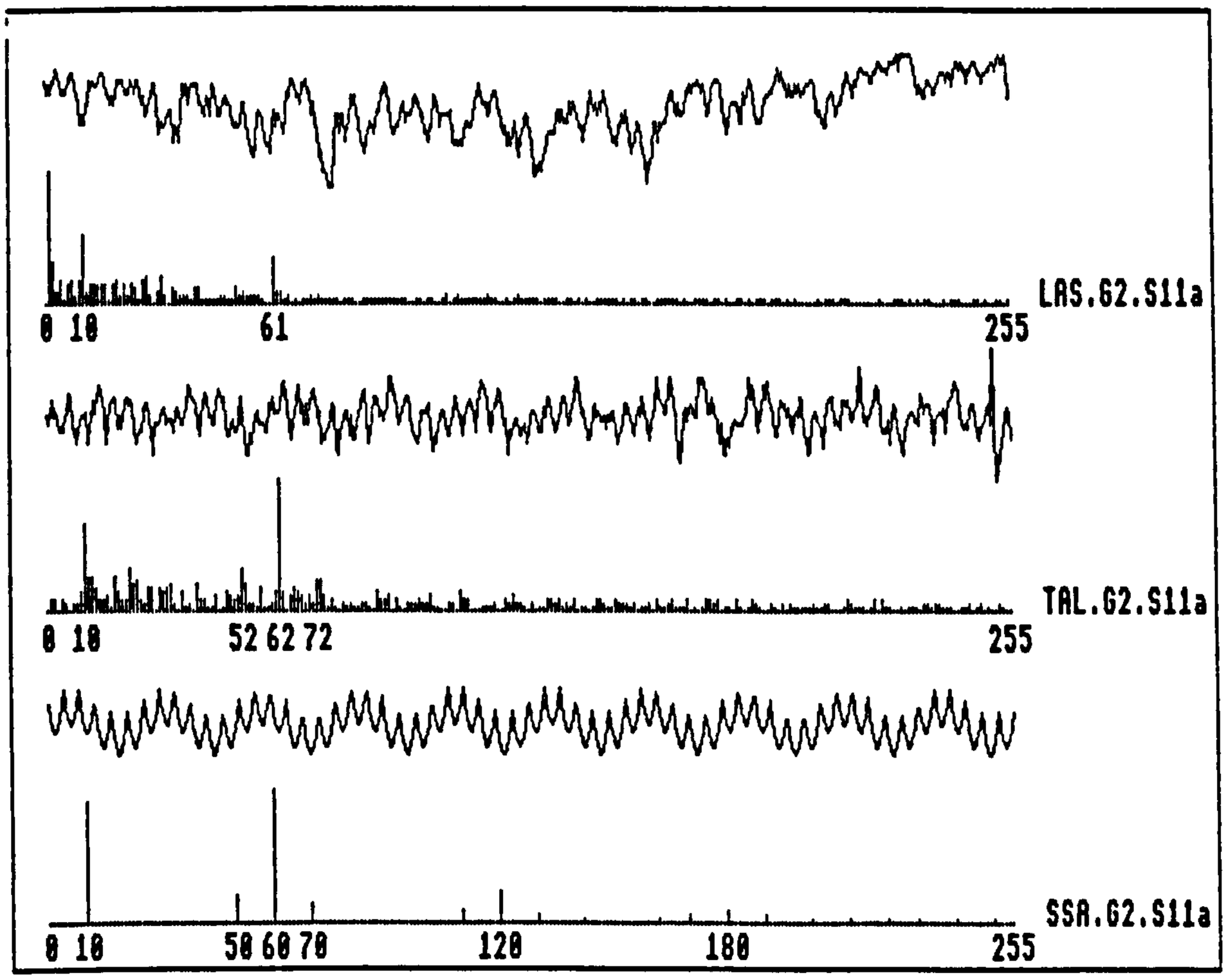

MACHINING PARAMETERS		PRINCIPAL PEAK HARMONICS
No. of knives	6	h1 = 10 h2 = 20 hj = 60
Feed speed	75 m/min	
Cutter Speed	6000 rpm	
Vib. rate	0	
Proud Knives	0	
Ecc.rate/rev	1	
Spindle Runout	2 microns	

ANALYSIS OF FFT's USING FAULT FINDING ALGORITHM (FFA)		
FFA ON LASER DATA THRESHOLD=0.4	FFA ON TALY DATA THRESHOLD=0.4	FFA ON SSA DATA THRESHOLD=0.4
(0.balance 1) Harmonic 10 (Multi-knife) Harmonic 61 (Unknown Faults) Harmonic 27	(0.balance 1) Harmonic 10 (Multi-knife) Harmonic 62	(0.balance 1) Harmonic 10 (Multi-knife) Harmonic 60

Figure 7.G2.S11a: RESULTS FOR TIMBER SAMPLE NUMBER G2.S11a

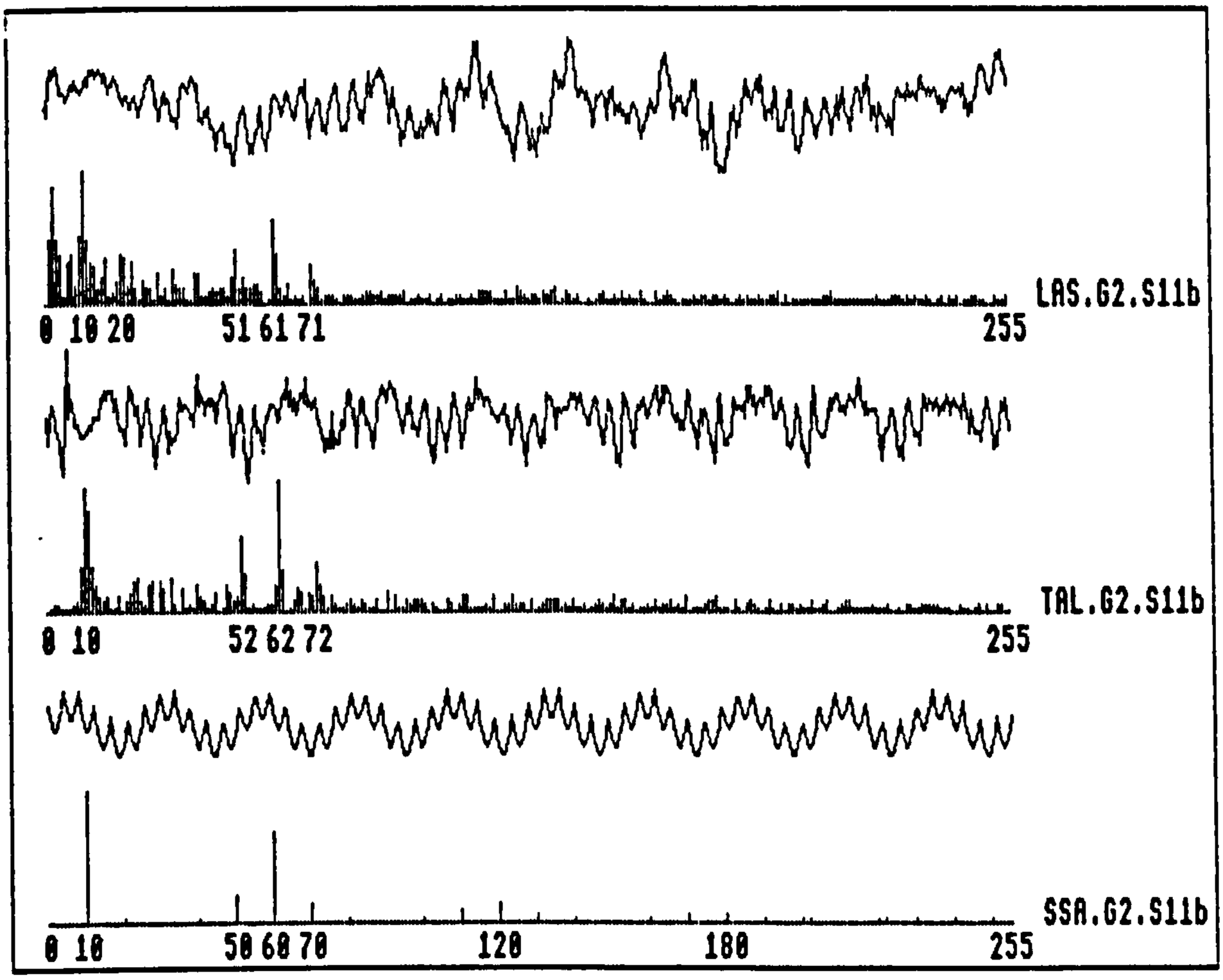

MACHINING PARAMETERS	PRINCIPAL PEAK HARMONICS
No. of knives 6 Feed speed 75 m/min Cutter Speed 6000 rpm Vib. rate 0 Proud Knives 0 Ecc.rate/rev 1 Spindle Runout 3 microns	h1 = 10 h2 = 20 hj = 60

ANALYSIS OF FFT's USING FAULT FINDING ALGORITHM (FFA)		
FFA ON LASER DATA THRESHOLD=0.4	FFA ON TALY DATA THRESHOLD=0.4	FFA ON SSA DATA THRESHOLD=0.4
(0.balance 1) Harmonic 10 (Multi-knife) Harmonic 61 (Unknown Faults) Harmonic 51	(0.balance 1) Harmonic 10 (Multi-knife) Harmonic 62 (Unknown Faults) Harmonic 52	(0.balance 1) Harmonic 10 (Multi-knife) Harmonic 60

Figure 7.G2.S11b: RESULTS FOR TIMBER SAMPLE NUMBER G2.S11b

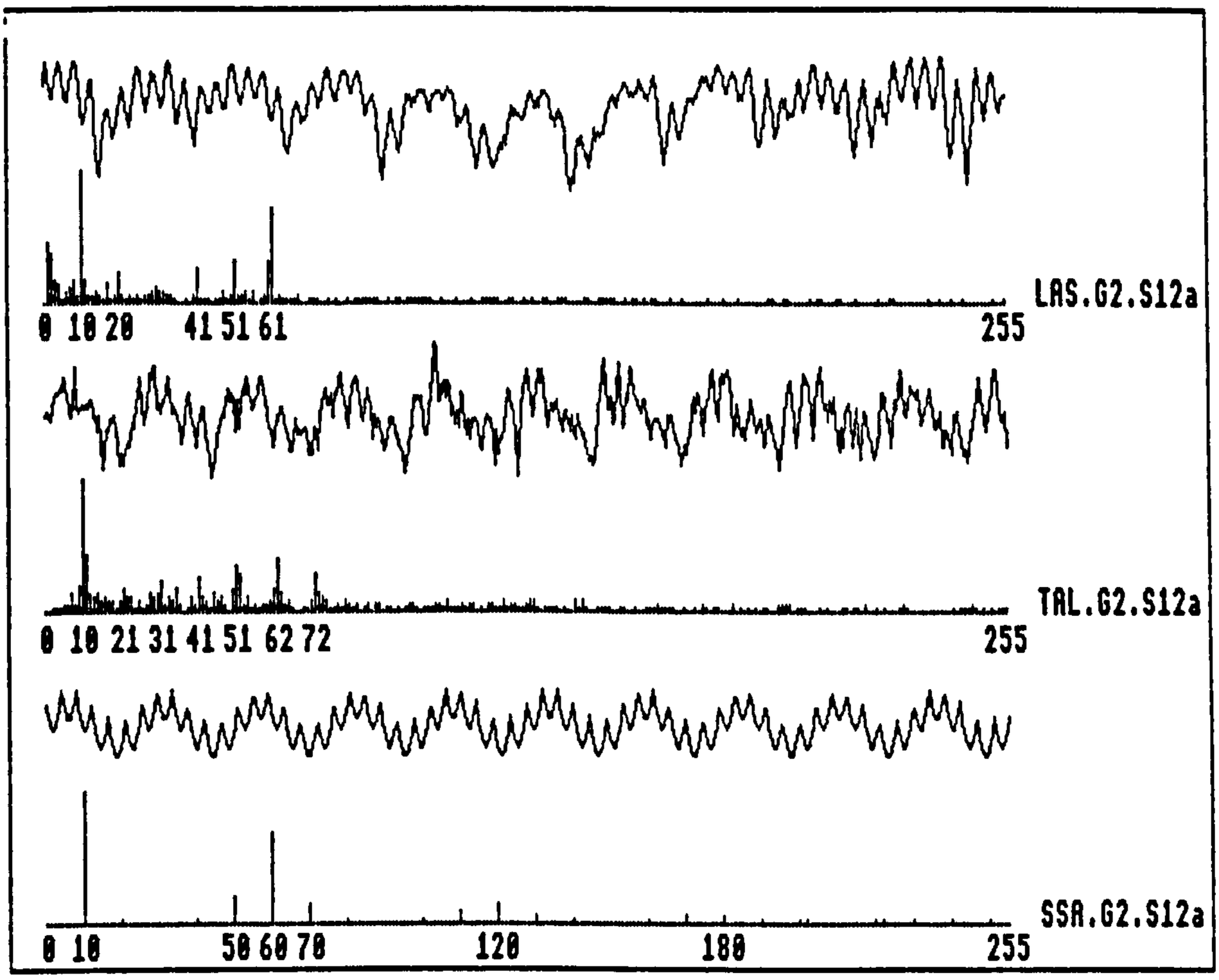

MACHINING PARAMETERS	PRINCIPAL PEAK HARMONICS
No. of knives 6 Feed speed 75 m/min Cutter Speed 6000 rpm Vib. rate 0 Proud Knives 0 Ecc.rate/rev 1 Spindle Runout 3 microns	h1 = 10 h2 = 20 hj = 60

ANALYSIS OF FFT's USING FAULT FINDING ALGORITHM (FFA)		
FFA ON LASER DATA THRESHOLD=0.4	FFA ON TALY DATA THRESHOLD=0.4	FFA ON SSA DATA THRESHOLD=0.4
(O.balance 1) Harmonic 10 (Multi-knife) Harmonic 61	(O.balance 1) Harmonic 10 (Multi-knife) Harmonic 62	(O.balance 1) Harmonic 10 (Multi-knife) Harmonic 60

Figure 7.G2.S12a: RESULTS FOR TIMBER SAMPLE NUMBER G2.S12a

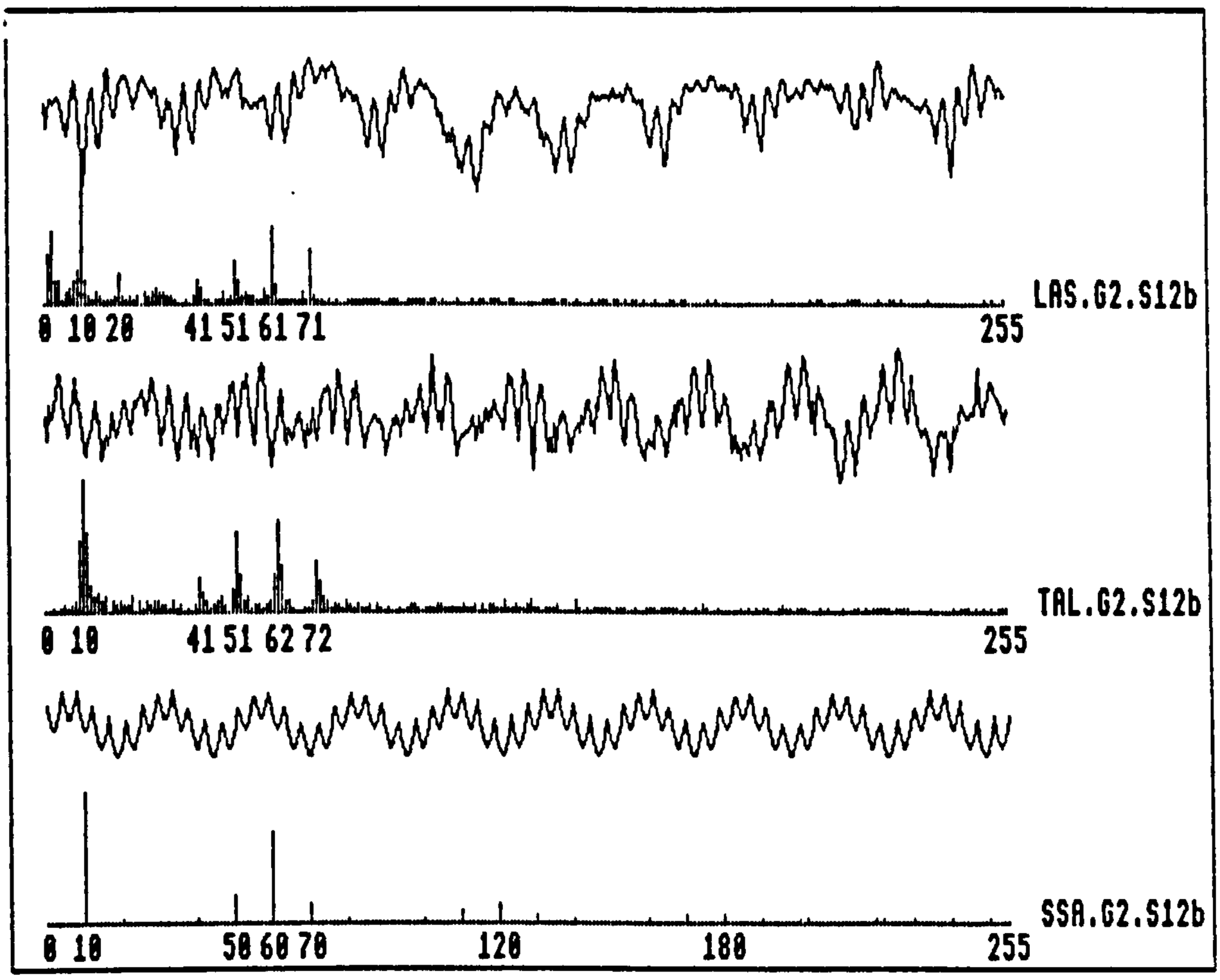

MACHINING PARAMETERS	PRINCIPAL PEAK HARMONICS
No. of knives 6 Feed speed 75 m/min Cutter Speed 6000 rpm Vib. rate 0 Proud Knives 0 Ecc.rate/rev 1 Spindle Runout 3 microns	h1 = 10 h2 = 20 hj = 60

ANALYSIS OF FFT's USING FAULT FINDING ALGORITHM (FFA)		
FFA ON LASER DATA THRESHOLD=0.4	FFA ON TALY DATA THRESHOLD=0.4	FFA ON SSA DATA THRESHOLD=0.4
(0.balance 1) Harmonic 10 (Multi-knife) Harmonic 61 (Unknown Faults) Harmonic 71	(0.balance 1) Harmonic 10 (Multi-knife) Harmonic 62 (Unknown Faults) Harmonic 51	(0.balance 1) Harmonic 10 (Multi-knife) Harmonic 60

Figure 7.G2.S12b: RESULTS FOR TIMBER SAMPLE NUMBER G2.S12b

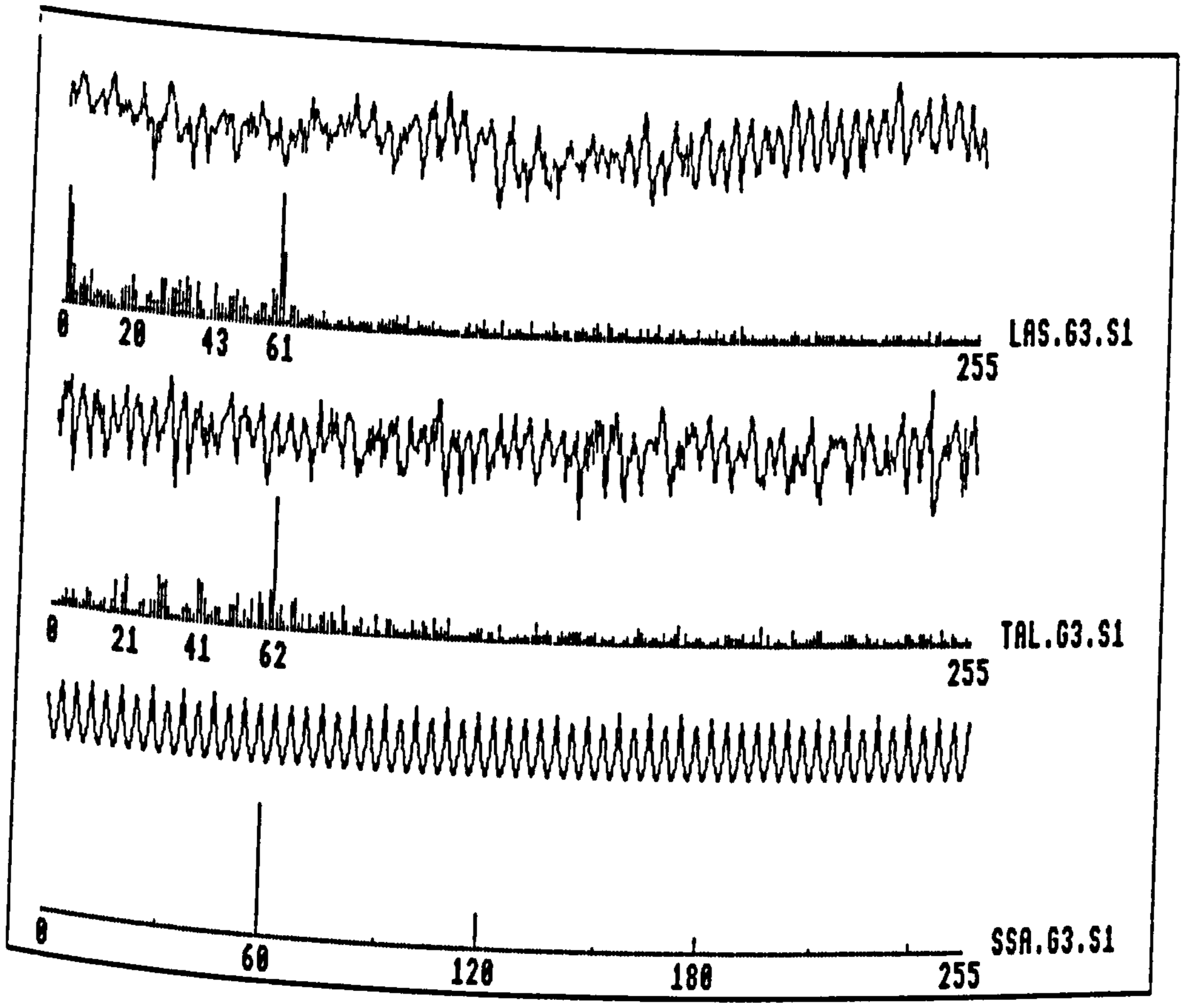

MACHINING PARAMETERS		PRINCIPAL PEAK HARMONICS
No. of knives	6	h1 = 10 h2 = 20 hj = 60
Feed speed	75 m/min	
Cutter Speed	6000 rpm	
Vib. rate	0	
Proud Knives	0	
Ecc.rate/rev	0	
Spindle Runout	0 microns	

ANALYSIS OF FFT's USING FAULT FINDING ALGORITHM (FFA)		
FFA ON LASER DATA THRESHOLD=0.4	FFA ON TALY DATA THRESHOLD=0.4	FFA ON SSA DATA THRESHOLD=0.4
(Multi-knife) Harmonic 61	(Multi-knife) Harmonic 62	(Multi-knife) Harmonic 60

Figure 7.G3.S1: RESULTS FOR TIMBER SAMPLE NUMBER G3.S1

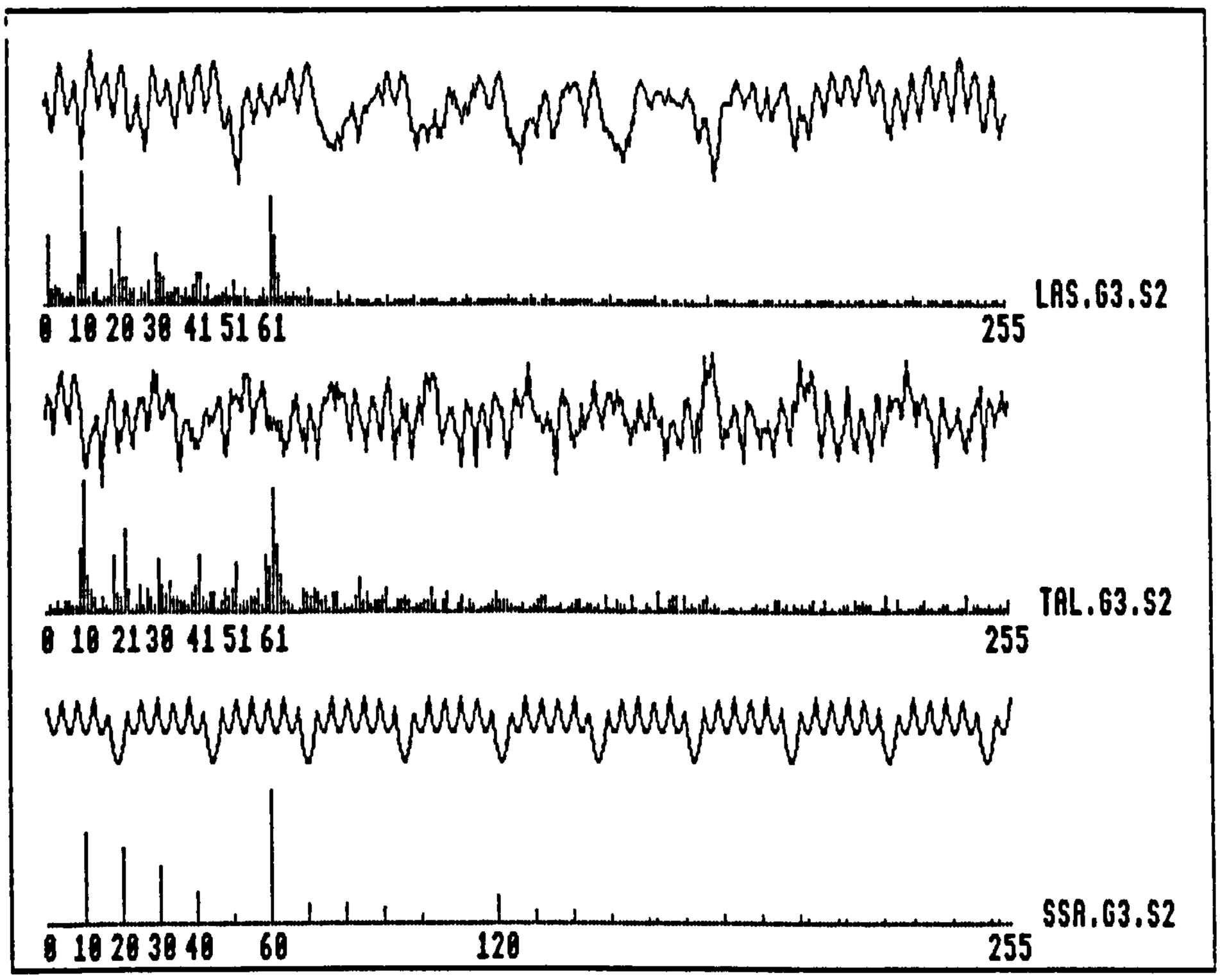

MACHINING PARAMETERS	PRINCIPAL PEAK HARMONICS
No. of knives 6 Feed speed 75 m/min Cutter Speed 6000 rpm Vib. rate 0 Proud Knives 1 >>> 1 Ecc.rate/rev 0 Spindle Runout 0 microns	h1 = 10 h2 = 20 hj = 60

ANALYSIS OF FFT's USING FAULT FINDING ALGORITHM (FFA)		
FFA ON LASER DATA THRESHOLD=0.4	FFA ON TALY DATA THRESHOLD=0.4	FFA ON SSA DATA THRESHOLD=0.4
(Proud Knife) Harmonic 10 Harmonic 20 (Multi-knife) Harmonic 61	(Proud Knife) Harmonic 10 Harmonic 21 Harmonic 30 Harmonic 41 (Multi-knife) Harmonic 61	(Proud Knife) Harmonic 10 Harmonic 20 Harmonic 30 (Multi-knife) Harmonic 60

Figure 7.G3.S2: RESULTS FOR TIMBER SAMPLE NUMBER G3.S2

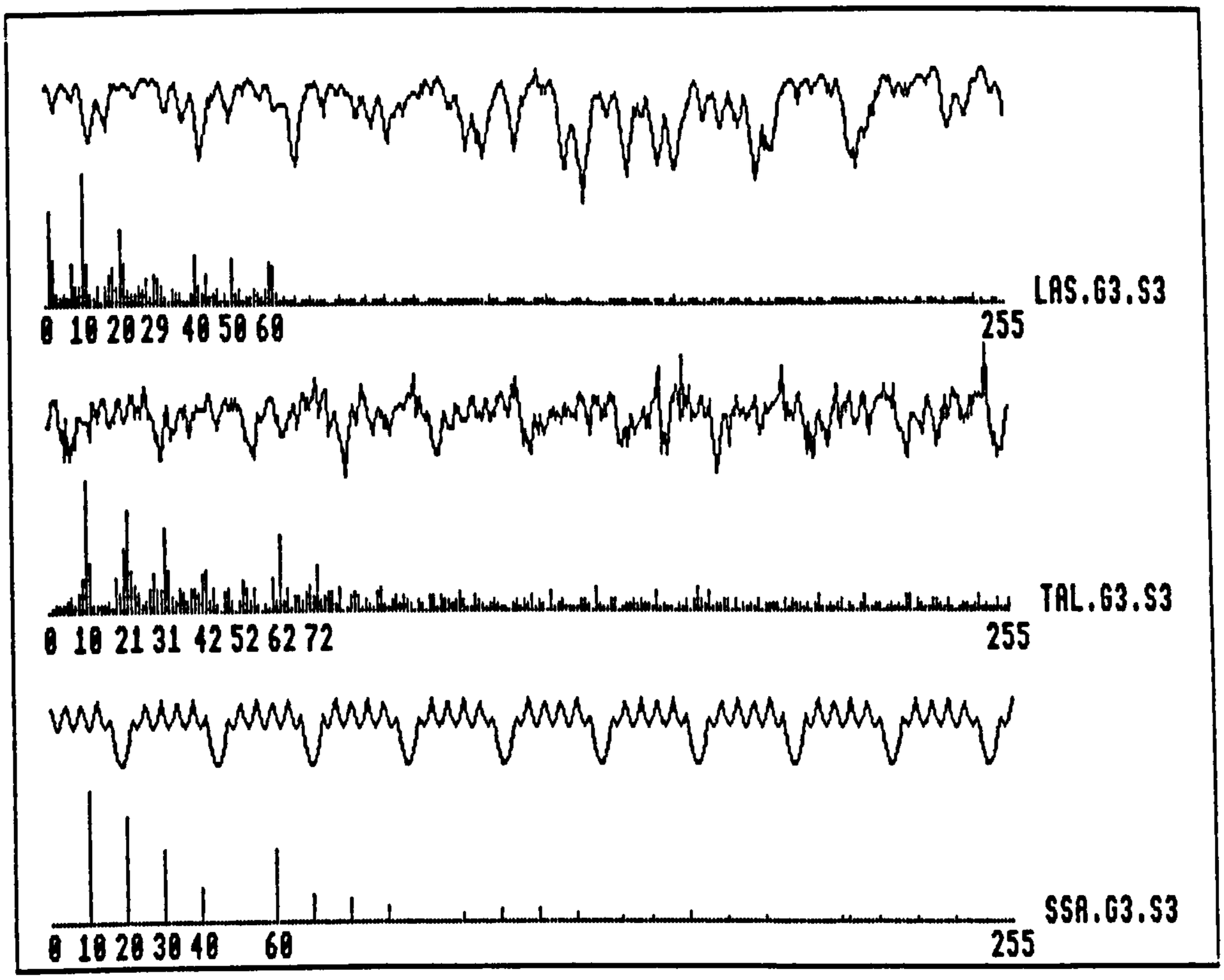

MACHINING PARAMETERS	PRINCIPAL PEAK HARMONICS
No. of knives 6 Feed speed 75 m/min Cutter Speed 6000 rpm Vib. rate 0 Proud Knives 1 >>> 1 Ecc.rate/rev 0 Spindle Runout 0 microns	h1 = 10 h2 = 20 hj = 60

ANALYSIS OF FFT's USING FAULT FINDING ALGORITHM (FFA)		
FFA ON LASER DATA THRESHOLD=0.4	FFA ON TALY DATA THRESHOLD=0.4	FFA ON SSA DATA THRESHOLD=0.4
(Proud Knife) Harmonic 10 Harmonic 20	(Proud Knife) Harmonic 10 Harmonic 21 Harmonic 31 (Multi-knife) Harmonic 62	(Proud Knife) Harmonic 10 Harmonic 20 Harmonic 30 (Multi-knife) Harmonic 60

Figure 7.G3.S3: RESULTS FOR TIMBER SAMPLE NUMBER G3.S3

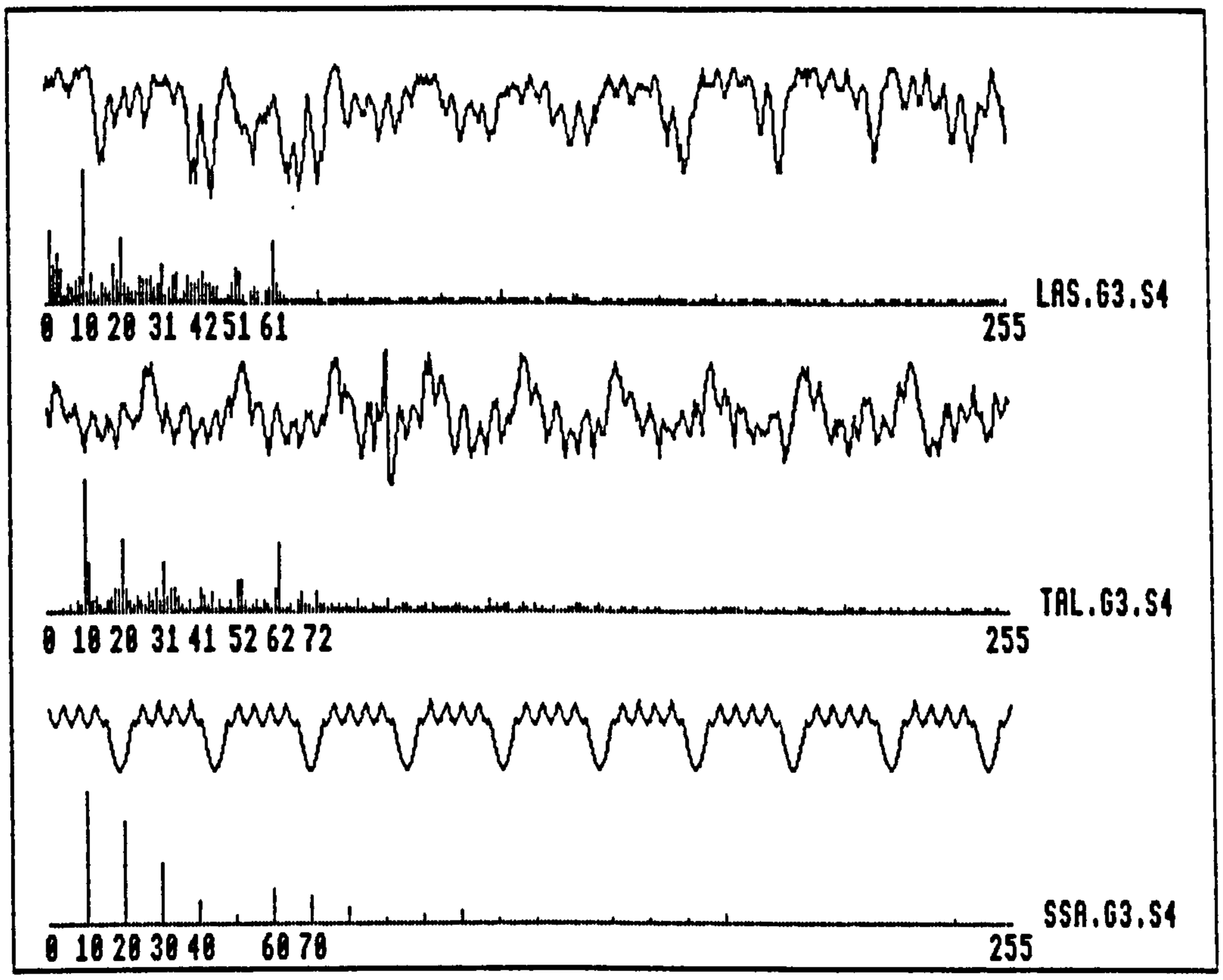

MACHINING PARAMETERS	
No. of knives 6 Feed speed 75 m/min Cutter Speed 6000 rpm Vib. rate 0 Proud Knives 1))) 1 Ecc.rate/rev 0 Spindle Runout 0 microns	PRINCIPAL PEAK HARMONICS h1 = 10 h2 = 20 hj = 60

ANALYSIS OF FFT's USING FAULT FINDING ALGORITHM (FFA)		
FFA ON LASER DATA THRESHOLD=0.4	FFA ON TALY DATA THRESHOLD=0.4	FFA ON SSA DATA THRESHOLD=0.4
(Proud Knife) Harmonic 10 Harmonic 20 (Multi-knife) Harmonic 61	(Proud Knife) Harmonic 10 Harmonic 20 (Multi-knife) Harmonic 62	(Proud Knife) Harmonic 10 Harmonic 20 Harmonic 30

Figure 7.G3.S4: RESULTS FOR TIMBER SAMPLE NUMBER G3.S4

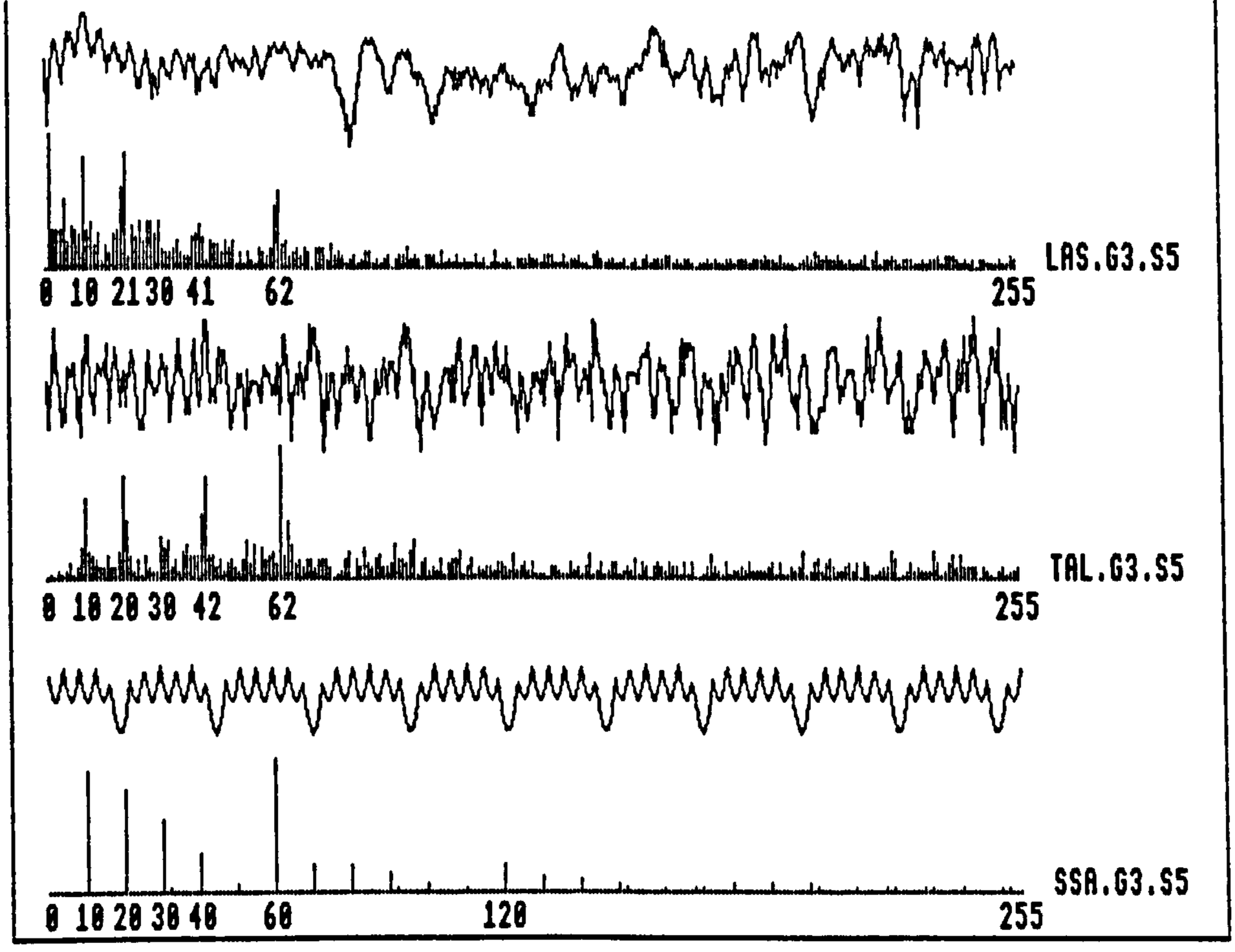

MACHINING PARAMETERS		PRINCIPAL PEAK HARMONICS
No. of knives	6	h1 = 10 h2 = 20 hj = 60
Feed speed	75 m/min	
Cutter Speed	6000 rpm	
Vib. rate	0	
Proud Knives	1 >>> 1	
Ecc.rate/rev	0	
Spindle Runout	0 microns	

ANALYSIS OF FFT's USING FAULT FINDING ALGORITHM (FFA)		
FFA ON LASER DATA THRESHOLD=0.4	FFA ON TALY DATA THRESHOLD=0.4	FFA ON SSA DATA THRESHOLD=0.4
(Proud Knife) Harmonic 10 Harmonic 21 (Multi-knife) Harmonic 62	(Proud Knife) Harmonic 10 Harmonic 20 (Multi-knife) Harmonic 62 (Unknown Faults) Harmonic 42	(Proud Knife) Harmonic 10 Harmonic 20 Harmonic 30 (Multi-knife) Harmonic 60

Figure 7.G3.S5: RESULTS FOR TIMBER SAMPLE NUMBER G3.S5

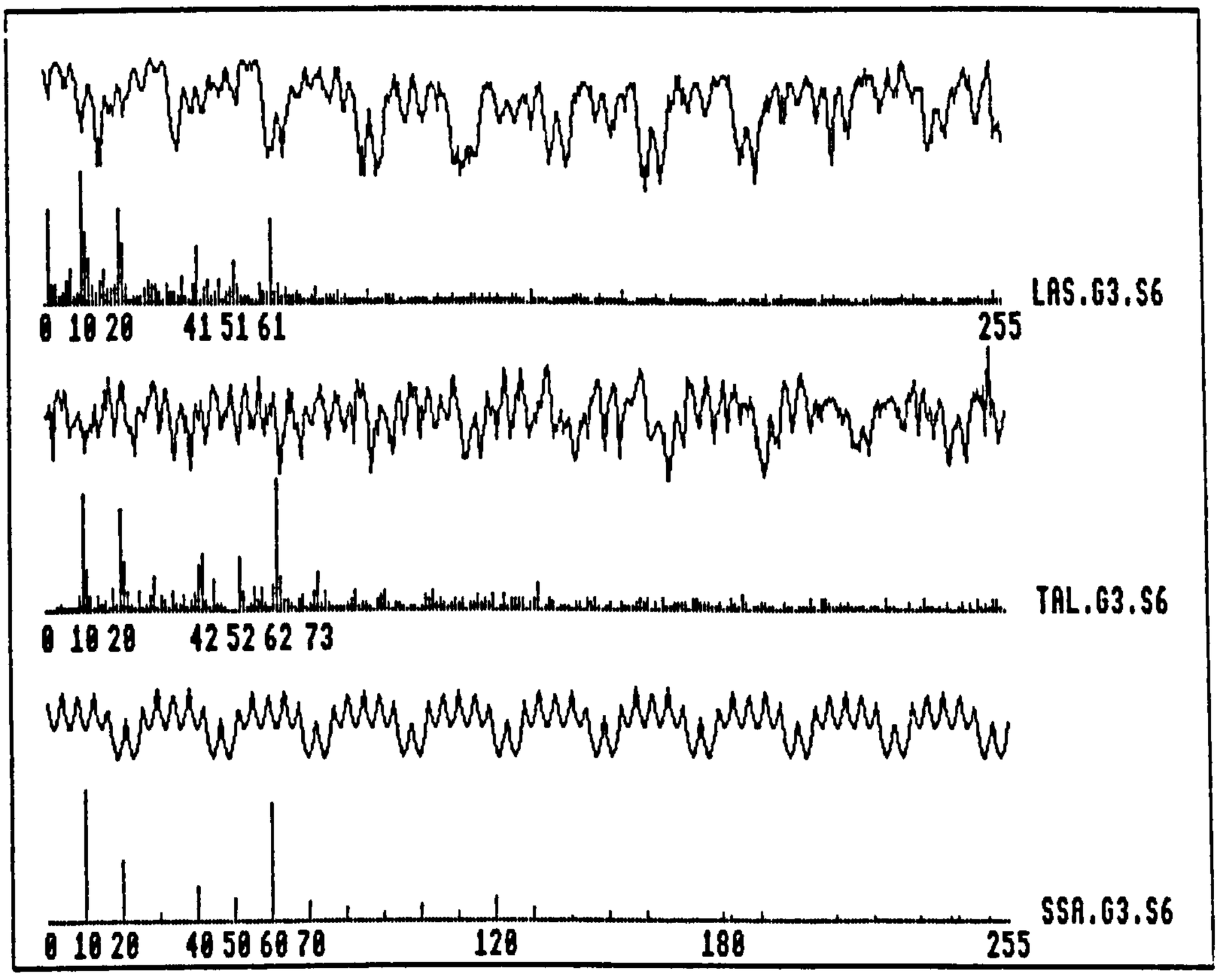

MACHINING PARAMETERS	PRINCIPAL PEAK HARMONICS
No. of knives 6 Feed speed 75 m/min Cutter Speed 6000 rpm Vib. rate 0 Proud Knives 2 >>> 1 2 Ecc.rate/rev 0 Spindle Runout 0 microns	h1 = 10 h2 = 20 hj = 60

ANALYSIS OF FFT's USING FAULT FINDING ALGORITHM (FFA)		
FFA ON LASER DATA THRESHOLD=0.4	FFA ON TALY DATA THRESHOLD=0.4	FFA ON SSA DATA THRESHOLD=0.4
(Proud Knife) Harmonic 10 Harmonic 20 (Multi-knife) Harmonic 61 (Unknown Faults) Harmonic 41	(Proud Knife) Harmonic 10 Harmonic 20 (Multi-knife) Harmonic 62 (Unknown Faults) Harmonic 42 Harmonic 52	(Proud Knife) Harmonic 10 Harmonic 20 (Multi-knife) Harmonic 60

Figure 7.G3.S6: RESULTS FOR TIMBER SAMPLE NUMBER G3.S6

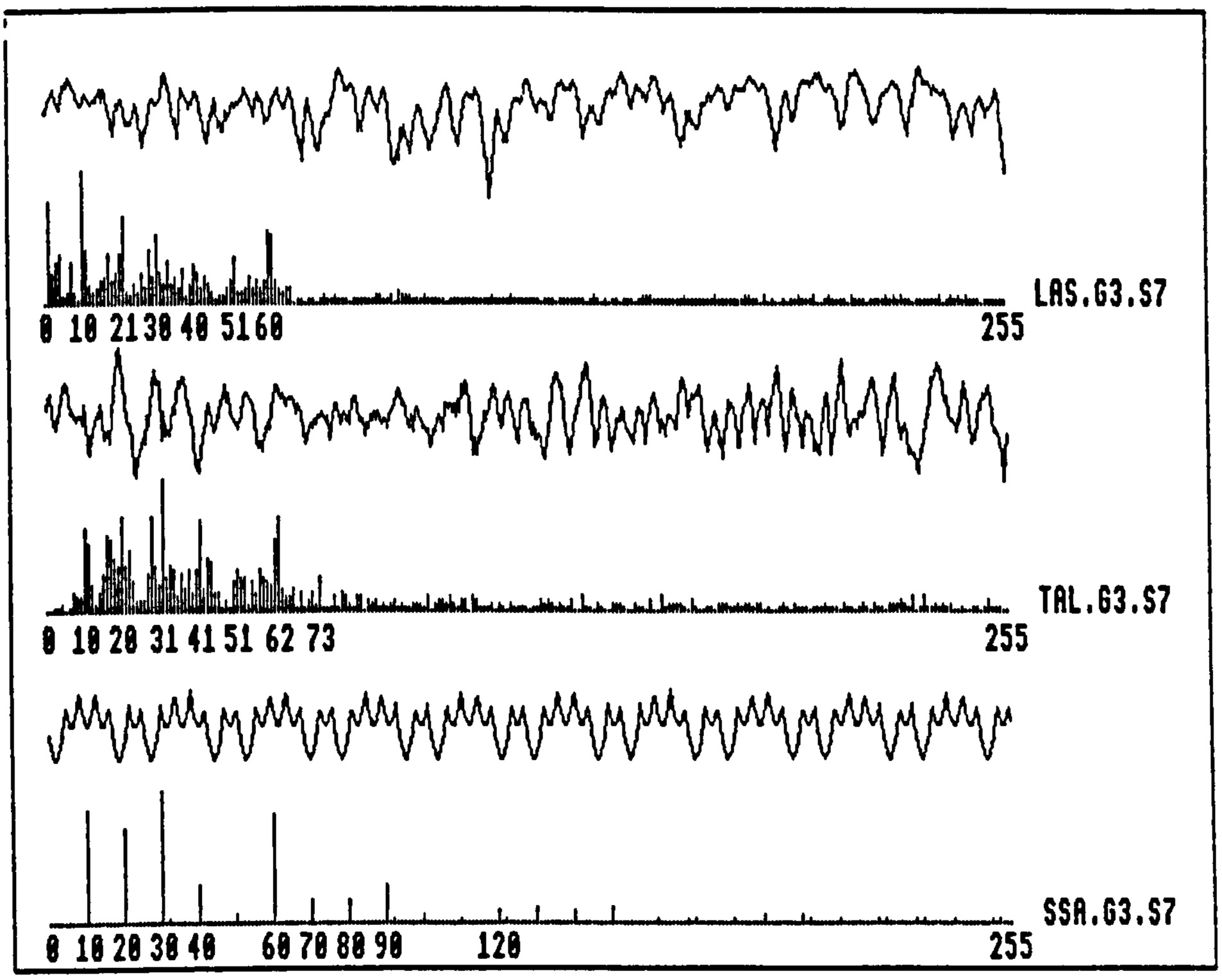

MACHINING PARAMETERS	PRINCIPAL PEAK HARMONICS
No. of knives 6 Feed speed 75 m/min Cutter Speed 6000 rpm Vib. rate 0 Proud Knives 2))) 1 3 Ecc.rate/rev 0 Spindle Runout 0 microns	h1 = 10 h2 = 20 hj = 60

ANALYSIS OF FFT's USING FAULT FINDING ALGORITHM (FFA)		
FFA ON LASER DATA THRESHOLD=0.5	FFA ON TALY DATA THRESHOLD=0.5	FFA ON SSA DATA THRESHOLD=0.5
(Proud Knife) Harmonic 10 Harmonic 21 Harmonic 30 (Multi-knife) Harmonic 60	(Proud Knife) Harmonic 10 Harmonic 20 Harmonic 31 Harmonic 41 (Multi-knife) Harmonic 62 (Unknown Faults) Harmonic 16	(Proud Knife) Harmonic 10 Harmonic 20 Harmonic 30 (Multi-knife) Harmonic 60

Figure 7.G3.S7: RESULTS FOR TIMBER SAMPLE NUMBER G3.S7

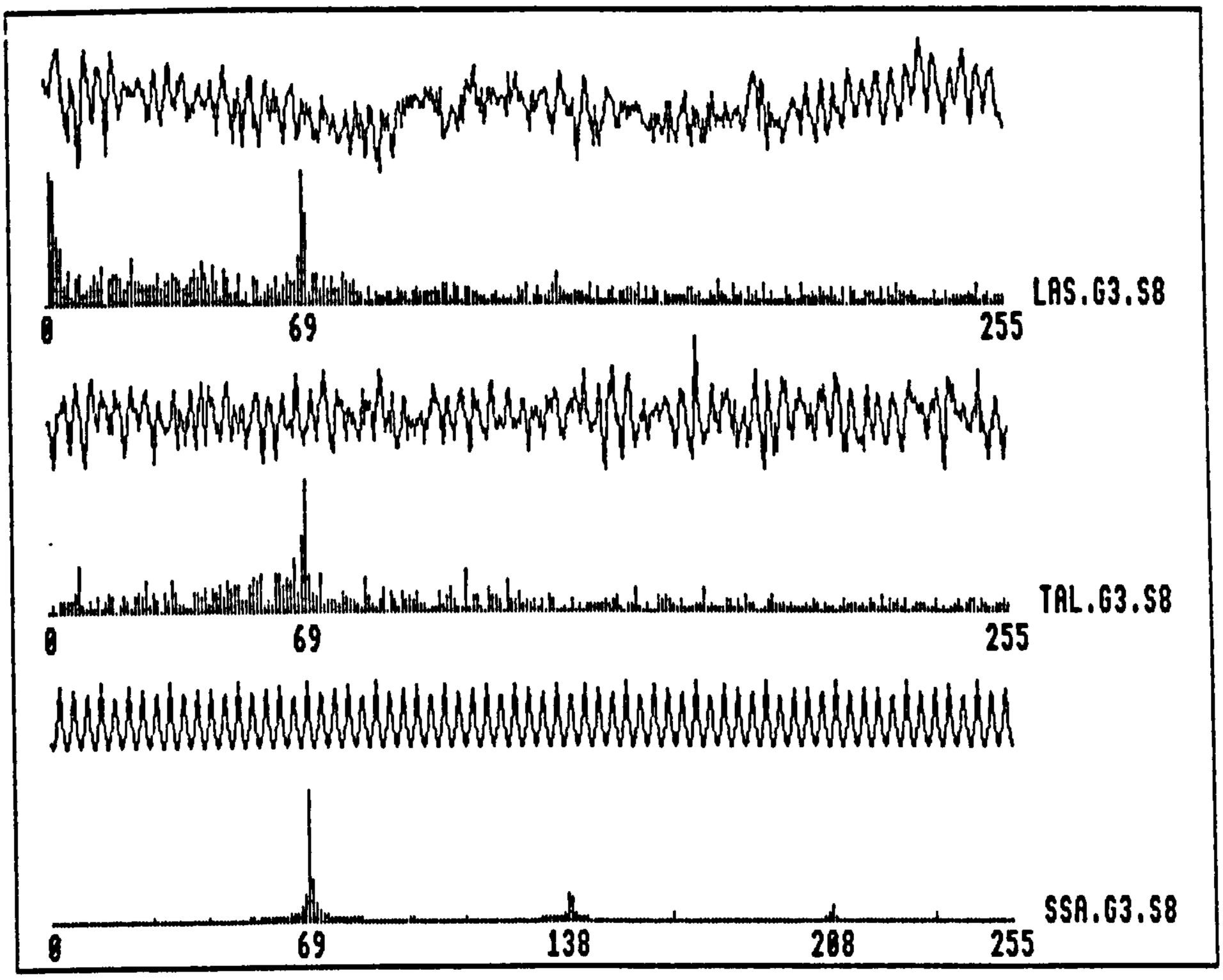

MACHINING PARAMETERS		PRINCIPAL PEAK HARMONICS
No. of knives	6	h1 = 11 h2 = 22 hj = 69
Feed speed	65 m/min	
Cutter Speed	6000 rpm	
Vib. rate	0	
Proud Knives	0	
Ecc.rate/rev	0	
Spindle Runout	0 microns	

ANALYSIS OF FFT's USING FAULT FINDING ALGORITHM (FFA)		
FFA ON LASER DATA THRESHOLD=0.4	FFA ON TALY DATA THRESHOLD=0.4	FFA ON SSA DATA THRESHOLD=0.4
(Multi-knife) Harmonic 69	(Multi-knife) Harmonic 69	(Multi-knife) Harmonic 69

Figure 7.G3.S8: RESULTS FOR TIMBER SAMPLE NUMBER G3.S8

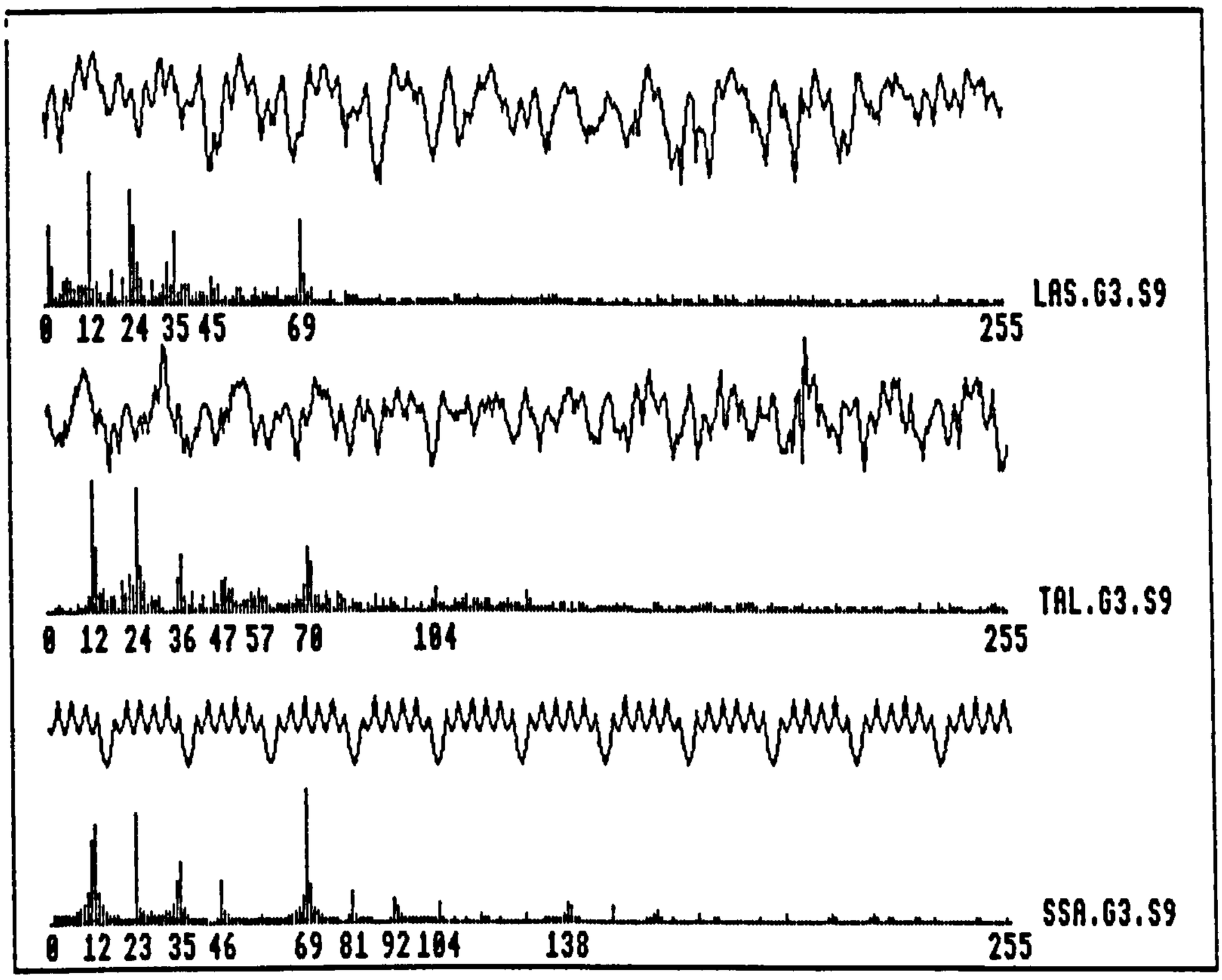

MACHINING PARAMETERS		PRINCIPAL PEAK HARMONICS
No. of knives	6	h1 = 11 h2 = 22 hj = 69
Feed speed	65 m/min	
Cutter Speed	6000 rpm	
Vib. rate	0	
Proud Knives	1)))) 1	
Ecc.rate/rev	0	
Spindle Runout	0 microns	

ANALYSIS OF FFT's USING FAULT FINDING ALGORITHM (FFA)		
FFA ON LASER DATA THRESHOLD=0.4	FFA ON TALY DATA THRESHOLD=0.4	FFA ON SSA DATA THRESHOLD=0.4
(Proud Knife) Harmonic 12 Harmonic 23 Harmonic 35 (Multi-knife) Harmonic 69	(Proud Knife) Harmonic 12 Harmonic 24 Harmonic 36 (Multi-knife) Harmonic 78	(Proud Knife) Harmonic 12 Harmonic 23 Harmonic 35 (Multi-knife) Harmonic 69

Figure 7.G3.S9: RESULTS FOR TIMBER SAMPLE NUMBER G3.S9

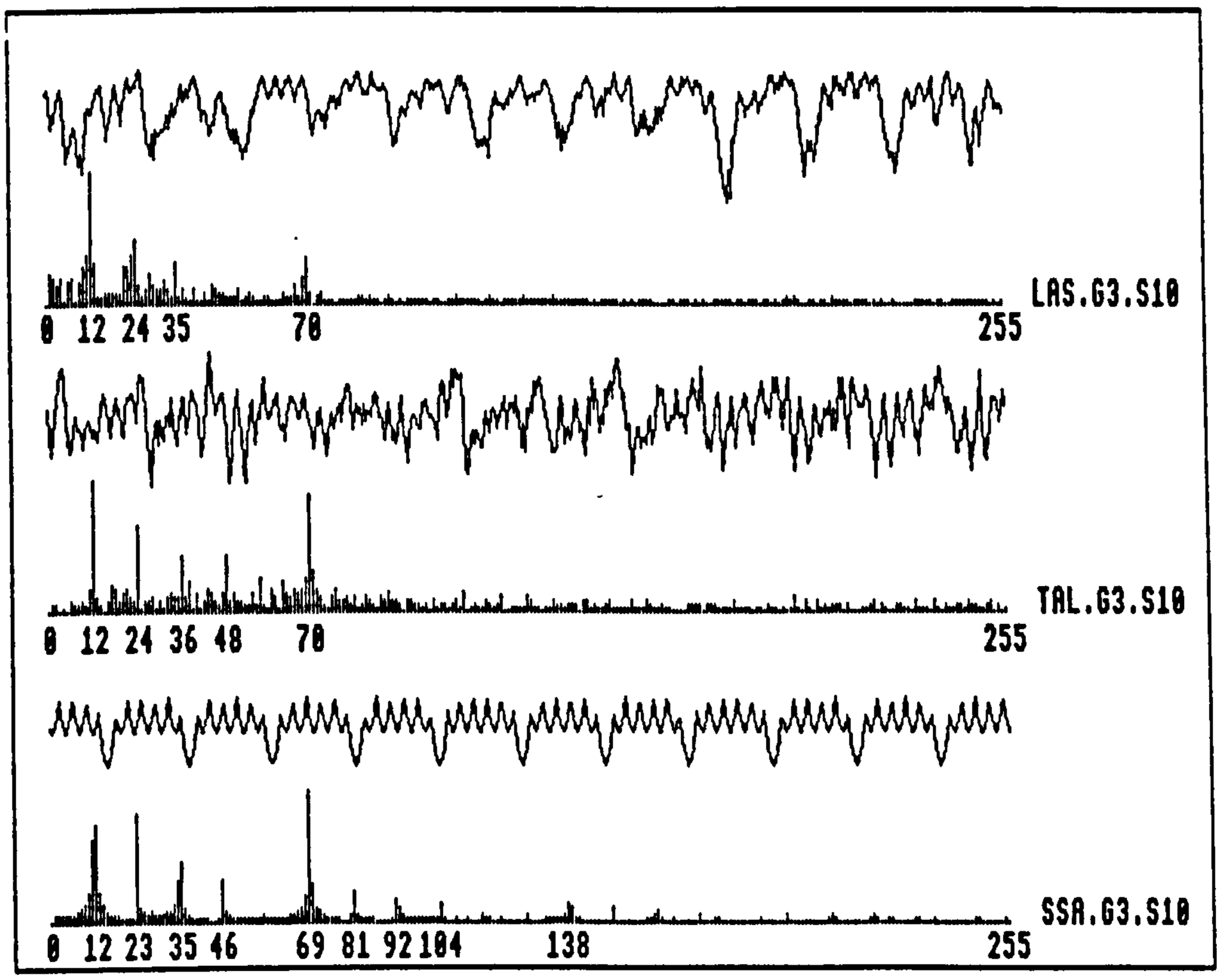

MACHINING PARAMETERS	PRINCIPAL PEAK HARMONICS
No. of knives 6 Feed speed 65 m/min Cutter Speed 6000 rpm Vib. rate 0 Proud Knives 1))) 1 Ecc.rate/rev 0 Spindle Runout 0 microns	h1 = 11 h2 = 22 hj = 69

ANALYSIS OF FFT's USING FAULT FINDING ALGORITHM (FFA)		
FFA ON LASER DATA THRESHOLD=0.4	FFA ON TALY DATA THRESHOLD=0.4	FFA ON SSA DATA THRESHOLD=0.4
(Proud Knife) Harmonic 12 Harmonic 24	(Proud Knife) Harmonic 12 Harmonic 24 Harmonic 36 Harmonic 48 (Multi-knife) Harmonic 70	(Proud Knife) Harmonic 12 Harmonic 23 Harmonic 35 (Multi-knife) Harmonic 69

Figure 7.G3.S10: RESULTS FOR TIMBER SAMPLE NUMBER G3.S10

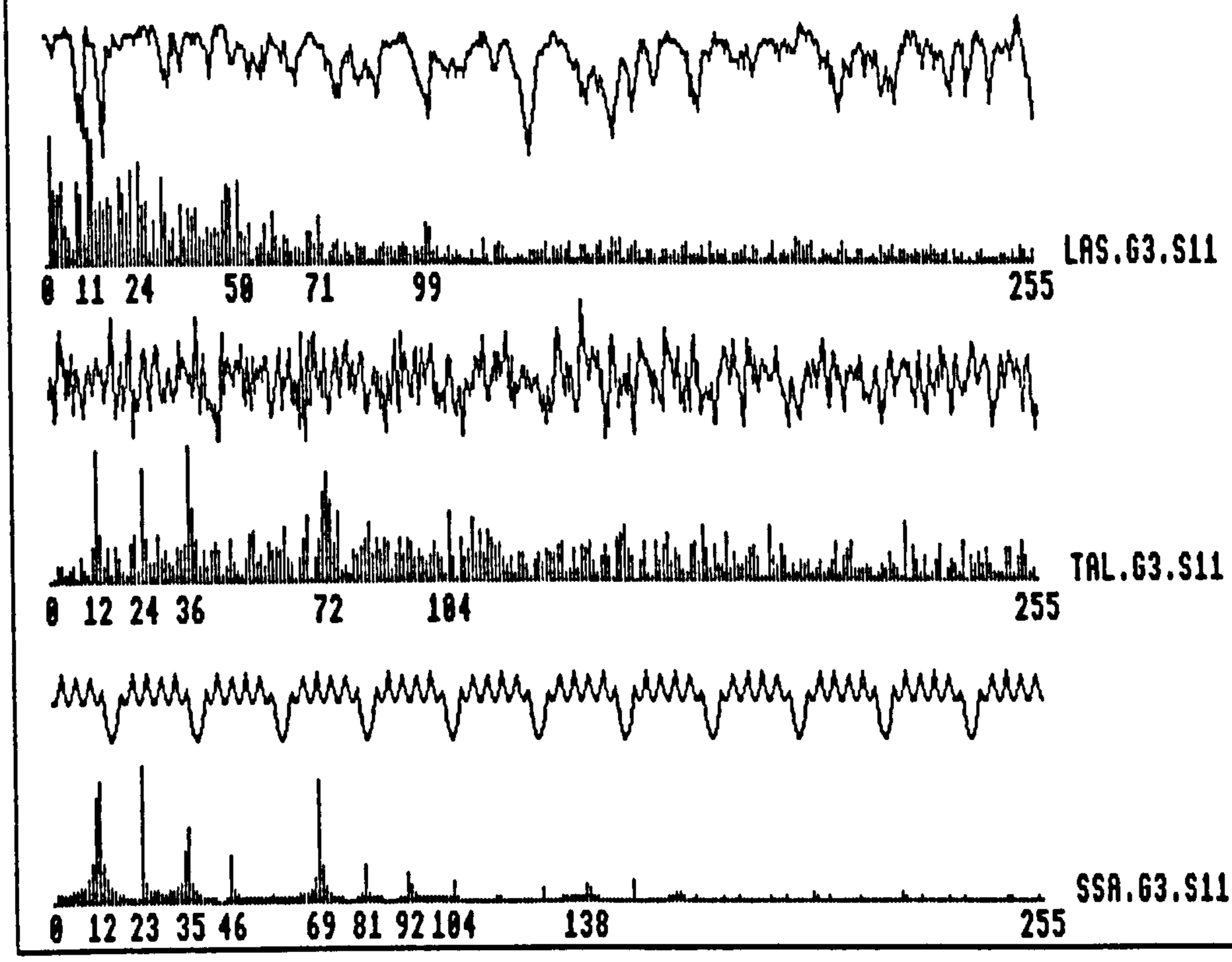

MACHINING PARAMETERS	PRINCIPAL PEAK HARMONICS
No. of knives 6 Feed speed 65 m/min Cutter Speed 6000 rpm Vib. rate 0 Proud Knives 1)))) 1 Ecc.rate/rev 0 Spindle Runout 0 microns	h1 = 11 h2 = 22 hj = 69

ANALYSIS OF FFT's USING FAULT FINDING ALGORITHM (FFA)		
FFA ON LASER DATA THRESHOLD=0.5	FFA ON TALY DATA THRESHOLD=0.5	FFA ON SSA DATA THRESHOLD=0.5
(Proud Knife) Harmonic 11 Harmonic 24 (Unknown Faults) Harmonic 30 Harmonic 50	(Proud Knife) Harmonic 12 Harmonic 24 Harmonic 36 (Multi-knife) Harmonic 67 (Digital noise) Harmonic 104 (Unknown Faults) Harmonic 72	(Proud Knife) Harmonic 12 Harmonic 23 Harmonic 35 (Multi-knife) Harmonic 69

Figure 7.G3.S11: RESULTS FOR TIMBER SAMPLE NUMBER G3.S11

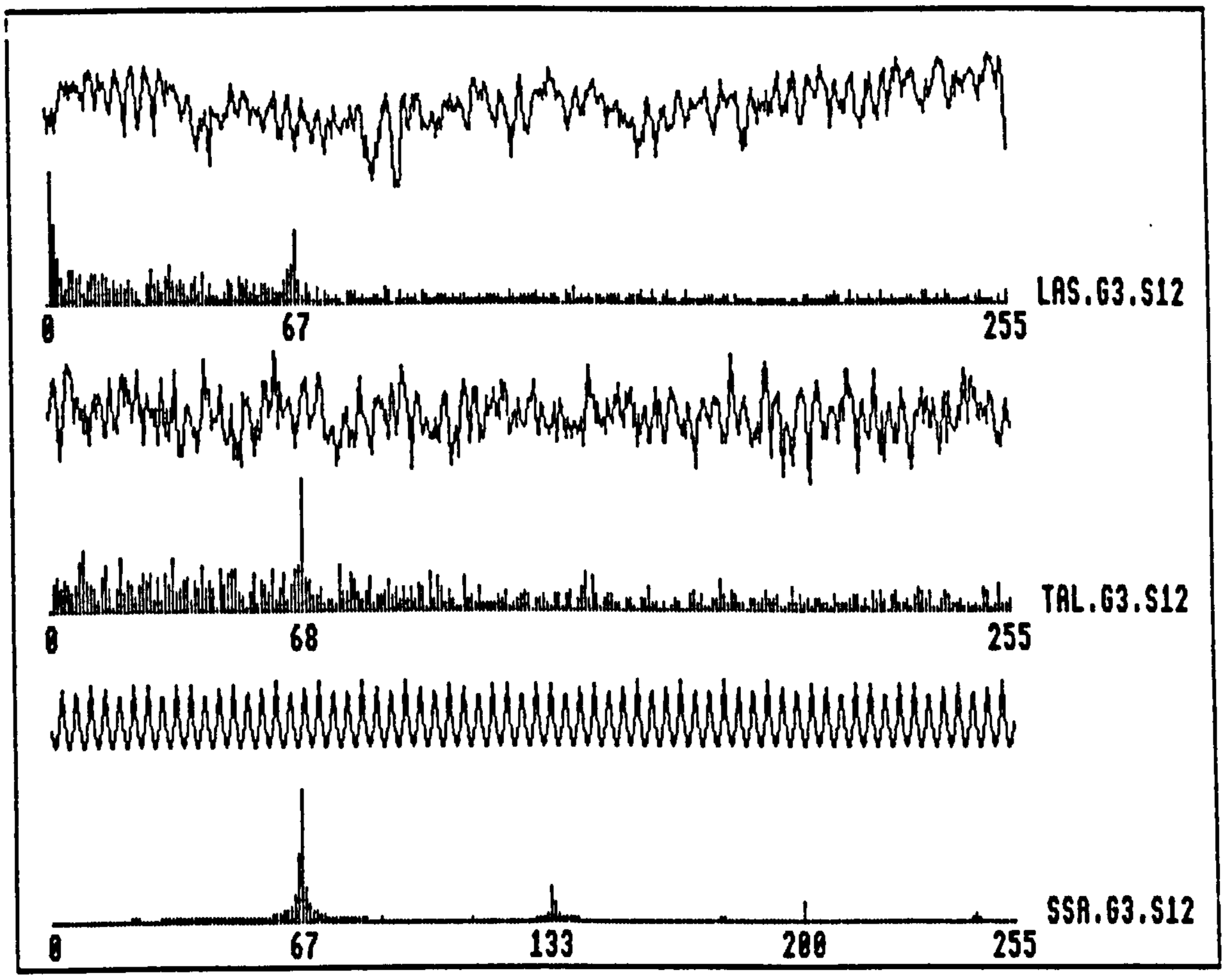

MACHINING PARAMETERS	PRINCIPAL PEAK HARMONICS
No. of knives 8 Feed speed 90 m/min Cutter Speed 6000 rpm Vib. rate 0 Proud Knives 0 Ecc.rate/rev 0 Spindle Runout 0 microns	h1 = 8 h2 = 16 hj = 66

ANALYSIS OF FFT's USING FAULT FINDING ALGORITHM (FFA)		
FFA ON LASER DATA THRESHOLD=0.4	FFA ON TALY DATA THRESHOLD=0.4	FFA ON SSA DATA THRESHOLD=0.4
(Multi-knife) Harmonic 67 (Unknown Faults) Harmonic 28 Harmonic 33 Harmonic 42	(Proud Knife) Harmonic 9 Harmonic 19 (Multi-knife) Harmonic 68 (Unknown Faults) Harmonic 33	(Multi-knife) Harmonic 67

Figure 7.G3.S12: RESULTS FOR TIMBER SAMPLE NUMBER G3.S12

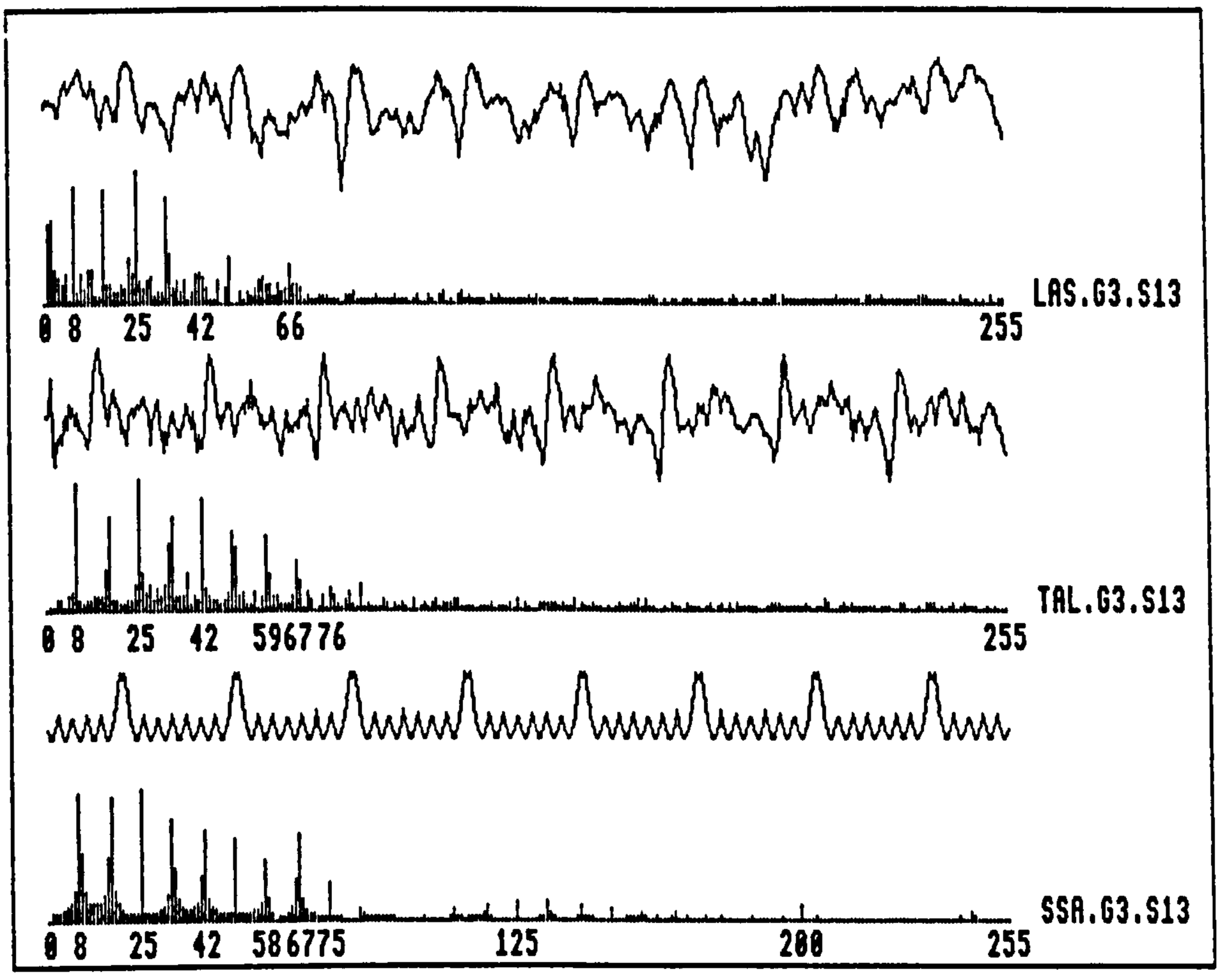

MACHINING PARAMETERS	PRINCIPAL PEAK HARMONICS
No. of knives 8 Feed speed 90 m/min Cutter Speed 6000 rpm Vib. rate 0 Proud Knives 7 >>> 1 2 3 4 5 6 7 Ecc.rate/rev 0 Spindle Runout 0 microns	h1 = 8 h2 = 16 hj = 66

ANALYSIS OF FFT's USING FAULT FINDING ALGORITHM (FFA)		
FFA ON LASER DATA THRESHOLD=0.5	FFA ON TALY DATA THRESHOLD=0.5	FFA ON SSA DATA THRESHOLD=0.5
(Proud Knife) Harmonic 8 Harmonic 16 Harmonic 25 Harmonic 33	(Proud Knife) Harmonic 8 Harmonic 17 Harmonic 25 Harmonic 34 Harmonic 42 Harmonic 50 Harmonic 59	(Proud Knife) Harmonic 8 Harmonic 17 Harmonic 25 Harmonic 33 Harmonic 42 Harmonic 50 (Multi-knife) Harmonic 67

Figure 7.G3.S13: RESULTS FOR TIMBER SAMPLE NUMBER G3.S13

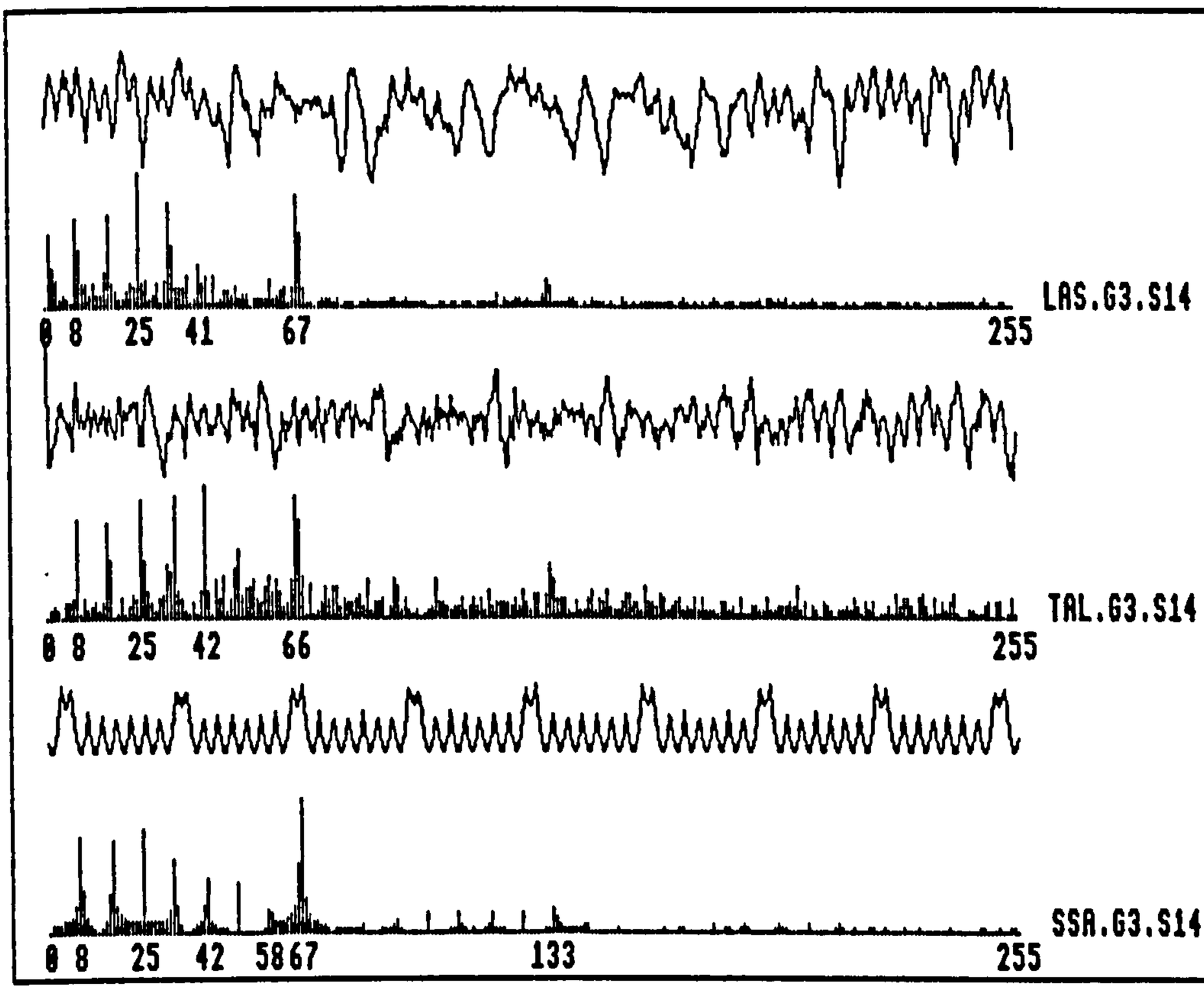

MACHINING PARAMETERS		PRINCIPAL PEAK HARMONICS
No. of knives	8	h1 = 8 h2 = 16 hj = 66
Feed speed	90 m/min	
Cutter Speed	6000 rpm	
Vib. rate	0	
Proud Knives	7)))) 1 2 3 5 6 7 8	
Ecc.rate/rev	0	
Spindle Runout	0 microns	

ANALYSIS OF FFT's USING FAULT FINDING ALGORITHM (FFA)		
FFA ON LASER DATA THRESHOLD=0.5	FFA ON TALY DATA THRESHOLD=0.5	FFA ON SSA DATA THRESHOLD=0.5
(Proud Knife) Harmonic 8 Harmonic 17 Harmonic 25 Harmonic 33 (Multi-knife) Harmonic 67	(Proud Knife) Harmonic 8 Harmonic 16 Harmonic 25 Harmonic 34 Harmonic 42 Harmonic 51 (Multi-knife) Harmonic 66	(Proud Knife) Harmonic 8 Harmonic 17 Harmonic 25 Harmonic 33 (Multi-knife) Harmonic 67

Figure 7.G3.S14: RESULTS FOR TIMBER SAMPLE NUMBER G3.S14

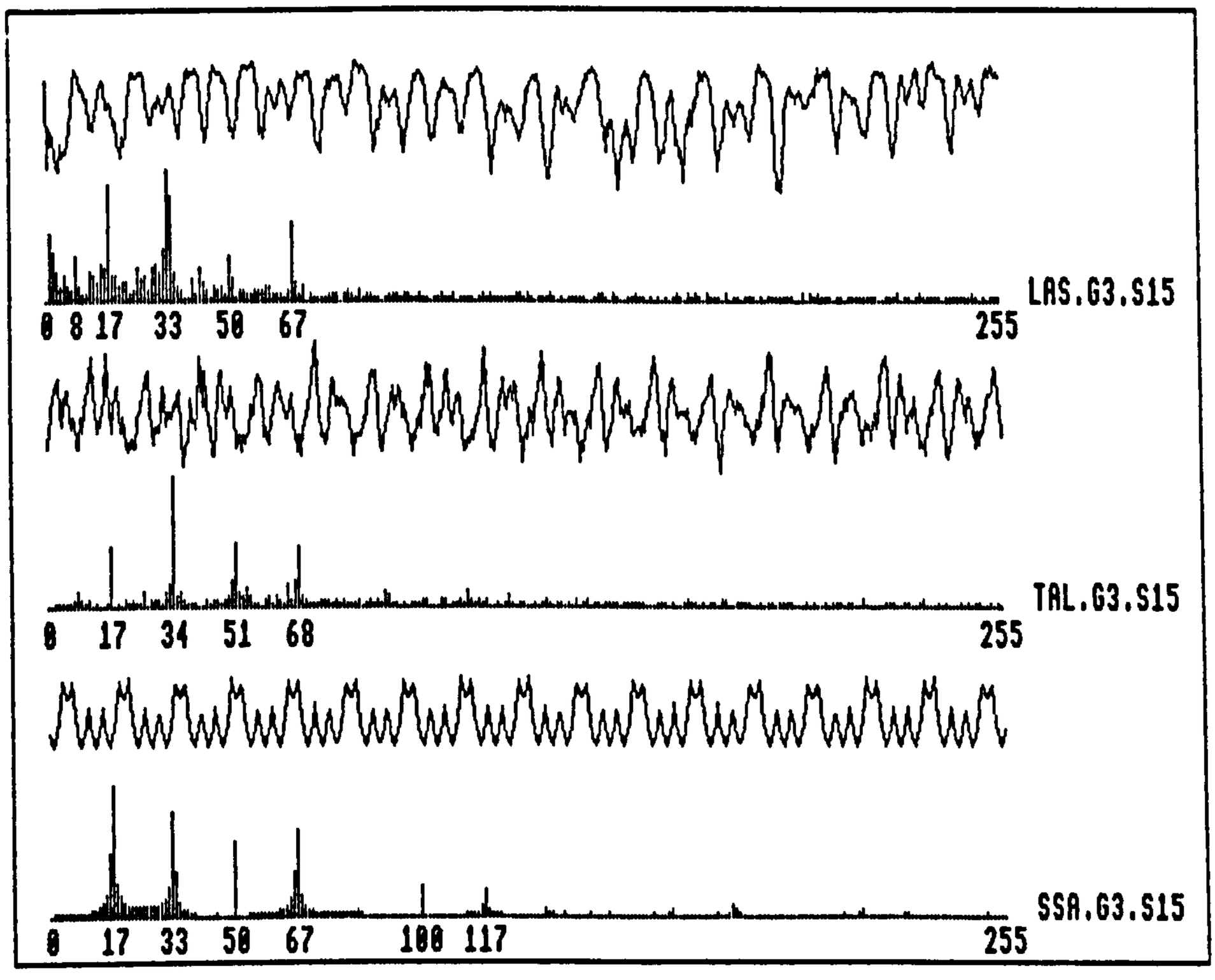

MACHINING PARAMETERS	PRINCIPAL PEAK HARMONICS
No. of knives 8 Feed speed 90 m/min Cutter Speed 6000 rpm Vib. rate 0 Proud Knives 6 >>> 1 2 3 5 6 7 Ecc.rate/rev 0 Spindle Runout 0 microns	h1 = 8 h2 = 16 hj = 66

ANALYSIS OF FFT's USING FAULT FINDING ALGORITHM (FFA)		
FFA ON LASER DATA THRESHOLD=0.4	FFA ON TALY DATA THRESHOLD=0.4	FFA ON SSA DATA THRESHOLD=0.4
(0.balance 2) Harmonic 17 (Multi-knife) Harmonic 67 (Unknown Faults) Harmonic 33	(0.balance 2) Harmonic 17 (Multi-knife) Harmonic 68 (Unknown Faults) Harmonic 34 Harmonic 51	(0.balance 2) Harmonic 17 (Multi-knife) Harmonic 67 (Unknown Faults) Harmonic 33 Harmonic 50

Figure 7.G3.S15: RESULTS FOR TIMBER SAMPLE NUMBER G3.S15

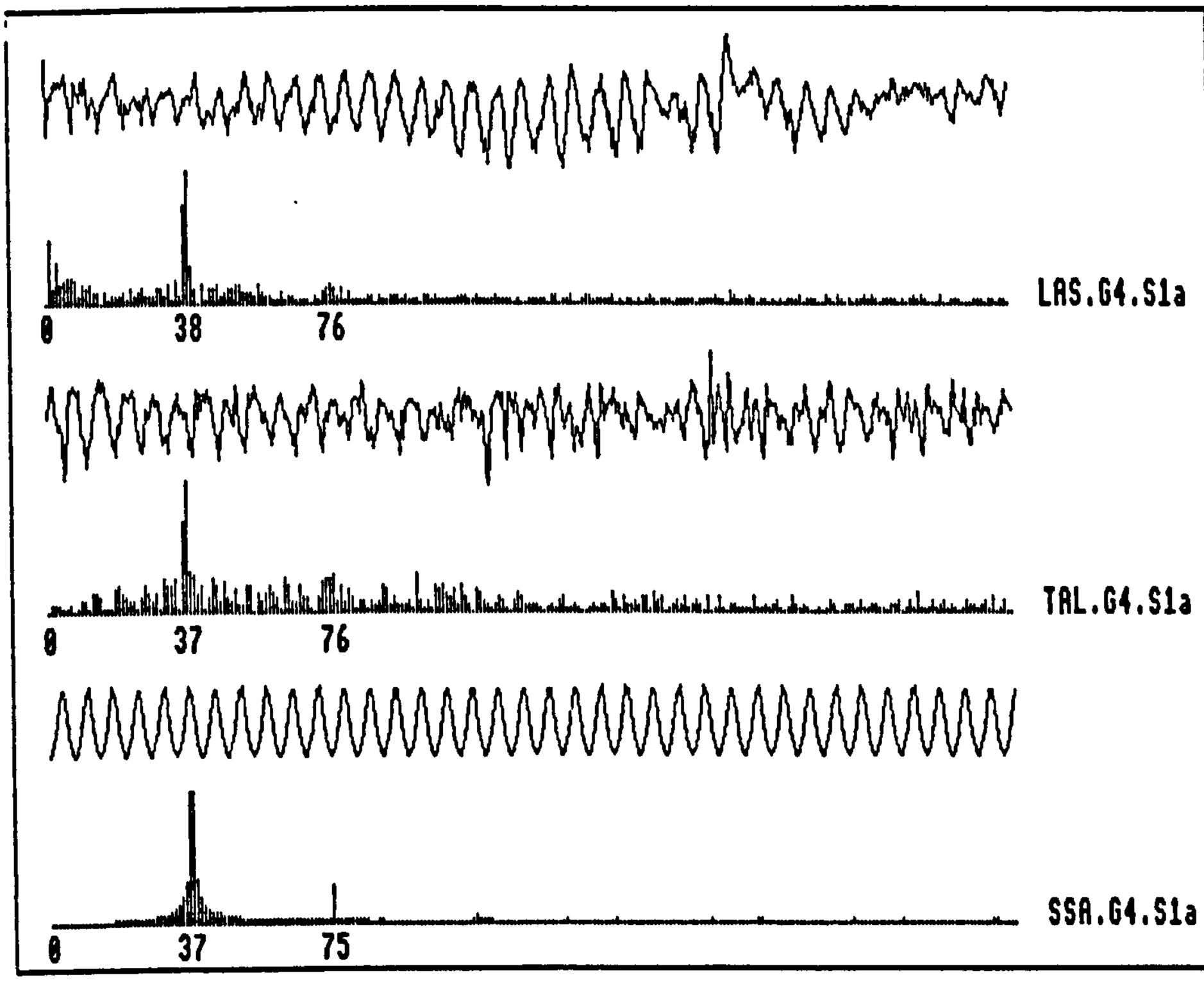

MACHINING PARAMETERS		PRINCIPAL PEAK HARMONICS
No. of knives	4	h1 = 37 h2 = 74 hj = 149
Feed speed	15 m/min	
Cutter Speed	4500 rpm	
Vib. rate	0	
Proud Knives	1 >>> 1	
Ecc.rate/rev	0	
Spindle Runout	0 microns	

ANALYSIS OF FFT's USING FAULT FINDING ALGORITHM (FFA)		
FFA ON LASER DATA THRESHOLD=0.4	FFA ON TALY DATA THRESHOLD=0.4	FFA ON SSA DATA THRESHOLD=0.4
(Single knife) Harmonic 38	(Single knife) Harmonic 37	(Single knife) Harmonic 38

Figure 7.G4.S1a: RESULTS FOR TIMBER SAMPLE NUMBER G4.S1a

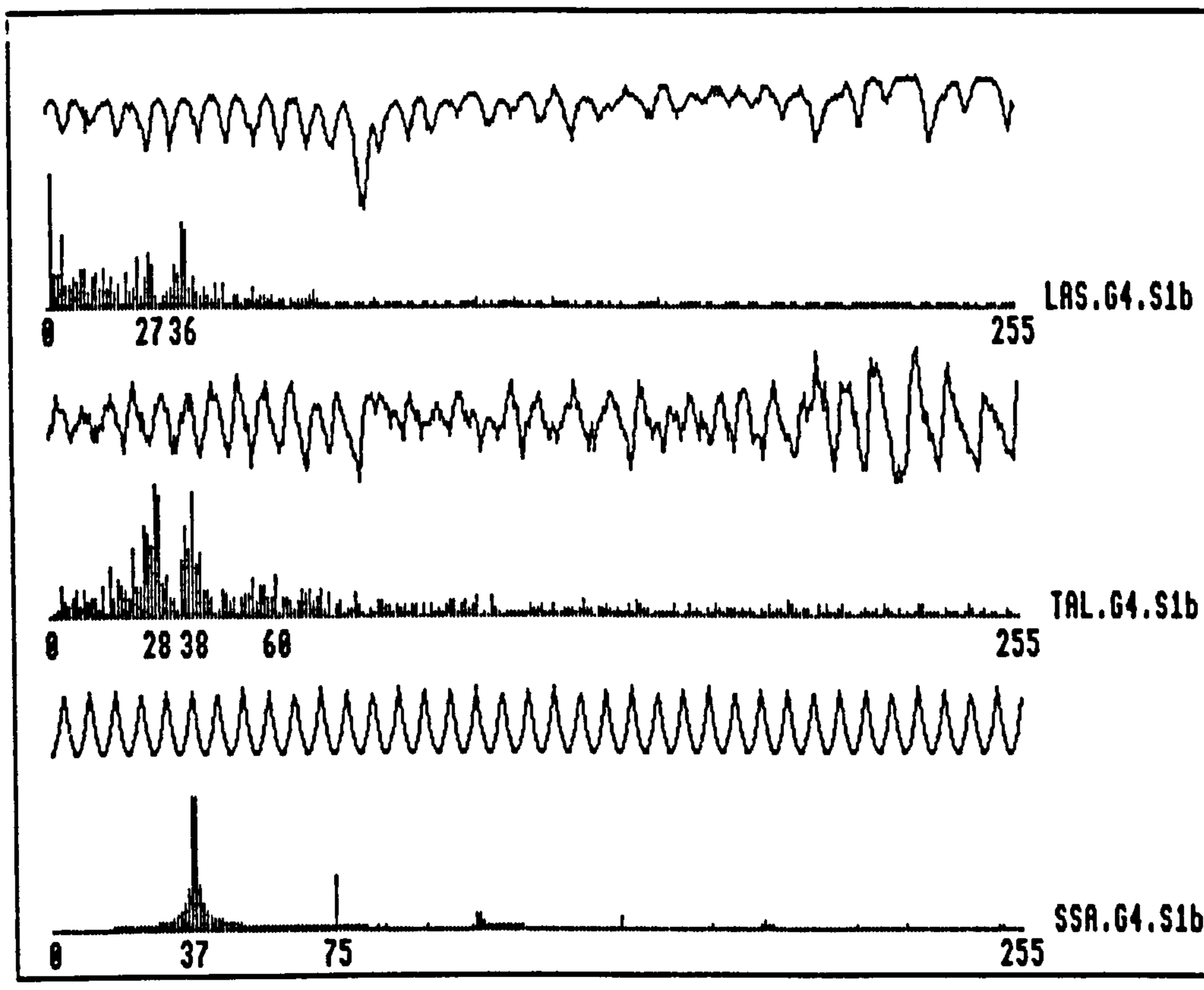

MACHINING PARAMETERS	PRINCIPAL PEAK HARMONICS
No. of knives 4 Feed speed 15 m/min Cutter Speed 4500 rpm Vib. rate 0 Proud Knives 1 >>> 1 Ecc.rate/rev 0 Spindle Runout 0 microns	h1 = 37 h2 = 74 hj = 149

ANALYSIS OF FFT's USING FAULT FINDING ALGORITHM (FFA)		
FFA ON LASER DATA THRESHOLD=0.4	FFA ON TALY DATA THRESHOLD=0.4	FFA ON SSA DATA THRESHOLD=0.4
(Single knife) Harmonic 36	(O.balance 1) Harmonic 38 (Unknown Faults) Harmonic 40	(Single knife) Harmonic 38

Figure 7.G4.S1b: RESULTS FOR TIMBER SAMPLE NUMBER G4.S1b

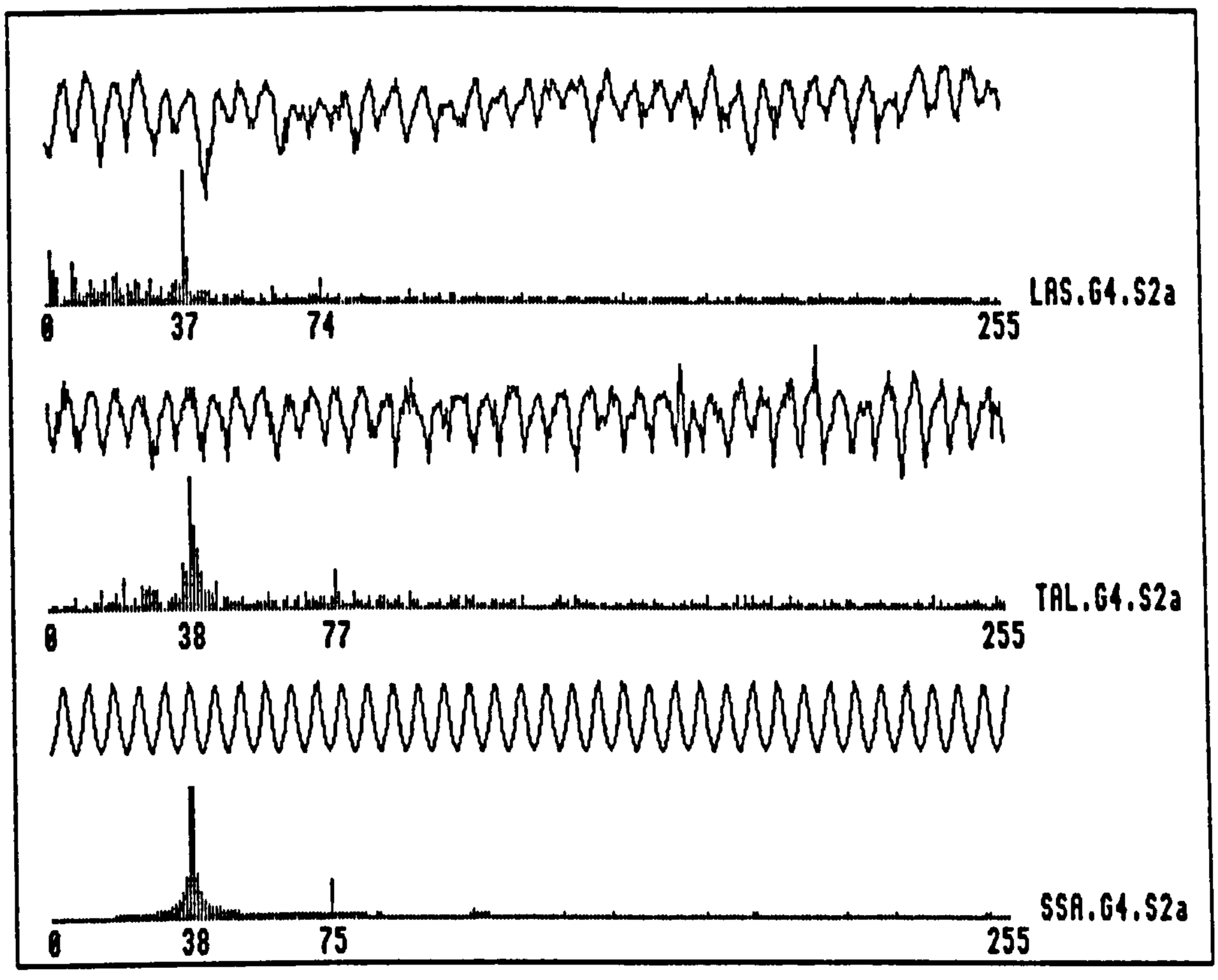

MACHINING PARAMETERS		PRINCIPAL PEAK HARMONICS
No. of knives	4	h1 = 9 h2 = 18 hj = 37
Feed speed	60 m/min	
Cutter Speed	4500 rpm	
Vib. rate	0	
Proud Knives	0	
Ecc.rate/rev	0	
Spindle Runout	0 microns	

ANALYSIS OF FFT's USING FAULT FINDING ALGORITHM (FFA)		
FFA ON LASER DATA THRESHOLD=0.4	FFA ON TALY DATA THRESHOLD=0.4	FFA ON SSA DATA THRESHOLD=0.4
(Multi-knife) Harmonic 37	(Multi-knife) Harmonic 38	(Multi-knife) Harmonic 38

Figure 7.G4.S2a: RESULTS FOR TIMBER SAMPLE NUMBER G4.S2a

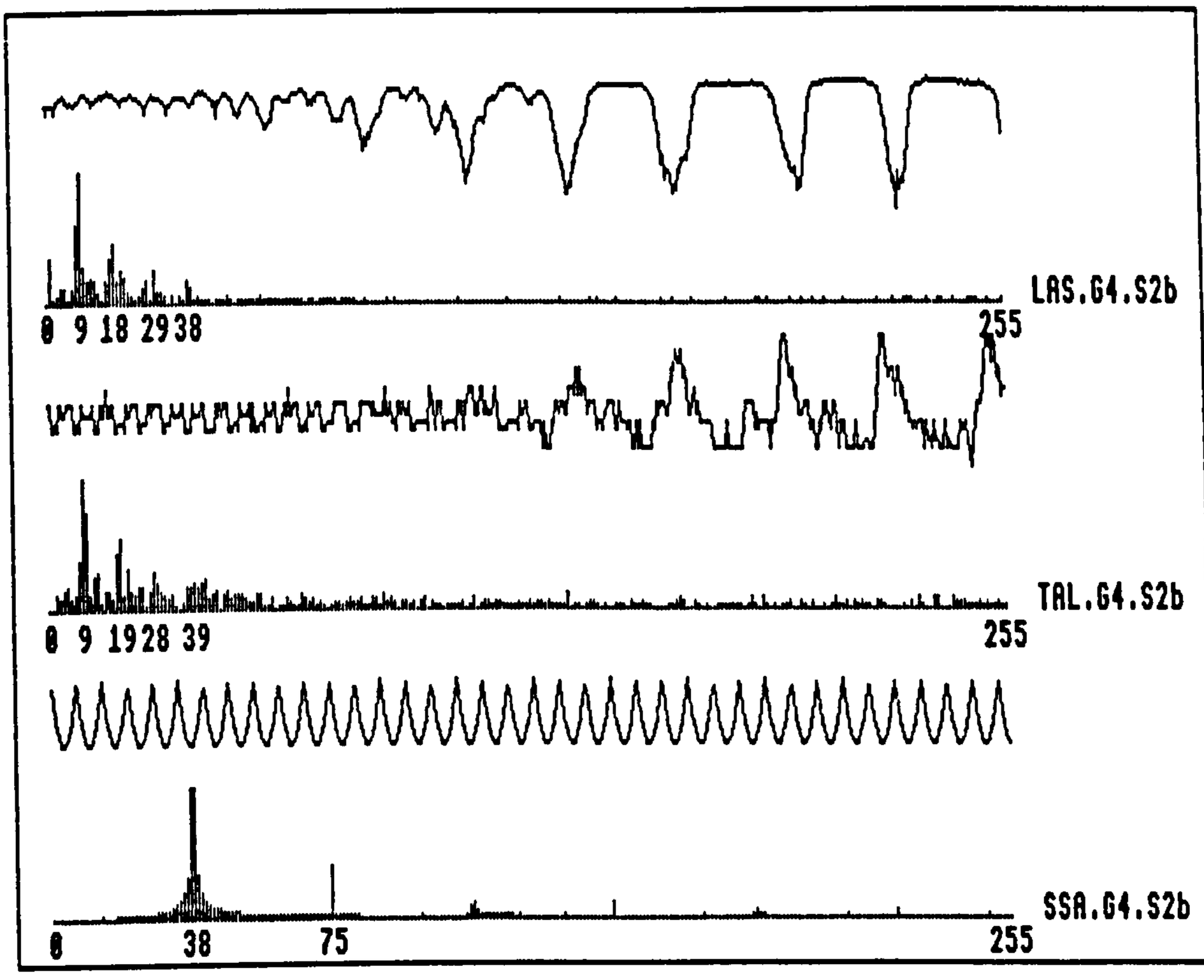

MACHINING PARAMETERS		PRINCIPAL PEAK HARMONICS
No. of knives	4	h1 = 9 h2 = 18 hj = 37
Feed speed	60 m/min	
Cutter Speed	4500 rpm	
Vib. rate	0	
Proud Knives	0	
Ecc.rate/rev	0	
Spindle Runout	0 microns	

ANALYSIS OF FFT's USING FAULT FINDING ALGORITHM (FFA)		
FFA ON LASER DATA THRESHOLD=0.4	FFA ON TALY DATA THRESHOLD=0.4	FFA ON SSA DATA THRESHOLD=0.4
(Proud Knife) Harmonic 9 Harmonic 18	(Proud Knife) Harmonic 9 Harmonic 19	(Multi-knife) Harmonic 38

Figure 7.G4.S2b: RESULTS FOR TIMBER SAMPLE NUMBER G4.S2b

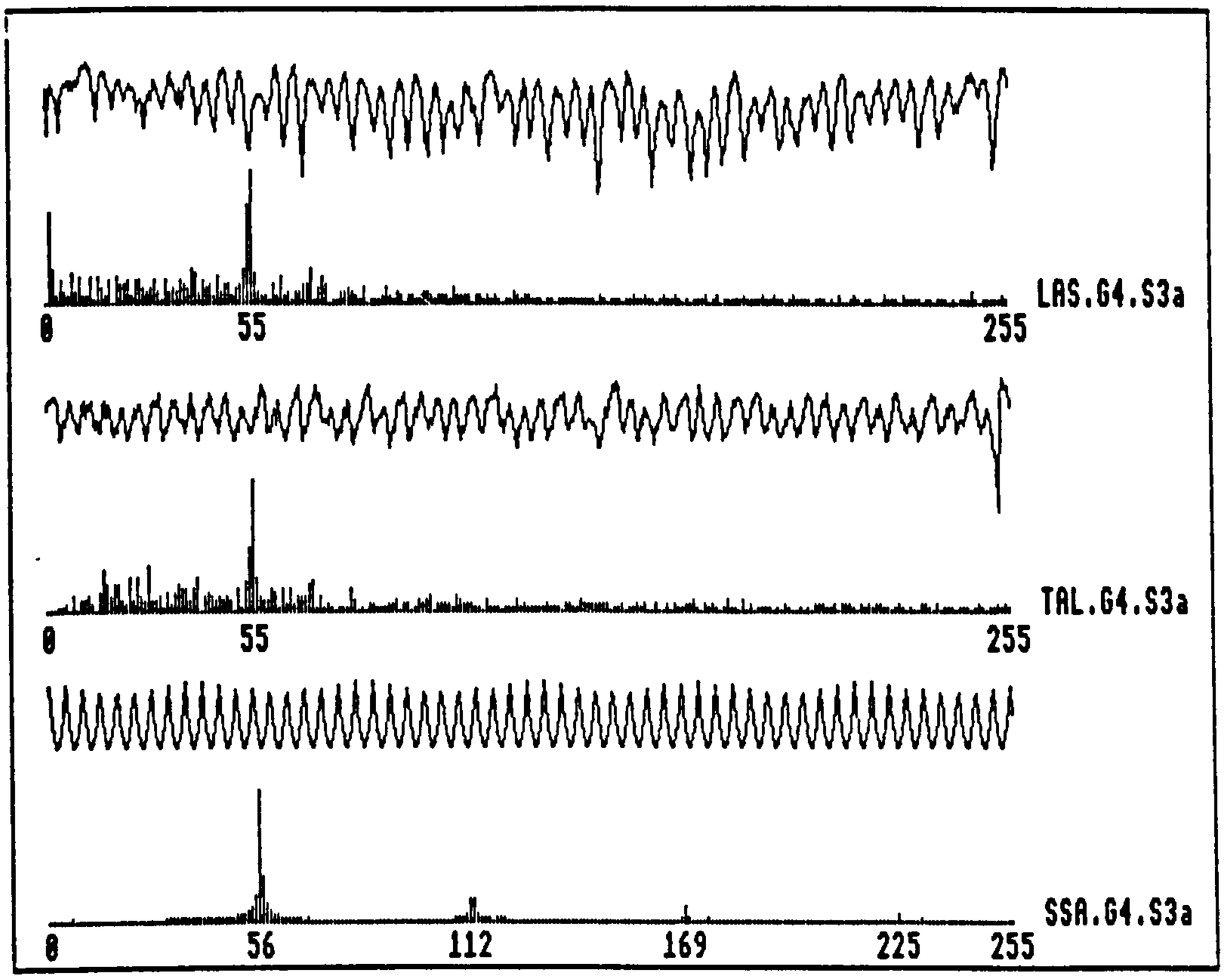

MACHINING PARAMETERS		PRINCIPAL PEAK HARMONICS
No. of knives	6	h1 = 9 h2 = 18 hj = 56
Feed speed	80 m/min	
Cutter Speed	6000 rpm	
Vib. rate	0	
Proud Knives	0	
Ecc.rate/rev	0	
Spindle Runout	0 microns	

ANALYSIS OF FFT's USING FAULT FINDING ALGORITHM (FFA)		
FFA ON LASER DATA THRESHOLD=0.4	FFA ON TALY DATA THRESHOLD=0.4	FFA ON SSA DATA THRESHOLD=0.4
(Multi-knife) Harmonic 55	(Multi-knife) Harmonic 55	(Multi-knife) Harmonic 56

Figure 7.G4.S3a: RESULTS FOR TIMBER SAMPLE NUMBER G4.S3a

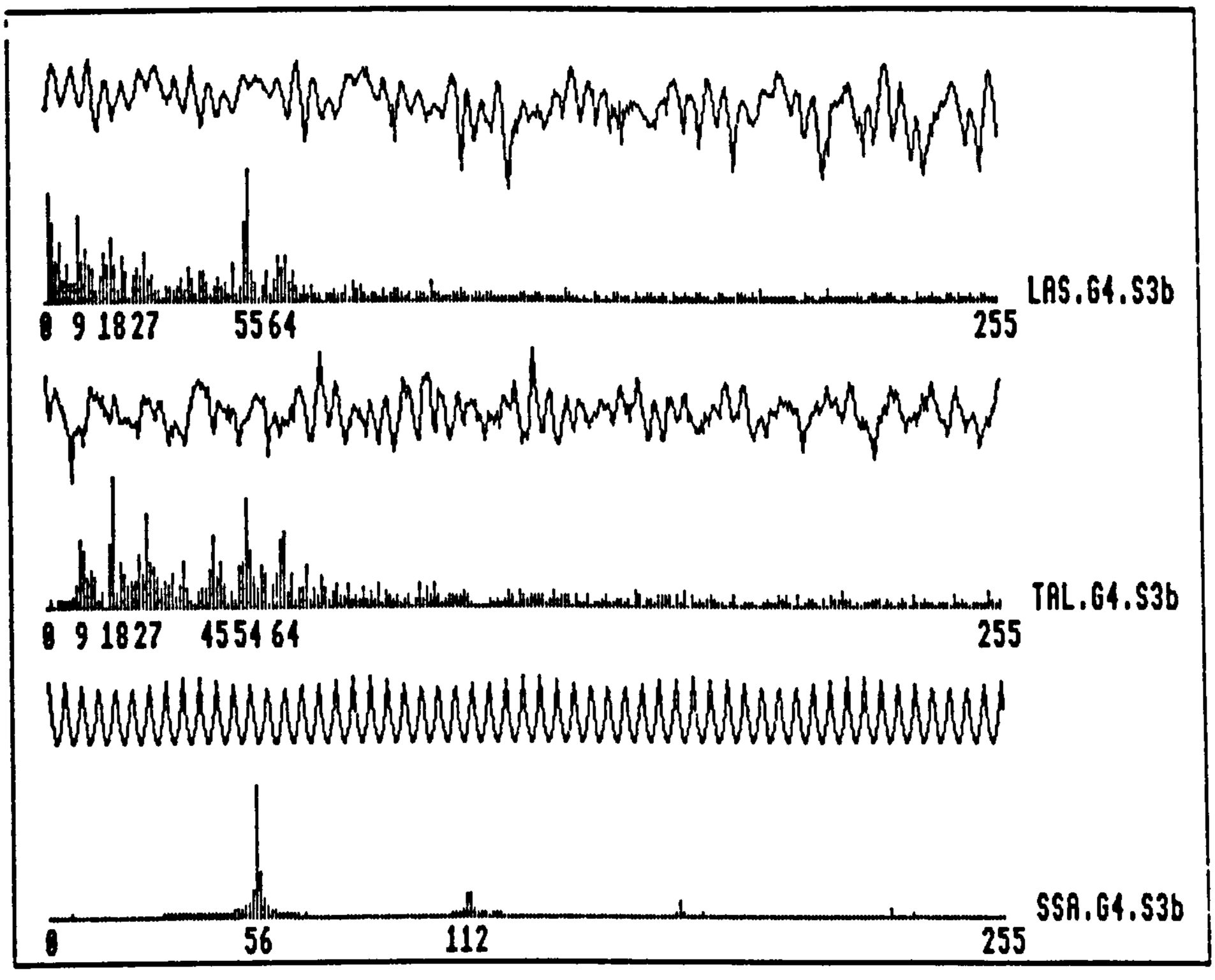

MACHINING PARAMETERS		PRINCIPAL PEAK HARMONICS
No. of knives	6	h1 = 9 h2 = 18 hj = 56
Feed speed	80 m/min	
Cutter Speed	6000 rpm	
Vib. rate	0	
Proud Knives	0	
Ecc.rate/rev	0	
Spindle Runout	0 microns	

ANALYSIS OF FFT's USING FAULT FINDING ALGORITHM (FFA)		
FFA ON LASER DATA THRESHOLD=0.4	FFA ON TALY DATA THRESHOLD=0.4	FFA ON SSA DATA THRESHOLD=0.4
(Proud Knife) Harmonic 9 Harmonic 18 (Multi-knife) Harmonic 55	(Proud Knife) Harmonic 9 Harmonic 18 Harmonic 27 (Multi-knife) Harmonic 54 (Unknown Faults) Harmonic 45 Harmonic 64	(Multi-knife) Harmonic 56

Figure 7.G4.S3b: RESULTS FOR TIMBER SAMPLE NUMBER G4.S3b

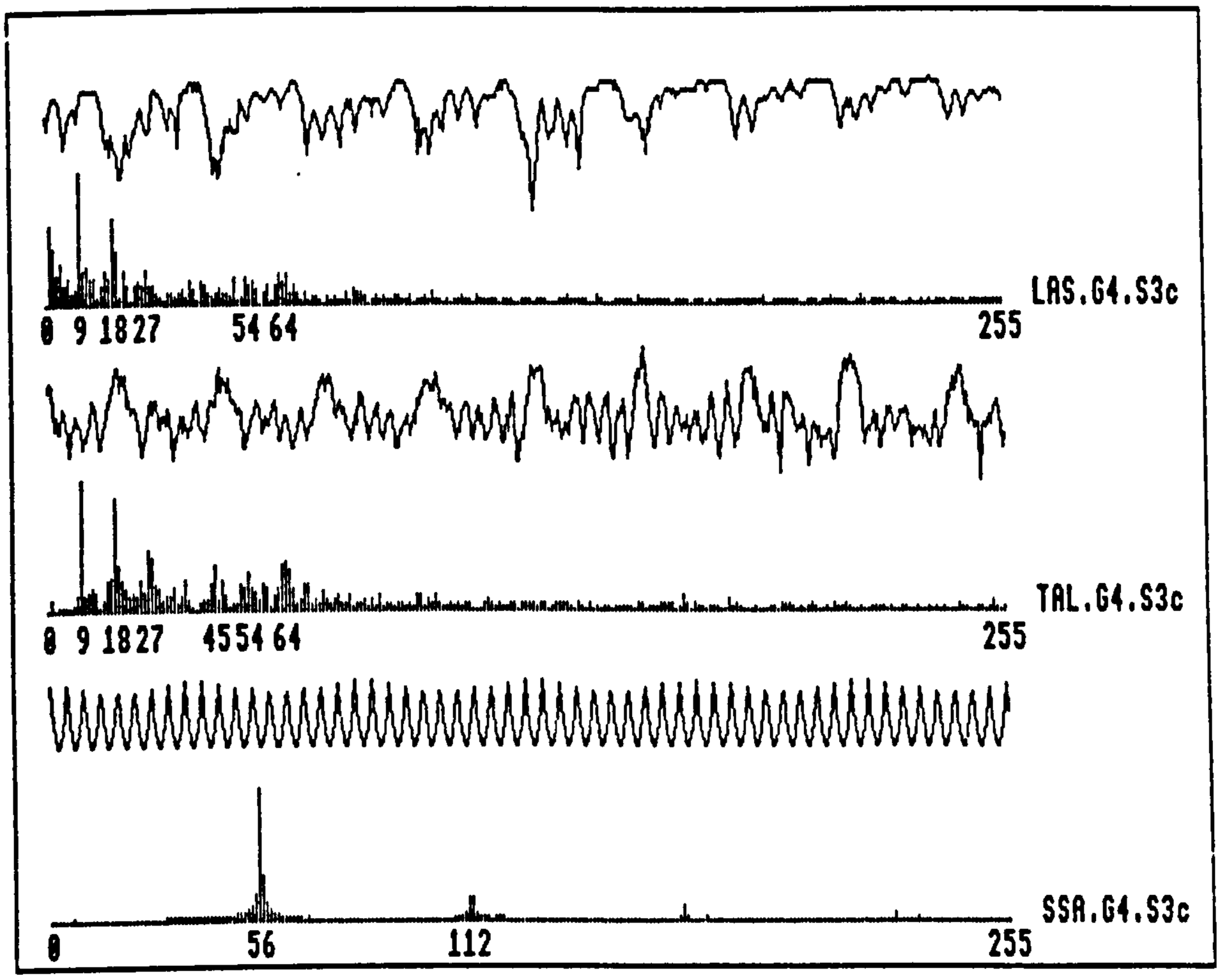

MACHINING PARAMETERS	PRINCIPAL PEAK HARMONICS
No. of knives 6 Feed speed 80 m/min Cutter Speed 6000 rpm Vib. rate 0 Proud Knives 0 Ecc.rate/rev 0 Spindle Runout 0 microns	h1 = 9 h2 = 18 hj = 56

ANALYSIS OF FFT's USING FAULT FINDING ALGORITHM (FFA)		
FFA ON LASER DATA THRESHOLD=0.4	FFA ON TALY DATA THRESHOLD=0.4	FFA ON SSA DATA THRESHOLD=0.4
(Proud Knife) Harmonic 9 Harmonic 18	(Proud Knife) Harmonic 9 Harmonic 18 Harmonic 27	(Multi-knife) Harmonic 56

Figure 7.G4.S3c: RESULTS FOR TIMBER SAMPLE NUMBER G4.S3c

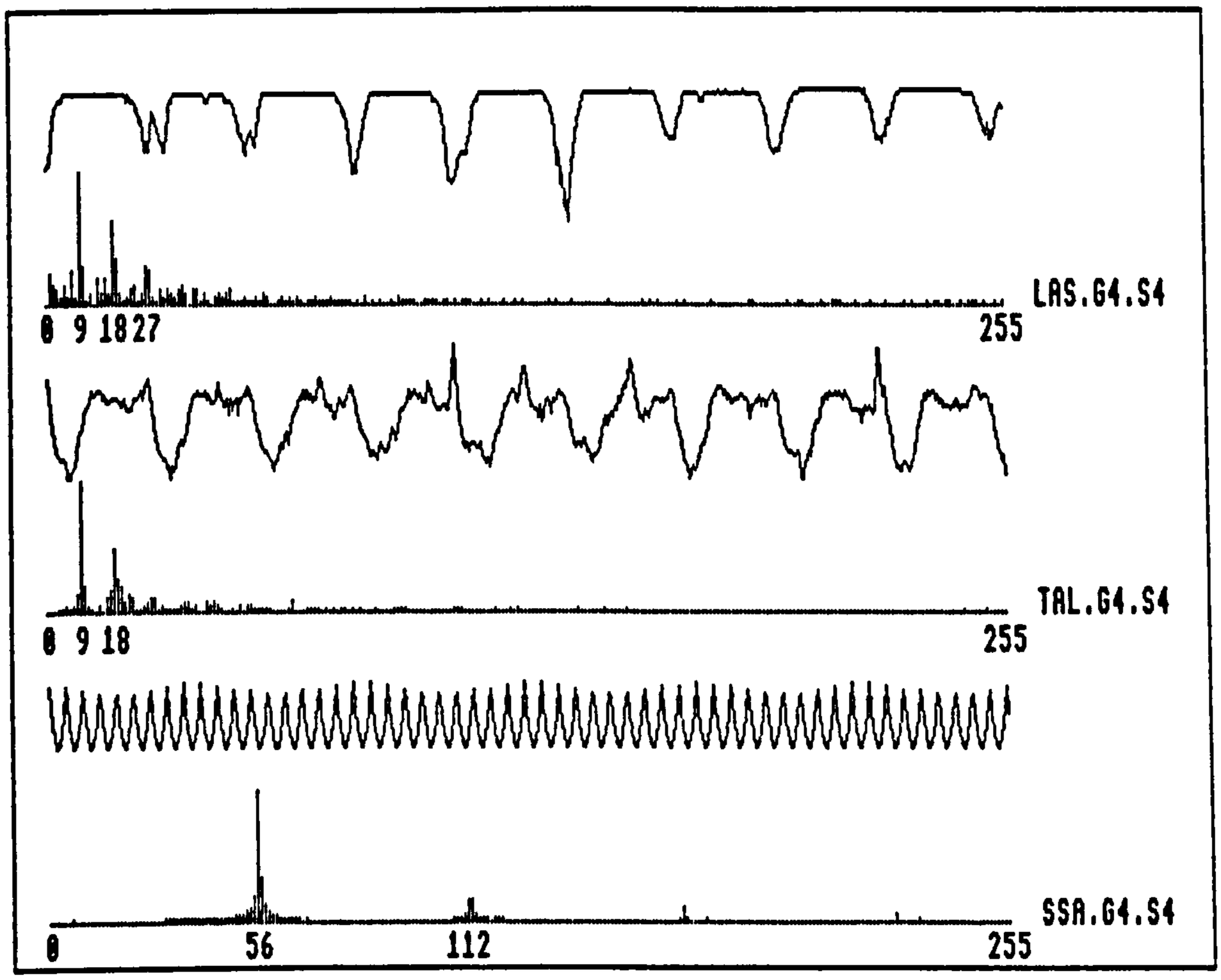

MACHINING PARAMETERS		PRINCIPAL PEAK HARMONICS
No. of knives	6	h1 = 9 h2 = 18 hj = 56
Feed speed	80 m/min	
Cutter Speed	6000 rpm	
Vib. rate	0	
Proud Knives	0	
Ecc.rate/rev	0	
Spindle Runout	0 microns	

ANALYSIS OF FFT's USING FAULT FINDING ALGORITHM (FFA)		
FFA ON LASER DATA THRESHOLD=0.4	FFA ON TALY DATA THRESHOLD=0.4	FFA ON SSA DATA THRESHOLD=0.4
(Proud Knife) Harmonic 9 Harmonic 18	(Proud Knife) Harmonic 9 Harmonic 18	(Multi-knife) Harmonic 56

Figure 7.G4.S4: RESULTS FOR TIMBER SAMPLE NUMBER G4.S4

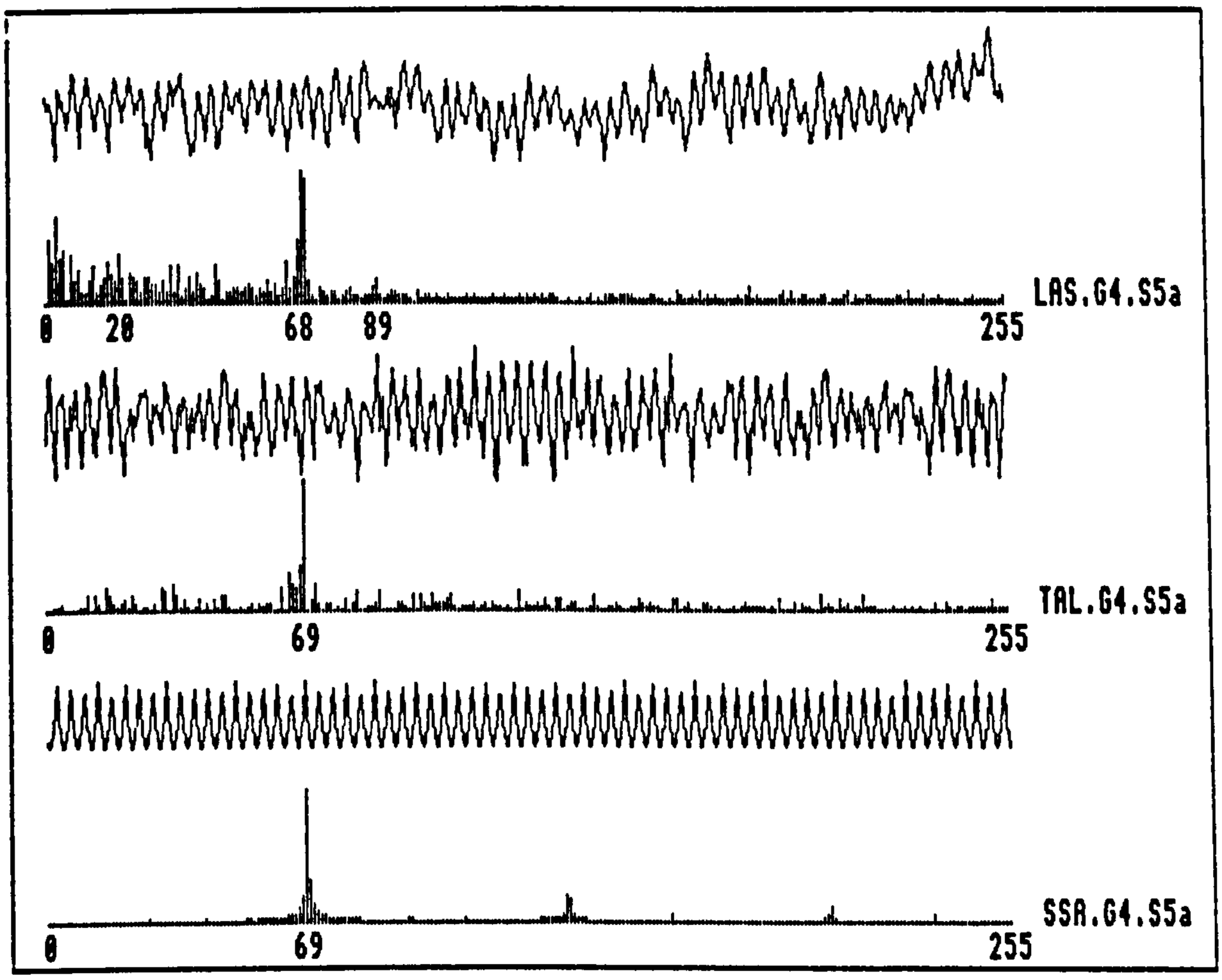

MACHINING PARAMETERS		PRINCIPAL PEAK HARMONICS
No. of knives	6	h1 = 11 h2 = 22 hj = 69
Feed speed	65 m/min	
Cutter Speed	6000 rpm	
Vib. rate	0	
Proud Knives	0	
Ecc.rate/rev	0	
Spindle Runout	0 microns	

ANALYSIS OF FFT's USING FAULT FINDING ALGORITHM (FFA)		
FFA ON LASER DATA THRESHOLD=0.4	FFA ON TALY DATA THRESHOLD=0.4	FFA ON SSA DATA THRESHOLD=0.4
(Multi-knife) Harmonic 69	(Multi-knife) Harmonic 69	(Multi-knife) Harmonic 69

Figure 7.G4.S5a: RESULTS FOR TIMBER SAMPLE NUMBER G4.S5a

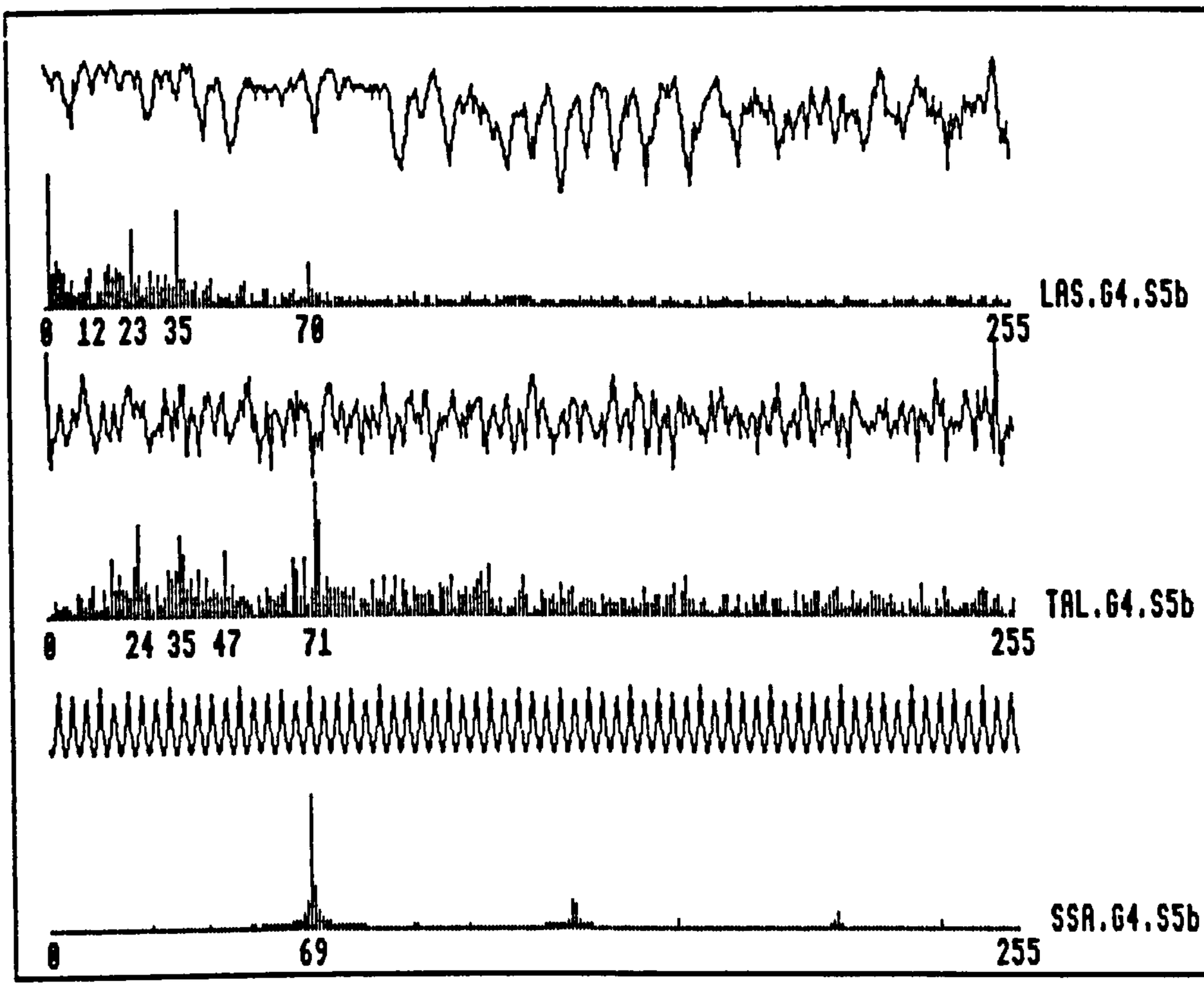

MACHINING PARAMETERS		PRINCIPAL PEAK HARMONICS
No. of knives	6	h1 = 11
Feed speed	65 m/min	h2 = 22
Cutter Speed	6000 rpm	hj = 69
Vib. rate	0	
Proud Knives	0	
Ecc.rate/rev	0	
Spindle Runout	0 microns	

ANALYSIS OF FFT's USING FAULT FINDING ALGORITHM (FFA)		
FFA ON LASER DATA THRESHOLD=0.4	FFA ON TALY DATA THRESHOLD=0.4	FFA ON SSA DATA THRESHOLD=0.4
(Proud Knife) Harmonic 12 Harmonic 23 Harmonic 35 (Multi-knife) Harmonic 70 (Unknown Faults) Harmonic 17 Harmonic 19	(Multi-knife) Harmonic 71 (Unknown Faults) Harmonic 17 Harmonic 24 Harmonic 35 Harmonic 47 Harmonic 65	(Multi-knife) Harmonic 69

Figure 7.G4.S5b: RESULTS FOR TIMBER SAMPLE NUMBER G4.S5b

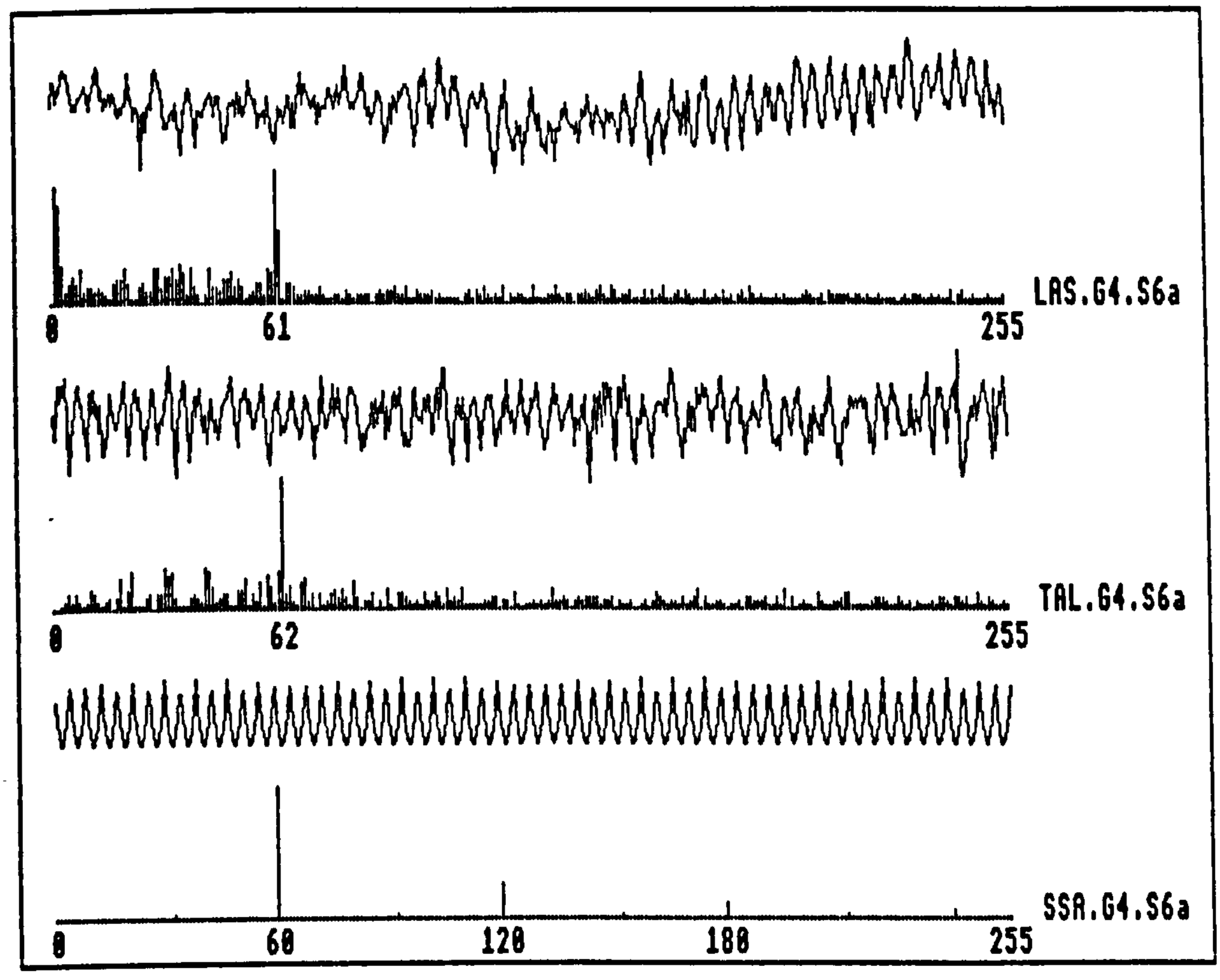

MACHINING PARAMETERS		PRINCIPAL PEAK HARMONICS
No. of knives	6	h1 = 10 h2 = 20 hj = 60
Feed speed	75 m/min	
Cutter Speed	6000 rpm	
Vib. rate	0	
Proud Knives	0	
Ecc.rate/rev	0	
Spindle Runout	0 microns	

ANALYSIS OF FFT's USING FAULT FINDING ALGORITHM (FFA)		
FFA ON LASER DATA THRESHOLD=0.4	FFA ON TALY DATA THRESHOLD=0.4	FFA ON SSA DATA THRESHOLD=0.4
(Multi-knife) Harmonic 61	(Multi-knife) Harmonic 62	(Multi-knife) Harmonic 60

Figure 7.G4.S6a: RESULTS FOR TIMBER SAMPLE NUMBER G4.S6a

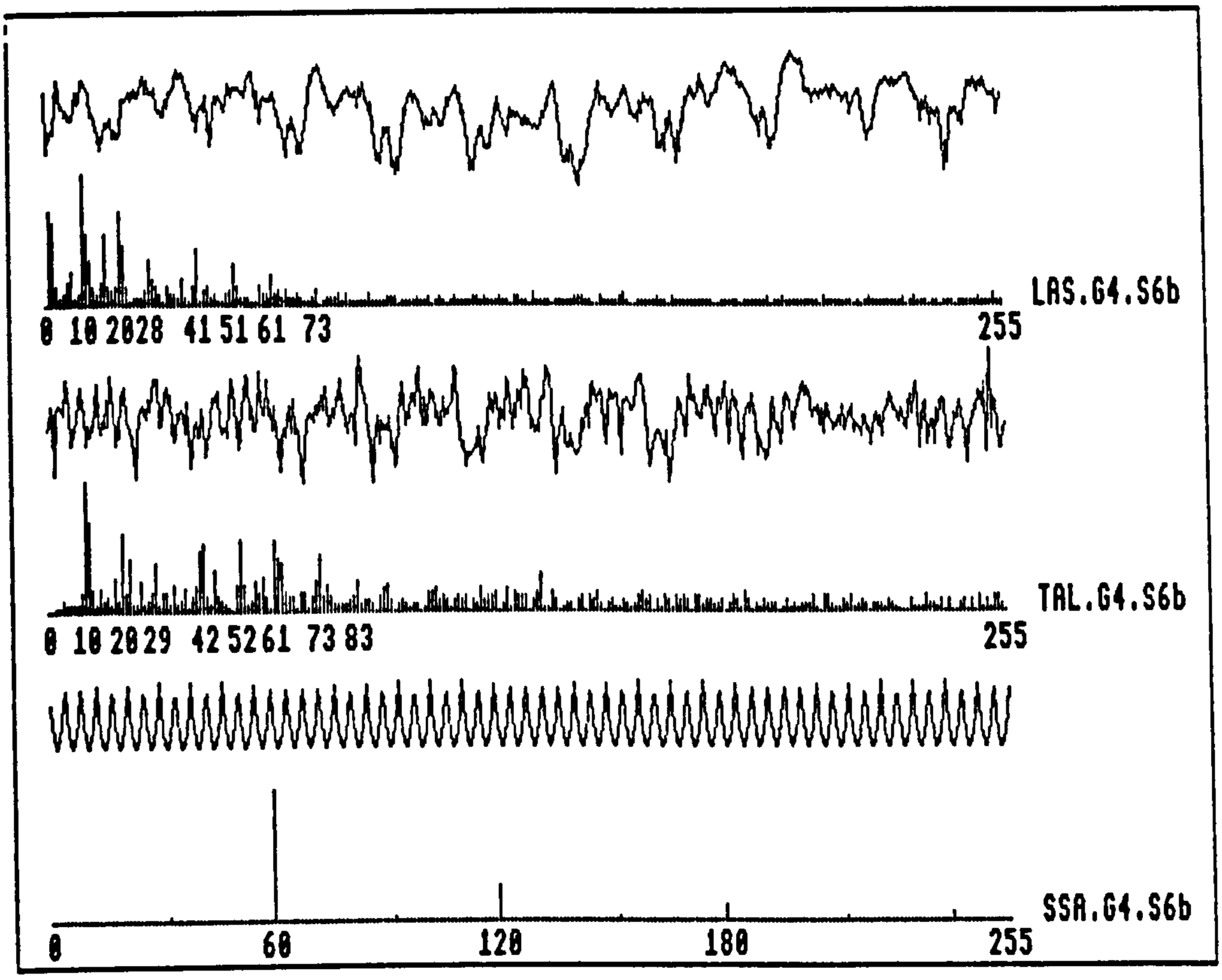

MACHINING PARAMETERS	PRINCIPAL PEAK HARMONICS
No. of knives 6 Feed speed 75 m/min Cutter Speed 6000 rpm Vib. rate 0 Proud Knives 0 Ecc.rate/rev 0 Spindle Runout 0 microns	h1 = 10 h2 = 20 hj = 60

ANALYSIS OF FFT's USING FAULT FINDING ALGORITHM (FFA)		
FFA ON LASER DATA THRESHOLD=0.4	FFA ON TALY DATA THRESHOLD=0.4	FFA ON SSA DATA THRESHOLD=0.4
(Proud Knife) Harmonic 10 Harmonic 20 (Unknown Faults) Harmonic 16 Harmonic 41	(Proud Knife) Harmonic 10 Harmonic 20 (Multi-knife) Harmonic 61 (Unknown Faults) Harmonic 22 Harmonic 42 Harmonic 52 Harmonic 73	(Multi-knife) Harmonic 60

Figure 7.G4.S6b: RESULTS FOR TIMBER SAMPLE NUMBER G4.S6b

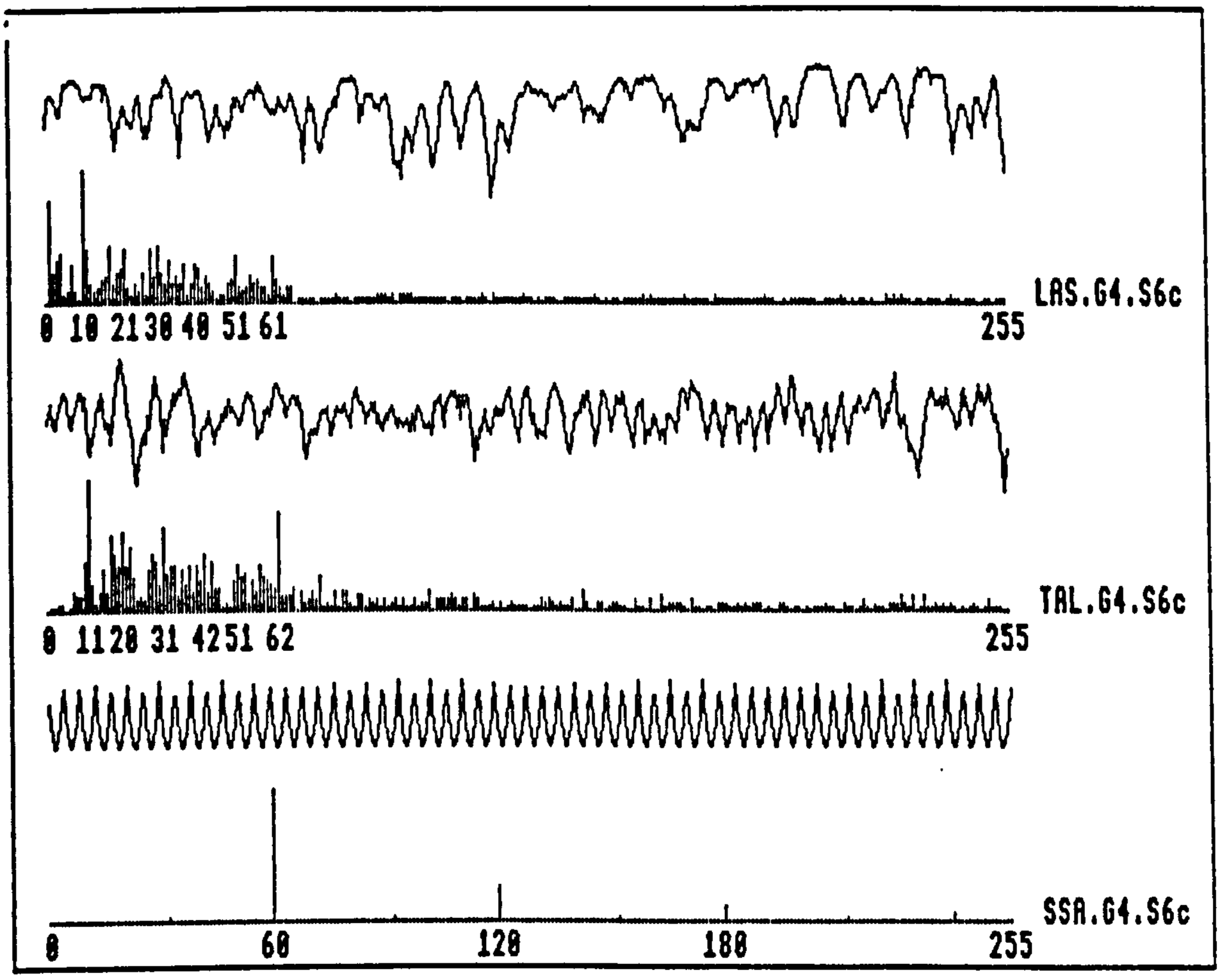

MACHINING PARAMETERS	PRINCIPAL PEAK HARMONICS
No. of knives 6 Feed speed 75 m/min Cutter Speed 6000 rpm Vib. rate 0 Proud Knives 0 Ecc.rate/rev 0 Spindle Runout 0 microns	h1 = 10 h2 = 20 hj = 60

ANALYSIS OF FFT's USING FAULT FINDING ALGORITHM (FFA)		
FFA ON LASER DATA THRESHOLD=0.4	FFA ON TALY DATA THRESHOLD=0.4	FFA ON SSA DATA THRESHOLD=0.4
(Proud Knife) Harmonic 10 Harmonic 21 Harmonic 30 (Unknown Faults) Harmonic 17	(Proud Knife) Harmonic 11 Harmonic 20 Harmonic 31 Harmonic 42 (Multi-knife) Harmonic 62 (Unknown Faults) Harmonic 22	(Multi-knife) Harmonic 60

Figure 7.G4.S6c: RESULTS FOR TIMBER SAMPLE NUMBER G4.S6c

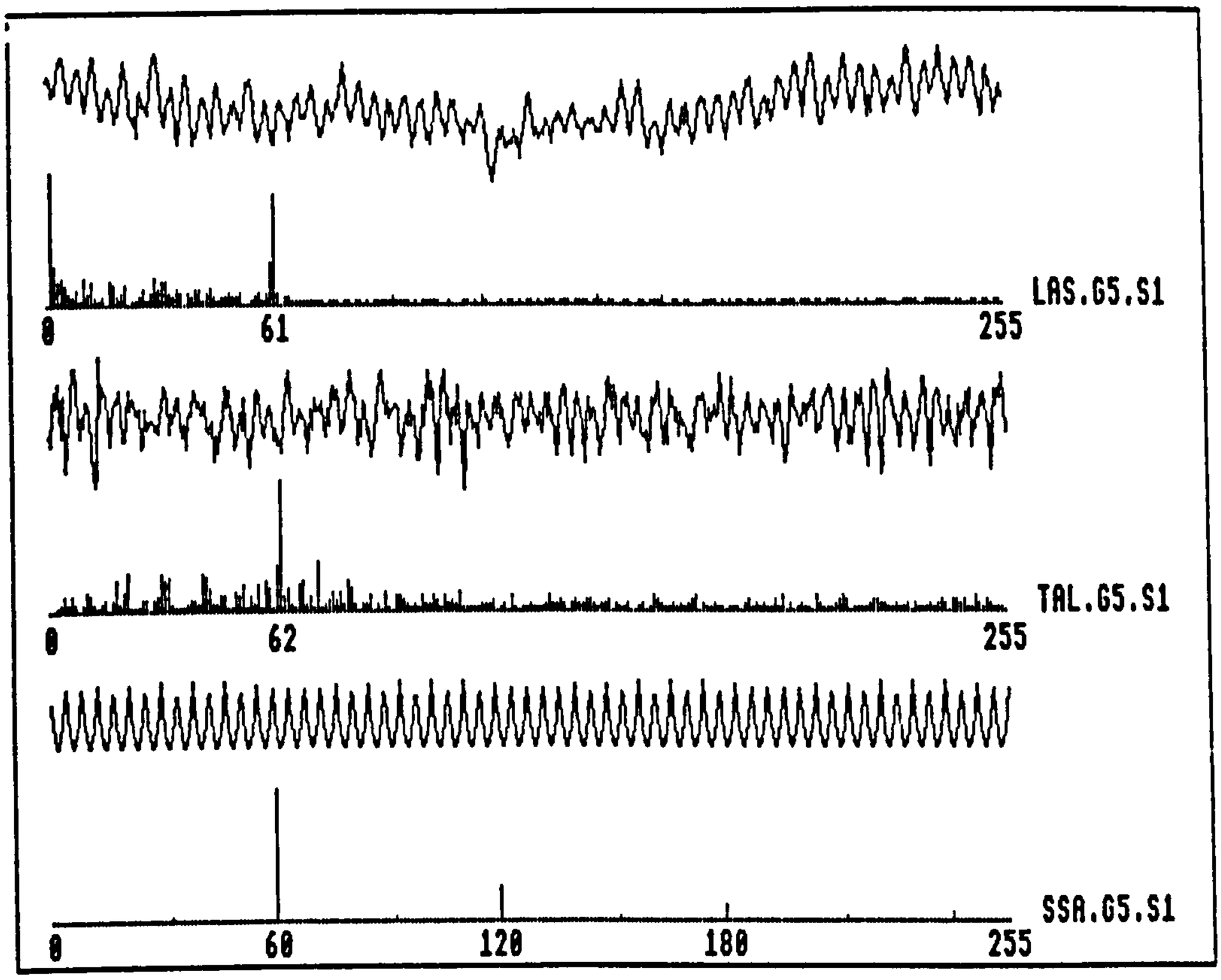

MACHINING PARAMETERS		PRINCIPAL PEAK HARMONICS
No. of knives	6	h1 = 10 h2 = 20 hj = 60
Feed speed	75 m/min	
Cutter Speed	6000 rpm	
Vib. rate	0	
Proud Knives	0	
Ecc.rate/rev	0	
Spindle Runout	0 microns	

ANALYSIS OF FFT's USING FAULT FINDING ALGORITHM (FFA)		
FFA ON LASER DATA THRESHOLD=0.4	FFA ON TALY DATA THRESHOLD=0.4	FFA ON SSA DATA THRESHOLD=0.4
(Multi-knife) Harmonic 61	(Multi-knife) Harmonic 62	(Multi-knife) Harmonic 60

Figure 7.G5.S1: RESULTS FOR TIMBER SAMPLE NUMBER G5.S1

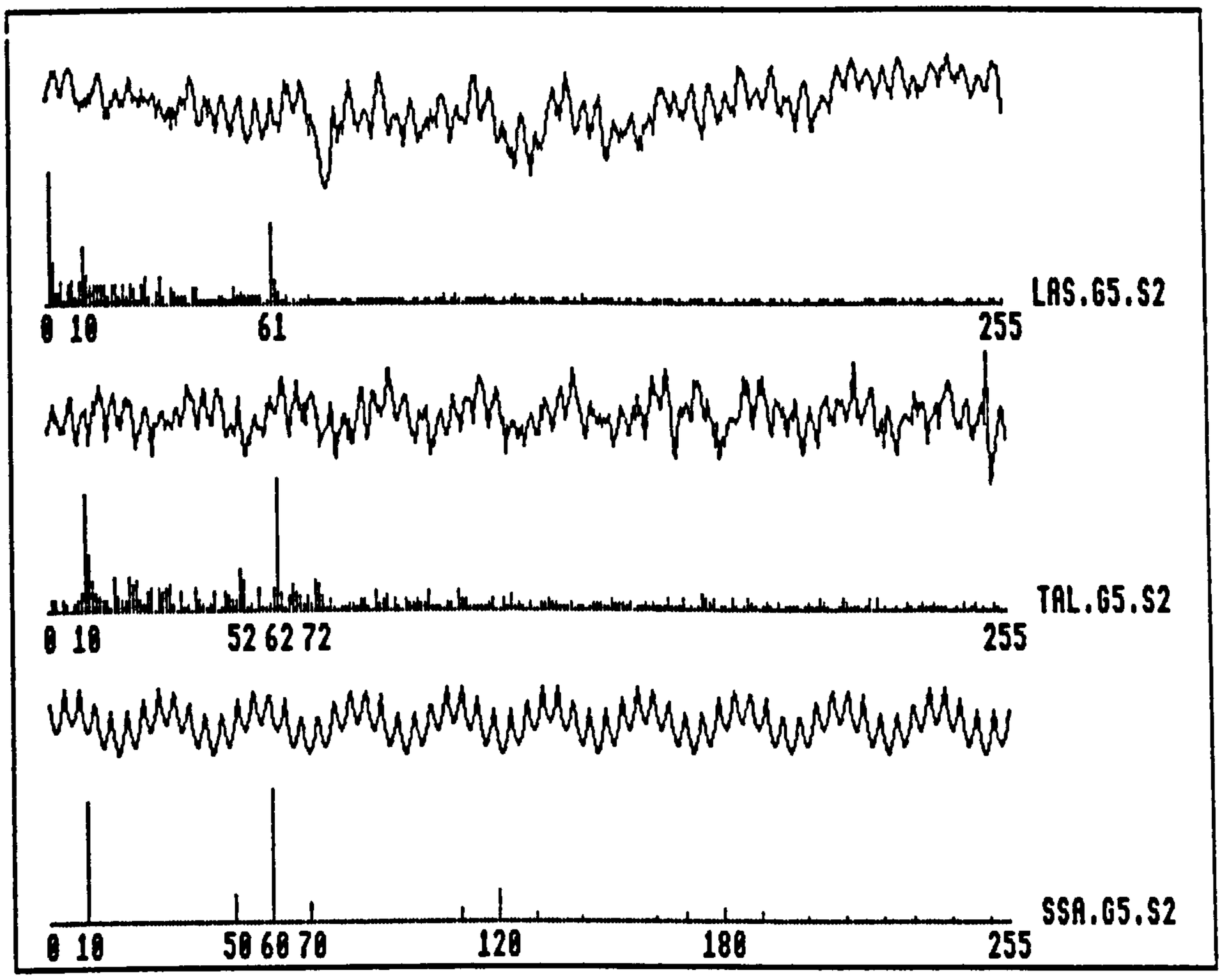

MACHINING PARAMETERS	PRINCIPAL PEAK HARMONICS
No. of knives 6 Feed speed 75 m/min Cutter Speed 6000 rpm Vib. rate 0 Proud Knives 0 Ecc.rate/rev 1 Spindle Runout 2 microns	h1 = 10 h2 = 20 hj = 60

ANALYSIS OF FFT's USING FAULT FINDING ALGORITHM (FFA)		
FFA ON LASER DATA THRESHOLD=0.4	FFA ON TALY DATA THRESHOLD=0.4	FFA ON SSA DATA THRESHOLD=0.4
(0.balance 1) Harmonic 10 (Multi-knife) Harmonic 61	(0.balance 1) Harmonic 10 (Multi-knife) Harmonic 62	(0.balance 1) Harmonic 10 (Multi-knife) Harmonic 60

Figure 7.G5.S2: RESULTS FOR TIMBER SAMPLE NUMBER G5.S2

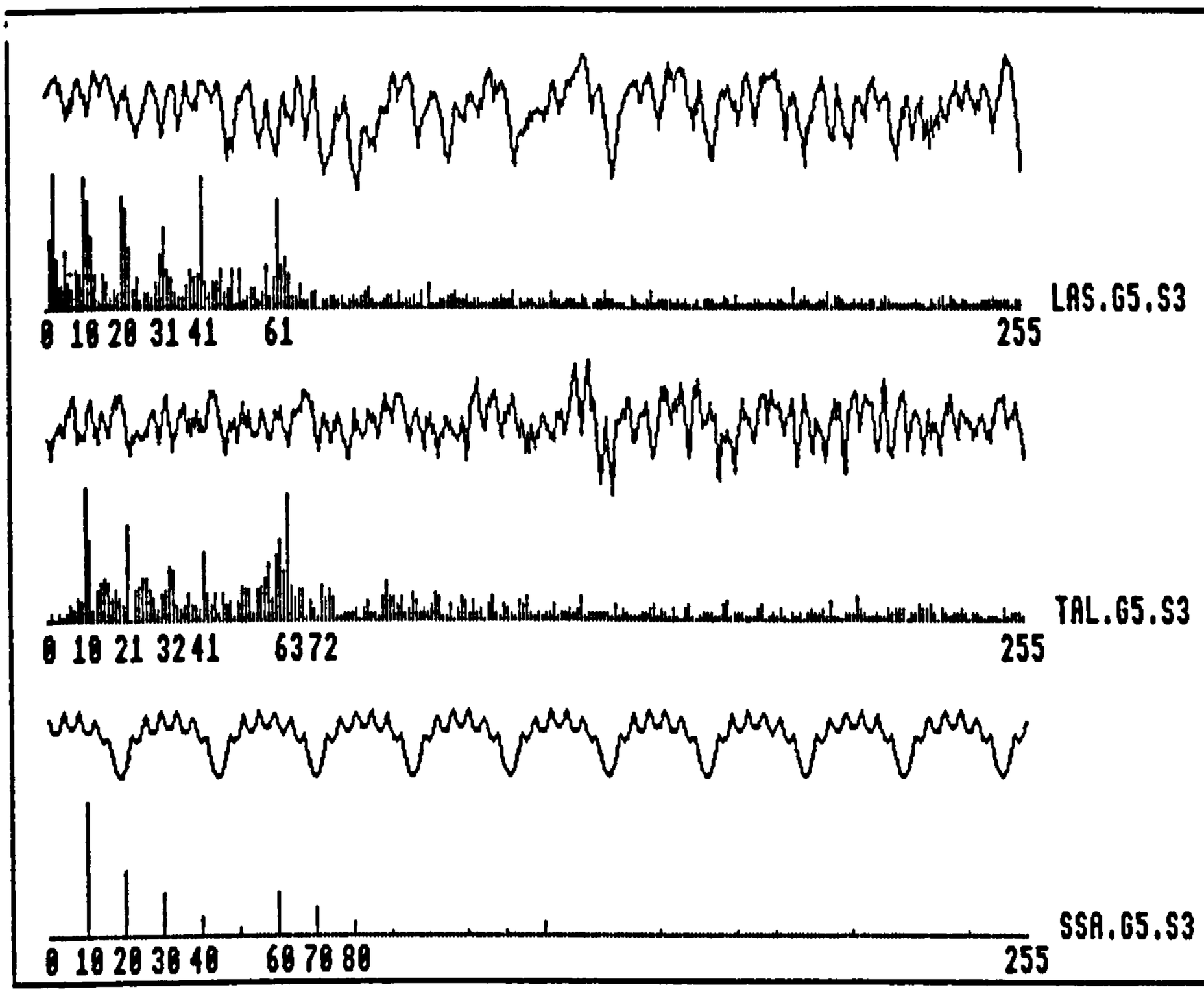

MACHINING PARAMETERS	PRINCIPAL PEAK HARMONICS
No. of knives 6 Feed speed 75 m/min Cutter Speed 6000 rpm Vib. rate 0 Proud Knives 1 >>> 1 Ecc.rate/rev 1 Spindle Runout 2 microns	h1 = 10 h2 = 20 hj = 60

ANALYSIS OF FFT's USING FAULT FINDING ALGORITHM (FFA)		
FFA ON LASER DATA THRESHOLD=0.4	FFA ON TALY DATA THRESHOLD=0.4	FFA ON SSA DATA THRESHOLD=0.4
(Proud Knife) Harmonic 10 Harmonic 20 Harmonic 31 Harmonic 41 (Multi-knife) Harmonic 61	(Proud Knife) Harmonic 10 Harmonic 21 Harmonic 32 Harmonic 41 (Multi-knife) Harmonic 63	(Proud Knife) Harmonic 10 Harmonic 20

Figure 7.65.S3: RESULTS FOR TIMBER SAMPLE NUMBER G5.S3

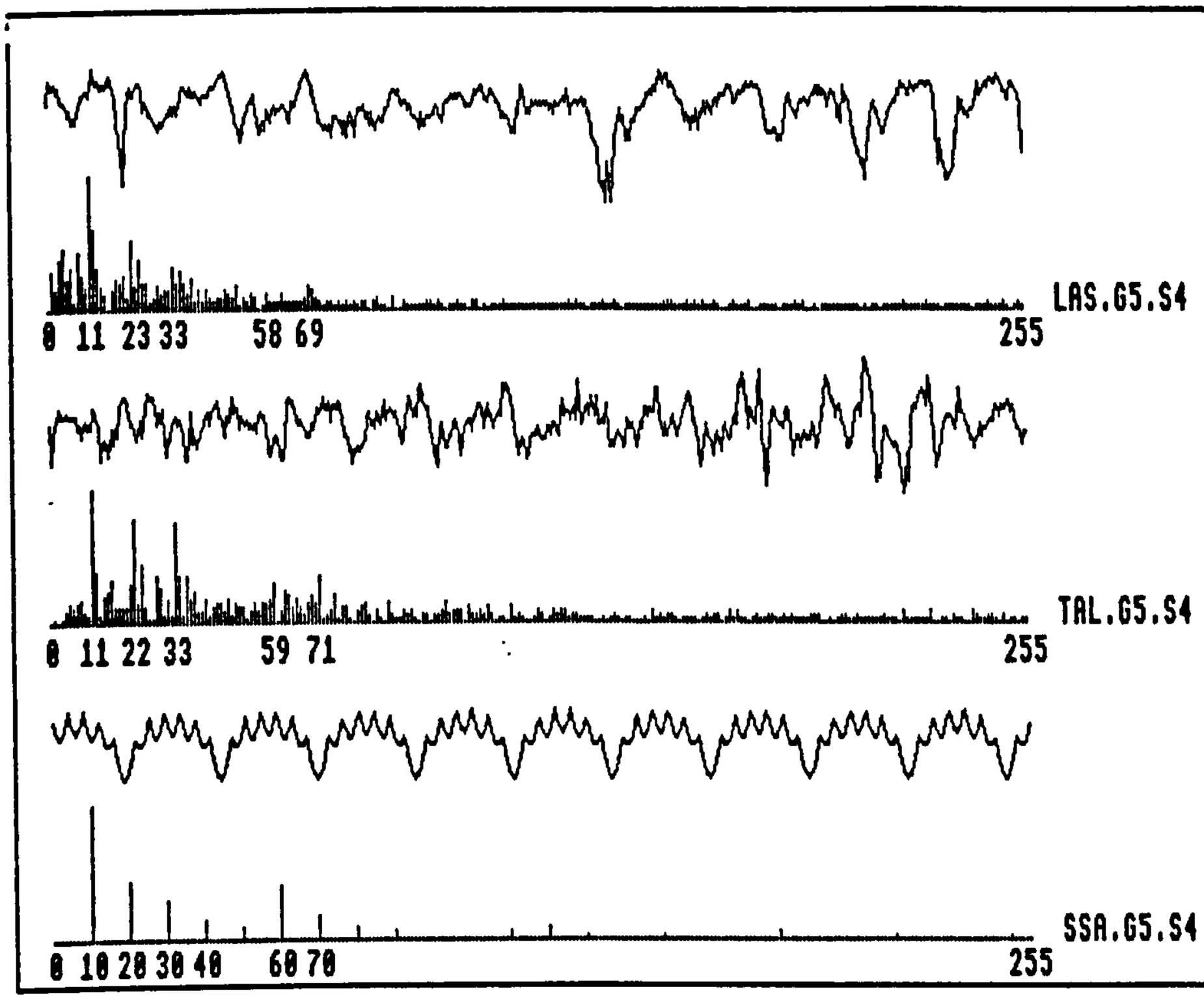

MACHINING PARAMETERS	PRINCIPAL PEAK HARMONICS
No. of knives 6 Feed speed 75 m/min Cutter Speed 6000 rpm Vib. rate 0 Proud Knives 1 >>> 1 Ecc.rate/rev 1 Spindle Runout 2 microns	h1 = 10 h2 = 20 hj = 60

ANALYSIS OF FFT's USING FAULT FINDING ALGORITHM (FFA)		
FFA ON LASER DATA THRESHOLD=0.4	FFA ON TALY DATA THRESHOLD=0.4	FFA ON SSA DATA THRESHOLD=0.4
(Proud Knife) Harmonic 11 Harmonic 22	(Proud Knife) Harmonic 11 Harmonic 22 Harmonic 33 (Unknown Faults) Harmonic 24	(Proud Knife) Harmonic 10 Harmonic 20 (Multi-knife) Harmonic 60

Figure 7.65.S4: RESULTS FOR TIMBER SAMPLE NUMBER G5.S4

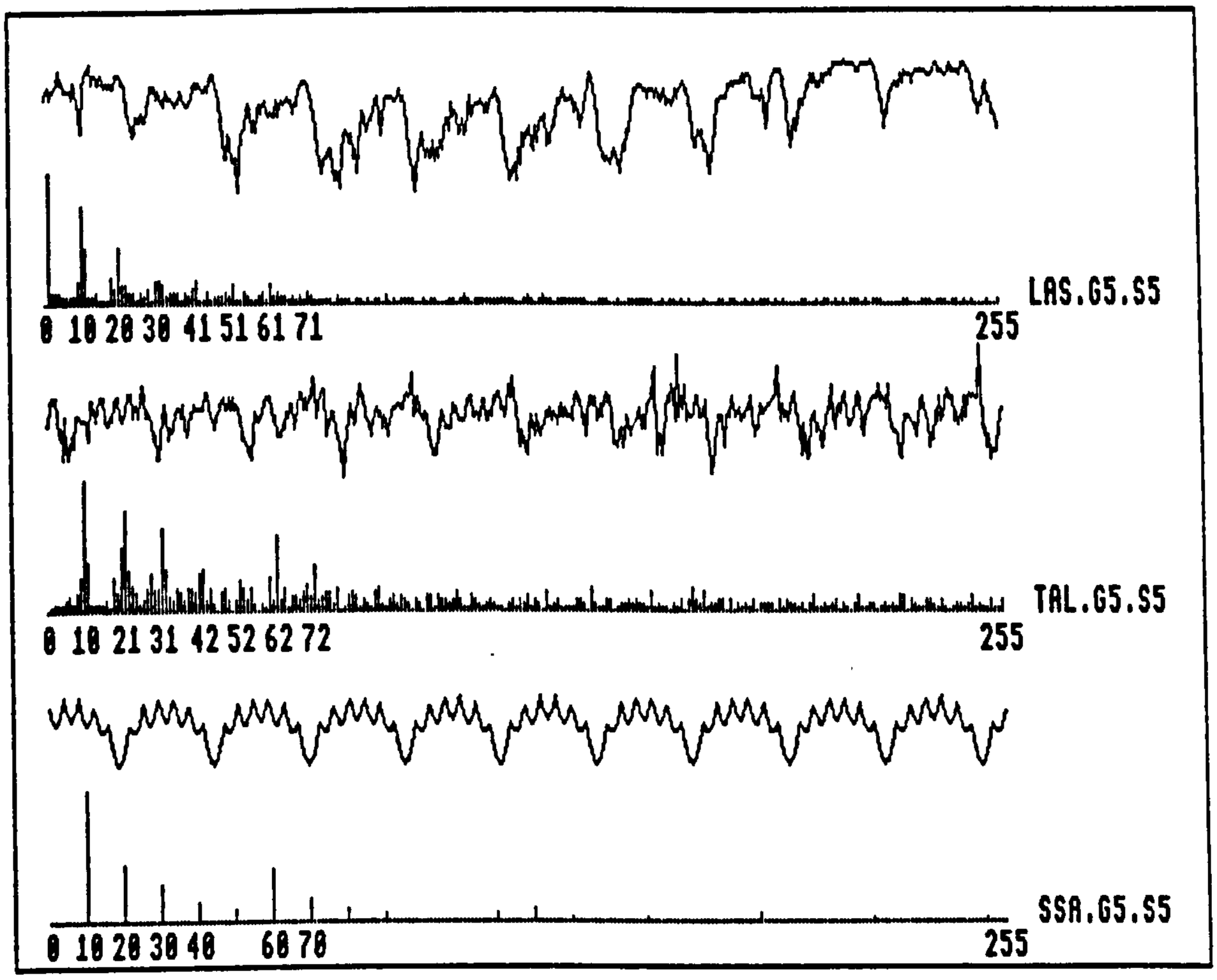

MACHINING PARAMETERS	PRINCIPAL PEAK HARMONICS
No. of knives 6 Feed speed 75 m/min Cutter Speed 6000 rpm Vib. rate 0 Proud Knives 1 >>> 1 Ecc.rate/rev 1 Spindle Runout 2 microns	h1 = 10 h2 = 20 hj = 60

ANALYSIS OF FFT's USING FAULT FINDING ALGORITHM (FFA)		
FFA ON LASER DATA THRESHOLD=0.4	FFA ON TALY DATA THRESHOLD=0.4	FFA ON SSA DATA THRESHOLD=0.4
(Proud Knife) Harmonic 10 Harmonic 20	(Proud Knife) Harmonic 10 Harmonic 21 Harmonic 31 (Multi-knife) Harmonic 62	(Proud Knife) Harmonic 10 Harmonic 20 (Multi-knife) Harmonic 60

Figure 7.G5.S5: RESULTS FOR TIMBER SAMPLE NUMBER G5.S5

TABLES

Table 1

Calibration Table for micrometer-controlled Angle of Incidence of Timber Illumination

Barrel	Transverse Distance	Angle of Incidence	Angle of Incidence
0	0	0	0°-0'-0"
1	6.0	0.1261	0°-7'-34"
2	12.5	0.2627	0°-15'-46"
3	19.5	0.4098	0°-24'-35"
4	25.5	0.5360	0°-23'-09"
5	32.5	0.6831	0°-40'-59"
6	39.0	0.8197	0°-49'-11"
7	45.5	0.9562	0°-57'-22"
8	52.0	1.0928	1°-5'-34"
9	58.5	1.2294	1°-13'-46"
10	65.0	1.3659	1°-21'-57"
11	71.0	1.5025	1°-30'-09"
12	78.0	1.6390	1°-38'-20"
13	84.0	1.7650	1°-45'-54"
14	90.5	1.9015	1°-54'-05"
15	97.0	2.0379	2°-02'-16"
16	103.5	2.1743	2°-10'-28"
17	110.0	2.3108	2°-18'-39"
18	116.0	2.4366	2°-26'-12"
19	122.0	2.5625	2°-33'-45"
20	129.0	2.7093	2°-42'-34"

Table 2

Example of Bit Reversal for 3 bits

Natural Order		Bit - reversed Order	
Decimal	Binary	Binary	Decimal
0	000	000	0
1	001	100	4
2	010	010	2
3	011	110	6
4	100	001	1
5	101	101	5
6	110	011	3
7	111	111	7

TABLE G1: SINGLE KNIFE FINISH

Sample Number	Number of Knives	Head speed (rpm)	Feed speed (m/min)	Machine Condition
G1.S1	4	4500	15	Fully set Skf
G1.S2	4	4500	15	Fully set Skf
G1.S3	4	4500	30	Fully set Skf
G1.S4	4	9000	30	Fully set Skf
G1.S5	4	9000	30	Fully set Skf
G1.S6	4	9000	30	Fully set Skf
G1.S7	4	6000	17	Fully set Skf
G1.S8	4	6000	17	Fully set Skf

TABLE G2: UNBALANCED CUTTERHEAD

Sample Number	Number of Knives	Head speed (rpm)	Feed speed (m/min)	Machine Condition
G2.S1	4	4500	60	Fully set
G2.S2	4	4500	60	Fully set
G2.S3	4	4500	60	Fully set
G2.S4a	4	4500	60	O-bal:1 screw
G2.S4b	4	4500	60	O-bal:3 screws
G2.S4c	4	4500	60	O-bal:5 screws
G3.S5	6	6000	80	Fully set
G2.S6	6	6000	80	Fully set
G2.S7a	6	6000	80	O-bal:3 screws
G2.S7b	6	6000	80	O-bal:5 screws
G2.S8a	6	6000	80	O-bal:3 screws
G2.S8b	6	6000	80	O-bal:5 screws
G2.S9a	6	6000	80	O-bal:3 screws Wet timber
G2.S10a	6	6000	75	Fully set
G2.S10b	6	6000	75	O-bal:3 screws
G2.S11a	6	6000	75	O-bal:2 screws
G2.S11b	6	6000	75	O-bal:3 screws
G2.S12a	6	6000	75	O-bal:3 screws
G2.S12b	6	6000	75	O-bal:3 screws

TABLE G3: PROUD KNIFE

Sample Number	Number of Knives	Head speed (rpm)	Feed speed (m/min)	Machine Condition
G3.S1	6	6000	75	Fully set
G3.S2	6	6000	75	1 proud:+4µm
G3.S3	6	6000	75	1 proud:+8µm
G3.S4	6	6000	75	1 proud:+12µm
G3.S5	6	6000	75	1 proud:+8µm
G3.S6	6	6000	75	1,2 proud:+8µm
G3.S7	6	6000	75	1,3 proud:+8µm
G3.S8	6	6000	65	fully set
G3.S9	6	6000	65	1 proud:+4µm
G3.S10	6	6000	65	1 proud:+8µm
G3.S11	6	6000	65	1 proud:+12µm
G3.S12	8	6000	90	fully set
G3.S13	8	6000	90	1 proud: -4µm
G3.S14	8	6000	90	1 proud: -8µm
G3.S15	8	6000	90	4,8 proud: -8µm

TABLE G4: TIMBER VIBRATION

Sample Number	Number of Knives	Head speed (rpm)	Feed speed (m/min)	Machine Condition
G4.S1a	4	4500	15	Fully set Single knife finish
G4.S1b	4	4500	15	No chipbreaker Skf
G4.S2a	4	4500	60	Fully set
G4.S2b	4	4500	60	No top pressure No chipbreaker
G4.S3a	6	6000	80	Fully set
G4.S3b	6	6000	80	Outboard bearing tied but un-pressurised
G4.S3c	6	6000	80	Outboard bearing untied and un-pressurised
G4.S4	6	6000	80	No outboard bearing
G4.Sea	6	6000	65	Fully set
G4.S5b	6	6000	65	chipbreaker:1Bar
G4.S6a	6	6000	75	Fully set
G4.S6b	6	6000	75	chipbreaker:2Bar
G4.S6c	6	6000	75	chipbreaker:1Bar

TABLE G5: FAULT COMBINATION

Sample Number	Number of Knives	Head speed (rpm)	Feed speed (m/min)	Machine Condition
G5.S1	6	6000	65	fully set joint
G5.S2	6	6000	65	O-bal:2 screws
G5.S3	6	6000	65	O-bal:2 screws 1 proud:+8µm
G5.S4	6	6000	65	O-bal:2 screws 1 proud:+8µm Chipbreaker: 1 Bar
G5.S5	6	6000	65	O-bal:2 screws 1 proud:+8µm Chipbreaker: 1 Bar Outboard Bearing: untied

APPENDICES

APPENDIX A: COMPUTER SOFTWARE

APPENDIX A0: LOCI-0

APPENDIX A1: LOCI-1

APPENDIX A2: LOCI-2

APPENDIX A3: LOCI-3

APPENDIX A4: Surface Simulation Algorithm (SSA)

APPENDIX A5: Data Capture Software

APPENDIX A6: FFT Algorithm: BBC BASIC Version

APPENDIX A7: FFT Algorithm: Machine Code Version

APPENDIX A8: Fault Finding Algorithm (FFA)

APPENDIX B: LASER; PHOTODIODE; TALYROND 200

APPENDIX B1: Helium-Neon Laser data sheet

APPENDIX B2: Laser light Production

APPENDIX B3: Photodiodes

APPENDIX B4: Talyrond 200

APPENDIX C: CIRCUIT DIAGRAMS

APPENDIX C1: Electronic Hardware

APPENDIX D:

APPENDIX D1: Cutterhead Balancing

APPENDIX E: PUBLISHED PAPERS

Appendix A0: LOCI-0

```
10 REM LOCI-0
20 XORG=0: YORG=0
30 INPUT "NO OF KNIVES" N1
40 V1=300: W1=2
50 H1=450:R1=200:Tw=275:F1=PI+ASN((H1-Tw)/R1)
60 MOVE XORG,YORG:DRAW XORG,YORG+Tw:
    MOVE XORG,YORG+Tw:DRAW XORG+1280,YORG+Tw
70 Lb=2*PI/N1
80 YORG=YORG+H1
90 XORG=XORG+R1
100 FOR I=1 TO N1
110     Lg=(I-1)*Lb
120     X=R1*(COS(F1-Lg)-COS(PI/2))
130     Y=R1*SIN(F1-Lg)-SIN(0)
140     MOVE XORG,YORG: DRAW XORG+X,YORG+Y
150     FOR dt=0.1 TO PI STEP 0.1
160         Y=R1*SIN(F1-Lg+W1*dt)-R1*SIN(0)
170         X=R1*(COS(F1-Lg+W1*dt)-COS(PI/2))+V1*dt
180         DRAWXORG+X,YORG+Y
190     NEXT dt
200 NEXT I
```

Appendix A1: LOCI-1

```
 10 REM LOCI-1
 20 XORG=0:YORG=0
 30 INPUT "NO OF KNIVES" N1%
 40 V1=400: W1=2
 50 H1=400:R1=200:Tw=250:F1=PI+ASN((H1-Tw)/R1)
 60 MOVEXORG,YORG:DRAWXORG,YORG+Tw:
      MOVEXORG,YORG+Tw:DRAWXOR G+1280,YORG+Tw
 70 Lb=2*PI/N1%
 80 YORG=YORG+H1
 90 XORG=XORG+R1
100 FOR I=1 TO N1%
110    Lg=(I-1)*Lb
120    X=R1*(COS(F1-Lg)-COS(PI/2))
130    Y=R1*SIN(F1-Lg)-SIN(0)
140    MOVE XORG,YORG: DRAW XORG+X,YORG+Y
150    FOR dt=0 TO PI STEP .03
160       Y=R1*SIN(F1-Lg+W1*dt)-R1*SIN(0)
170       X=R1*(COS(F1-Lg+W1*dt)-COS(PI/2))+V1*dt
180       MOVE XORG+X,YORG+R1: DRAW XORG+X,YORG+Y
190    NEXT
200 NEXT
```

Appendix A2: LOCI-2

```
10REM LOCI-2
20 xx=150:yy=600: VDU28,0,25,79,0
30 XORG=200: YORG=200
40 INPUT "NO. OF KNIVES " N1
50 INPUT "POSITION OF PROUD  KNIFE " kp:IF kp>N1 THEN 50
60 IF kp<1 THEN 50 ELSE kp=kp-1
70 V1=10: W1=150: R=0.2:R1=R:Rp=R+0.05:H=0.2:Tw=0.19
80 Lb=2*PI/N1
90 FOR I=0 TO 2*N1
100    IF I= kp + (I DIV N1)*N1 THEN R1=Rp ELSE R1=R
110    th=2*ACS((H-Tw)/R1):F1=PI+ASN((H-Tw)/R1)
120    Lg=(I-1)*Lb
130    Xs=V1*Lg/W1: Xe=R1*(COS(F1+th)-COSF1)+V1*(Lg+th)/W1
140    IF I=0 THEN step=ABS(Xe-Xs)/16
150    dt=0
160    FOR x=Xs TO Xe STEP step
170       a=-(W1*R1*SINF1-V1)/(W1*R1*COSF1)
180       b=SQR((2*(W1*R1*SINF1-V1))^2
              -4*W1*R1*COSF1*2*(x-V1*Lg/W1))/(2*W1*R1*COSF1)
190       A=a+b:B=a-b
200       IF B>0 THEN dt=B
210       IF A>0 THEN dt=A
220       Y=R1*(SIN(F1+W1*dt)-SIN(F1))
230       X=R1*(COS(F1+W1*dt)-COSF1)+V1*(Lg+W1*dt)/W1
240       MOVE XORG+X*xx,YORG:DRAW XORG+X*xx,YORG+Y*yy
250    NEXT
260 NEXT
```

Appendix A3: LOCI-3

```
10 REM LOCI-3
20  MODE 0
30  m=1: DIM Y(1000),kp(20): VDU28,0,12,79,0
40  xx=600*2: yy=18000*2
50 XORG=0: YORG=350
60 INPUT "Number of Knives " N%
70 REPEAT:
          INPUT "Number of Proud Knives "Nokp%:
     UNTIL Nokp%>0 AND Nokp%<N%+1: Nokp%=Nokp-1
80 FOR J=1 TO Nokp%:
               INPUT "Position of Proud Knives " kp:
               kp(J)= kp-1:
       NEXT
  90  INPUT "MULT. REVS n1 " n1
 100  Lb=2*PI/N%
 110  V1=20: W1=190
 120  r1=0.2:d=0.0002:R=r1:r2=r1+0.003:H1=0.4:T=0.202
 130  IF n1=0 THEN r=0 ELSE r=0.0005:R1=R1+r
 140  th=2*ACS((H1-T)/R1):F1=PI+ASN((H1-T)/R1)
 150  Es=F1+(n1-1)*PI
 160  Xs=0
 170  Xe=R1*(COS(F1+th)-COSF1)+r*(COS(Es+n1*th)-COSEs)+V1*(Lb+th)/W1
 180  step=(Xe-Xs)/16: m=1/step:
 190  V1=V1*m:r1=r1*m:d=d*m:R1=R1*m:
 200  r2=r2*m:r=r*m:H1=H1*m:T=T*m
 210  MOVE XORG,YORG+T/m:DRAW XORG+200,YORG+T/m
 220  step=1
 230  FOR I=0 TO 4*N%:
              IF Nokp%=0 THEN 250
 240          FOR J=1 TO Nokp%:
                        R=r1:
                       IF I=kp(J)+(I DIV N%)*N% THEN R=r2:J=Nokp%:
               NEXT
 250          th=2*ACS((H1-T)/R1):F1=PI+ASN((H1-T)/R1)
 260          Lg=I*Lb :E=Es-Lg*n1
 270          Xs=INT(V1*Lg/W1):
               Xe=INT(R1*(COS(F1+th)-COSF1)
                                          +r*(COS(E+n1*th)-COSE)+V1*(Lg+th)/W1)
 280          xs=(V1*Lg/W1):
               xe=(R1*(COS(F1+th)-COSF1)
                                          +r*(COS(E+n1*th)-COSE)+V1*(Lg+th)/W1)
 290      FOR x=Xs TO Xe STEP step
 300          a=-(W1*(R1*SINF1+r*n1*SINE)-V1)/(W1^2*(R1*COSF1+r*n1^2*COSE))
 310          b=SQR((W1*(R1*SINF1+n1*r*SINE)-V1)^2
                          -2*W1^2*(R1*COSF1+r*n1^2*COSE)*(x-V1*Lg/W1))/
                                                  (W1^2*(R1*COSF1+r*n1^2*COSE))
 320          A=a+b:B=a-b:dt=0
 330          IF B>0 THEN dt=B
 340          IF A>0 THEN dt=A
 350          Y=R1*(SIN(F1+W1*dt)-SIN(F1))+r*SIN(E+n1*W1*dt)
 360           IF Y < Y(x) THEN Y(x)=Y
 370           X=R1*(COS(F1+W1*dt)-COSF1)+
                                       r*(COS(E+n1*W1*dt)-COSE)+V1*(Lg+W1*dt)/W1
 380            MOVE XORG+x*xx/m,YORG:
                 DRAW XORG+x*xx/m,YORG+Y*yy/m
 390     NEXT
 400 NEXT
 410 CLS :CLG
```

```
420 FOR X=0 TO 1000
430     MOVE XORG+X*xx/m,YORG:
        DRAW XORG+X*xx/m,YORG+Y(X)*yy/m
440 NEXT
```

Appendix A4: SSA (Surface Simulation Algorithm)

```
4570DEF PROC SSA (Surface Simulation Algorithm)
4571 NOS=0
4580 m=1: ASUM=0:SCALE=0 :VDU28,40,26,79,8
4590 xx=32000/16*3*4/6*2
4600 yy=400000
4610 XORG=0 :TX=0:BLK$="                              "
4620 YORG=1000:TY=10
4630 VDU31,TX,0:PRINT"No of knives":
                PRINT"Feed speed":
                PRINT"Cutter Speed":
                PRINT"Vib rate":
                PRINT"Proud Knives":
                PRINT"Mult. of Revs":
                PRINT"Spindle Runout"
4640 VDU31,15,0:PRINT;nN%:
          VDU31,15,1:PRINT;V*60:
          VDU31,15,2:PRINT;rpm:
          VDU31,15,3:PRINT;rate:
          VDU31,15,4:PRINT;Nokp%:
          VDU31,15,5:PRINT;n:
          VDU31,15,6:PRINT;r/10^-6
4650 TXX=18:TYY=4:IF Nokp%=0 THEN 4670
4660 FOR J=1 TO Nokp%:VDU31,TXX,TYY:PRINT;kp(J)+1:TXX=TXX+2:NEXT
4670 smplth=0.125
4680 CHANGE=0
4690 REPEAT
4700       IF FIRST=1 OR SCALE=4 THEN 4710 ELSE 4910
4710      VDU31,TX,TY:PRINT"f0 - change data              "
4720      PRINT"f9 - to run                    "
4730     CHANGE= GET
4740     IF CHANGE=130 THEN 4750 ELSE 4900
4750     REPEAT:VDU31,TX,TY:PRINT"Select function button "
4760       REPEAT:CHANGE=GET:UNTIL CHANGE>130 AND CHANGE<140
4770            ON CHANGE-130 GOTO 4780,4790,4800,4810,4820,4860,4860,4880,4890
4780            VDU31,TX,TY:INPUT "NO. OF KNIVES " nN%:
                IF nN%=0 THEN 4780 ELSE VDU31,15,0:PRINTBLK$:
                        VDU31,15,0:PRINT;nN%:GOTO 4890
4790                    VDU31,TX,TY:PRINTBLK$:
                        VDU31,TX,TY: INPUT "WOOD FEEDSPEED m/min"V:
                 IF V=0  THEN 4790 ELSE
                        VDU31,15,1:PRINTBLK$:V=V/60
                        VDU31,15,1:PRINT; V*60: GOTO 4890
4800      VDU31,TX,TY:PRINTBLK$:
            VDU31,TX,TY:INPUT "CUTTER  SPEED rpm " rpm:
             IF rpm=0 THEN 4800 ELSE W=2*PI*rpm/60:
                                                VDU31,15,2:PRINTBLK$:
                                                VDU31,15,2:PRINT ;rpm :
                                                GOTO 4890
4810      VDU31,TX,TY:PRINTBLK$:
            VDU31,TX,TY:INPUT "VIBRATION rate " rate:
            VDU31,15,3 :PRINTBLK$:
            VDU31,15,3:PRINT ;rate:GOTO 4890
4820      VDU31,TX,TY:PRINTBLK$:
            VDU31,TX,TY: INPUT "NUMBER OF PROUD KNIVES "Nokp%:
            VDU31,15,4 :PRINTBLK$:
            VDU31,15,4 :PRINT;Nokp%:
            FOR J=0 TO 20:kp(J)=0:NEXT:REM zero store proud knife
4830       IF Nokp% <>0  THEN 4840 ELSE 4890
```

```
4840    TXX=18:TYY=4:REM start position to display position of proud knife
4850    FOR J=1TO Nokp%:
        REPEAT:
            VDU31,TX,TY:PRINTBLK$:
            VDU31,TX,TY:
            INPUT"POSITION OF PROUD KNIFE" kp:
        UNTIL kp>0 AND kp<nN%+1:
        VDU31TXX,TYY:PRINT;kp:kp(J)=kp-1:TXX=TXX+2:
          NEXT:GOTO 4890
4860    VDU31,TX,TY:PRINTBLK$:
          VDU31,TX,TY:INPUT"MULT. of REVS for spindle runout n" n:
          VDU31,15,5:PRINTBLK$:
          VDU31,15,5:PRINT;n :GOTO 4890
4870    IF n<>0 THEN 4880 ELSE r=0:GOTO 4890
4880                  VDU31,TX,TY:PRINT;BLK$:
                        VDU31,TX,TY:INPUT"Spindle runout (microns)"r:
                        VDU31,15,6 :PRINTBLK$:
                        VDU31,15,6 :PRINT;r:r=r*10^-6:GOTO 4890
4890  UNTIL CHANGE=139
4900  GOTO 5030
4910  FIRST=1
4920  VDU31,TX,TY:INPUT "NO. OF KNIVES " nN%:
          IF nN%=0 THEN 4920 ELSE  VDU31,15,0 :PRINT BLK$ :
                                                VDU31,15,0 :PRINT ;nN%
4930  VDU31,TX,TY:PRINTBLK$:
          VDU31,TX,TY:INPUT "WOOD FEEDSPEED m/min " V:
          IF V=0 THEN 4930 ELSE
            VDU31,15,1:PRINT BLK$:
            VDU31,15,1:V=V/60:PRINT;V*60
4940   VDU31,TX,TY:PRINTBLK$:
          VDU31,TX,TY:INPUT "CUTTER  SPEED rpm " rpm:
          IF rpm=0 THEN 4940 ELSE W=2*PI*rpm/60:
                            VDU31,15,2:PRINT BLK$:
                            VDU31,15,2:PRINT ;rpm
4950   VDU31,TX,TY:PRINTBLK$:
          VDU31,TX,TY:INPUT "VIBRATION rate " rate:
          VDU31,15,3 :PRINTBLK$:VDU31,15,3:PRINT ;rate
4960   VDU31,TX,TY:PRINTBLK$:
          VDU31,TX,TY:INPUT"NUMBER OF PROUD KNIVES "Nokp%:
          VDU31,15,4 :PRINTBLK$:
          VDU31,15,4 :PRINT;Nokp%:
           IF Nokp% =0 THEN 4980
4970   TXX=18:TYY=4:
          FOR J=1TO Nokp%:
                  REPEAT:VDU31,TX,TY:PRINTBLK$:
                                  VDU31,TX,TY:
                                  INPUT"POSITION OF PROUD KNIFE "kp:
                  UNTIL kp>0 AND kp<nN%+1:
                   VDU31,TXX,TYY:PRINT;kp:kp(J)=kp-1:TXX=TXX+2:
          NEXT:
4980   VDU31,TX,TY:PRINTBLK$:
          VDU31,TX,TY:INPUT "MULT.of REVS for spindle runout n " n:
          VDU31,15,5 :PRINTBLK$:
          VDU31,15,5:PRINT;n
4990   IF n<>0 THEN 5010 ELSE r=0:GOTO 5030
5010   VDU31,TX,TY:PRINT;BLK$:
          VDU31,TX,TY:
           INPUT "INPUT Spindle runout in microns " r:
           VDU31,15,6 :PRINTBLK$:
           VDU31,15,6:PRINT;r
```

```
5020     r=r*10^-6: REM out of true radus of spindle
5030 UNTIL CHANGE=139
5040 Lb=2*PI/nN% :c=smplth *W/(2*PI*V)
5050 r1=0.1:d=0.0002:R=r1:r2=r1+.05*d:H=r1+0.2*d:vib=0.000003
5060 th=2*ACS((R-d)/R):F=PI+ASN((R-d)/R)
5070 Es=F+(n-1)*PI :REMstart angle for out of balance term
5080 Xs=0:Xe=R*(COS(F+th)-COSF)+r*(COS(Es+th)-COSEs)+V*(Lb+th)/W
5090 step=smplth /256:m=1/step: :REM increment of 1 for each step
5100 V=V*m:r1=r1*m:d=d*m:R=R*m:r2=r2*m:r=r*m:
        H=H*m:SMPLTH=smplth*m:vib=vib*m
5110 step=1:I=-1:Yhi=-10000:Ylo=100000::REM Y values for determine peaks later
5120 REPEAT
5130   I=I+1 :IF Nokp%=0 THEN 5180
5140   FOR J= 1 TO Nokp%
5150     R=r1
5160     IF I= kp(J)+(I DIV nN%)*nN% THEN R=r2:J=Nokp%:REM detect Proud knife
5170   NEXT
5180   th=2*ACS((R-d)/R):F=PI+ASN((R-d)/R)
5190   L=I*Lb :E=Es-L*n
5200   Xs=INT(V*L/W):Xe=INT(R*(COS(F+th)-COSF)+r*(COS(E+th)-COSE)+V*(L+th)/W)
5210   Ys=H+R*SINF+r*SINE
5220   MOVE XORG,YORG:DRAW XORG+Xs/m,YORG+Ys/m
5240   dt=0:xMAX=V*F/W+(1/(W^2*COSF)*(W*SINF-V/R)^2-2*(COSF-1))*R/2
5250   FOR x=Xs TO Xe STEP step
5260     a=-(W*(R*SINF+r*n*SINE)-V)/(W^2*(R*COSF+r*n^2*COSE))
5270     b= SQR((W*(R*SINF+n*r*SINE) -V)^2 -2*W^2*(R*COSF+r*COSE)*(x-V*L/W))
                    /(W^2*(R*COSF+r*n^2*COSE))
5280     A=a+b:B=a-b
5290     IF B>0 AND A>B THEN dt=BELSE IFA>0 THEN dt=A ELSE dt=B
5300     Y=H+R*SIN(F+W*dt)+r*SIN(E+n*W*dt)+vib*SIN(F+rate*W*dt)
5310     Y= Y-1*d:REM invert value
5320     X=R*(COS(F+W*dt)-COSF)+r*(COS(E+n*W*dt)-COSE)+V*(L+W*dt)/W
5330     IF x<extra OR x>255+extra GOTO5390
5340     IF Y < Y(x) THEN Y(x)=Y :REM store lowest current value of over lap cusps
5350     IF Y(x)>Yhi THEN Yhi=Y(x):Xhi=x-extra
5360     IF Y(x)+1*d < Ylo THEN Ylo=Y(x)+1*d :Xlo=x-extra
5370     a=x-extra:XR(a)=Y(x):XI(a)=0:
5380     MOVE XORG+(x*xx/m)-(extra*xx/m),YORG:
           DRAW XORG+(x*xx/m)-(extra*xx/m),YORG+Y(x)*yy/m
5390     REM PRINTx;" ",X;" ",Y;" ",I
5400   NEXT
5420   nc=(I-1)/nN%
5430 UNTIL nc>c+1
5440 IF A$="" THEN A$="SIMULATION"
5450 VDU31,TX,TY+6:PRINT"h1= ";m*W*smplth/(2*PI*V)
5460 VDU31,TX,TY+7:PRINT"hp= ";m*W*smplth*nN%/(2*PI*V)
5470 h1=m*W*smplth/(2*PI*V):h2=m*W*smplth/(PI*V):hp=m*W*smplth*nN%/(2*PI*V)
5480 hs=h1
5490 hv=2*hp
5500 V=V/m :r=r/m:SCALE=4
5510ENDPROC
```

Appendix A5
Data Capture Software

A5.0 Computer Initilisation

```
 70DEF PROCinitial
 80 yy=400000:m=1:xx=512000
 90 extra=20:TX=0:TY=8:BLK$="                                    ":ADD=&23000
100 VDU 28,40,20,79,17
110 FLAG=0:WHICH=0:*FX225,129
120 DIMC(790),S(790),Y(256+extra),kp(20),
    XRR(1024),Hx(255),Hy(255),fft(128)
130 DIM code% &FF
140 DIM screenDump 2000
150 Z%=code%+&20
160 black=&00:mode=0:print=1:colAcc1=1:colAcc2=2:
    colAcc3=3:mask=4:row=5:across=6:partByte=7:pinIdent=8:downCol=9
    pointer=10:SP=13
165 ivhi=&207:ivlo=&206:pcr=&FE6C:ifr=&FE6D:ier=&FE6E:ddrb=&FE62:
    orb=&FE60
170 SCL=6:XORG=50:LTH=4:inv=0
180 N%=1024/LTH:J%=LN(N%)/LN2
190
200 DIM XR(N%+extra),XI(N%+extra)
210REM Set Function Keys
220 *FX 225,130
230REM State Addresses
240 A%=0:B%=0:VDU 21
250 PROCassemble
260 PROCdumper
270 VDU 6
280 BLANK$="                                                    "
290 PRINT"LOADING SINE AND COSINE TABLES":PROClookup:CLS
300 nN%=0:V=0:rpm=0:rate=0:Nokp%=0:n=0:r=0
310ENDPROC
```

A5.1 Laser Instrument

```
470DEFPROClaser
480 REM Saturation Voltage
490 V=&20
500 CLG
510 C%=0:Z%=0:Cn=0:dt%=0
520 REM Repeat 1
530           C%=C%+2000
540           Xo=&3F:Xi=&3F
550           REPEAT
560              CLS:PRINT"LASER MEASUREMENT IN PROGRESS"
570              Cn=Cn+1:dt%=0
580              IF Cn=1 THEN 620
590                      IF Xo=Xi THEN Xi=Xi+1
600                      dt%=(Xi-V)*(C%-Z%)/(Xo-Xi):Z%=C%
610                      IF dt%=0 THEN 730
620                 C%=C%+dt%
630                 CALL start
640                 TIME=0
650                 FOR D= 0 TO C% :NEXT
660                     T=TIME
670                     CALL start
680REM               if 1
690                 IF ?flag=0 THEN 690
700REM               endif1
710                 Xo=Xi:Xi=?storelo
720           UNTIL ABS(V-Xi)<=1
730           Cn=0:VDU5:MOVE 0,1000
740 PRINT"C%=";C%,
          "INTEGRATION TIME=";T/100"  ;"SEC.",":
          "Z%=";Z%,"dt%=";dt%,
          "Xi=";Xi,"Xo=";Xo;" V=";V:VDU4
750 PROCPLOT(500,1)
760 ENDPROC
```

A5.2 Talyrond 200

```
1120DEF PROCtallyrond
1130 CLG:CLS:*FX 15,0
1140 PRINT"Press any key after starting traverse"
1150 delay=25000:x=GET
1160 ?latchlo=delay MOD 256
1170 ?latchhi=delay DIV 256
1180 CALL start2
1190 ?counthi=delay DIV 256:TIME=0
1200 CLS:PRINT"TALYROND MEASUREMENT IN PROGRESS":PRINT
1210 IF FLAG=1 THEN 1230
1220 PRINT" AND LOADING SINE & COSINE TABLE":
     PROClookup:FLAG=1:VDU31,0,2:PRINT BLANK$
1230 REPEAT:UNTIL ?Xstore=0
1240 XORG=50:YORG=500
1250 CLS:MOVE XORG,YORG
1260 FOR I=0 TO 1023
1270   DRAW XORG+I,YORG+?(&1300+I)*SCL
1280 NEXT
1290ENDPROC
```

A5.3 Interrupt Service Routine

```
2540DEF PROCassemble1
2550 DIM Z% 400
2560 FOR opt%=0 TO 2 STEP 2
2570 P%=Z%
2580[
2590 OPT opt%
2600.init   SEI                 ;DIS INT
2610        LDA  ivhi           ;check
2620.if     CMP  #&E6           ;chech if already initiated
2630        BNE  els            ;yes. THEN branch to els
2640        STA  oldv+1         ;save old vec
2650        LDA  ivlo           ;save old vec
2660        STA  oldv           ;save old vec
2670        LDA  #int MOD256    ;new vec lobyte
2680        STA  ivlo           ;instate new NEWvec lo
2690        LDA  #int DIV256    ;new vec hibyte
2700        STA  ivhi           ;instate new vec hi
2710.els    CLI                 ;clear int disable
2720        RTS                 ;return
2730
2740.int    LDA  &FC            ;save reg's
2750        PHA                 ;A
2760        PHX                 ;X
2770        PHY                 ;Y
2780        LDA  ifr            ;did CB1 interrupt?
2790        AND  #&10           ;check CB1
2800.ifCB1  BEQ  exit           ;if CB1 load array data ELSE exit
2810.then   LDA  #&FF           ;then
2820        STA  orb            ;clear int by writing to PORT B
2830.page   LDA  #&00           ;first page lobyte
2840        STA  &70            ;install lobyte
2850        LDA  #&13           ;first page hibyte
2860        STA  #&71           ;install hibyte
2870        LDA  #&3F           ;min data=&0,max data=&3F
2880        STA  storelo        ;store for min data
2890        STZ  storehi
2900        LDX  #&04           ;page count
2910        LDY  #&00           ;page line pointer
2920.rpt1   LDA  #&00           ;REPEAT
2930        STA  orb            ;clk array RAM
2940        LDA  #&40           ;clk array RAM
2950        STA  orb            ;clk array RCM
2960        LDA  orb            ;load data
2970        AND  #&3F           ;&3F because 6 bits only
2980        STA  (&70),Y        ;store data
2990        CMP  storelo        ;compare data with current min
3000.if1    BPL  else1          ;if larger ignore
3010        STA  storelo        ;if smaller save in storelo
3020.else1  CMP  storehi        ;compare data with current max
3030.if2    BMI  else2          ;if smaller ignore
3040        STA  storehi        ;if larger save in storehi
3050.else2 INY                  ;point to nextline on current
                                                          page
3060.unt1   BNE  rpt1           ;UNTIL Y=0
3070        INC  &71            ;point to next page
3080        DEX                 ;dec page count
3090        BNE  rpt1           ;UNTIL X=0
3100        LDA  &1300          ;fill-in "missing" data
3110        STA  &16FF          ;at &16FF
3120        INC  flag           ;signal end of data transfer
3130        JMP  exit2
3140.oldv   NOP                 ;reserve space for old vec add
3150        NOP                 ;reserve space for old vec add
3180.exit   LDA  ifr            ;get system VIA interrupt
                                                        status
3190        AND  #&40
3200        CMP  #&40           ;if timer 1 interrupt then
3210        BNE  exit2
3220        LDA  countlo        ;clear interrupt
3230        LDY  Ystore
3240        LDA  #&20
```

```
3250          STA  orb          ;line 6 hi
3260          LDA  orb
3270          AND  #&1F         ;read data
3280          STA  temploc      ;store data
3290          LDA  #&10         ;get ready for BIT test
3300          STZ  orb          ;line 6 lo
3310          BIT  orb
3320.if3      BNE  else3
3330.then3    SEC
3340          JMP  endif3
3350.else3    CLC
3360.endif3   ROL  temploc
3370          LDA  temploc
3380          STA  (addlo),Y
3390          INC  Ystore
3400          BNE  exit2
3410          INC  addhi
3420          DEC  Xstore
3430          BNE  exit2
3440          SEI
3450          LDA  ier
3460          AND  #&40
3470          STA  ier
3480          CLI
3490 exit2    PLY
3500          PLX
3510          PLA
3520          STA  &FC
3530          JMP  (oldv)       ;continue interrupt chain
3540.start    SEI
3550          LDA  #&90         ;enable int.
3560          STA  ier          ;enable int
3570          LDA  pcr          ;load pcr
3580          ORA  # &F0        ;conserve port A CA1/CA2
3590          STA  pcr          ;configure port B CB1 +edge
                                                      CB2 hi
3600          LDA orb           ;dummy load to clear interrupt
                                                    if any occured
3610          LDA #&FF          ;all outputs hi
3620          STA orb           ;all outputs hi
3630          LDA #&C0          ;configure PORT B direction as
3640          STA ddrb          ;6 inputs,2 outputs
3650          CLI
3660          STZ flag          ;flag to signal data transfer
                                                          end
3670          LDA pcr           ;SEND start pulse
3680          AND #&DF          ;by conserving PORT A
                                                   directives
3690          STA pcr           ;and strobing CB2
3700          ORA #&20          ;
3710          STA pcr           ;DONE
3720          RTS               ;Return
3730
3740.start2   LDA #&20
3750          STA ddrb          ;configure output port
3770          STZ addlo         ;start address
3780          LDA #&13
3790          STA addhi
3800          STZ Ystore
3810          LDA #&4
3820          STA Xstore
3830          LDA #&40          ;set aux. cont reg
3840          ORA acr
3850          AND #&7E
3860          STA acr
3870          LDA #&20
3880          STA ddrb
3890          SEI
3900          LDA #&C0
3910          ORA ier           ;set int. enable reg
3920          STA ier
3930          CLI
3940          RTS
```

```
3170 ]
3970 NEXTopt%
3980ENDPROC
```

Appendix A6
FFT Algorithm :BBC BASIC

```
481 REM>FFTTHE
482
490 DEF FNrbitr=USR sss
511
520 DEFPROCassemble
530 FOR pass=0 TO 3 STEP 3
540 P%=Z%
550 [OPT pass
560 .sss
570         STMFD   (SP)!,{R1,R9,R14}
580         MOV     R9, #&A
590         MOV     R1, #0
600 .loop
610         MOVS     R0,R0,LSR #1
620         ADCS    R1,R1,R1
630         SUBS    R9,R9,#1
640         BNE loop
650 ;
660         MOV     R0,R1
670         LDMFD   (SP)!,{R1,R9,pc}
680 ]
690 NEXT pass
700 ENDPROC
751
760 DEF PROCfft(DELTA,SIGN)
770
780 PN=2*PI/N%
790 L%=N%/2
800 IR1%=IR%-1
810 K%=0
830 FOR IS%= 1 TO IR%
840    REPEAT
850       FOR I%=1 TO L%
860          REM      K%=K%+1 N/A SEE LINE 1000
870          KPL%=K%+L%
880          A%=K%/(2^IR1%)
890          AM%=FNrbitr
900          IF AM%=0 THEN 910 ELSE 930
910                   XR1=XR(KPL%):XI1=XI(KPL%)
920                   GOTO 980
930          ARG=AM%*PN
940          ARG1=(AM%-N%/4)*PN
950          C=COS(ARG)
960          S=-SIGN*COS(ARG1)
970          XR1=C*XR(KPL%)-S*XI(KPL%):XI1=C*XI(KPL%)+S*XR(KPL%)
980          XR(KPL%)=XR(K%)-XR1:XI(KPL%)=XI(K%)-XI1
990          XR(K%)=XR(K%)+XR1:XI(K%)=XI(K%)+XI1
1000         K%=K%+1
1010      NEXT I%
1020      K%=K%+L%
1030   UNTIL K%>=N%
1040   K%=0
1050   IR1%=IR1%-1
1060      L%=L%/2
1070 NEXT IS%
1080 FOR K%=0 TO N%-1
1090      A%=K%
1100      K1%=FNrbitr
1110      IF K1%>K% THEN 1120 ELSE 1150
1120                 XR1=XR(K%):XI1=XI(K%)
1130                 XR(K%)=XR(K1%):XI(K%)=XI(K1%)
1140                 XR(K1%)=XR1:XI(K1%)=XI1
1150 NEXT K%
1160 IF DELTA<>1 THEN 1170 ELSE ENDPROC
1170              FOR K%=0 TO N%-1
1180                  XR(K%)=DELTA*XR(K%):XI(K%)=DELTA*XI(K%)
1190              NEXT K%
1210 ENDPROC
```

AppendixA7
FFT Algorithm:AssemblyLanguage

```
 5 CN=0
10 IF PAGE<>&2800 THEN PAGE=&2800:CHAIN"TEST3"
20 REM A.FFT256WOOD ASSEMBLY LANGUAGE
30 MODE128
40 LTH=4  :complo=PAGE-1:comphi=PAGE-2:countlo=PAGE-3:counthi=PAGE-4
41 nnn=PAGE-5:cn=PAGE-6:aa=PAGE-7:nn1=PAGE-8:is=PAGE-9:
     count4=PAGE-10:REM*
45 ?countlo=0:?counthi=0 :?cn=0
46 INPUT "IScount" nn: ?is=nn-1:INPUT "Icount" nn: ?nnn=nn-1:
     INPUT "A%" nn:?aa=nn MOD 256:?nn1=nn DIV 256
 50 SCL=6:
 60 XORG=50:YORG=800
 70 ADD=&1300
 80 reallo=&1700
 90 realhi=&1801
100 imaglo=&1902
110 imaghi=&1A03
120 sinlo=&1B04
130 sinhi=&1E06
140 coslo=&2108
150 coshi=&240A
160 XR1lo=&1800
170 XR1hi=&1901
180 XI1lo=&1A02
190 XI1hi=&1B03
192 sinl =&74:?sinl=sinlo MOD 256:?(sinl+1)=sinlo DIV 256
194 sinh =&76:?sinh=sinhi MOD 256:?(sinh+1)=sinhi DIV 256
196 cosl =&78:?cosl=coslo MOD 256:?(cosl+1)=coslo DIV 256
198 cosh =&7A:?cosh=coshi MOD 256:?(cosh+1)=coshi DIV 256
200 storelo = &72
210 storehi = &73
220 mpdlo = &270C
230 mpdhi = &270D
240 mprlo = &270E
250 mprhi = &270F
260 prod1 = &2710
270 prod2 = &2711
280 prod3 = &2712
290 prod4 = &2713
300 divlo = &7C
310 divhi = &7D
320 pdivlo = &80
330 divqlo = &7E
340 divqhi = &7F
350 pdivhi = &81
360  l=&82
370 Icount=&83
380 k=&84
390 kpl=&85
400 aA=&86
410 IScount=&87
420 flag = &88
430 addlo=&89
440 addhi=&8A
450 adrlo=&8B
460 adrhi=&8C
470 IR1=&8D
```

```
480 loo=&8E
490 ivhi = &207
500 ivlo = &206
510 pcr = &FE6C
520 ifr = &FE6D
530 ier = &FE6E
540 ddrb = &FE62
550 orb = &FE60
555 IF CN>0 THEN 590
560 PROClookup:CN=1
570 FOR I%=0 TO 255 : A=A+(63-?(ADD+LTH*I%)):NEXT
580 AVE=A/256:MOVE XORG,YORG
590 FOR I%=0 TO 255
640       ?(reallo+I%)=4*SIN(8*PI*I%/256)+4:?(realhi+I%)=0
650     ?(imaglo+I%)=0:?(imaghi+I%)=0
740     DRAW XORG+LTH*I%,YORG+?(reallo+I%)*5
760 NEXT
765 IF CN=2 THEN 4600
770 DIM Z% 1000
780 FOR pass%=0 TO 2 STEP 2
790 P%=Z%
800[
810 OPT pass%
820\
830  .fft          LDA    #128
840                STA     l
850                LDA    #7
860                STA    IR1     \IR1%=IR%-1
880                STZ    k
890                STZ    aA
910                STZ    IScount
920  .rept1        NOP           \FOR IS%=1 TO IR%
930  .rept2        NOP           \REPEAT
940                STZ    Icount   \FOR I%=1TO L%
950   .rept3       LDA    l
960                CLC
970                ADC    k
980                STA    kpl     \KPL%=K%+L%
990                LDA    k
1000               LDX    IR1
1002               BEQ    endif0
1010       .loop1  LSR    A
1020               DEX
1030               BNE     loop1  \K%/(2^IR1)
1110       .endif0 STA    loo
1120               JSR    rbitr    \AM%=RBITR%
1130               LDA    loo
1140               BNE    else1   \IF AM%=0 then1 else1
1150               LDX    kpl
1160               LDA    reallo,X
1170               STA    XR1lo
1180               LDA    realhi,X
1190               STA    XR1hi    \XR1=XR(KPL%)
1200\
1210               LDA    imaglo,X
1220               STA    XI1lo
1230               LDA    imaghi,X
1240               STA    XI1hi     \XI1=XI(KPL%)
1250               JMP    enif1
1260  .else1       LDX    kpl
```

```
1270            LDA   imaglo,X
1280            STA   mprlo
1290            LDA   imaghi,X
1300            STA   mprhi
1310            LDY   aA
1320            LDA   (sinl),Y
1330            STA   mpdlo
1340            LDA   (sinh),Y
1350            STA   mpdhi
1360            JSR   mult16   \S(A%)*XI(KPL%)
1370\
1375            JSR   shift4
1380            LDA   prod2
1390            STA   complo
1400            LDA   prod3
1410            STA   comphi
1420            JSR   twocmp   \2's comp for subtraction
1430\
1440            LDA   complo
1450            STA   adrlo
1460             LDA   comphi
1470            STA   adrhi   \ store for "addition"
1480\
1490            LDA   reallo,X
1500            STA   mprlo
1510            LDA   realhi,X
1520            STA   mprhi
1530            LDA   (cosl),Y
1540            STA   mpdlo
1550            LDA   (cosh),Y
1560            STA   mpdhi
1570            JSR   mult16    \C(A%)*XR(KPL%)
1580\
1585            JSR   shift4
1590            LDA   prod2
1600            STA   addlo
1610            LDA   prod3
1620            STA   addhi     \store for "addition"
1630            JSR   add16     \do "addition"
1640\
1650            LDA   addlo
1660            STA   XR1lo
1670            LDA   addhi
1680            STA   XR1hi     \XR1=C(A%)*XR(KPL)-S(A%)*XI(KPL)
1690\
1700            LDA   imaglo,X
1710            STA   mprlo
1720            LDA   imaghi,X
1730            STA   mprhi
1740            LDA   (cosl),Y
1750            STA   mpdlo
1760            LDA   (cosh),Y
1770            STA   mpdhi
1780            JSR   mult16   \C(A%)*XI(KPL)
1790\
1795            JSR   shift4
1800            LDA   prod2
1810            STA   addlo
1820            LDA   prod3
1830            STA   addhi     \store for addition
```

```
1840\
1850            LDA   reallo,X
1860            STA   mprlo
1870            LDA   realhi,X
1880            STA   mprhi
1890            LDA   (sinl),Y
1900             STA   mpdlo
1910            LDA   (sinh),Y
1920            STA   mpdhi
1930            JSR   mult16   \S(A%)*XR(KPL)
1940\
1945            JSR   shift4
1950            LDA    prod2
1960            STA   adrlo
1970            LDA    prod3
1980            STA   adrhi    \store for addition
1990            JSR   add16    \do addition
2000\
2010            LDA    addlo
2020            STA   XI1lo
2030            LDA    addhi
2040            STA   XI1hi    \XI1=C(A%)*XI(KPL)+S(A%)*XR(KPL)
2041            LDA cn
2042            CMP nn1
2043            BNE rrr
2044            LDA aA
2045            CMP aa
2046            BNE rrr
2047            LDA Icount
2048            CMP nnn
2049            BNE rrr
2050            LDA IScount
2051            CMP is
2052            BNE rrr
2053            RTS
2054\
2060 .rrr       INC   aA       \A%=A%+1
2062            BNE    enif1
2064            INC   sinl+1
2066            INC   sinh+1
2067            INC   cosl+1
2068            INC   cosh+1
2069            INC cn
2070 .enif1     LDA cn
2071            CMP nn1
2072            BNE eee
2073            LDA aA
2074            CMP aa
2075            BNE eee
2076            LDA Icount
2077            CMP nnn
2078            BNE eee
2079            LDA IScount
2080            CMP is
2081            BNE eee
2082            RTS
2088 .eee       LDY   k
2089            LDA   XR1lo
2090            STA    complo
2100            LDA    XR1hi
```

```
2110            STA   comphi
2120            JSR   twocmp  \two's comp XR1 for subtraction
2130\
2140            LDA   complo
2150            STA   adrlo
2160            LDA   comphi
2170            STA   adrhi    \store XR1 for subtraction
2180\
2190            LDA   reallo,Y
2200            STA   addlo
2210            LDA   realhi,Y
2220            STA   addhi    \store XR(K%) for subtraction
2230\
2240            JSR   add16    \do subtraction
2250            LDA   addlo
2260            STA   reallo,X
2270            LDA   addhi
2280            STA   realhi,X \storeresultXR(KPL)=XR(K%)-XR1
2290\
2300            LDA   XI1lo
2310            STA   complo
2320            LDA   XI1hi
2330            STA   comphi
2340            JSR   twocmp   \2's comp XI1 for subtraction
2350            LDA   complo
2360            STA   adrlo
2370            LDA   comphi
2380            STA   adrhi    \ store XI1 for subtraction
2390\
2400            LDA   imaglo,Y
2410            STA   addlo
2420            LDA   imaghi,Y
2430            STA   addhi    \store XI(K%) for subtraction
2440            JSR   add16    \ do subtraction
2450\
2460            LDA   addlo
2470            STA   imaglo,X
2480            LDA   addhi
2490            STA   imaghi,X \store result XI(KPL)=XI(K%)-XI1
2500\
2510            LDA   reallo,Y
2520            STA   addlo
2530            LDA   realhi,Y
2540            STA   addhi    \store XR(K%) for addition
2550\
2560            LDA   XR1lo
2570            STA   adrlo
2580            LDA   XR1hi
2590            STA   adrhi    \store XR1 for addition
2600            JSR   add16    \do addition
2610\
2620            LDA   addlo
2630            STA   reallo,Y
2640            LDA   addhi
2650            STA   realhi,Y \store result XR(K%)=XR(K%)+XR1
2660\
2670            LDA   imaglo,Y
2680            STA   addlo
2690            LDA   imaghi,Y
2700            STA   addhi    \store XI(K%) for addition
```

```
2710\
2720            LDA   XI1lo
2730            STA   adrlo
2740            LDA   XI1hi
2750            STA   adrhi     \store XI1 for addition
2760            JSR   add16     \ do addition
2770            LDA   addlo
2780            STA   imaglo,Y
2790            LDA   addhi
2800            STA   imaghi,Y \store result XI(K%)=XI(K%)+XI1
2801            JMP bbb          \ LDA cn
2802            CMP nn1
2803            BNE bbb
2804            LDA aA
2805            CMP aa
2806            BNE bbb
2807            LDA countlo
2808            CMP nnn
2809            BNE bbb
2810            RTS
2811\
2820 .bbb       INC   k         \K%=K%+1
2821
2830\
2840            INC   Icount
2850            LDA   Icount
2860            CMP   1
2870            BNE   here1     \FOR I%=1TO L%     NEXT
2880\
2890            LDA   k
2900            CLC
2910            ADC   1
2920            STA   k         \ K%=K%+L%
2930\
2950            BCC   here      \UNTIL K%>=N%
2960\
2970            STZ   k         \K%=0
2980            DEC   IR1       \IR1%=IR1%-1
2990            LSR   1         \L%=L%/2
3000\
3010            INC   IScount
3020            LDA   IScount
3030            CMP   #8
3040            BNE   here      \FOR IS%=1 TO IR%    NEXT
3050            JMP   rept4
3060 .here      JMP rept1
3065 .here1     JMP   rept3
3070 .rept4     LDY   k
3080            STY   loo
3100            JSR   rbitr      \PROCRBITR
3110            LDX   loo
3130            CPX   k
3140            BMI   else2     \IF K1%>K% then2 else2
3150            LDA   reallo,Y
3160            STA   XR1lo
3170            LDA   realhi,Y
3180            STA   XR1hi     \XR1=XR(K%)
3190\
3200            LDA   imaglo,Y
3210            STA   XI1lo
```

```
3220                LDA   imaghi,Y
3230                STA   XI1hi     \XI1=XI(K%)
3240\
3250                LDA   reallo,X
3260                STA   reallo,Y
3270                LDA   realhi,X
3280                STA   realhi,Y  \XR(K%)=XR(K1%)
3290\
3300                LDA   imaglo,X
3310                STA   imaglo,Y
3320                LDA   imaghi,X
3330                STA   imaghi,Y \XI(K%)=XI(K1%)
3340                LDA   XR1lo
3350                STA   reallo,X
3360                LDA   XR1hi
3370                STA   realhi,X  \XR(K1%)=XR1
3380\
3390                LDA   XI1lo
3400                STA   imaglo,X
3410                LDA   XI1hi
3420                STA   imaghi,X \XI(K1%)=XI1
3430\
3440.     else2     INC   k
3450                LDA   k
3455                CLC
3460                ADC   #1
3470                BCC   rept4     \NEXT K%
3480                RTS
3490\
3500 .twocmp        LDA   comphi
3510                EOR   #&FF
3520                STA   comphi
3530                LDA   complo
3540                EOR   #&FF
3550                CLC
3560                ADC   #1
3570                STA   complo
3580                BCC   end
3590                INC   comphi
3600 .end           RTS
3610\
3620 .rbitr         PHX
3630                PHY
3640                LDX   #8
3650 .loop2         ROR   loo
3660                ROL   A
3670                DEX
3680                BNE   loop2
3690                STA   loo
3700                PLY
3710                PLX
3720                RTS
3730 .mult16        PHX
3740                PHY
3741                JMP mult
3750                LDA    mprhi
3760                AND    mpdhi
3770                BPL    mult
3780                LDA    mprlo
3790                STA    complo
```

```
3800            LDA   mprhi
3810            STA   comphi
3820            JSR   twocmp
3830            LDA   complo
3840            STA   mprlo
3850            LDA   comphi
3860            STA   mprhi
3870\
3880            LDA   mpdlo
3890            STA   complo
3900            LDA   mpdhi
3910            STA   comphi
3920            JSR   twocmp
3930            LDA   complo
3940            STA   mpdlo
3950            LDA   comphi
3960            STA   mpdhi
3970\
3980 .mult      LDA   #&0
3990            STA   prod3   \;hi byte of product = 0
4000            STA   prod4   \;hi byte of product = 0
4010            LDX   # 16    \;set bit counter
4020 .next1     LSR   mprhi   \ ;shift hi-byte of multplier
4030            ROR   mprlo   \;catch carry/next multplier bit intocarry
4040            BCC   rotate  \;branch if multplier bit was zero
4050            LDA   prod3   \;get third byte of product
4060            CLC           \;prepare to add
4070            ADC   mpdlo   \;add to low byte of multplicand
4080            STA   prod3   \;store new third byte of product
4090            LDA   prod4   \;get forth byte of product
4100            ADC   mpdhi   \;add to hi byte of multplicand
4110 .rotate    ROR   A
4120            STA   prod4   \;store new forth byte of product
4130            ROR   prod3   \;rotate third byte of product
4140            ROR   prod2   \;rotate second byte of product
4150            ROR   prod1   \;rotate first byte of product
4160            DEX           \;dec;ent counter
4170            BNE   next1    \;loop back if more bits
4180            PLY
4190            PLX
4200            RTS
4210\
4220 .div16     PHX
4230            PHY
4240            LDA   #&0
4250            STA   pdivlo  \;set lo partial dividend
4260            STA   pdivhi  \;set hi partial dividend
4270            LDX   #16
4280 .next2     ASL   divqlo  \ ;shift dividend/quotent left
4290            ROL    divqhi \;shift dividend/quotent left
4300            ROL    pdivlo \;shift bits into partial dividend
4310            ROL    pdivhi \;shift bits into partial dividend
4320            LDA    pdivlo \;load lo byte of partial dividend
4330            SEC           \;prepare to subtract lo bytes
4340            SBC    divlo  \;subtrect lo divisor
4350            TAY           \;save result in Y
4360            LDA    pdivhi \;load hi partial dividend
4370            SBC    divhi  \;subtract hi divisor
4380            BCC    done   \;skip subtraction if dividend less than divisor
4390            INC    divqlo \;incriment quotent
```

```
4400                STA   pdivhi  \;save new hi pratial dividend
4410                STY   pdivlo  \;save new lo pratial dividend
4420 .done          DEX           \ ;dec;ent counter
4430                BNE   next2   \;loop back if more bits to deal with
4440                PLY
4450                PLX
4460                RTS
4470\
4480 .add16
4490                LDA   addlo   \load lo-byte of first No
4500                CLC           \Clear carry fir low-byte addition
4510                ADC   adrlo   \Add low-byte of first No to Accum.
4520                STA   addlo   \store lo-byte of result
4530                LDA   addhi   \load hi-byte of first No
4540                ADC   adrhi   \Add hi-byte of first No to Accum.
4550                STA   addhi   \store hi-byte of result
4560                RTS
4570\
4571 .shift4       LDA   #1
4572                STA   count4
4573 .rept         ASL   prod1
4574                ROL   prod2
4575                ROL   prod3
4576                DEC   count4
4577                BNE   rept
4578                RTS
4580 ]
4590      NEXT pass%
4595 CN=2
4600 REM FOR I=0TO255 :PRINT~?(reallo+I):NEXT
4601 REM PROCmathstest:GOTO4601
4610 TIME=0:CALL fft
4612 PRINT"TIME=";TIME/100;"sec"
4613PRINT"XR(KPL)=";~?(reallo+?kpl)+?(realhi+?kpl)*256;
        TAB(20);"XI(KPL)=";~?(imaglo+?kpl)+?(imaghi+?kpl)*256
4614 PRINT"XR(K)=";~?(reallo+?k)+?(realhi+?k)*256;
         TAB(20);"XI(K)=";~?(imaglo+?k)+?(imaghi+?k)*256
4615 PRINT"XR1=";~?XR1lo+?XR1hi*256;TAB(20);"XI1=";~?XI1lo+?XI1hi*256
4616 PRINT"K=";?k,"KPL=";?kpl
4617 PRINT"A%=";?aA+?cn*256
4618 PRINT"I%=";?Icount+1
4619 PRINT"IS%=";?IScount+1
4620  PRINT"C(A%)=";~?(coslo+?cn*256+?aA)+?(coshi++?cn*256+?aA)*256;"
                    ";"XI(KPL%)=";~?(imaglo+?kpl)+?(imaghi+?kpl)*256;"
                    ";"S(A%)=";~?(sinlo+?cn*256+?aA)+?(sinhi+?cn*256+?aA)*256
4629 REM FOR I=0TO255 :PRINT~?(reallo+I)+?(realhi+I)*256:NEXT
4630 YORG=200:MOVE XORG,YORG
4640 FOR I=0TO255
4650        real=(?(reallo+I)+?(realhi+I)*256):imag=(?(imaglo+I)+?(imaghi+I)*256)
4660        IF real>&7FFF THEN real=real OR &FFFF0000
4670        IF imag>&7FFF THEN imag=imag OR &FFFF0000
4680       MOVE XORG+I*LTH,YORG:
              DRAW XORG+I*LTH,YORG+(SQR(real^2+imag^2))/200
4690 NEXT
4700 GGGGG=GET :GOTO10

4710 DEFPROClookup
4720 Y=OPENIN "LC"
4730 X=OPENIN "LS"
4740 FOR I=0 TO 769
```

```
4750    INPUT#Y ,C%
4770    ?(coslo+I)=(C% AND &FFFF) MOD 256:
           ?(coshi+I)=(C% AND &FFFF) DIV 256
4780    INPUT#X ,S%
4800    ?(sinlo+I)=(S% AND &FFFF) MOD 256:?(sinhi+I)=(S% AND &FFFF) DIV 256
4805    REM PRINT TAB(0);"C=";~(?(coslo+I)+(?(coshi+I))*256);TAB(20);
           TAB(40);"S=";~(?(sinlo+I)+(?(sinhi+I))*256);TAB(60)
4810 NEXT:CLS
4820 CLOSE# Y
4830 CLOSE# X
4840ENDPROC

4999DEFPROClooksin
5000    A=0 :CN=0
5010    sinh=&1E06
5020    sinl=&1B04
5030    REPEAT
5040        PRINTA,CN,~?(sinl+A)+?(sinh+A)*256
5050        A=A+1 :CN=CN+1
5060        IF A=256 THEN sinl=sinl+&100:sinh=sinh+&100:A=0
5070     UNTIL CN=770
5080 ENDPROC

6000DEFPROCmathstest
6010 INPUT"FIRST" FFFF
6020 INPUT"SECOND" SSSS
6030 ?mprhi= (FFFF AND &FFFF) DIV 256:PRINT"mprhi=";~?mprhi
6040 ?mprlo= (FFFF AND &FFFF) MOD 256:PRINT"mprlo=";~?mprlo
6050 ?mpdhi= (SSSS AND &FFFF) DIV 256:PRINT"mpdhi=";~?mpdhi
6060 ?mpdlo= (SSSS AND &FFFF) MOD 256:PRINT"mpdlo=";~?mpdlo
6070 CALL mult16
6080 PRINTFFFF;"*";SSSS;"=";~?prod1+?prod2*256,~SSSS*FFFF
6090 PRINT"prod1=";~?prod1,"prod2=";~?prod2
6999ENDPROC
```

Appendix A8
Fault Finding Algorithm FFA

```
13390 DEF PROC FFA fault finding algorithm
13400 IF NOS=0 THEN INPUT"THRESHOLD "thresh
13410 VDU31,0,0:PRINT "                ":
13420 VDU31,0,0:IF NOS=0 THEN PRINT"FFA ON LASER DATA"
13430          IF NOS=1 THEN PRINT"FFA ON TALY  DATA"
13440          IF NOS=2 THEN PRINT"FFA  ON SSA  DATA"
13450 VDU31,0,1:PRINT"  THRESHOLD=";thresh
13460 peak=0 :h1=INT(h1):hj=INT(hj)
13470 FOR I=INT(h1-3) TO N%/2-1
13480    IF fft(I) > peak THEN peak=fft(I):hp=I
13490 NEXT
13500 VDU31,0,3
13510 problem=0
13520 X=0:f1=1:f2=2:f3=4:f4=8:f5=16:f6=32:f7=64:f8=128:
13530 lock1=0:lock2=0:lock3=0:lock4=0
13540 single=0:exist=0:hjfound=0:LL=0:MM=0:NN=0:PP=0
13550 Jp1=0:Jp2=0:Jp3=0:pk1=0:pk2=0:pk3=0:peakj=0:
13560 FOR I=0 TO N%-1:Hx(I)=0:Hy(I)=0:Hz(I)=0:Hp(I)=0:NEXT
13570 FOR I=INT(h1-5) TO N%/2-3
13580    REM IF1 local max
13590    IF(fft(I+1)-fft(I))>0AND(fft(I+2)-fft(I+1))<0
                ANDfft(I+3)<fft(I+1)ANDfft(I+4)<fft(I+1)
                ANDfft(I-1)<fft(I+1) AND fft(I-2)<fft(I+1)
                AND fft(I-3)<fft(I+1)
                THEN 13600 ELSE 14610
13600          REM THEN1 compare with threshold
13610          REM IF2
13620          IF fft(I+1)> peak*thresh
                     THEN 13630 ELSE 14590:
                     REM THEN2
13630               REM IF3 peak is h1 then check for proud knife OR Ob1
13640               IF ABS(I+1-h1)<=2
                          THEN 13650 ELSE 14340:REM THEN3
13650                    REM search for other peaks between h1 and hj
13660                     peak1=0:peak2=0:peak3=0:LL=0
13670                    Hy(LL)=I+1
13680                    FOR J=INT(I+1) TO INT(hj-4):
13690                         IF (fft(J+1)-fft(J))>0 AND (fft(J+2)-fft(J+1))<0
                                  AND fft(J+3)<fft(J+1) AND fft(J+4)<fft(J+1)
                                  THEN 13700 ELSE 13760
13700                             IF fft(J+1)> peak*threshstorepeak
13710                                  IF pk1>peak1
                                            THEN peak1=pk1:Jp1=J+1:
13720                             IF fft(J+1)< peak1 AND fft(J+1)> peak1*thresh
                                       THEN pk2=fft(J+1):
13730                             IF pk2>peak2
                                       THEN peak2=pk2:Jp2=J+1:
13740                             IF fft(J+1)< peak2 AND fft(J+1)> peak2*thresh
                                       THEN pk3=fft(J+1):
13750                          IF pk3>peak3
                                       THEN peak3=pk3:Jp3=J+1:
13760                    NEXT:
13770                    REM keep record of any peaks between h1 and hj
13780                    REM IF4 If no peaks found - Ob1 or Sk
13790                    REM THEN4 check for Ob1 ie. hj
13800                    IF LL=0
                              THEN 13810 ELSE 14040
```

```
13810                peakK=0
13820               FOR K= INT(hj/2) TO INT(1.5*hj):REM PRINT K
13830                    IF fft(K)>peakK THEN peakK=fft(K):Kp=K
13840              NEXT :peakj=0:REM PRINT"peakK="peakK,Kp
13850              IF ABS(Kp-hj)>3
                         THEN 13860 ELSE 13950
13860                      FOR K=INT(hj/2) TO INT(1.5*hj):REM PRINT K
13870                          IF (fft(K+1)-fft(K))>0 AND (fft(K+2)-fft(K+1))<0
                                   AND fft(K+3)<fft(K+1)
                               THEN 13880 ELSE 13940
13880                            IF fft(K+1)>thresh*thresh*peakK
                                     THEN 13890 ELSE 13940
13890                                IF ABS(K+1-hj)<3
                                   THEN 13900 ELSE 13940
13900                               Kj=K+1:peakj=fft(Kj):
                                      hjfound=1:Kjj=Kj:
                                      K=INT(1.5*hj):
                                    :GOTO 13940

13910                                       REM else
                                              endif
13920                                  REM elseendif
13930                              REM else endif
13940                        NEXT: GOTO 13970
                             REM else
13950                      Kj=Kp:peakj=fft(Kj):GOTO 13970
13960                  REM IF5
13970                IF peakj> thresh*thresh*peak
                           THEN 13980 ELSE 14000:REM THEN5
13980          X=X+f1:lock1=1:PRINT"  (O.balance 1)":PRINT"   Harmonic ";I+1
13990                      PRINT"  (Multi-knife)":PRINT"   Harmonic ";Kj:
                             X=X+f5:lock2=1:Kjj=Kj:hjfound=1:
                             GOTO 14030:REM TO ENDIF5
14000                    REM ELSE5
14010                    X=X+f8:lock3=1:PRINT" (Single  knife)":
                           PRINT"  Harmonic ";I+1:GOTO 14030:REM TO ENDIF5
14020                  REM ENDIF5
14030                GOTO 14320:REM TO ENDIF4
14040          REM ELSE4 could be proud knives, check for proud knives
14050          IF lock1=0 AND lock3=0 THEN 14060 ELSE 14310:REM ELSE4
14060            RR=LL:pcount=0
14070            FOR M=0 TO LL-1:REM RR-1
14080              Proud=0
14090              IF M+1>RR THEN GOTO 14180
14100              REPEAT
14110                IF ABS(Hy(M)-Hy(M+1))>(Hy(0)-2.5)
                         AND ABS(Hy(M)-Hy(M+1))<(Hy(0)+2.5)
                       THEN 14120 ELSE 14130
14120                    PP=PP+1:Hp(PP)=Hy(M+1):pcount=pcount+1:
                           Hp(0)=Hy(0):Proud=1:GOTO 14160
14130                  NN=NN+1:Hx(NN)=Hy(M+1):REM Unknown fault
14140                  FOR QQ=M+1 TO RR:Hy(QQ)=Hy(QQ+1):NEXT
14150                  RR=RR-1
14160                UNTIL Proud=1 OR RR=0
14170                IF RR=0 AND pcount=0 THEN M=LL-1
14180              NEXT:REM FOR QQ=0 TO LL:PRINTQQ;" ";Hy(QQ):NEXT
14190          REM IF6
14200          IF pcount>0
                   THEN 14220 ELSE 14270
14210              REM THEN6
```

```
14220                PRINT"  (Proud Knife)":lock1=1
14230                FOR M=0 TO pcount
14240                   PRINT"   Harmonic ";Hp(M)
14250                NEXT
14260                GOTO 14310:TO ENDIF6
14270              REM ELSE6
14280              IF lock1=0 THEN 14290 ELSE 14310
14290              PRINT"  (O.balance 1)":PRINT"   Harmonic ";I+1
14300              lock1=1:X=X+f1
14310            REM ENDIF6
14320          REM ENDIF4
14330          GOTO 14580:REM TO ENDIF3
14340        REM ELSE3 must be some other fault
14350        REM IF7 Try the Principal Harmonics
14360        IF lock1=0  THEN 14380 ELSE 14400:
14370      REM THEN7
14380      IF ABS(I+1-h2)<2 THEN 14390 ELSE 14400
14390    X=X+f4:lock1=1:PRINT"  (O.balance 2)": PRINT"   Harmonic ";I+1:GOTO 14490
14400          IF lock2=0  THEN 14410 ELSE 14430
14410           IF ABS(I+1-hj)<4 THEN 14420 ELSE 14430
14420                                          X=X+f5:PRINT"(Multi-knife)":hjfound=1:
                                                PRINT" Harmonic ";I+1:lock2=1:GOTO 14490
14430           IF I+1>hj+15
                                  THEN X=X+f7:MM=MM+1:Hz(MM)=I+1:
                                   GOTO 14490:REM Dig noise
14440           IF lock1=0 AND lock2=0 AND lock3=0 AND lock4=0
                                  THEN 14450 ELSE 14460
14450            IF ABS(hs-I+1)<2 THEN single=single+1:sk=I+1:GOTO 14490
14460           IF lock1=0 THEN 14470 ELSE 14500
14470              IF ABS(I+1-h1)<1.5THEN 14480 ELSE 14500
14480                                          X=X+f1:lock1=1:PRINT"  (O.balance 1)":
                                                  PRINT"  Harmonic ";I+1:GOTO 14490
14490               GOTO 14570 :REM TO ENDIF7
14500              REM ELSE7
14510              exist=0
14520              FOR SS=0 TO NN
14530                IF Hx(SS)=I+1 THEN exist=1
14540              NEXT
14550              IF exist=0 THEN 14560 ELSE 14570
14560                NN=NN+1:Hx(NN)=I+1:
14570            REM ENDIF7
14580           REM ENDIF3
14590         REM ELSE2
14600       REM ENDIF2
14610      REM ELSE1
14620    REM ENDIF1
14630 NEXT
14640 IF single>0 AND lock1=0 AND lock2=0 AND lock3=0 AND lock4=0
                                  THEN X=X+f8:PRINT" (Single  Knife)":PRINT"   Harmonic ";sk:
14650 IF MM>0 THEN 14660 ELSE 14700
14660         PRINT" (Digital noise)":
14670         FOR I=1 TO MM
14680            PRINT"   Harmonic ";Hz(I)
14690         NEXT
14700 IF NN>0 THEN 14710 ELSE 14840
14710    first=1
14720    FOR I=1 TO NN
14730     exist=0
14740     IF LL>0  THEN 14750 ELSE 14780
14750         FOR J=1 TO LL
```

```
14760          IF Hy(J)=Hx(I) THEN exist=1
14770        NEXT
14780        IF hjfound=1 THEN 14790 ELSE 14800
14790        IF Kjj=Hx(I) THEN exist=1:
14800        IF exist=1 THEN 14830
14810         IF first=1 PRINT"(Unknown  Faults)":first=0
14820        PRINT"   Harmonic ";Hx(I)
14830    NEXT
14840 vpos=VPOS:IF vpos>Vpos THEN Vpos=vpos:
14850ENDPROC
14860
```

APPENDIX B

COHERENT LIGHT, LASERS and PHOTODIODE

Contents

APPENDIX B1: The Helium-Neon Laser

APPENDIX B2: The Production of Coherent Light

APPENDIX B3: Photodiodes

APPENDIX B4: Talyrond 200

Appendix B1

Helium-Neon Laser Data Sheet

Spectra·Physics
Model 105
5mW Helium-Neon Laser

Features

- Hard Sealed Plasma Tube
- Typical Lifetime Exceeding 22,000 Hours
- Outstanding Beam Pointing Performance
- Low Amplitude Noise
- Consistent Level of Power Output Over the Life of the Laser

Spectra-Physics' Model 105 laser head with the Model 205 power supply delivers performance unmatched in a 5mW Helium-Neon laser system. The Model 105 is based on the Model 089 plasma tube, a hard-seal tube with a solid reputation among our most sophisticated OEM customers. This tube delivers remarkably constant output power over an extended life, a characteristic exclusive to Spectra-Physics hard-seal plasma tubes. This unique feature minimizes service calls and eliminates expensive system elements required to compensate for power degradation seen in other lasers. The Model 105 has driven dynamic beam pointing performance and static beam alignment precision beyond the demands of most OEM optical systems. In many cases, this eliminates costly realignment steps each time a laser is installed. The Model 105 is both physically and electrically compatible with standard OEM 5mW He-Ne's, making improved performance easily available to current 5mW users.

Model 105 Laser Head

The Model 105 Helium-Neon laser head delivers 5mW of power output at 632.8nm. The plasma tube is hard-sealed to permit high temperature bakeout of the tube, yielding a contaminant-free product and an extended lifetime of nominally 22,000 hours. Proprietary cathode processing leads to a constant power output level over the life of the laser, a characteristic exclusive to Spectra-Physics hard-seal plasma tubes.

Using advanced tooling techniques, the plasma tube is packaged in a cylindrical aluminum housing to provide static beam alignment precision unequaled in 5mW He-Ne lasers. The tube is heat shielded and the housing specially finished to minimize thermal gradients. The result is outstanding dynamic beam pointing performance. The laser head is equipped with a beam attenuator to block laser emission while the unit is in operation.

The Model 105 comes in both polarized (Model 105-1) and non-polarized (Model 105-2) versions. In addition, an optional 1"-32 accessory bezel is available to attach directly to the front face plate of the laser head. The bezel provides a convenient method of mounting special optics to be used with the laser.

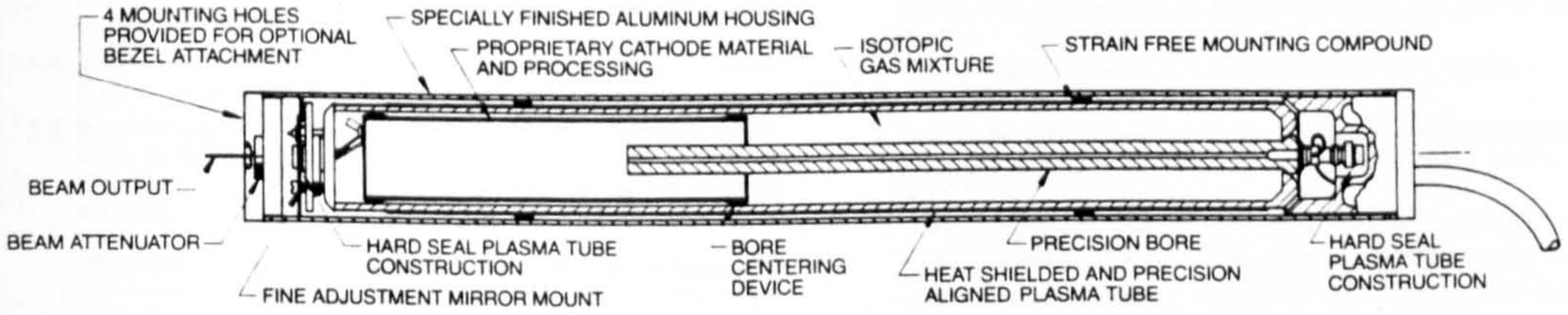

Model 105 Performance Specifications

1. Optical Parameters

1.1	Power Output, TEM_{00} (632.8 nm)	>5mW
1.2	TEM_{00} Mode Purity	>95%
1.3	Polarization Extinction Ratio (Model 105-1 only)	500:1 minimum
1.4	Beam Diameter	0.83 ± .02 mm
1.5	Beam Divergence Angle	1.0 mRad. nominal
1.6	Beam Quality	
	Random Spatial Noise	<1%
	A/R Spot Intensity	<0.25%
1.7	Longitudinal Mode Spacing	413 MHz
1.8	Beam Waist Location	See Outline Drawing

2. Dynamic Output Parameters

2.1	Warm-up Characteristics (Expressed as a percentage of the steady state power)	
	Power at Turn-on	>80%
	Power at 6 Minutes After Turn-on	>90%
	Power at 15 Minutes After Turn-on	>95%
2.2	Long-term Power Drift Under Constant Ambient Conditions	± 5% maximum
2.3	Mode Sweeping Contribution	± 2% maximum
2.4	Power Changes Over the Specified Operating Environmental Range with Respect to the Value at 25°C	± 5% maximum
2.5	Beam Amplitude Noise	
	Beam Amplitude Noise, Broadband (20Hz-2MHz)	0.5% rms maximum
	Beam Amplitude Noise, Typical Spectral Density	See Figure 1

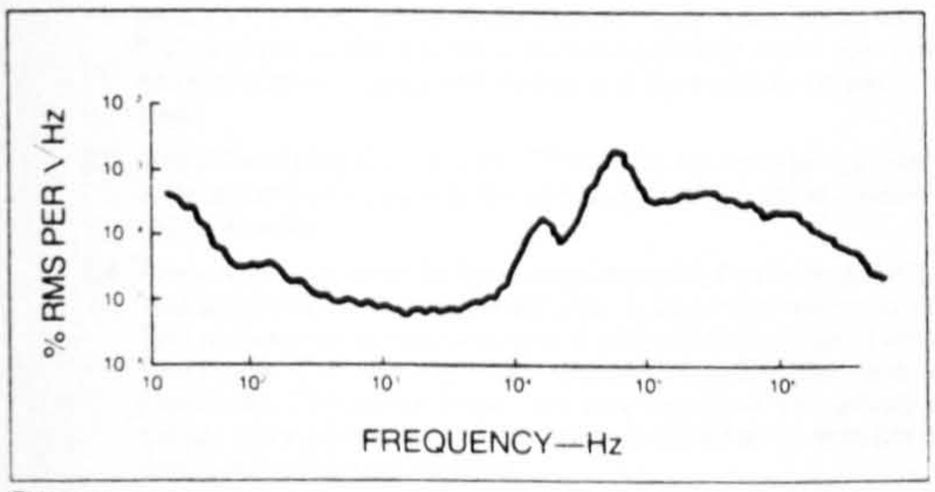

Figure 1

3. Beam Alignment Parameters

3.1	Static Alignment	
	Beam Location at Exit Aperture	<0.004" (0.1mm)
	Beam Angle	<400 microradians
3.2	Beam Angle Stability	
	Beam Angle Drift From Cold Start	<100 microradians
	Steady State Beam Angle Fluctuations	<20 microradians peak

4. Environmental Limits

4.1	Operating	
	Temperature	10°C to 60°C
	Altitude	0 to 10,000 feet
	Humidity	0 to 95%
	Vibration	
	Temporary power degradation due to sinusoidal vibration in the given frequency range and with the specified amplitude:	
	5-1000Hz, 0.5G	<5%
	5-1000Hz, 1.0G	<10%
	5-1000Hz, 1.5G	<25%
	Permanent power change due to sinusoidal vibration in the frequency range 5-200Hz, at a level of 1.5G:	<5%
4.2	Non-operating	
	Temperature	– 40°C to 80°C
	Altitude	0 to 70,000 feet
	Humidity	0 to 95%
	Vibration	1.5G, 5-200Hz
	Shock	15G, 11msec.

5. Electrical Parameters

5.1	Operating Current	6.5 ± 0.1mA
5.2	Operating Voltage	2350 ± 100 Volts
5.3	Starting Voltage	<10 kV
5.4	Drop-out Current	<5.5 mA

6. Mechanical Parameters

6.1	Weight	1.94 lbs/880 g.
6.2	Dimensions	See Outline Drawing

Notes

The following notes provide supporting details to the Model 105 and 205 performance specifications. The notes are numbered to correspond with the specification to which they refer.

Model 105 Laser Head

Unless otherwise noted or implied, all performance specifications apply after the completion of a 15 minute warm-up period.

1.3 Polarization Extinction Ratio: Less than one part in 500 (0.2%) of the total output power is contained in a plane at right angles to the primary plane of polarization.

1.4 Beam Diameter: The beam diameter is as measured at the front face plate of the laser and at the $1/e^2$ intensity points of the beam.

1.5 Beam Divergence: The stated value is the full cone angle divergence. In the far field (roughly, greater than 100 cm from the laser front face plate) the $1/e^2$ beam diameter can be estimated by the following equation:

$$w(z) \simeq z\theta$$

where θ is the full cone angle divergence in radians and w(z) is the $1/e^2$ beam diameter at a distance z from the front face plate of the laser. At any distance from the laser, the $1/e^2$ beam diameter can also be determined by the following exact equation:

$$w(z) = w(o)\sqrt{1 + (4z\lambda/\pi w(o)^2)^2}$$

where $\lambda = 632.8 \times 10^{-6}$mm and w(o) is the $1/e^2$ beam diameter at the front face plate of the laser.

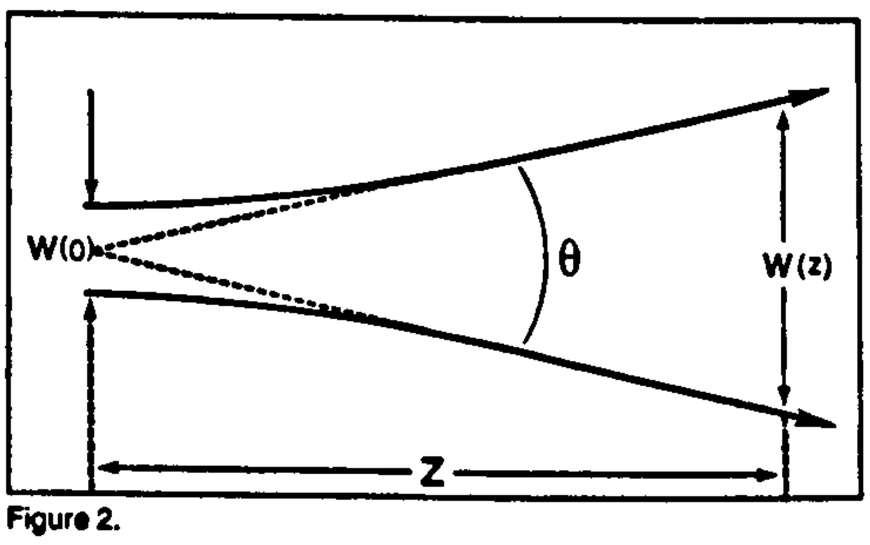

Figure 2.

1.6 Beam Quality; Random Spatial Noise: Percent of output power lying outside a disk capable of occulting more than 99.9% of the theoretically perfect Gaussian intensity distribution; includes A/R spot intensity.

Beam Quality; A/R Spot Intensity: Percentage of output power contained in multiple reflections from the anti-reflection coating of the output coupler.

2.1 Warm-up Characteristics: The powers listed are percentages of the steady state power of the fully warmed-up unit. The steady state power is determined by averaging the power over a minimum period of one hour after a warm-up period of 30 minutes. After 15 minutes, the power will fall within 95% of the steady state power, i.e., within the band defined by the long-term power drift specification of ± 5%.

2.2 Long-term Power Drift: This stated value gives the maximum percentage change in power relative to the steady state power (see Note 2.1) during a period of continuous operation and under constant ambient conditions. Long-term refers to a time period on the order of days.

2.3 Mode Sweeping Contribution: Of the total 5% long-term power drift, a maximum of 2% is due to the sweeping of longitudinal modes under the gain curve.

2.4 Power Changes Over the Specified Operating Environmental Range: The specification is determined after a 30 minute warm-up period. The ambient temperature is cycled through the operating temperature range at a rate less than 10°C per hour and the laser output monitored. The output power will vary less than 5% relative to the steady state power at 25°C (see Note 2.1). All other ambient conditions are maintained constant.

2.5 Beam Amplitude Noise: The beam amplitude noise is partially contributed by noise inherent in the power supply (see Model 205, Note 7). These specifications, therefore, are applicable only when the Model 205 power supply is used to drive the Model 105 laser head.

Beam Amplitude Noise, Typical Spectral Density: This plot is intended to provide typical narrow band frequency information; the data is not guaranteed. The typical beam amplitude noise for a particular frequency range F_{n-1} to F_n over which the spectral density has a constant value $S.D._n$ can be estimated by the following equation:

$$\text{Beam Amplitude Noise (\%rms)} = RMS_n = (S.D.)_n\sqrt{F_n - F_{n-1}}$$

The total noise over several frequency ranges can then be found from:

$$\text{Total Beam Amplitude Noise (\%rms)} = \sqrt{RMS_1^2 + RMS_2^2 + \ldots + RMS_n^2}$$

To illustrate, the noise from 1 kHz to 10 kHz can best be estimated by dividing the frequency range into two parts (Note: scales are logarithmic):

RMS_1 (1 kHz to 5 kHz) $= (5 \times 10^{-6}) \times \sqrt{(4 \times 10^3)} = 0.0003\%$ rms

RMS_2 (5 kHz to 10 kHz) $= (1.5 \times 10^{-5}) \times \sqrt{(5 \times 10^3)} = 0.001\%$ rms

Total Beam Amplitude Noise (1 kHz to 10 kHz) $= \sqrt{(0.0003)^2 + (0.001)^2} \simeq 0.001\%$ rms

The data given in this section is a worst case situation for any frequency band when observed over a long time period relative to the time scale of longitudinal mode sweeping. Over this time period, noise resulting from intermode competition will move over several frequency bands and is therefore counted more than once. As a result, the total noise calculated from 20 Hz to 2 MHz may well exceed the broadband value, 0.5%.

3. Beam Alignment Parameters: The specifications under this section define the beam alignment accuracies of the Model 105 laser head with respect to the recommended mounting areas at the two ends of the laser housing (see Outline Drawing, Model 105 Laser Head). The values listed are valid at constant 25° ambient temperature and are taken with respect to a mean best centerline defined by the recommended mounting bands. The mean best centerline is that stationary axis which traces out the smallest possible patterns on two imaginary planes at the mounting bands as the laser is rotated through 360° on the mounting surfaces. If the mounting bands were perfectly circular, both patterns would shrink to points and would define a centerline in the usual sense. The specifications in this section include the beam displacement effects of housing eccentricity in the mounting areas, but not the effects of tolerance in the laser housing diameter. This tolerance (± 0.001"), must be considered along with the user's specific mounting scheme when determining the exact tolerance in beam position relative to the user's mounting surfaces.

3.1 Static Alignment: This specification describes the steady state location in both angle and position of the laser beam. This steady state location is determined by averaging over a period of one hour after a warm-up period of 30 minutes.

Beam Location at Exit Aperture: This specification describes the tolerance in steady state beam position at the front face plate of the laser. The beam will therefore fall within 0.004" of the mean best centerline.

Beam Angle: The steady state angle at which the beam exits the laser can fall within a cone of half angle 400 microradians. To illustrate, observe the cross sectional view taken at 1000" from the front face plate of the laser. At this distance, the effect of the tolerance in steady state beam position (0.004") will be negligible relative to the displace-

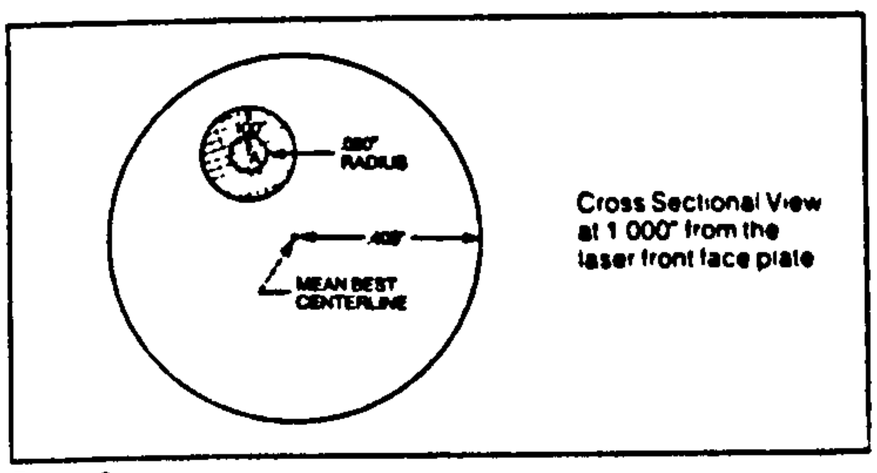

Figure 3

ment due to the steady state beam angle tolerance. The beam will therefore fall within a circle of radius 0.400" (400 x 10^{-6} radians x 1,000") of the mean best centerline or within the shaded area as illustrated in Figure 3.

3.2 Beam Angle Drift From Cold Start: During the period from cold start to steady state, the beam angle will fall within a cone of half angle 100 microradians relative to the steady state (see Note 3.1 static alignment) beam direction. At 1,000" from the laser front face plate, assume that the steady state position of the beam is at point A. Prior to reaching steady state, the beam will fall within a circle of radius 0.100" (100 x 10^{-6} radians x 1,000") about point A, or within the cross hatched area in Figure 3.

Steady State Beam Angle Fluctuations: After a 30 minute warm-up, the beam will remain within a cone of half angle 20 microradians relative to the steady state beam direction (see Note 3.1 static beam alignment). At 1,000" from the laser front face plate, the beam will fall within 0.020" (20 x 10^{-6} radians x 1,000") of the steady state beam position A.

4.1 Operating Environmental Limits:

Temperature, Altitude, Humidity: Unless otherwise stated, all specifications will be met over the entire operating range. The humidity range given is in a non-condensing environment.

Vibration, Temporary Power Degradation: The values given are worst case values observed at resonances when the sinusoidal vibration is produced along any of three mutually perpendicular axes.

Vibration, Permanent Power Change: This specification is stated per MIL-STD-810C Method 514.2 Category g. If a permanent power change does occur as a result of vibration, all specifications which are expressed relative to power (e.g., long-term power drift, beam amplitude noise) will then be based on the new steady state power output.

4.2 Non-operating Environmental Limits:

Humidity: The humidity range given is in a non-condensing environment.

Vibration: The laser will meet all performance specifications after the unit is subjected to a sinusoidal vibration at 1.5G amplitude over the frequency range of 5-200 Hz per MIL-STD-810C Method 514.2 Category g.

Shock: The laser will meet all performance specifications after withstanding three 15G 11 msec. shocks along each of three mutually perpendicular axes per MIL-STD-810C.

5.1 Operating Current: The laser must be driven by a current source with current output 6.5 ± 0.1mA.

5.3 Starting Voltage: The voltage required to start the head will be less than 10kV. If using a power supply other than the Model 205, the start pulse must be 10kV or greater to provide the capability of starting all possible laser heads satisfying the start voltage specification. The user should also be aware that factors other than the magnitude of the start pulse (e.g., the pulse risetime and environmental conditions) will affect the exact starting characteristics of the laser. If using a power supply other than the Model 205, these factors must be considered.

5.4 Drop-out current: Current below which the laser will cease to operate. Use of a power supply other than the Model 205 may change the drop-out characteristics of the laser.

Model 205 Power Supply

1. Input Voltage: The Model 205-0 or 205-1 power supply must be wired to a fuse protected AC power cord for operation on the user's available AC line voltage. Refer to the Model 205 Outline Drawing for the correct wiring scheme for 100, 110, 200 and 220 volt operation. All three connections (hot, neutral, and ground) must be made for proper operation of the laser. *CAUTION: The green lead must be connected to ground through the AC line. Failure to do so will create a safety hazard and may damage the power supply.* A 100 ohm resistor may be wired in series between the green lead and ground in order to avoid any potential ground loops.

3. Recommended Fusing: A 0.5 Amp fuse should be wired in series with the hot lead. Fusing will protect the power supply from continuous high input current and safeguard against shorting of the AC line

4. Start Voltage: Feedback regulation of the start voltage assures a constant voltage start pulse independent of line voltage and leakage currents.

5. Output Voltage Compliance Range: The Model 205 power supply is a current source. The laser head load will therefore determine the operating voltage. If this operating voltage remains within the stated compliance range, the output current will be regulated. The Model 105 laser head's allowed range of running voltages assures that this condition is met.

6. Output Current: The output current regulation of .1mA refers to a worst case situation which would result from combined 10% line and 10% load voltage changes. This assumes that the operating voltage falls within the compliance range. It is possible to estimate the actual change in laser output which is directly attributable to changes in the power supply output current. The following rule of thumb applies:

$$\text{Laser Amplitude Change (\%) Attributable to Changes in Power Supply Output Current} \approx \frac{\text{Change in Power Supply Output Current (\%)}}{6}$$

Therefore, a ± 0.1mA or ±1.5% change in current will produce approximately a ± 0.3% (1.5%/6) change in laser output.

7. Output Current Amplitude Ripple: The amplitude ripple of 2% peak to peak (.7% rms) refers to both random and repetitive noise in the power supply output current at frequencies greater than 10Hz. Using the above rule of thumb (see note 6), this amplitude ripple will produce a noise in laser output power of approximately 0.1% rms.

9. BRH Time Delay: The Bureau of Radiological Health requires that any laser system maintain a sufficient time delay (~3 sec.) between system turn-on and emission of laser radiation, to warn the user of potential radiation exposure. The Model 205 can provide a 3.5 sec. time delay if the user so desires. To activate the time delay, the violet wire indicated in the Model 205 Outline Drawing should remain shorted. Cutting this wire will eliminate the time delay.

Model 205 Power Supply

The Spectra-Physics Model 205 is a feedback-regulated current supply which drives the Model 105 laser head to produce a reliable, high-performance system. Utilizing high-frequency switching regulator technology, the supply features efficient, cool operation without the need for a heat sink. Feedback current regulation and an electronic output filter yield a very stable, low-ripple output current to the laser. Complete dielectric isolation is provided between the AC line and the output circuits. Full protection is provided against both short and open circuits at the output.

The Model 205 contains an optional time delay circuit which inhibits laser ignition for approximately 3.5 seconds after the input power is applied. The time delay, which can be activated by the user at his option (see Model 205 Outline Drawing), is one feature required by the Bureau of Radiological Health for laser devices. The Model 205 is available in two versions; the Model 205-0 which operates on 110 or 220 VAC power and the Model 205-1 which operates on 100 or 200 VAC power.

Model 205 Performance Specifications

1.	Input Voltage Model 205-0 Model 205-1	 110/220 VAC ± 10%; 50-400 Hz 100/200 VAC ± 10%; 50-400 Hz
2.	Input Current (average)	120mA at 100/110 VAC 60mA at 200/220 VAC
3.	Recommended Fusing	0.5 Amp.
4.	Start Voltage (feedback regulated)	>10 kVDC
5.	Output Voltage Compliance Range	1850 VDC–2450 VDC
6.	Output Current	6.5 ± 0.1 mA
7.	Output Current Amplitude Ripple	<2% peak to peak
8.	Conversion Efficiency	>87%
9.	BRH Time Delay	~3.5 Sec.
10.	Operating Temperature (No heat sinking required)	–20°C to +50°C
11.	Weight	1.3 lbs/580 g.
12.	Dimensions	See Outline Drawing

Outline Drawings

Dimensions in inches
Dimensions in parentheses in millimeters

Model 105 Laser Head

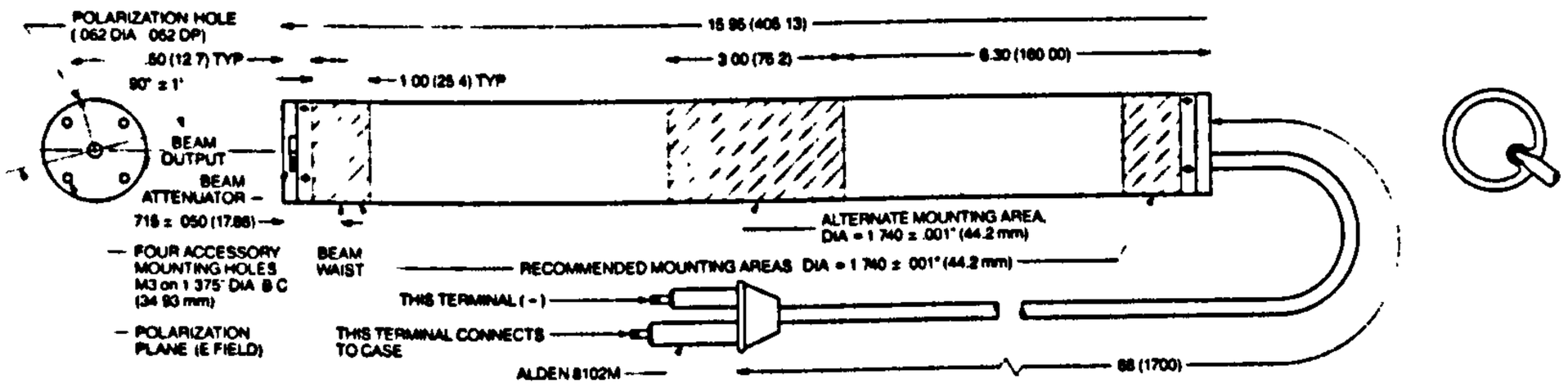

Model 205 Power Supply

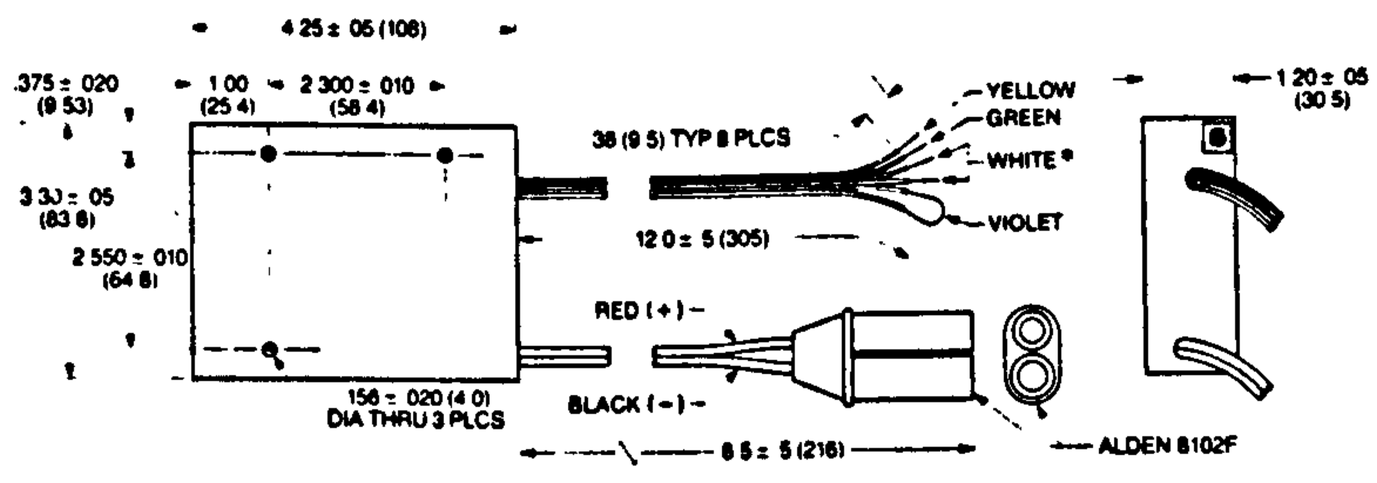

*Red leads are substituted for white in the Model 205-1 100-200 VAC power supply

MODEL #	AC LINE VOLTAGE	AC POWER CONNECTIONS HOT	NEUTRAL	GROUND
205-0	110V	Either White	Yellow	Green
	220V	White	White	Green
205-1	100V	Either Red	Yellow	Green
	200V	Red	Red	Green

BRH DELAY	DELAY CIRCUIT CONNECTIONS VIOLET	VIOLET
3.5 Sec	Shorted	
None	Open	

1) Green lead must be connected to ground through the AC line. Failure to do so will create a safety hazard and may damage the power supply.
2) A 100 Ohm resistor may be wired in series between the green lead and ground in order to avoid any potential ground loops.
3) High side of AC line must be fuse protected. Recommended fusing .05 amps.
4) Insulate all unused leads.

Appendix B2: Laser light Production

The Production of Coherent Light - The Laser Beam

For their operation, lasers rely on the phenomenon of stimulated emission of radiation. This is achieved by forcing atoms into an excited energy state; an electron in an excited atom may decay to a lower energy level, and, in so doing, it will emit a photon of energy, E, given by:-

$$E = hv \qquad \text{(B2.1)}$$

where:-

h is Plancks Constant

v is the photon frequency

This constitutes spontaneous emission of radiation. The emitted photon may pass close to another atom in a similar excited state and it may induce an identical transition; the emitted and stimulating photons will be the same in every aspect, having the same frequency, phase, direction and polarisation.

LASER is the acronym for Light Amplification by Stimulated Emission of Radiation. Laser oscillation can only be achieved if the probability of stimulated emission is greater than that of spontaneous emission and absorbtion. This is done by a process known as inversion, in which more atoms exist in an excited energy state than in some lower state to which direct transition is possible. This imbalance must be maintained or laser oscillation will fail.

The Helium-Neon Laser

In the Helium-Neon Laser a mixture of helium and neon gases is contained in a narrow tube. The mixture is predominantly helium - about 90%. An electrical discharge ionises the gas in the narrow tube. The plasma, thus formed, contains many helium atoms in metastable states. In these states, one of the valence electrons has been raised to the 1s and 2s levels where it will remain for a long time, the downward transition being forbidden by the rules of quantum mechanics.

Neon, having an atomic number of 10, normally has 10 electrons residing in the 1s 2s 2p configuration. Collisions between the metastable helium atoms and neon atoms cause one of the neon electrons in the 2p level to be raised to the 4s and 5s levels. The energy match between the 2s helium levels and the 4s and 5s neon levels is very close and it is therefore more probable that this excitation will take place than one to the 3s or 3p levels. When a neon atom is excited in this way, the helium atom drops back to the ground state but, because there are many more helium atoms than neon atoms, the metastable collision probability remains very high.

For helium laser action to occur, the majority of neon atoms must remain with electrons in the 4s and 5s energy levels than the 3p level. There are many downward transitions available in the excited neon electrons; the major neon laser line transitions are shown in the energy level diagram (figure B2.1).

Some of the radiation will be emitted in a direction parallel to the axis of the narrow tube; the rest is emitted through the tube walls and does not take part in the laser action. A photon travelling along the tube has a probability of passing close to a second excited neon atom and stimulating the emission of another identical photon. The probability of this happening depends on the gas density and the length of the tube; a single pass of a photon along the tube constitutes a probability of 0.1 (10%).

Mirrors are placed at both ends of the tube, reflecting the photons many times along its length, thus increasing the probability of further stimulated emission. Each stimulated photon is capable of stimulating another photon which is coherent with itself and those already present, thus, light amplification is achieved.

The two mirrors are coated to have a high reflectance of the laser wavelength of interest, but to transmit unwanted laser lines, thus amplification is restricted to the desired wavelength. Misdirected photons of the desired wavelength escape from the tube and are not amplified, which gives rise to the highly directional characteristic of laser output.

In order to utilise the desired laser radiation, some of it must be allowed to escape from the tube as a beam. This is done by coating one of the mirrors to permit about 1% transmission of the laser wavelength. This 1% of light which escapes constitutes the usable output of the laser.

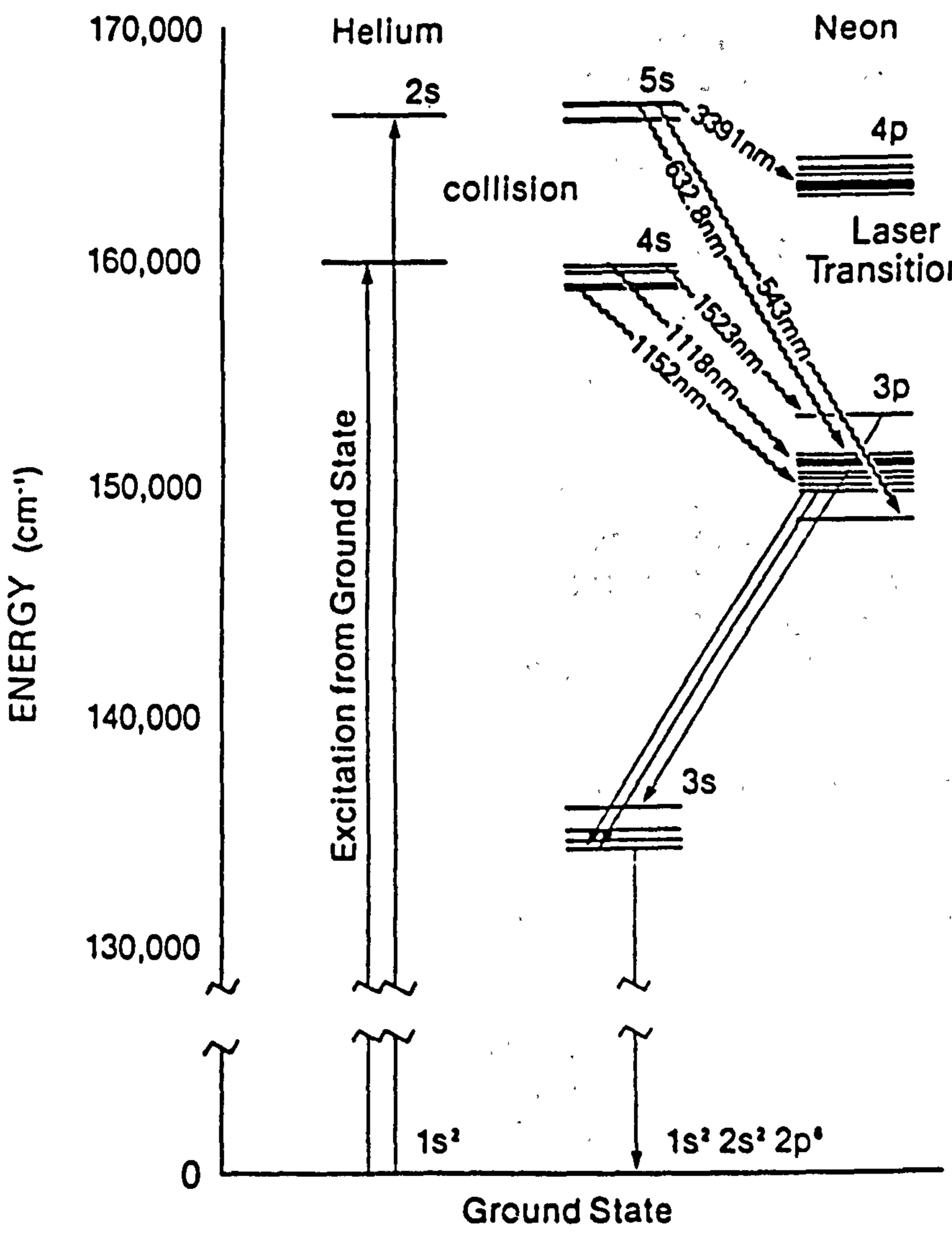

Figure B2.1: Energy Level Diagrams for Helium and Neon

Appendix B3

The Photodiode

The initial stage in the action of a photoelectric semiconductor device is that the radiation quanta are absorbed, and free charge carriers are generated, in the semiconductor. These carriers immediately cause the conductivity of the semiconductor to increase; a phenomenon called photoconductivity.

Silicon photoconductors have a number of advantages over the germanium type. The resistivity of silicon can be much higher (of the order of several thousand ohm/cm) with the consequence that photoconductors of much higher resistance can be obtained. The temperature dependence of the resistance is also many times smaller.

A photodiode is a device which makes use of the variations that occur in the current-voltage characteristics of a photoconductor p-n junction under the action of electromagnetic radiation. The effect of such radiation on this characteristic of the p-n junction depends on factors such as :-

1) the intensity and wavelength of the incident radiation.
2) the geometrical dimensions and physical parameters of the p-n junction
3) the direction of incidence of the radiation with respect to the plane of the junction.

In photodiodes, effective absorbtion of radiation occurs in a very thin surface layer (about 1 micron thick), and most of the carriers are generated in this layer. Referring to the junction shown in figure B3.1, the photon flux, Q, is perpendicular to the plane of the junction. The equations for the characteristics of the photodiode, so illuminated, have been derived by Cummerow (Ref. B3.1).

The relationship between the current, **I**, and voltage, **V**, in a photodiode is given by:-

$$I = I_s (e^{qV/KT} - 1) + I_{ph} \quad = (I_d + I_{ph}) \qquad \text{(B3.1)}$$

where:-

I_s = saturation current of p-n junction
q = electronic charge (1.6x10 Coulomb)
K = Boltzmanns constant (1.38x10 J/C)
T = absolute temperature
I_{ph} = photoelectric current

The first term of equation B3.1 determines the characteristic of an unilluminated photodiode; this is known as the dark current I_d. The second term which, as can be seen, is independent of the voltage applied, represents the current due to carriers generated by radiation, I_{ph}.

Typical characteristics of a photodiode, represented by equation B3.1, are plotted in figure B3.2. A photodiode is normally operated in the region to the

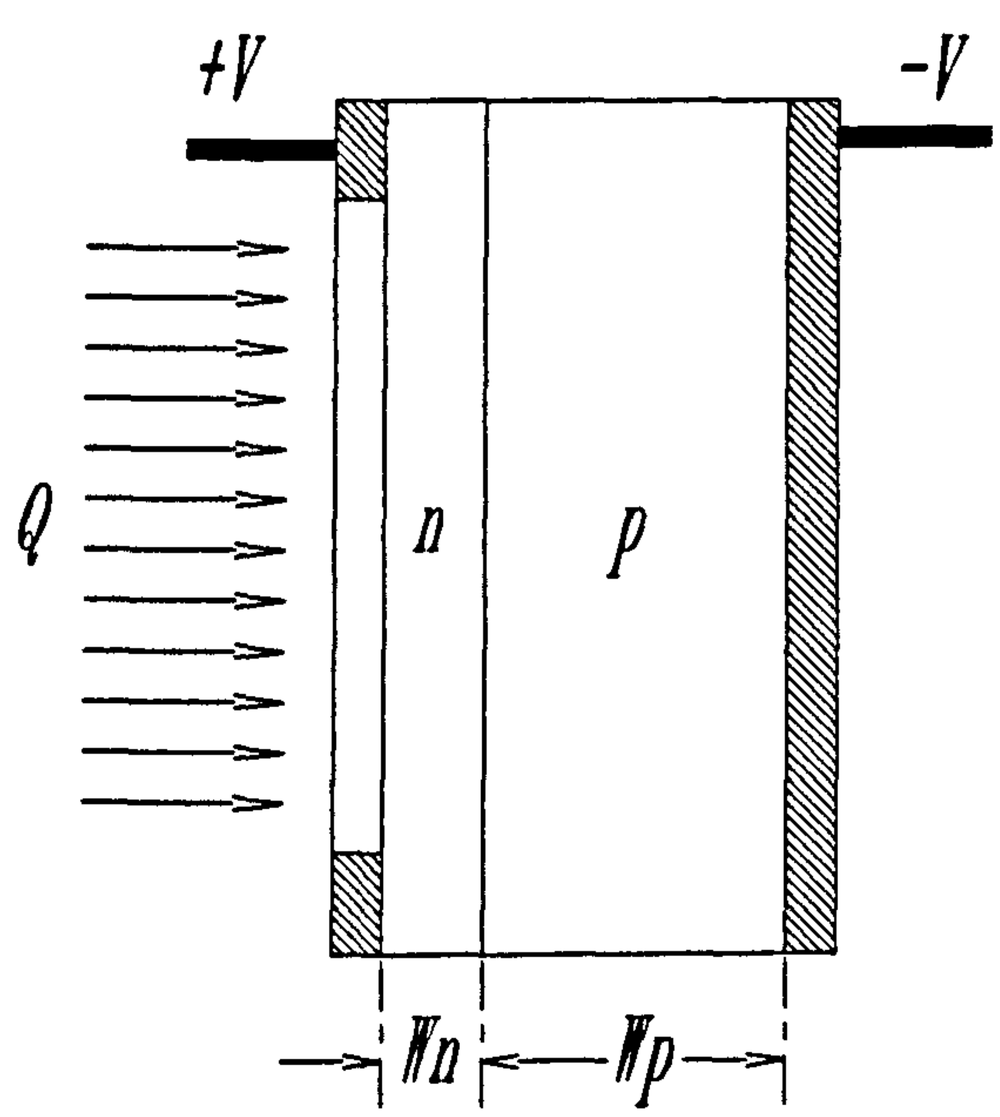

P-N JUNCTION PHOTODIODE

Illumination perpendicular to the junction plane

Figure B3.1

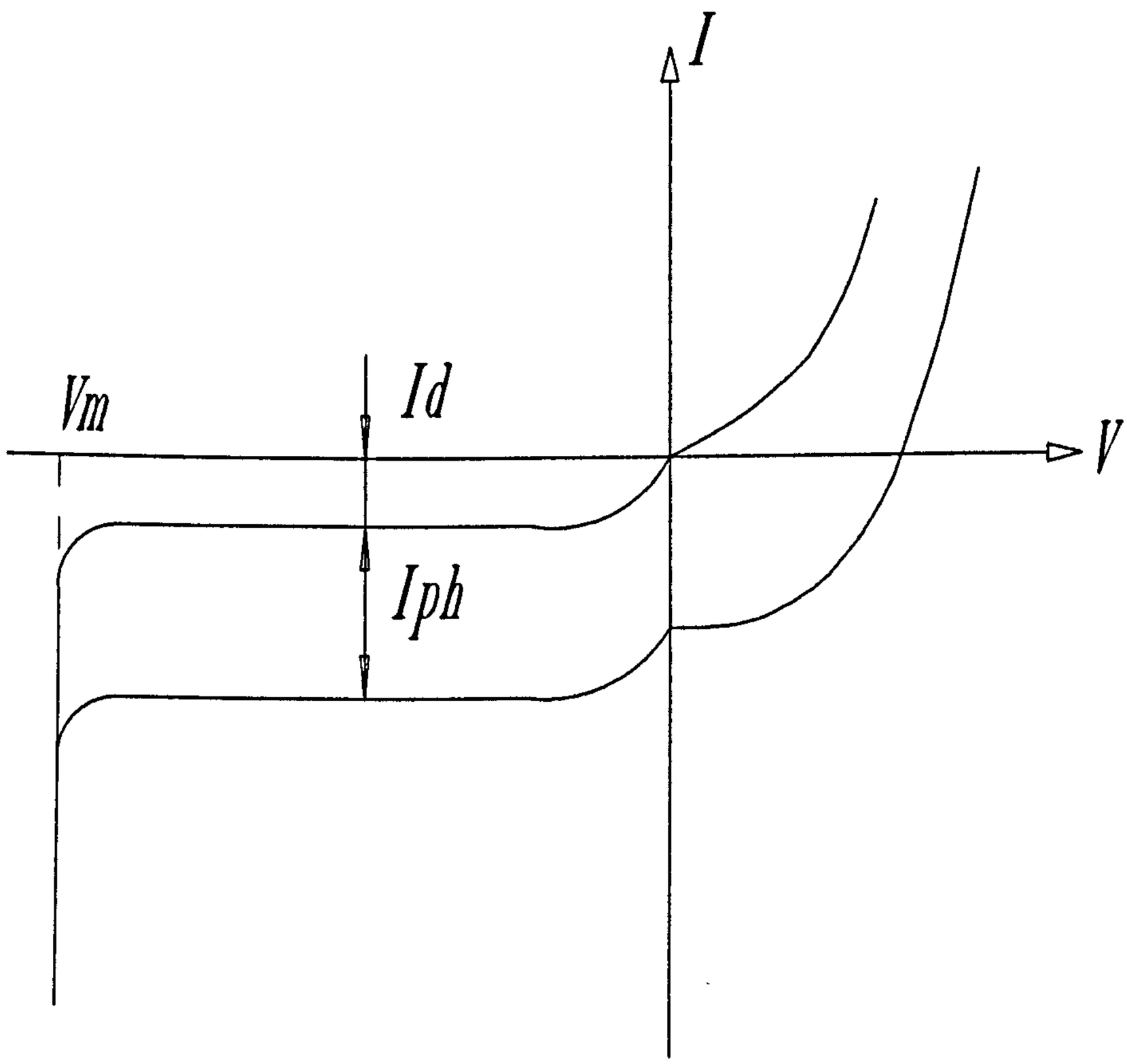

VOLTAGE - CURRENT CHARACTERISTIC FOR p-n JUNCTION

Figure B3.2

left of the **I** axis on this diagram, ie. under reverse bias conditions.

References

B3.1 Cummerow R L,Photovoltaic Effect in P-N Junctions
Physical Review 95 No 1, 1954

Appendix B4

Talyrond 200
Mode of Operation

Amongst its many features, the Talyrond 200 has a 300mm straightnes column (figure B4.1) with motorised vertical traverse. This has two travese speeds, giving rise to "horizontal" magnification of x1 and x5.

The output signal from the stylis, which would normally be used to drive the linear recorder, was intercepted and gated through a 10-bit Analogue to Digital Converter (ADC) (figure B4.2). The synchronizing of the analogue to digital conversions was controlled by an algorithm (see Appendix A5.2 and A5.3) in the BBC micro-computer to which the ADC was connected (see figure B4.2). The algorithm used the programmable timers in the 6522 VIA in conjunction with part of the interrupt service routine (see lines 3200 to 3300, appendix A5.3) to send precice timing signals which identified distances along the timber sample length (=125mm) in increments of 0.122mm. The number of sample points per sample length was 1024. Hence the profile of the machined timber could be captured in the form of a digitised series of numbers. The data caputred was stored in the computer's RAM for future analysis.

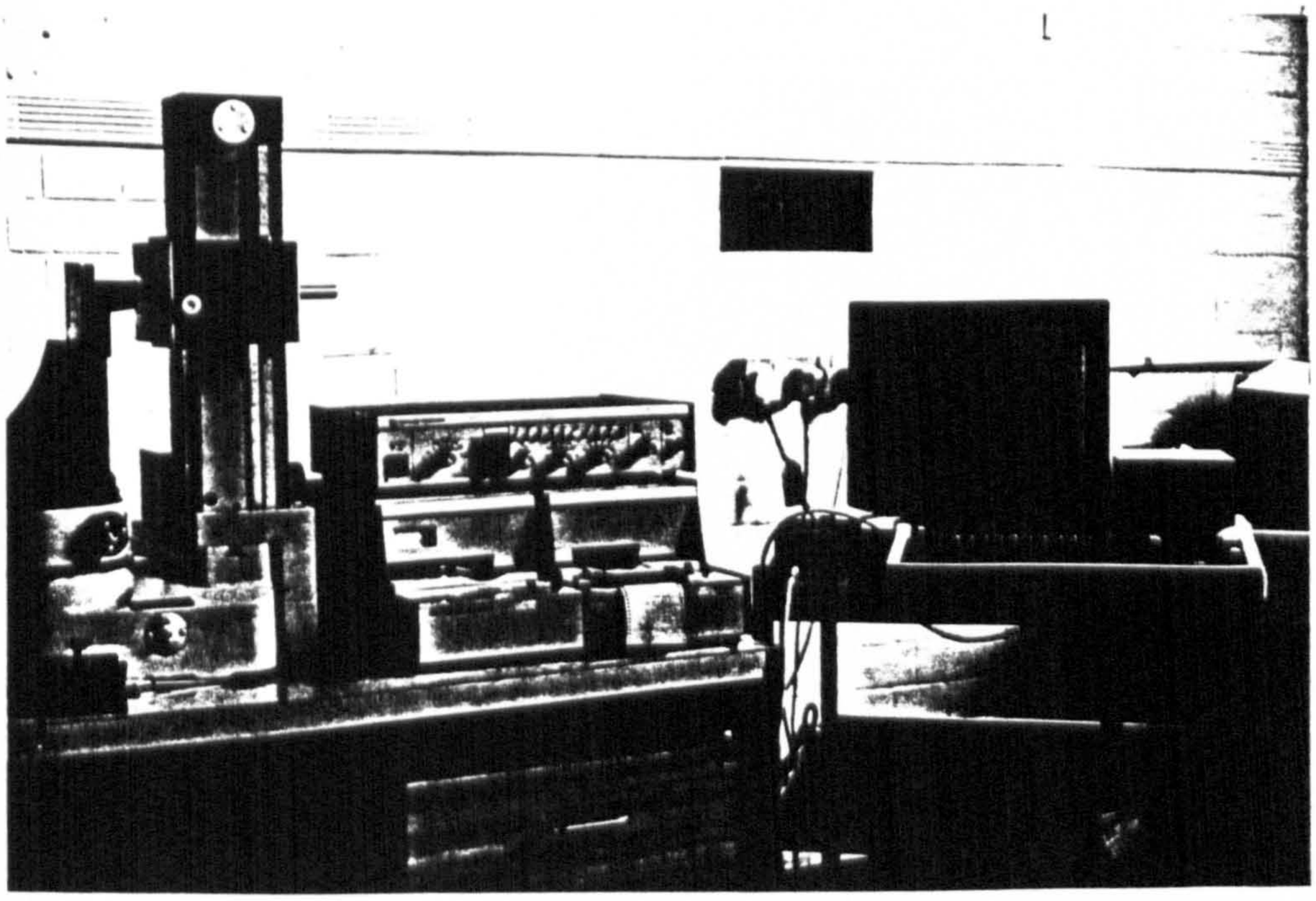

Figure B4.1: Talyrond 200 data capture.

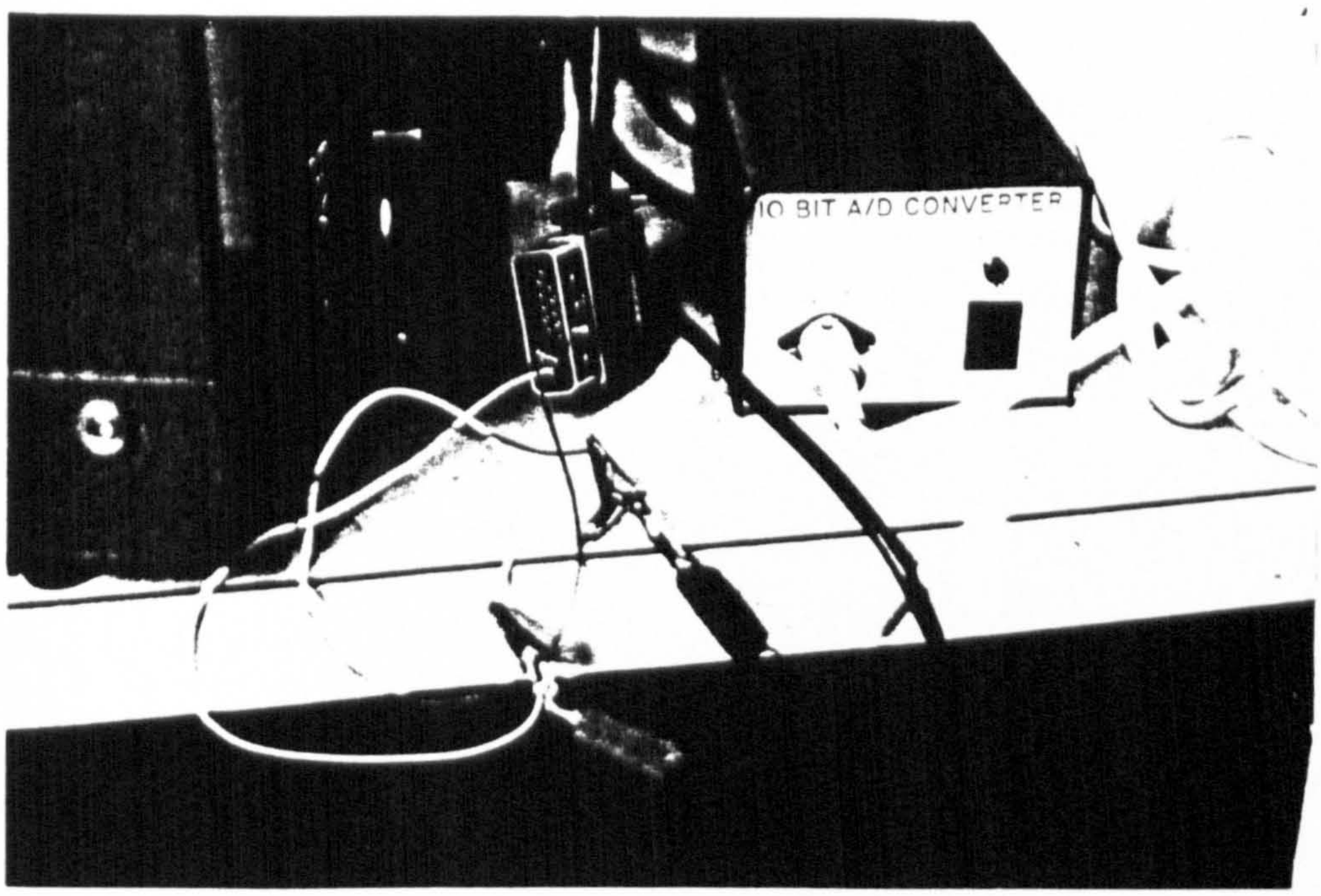

Figure B4.2: Analogue to Digital Converter used with Talyrond 200.

Appendix C

APPENDIX C1

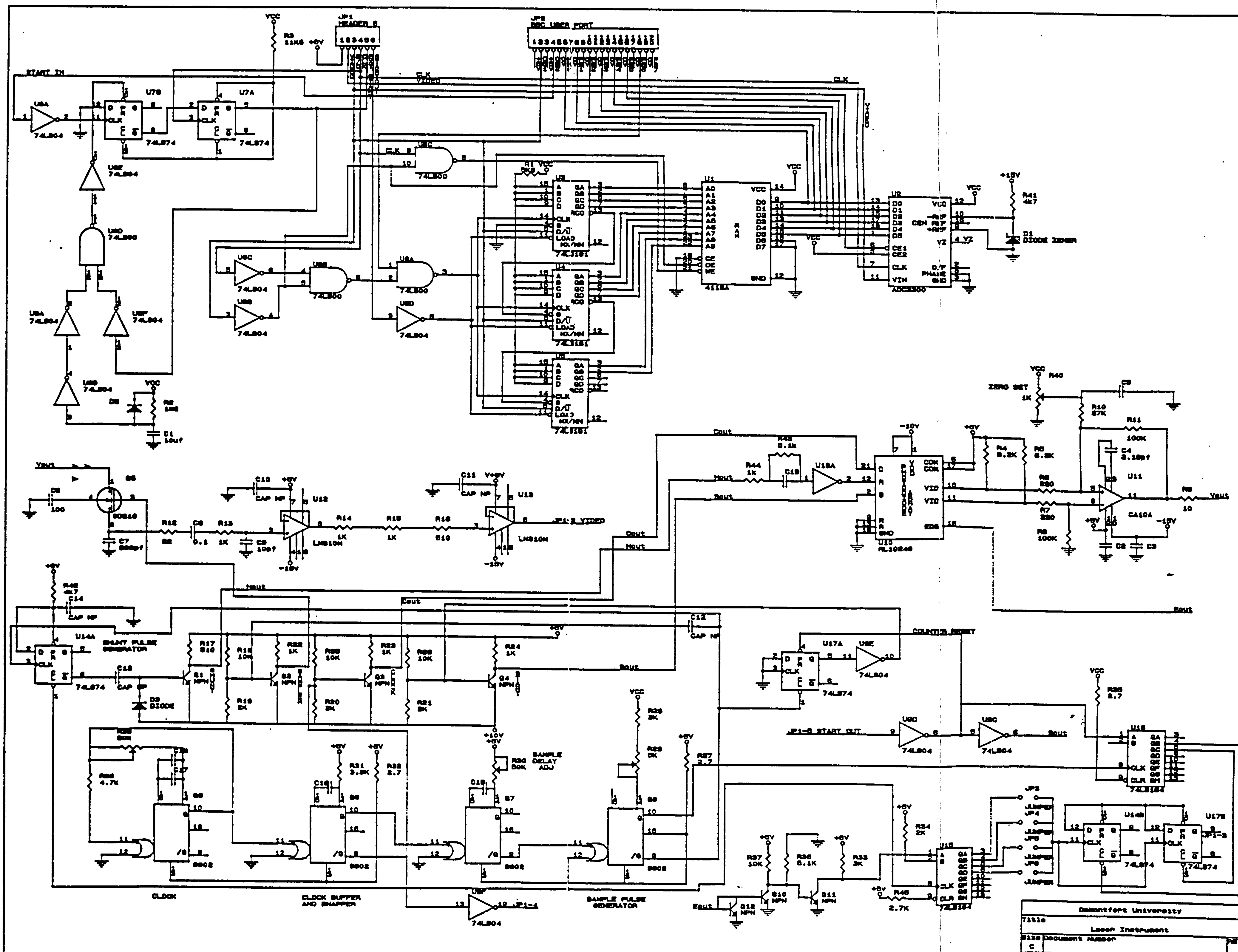
START IN
JP1
HEADER 6
JP2
BBC USER PORT
CLK
VIDEO
74LS04
74LS74
74LS00
74LS191
ADC0300
Vout
LM310H
Cout
Mout
Sout
COUNTER RESET
SHUNT PULSE GENERATOR
SAMPLE DELAY ADJ
JP1-5 START OUT
74LS164
JUMPER
CLOCK
CLOCK BUFFER AND SHAPPER
SAMPLE PULSE GENERATOR
JP1-4
DeMontfort University
Title
Laser Instrument
Size
C
Document Number
REV
Date:
April 20, 1998
Sheet
1 of
1

Appendix D

APPENDIX D1

6000 R.P.M.
40.00 mm

MAXIMUM PERMISSIBLE RESIDUAL UNBALANCE TO G2.5

C/HEAD DIA	LENGTH OF CUTTERHEAD														
	25	40	50	60	80	100	130	150	160	180	230	260	300	310	320
101	5	8	11	13	17	21	28	32	34	38	49	55	64	66	68
122	8	13	16	20	26	33	43	49	52	59	75	85	98	102	105
137	11	17	21	25	34	42	55	64	68	76	97	110	127	131	135
150	13	21	26	31	41	52	67	77	82	93	119	134	155	160	165
163	15	25	31	37	49	62	80	92	99	111	142	160	185	191	197
177	18	29	37	44	59	73	95	110	117	132	169	191	220	227	235
195	22	36	45	54	72	90	117	135	144	162	207	234	269	278	287
215	28	44	55	66	88	110	143	165	176	198	253	286	330	341	352
230	32	51	63	76	101	127	164	190	202	228	291	329	380	392	405
300	55	87	109	131	174	218	283	327	349	392	501	567	654	676	698

9000 R.P.M.
40.00 mm

MAXIMUM PERMISSIBLE RESIDUAL UNBALANCE TO G2.5

C/HEAD DIA	LENGTH OF CUTTERHEAD														
	25	40	50	60	80	100	130	150	160	180	230	260	300	310	320
101	4	6	7	8	11	14	18	21	23	25	33	37	42	44	45
122	5	9	11	13	17	22	28	33	35	39	50	57	66	68	70
137	7	11	14	17	23	28	37	42	45	51	65	73	85	88	90
150	9	14	17	21	27	34	45	52	55	62	79	89	103	107	110
163	10	16	21	25	33	41	53	62	66	74	94	107	123	127	131
177	12	20	24	29	39	49	64	73	78	88	112	127	147	152	156
195	15	24	30	36	48	60	78	90	96	108	138	156	180	186	192
215	18	29	37	44	59	73	95	110	117	132	169	191	220	227	235
230	21	34	42	51	67	84	110	127	135	152	194	219	253	261	270
300	36	58	73	87	116	145	189	218	233	262	334	378	436	451	465

Appendix E: Published Papers

LAMDAMAP 93, SOUTHAMPTON
Laser Metrology and Machine Performance
Int. Symp. pp. 147-154 July 1993

A Laser Based Method for the Assessment of Machine Tool Performance

K.M. Maycock and R. Parkin
Department of Mechanical and Manufacturing Engineering, De Montfort University, Leicester, UK

ABSTRACT

The problems of in process assessment of the surface quality of machined timber (high levels of vibration etc.) render most data acquisition methods inadequate. This paper describes the development and validation of a post process measurement system, capable of being transferred to the "in process" environment. The system uses a novel Laser illumination and Machine Vision technique. The signal processing analyses the surface information using Fourier techniques to produce frequency "signature". These are then analysed to provide data on product quality.

INTRODUCTION

The wood-working industry need a reliable method to quantify and categorise the surface quality of its planed and spindle moulded products. The current practice, that of visual and tactile inspection, results in a wide variance in what may be classed as acceptable or defective surface finish. These methods are very subjective and restricted to post process application.

Modern wood-working machines "extrude" timber at extremely high rates, often in excess of 140m/min. When the process develops a significant fault a large quantity of defective timber is produced before the symptoms are detected by post process inspection. Evidently, to ensure consistent quality and economy, it is necessary to develop sensors capable of monitoring the quality of the product, at the instant that it is produced, so that any necessary remedial action may be effected immediately. Meanwhile, a practical and more precise method of specifying machined wood finish is required to ensure consistent quality of production.

Current surface analysis instrumentation is biased toward metalworking, has relatively short traverse lengths and use parameters which have little relevance to wood-working. Within the context of wood machining, with its high levels of vibration, the in process monitoring of surface quality using delicate stylus instruments is impossible. A fast-response, non-contact method of surface quality assessment, including parameters that can readily indicate and identify

machining defects, is required.

MACHINING PROCESS

The timber industry uses the up-cutting mode for machining its products. Due to the kinematics of the planing process, the geometry of the machined surface consists of a series of cusps; their distribution and linear spacing being dependant largely on the linear feed speed of the timber, the number of knives on cutterhead, the rotational speed of the cutterhead, etc. In practice, the ideal surface is not achieved; vibration, spindle dynamic imbalance, proud knives, etc., all affect the locus of the knives and therefore the surface form.

ASSESSMENT PARAMETERS

The cutting circle radius used on planing machines is relatively large (typically 150mm) and the depth of the cusps produced on the surface, is few microns (typically 10 μm). These very small amplitude variations are not detectable by the naked eye and do not account for any perceived "defects". The eye, however, is extremely sensitive to changes of slope (Gonzalez[1]). The eye detects the change from positive to negative slope at the apex of each cusp. It is the consistency with which the apexes repeat that affect the aesthetic qualities of the machined surface; any variation in the surface wavelength, or long periodic "beats" superposed there on are noticed and render the surface quality defective (Brown[2] and Elmdorf[6]). Therefore it seems reasonable to develop an instrument that could analyse the frequency information inherent on machined timber surfaces.

PROPOSED INSTRUMENT

The principles of the proposed laser instrument are as follows. A broad beam of laser light would be directed at grazing incidence to the surface being machined, and in the same plane as the traversing workpiece (figure 1). This would have the effect of producing a pattern of bright and dark regions on the surface to be assessed. This pattern, which contains the frequency information of interest, would move past a single photodiode as the workpiece is traversed. The output voltage of a photodiode would be sampled (using a rotary position encoder to define precisely the sampling points), digitised (using an Analogue to Digital Convertor) and stored for subsequent analysis.

With appropriate sampling frequency, the data captured over a given length of timber could be analysed in terms of its frequency content. This would involve transforming the data from the "time" domain to the "frequency" domain using a fast Fourier Transform (FFT) algorithm, then using a "fault finding algorithm" (FFA) to analyse the

frequency signature to detect any machining defects that may have been induced on the timber surface.

DEVELOPMENT OF LASER INSTRUMENT

For financial and practical reasons the philosophy adopted was to develop the instrument using stationary, pre-machined timber samples. This was accomplished by employing a linear array of photodiodes (instead of a single diode), "traversing" being achieved by scanning the diode array, as opposed to moving the timber. Optical lenses were used to focus the image of a given illuminated length of timber on to the photodiode array. Scanning of the array provided data, which was captured and stored for subsequent analysis. The device, thus investigated, was a post process instrument but established using the principles of in process measurement.

Mathematical Model

The geometry of, and the mechanics associated with, the production process was also investigated to generate a mathematical model that could be used to represent the profile of a machined timber surface. The rigorous mathematical model developed formed the nucleus of a computer surface simulation algorithm (SSA); the SSA was used to test the hypothesis of, and substantiate the philosophy behind, the proposed surface assessment method. It was also used to predict surface profiles and therefore FFT templates (or frequency signatures) for machine performance determination or surface profile comparisons.

DEFECT IDENTIFICATION FROM FFT SIGNATURES

The frequency signature of an ideal machined timber surface will contain a single peak (or local maxima) because the pitch (or knife mark distribution) of an ideal surface is uniform. The expected number of knife-marks, h_j, in a given sample length, L_s, is given by

$$h_j = \frac{WL_s}{2\pi V} N \qquad (1)$$

where **W** is angular velocity of the cutterhead, **V** is linear feed velocity of the timber , **N** is number of knives on the cutterhead and the suffix **j** indicate a jointed, multi-knife finish.

Cutterheads that are not dynamically balanced produce planed surfaces that exhibit a "once-per-revolution" defect due to lack of spindle concentricity. Such a profile will feature the expected number of knife marks, h_j, superposed onto a surface that undulates sinusoidally because of the imbalance. The frequency signature of a sample length of such a surface will contain two major peaks; one at principal

harmonic h_j (see Equation 1), the other at h_1 (the principal harmonic which represents the surfaces undulation) given by

$$h_1 = \frac{WL_s}{2\pi V} \qquad (2)$$

where the symbols are as defined in Equation 1 and where the suffix 1 indicate a once-per-revolution defect.

A single proud knife on otherwise ideal cutterhead, would cause it to machine a surface whose frequency signature contain additional peak harmonics to that of an ideal finish. The peaks that characterise such a profile was illustrated by using the SSA to generate a "proud-knife" surface and transforming it to a frequency signature (see figure 2). The harmonic number of the peaks can be seen to follow an arithmetically progressing series that start at h_1 (Equation 2), the amplitude of the successive peaks diminishing with increase in harmonic number.

INDUCED DEFECTS AND SURFACE ANALYSIS

Four categories of "faults" were investigated: Ideal machining (no defects); cutterhead imbalance; proud knives; poor workpiece support and control. Timber samples were produced using machining conditions that reflected these faults; the machining parameters and machine conditions being recorded for each sample in Table 1 and corresponding data plotted in figures 3 to 6.

TABLE 1

Sample No.	No. Knives	Head speed	Feed speed	Machine Condition
G2.S1	4	4500 rpm	60 m/min	ideal
G2.S4	4	4500 rpm	60 m/min	out-of-balance
G3.S9	6	6000 rpm	65 m/min	1 proud knife
G4.S4	6	6000 rpm	80 m/min	poor timber support

Three surface waveform data sets were generated from each timber sample; the first came from the Laser Instrument (LAS), the second from the Talyrond 200 (TAL) and the third from the surface simulation algorithm (SSA). Each data set was transformed into the frequency domain. The frequency signature was then analysed, using the FFA which examined it with respect to the number of significant peaks present (significance being determined by comparison with a preset threshold value), and the position that the peaks occupied in the harmonic spectrum. This showed the type of defects present in the surface and the machining faults from which they may have originated.

DISCUSSION

For sample number G2.S1 (see figure 3), the frequency signature resulting from the laser instrument and the talyrond 200 both have a peak at harmonic 40±1, compared to the expected peak at harmonic 38±1 (=h_j) in the SSA generated data set. The difference in can be explained in terms of timber slippage during machining. However, harmonic 40 falls within the tolerance band of h_j±2 specified in the FFA with harmonic 41 just outside it. Hence, FFA analysis of the laser instrument's FFT signature produced the "multi-knife-finish" verdict, while that of the talyrond resulted in "unknown fault". The peak at harmonic 1 is due to variations in the timber's reflectivity because of its resinous condition. This is not a major drawback to the analysis technique, because, in timber the resinous grains are always "very-long-wavelength" in nature, compared to the surface waves produced by the machining operation. Consequently, in developing the philosophy behind the FFA, the very low peak harmonics in the FFT signature were ignored.

Similar results are shown for sample G2.S4 (figure 4), where, as expected there are two significant peaks in the FFT signature, one due to cutterhead imbalance, the other to multi-knife finish. With the proud knife sample, G3.S9 (figure 5), the characteristic arithmetically-progressing, diminishing-harmonic phenomenon is present and was detected by the FFA for each data set. The poorly supported timber sample, G4.S4 (figure 6), could not be accurately simulated because of the large number of unknowns (forcing frequency, mode of vibration, timber stiffness, etc.). So, although some fault was obviously present, the ill equipped FFA, highlighted, but incorrectly identified, the fault.

CONCLUSIONS

The system is successful in quantifying timber surface quality and, to some extent, identifying the causes of defects. This is a considerable step forward as it provides a basis for establishing standards and removing the subjective human link. Future work will attempt to realise an in process device with a view to adaptive process control.

References

1. Gonzalez, R.C and Wintz P., *Digital Image Processing* Addison-Wesley Publishing Company, Inc. 1977

2. Brown, I.D. "Visual and Tactile Judgments of Surface Roughness." *Ergonomics*, Vol 3, Part 1.

3. Elmdorf, A and Vaughan, T.W. "A Survey of Methods of Measuring Smoothness of Wood." *Forest Products Journal*, Vol 8, 1958

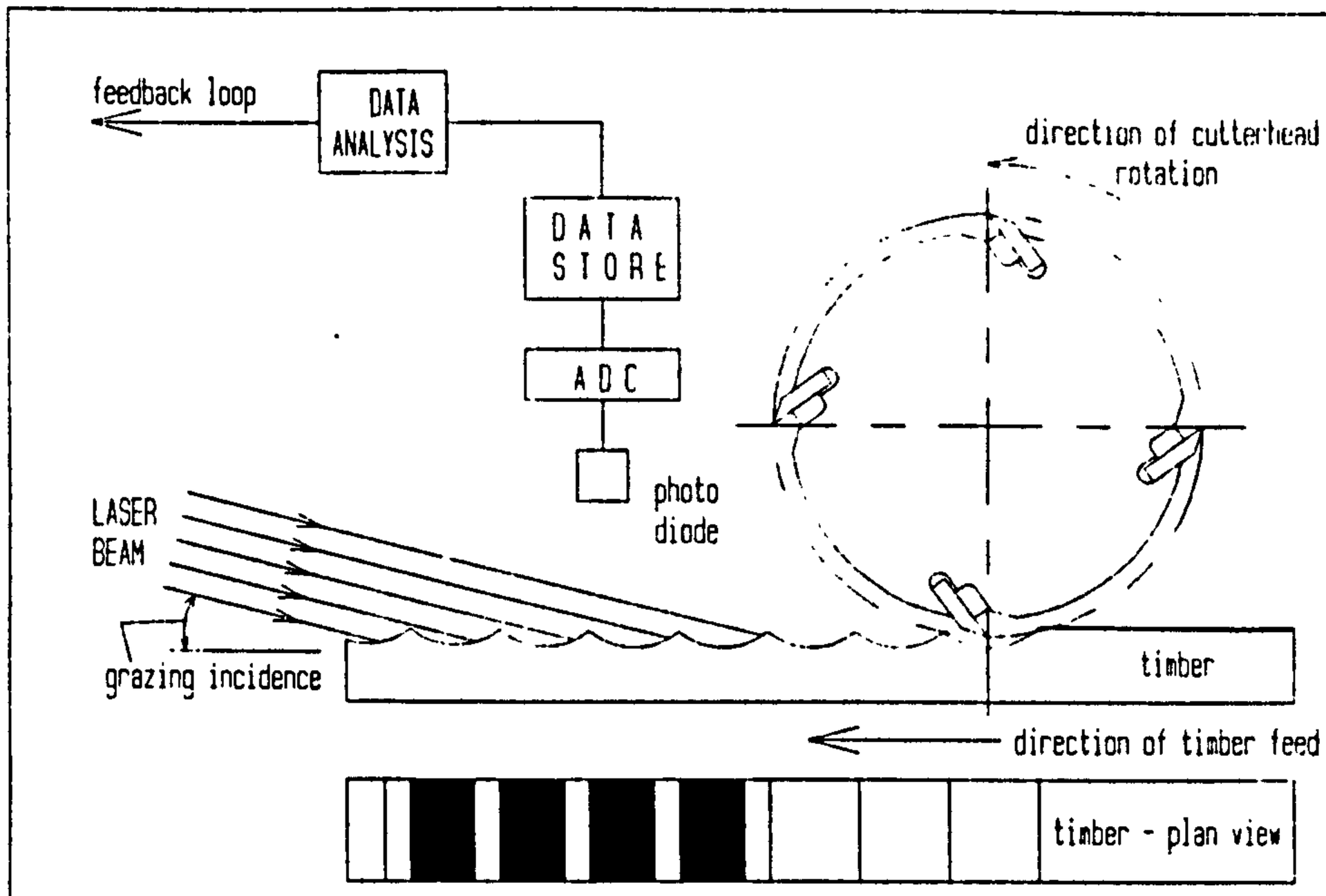

Figure 1: Schematic Diagram of the Proposed Technique

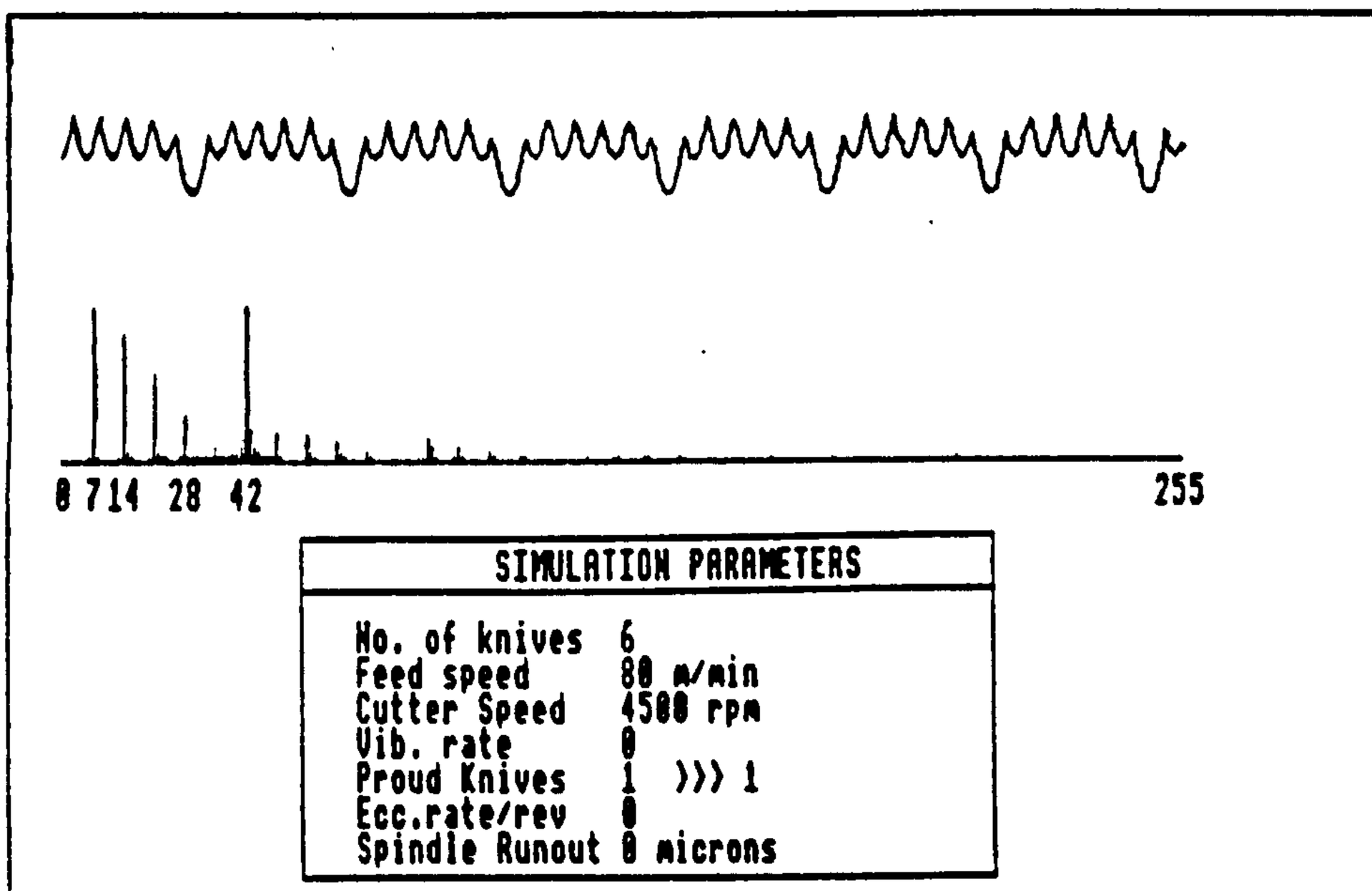

Figure 2: Results for Profile Simulation of Proud Knife

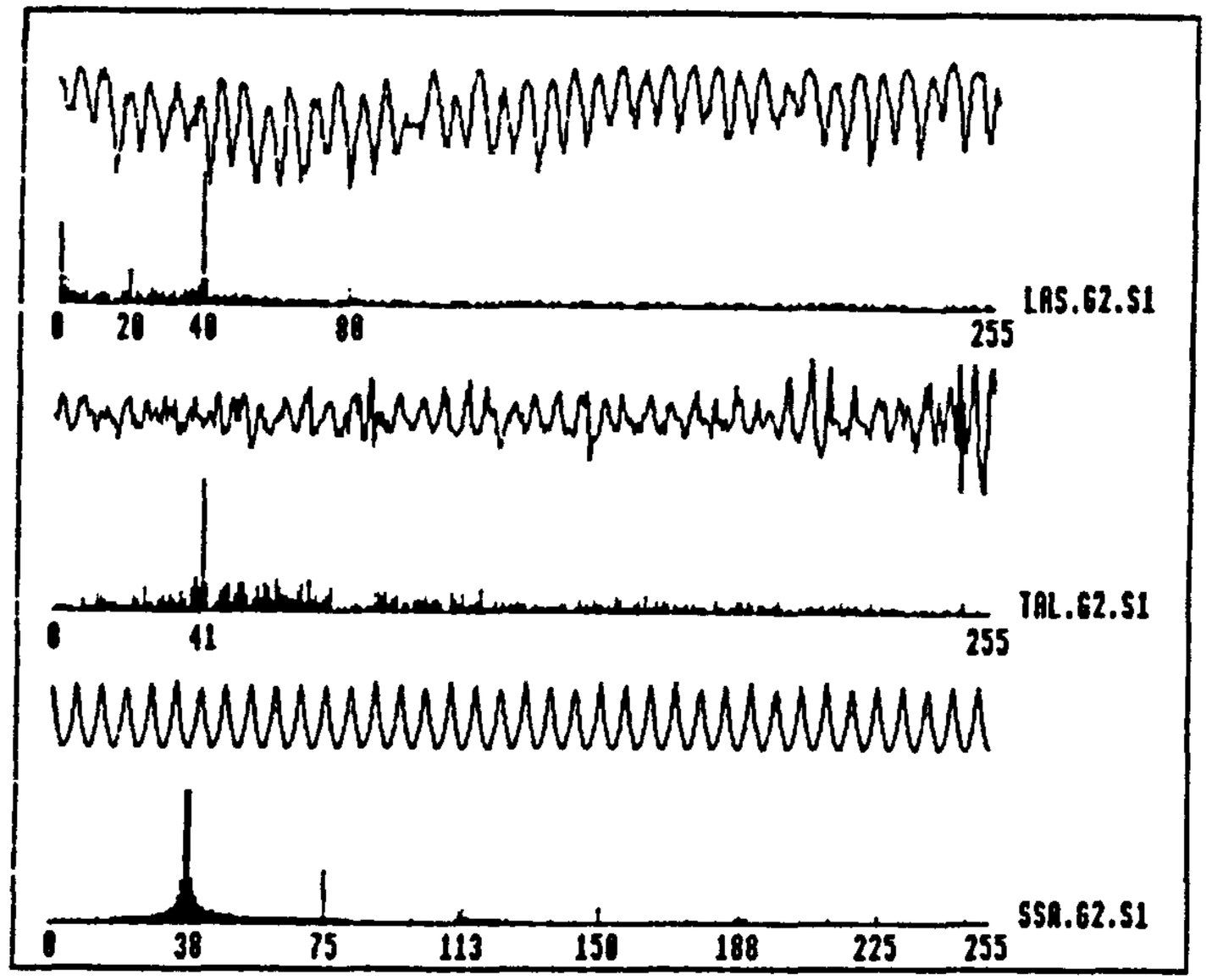

PRINCIPAL PEAK HARMONICS
h1 = 9 h2 = 18 hj = 37

ANALYSIS OF FFT's USING FAULT FINDING ALGORITHM (FFA)		
FFA ON LASER DATA THRESHOLD=0.5	FFA ON TALY DATA THRESHOLD=0.5	FFA ON SSA DATA THRESHOLD=0.5
(Multi-knife) Harmonic 40	(Unknown Faults) Harmonic 41	(Multi-knife) Harmonic 38

Figure 3: Results for Timber Sample Number G2.S1

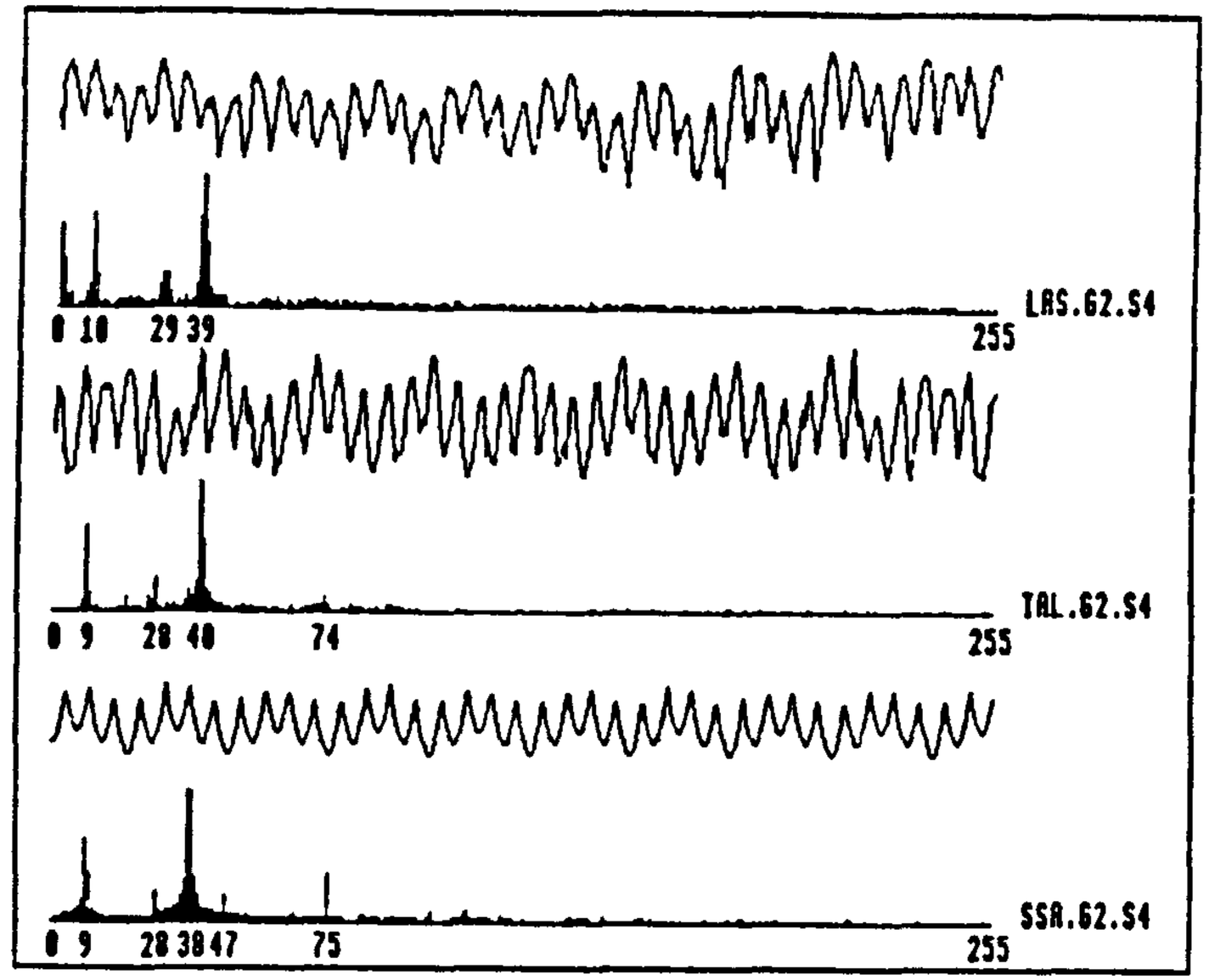

PRINCIPAL PEAK HARMONICS
h1 = 9 h2 = 18 hj = 37

ANALYSIS OF FFT's USING FAULT FINDING ALGORITHM (FFA)		
FFA ON LASER DATA THRESHOLD=0.4	FFA ON TALY DATA THRESHOLD=0.4	FFA ON SSA DATA THRESHOLD=0.4
(0.balance 1) Harmonic 18 (Multi-knife). Harmonic 40	(0.balance 1) Harmonic 9 (Multi-knife) Harmonic 40	(0.balance 1) Harmonic 9 (Multi-knife) Harmonic 38

Figure 4: Results for Timber Sample Number G2.S4

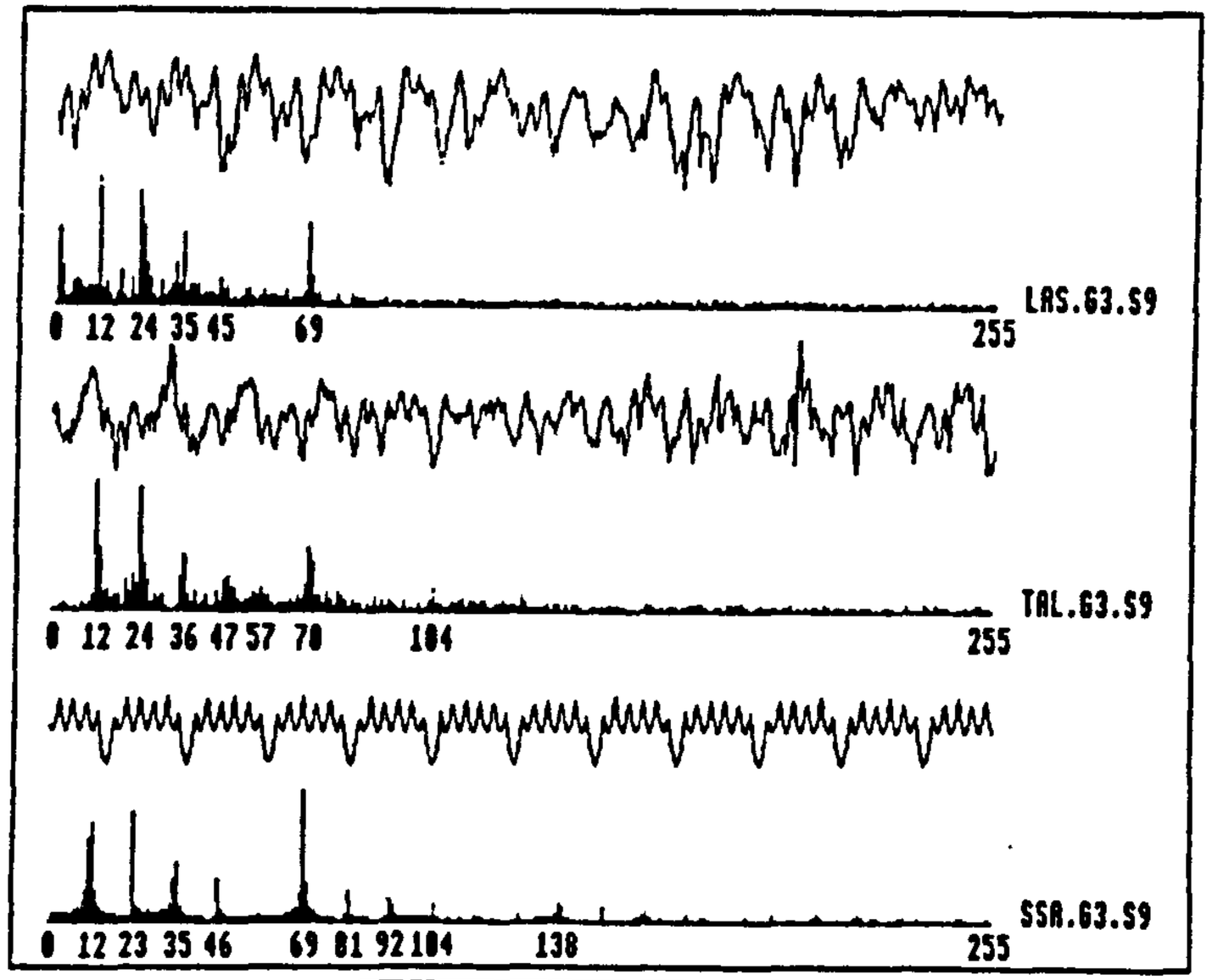

PRINCIPAL PEAK HARMONICS
h1 = 11 h2 = 22 hj = 69

ANALYSIS OF FFT's USING FAULT FINDING ALGORITHM (FFA)		
FFA ON LASER DATA THRESHOLD=0.4	FFA ON TALY DATA THRESHOLD=0.4	FFA ON SSA DATA THRESHOLD=0.4
(Proud Knife) Harmonic 12 Harmonic 23 Harmonic 35 (Multi-knife) Harmonic 69	(Proud Knife) Harmonic 12 Harmonic 24 Harmonic 36 (Multi-knife) Harmonic 70	(Proud Knife) Harmonic 12 Harmonic 23 Harmonic 35 (Multi-knife) Harmonic 69

Figure 5: Results for Timber Sample Number G3.S9

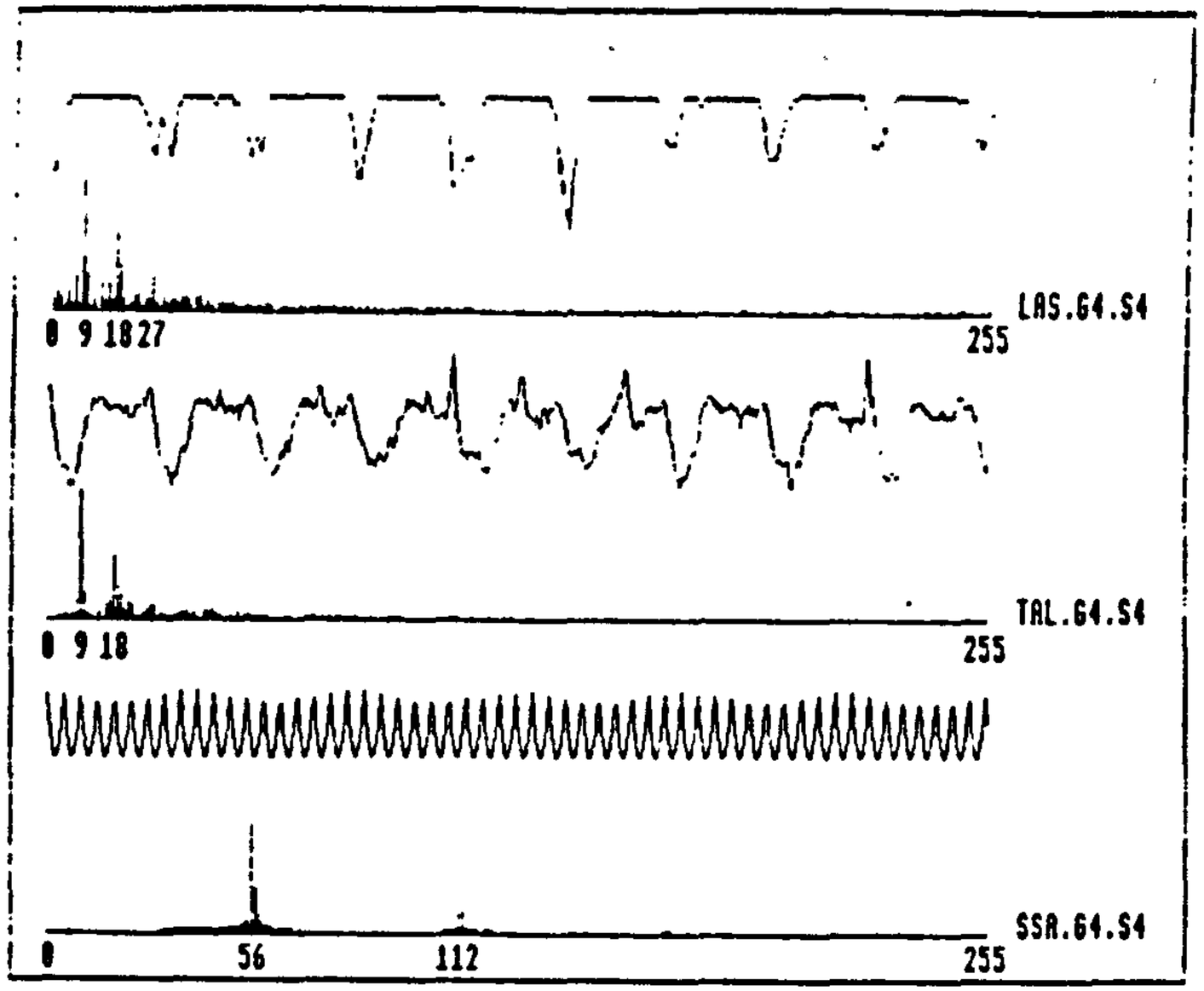

PRINCIPAL PEAK HARMONICS
h1 = 9 h2 = 18 hj = 56

ANALYSIS OF FFT's USING FAULT FINDING ALGORITHM (FFA)		
FFA ON LASER DATA THRESHOLD=0.4	FFA ON TALY DATA THRESHOLD=0.4	FFA ON SSA DATA THRESHOLD=0.4
(Proud Knife) Harmonic 9 Harmonic 18	(Proud Knife) Harmonic 9 Harmonic 18	(Multi-knife) Harmonic 56

Figure 6: Results for Timber Sample Number G4.S4

Sensors and Actuators A, 25–27 (1991) 433–437

Surface Measurement of Planed and Moulded Timber Products

F. CUTRI, K. MAYCOCK and R. PARKIN

School of Engineering and Manufacture, Department of Mechanical and Production Engineering, Leicester Polytechnic, PO Box 143, Leicester LE1 9BH (U.K.)

Abstract

The surface quality of planed and moulded wooden components is primarily affected by machine performance during manufacture. Woodworking machinery has unique problems due to high speeds of operation. With raw material throughput rates of 180 m/min and cutter head speeds of 15000 rev/min, large quantities of poor-quality material can arise in short periods if machine faults are allowed to develop. At present the quality of the product is principally assessed by subjective visual/tactile means.

Preceding research has explored specific types of machine fault that give rise to identifiable surface waveforms, inherently found on moulded wooden components.

With the present deficiency of in-process surface monitoring systems for moulded artifacts, the aim of this work is the development of an optical non-contact measuring transducer. The in-process system will be used to measure the surface waveforms of the timber sections produced in order to identify machine faults prior to taking corrective action.

Contact measurement methods are inadequate for this application due to the high levels of vibrations and feed speeds present in the process. This paper discusses the underlying principles of the overall measuring system, and the novel laser/photodiode combination.

With the quality of the process being reflected in the resultant surface finish, fast Fourier analysis is performed on accumulated surface data. The surface data samples are transformed to associate harmonic frequencies for surface evaluation.

The possible applications of the system are widespread, i.e., any process where surface wavelengths of 1 mm or more are important.

Introduction

As current trends of technology advance, machines and processes becomes more complex and sophisticated. It is usually desirable for duty cycles, where possible, to be optimized and waste materials to be curtailed. However, the quality of the end commodity will always remain one of the highest production constraints. Within woodworking machinery manufacturing, competitiveness and saleability are essential [1]. Therefore it is always paramount that the machinery produced is economic, moderate in setting times and capable of high material throughput in addition to yielding good-quality artifacts.

The emphasis of this paper is that of material quality, as produced by planers and spindle moulders. It is possible for a variety of these machines to extrude timber up to a maximum rate of 180 m/min. Allowing such a process to develop operational faults would result in large quantities of sub-standard timber being produced in a short period of time.

Palpably, to ensure consistent high quality and efficiency, a system capable of monitoring the surface quality of machined material is essential. The monitoring system would evidently have to be an optical non-contact solution due to the inherent high speeds and excessive vibration levels of the process. A

0924-4247/91/$3.50

complete appreciation of the process and the surface geometry of the product is required before developing such a measurement system.

The Process

When planing or moulding components, the feed material is not clamped to the machine table. The workpiece is pressed to the table, using pressurized feed rollers, as it passes the cutter heads (Fig. 1). The machine bed of the planar moulder is fixed and the workpiece traverses the rotating cutter heads.

Due to the physics of the process, the geometry of the machined product surface consists essentially of circular arcs [2]. As can be expected, in practice, the ideal is never achieved: vibration, spindle dynamic imbalance and proud knives all affect the cutter locus and hence the surface profile. Obviously, the greater the level of vibration, dynamic imbalance, etc., the further the surface departs from the ideal.

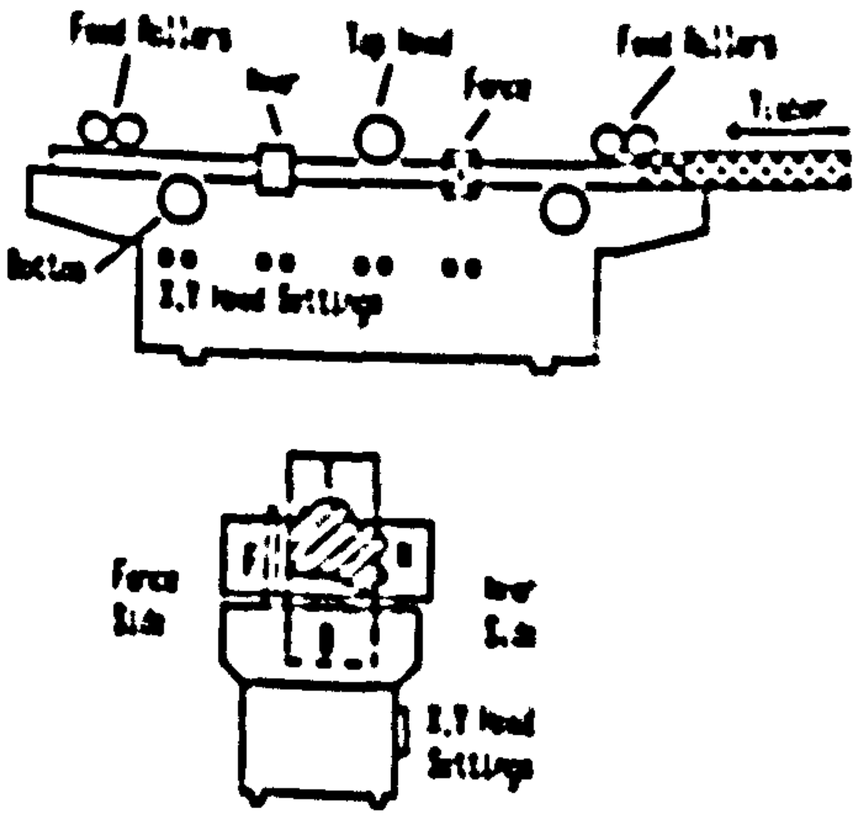

Fig. 1. Diagram of a typical planer moulder. T = top head, B = bottom head, F = fence head, N = near head.

Surface Generation

The wood removal process of planing/moulding machines is intermittent, as shown in Fig. 2 [3]. The locus taken by a cutter-head knife tip, while in the process of chip severance, is actually cycloidal or, more broadly speaking, trochoidal [4].

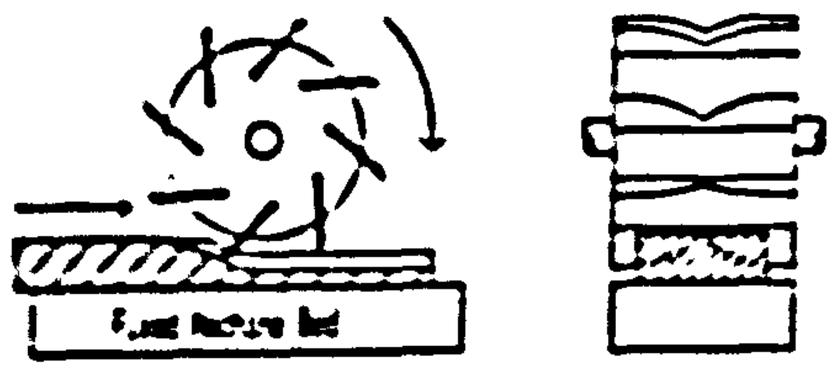

Fig. 2. Moulding process showing single cutter head. The workpiece is traversed past the cutter head.

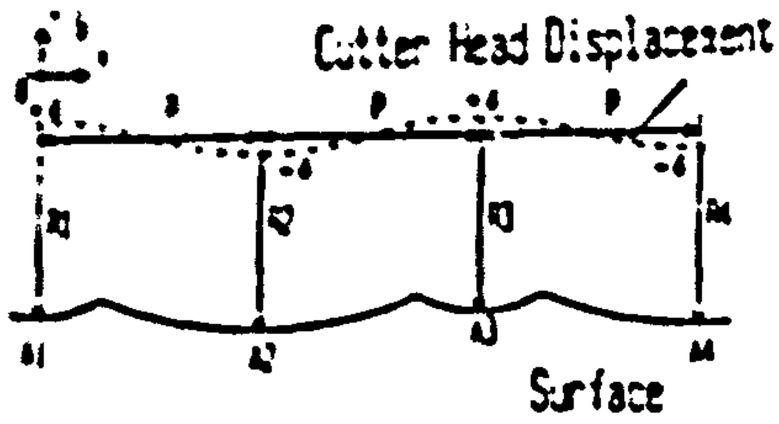

Fig. 3. Surface profile obtained when the cutter head is displaced once every two revolutions.

In practice it is difficult to reproduce ideal machine-operating conditions. The resultant arcs produced on the machined part give rise to many different perturbations of shape due to the practical effects already mentioned. Figure 3 shows a common surface profile obtained with a displacement effect of the cutter head once every two revolutions.

As the planing and spindle moulding process generates a variety of surface shapes on the product, which are dependent on the machine operating conditions, monitoring of the product's surface profile is important.

Surface Assessment Instrumentation

At present there are several types of surface measurement instruments and techniques capable of post-process assessment of surface finish. These range from visual/tactile and optical techniques to precision stylus instrumentation, the latter being capable of calculating surface roughness values with permanent recording facilities. Obviously each method of surface assessment has its own merits and drawbacks.

Although a variety of techniques and instrumentation capable of post-process measurement of surface irregularities exist, they are either very subjective or very time consuming. Contact instrumentation is inadequate for the measurement of in-process surface profiles, as traversing rates are of the order of millimetres per minute (typical machining rates being hundreds of metres per minute for the moulding process).

It is therefore evident, mainly because of the production speeds, that a non-contact in-process surface monitoring system needs to be developed and evaluated.

In-process Measurement Proposal

The monitoring system has been designed to measure the surface characteristics of the wooden component as it is processed. Figure 4 represents the basis of the in-process measurement system. A broad laser beam illuminates the machined surface at grazing incidence ($\theta < 1.5$). The illumination is in the same plane as the traversing workpiece, which gives prominence to the leading slope faces of each surface cusp. A fringe pattern of bright and dark regions is readily observed, representing the surface slope along the product.

A single-element silicon photodiode is used to detect variations in diffusely reflected laser light as the timber passes from the machine. Automatic gain control and signal-conditioning circuitry is used to amplify and filter the output voltage of the photodiode to give maximum dynamic range to the analog-to-digital converter. The sampled output voltage of the photodiode is synchronized using the output of a rotary position encoder as the system clock for the analog-to-digital converter. Additional electronics control the clock signal for correct read/write operations and memory sequencing. As soon as the periodic surface information has been captured (in real time) in the computer memory, it can be analysed in terms of its frequency content using Fourier analysis techniques. The data captured are not prone to distortion due to vibration, as the plane of vibration is almost perpendicular to the illumination. As the laser beam is broad and of grazing incidence to the surface, the vibration levels do not exceed the outer limits of the beam. This phenomenon only occurs because diffuse and not specular reflection is being monitored.

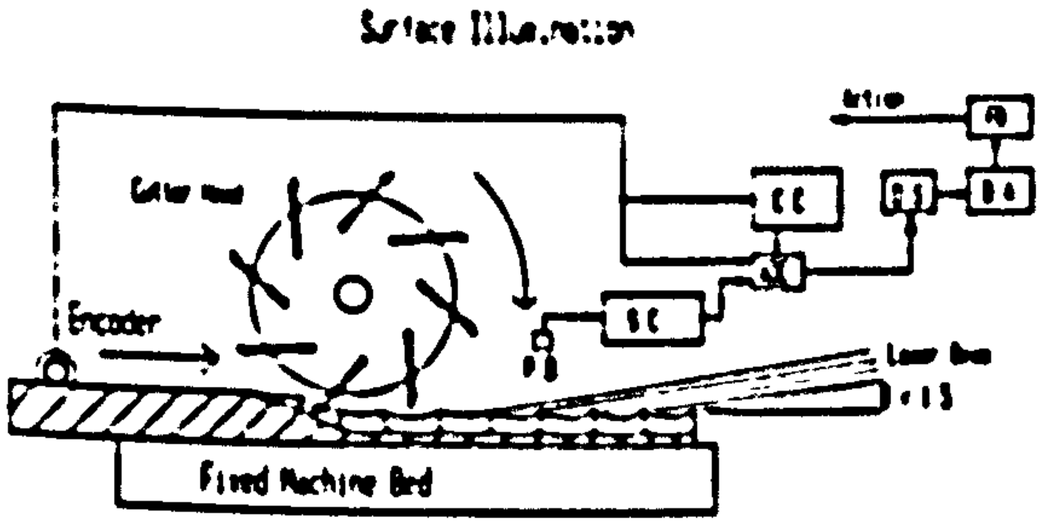

Fig. 4. Basis of the surface characterization system for a workpiece traversed past a single cutter head. P.D. = photodiode; S.C. = signal conditioning; C.C. = control circuitry; D.S. = data store; D.A. = data analysis; FB = feedback; ADC = analog digital converter.

At present, actual material throughput is in the region of 2–2.5 m/s. The new system has been designed to cope with a maximum material movement of 5 m/s, thus allowing increased capacity as machine operating conditions improve. The system is capable of monitoring wavelengths of 1 mm and longer (a 1 mm wavelength represents a very fine planed surface, suitable for furniture manufacturers' requirements).

With appropriate sampling frequency, the data captured over a given sample length can be analysed in terms of frequency content using Fourier analysis techniques.

Results

Figure 5(a, b) shows the resultant surface profiles and associated frequency spectra of a machined surface, obtained using a Talyrond and the novel laser monitoring system respecively. Figures 6 and 7, in the same manner, show other machined surfaces.

To obtain the results in Fig. 5, the machine's cutter head was set up containing six

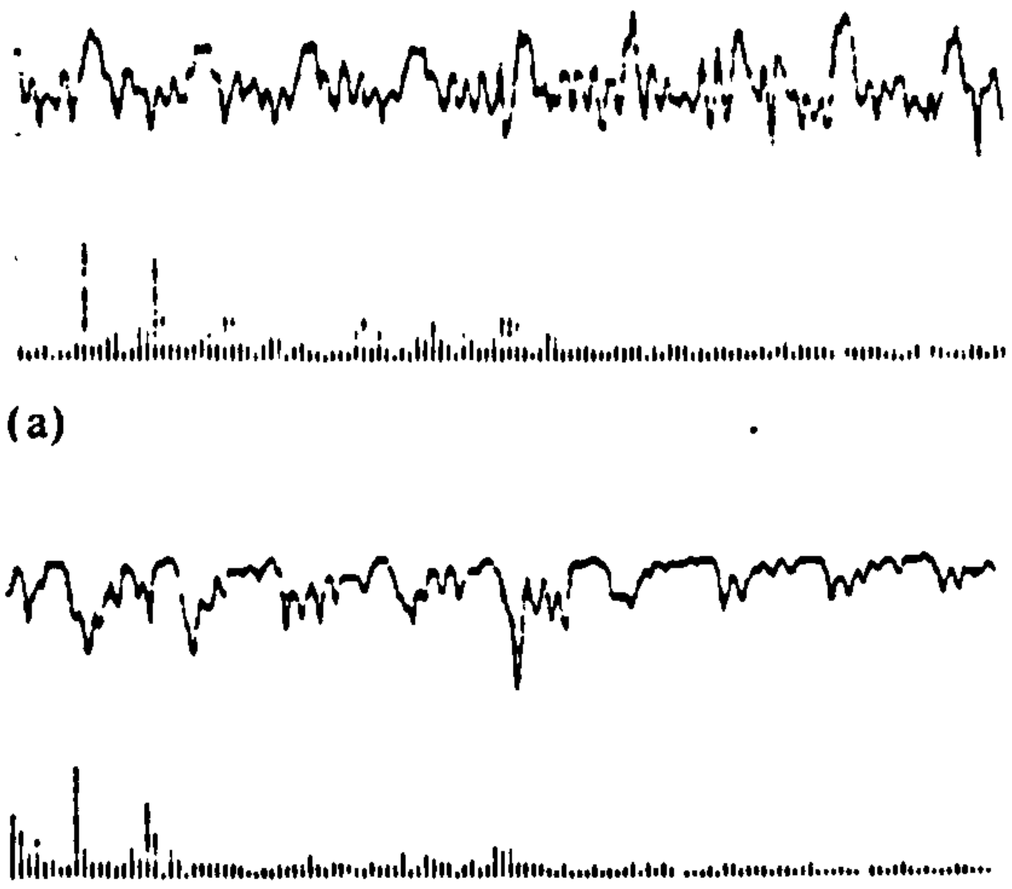

(a)

(b)

Fig. 5. Resultant surface profiles and associated frequency spectra (harmonic nos. 1–128) obtained using (a) a Talyrond and (b) the laser monitoring system.

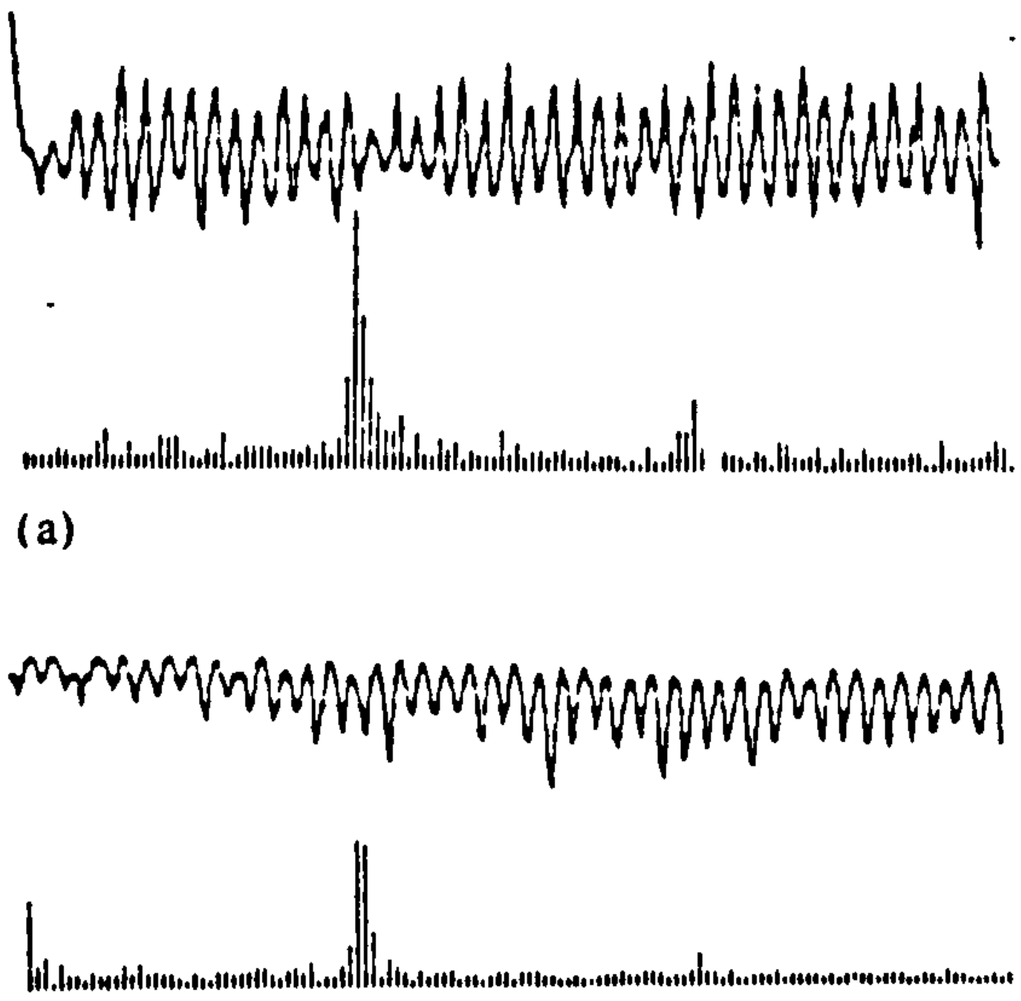

(a)

(b)

Fig. 6. As Fig. 5, but with a once per revolution effect caused on a four-knife cutter head and a slower feed speed.

knives and a deliberate out-of-balance effect was generated at knife number three (added weights).

With a sample length of 125 mm and 128 frequency harmonics shown, wavelengths of 125 mm down to approximately 1 mm can be represented. The dominant frequency harmonics present in Fig. 5(b) are numbers ten and nineteen. These peaks are caused by the out-of-balance effect and individual cutter head knife markings of the process.

Figure 6 shows similar conditions to those in Fig. 5. Again there is a deliberate effect caused on a four-knife cutter head once per revolution. In this case the feed speed of the machine is much slower.

Figure 7 shows a single-knife surface finish. This surface was obtained using a four-knife cutter head with three of the knives used as balancing masses only. With no out-of-balance effect present, the dominant frequency in the frequency spectra is now due to the cutter knife marks on the surface.

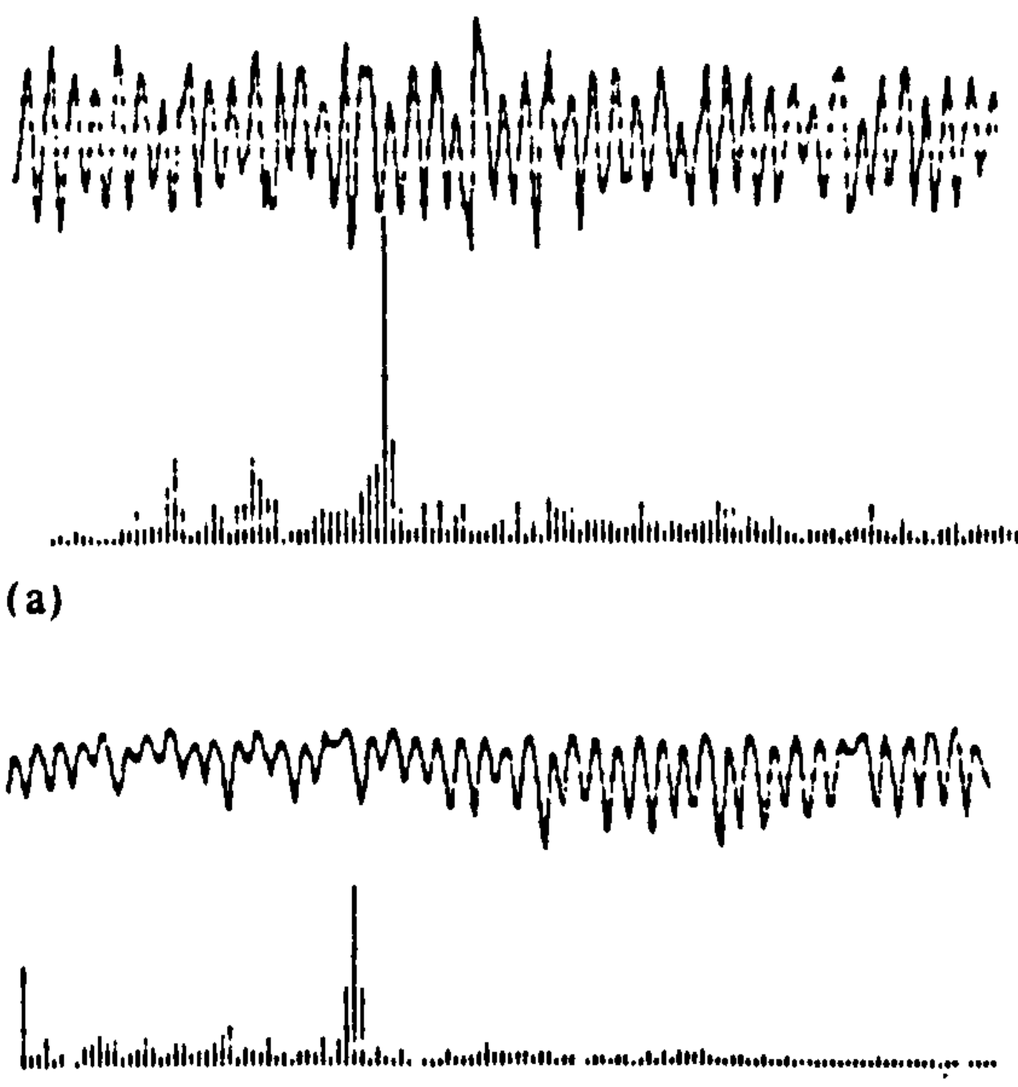

(a)

(b)

Fig. 7. As Fig. 5, but for a single-knife surface finish.

Conclusions

Good correlation between existing surface measuring systems (Talyrond) and the novel laser measurement system has been obtained using harmonic analysis. This comparison has been achieved using a fast Fourier algorithm to convert real-time surface data to the frequency domain.

References

1 B. Garratt. *Business Development Seminar*, Nov. 1988. Wadkin PLC, Green Lane Road, Leics., U.K.

2 M. R. Jackson. Some effects of machine characterisation in planed and spindle mounted wooden products. *Ph.D. Thesis*, Department of Mechanical and Production Engineering, Leicester Polytechnic, June 1986.

3 M. E. Martellotti. An analysis of the milling process. *Trans. ASME.* (Nov. 1941) 255–264.

4 P. Koch. An analysis of the lumber planing process. *For. Prod. J.*, (Aug. 1955) 677–700.

The Use of In-Process Surface Topography Measurements as a Predictor of Machine Performance and Condition

by FA Cutri, RM Parkin and K Maycock

As manufacturing industries become progressively automated emphasis is increasingly placed on machine or process control. To this end research work presently under way at Leicester Polytechnic has concentrated on an automatic surface monitoring system for in-process production control.

Recent woodworking machinery has achieved large increases in material feed rates and cutter head spindle speeds. Typical spindle speeds of modern machinery is in the region of 6000 rev/min. For high quality machined components, spindle speeds of 15000 rev/min (max) are required with multi knife cutter head assemblies.

Advancements in technology contribute dominantly to the high production rates and associated component quality which can now be produced. However, the adoption of technology has brought with it some undesirable and expensive problems. As the quality of the process is reflected in the surface finish of the artifact, and production rates are very high, the development of a non-contact surface monitoring system is examined.

Consideration is given to machine vibration origins, with correlation of specific topographical anomalies to machined surfaces. Prediction software and Fourier analysis have been used to attain encouraging results from machinery exhibiting known operational parameters.

1. Background

Manufacturing industries are becoming increasingly automated, using complex computers for the control of production processes and machinery[1]. However, the processes and machines still propagate functional vibrations to the components under production. The period and energy content of the inherent cyclic undulations, when analysed, build up a frequency signature which is representative of characteristic operational conditions.

The repetition and amplitude of generated vibrations are usually unique for individual machines. However a machine vibration frequency spectrum can generally be predicted when analysing the design specifications. Distinctive periodic peaks, present within resultant frequency spectra, can be detected and, usually, associated with specific system mechanisms. Important, machine related, period information can be utilised as a basis for machine condition evaluation.

Machine vibration can be segregated into low, medium and high frequency ranges, dependent on origin. Usually large periodic oscillations are produced from such mechanisms as out of balance rotating masses, misalignments or bent shafts. Medium range undulation components such as meshing gears within gearboxes give rise to multiple shaft revolution frequencies. Short wavelength fluctuations generally originate from areas such as rolling element bearings.

2. Vibration Origins

A rotating system and resultant frequency spectrum can be seen in Figure 1 illustrating the origins of typical periodic undulations. Point A on the spectrum identifies a spectral peak produced from an out of balance; this type of fault appears at shaft revolution frequencies. Point B (Figure 1) correlates the spectral crest to gear teeth meshing. The frequency of tooth mesh corresponds to rotational speed multiplied by the number of teeth located on the gear. As imperfect rolling action (sliding due to wear), loading and deflection (dependent on the number of teeth in mesh) vary, then high harmonics, in addition to the tooth meshing frequency, are present (Figure 2).

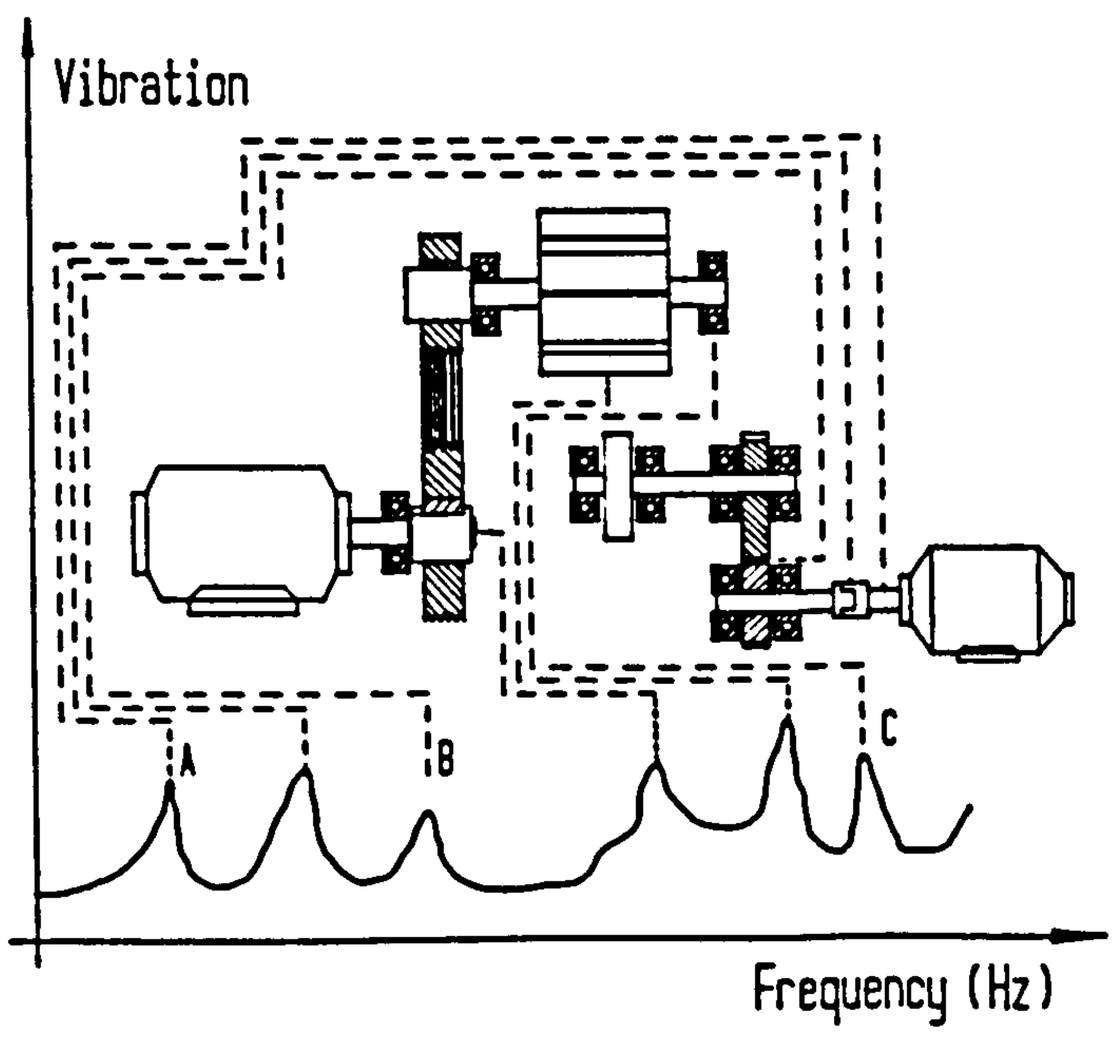

Fig 1 Machine Element Frequency Ranges

If local incipient faults such as a cracked (but not fully broken) tooth occurs on a gear wheel, then the resultant time and frequency spectra are affected. The damaged tooth will deflect more in mesh altering normal operational vibration characteristics as shown in Figure 3(a). The effect of a single cracked tooth in the time domain signal is that of a healthy, or maybe worn gearbox signal with a series of superimposed pulses upon it. This type of local fault generates low level sidebands in the frequency domain spectrum (Figure 3(b)). As this type of fault propagates (ie several faulty teeth in mesh) then the periodic characteristics alter (Figure 4(a)). An amplitude modulated effect transpires transforming the time domain signal. The effect of this change in the frequency

Frank Cutri graduated with his BEng Engineering Technology Degree in 1988 at Leicester Polytechnic. He is presently consolidating his Doctorate research in the field of Mechatronics and Systems Engineering.

Rob Parkin BSc, PhD, CEng, MIEE, FIMechE is a Reader in Mechatronics and Principal Lecturer in the School of Engineering & Manufacture, Leicester Polytechnic.

Keith Maycock BSc is a time-served draughtsman, who graduated in Engineering Technology at Leicester Polytechnic in 1985. He is now a Lecturer II at Leicester Polytechnic.

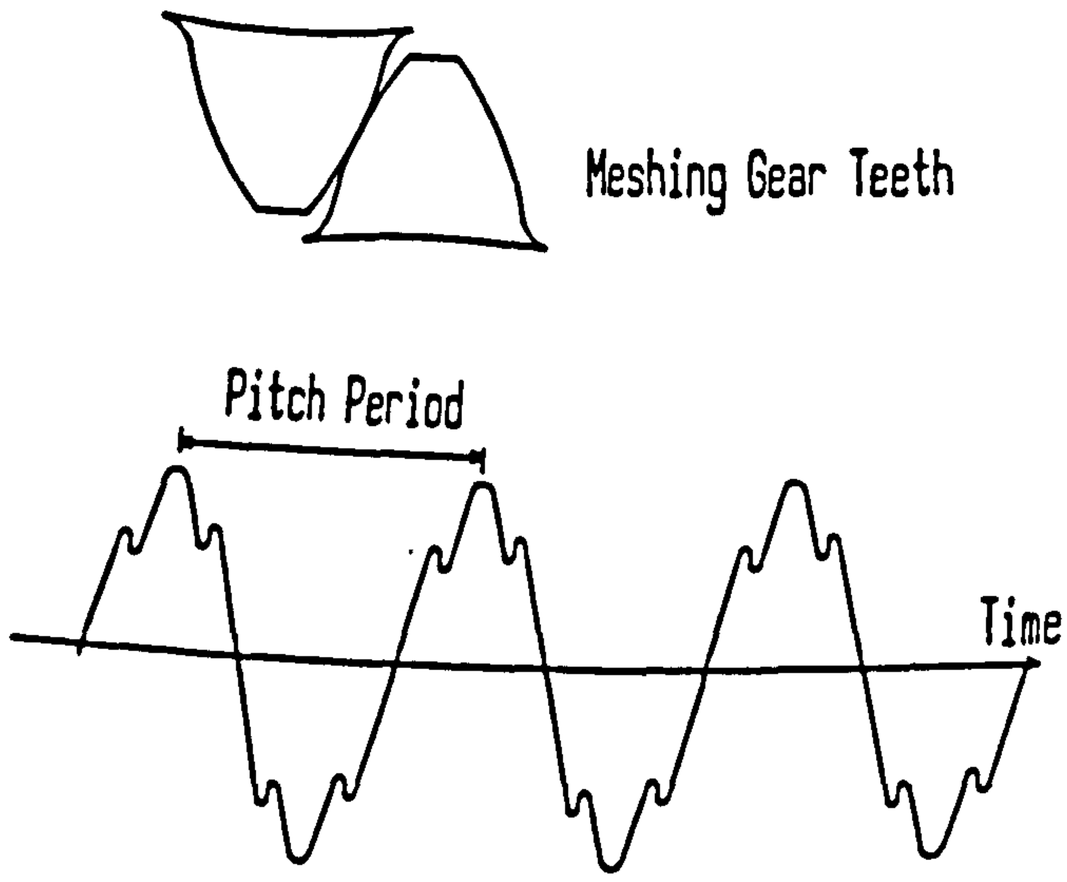

Fig 2 Typical Gearmesh Waveform

domain being an increase in the sideband amplitudes (Figure 4(b)).

Point C of Figure 1 represents a typical defect frequency generated from rolling element bearings. There are several defects possible within rolling element bearings (Figure 5(a)). Faults such as cracks or blemishes (corrosion pits) can develop on either of the bearing races or even on the rolling elements themselves. If a fault occurs on the surface of the outer race (outer race fixed) then small amplitude impulses arise every time a rolling element passes

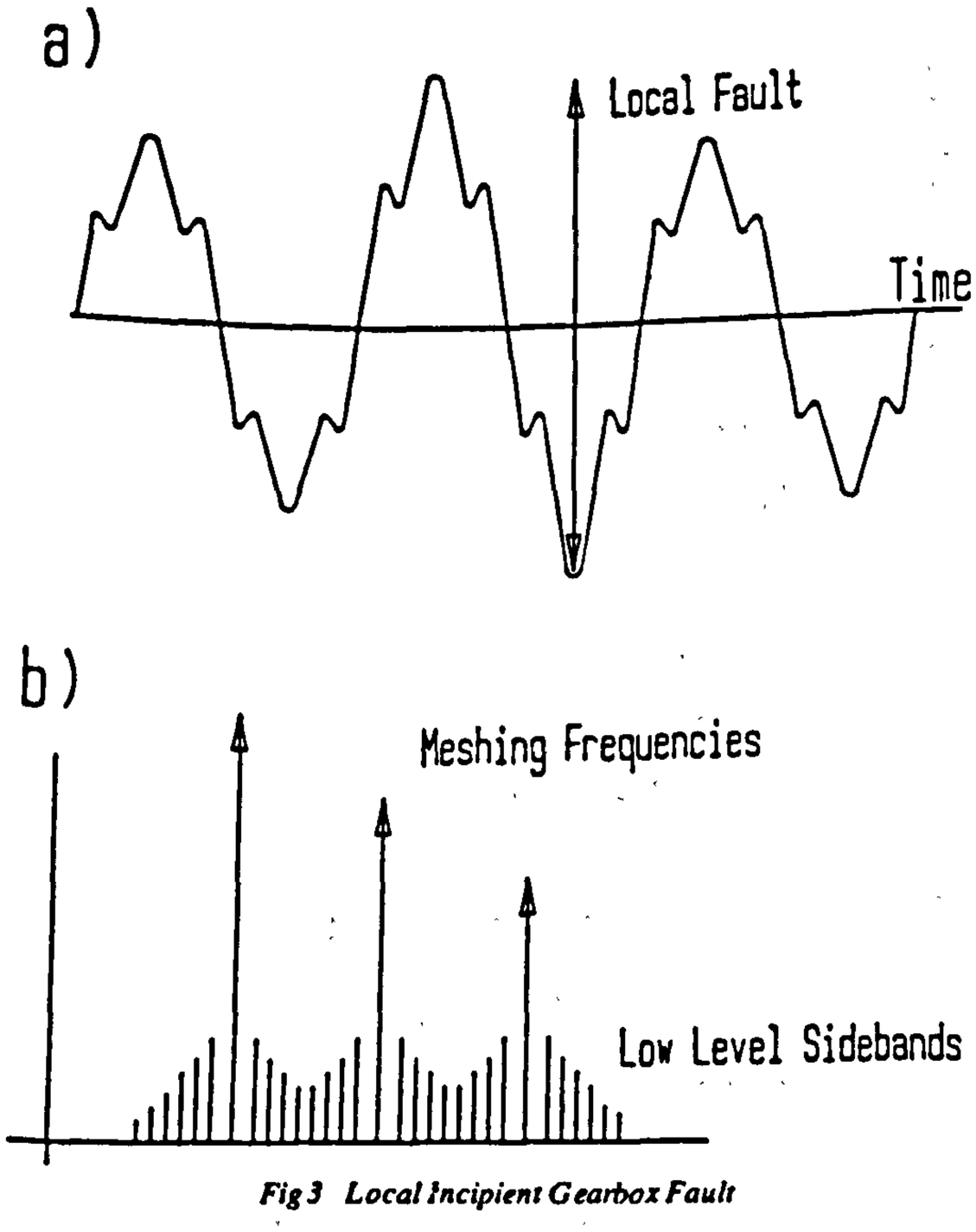

Fig 3 Local Incipient Gearbox Fault

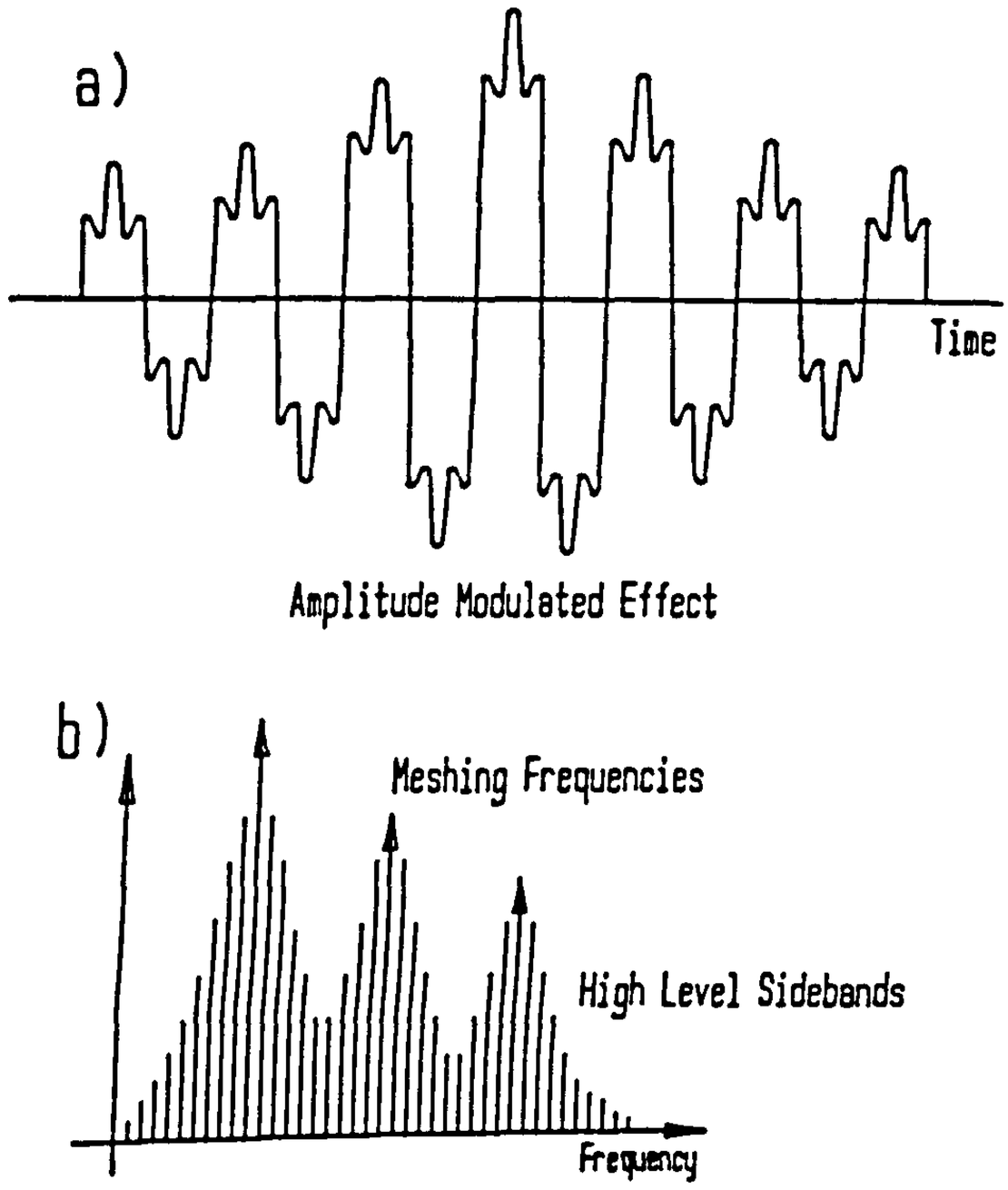

Fig 4 Fault Propagation Within Gearbox

over the affected area. The amplitude of these impulses are constant (Figure 5(b)), with frequency rates as indicated in Figure 6. If an imperfection arises on the surface of the inner race (rotating race), then the resultant energy impulses vary in amplitude with the changes in rolling element load (Figure 5(c)). In both cases the energy impulses are transmitted to the bearing housing, which in turn vibrates at its natural frequency.

As vibration origins can be identified using machine frequency spectra, it is possible to monitor machine status. Transitions between initial "healthy" and eventual worn or failed machine spectra can be recorded. As the operation time of the system increases and the frequency spectrum alters, thresholds can be established on required operating conditions. The thresholds imposed can be used to initialise planned preventative maintenance work, before eventual failure occurs.

As incipient operational vibrations can, and are, transferred to the workpiece, analysis of the machined commodity surface can provide (using suitable measurement/monitoring facilities) important machine operating status information.

3. The Process

This paper will investigate planed and spindle moulding of wooden artifacts. The woodworking industry desperately requires a reliable method by which to quantify and categorise the surface quality of its planed and spindle moulded products. The current practice is that of visual tactile inspection, which results in a wide variance in what is classed as an acceptable or defective surface finish: what one manufacturer may reject as an unacceptable standard, another may accept as "good". These methods, by their very nature, are subjective and restricted to post process applications.

Woodworking machinery has unique problems due to high speeds of operation. Modern woodworking machines "extrude"

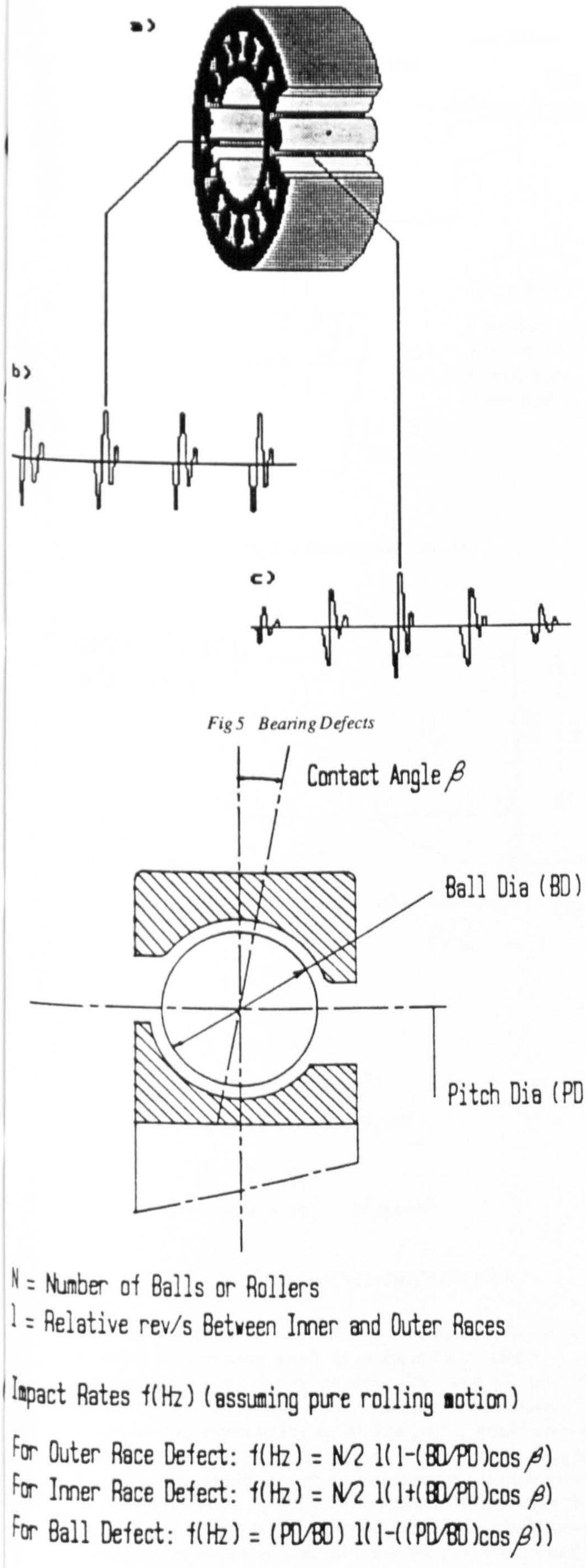

Fig 5 Bearing Defects

Fig 6 Rolling Element Bearing Frequencies

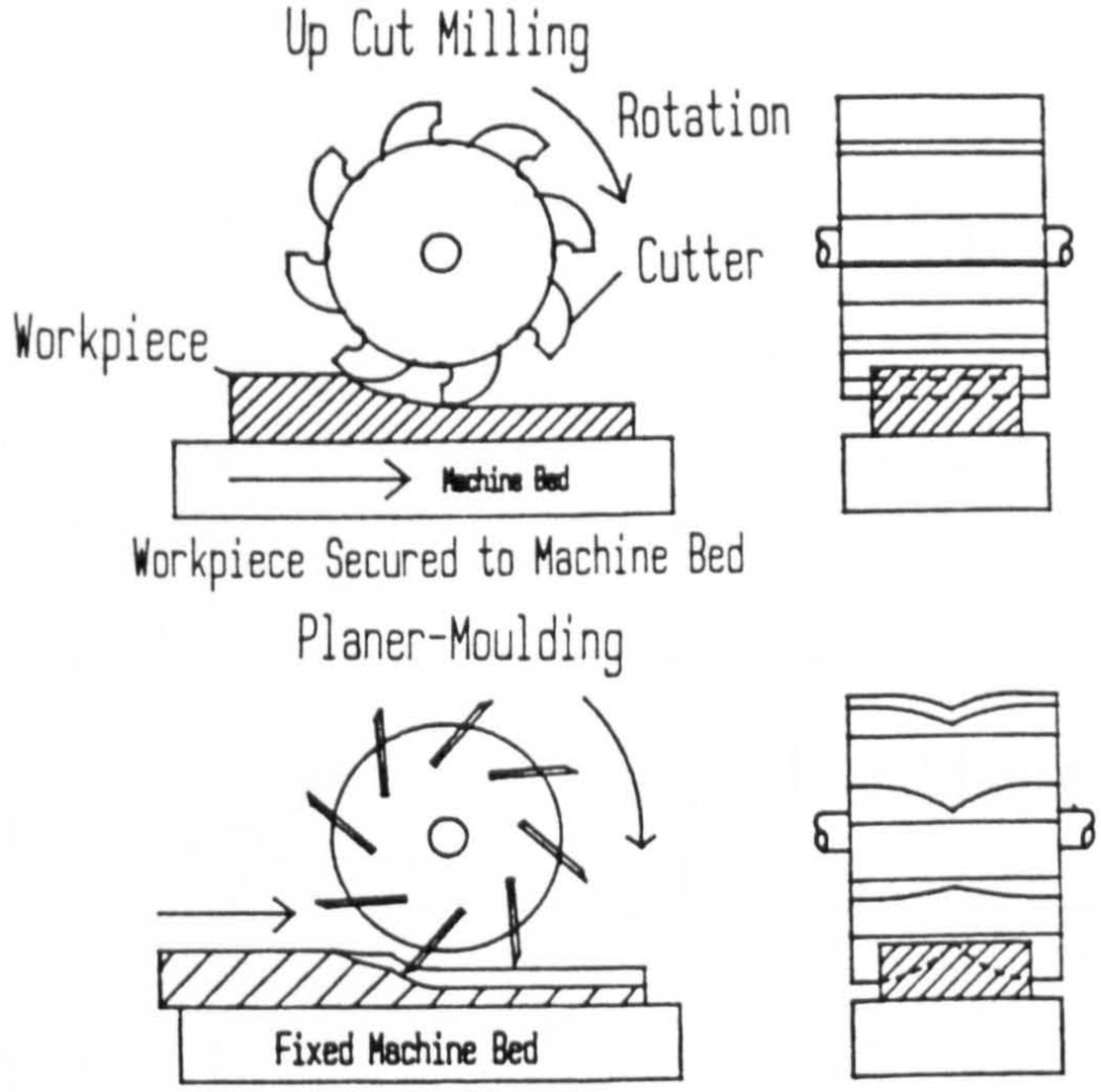

Fig 7

timber at extremely high rates, often in excess of 140 m/min. To achieve these rates, high cutter head rotational speeds are used (up to 15000 rev/min) resulting in high levels of noise and vibration with attendant risk of machine bearing failure. Thus if the process develops a fault; eg, blunt cutters, imbalance, then a considerably large quantity of sub standard (defective surface finish) timber can be produced before the symptoms are detected. It is evident, due to these operational speeds, that non-contact sensors capable of monitoring the quality of the product require development.

The planed and spindle moulding process is comparable with the milling of metals in the up cutting mode (Figure 7). Although these operations are analogous, there are some fundamental differences. The major discrepancy is that milled components are firmly clamped to the machine bed, while the bed is traversed past the cutting head. With planing and spindle moulding, the bed and the cutter heads are fixed and the workpiece is traversed using pressurised feed rollers (Figure 8). Also material machining speeds are extremely high when compared to the milling process.

Because the cutting circle diameter used on planing machines is relatively large (typically 200mm), the depth, h (Figure 9) of each cusp, produced on the surface of the product, is of the order of a few microns. Due to the surface amplitudes being small, height variations, as such, are undetectable by the naked eye. Investigations[2] have shown that it is the consistency with which the apexes repeat that affect the aesthetic qualities of the machined surface. It is then surface wavelength, or periodic beat, information that is essential for product evaluation by the manufacturer.

4. Surface Finish

As faults develop within the system, the surface contours generated on the artifact depart from the ideal. This departure contains information regarding the corresponding anomalies. As machine faults develop, changes in the surface parameters may be

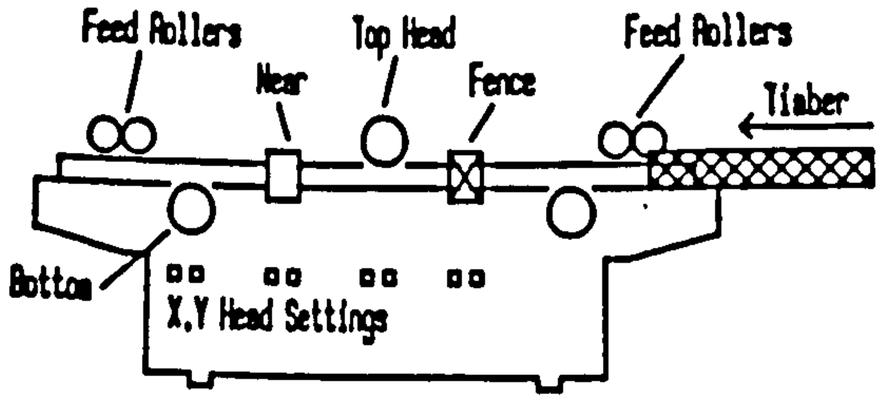

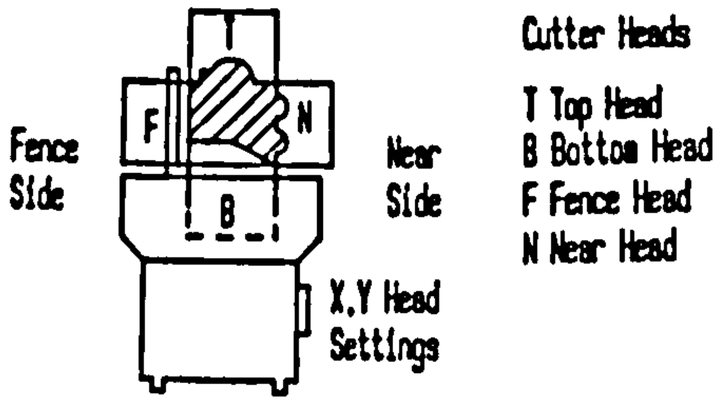

Fig 8 4 Head Planer - Moulder

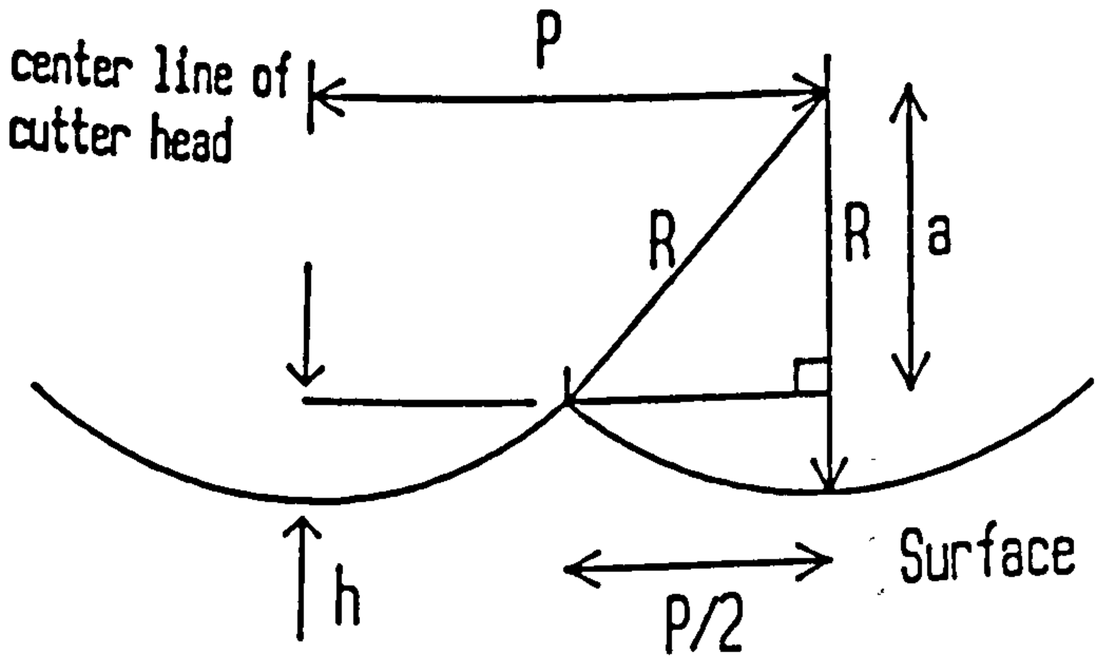

$a = R - h$

$a^2 = R^2 - (P/2)^2$

$a = (R^2 - (P/2)^2)^{1/2}$

$h = R - a$

$h = R - (R^2 - P^2/4)^{1/2}$

$P = (f.\ 10^3)/nN$

Fig 9 Surface Profile Height and Pitch

analysed to predict the mechanism of the defect. The defects may be either slow moving trends or catastrophic in nature.

If machine cutting conditions were ideal, with all operational factors known, the profile of the resultant manufactured surface would be that shown in Figure 10. The profile would consist of knife traces (arcs), detailed A_1 to A_n, with corresponding arc radii R_1 to R_n. The origin of each arc being separated by a theoretical feed pitch per knife (identical wavelengths[3]). However, in practice, the ideal is rarely achieved; vibration, spindle dynamic imbalance, proud knives, etc all affect the cutter locus and hence surface profile. The greater the level of vibration, dynamic

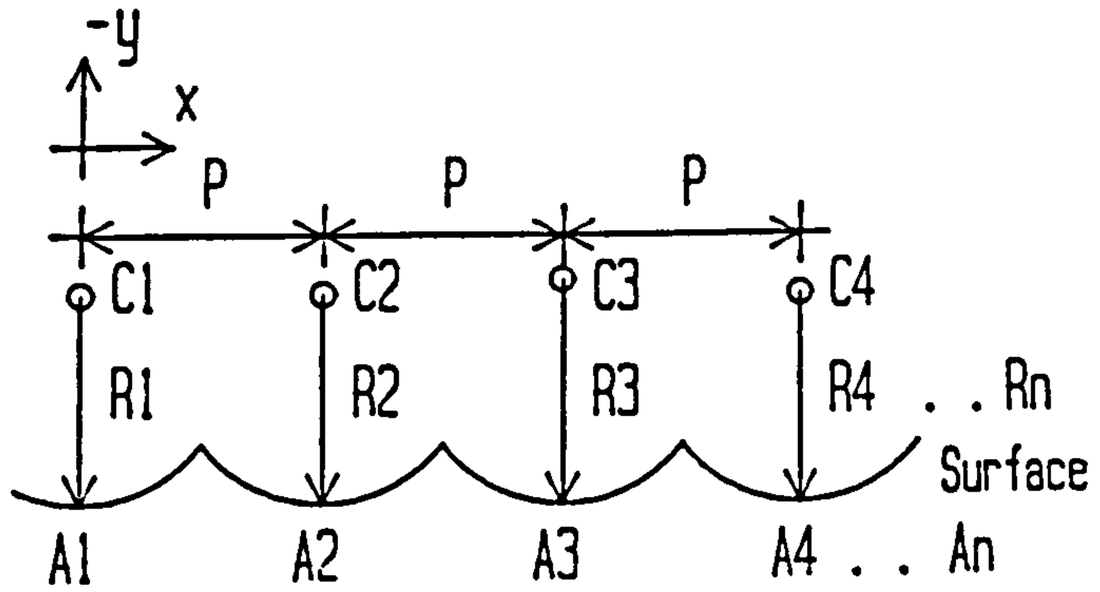

Fig 10 Surface Profile

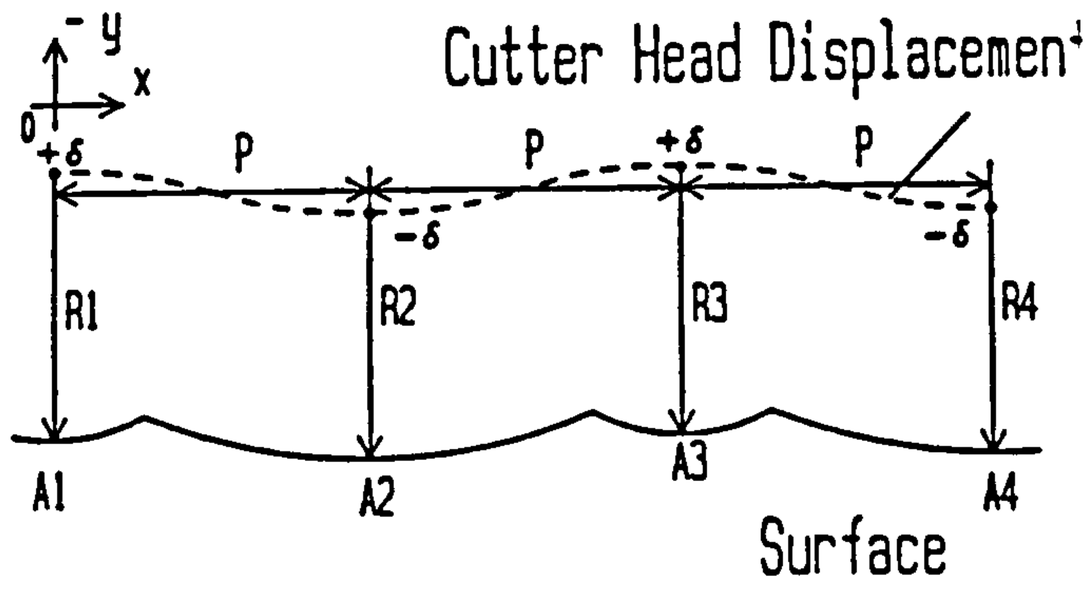

Fig 11 Once Every Two Revolution Effect

imbalance, etc the further the surface departs from the ideal. A more typical profile of a planed surface is shown in Figure 11. With a single knife finish the displacement (δ) of the cutter head occurs every two revolutions of the cutter head (2P). With a total head displacement of (2δ) between the theoretical feed pitch (P), an imperfect surface profile results. Instead if identical wavelengths of (P) (ideal surface profile), the wavelengths of arc A_2 and A_3 are in fact equal to;

$(P + (4R\delta/P))$

and

$(P - (4R\delta/P))$

respectively[4]. Where (R) is the radius of the cutter head and (δ) is the instantaneous cutter head displacement.

This type of effect could be generated if an out of balance drive motor pulley was run at half the angular velocity of the cutter head spindle (2:1 pulley ratio). Amplification of the drive motor pulley imbalance, due to structural resonance, could create significant cutter head displacement.

As machine setup and operational conditions vary widely, it is evident that many surface contours are achievable on the product. With the realisation of this phenomenon, two stages of research were undertaken. Initially simulation software was written, for the prediction of surface profiles obtainable on moulding machines exhibiting known operating conditions. In conjunction with this research, an opto-electronic non-contact, in-process surface measurement/monitoring system was developed.

5. Surface Simulation

Extensive software has been developed which explored the geometric trochoidal relationship between the cutter locus and the workpiece traverse. All practical operating conditions, such as out of balances, proud knives, revolution effects, etc were incorporated

within the software.

The programs allowed Fourier analysis of the simulated data, for data conversion from the time domain to that of the frequency domain (wavelength being essential surface information). Real data, gathered from the optical measuring system and a more classical stylus system (contact, post process), could also be processed by the software to establish the frequency content of real surface data. With the whole process accurately modelled the simulation software could be used to predict machined surface profiles. The accuracy of the model was evaluated against the existing surface measurement systems and the novel opto-electronic surface measurement system mentioned previously. The results and comparisons of the simulated data are discussed and illustrated later with correlation to the advanced opto-electronic surface measurement system.

6. Optical Surface Measurement System

6.1 Objective

The foregoing discussion clearly indicates the requirement for a fast-response non-contact, method of measuring the surface quality of machined timber; an integral part of this requirement is the determination of parameter(s) which can readily indicate and identify defects.

The "non-contact-rapid-response" nature of light, coupled with recent advances in laser and opto-electronic technology, has brought about interesting and new possibilities for in-process assessment of product quality.

6.2 Realisation

Previous work has investigated certain types of machine faults that give rise to identifiable surface waveforms on produced timber[5]. The monitoring system has been designed to measure the surface characteristics of the wooden component in-process. Figure 12 represents the basis of the in-process measurement system. A broad laser beam illuminates the machined surface at grazing incidence (θ <1.5°). The illumination is in the same plane as the traversing workpiece, which gives prominence to the leading slope faces of each surface cusp. A fringe pattern of bright and dark regions is readily observed representing the surface slope along the product.

A single element silicon photo diode is used to detect variations in diffusely reflected surface laser light as the timber passes from the machine. Automatic gain control and signal conditioning circuitry is used to amplify and filter the output voltage of the photo diode to give maximum dynamic range to the analogue to digital convertor. The sampled output voltage of the photo diode is synchronised using the output of a rotary position encoder, as the system clock for the analogue to digital convertor. Additional electronics control the clock signal for correct read/write operations and memory sequencing. As soon as the periodic surface information has been captured (in real time) in the computer memory, it can be analysed in terms of its frequency content, using Fourier Analysis Techniques. The data captured is not prone to distortion due to vibration, as the plane of vibration is almost perpendicular to the illumination. As the laser beam is broad and of grazing incidence to the surface the vibration levels do not exceed the outer limits of the beam. This phenomenon only occurs because diffuse and not specular reflection is being monitored.

At present, actual material throughput is in the region of two to two and a half metres per second. The new system has been designed to cope with a maximum material movement of five metres per second, thus allowing increased capacity as machine operating conditions improve. The system is capable of monitoring wavelengths of one millimetre and greater (one millimetre being a very fine planed surface suitable for furniture manufacturers requirements).

6.3 Results

Figure 13(a,b,c) shows the resultant surface profiles and associated frequency spectra of a machined surface, obtained using a Talyrond, the novel laser monitoring system and simulation software respectively. Figures 14 and 15, in the same manner, show other machined surfaces. To obtain the results in Figure 13, the responsible machines cutter head was set up containing six knives and was run at six thousand rev/min. With a material feed speed of ninety metres per minute and a deliberate out of balance effect generated at knife number three (added weights), Figure 13(b) was recorded using the laser system.

With a sample length of one hundred and twenty five millimetres and one hundred and twenty eight frequency harmonics shown; wavelengths of one hundred and twenty five millimetres down to approximately one millimetre can be represented. The dominant frequency harmonics present in Figure 13(b) are numbers ten and

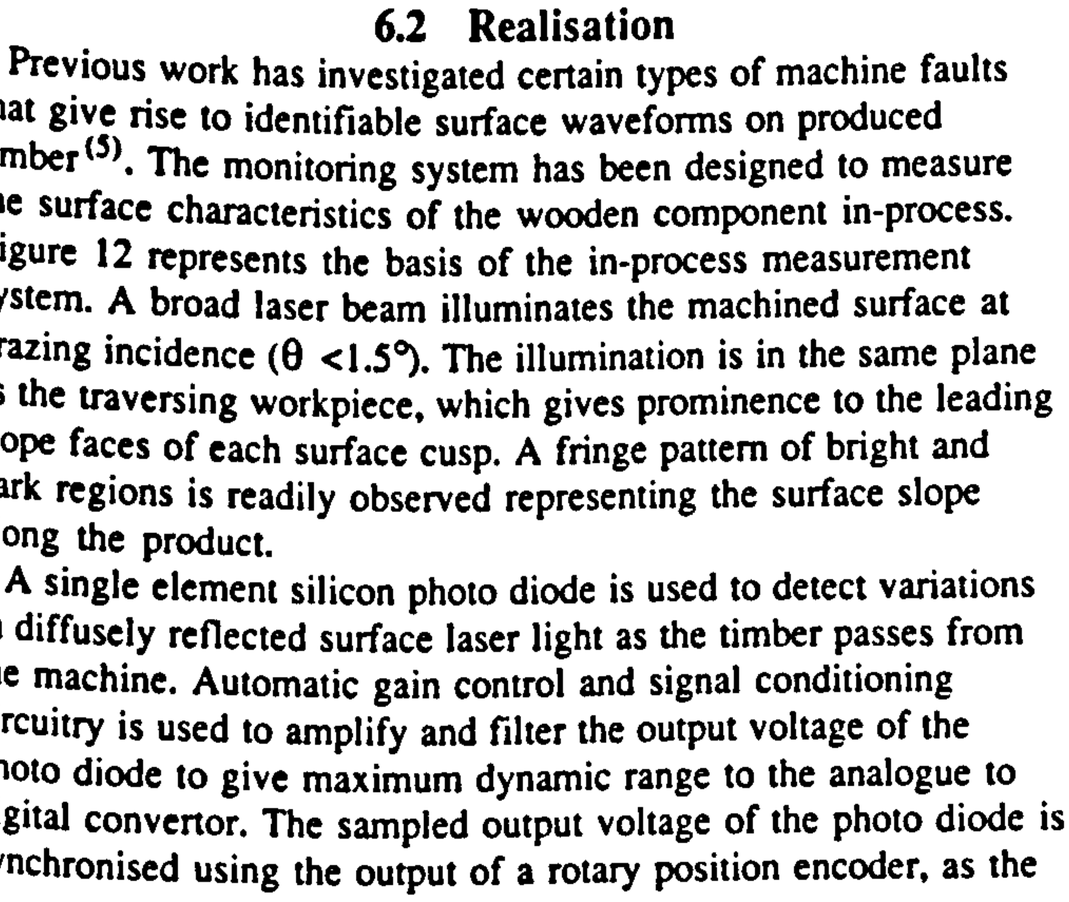

Workpiece Traversed Past the Cutter Head
Moulding Process Showing Single Cutter Head

Fig 12 Surface Illumination

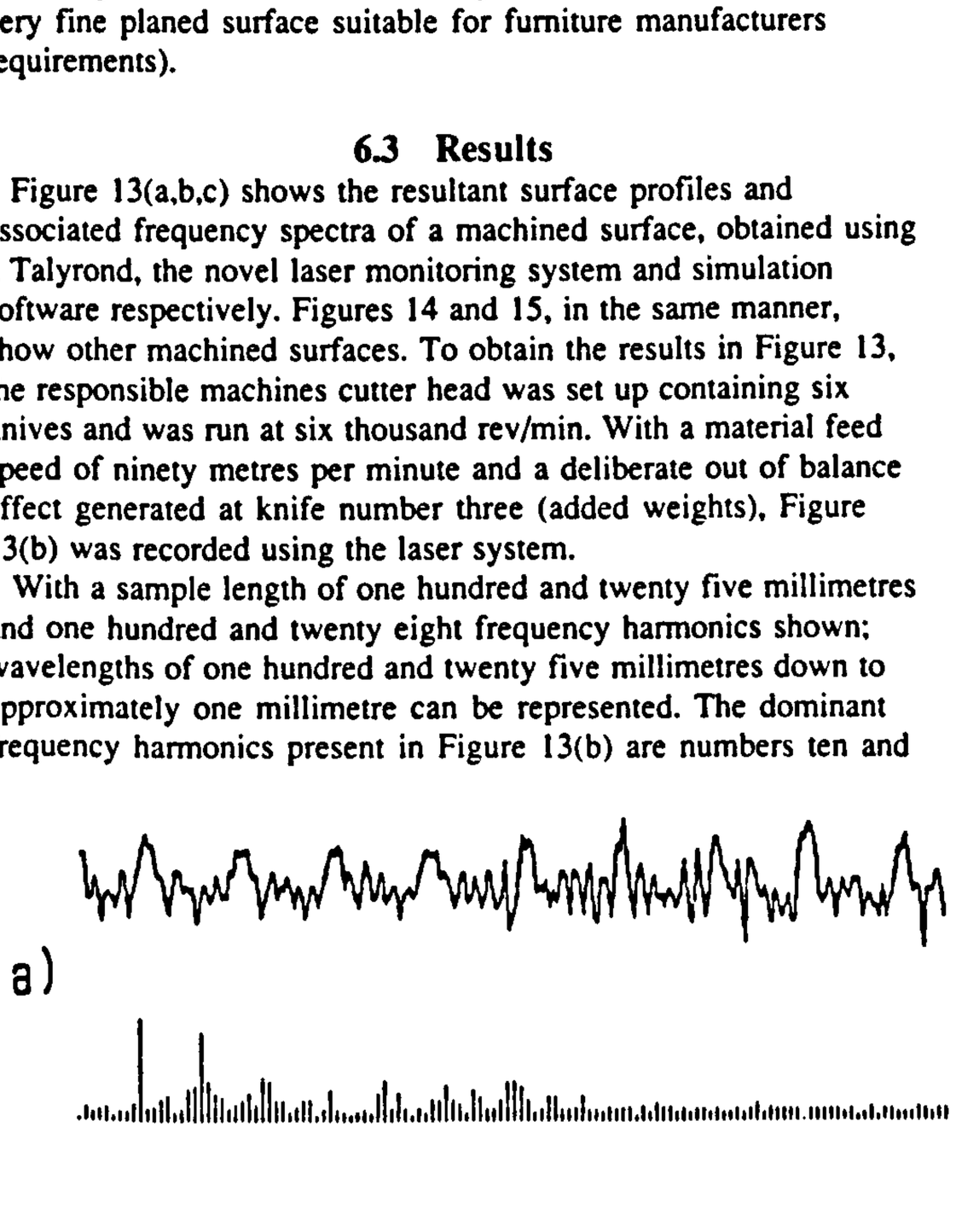

Fig 13 Surface Data

Text cut off in original

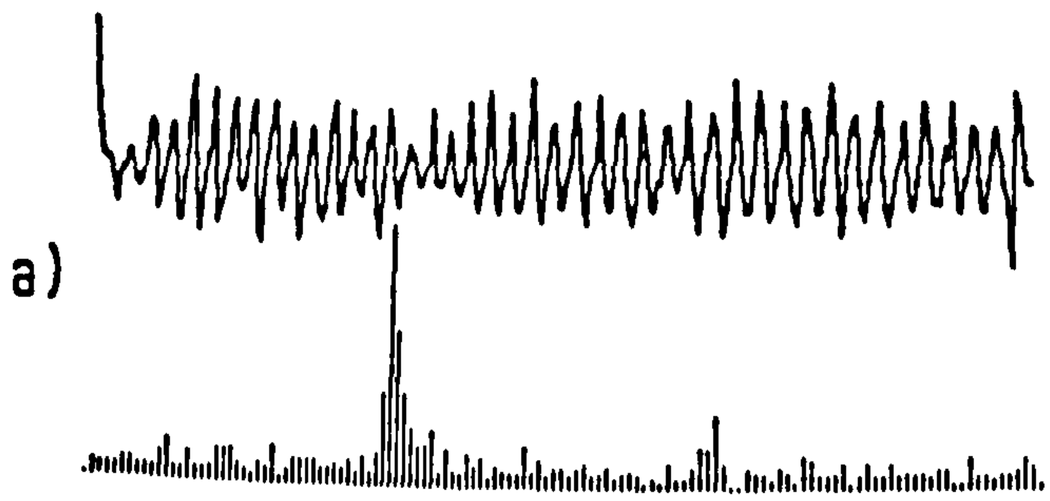

Fig 14 Surface Data

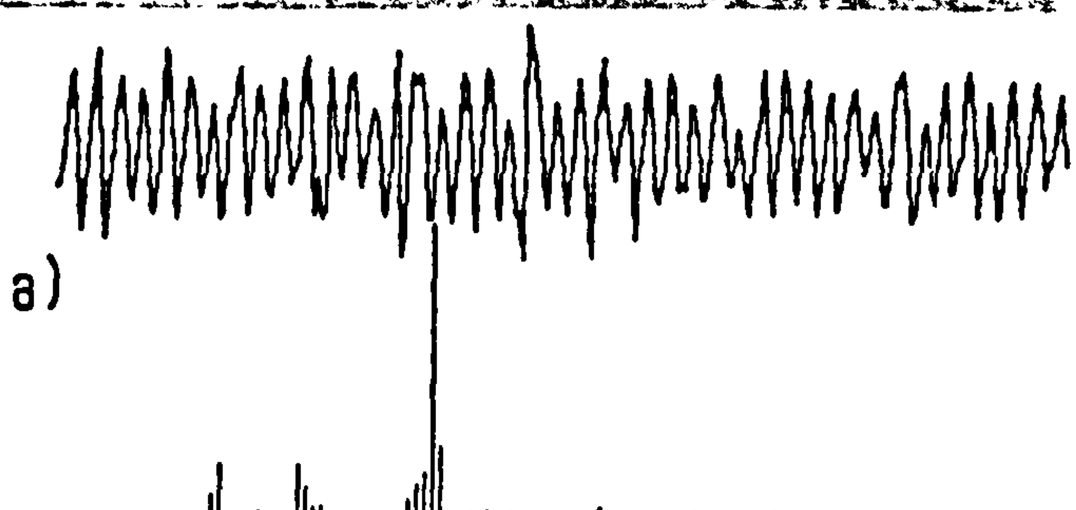

Fig 15 Surface Data

nineteen (12.5mm and 6.58mm wavelengths). These peaks are caused by the out of balance effect and individual cutter head knife markings of the process. Because the out of balance effect occurs once every revolution of the cutter head it would be expected for the frequency harmonic to be approximately number eight or nine with these specific operating conditions. It would take 8.33 seconds to pass one hundred and twenty five millimetres of material, through the machine, at a feed rate of ninety metres per minute. With a cutter head speed in the order of six thousand rev/min there would be approximately eight and one half revolutions within the sample length. In fact from Figure 13(b) it can be seen that there are ten revolutions present. This small discrepancy is due to inaccuracies arising from the feed and cutter head speed equipment. As there is an out of balance effect, the knife marks vary in surface wavelength, thus in the frequency spectrum the knife marks are spread over several rather than a single harmonic (eg harmonic numbers 10, 19, etc).

Figure 14 shows similar conditions as that in Figure 13. Here again there is a deliberate once per revolution effect caused on a four knife cutter head. In this instant the feed speed of the machine (eighteen metres per minute) is much slower, but the cutter head speed of six thousand rev/min remains the same. The effect of the slow feed speed on the surface is the translation of the out of balance dominant frequency along the frequency spectrum (Higher frequency due to slower moving feed material). A second effect being the smoothing of knife marks on the surface, which is indicated in the frequency spectrum due to a lack of other higher dominant frequency harmonics.

Figure 15 shows a single knife finish surface. This surface was obtained using a four knife cutter head with three of the knives used as balancing masses only. With no out of balance effect present, the dominant frequency in the frequency spectra is now due to the cutter knife marks on the surface. With a feed speed of eighteen metres per minute it would take 0.416 seconds to pass one hundred and twenty five millimetres of timber past the cutter head. Again with a six thousand rev/min cutter head there would be 41.6 revolutions of the cutter head (with a single knife this would be 41.6 identical knife marks) in the sample length. As shown in each of the frequency spectra the dominant harmonic is number forty five (wavelengths of 3mm). This small discrepancy resulting again from feed and cutter head equipment inaccuracie

7. Conclusions

This paper has discussed typical vibration origins of machines and the effects they have on the surface of the manufactured component. Prediction software as well as non-contact measuring/monitoring hardware has been developed to control t quality of the artifacts and the process. Good correlation betwee existing surface measuring systems (Talyrond) and the novel lase measurement system has been obtained using harmonic analysis This comparison has been achieved using a Fast Fourier Algorithm to convert real time surface data to the frequency domain. Faults such as corrosion pits or cracks on bearing races gears will be present at higher harmonics of the frequency spectr Future work regarding the frequency spectra of trend or catastrophic failures is required for correct initialisation of feedback action.

8. References

1. LR Rakowoski. Blasting Off with CIM. Machine and Tool Blue Book. June 1987.
2. B Garratt. Business Development Seminar. Nov 1988. Wadkin Plc, Green Lane Road, Leics
3. R Goodchild. Investigating Finish of Rotary Planing. Engineering. Jan 25th 1963.
4. MR Jackson. Some effects of machine characterisation in planed and spindle moulded wooden products. PhD Thesi Dept of Mechanical and Production Engineering, Leicest Polytechnic. June 1986.
5. MS Hundral. Mechanical Signature Analysis. Dept of Mechanical Engineering, University of Vermont, Burlingt

Measurement and Control Techniques for Timber Production Processes

K M Maycock and R Parkin

School of Mechanical and Production Engineering, Leicester Polytechnic, UK

Abstract

Woodworking machinery has unique problems due to the high speed of operation. The production rate of planed and spindle moulded timber products is currently running at approximately 1 m/s. To achieve these rates high speed cutters are used (up to 15000 rev/min) resulting in high levels of noise and vibration and risk of bearing failures. Faults in the machine result in a poor quality product. The quality of the product is normaly assessed by subjective visual means, i.e. does it look alright?

Previous work has investigated certain types of machine fault that give rise to identifiable surface waveforms of the produced timber. This paper proposes a system for the management and control of the production process to identify and rectify product defects.

An important feature of this work is the development of a "smart" sensor to measure the surface waveforms of the timber sections produced, in order to identify machine faults, prior to taking corrective action.

Contact measurement methods are inappropriate due to high speeds and vibration levels present in the process. This paper describes a microprocessor controlled, non contact, measuring "block" for incorporation into the overall machine management and control system.

The measurement system incoporates a novel laser and photodiode array combination and utilises real time Fast Fourier analysis techniques. The possible applications of the system are widespread, i.e. any process in which the surface waviness (wavelength => 1mm) is important (e.g. steel production, plating/coating industry). The sensor system is the subject of a patent application.

1.0 Introduction

1.1 Background

The woodworking industry desperately needs a reliable method by which to quantify and categorise the surface quality of its planed and spindle moulded products. The current practice is that of visual and tactile inspection, which results in a wide variance in what is classed as an acceptable or defective surface finish; what one manufacturer may reject as an unacceptable standard, another may accept as "good". These methods, by their very nature, are subjective and are restricted to post-process application.

Modern woodworking machines "extrude" timber at extremely high rates, often in excess of 140m/min. Thus, when the process develops a fault, eg blunt cutters, a considerably large quantity of sub-standard (defective surface finish) timber is produced before the symptoms are detected by post-process inspection.

Evidently, to ensure consistent quality and economy, it is necessary to develop sensors capable of monitoring the quality of the product, at the instant that it is produced, so that any necessary remedial action may be effected immediately.

1.2 Surface Geometry

Machined timber production has some similarities with the milling of metals; the revolving cutter shears chips from the surface in the up-cutting mode. However, with wood, the feed (typically 100 m/min) and cutter speeds (typically 15000 rev/min) far exceed those of milling; also, machining the workpiece is clamped to a moving bed, whilst in wood machining the bed is fixed and the workpiece is traversed.

Due to the physics of the process, the geometry of the machined surface consists of a series of, essentially, cicular arcs. As can be expected, in practice, the ideal is never achieved; vibration, spindle dynamic imbalance, proud knives, etc, all affect the cutter locus and hence surface profile. Obviously, the greater the level of vibration, dynamic imbalance, etc, the further the surface form departs from the ideal.

1.3 Current Surface Metrology

On considering the methods of surface analysis currently available (ie.stylus, visual/tactile, opotical and laser/optoelectronic techniques) none was found which would satisfy the criterion demanded by wood machining:-

i) Stylus instruments proved too delicate and possessed too small a bandwidth.
ii) Optical techniques are too time consuming.
iii) Laser/Optoelectronic techniques proved prone to object surface vibration which is inhrent in wood machining.

2.0 Objective

2.1 Requirements

The foregoing discussion indicates the requirement for a fast-response, non-contact, method of measuring the surface quality of machined timber; an integral part of this requirement is the determination of parameter(s) which can readily indicate and identify defects.

The "non-contact-rapid-response" nature of light, coupled with recent advances in laser and opto-electronic technology, has brought about interesting and new possiblities for in-process assessment of product quality.

2.2 Proposed Parameters

Because the cutting circle diameter used on planing machines is relatively large (typically 200mm), the depth of each cusp produced on the surface is of the order of a few microns (typically 10 μm). These are very small amplitude variations and, as such, are not detectable by the naked eye. Amplitude variation, then, cannot account for any perceived "defects". However, the eye is extremely sensitive to changes in slope (Rafael 1977) ie boundaries or lines on the surface. Hence the eye readily detects the change, from positive to negative slope, where the cicular arcs intercept, ie the apexes.

Investigations have shown that it is the consistency with which the apexes repeat that affect the aesthetic qualities of the machined surface; ie any variation in the surface wavelength, or long periodic "beats" superposed thereon, are detectable by the eye and, as such, render the surface quality defective (Knidsen 1928, Schmaltz 1936).

Therefore it would seem reasonable to analyse the surface form in terms of the frequency information inherent on any machined (planed) wooden surface.

3.0 Proposed Instrument

The technique proposed uses laser light to highlight the apexes at the intersection of the surface arcs (Figure 1). A broad beam of laser light is directed at grazing incidence (0 < 1.5 degrees) to the surface being machined, and in the plane of traverse of the workpiece. This has the effect of highlighting the leading slopes of each cusp in the beams path and produces a pattern of bright and dark regions on the surface of the workpiece. This pattern, which contains the periodic information of interest, is traversed past a single photodiode.

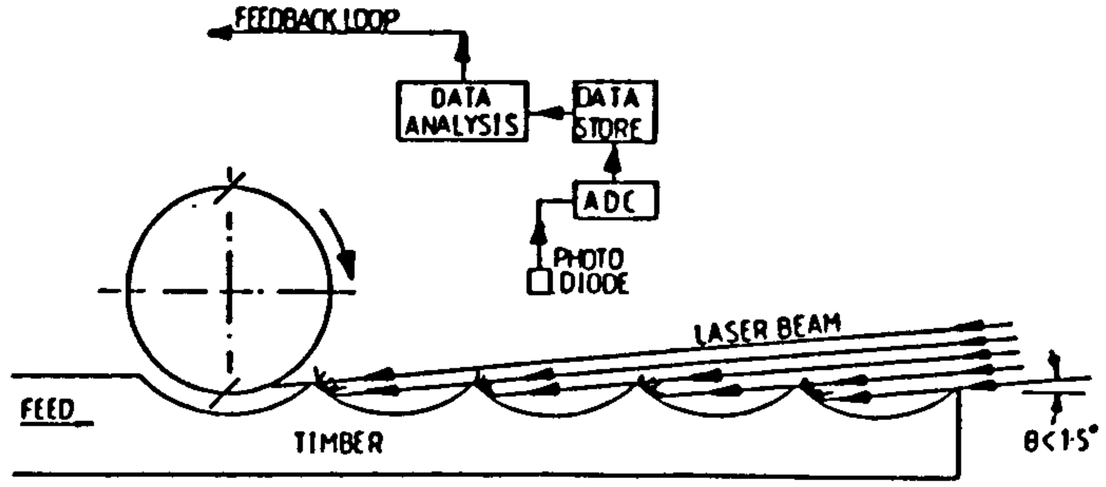

PROPOSED METHOD

Figure 1.

The output voltage of the photodiode is proportional to the intensity of the light incident upon it. This voltage is sampled (utilising a position encoder to define sample points), digitised using an Analogue to Digital Convertor, and stored in a computer's memory for subsequent analysis. The data captured is not prone to distortion due to vibration because the monitored reflectoin is diffuse, rather than specular, and the plane of vibration is almost perpendicular to the broad incident beam.

With appropriate sampling frequency, the data captured over a given length can be analysed, in terms of its frequency content, using Fourier Analysis Techniques.

The initial investigations into the technique outlined above were undertaken in a microprocessor/instrumentation laboratory with no access to woodworking machinery. The high cost of operating such machinery also means that even the collaborating machinery manufacturers do not produce any significant amounts of machined timber.

The philosophy adopted, therefore, was to use and develop the technique on stationary, pre-machined timber samples. This was accomplished by utilising

linear array of photodiodes rather than a single diode. Traversing was achieved by scanning the diode array instead of traversing the timber. Optical lenses are used to focus the image of a given length of timber on to the photodiode array. Scanning of the array provides data which is then captured for subsequent analysis.

4.0 Results

4.1 Data Capture

Figure 2(b) shows a typical graphical display of surface data captured from a timber sample (relative lightintensity being plotted against lateral position) which had been planed using a feedspeed of 106 m/min, cutterspeed of 6000 rpm and 6 knives on the cutter head. Figure 2(a) shows the corresponding Talysurf trace of the same sample.

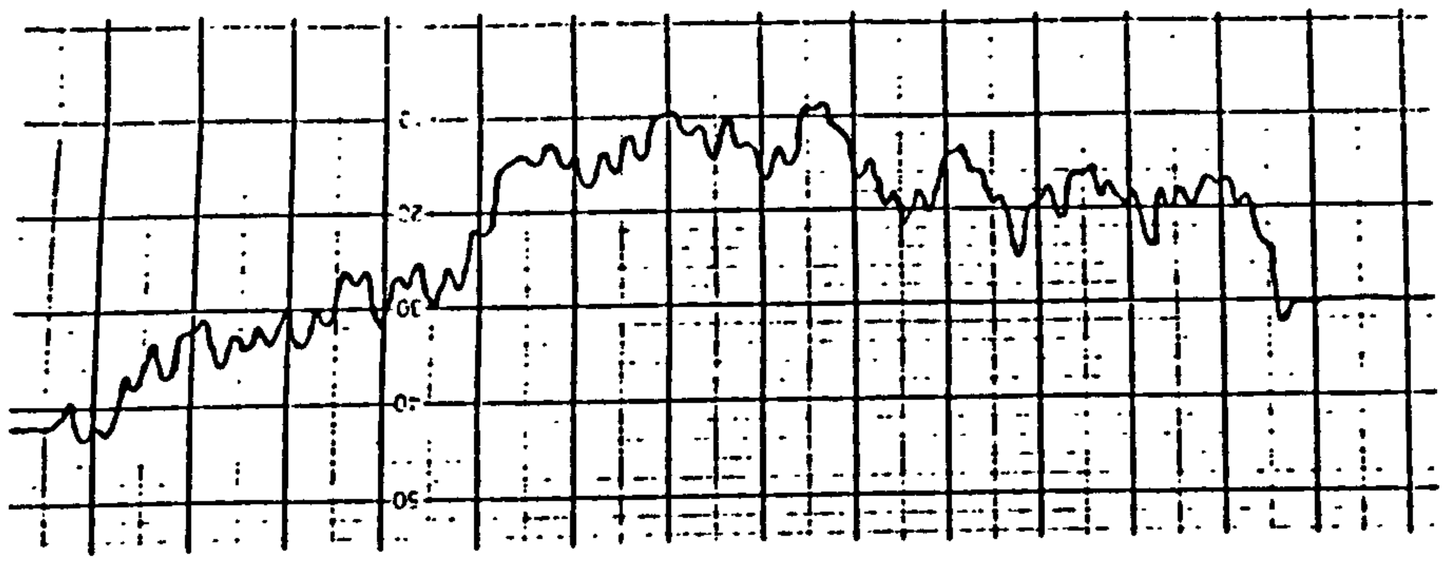

Figure 2(a) Talysurf Trace

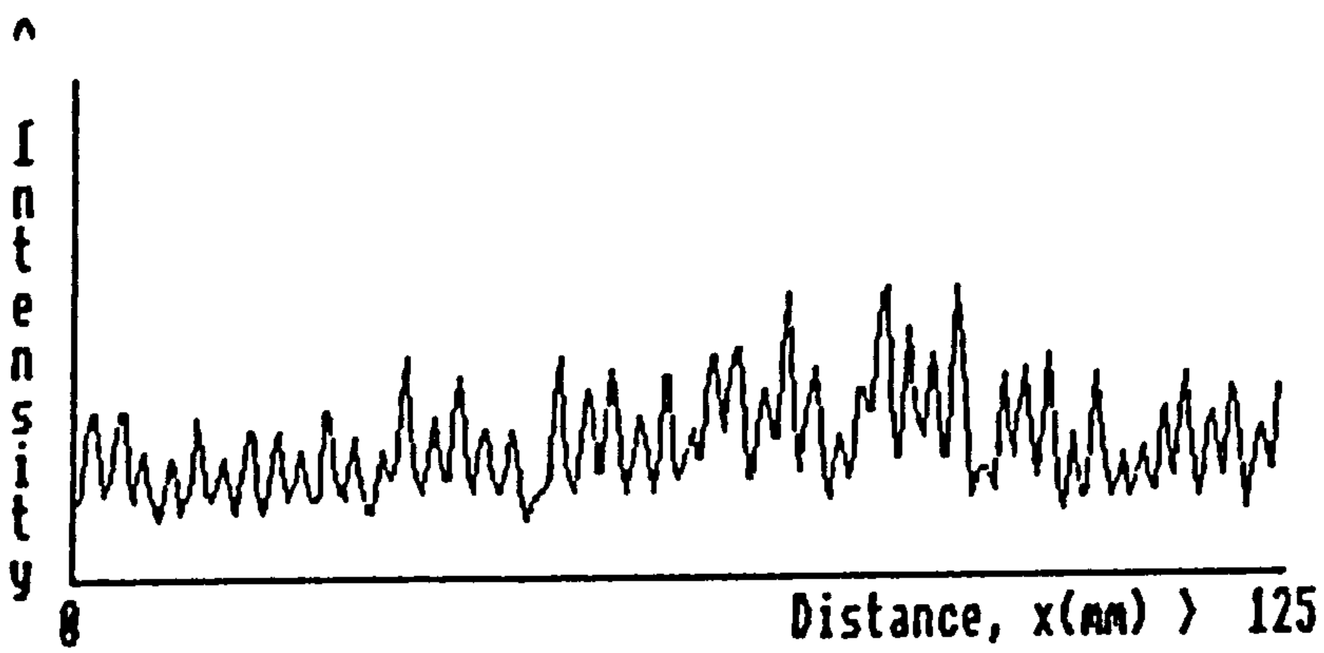

Figure 2(b) Light Intensity

4.2 Frequency Spectra of Surface Data

The surface data set obtained from the timber sample was transformed to the frequency domain using an FFT algorithm. The resulting frequency spectrum is shown in Figure 2(c).

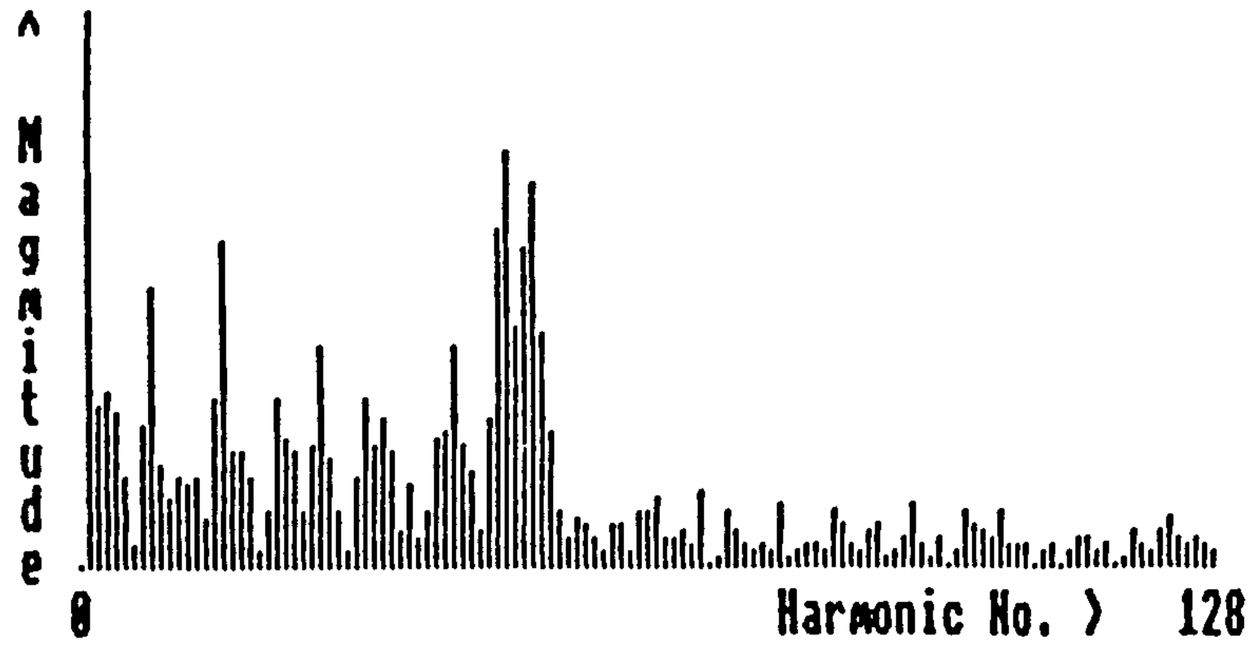

Figure 2(c) Spectrum

5.0 Discussion

There is close correlation between the peaks of the Talysurf trace and the peaks of the captured light intensity data.

The data set was analysed in terms of its harmonic content using an FFT algorithm. The result is shown in Figure 2(c) which clearly show maximum magnitude at the dominant harmonics. Notice there are 48 local maxima in the plot of light intensity verses distance - the spectrum reveals this fact with a maxima at harmonic 48. The low, undesirable frequency beats present are clearly visable in the plot and are highlighted in the spectrum.

6.0 Conclusion

An optical in-process sensor for assessing the surface quality of planed timber was introduced. Due to the growing intrest in product quality, the automation of measurement and development of accurate measurement techniques are urgently needed. The method introduced has been applied to materials other than wood eg alumiium, plastics which indicates the possible diversity of its application.

7.0 Future Work

Future work will include the relating of known process faults and associated defective surface finish with frequency spectra "signatures"; this will enable the indentification of specific faults when they occur.

The in-process application of the technique will be pursued; this necessitates dispensing with the use of a general purpose computer, replacing it with a dedicated "chip-level" device in order to achieve the speed required, incorporating the use of maths coprocessors and FFT analysers.

8.0 Bibliography

Knidsen V O, "Hearing" With a Sense of Touch, Journal of General Psychology, V1, 1928

Rafael C. Gonzalez, Paul Wintz, Digital Image Processing, Addison-Wesley Publishing Company, Inc. 1977

Schmaltz G, Technische Oberflachenkunde, Springer, Berlin, 1936

BHRA Cond Monitoring Journal Tech Note
Vol 4, No1, Jan1991

In-Process Surface Topography Measurements Predict Machine Performance and Condition.

F. Cutri B.Eng
R. Parkin B.Sc, PhD, CEng, MIEE, MIMechE
K. Maycock B.Sc

Leicester Polytechnic School of Engineering and Manufacture
Department of Mechanical and Production Engineering

Introduction

This review investigates planed and spindle moulding of wooden artifacts (Figure (1)). The woodworking industry desperately requires a reliable method by which to quantify and categorise the surface quality of its planed and spindle moulded products. The current practice is that of visual tactile inspection, which results in a wide variance in what is classed as an acceptable or defective surface finish; what one manufacturer may reject as an unacceptable standard, another may accept as "good". These methods, by their very nature, are subjective and restricted to post process applications.

Woodworking machinery has unique problems due to high speeds of operation. Modern woodworking machines "extrude" timber at extremely high rates, often in excess of 100 m/min. To achieve these rates, high cutter head rotational speeds are used (up to 15000 rev/min) resulting in high levels of noise and vibration with attendant risk

of machine bearing failure. Thus if the process develops a fault; eg, blunt cutters, imbalance, then a considerably large quantity of sub standard (defective surface finish) timber can be produced before the symptoms are detected. It is evident, due to these operational speeds, that non-contact sensors capable of monitoring the quality of the product require development.

Because the cutting circle diameter used on planing machines is relatively large (typically 200mm), the depth, h (Figure (2)) of each cusp, produced on the surface of the product, is of the order of a few microns. Due to the surface amplitudes being small, height variations, as such, are undetectable by the naked eye. Investigations have shown that it is the consistency with which the apexes repeat that affect the aesthetic qualities of the machined surface. It is then surface wavelength, or periodic beat, information that is essential for product evaluation by the manufacturer.

Realisation

The foregoing introduction clearly indicates the requirement for a fast-response non contact, method of measuring the surface quality of machined timber. Thus the "non-contact-rapid-response" nature of light, coupled with recent advances in laser and opto-electronic technologies, brings about interesting and new possibilities for the in-

process assessment of product quality.

Previous work has investigated certain types of machine faults that give rise to identifiable surface waveforms on produced timber. The monitoring system has been designed to measure the surface characteristics of the wooden component in-process. Figure (3) represents the basis of the in-process measurement system. A broad laser beam illuminates the machined surface at grazing incidence ($\theta<1.5°$). The illumination is in the same plane as the traversing workpiece, which gives prominence to the leading slope faces of each surface cusp. A fringe pattern of bright and dark regions is readily observed representing instantaneous surface slope along the product.

A single element silicon photo diode is used to detect variations in diffusely reflected surface laser light as the timber passes from the machine. Automatic gain control and signal conditioning circuitry is used to amplify and filter the output voltage of the photo diode to give maximum dynamic range to the analogue to digital convertor. The sampled output voltage of the photo diode is synchronised using the output of a rotary position encoder, as the system clock for the analogue to digital convertor. Additional electronics control the clock signal for correct read/write operations and memory sequencing.

As soon as the periodic surface information has been captured (in real time) in the computer memory, it is analysed in terms of its frequency content, using Fourier Analysis Techniques (Fast Fourier Transforms). The data captured is not prone to distortion due to vibration, as the plane of vibration is almost perpendicular to the laser illumination. As the laser beam is broad and of grazing incidence to the surface the vibration levels do not exceed the outer limits of the beam. This phenomenon only occurs because diffuse and not specular reflection is being monitored.

At present, actual material throughput is in the region of two to two and a half metres per second. The new system has been designed to cope with a maximum material movement of five metres per second, thus allowing increased capacity as machine operating conditions improve. The system is capable of monitoring wavelengths of one millimetre and greater (one millimetre being a very fine planed surface suitable for furniture manufacturers requirements).

Results

Figure ((4)a,b,) show the resultant surface and illumination profiles with their associated frequency spectra of a machined timber surface, obtained using a Talyrond and novel laser monitoring system respectively. Figures (5)

and (6), in the same manner, show other typical machined timber surfaces. The resulting profiles in figure ((4)a,b) were obtained on a six knife cutter head machine. The cutter head was run at six thousand rev/min with a corresponding material feed speed of ninety metres per minute. A deliberate out of balance effect was generated at knife number three on the cutter head (added weights), which resulted in the creation of particular frequency harmonics.

With sample lengths of one hundred and twenty five millimetres and one hundred and twenty eight frequency harmonics shown; wavelengths of one hundred and twenty five millimetres down to approximately one millimetre are representable. The dominant frequency harmonics present in Figure ((4)a,b) are numbers ten and nineteen (12.5mm and 6.58mm wavelengths). These peaks are caused by the out of balance effect and individual cutter head knife markings respectively. Because the out of balance effect occurred once every revolution of the cutter head the approximate frequency harmonic expected was number eight or nine, with these specific operating conditions. It would take 0.0833 seconds to pass one hundred and twenty five millimetres of material, through the machine, at a feed rate of ninety metres per minute. With a cutter head speed in the order of six thousand rev/min there would be

approximately eight and one half revolutions within the sample length. In fact from Figure ((4)a,b) it can be seen that there are ten revolutions present. This discrepancy is due to inaccuracies arising from the feed and cutter head speed equipment. As there is an out of balance effect, the knife marks vary in surface wavelength, thus in the frequency spectrum the knife marks are spread over several rather than a single harmonic (eg harmonic numbers 10, 19, etc).

Figure (5) shows similar conditions as that in Figure (4). Here again there is a deliberate once per revolution out of balance effect caused, however, now on a four knife cutter head. In this instant the feed speed of the machine (eighteen metres per minute) is much slower, but the cutter head speed of six thousand rev/min remains the same. The effect of the slow feed speed on the surface is the translation of the out of balance dominant frequency along the frequency spectrum (Higher frequency due to slower moving feed material). As it would take 0.4166 seconds to pass one hundred and twenty five millimetres of timber at eighteen meters per minute. An out of balance frequency would now be generated at approximately harmonic No forty two (Figure((5)a,b)) in the frequency spectra. In addition to the out of balance phenomenon there is a secondary effect resulting in smoothed surface knife

marks, this event is indicated in the frequency spectrum due to a lack of other higher dominant frequency harmonics.

Figure ((6)a) shows a single knife finish surface. This surface was obtained using a four knife cutter head with three of the knives used as balancing masses only. With no out of balance effect present, the dominant frequency in the frequency spectra is now due solely to the cutter knife marks on the surface. With a feed speed of eighteen metres per minute it would again take 0.416 seconds to pass one hundred and twenty five millimetres of timber past the cutter head. With a six thousand rev/min cutter head there would be 41.6 revolutions of the cutter head (with a single knife this would be 41.6 identical knife marks) in the sample length. As shown in each of the frequency spectra (figure ((6)a,b)) the dominant harmonic No is number forty five (wavelength of 3mm). The discrepancy resulting again from feed and cutter head equipment inaccuracies.

Conclusion

Non-contact measuring/monitoring hardware and software has been developed to control the quality of planed artifacts. Good correlation between existing surface measuring systems (Talyrond) and the novel laser measurement system has

been obtained using harmonic analysis. This comparison has been achieved using a Fast Fourier Algorithm to convert real surface data from the time to the frequency domain. Results have shown that certain machine fault signatures are inherent within manufactured product surface contours. Future work regarding the frequency spectra of trend or catastrophic failures is required for correct initialisation of machine feedback action.

Figure 1

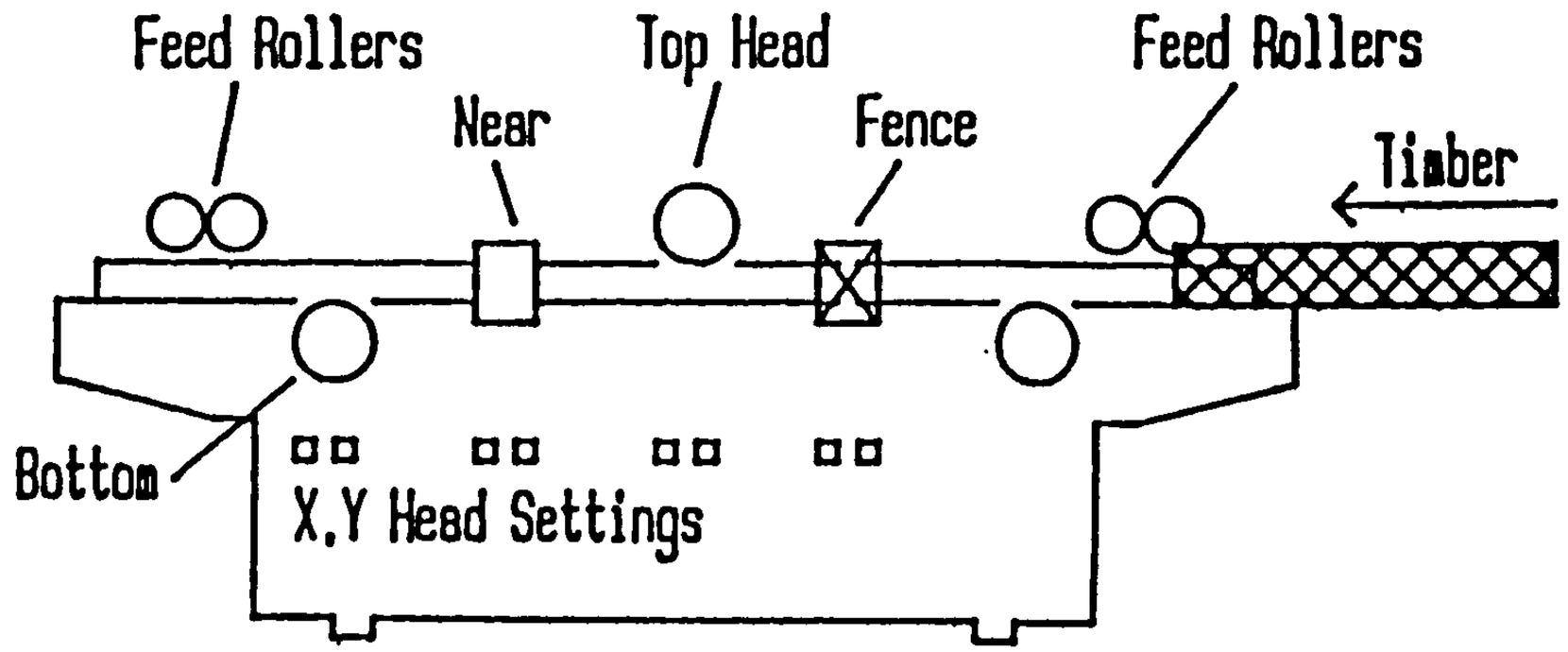

4 Head Planer - Moulder

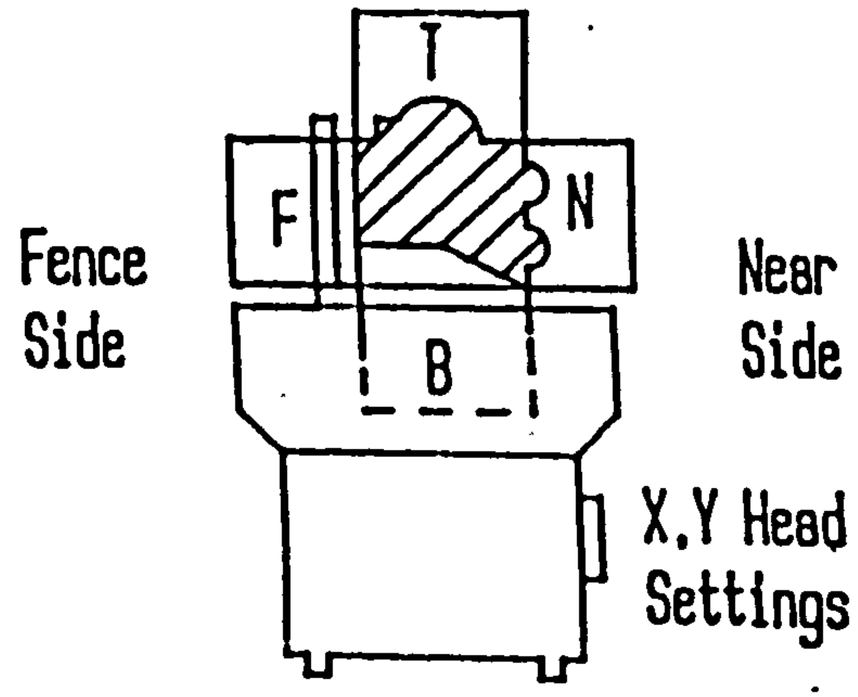

Cutter Heads

T Top Head
B Bottom Head
F Fence Head
N Near Head

Surface Profile Height and Pitch

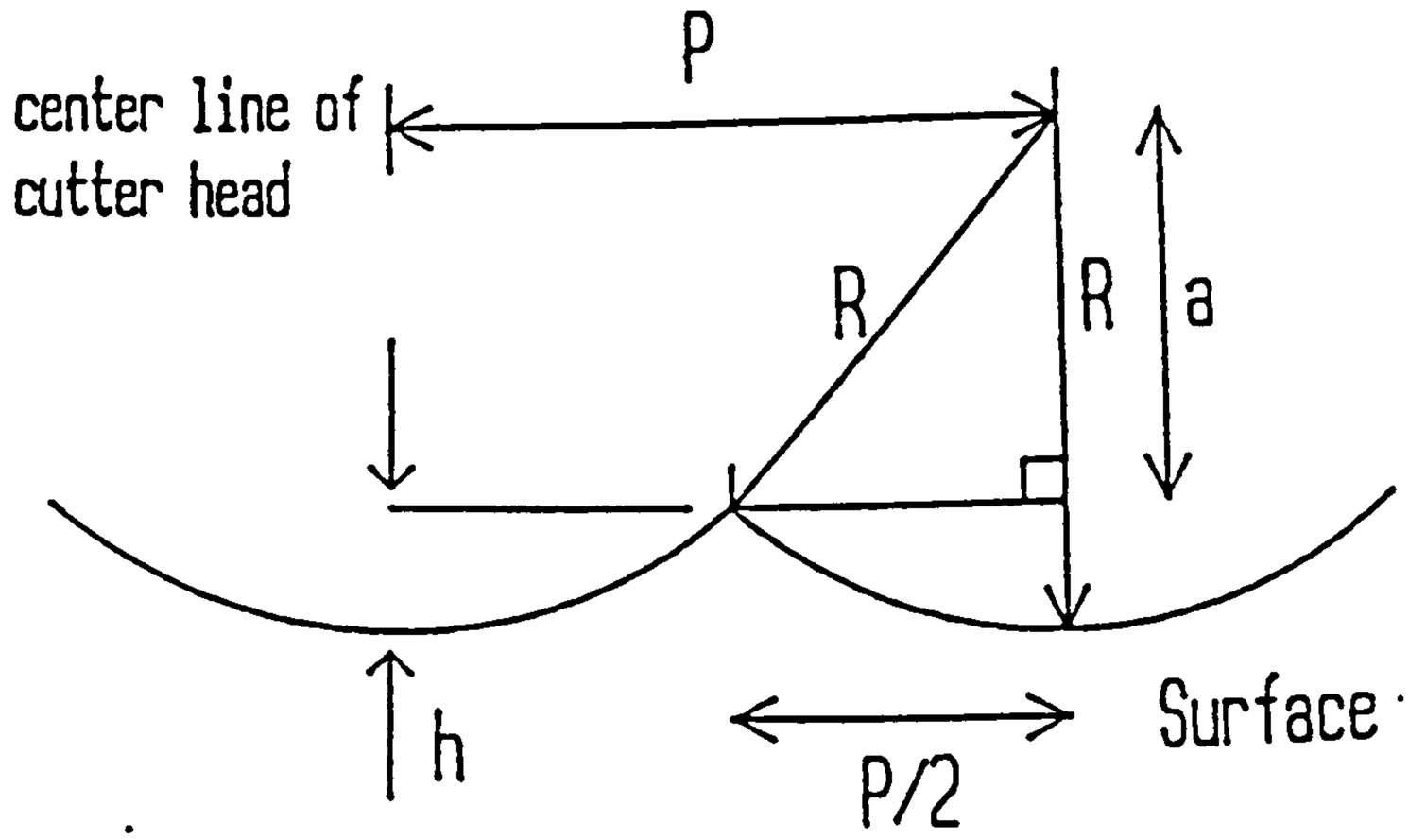

$a = R - h$

$a^2 = R^2 - (P/2)^2$ $\qquad P = (f. 10^3)/nN$

$a = (R^2 - (P/2)^2)^{1/2}$

$h = R - a$

$h = R - (R^2 - P^2/4)^{1/2}$

Figure 2

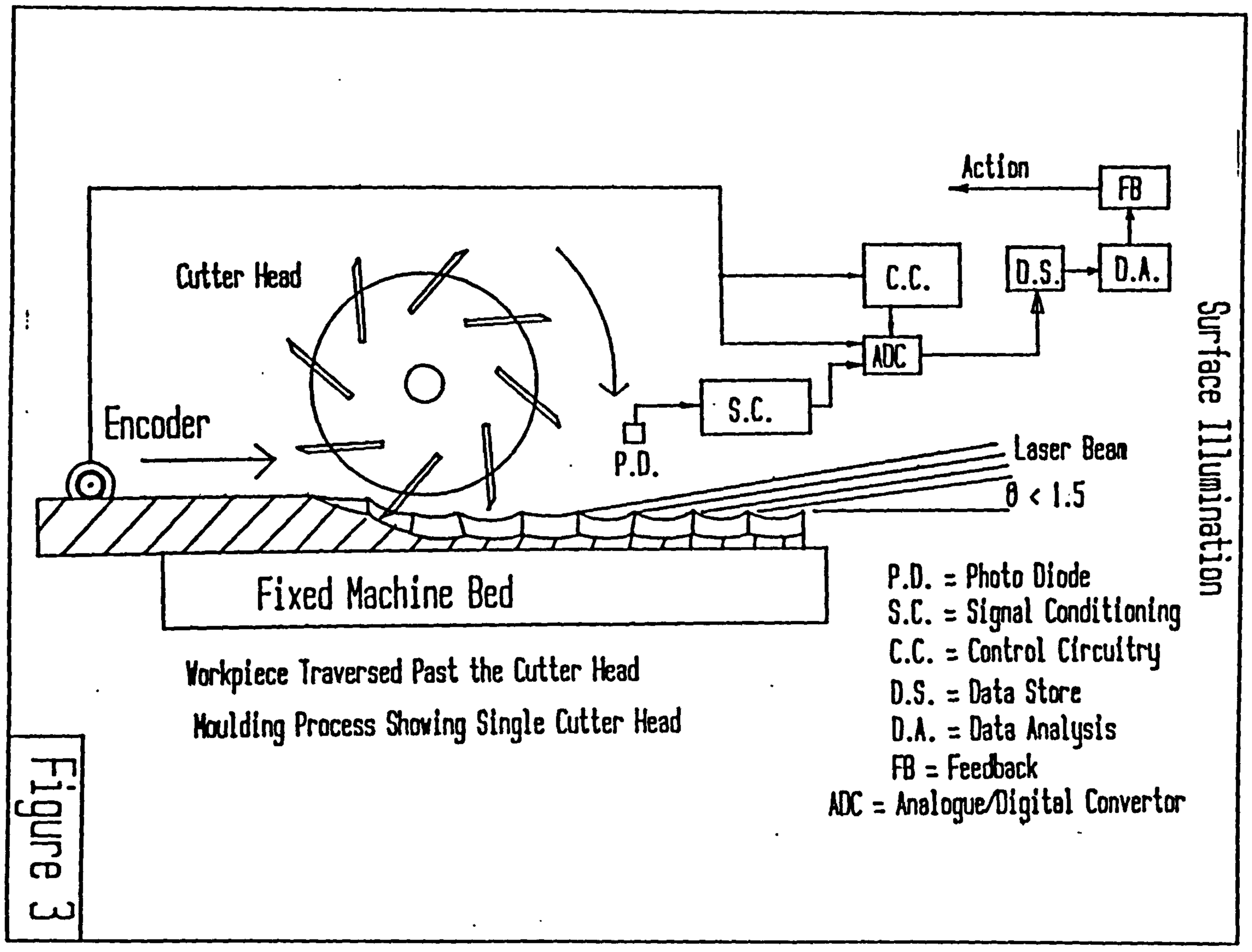
Action
FB
C.C.
D.S.
D.A.
Cutter Head
ADC
S.C.
Encoder
P.D.
Laser Beam
θ < 1.5
Fixed Machine Bed
Workpiece Traversed Past the Cutter Head
Moulding Process Showing Single Cutter Head
P.D. = Photo Diode
S.C. = Signal Conditioning
C.C. = Control Circuitry
D.S. = Data Store
D.A. = Data Analysis
FB = Feedback
ADC = Analogue/Digital Convertor
Surface Illumination

Figure 3

Talyrond Surface Data

4a)

Laser Slope Intensity Data

4b)

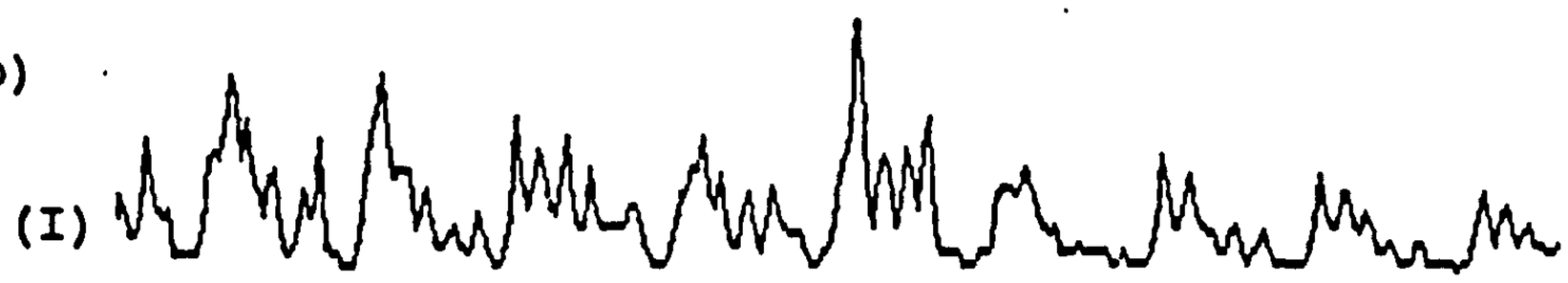

(A) Amplitude
(I) Intensity

Figure 4

Talyrond Surface Data

5a)

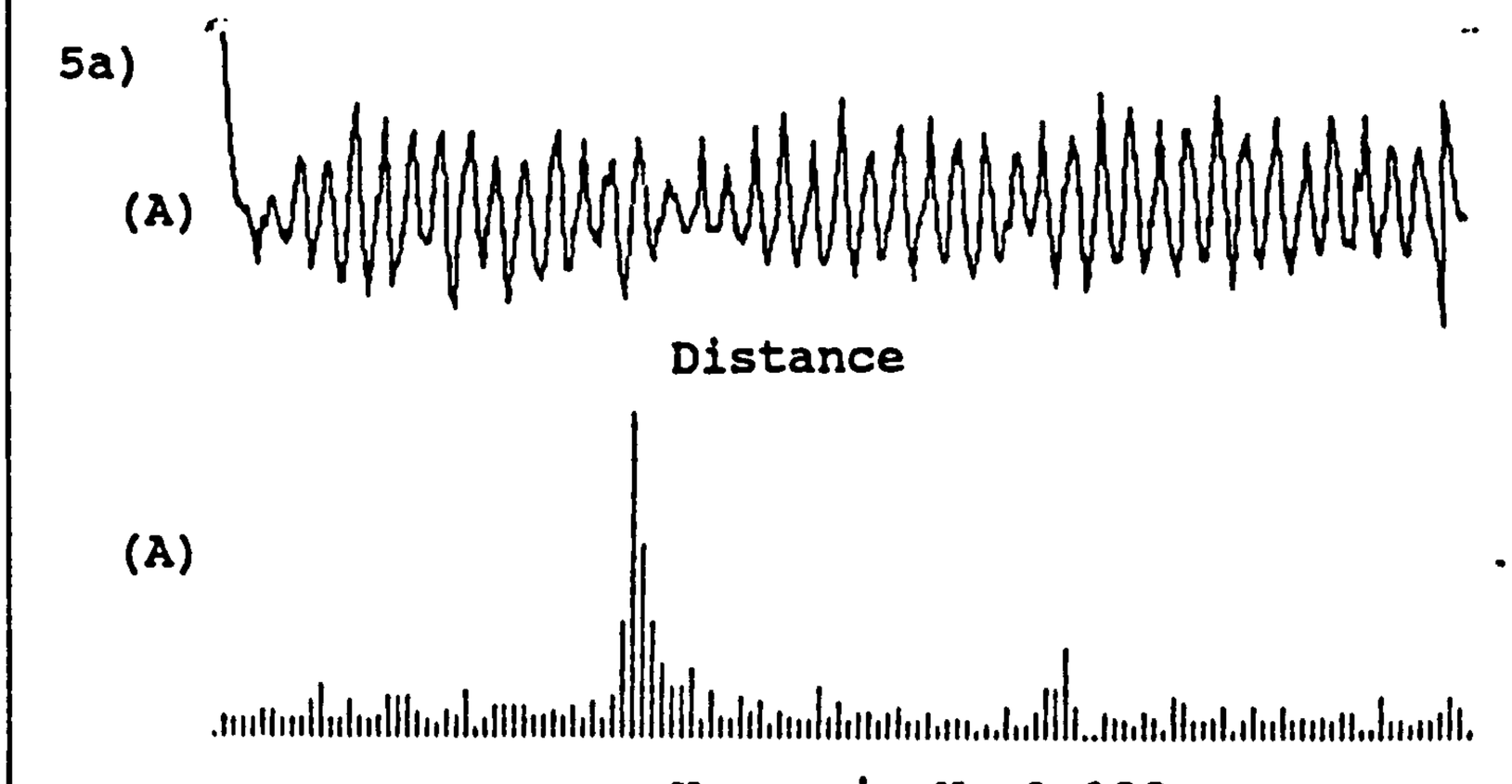

Laser Slope Intensity Data

5b)

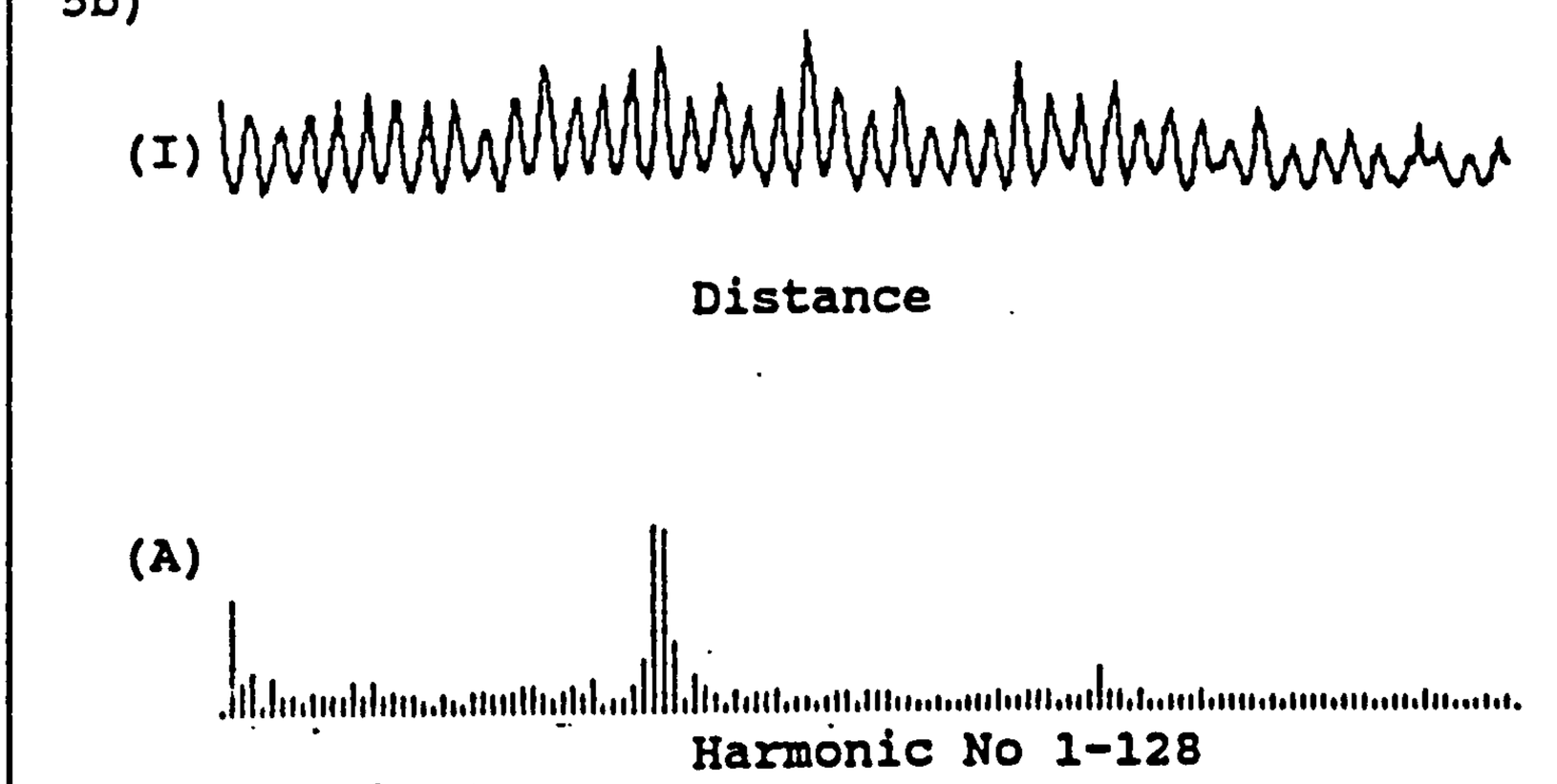

(A) Amplitude
(I) Intensity

Figure 5

Talyrond Surface Data

6a)

Laser Slope Intensity Data

6b)

(A) Amplitude
(I) Intensity

Figure 6